

**GEOLOGY AND GEOHYDROLOGY OF THE PALO DURO BASIN,  
TEXAS PANHANDLE**

**A Report on the Progress of Nuclear Waste Isolation Feasibility Studies (1983)**

**Annual Report**

**for period October 1, 1982 - September 30, 1983**

**edited by**

**T. C. Gustavson**

**contributions by**

**R. W. Baumgardner, Jr., R. T. Budnik, S. C. Caran, E. W. Collins, R. D. Conti,  
S. D. Davis, A. R. Dutton, S. P. Dutton, R. S. Fisher, G. E. Fogg, M. A.  
Fracasso, T. C. Gustavson, S. D. Hovorka, D. A. Johns, A. Kolker, C. W. Kreidler,  
B. A. Luneau, M. D. Machenberg, D. A. McGookey, H. S. Nance, R. W. Neck,  
E. D. Orr, W. D. Pennington, B. C. Richter, S. C. Ruppel, R. K. Senger, W. W.  
Simpkins, D. A. Smith, S. Thomas, and P. Wirojanagud**

**Prepared for the U.S. Department of Energy  
Salt Repository Project Office  
Contract No. DE-AC97-83WM46651**

**Bureau of Economic Geology  
W. L. Fisher, Director  
The University of Texas at Austin  
University Station, Box X  
Austin, Texas 78713**

**1987**

## CONTENTS

Purpose and Scope by Research Staff . . . . .	1
Palo Duro Basin Studies--A Summary of Sixth-Year Research Activities by Research Staff . . . . .	4
Seismic Reflection Surveys for Siting a Proposed Nuclear Waste Isolation Facility, Texas Panhandle by Roy T. Budnik . . . . .	13
Evidence of Basin and Range-Age Deformation in the Texas Panhandle by Roy T. Budnik . . . . .	22
Occurrence of Clastic Dikes in the Texas Panhandle by Edward W. Collins . . . . .	40
Geometry and Origin of Synclinal Depressions at Caprock Canyons State Park, Briscoe County, Texas by Edward W. Collins . . . . .	43
Mississippian Conodont Biostratigraphy in the Palo Duro Basin Area by Stephen C. Ruppel . . . . .	47
Pre-Pennsylvanian Carbonates as Potential Hydrocarbon Source Rocks, Palo Duro and Dalhart Basins, Texas by Stephen C. Ruppel . . . . .	57
Regional Correlation and Cyclicity of the San Andres Formation (Permian, Guadalupian), Palo Duro Basin, Texas Panhandle by Michael A. Fracasso . . . . .	69
Late Permian Volcanic Ash Beds in the Quartermaster-Dewey Lake Formations, Texas Panhandle by Allan Kolker and Michael A. Fracasso . . . . .	78
Preliminary Stratigraphic Correlations and Structural Implications of the Dockum Group, Palo Duro Basin, Texas by David A. Johns . . . . .	89
Lithostratigraphic Sections: Stone and Webster Engineering Corporation Harman No. 1 and Zeeck No. 1, Swisher County, Texas by Susan D. Hovorka, Sterling Thomas, Barbara A. Luneau, and Stephen C. Ruppel . . . . .	98
Correlation of Clean, Muddy, and Anhydritic Zones in Halite, San Andres Formation Units 4 and 5, Deaf Smith County, Texas by Susan D. Hovorka, Barbara A. Luneau, and Sterling Thomas . . . . .	110
Evidence of Halite Dissolution in Core from beneath the Southern High Plains, Texas by Susan D. Hovorka . . . . .	114



Textural Classification of Salt with Genetic Significance by Susan D. Hovorka . . . . .	128
Cyclicality in the San Andres Formation by Susan D. Hovorka . . . . .	141
Geochemical and Textural Evidence of Primary and Altered Halite, Permian San Andres Formation, Palo Duro Basin, Texas by R. Stephen Fisher and Susan D. Hovorka . . . . .	151
Clay Mineral Assemblages in Evaporite Host Rocks, Palo Duro Basin, Texas by R. Stephen Fisher . . . . .	159
Petrology and Depositional Environments of Post-Wichita/Pre-Dockum Siliciclastic Rocks (Leonardian-Ochoan), Palo Duro Basin by Allan Kolker, Susan D. Hovorka, Douglas A. McGookey, and H. Seay Nance . . . . .	165
Thermal Maturity of Some Source Rocks in the Palo Duro Basin by Shirley P. Dutton. . . . .	175
Oil Fields in the Northwestern Palo Duro Basin by Shirley P. Dutton. . . . .	181
Comparison of Neutron-Density and Neutron-Sonic Crossplotting Methods in Determining Lithology and Porosity in Wolfcamp Carbonates by Robert D. Conti . . . . .	187
Hydrogeologic Testing of the San Andres Formation in the Palo Duro Basin, Texas Panhandle by Alan R. Dutton . . . . .	194
Water Sampling and Hydrologic Testing in the Salt-Dissolution Zone of the Texas Panhandle by Alan R. Dutton . . . . .	198
Potentiometric Surface of the Upper Pennsylvanian Aquifer, Texas Panhandle by D. Anderson Smith . . . . .	209
Interpretation of Pressure-Depth Data from Confined Aquifers by Elizabeth D. Orr and Charles W. Kreitler . . . . .	215
Vertical Components of Ground-Water Flow in the Palo Duro Basin by Elizabeth D. Orr and Charles W. Kreitler . . . . .	222
Numerical Modeling of the Wolfcamp Aquifer, Palo Duro Basin by Prakob Wirojanagud, Charles W. Kreitler, and D. Anderson Smith . . . . .	231
Modeling of Vertical Ground-Water Flow in the Palo Duro Basin: A Progress Report by Rainer K. Senger and Graham E. Fogg. . . . .	237
Geochemical Characteristics of Salt Spring and Shallow Subsurface Brines in the Rolling Plains of Texas and Southwestern Oklahoma by Bernd C. Richter and Charles W. Kreitler. . . . .	245

Isotopic Composition of Shallow Ground Water in Eastern New Mexico and the Texas Panhandle by Rainer K. Senger, Bernd C. Richter, and Charles W. Kreitler . . . . .	257
A Review of Research on Borehole Sealing and Its Application to a Proposed Repository in the Palo Duro Basin by William W. Simpkins . . . . .	263
Water Content of Bedded Salt, Palo Duro Basin, Texas by R. Stephen Fisher . . . . .	268
Hydrogeochemistry of Sub-Salt Brines from the Sawyer, Mansfield, and Zeeck Wells, Palo Duro Basin, Texas by R. Stephen Fisher . . . . .	270
Structural Control of Physiography, Geomorphic Processes, and Lithofacies, Texas Panhandle by Thomas C. Gustavson and Roy T. Budnik . . . . .	279
Stratigraphy of an Extensive Quaternary Sedimentary Sequence--Briscoe, Floyd, Hall, and Motley Counties, Texas by S. Christopher Caran and Robert W. Baumgardner, Jr. . . . .	286
Quaternary Faulting in Southeastern Briscoe County, Texas by Robert W. Baumgardner, Jr., and S. Christopher Caran . . . . .	295
Long-Term Rates of Denudation based on Hypsometric Analysis of Drainage Basins and Underlying Salt Beds, Texas Panhandle by Robert W. Baumgardner, Jr. . . . .	301
Statistical Analysis of Erosion Pin Measurements: Description of Erosion and Deposition by William W. Simpkins . . . . .	307
Statistical Analysis of Erosion Pin Measurements: Calculation and Projection of Erosion and Deposition Rates by William W. Simpkins . . . . .	319
Modern Eolian Processes on the Southern High Plains and Adjacent Areas by Marcie D. Machenberg and S. Christopher Caran. . . . .	329
Analysis of Dust-Trap Samples Collected on the Southern High Plains and Adjacent Areas by Marcie D. Machenberg . . . . .	337
Late Quaternary Paleoclimatology of Northwestern Texas--Implications for Disposal of Nuclear Waste by S. Christopher Caran and Raymond W. Neck . . . . .	344
Historic Seismicity in and around the Texas Panhandle by Wayne D. Pennington and Scott D. Davis . . . . .	350
References. . . . .	356

## Figures

1. Organizational structure of the West Texas Waste Isolation Program (FY 1983) . . . . .	3
2. Location map of seismic reflection surveys and Department of Energy test wells, Palo Duro Basin . . . . .	16
3. Portion of line SWEC G-1 in central Swisher County . . . . .	17
4. Portion of line SWEC J in central Randall County . . . . .	18
5. Portion of line SWEC G-3 in central Swisher County . . . . .	19
6. Portion of line SWEC H-2 in northern Swisher County . . . . .	20
7. Distribution of syntectonic Neogene sediments of the High Plains and Rio Grande Rift . . . . .	25
8. Isopach map, Ogallala Formation . . . . .	26
9. Structure-contour map on top of basement, Whittenburg trough and flanking uplifts . . . . .	27
10. Distribution of salt and isopach of Middle and Upper Permian strata, Carson basin . . . . .	28
11. Isopach map of the Dockum Group (Triassic) in the Carson basin . . . . .	29
12. a. Structure map of base of the Ogallala Formation, Carson basin . . . . .	30
b. Structure map of top of the Alibates Formation, Carson basin . . . . .	31
13. a. Structure map of top of the Tubb Formation, Carson basin . . . . .	32
b. Structure map of top of Wolfcamp, Carson basin . . . . .	33
c. Structure map of top of basement, Carson basin . . . . .	34
14. Isopach map of the Pennsylvanian and Lower Permian, Carson basin . . . . .	35
15. Schematic illustration of Ogallala depositional facies and sediment dispersal systems . . . . .	36
16. Log length versus log width for 70 pull-apart basins or rhomb grabens and horsts associated with major strike-slip faults of the world . . . . .	37
17. Structure-contour map on the base of the Ogallala Formation at the western end of the Amarillo Uplift . . . . .	38
18. Seismicity in the Texas Panhandle . . . . .	39

19. Comparison of clastic dikes and joint orientations in the Texas Panhandle and eastern New Mexico. . . . .	42
20. Structure map exhibiting the geometry of folds at Caprock Canyons State Park, Briscoe County. . . . .	45
21. (a) Rose diagram exhibiting trends of vertical gypsum veins, (b) Schmidt net plot of poles to inclined veins . . . . .	46
22. Conventional subdivision of Mississippian rocks in Palo Duro Basin . . . . .	50
23. Map of the Texas Panhandle showing the location of the Palo Duro and Hardeman Basins and four cored wells . . . . .	51
24. Probable correlation of four wells from which conodonts were recovered . . . . .	52
25. Reported hydrocarbon shows, discoveries, and fields in the Ellenburger Group (Ordovician) in the Texas Panhandle . . . . .	60
26. Reported hydrocarbon shows, discoveries, and fields in the Mississippian rocks of the Texas Panhandle . . . . .	61
27. Distribution of Ordovician (Ellenburger Group) deposits and wells in the Texas Panhandle area that were sampled for total organic carbon . . . . .	62
28. Distribution of Mississippian deposits and wells in the Texas Panhandle area that were sampled for total organic carbon. . . . .	63
29. Frequency distribution of total organic carbon abundance in pre-Pennsylvanian carbonates from the Palo Duro, Dalhart, and Hardeman Basins . . . . .	64
30. Plot of vitrinite reflectance with depth . . . . .	65
31. Palo Duro Basin and surrounding structural elements, Texas Panhandle . . . . .	73
32. Geophysical log pattern and lithology of lower San Andres Formation cycles 2, 3, and 4 . . . . .	74
33. Correlation section A-A', San Andres Formation, Dalhart and Palo Duro Basins, and northern shelf of the Midland Basin . . . . .	75
34. Correlation section B-B', San Andres Formation, western to eastern Palo Duro Basin . . . . .	76
35. Correlation section C-C', San Andres Formation, Tucumcari Basin to eastern Palo Duro Basin, New Mexico and Texas Panhandle . . . . .	77
36. Structural elements in Texas Panhandle region and locations of measured sections and volcanic ash beds in the Quartermaster and Dewey Lake Formations . . . . .	83
37. Measured sections K-3-83, K-4-83, and DOE-Gruy Federal Grabbe No. 1, Quartermaster and Dewey Lake Formations, Texas Panhandle. . . . .	84

38. Measured sections K-1-83, K-2-83, and K-5-83, Quartermaster Formation, Texas Panhandle . . . . .	85
39. Lower volcanic ash bed of the Permian Quartermaster and Dewey Lake Formations, Texas Panhandle . . . . .	86
40. Clay mineral X-ray diffraction analysis of lower volcanic ash bed, Quartermaster and Dewey Lake Formations, Texas Panhandle . . . . .	87
41. Stratigraphic column and general lithology of the Palo Duro Basin . . . . .	92
42. Outcrop of Dockum Group and locations of cross sections in the Palo Duro Basin . . . . .	93
43. West-east regional cross section 1-1' of post-Queen-Grayburg Formations . . . . .	94
44. North-south regional cross section 2-2' of post-Queen-Grayburg Formations. . . . .	95
45. Core description of the Dewey Lake Formation and Dockum Group correlated with geophysical well log patterns, Rex White No. 1 and Grabbe No. 1 . . . . .	97
46. Uppermost occurrence of halite in SWEC Harman No. 1 core composed of corroded halite crystals rimmed with anhydrite and dolomite . . . . .	103
47. Halite-filled vein in SWEC Harman No. 1 core . . . . .	103
48. Typical limestone of unit 4 of the San Andres Formation . . . . .	104
49. Possible supratidal dolomite at the top of San Andres unit 4 . . . . .	104
50. Tall, finely banded halite and anhydrite pseudomorphs after bottom-nucleated gypsum crystals. . . . .	105
51. Pseudomorphs after gypsum crystals radiating outward from an irregular bedding surface . . . . .	105
52. Typical fine sandstone with dissipation structures in the Queen-Grayburg Formations . . . . .	106
53. Halite-filled vertical fractures separated by thin horizontal partings of anhydrite in the uppermost occurrence of halite in SWEC Zeeck No. 1 core. . . . .	106
54. Unusual magnesite nodules indicating the probable penetration of diagenetic waters into the halite of the Salado-Tansill Formations. . . . .	107
55. Extremely coarse crystals in Salado-Tansill halite indicating the penetration of ground water deeper than the interval in which dissolution occurred . . . . .	107
56. Oncolite grainstone at the top of unit 4 carbonate, SWEC Zeeck No. 1 core . . . . .	108
57. Possible karst pits in an anhydrite bed within the unit 4 halite filled with mudstone and halite . . . . .	108

58. Cross-laminated carbonate grainstone in the Wolfcamp, SWEC Zeeck No. 1 core. . . . .	109
59. Example of detailed logs of SWEC J. Friemel No. 1, Detten No. 1, and G. Friemel No. 1 cores, San Andres Formation unit 5, showing correlation of two thin anhydrite beds . . . . .	112
60. Example of detailed logs of SWEC J. Friemel No. 1, Detten No. 1, and G. Friemel No. 1 cores, San Andres Formation unit 4, showing correlation of zones of anhydritic halite with primary fabric and the overlying zone of muddy halite with many mudstone interbeds . . . . .	113
61. Stratigraphic sections comparing features present in the dissolution zone of seven DOE stratigraphic test wells from the Palo Duro Basin. . . . .	117
62. Typical fabrics in the dissolution zone, Seven Rivers Formation SWEC Detten No. 1 core . . . . .	118
63. Insoluble residue breccia of mudstone, anhydrite, gypsum, and multifaceted dolomite in core, DOE-Gruy Federal Rex White No. 1 . . . . .	118
64. Photomicrograph of insoluble residue of mudstone, anhydrite, gypsum, and multifaceted dolomite . . . . .	119
65. Slickensided surfaces of fractures, some coated with gypsum vein-fillings . . . . .	120
66. Fibrous gypsum-filled veins, Salado-Tansill Formations, DOE-Gruy Federal Rex White No. 1 core . . . . .	120
67. Nodular anhydrite hydrated to gypsum in isolated spherical patches . . . . .	121
68. Photomicrograph of spherulitic, coarsely crystalline anhydrite in the dissolution zone, DOE-Gruy Federal Grabbe No. 1 core. . . . .	122
69. Coarsely crystalline halite texture characteristic of the uppermost halite preserved . . . . .	123
70. Dissolution zone in the G. Friemel No. 1 core at the base of the Seven Rivers Formation. . . . .	123
71. Euhedral gypsum replacing fine anhydrite mosaic . . . . .	124
72. Replacement of gypsum crystals by anhedral dolomite in anhydrite matrix in the Alibates Formation, DOE-Gruy Federal Grabbe No. 1 core. . . . .	125
73. Calcite cement in bimodal eolian sandstone, Dewey Lake Formation, DOE-Gruy Federal Grabbe No. 1 core . . . . .	126
74. Calcite replacing coarse euhedral gypsum crystals in mudstone, SWEC Mansfield No. 1 core. . . . .	127
75. Microfaulting and folding typical of Alibates Formation, SWEC Harman No. 1 core . . . . .	127

76. Minute fluid inclusions concentrated along relict growth faces of bottom-nucleated halite crystals defining chevron structures . . . . .	133
77. Typical chevron halite rock from unit 5 of San Andres Formation, SWEC Detten No. 1 core . . . . .	133
78. Photomicrograph of chevron halite truncated by a corrosion surface above which anhydrite has been deposited . . . . .	134
79. Dark pit filled with coarse, muddy halite and formed by dissolution, introduction of mudstone, and recrystallization of primary chevron halite rock along a vertical fracture . . . . .	135
80. Pit filled with coarse cavity-filling halite cement in color-banded, vertically oriented halite host . . . . .	135
81. Pit in color-banded, vertically oriented halite filled with, in succession (1) halite cement, (2) siliciclastic mudstone, and (3) displacive halite cubes . .	136
82. Typical chaotic mudstone-halite rock in which primary fabric has been destroyed . . . . .	136
83. Recrystallized muddy halite rock from a halite interval within the Queen-Grayburg Formations . . . . .	137
84. Displacive halite cubes in mudstone beds, unit 5, San Andres Formation, SWEC Mansfield No. 1 core . . . . .	138
85. Cavity-filling halite cement forms very coarse crystals in a pit in color-banded halite rock . . . . .	139
86. Fibrous halite fracture-fill in carbonate mudstone of unit 4, San Andres Formation, SWEC Mansfield No. 1 core . . . . .	139
87. Idealized San Andres cycle showing sequence of lithologies and sedimentary structures that would result from an uninterrupted increase in salinity . . .	144
88. Dark mudstone at the base of a cycle . . . . .	145
89. Correlation of San Andres Formation unit 4 carbonate showing that facies in the marine-limestone part of the interval are the result of variations in the energy of the depositional environment . . . . .	146
90. Examples of sequence lithologies in the anhydrite part of the cycle . . . .	147
91. Cyclicity in San Andres unit 5, SWEC Mansfield No. 1 core . . . . .	148
92. An incomplete cycle in the upper San Andres Formation, SWEC Detten No. 1 core . . . . .	149
93. Correlation of three thin cycles in the upper San Andres Formation across the northern Palo Duro Basin, showing the continuity of subtle variations in the nature of cyclicity . . . . .	150

94. Typical bromide-versus-depth profiles: (a) Permian Zechstein unit 2, (b) Salt unit 3. . . . .	153
95. Bromide versus depth, San Andres Formation, SWEC G. Friemel No. 1 . . . .	154
96. Bromide versus depth, San Andres Formation, DOE-Gruy Federal Rex White No. 1 . . . . .	155
97. Bromide versus depth, San Andres Formation, SWEC Sawyer No. 1 . . . .	156
98. Typical subcycle, SWEC Detten No. 1 core . . . . .	157
99. Type "B" halite with anhydritic bands, SWEC Detten No. 1. . . . .	158
100. Host-rock lithology and clay mineralogy of samples from (a) DOE-Gruy Federal Rex White No. 1, (b) DOE-Gruy Federal Grabbe No. 1 cores . . . . .	161
101. Histograms showing relative occurrence of clay minerals on three groups of samples: (a) no salt within 10 ft of sample, (b) non-salt samples within 10 vertical feet of bedded salt, (c) insoluble residue within salt rocks. .	162
102. Changes in concentrations of major ions during evaporation of average modern seawater . . . . .	163
103. Conceptual model of clay diagenesis in environments of increasing magnesium activity . . . . .	164
104. Representative grain size frequency distributions, (a) Lower Seven Rivers Formation, halite-influenced flat facies, SWEC Mansfield No. 1 core, (b) Queen-Grayburg Formations, eolian flat facies, DOE-Gruy Federal Grabbe No. 1 core, (c) Glorieta Formation, channel facies in flats, DOE-Gruy Federal Grabbe No. 1 core. . . . .	171
105. Bimodal very fine to medium sublitharenite . . . . .	172
106. Quartz:feldspar:rock fragment ratios for 33 Permian samples and 3 Dockum Group samples . . . . .	173
107. Trend of vitrinite reflectance with depth for two wells in the Palo Duro Basin . . . . .	177
108. A plot of pyrolysis T°C Max against the ratio $S_1/S_1 + S_2$ defining the oil generation zone . . . . .	178
109. Location of oil fields in Oldham and western Potter Counties . . . . .	183
110. Structure-contour map on the top of the upper granite wash, the reservoir for Lambert, Hryhor, and Sundance fields. . . . .	184
111. Neutron-porosity values plotted against the density-porosity values for "pure" dolomite . . . . .	190



112. Neutron-porosity values plotted against the density-porosity values for "pure" limestone . . . . .	191
113. Neutron-porosity values plotted against the sonic-transit-time values for pure dolomite . . . . .	192
114. Neutron-porosity values plotted against the sonic-transit-time values for "pure" limestone . . . . .	193
115. Locations of drill-stem tests in the San Andres Formation with values of salt-water head and permeability . . . . .	196
116. Locations of hydrochemical test wells in the salt dissolution zone in the Texas Panhandle . . . . .	202
117. Salt-dissolution zones, Texas Panhandle and eastern New Mexico . . . . .	203
118. Major zones of salt dissolution underlying the eastern margin of the Southern High Plains. . . . .	204
119. Stratigraphy and construction of the SWEC Sawyer No. 2 hydrochemical test well. . . . .	205
120. Stratigraphy and construction of the SWEC Mansfield No. 2 hydrochemical test well. . . . .	206
121. Stratigraphy and construction of the SWEC Detten No. 2 hydrochemical test well. . . . .	207
122. Stratigraphy and construction of the SWEC Harman No. 1 hydrochemical test well. . . . .	208
123. Semi-variogram of upper Pennsylvanian equivalent fresh-water heads calculated from drill-stem-test shut-in pressures in the Anadarko Basin . . . . .	212
124. Semi-variogram of upper Pennsylvanian equivalent fresh-water heads calculated from drill-stem-test shut-in pressures in the Palo Duro and Midland Basins . . . . .	213
125. Potentiometric surface map of equivalent fresh-water heads calculated from drill-stem-test shut-in pressures in upper Pennsylvanian strata . . . . .	214
126. Flow patterns and pressure-depth relationships for (a) a simple unconfined drainage basin, and (b) a confined hydrostatic aquifer . . . . .	218
127. Plot of pressure-depth drill-stem-test data in Hockley County. . . . .	219
128. Variations in configurations of plotted pressure-depth data due to changes in surface topography, aquifer structure, and the potentiometric surface . . . . .	220

129. Comparisons of drill-stem-test data and modeled pressure-depth data for the confined Deep-Basin Brine aquifer in areas east of the Caprock Escarpment: (a) eastern Motley County, north to southwestern Donley County, (b) Childress, Cottle, and northeastern King Counties . . . . .	221
130. Location of selected drill-stem tests in wells in the Deep-Basin Brine aquifer . . . . .	226
131. Reported shut-in pressure versus depth from selected wells in the Deep-Basin Brine aquifer, Palo Duro Basin . . . . .	227
132. Areas in Palo Duro Basin having similar pressure-depth relationships . . . . .	228
133. Pressure-depth plots for homogeneous regions of the Deep-Basin Brine aquifer . . . . .	229
134. Regions in Palo Duro Basin having potential vertical components of ground-water flow in the Deep-Basin Brine aquifer . . . . .	230
135. Transmissivity distribution of the best Wolfcampian aquifer simulation . . . . .	233
136. Computed head distribution from the best Wolfcampian aquifer simulation . . . . .	234
137. Streamlines and travel times from the best Wolfcampian aquifer simulation . . . . .	235
138. Potential for leakage from the upper unconfined aquifer down to the Deep-Basin Brine aquifer through the Evaporite aquitard . . . . .	236
139. Finite-element mesh representing the major hydrologic units . . . . .	241
140. Computed hydraulic head distribution. . . . .	242
141. Computed streamline distribution. . . . .	243
142. Location of salt-emission areas and the geographic distribution of samples belonging to Groups A, B, and C . . . . .	249
143. Plots of mNa/mCl ratios versus mCl . . . . .	250
144. Plot of Br/Cl weight ratio versus depth for four brine-emission areas. . . . .	251
145. Plot of $\delta D$ versus $\delta^{18}O$ for municipal wells, salt springs, test holes from the North Croton Creek area, and deep-basin brines from the Palo Duro Basin . . . . .	252
146. Hypothetical potentiometric-surface map of the Wolfcamp aquifer compared with fresh-water table . . . . .	253
147. Sampling locations of municipal wells in New Mexico and the Texas Panhandle . . . . .	259

148.	Map of the United States, showing the approximate contours of $\delta D$ and $\delta^{18}O$ of present-day meteoric water . . . . .	260
149.	Plot of $\delta^{18}O$ and $\delta D$ for shallow ground water from municipal wells in New Mexico and the Texas Panhandle . . . . .	261
150.	Potentiometric-surface map of the Wolfcampian carbonate aquifer, Texas Panhandle . . . . .	274
151.	Summary Piper diagrams showing the cationic and anionic compositions of the 10 deep-basin brine samples collected from DOE test wells . . . . .	275
152.	Piper diagrams showing the cationic compositions of the 10 water samples analyzed from DOE hydrologic test wells . . . . .	276
153.	Basement structure map of the northern part of the Palo Duro Basin . . . . .	281
154.	Isopach map of the Upper Permian Alibates Formation. . . . .	282
155.	Net-salt map of the Upper Permian Seven Rivers Formation . . . . .	283
156.	Structure-contour map on the base of the Ogallala Formation . . . . .	284
157.	Present-day topographic map of a part of the Southern High Plains of the Texas Panhandle . . . . .	285
158.	Area of investigation, western Rolling Plains of Texas . . . . .	291
159.	a. Representative sections through late Quaternary deposits of the western Rolling Plains . . . . .	292
	b. Explanation of symbols . . . . .	293
160.	Generalized composite section and paleoenvironmental interpretation of late Quaternary deposits, western Rolling Plains . . . . .	294
161.	Location of tilted lacustrine deposits and faulted sand and gravel deposits in southeastern Briscoe County, Texas . . . . .	298
162.	Tilted Quaternary sediments . . . . .	299
163.	Fault in Quaternary sediments . . . . .	300
164.	Dissolution fronts in Permian salt-bearing formations, Texas Panhandle and northeast New Mexico . . . . .	304
165.	Histogram of DG values for the study period. . . . .	312
166.	Histogram of DW values for the study period. . . . .	313
167.	Photograph of an erosion pin that showed very little activity during the study period . . . . .	314

168. Photograph of an erosion pin that showed a great amount of activity during the study period . . . . .	315
169. The standardized normal curve showing areas associated with common parameters . . . . .	324
170. Probability plots of erosion pin data . . . . .	325
171. Effects of deflation resulting from agricultural practices . . . . .	332
172. Infrared satellite image at 1800 GMT (12:00 noon CST) of a dust storm over the Texas Panhandle, April 2, 1982 . . . . .	333
173. (a) Abandoned homestead, located 5.2 km north of Needmore, in Bailey County, Texas, along State Highway 214, (b) Detail of exposed foundation, the lower half of which retains impressions of retains impressions of trowel marks and root traces. . . . .	334
174. General soil map of Bailey County, Texas, showing deflation-prone soils and sand dunes south of Muleshoe . . . . .	335
175. Physiography of the Texas Panhandle and location of dust collection sites . . . . .	340
176. Monthly mean dustfall at six collection sites. . . . .	341
177. Grain-size distributions of dust samples collected in the Southern High Plains and adjacent areas . . . . .	342
178. Relationship between monthly dustfall and rainfall . . . . .	343
179. Generalized measured section through late Quaternary deposits, Lake Theo archeological site, Caprock Canyons State Park, southeastern Briscoe County, Texas . . . . .	349
180. Epicentral locations, Texas Panhandle and vicinity . . . . .	353
181. Maximum seismic intensities within the Texas Panhandle from earthquakes in the Panhandle and nearby regions . . . . .	354

Plates (in pocket)

- I. Swisher County core-test well, SWEC Harman No. 1 test well
- II. Swisher County core-test well, SWEC Zeeck No. 1 test well

## Tables

1. List of DOE test wells and velocity data . . . . .	21
2. Conodonts recovered from Core 1, Hardeman County . . . . .	53
3. Conodonts recovered from Core 2, Hardeman County . . . . .	54
4. Conodonts recovered from Core 3, Childress County . . . . .	55
5. Conodonts recovered from Core 4, Donley County . . . . .	56
6. Total organic carbon . . . . .	66
7. Kerogen analysis . . . . .	67
8. Conodont color trends: Palo Duro and Hardeman Basins . . . . .	68
9. K/Ar ages and geochemical data from biotite in volcanic ash beds, Quartermaster and Dewey Lake Formations, Texas Panhandle . . . . .	88
10. Textural classification of halite with genetic significance . . . . .	140
11. Grain-size parameters and inferred depositional facies, Tubb through Dockum, Grabbe No. 1 core . . . . .	174
12. Total organic carbon content and vitrinite reflectance of wells in Oldham and Swisher Counties. . . . .	179
13. Results of pyrolysis from Zeeck No. 1. . . . .	180
14. Oil fields in the northwestern Palo Duro Basin . . . . .	185
15. San Andres hydrologic data from Palo Duro Basin test wells . . . . .	197
16. Hydraulic conductivity of the major hydrologic units, Texas Panhandle . . . . .	244
17. Chemical and isotopic analyses of Group A brines . . . . .	254
18. Chemical and isotopic analyses of Group B brines . . . . .	255
19. Chemical and isotopic analyses of Group C brines . . . . .	256
20. $\delta^{18}\text{O}$ and $\delta\text{D}$ for selected water wells in New Mexico and Texas Panhandle . . . . .	262
21. Chemical compositions of brine samples collected from DOE test wells . . . . .	277
22. Hypsometric integrals for five representative basins and volume of material removed from each since basin development began . . . . .	305
23. Erosion and salt dissolution for representative drainage basins. . . . .	306

24. DG statistics on six erosion monitoring stations in the Texas Panhandle . . . .	316
25. Statistics on stations from measurement periods 1 to 6 . . . . .	317
26. Repeated-measures analysis of variance . . . . .	318
27. (a) Statistics of pin-to-ground difference separated into erosion or deposition and then combined into an overall statistic. (b) Cumulative 3-yr statistics separated into erosion or deposition and combined into an overall statistic. . . . .	326
28. Comparison of DG (row amounts) statistics after 1, 2, and 3 yr of record . .	327
29. Comparison of DG rate statistics after 1, 2, and 3 yr of record . . . . .	328
30. Mean annual rates of deflation from around the base of abandoned structures, Bailey County, Texas . . . . .	336
31. Historical seismicity of the Texas Panhandle in the area bounded by 100°W-103°W, 34°N-36.5°N . . . . .	355

## PURPOSE AND SCOPE

### Research Staff

*This integrated study of the structure, tectonic history, physical stratigraphy, hydrogeology, geochemistry, natural resources, geomorphology, and paleoclimatology of the Palo Duro Basin in the Texas Panhandle is part of a continuing national evaluation of ancient salt basins as potential sites for isolation of nuclear waste.*

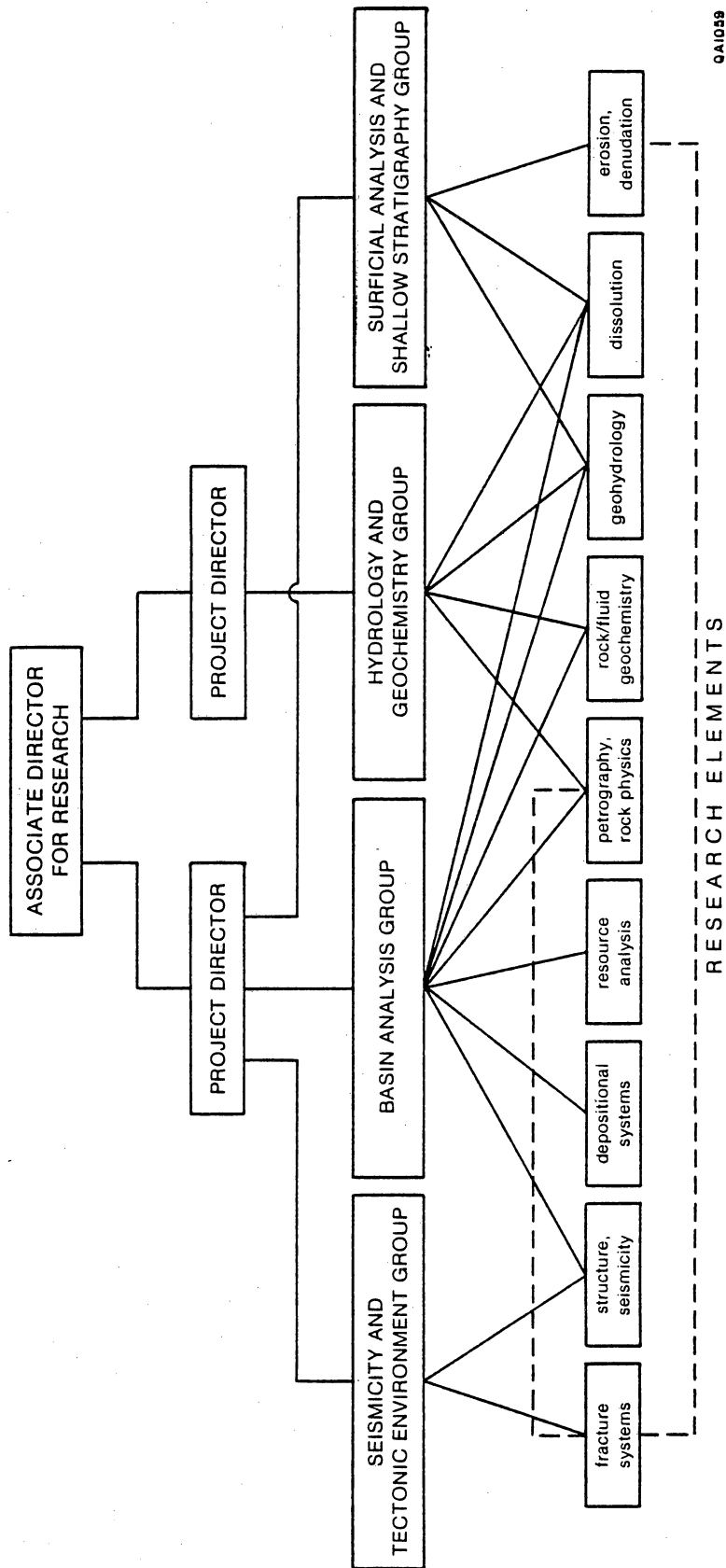
Since early 1977, the Bureau of Economic Geology has been evaluating the Palo Duro Basin in the Texas Panhandle as part of the national nuclear waste repository program. The Bureau, a research unit of The University of Texas at Austin, is conducting a long-term program to gather and interpret all geologic and hydrologic information necessary to describe, delineate, and evaluate salt-bearing and related strata in the Palo Duro Basin and vicinity.

The program in fiscal year 1983 (FY 83) includes four broad research tasks, which were addressed by a surficial analysis and shallow stratigraphy group, a hydrology and geochemistry group, and a seismicity and tectonic environment group and a basin analysis group (fig. 1). The surficial analysis and shallow stratigraphy group collected surface, subsurface, and remotely sensed data to describe salt dissolution, surface processes, and paleoclimatic history. The hydrology and geochemistry group continued analysis of shallow and deep fluid circulation within the basin and rock and fluid geochemistry within the salt-bearing and other stratigraphic units. The basin analysis group characterized the salt- and non-salt-bearing stratigraphic units within the basin, continued to assess the potential for generating and trapping hydrocarbons within the basin, and continued studies of salt quality and core. The seismicity and tectonic environment group continued to study regional seismicity, deep-basin structure and tectonic development, structural controls on sedimentation, and surface and subsurface fracture systems.

This report, a summary of progress during FY 83, represents principal conclusions, methods, and data and maps that were generated. Topical reports discussing various geological aspects of the Palo Duro Basin and vicinity are published as phases of study are

completed. This research was supported by the U.S. Department of Energy, Salt Repository Project Office, under contract no. DE-AC97-83WM46651.





9A1059

Figure 1. Organizational structure of the West Texas Waste Isolation Program (FY 1983).

## PALO DURO BASIN STUDIES--A SUMMARY OF SIXTH-YEAR RESEARCH ACTIVITIES

### Research Staff

*The sixth year of investigations was highlighted by analyses of structures and topographic features related to dissolution and collapse; studies of the relationship of fractures to structural trends; stratigraphic analyses of Mississippian, Pennsylvanian, Permian, Triassic, and Quaternary strata; analyses of organic carbon and vitrinite in Ordovician, Mississippian, and Pennsylvanian rocks; studies of evaporite cyclicity; analyses of core to determine sedimentary structures, diagenetic modifications, fabric, water content, clay mineral assemblages, and bromine content; studies of geophysical logs to estimate porosity distribution; isotopic analyses of water from the dissolution zone, saline springs, and the Dockum Group; hydrologic testing of the San Andres Formation; studies of pressure-depth relationships and vertical ground-water flow; the development of a regional vertical ground-water flow model; and studies of eolian processes and rates of denudation.*

Analyses of both outcrop and subsurface data in the vicinity of the Canadian River Valley and Amarillo Uplift indicate that Cenozoic structural deformation in the Texas Panhandle was extensive and apparently resulted from both tectonic movements and subsidence induced by dissolution of Permian bedded salt.

Comparison of surface and basement structures in eastern Randall County indicates that joint and fracture trends coincide with the dominant NW- and NE-trending basement faults. Clastic dikes cut strata throughout the Texas Panhandle, western Oklahoma Panhandle, and eastern New Mexico. The dikes tend to parallel regional joint orientations and appear to have been formed by filling subjacent fractures or fissures from above. Subsidence caused by evaporite dissolution appears to be the most likely mechanism by which horizontal strain and extension have opened the fractures or fissures. Folding of Permian strata above a salt dissolution zone has been identified in Caprock Canyons State Park, Texas Panhandle. Synclinal depressions have been mapped in that area, and the association between the structural basins, joints, and veins suggests that systematic, regional joints, which predate dissolution collapse, have influenced salt dissolution. Fractures may have acted as preferred paths for fluid movement. Stratigraphic analyses have confirmed ages, environments of deposition, and structural influences on deposition of various units.

Conodont faunas were recovered from four wells in the Palo Duro Basin area. Correlation of these faunas with well-established zonations elsewhere in the midcontinent suggests two things: (1) early (Osage) Mississippian deposition was restricted to the area of the Anadarko Basin axis, and (2) subsequently (during the Meramecian) deposition spread throughout the area as seas transgressed northward in response to the downwarping of the Ouachita geosyncline to the south.

Systematic variations in the completeness of sedimentary cycles and the vertical distribution of thin sheet siltstones in the San Andres Formation allow a subdivision into informal lower, middle, and upper genetic units. The fundamental mode of cyclicity is the same throughout, but the tempo differs in each of the units. These differences may reflect changes in structural control, frequency of eustatic sea-level change, or both.

Structural activity and orientation of structural trends have influenced deposition of lower San Andres strata in the Palo Duro Basin. Depositional facies, percent lithofacies, and lithofacies thickness of cycles 2, 3, and 4 have been affected.

The age of the Quartermaster and Dewey Lake Formations of the Permian Basin is problematic. Although they are generally considered Late Permian in age, the upper parts of these units may be Triassic. Discovery of volcanic ash beds in the Quartermaster and Dewey Lake Formations of the Palo Duro Basin, radiometrically dated as Late Permian, contributes to the resolution of this ambiguity.

Analyses of core from the Upper Permian salt-bearing sections in the Palo Duro Basin have led to interpretations of depositional environments and characteristics of insoluble residues resulting from dissolution. Cores from two new wells, the Stone and Webster Engineering Corporation (SWEC) Harman No. 1 and the SWEC No. 1 Zeeck, have allowed further examination of the stratigraphic column in Swisher County, including the base of the dissolution zone and top of salt, and the San Andres Formation. The Zeeck No. 1 core also contains parts of the Wichita and Wolfcamp shallow-water carbonates and Pennsylvanian starved basin deposits.

Detailed logging of cores from three DOE stratigraphic test wells in Deaf Smith County facilitates correlation of zones of mudstone beds, clean halite, and anhydritic halite within the halite rock of units 4 and 5 of the San Andres Formation.

Cores from seven of the stratigraphic test wells drilled by DOE in the northern Palo Duro Basin have been examined. Each of the cores contains evidence in the form of insoluble residues that halite formerly occurred stratigraphically higher than today. Dissolution beneath the Southern High Plains appears to have been a slow, noncatastrophic process in which rapid collapses did not occur. Two stages of diagenesis, probably accompanying two episodes of halite dissolution, can be identified.

A classification of halite based on crystal size, crystal shape, amount and composition of impurities, distribution of fluid inclusions, and characteristic sedimentary structures has been developed from examination of the Palo Duro Basin cores. Eight distinct classes of halite are characterized by a variety of fabrics, ranging from those that originated as primary brine-pool precipitates to those that formed during diagenesis.

Partial and complete regressive sequences, composed of (from the base upward) a basal black mudstone, limestone, dolomite, nodular anhydrite, bedded anhydrite, and halite, occur throughout most of the San Andres Formation. Even subtle variations in sediment character can be traced over large distances within the Palo Duro Basin. The continuity of these units reflects the extremely flat topography of the area during deposition and indicates that similar sediments formed contemporaneously throughout the area.

Units of thick-bedded halite in the San Andres Formation precipitated in shallow but regionally extensive, brine pools that episodically expanded and contracted. Previously unrecognized 1- to 6-ft-thick subcycles within salt units are characterized by primary textures and bromide contents of about 70 ppm at the base, altered textures and variable bromide concentrations near the top, and a thin mudstone cap containing halite veins with high bromide contents (as much as 342 ppm).

Middle to Upper Permian clastic sediments in the Palo Duro Basin were primarily deposited in eolian dune, eolian flat, intermittent-stream channel, wind-tidal (?) flat, shallow normal marine to hypersaline shelf, halite-influenced flat, and low-salinity pond environments. Source areas were probably granitic and medium-grade metamorphic terrains to the west and northwest of the Palo Duro Basin.

Clay minerals in clastic rocks, dolomite, anhydrite, and halite in the Palo Duro Basin consist of detrital illite; chlorite; diagenetic, mixed-layered chlorite-vermiculite; chlorite-smectite; chlorite-swelling chlorite; and saponite. Illite dominates the detrital suite; the relative occurrence of mixed-layered clays is sensitive to geochemical conditions in the diagenetic environment.

Exploration for hydrocarbons in the Palo Duro Basin has been successful only along the northern and southern margins. Recent analyses, however, indicate that both Mississippian and Ordovician basinal shales and carbonates have sufficient organic content and thermal maturity locally to have been hydrocarbon source rocks. Analysis of organic matter content and thermal maturation of Mississippian and Lower Ordovician carbonates in the Palo Duro and Dalhart Basins indicates that these rocks may also have acted as petroleum source rocks. Their source rock potential is far less, however, than equivalent rocks in the oil-producing Hardeman Basin to the east. Vitrinite reflectance of samples from Swisher and Oldham Counties indicates that shales in the Palo Duro Basin below depths of about 7,000 ft (2,100 m) are mature source rocks. Pyrolysis data support the interpretation that Pennsylvanian basinal shales reached the oil-generation zone.

Pennsylvanian granite wash and carbonates are important oil reservoirs in the northwestern Palo Duro Basin. Fields are primarily controlled by structure, and traps are provided by simple or faulted anticlines.

Studies related to basin hydrology include porosity determinations from cross plots of geophysical logs, testing of the deep-basin aquifer and dissolution zone, mapping of distributions of hydraulic head, analyzing pressure-depth relationships, and hydrologic

modeling. The neutron-density cross-plotting methods are superior to neutron-sonic methods for making quantitative carbonate-lithology and porosity determinations in Wolfcamp deep-basin aquifers. This is true because the former method can be used to detect secondary porosity and to determine lithology more accurately.

Quantitative estimates of porosity distributions within Wolfcampian strata of the Palo Duro Basin offer improved recognition of porous zones, which can be applied to (1) ground-water modeling simulations, (2) delineating porous fairways for hydrocarbon exploration, and (3) determining changes in porosity along locally or regionally correlatable units or hydrologic flow paths.

Hydrogeologic properties of the San Andres Formation within the Palo Duro Basin are being measured for verification of a regional ground-water flow model. Six drill-stem tests and one pumping test have provided estimates of hydraulic head and permeability in Deaf Smith, Randall, and Swisher Counties. Formation-water samples will be collected, after cleanup of drilling contamination, and analyzed to help determine the flow path of ground water in the San Andres in the Palo Duro Basin.

Test wells have been constructed in the Palo Duro Basin to provide data on the hydrogeology of the salt-dissolution zone. The bases of the test zones are within 7 to 49 ft of the upper surface of bedded salt. The test zone in three of the four wells was drilled with an air-mist foam to reduce the extent of contamination of strata to be tested. Hydrologic tests and chemical analyses of water samples will be conducted to determine the source of ground water that dissolves the salt and the rate and timing of the salt-dissolution processes.

The map of the potentiometric surface of the Wolfcampian aquifer has been updated using head data from the Stone and Webster Engineering Corporation J. Friemel No. 1 test well and using refined kriging parameters in the Palo Duro Basin area.

An objective geostatistical method was employed to map the hydraulic head distribution of heads measured in Upper Pennsylvanian rocks of the Palo Duro Basin and

surrounding areas. Geostatistical analysis was used to describe data variation. Kriging was then used to estimate head values based on available data with minimum estimate variance. Resulting estimates were contoured using CPS-1.

Pressure-depth data from drill-stem tests indicate that the Deep-Basin Brine aquifer is underpressured. Potential exists for downward flow from shallow aquifers, through the salt section, into the subsalt brine aquifer. Within the Deep-Basin Brine aquifer, potential for vertical flow varies across the Palo Duro Basin. These variations may affect the lengths of potential flow paths to the biosphere.

Several factors determine the reliability of pressure-depth plots for hydrologic interpretation in confined regional aquifers: the quality, quantity, and distribution of available data, and the variability in the components in the hydrogeologic setting, namely potentiometric surface, aquifer structure, and surface topography. Failure to recognize the effects of such factors can result in misinterpretation of pressure-depth plots and inaccurate analysis of the potential for vertical flow within the confined aquifer.

Ground waters in the Wolfcamp aquifer flow to the northeast toward the semi-impermeable granitic Amarillo Uplift. The Wolfcampian potentiometric surface can be reasonably simulated only when permeability of the granite wash that flanks the uplift is about 260 md. The best simulation results indicate a travel time across the basin from 1.2 to 2.0 m.y. Total discharge through the Wolfcampian aquifer is about 680,000 m<sup>3</sup>/yr.

A cross-sectional ground-water flow model was used to simulate stream lines in addition to the hydraulic heads in the Palo Duro Basin. The model indicates that the spatial distribution of relatively permeable granite wash largely controls the ground-water flow pattern in the deep-basin aquifer. In general, stream lines show downward flow into the basin in the center of the cross section. East of the basin, stratigraphically higher granite wash causes the stream lines to deflect upward and then to parallel the predominantly horizontal formations in the basin interior. Potential discharge of deep basinal brines is indicated by upward-trending stream lines in the eastern Rolling Plains.

Extensive research on borehole sealing has been done since the initial problems with the proposed Lyons, Kansas, nuclear waste repository site. Most emphasis has been placed on laboratory development and testing of grout plugs. The Bell Canyon Test at the Waste Isolation Pilot Project (WIPP) site near Carlsbad, New Mexico, is the only major in situ test to date. Information from that test indicates that flow rates in boreholes in the Palo Duro Basin will be greater as a result of a steeper hydraulic gradient than at WIPP.

Geochemical analyses of ground waters in the Texas Panhandle include determination of water content in salt, salinity and composition of deep-basin brines, and chemical and isotopic composition of shallow aquifers. A standardized procedure of soxhlet extraction in anhydrous methanol and Karl Fischer titration has been established for the analysis of water content in salt. Values determined on more than 100 Palo Duro Basin salt samples range from <0.2 to >15 weight percent water. Clay-rich salts typically contain an order of magnitude more water than samples with dolomite, anhydrite, or no impurities.

Highly saline Na-Cl brines from aquifers below the San Andres Formation at three sites in the Texas Panhandle are capable of dissolving both halite and anhydrite. Although there are not yet sufficient data for detailed evaluation of the chemical evolution of fluids along flow paths within specific units, results of analyses to date suggest that cross-formational mixing of brines may be significant.

The hydrogen ( $\delta D$ ) and oxygen ( $\delta^{18}O$ ) isotopic composition of shallow ground waters indicates typical meteoric water in the Palo Duro Basin area. Values of  $\delta D$  and  $\delta^{18}O$  range from  $-82\text{‰}$  to  $-41\text{‰}$  and  $-11.46\text{‰}$  to  $-5.36\text{‰}$ , respectively, showing a general increase toward the east, which reflects the general decrease in altitude and the heavier isotopic composition of precipitation in the Gulf Coast area. The isotopic composition of ground water from the Dockum Formation in Swisher County suggests an origin further to the west at higher elevations and the absence of significant mixing with isotopically heavier Ogallala water.



Chemical constituents and isotopic compositions of salt-spring and shallow-subsurface brines in the Rolling Plains show characteristics typical of halite dissolution by meteoric ground water as well deep-basin brine discharge. Geographic distribution of brine types correlates well with numerical modeling of ground-water flow.

Surface and Quaternary studies include investigations of the relationship of structure to dissolution, Quaternary sedimentation and surface physiography, analyses of rates of erosion and deposition, and further discussion of late Quaternary/Holocene paleoclimate. The vertical juxtaposition of structure, lithofacies, dissolution, and physiographic features, ranging in age from Paleozoic to Plio-Pleistocene, suggests continued control by the same structural elements in eastern Deaf Smith and western Randall Counties, Texas.

Quaternary alluvium as much as 250 ft (76.2 m) thick covers an area of more than 3,000 mi<sup>2</sup> (7,800 km<sup>2</sup>) on the western Rolling Plains of Texas. Neither the continuous extent nor the complex stratigraphy of these deposits had been recognized before the present study. Late Quaternary paleoclimatic and paleoenvironmental changes are reflected in this alluvial sequence. Deposition appears to have been structurally controlled in part, and the deposits themselves are faulted and downwarped locally. This new evidence of structural activity and effects on geomorphic processes during the late Pleistocene and Holocene Epochs may have implications for disposal of nuclear waste on the High Plains.

Downwarping and faulting contemporaneous with deposition of late Quaternary terrigenous sediment are recorded by exposures in southeastern Briscoe County, Texas. Deformation was probably caused by subsidence of the Permian subcrop owing to dissolution of bedded salt at depth. Fluvial sands and gravels and lacustrine clays filled the subsidence basin, producing a locally thickened Quaternary section. A well-developed paleosol above the lacustrine deposits was tilted and laterally truncated prior to modern eolian deposition at the site.

Hypsometric analysis of representative drainage basins indicates that when the effects of salt dissolution are removed from long-term estimates of denudation, present rates of denudation are considerably larger than previously estimated rates for periods longer than 100,000 years.

Statistical analysis of erosion-pin measurements indicates significant differences and variability both within and between monitoring stations. The data are normally distributed about a mean value of -0.135 cm. Field investigators have confirmed the existence of differing levels of pin activity, consistent with the magnitude/frequency concepts implied by the normal distribution. Analyses also suggest that increasing the length of the data record or measurement interval may not affect the frequency distribution of the data or its validity.

A statistical study of amounts and rates of erosion and deposition for the period 1978-1982 indicates that although mean net erosion has increased for a 3-year period, the mean rate at which it proceeds has effectively decreased. A probabilistic approach to rate projection provides an alternative to linear extrapolations of rates into the future. Geomorphic thresholds may be important factors to consider in any rate calculation.

Eolian processes have substantially modified the landscape on the Southern High Plains within historic time. The maximum inferred rate of deflation was 18.9 mm/yr at a site in Bailey County, Texas, a region of loose, sandy soils and frequent, seasonal dust storms. At least locally, agricultural land use practices have accelerated natural rates of erosion and deposition by winds.

Preliminary data derived from six dust traps installed on the Southern High Plains show that dust deposition varies locally and seasonally in response to natural and man-induced factors. Monthly rates of dustfall at individual stations ranged from 0.658 g/m<sup>2</sup> at Muleshoe to 13.441 g/m<sup>2</sup> at Palo Duro Canyon. Dust deposition contributes significantly to the renewal of the High Plains surface.

## SEISMIC REFLECTION SURVEYS FOR SITING A PROPOSED NUCLEAR WASTE ISOLATION FACILITY, TEXAS PANHANDLE

Roy T. Budnik

*The long-term geologic stability of an area is an important factor in the selection of a site for the disposal of high-level nuclear waste. Approximately 625 mi (1,000 km) of seismic reflection data have been acquired in the Texas Panhandle to assess the stability of the Palo Duro Basin.*

One of the aims of the West Texas Waste Isolation Project has been to determine the stability of the Palo Duro Basin during the past 1,500 m.y. The study entered a new phase in 1982 when the Department of Energy funded a program to acquire seismic reflection data to aid structural and stratigraphic interpretation in areas of poor well control, primarily in Deaf Smith and Swisher Counties. Stone and Webster Engineering Corporation (SWEC) contracted surveys specifically for the project and acquired proprietary surveys made for petroleum exploration.

The Palo Duro Basin comprises more than 4,000 ft (1,200 m) of Pennsylvanian and Lower Permian marine sediments and a comparable amount of Middle and Upper Permian evaporite and related strata (Dutton and others, 1982). The marine strata are marked by rapid lateral changes in lithology (velocity); the evaporite section has rapid vertical changes in lithology (impedance). Lateral changes in velocity complicate structural interpretations; large changes of impedance produce multiples and the loss of energy to deeper horizons. In addition, the top of the basement is not a good reflector, and the basement contains many internal primary reflectors. These problems have made elucidation of basement structure difficult.

The first body of data acquired for this study was a brokered proprietary twelvefold regional survey collected by Bendix-United Geophysical Company in 1972 (fig. 2). These data can be used to define large, deep structures but are too low frequency (12-40 Hz) to define smaller structures that may affect the host rock horizon (the San Andres Formation). Following preliminary interpretation of these data, a program for obtaining

additional data was proposed. A grid of four lines in Deaf Smith County and two perpendicular lines in Swisher County were recommended to tie into existing DOE test wells. G.J. Long and Associates, consultants to SWEC, recommended that the data be acquired with a high-frequency (20-110 Hz) source and a short geophone spread length to maximize the resolution of structures within the host rock.

Approximately 80 mi (125 km) of 24-fold data were collected in Deaf Smith County and 30 mi (48 km) in Swisher County during the summer of 1982. An additional 35 mi (55 km) were collected in Deaf Smith County in the spring of 1983 (fig. 2). Only short line segments could be permitted for certain parts of the SWEC survey. Western Geophysical Company was the contractor. An 85-mi (135-km) 48-fold proprietary line across Deaf Smith and Randall Counties in Texas and Curry and Quay Counties in New Mexico was also purchased from Western Geophysical (fig. 2). Two short lines were shot in central Randall County to tie together the Western and United proprietary lines (fig. 2). In addition, SWEC participated in the acquisition of four proprietary lines in Castro and Swisher Counties by STM Corporation (fig. 2).

Velocity control for interpretation of the seismic data is based on 14 proprietary velocity surveys and 12 integrated sonic logs from petroleum exploration wells, 4 velocity surveys, and 2 vertical seismic profiles for DOE wells, and 7 synthetic seismograms, also from DOE wells (table 1 and fig. 2).

Structural and stratigraphic interpretation of the data is continuing. As discussed earlier, the top of basement is very difficult to determine, especially on the lines acquired with a short geophone spread (figs. 2 and 3). The top of the Pennsylvanian and top of Wolfcampian (Lower Permian) are poor to fair reflectors. Tops of the San Andres and Tubb Formations are represented by moderate, relatively continuous reflectors. The tops of the Alibates, Seven Rivers, and Red Cave Formations produce strong, continuous reflections, as do the evaporite cycles within the lower San Andres. Few faults have been interpreted in the post-Pennsylvanian part of the section; vertical resolution limits recognition of

faults to those with throw greater than 150 ft (50 m). Deformation of the entire Paleozoic section was seen on line SWEC J in central Randall County (fig. 4). Apparent salt-dissolution structures are present on line SWEC G-3 in central Swisher County (figs. 2 and 5). Disruption of the Alibates reflector and loss of the San Andres reflector on line SWEC H-2 in northern Swisher County (figs. 2 and 6) also may be the result of salt dissolution.

Symbol	Shot by	For	Date	Energy Source	Fold	Spread Length
—	Western	SWEC	1982	Vibroseis	24	2860-220-0-220-2860
—	Western	SWEC	1983	Vibroseis	24	2860-220-0-220-2860
=====	Western	Proprietary	1982	Vibroseis	24	7150-825-0-825-7150
- - - - -	Bendix-United	Proprietary	1972	Vibroseis	12	4620-990-0-990-4620
=====	STM	Proprietary	1982-1983	Vibroseis	24	8250-330-0-330-8250
+++++	GEO X	Sundance	?	Dynamite	12	5280-220-0-220-5280
+++++	Petty Ray	Sundance	1981	Dynamite	8	6600-220-0-220-6600

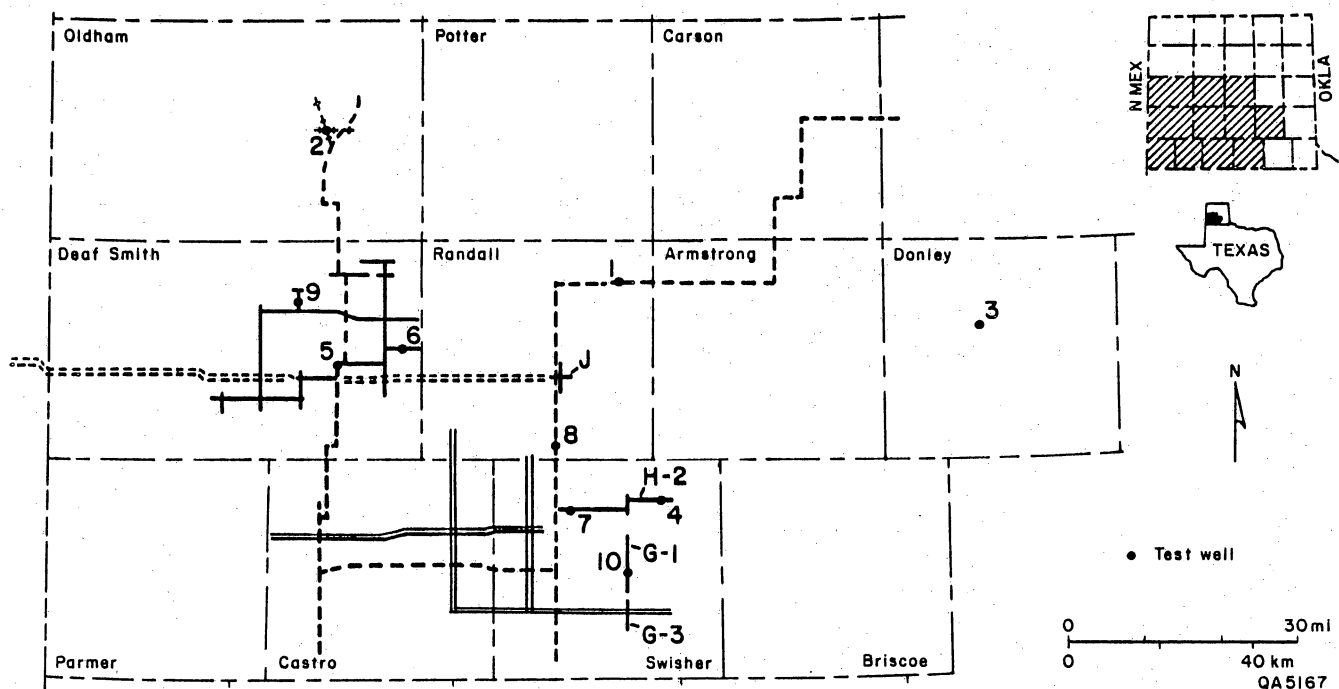
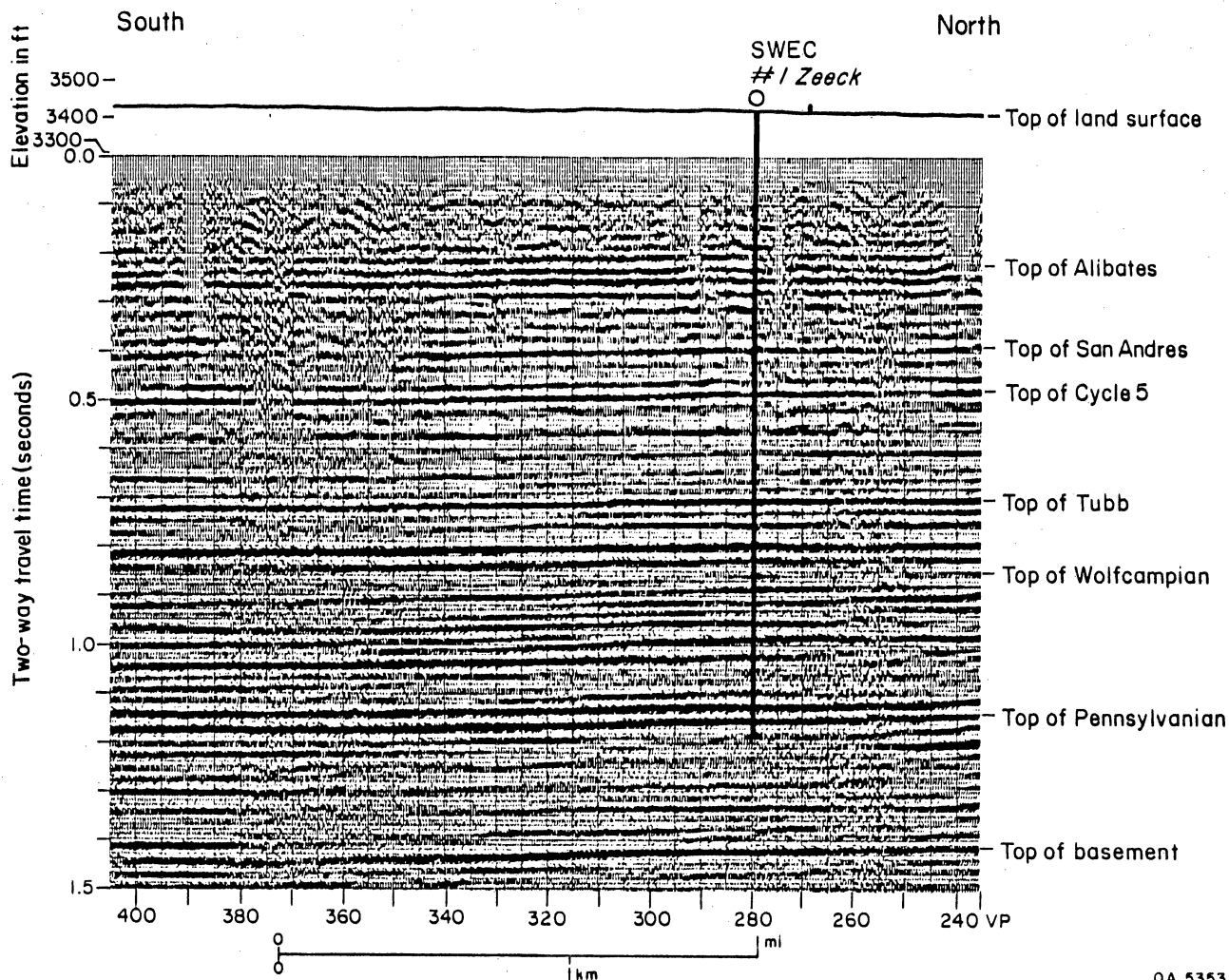


Figure 2. Location map of seismic reflection surveys and Department of Energy test wells, Palo Duro Basin. Well names listed in table 1.



QA 5353

Figure 3. Portion of line Stone and Webster Engineering Corporation G-1 in central Swisher County. Interpretation based on vertical seismic profile in Stone and Webster Engineering Corporation Zeeck No. 1 test well. Location given in figure 2.

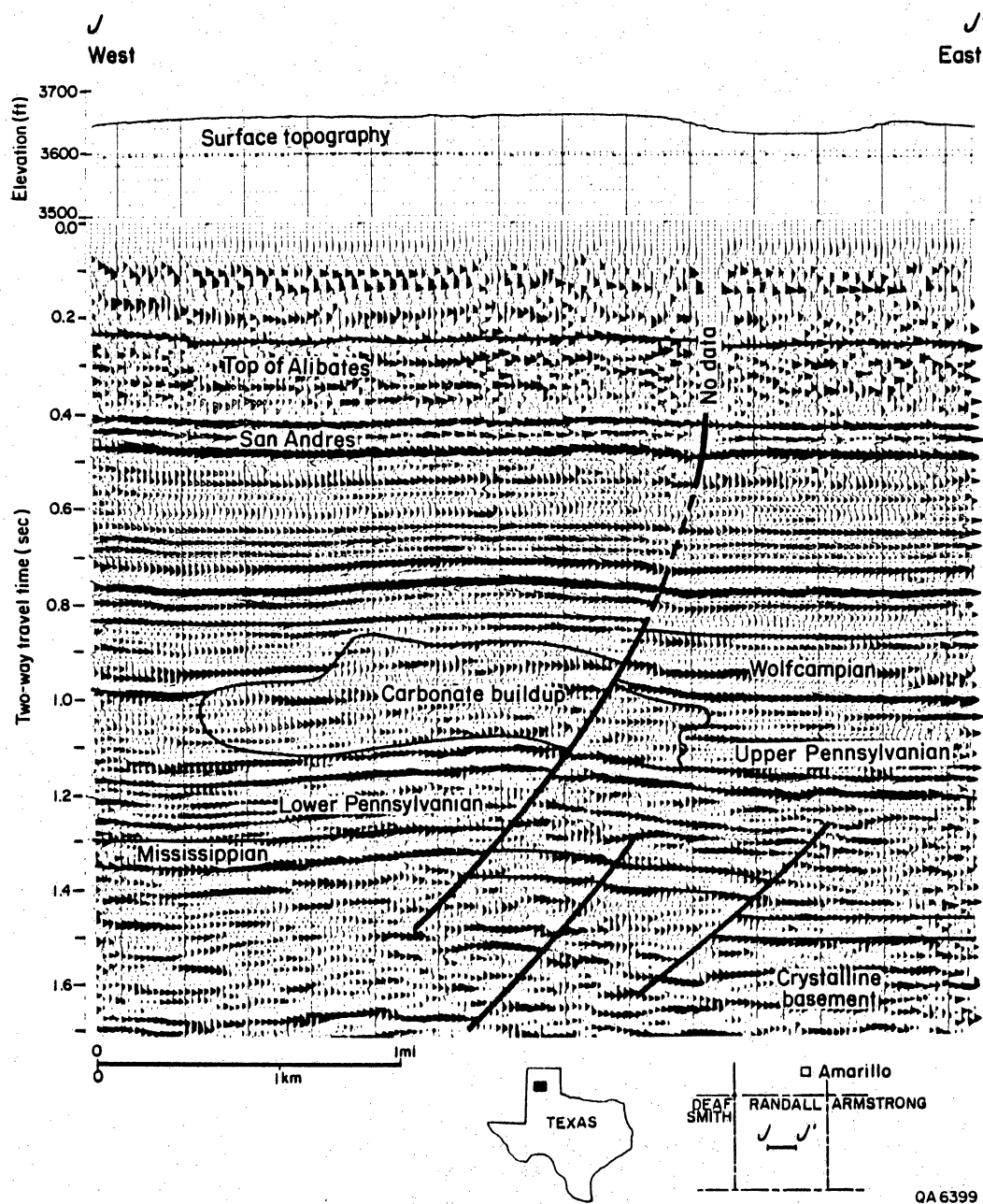


Figure 4. Portion of line Stone and Webster Engineering Corporation J in central Randall County. Basement faulting has affected the entire Paleozoic section. Location given in figure 2.



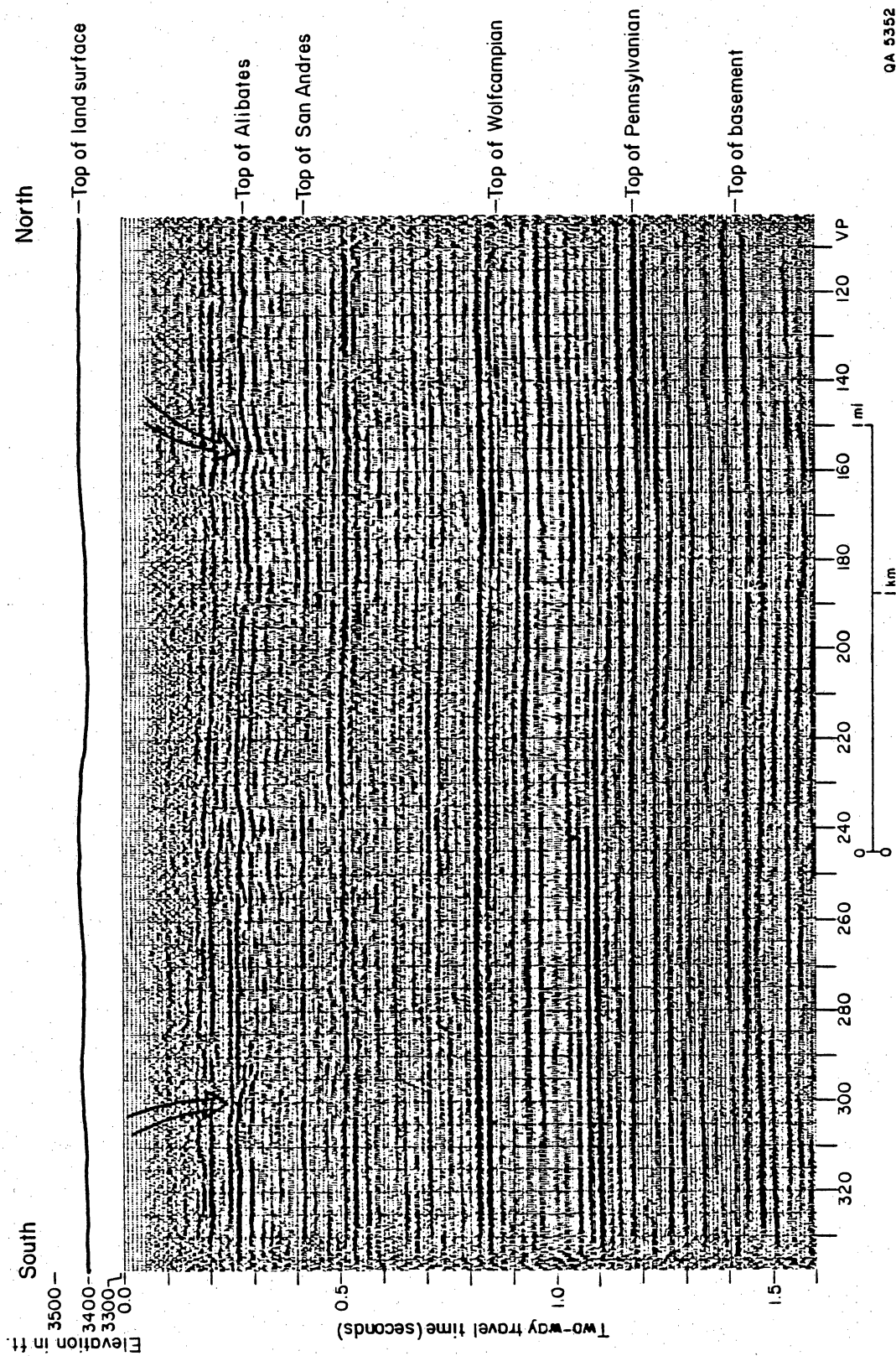


Figure 5. Portion of line Stone and Webster Engineering Corporation G-3 in central Swisher County. Salt dissolution (?) structures (arrows) appear as disrupted areas in the uppermost part of the Permian section. Location given in figure 2.

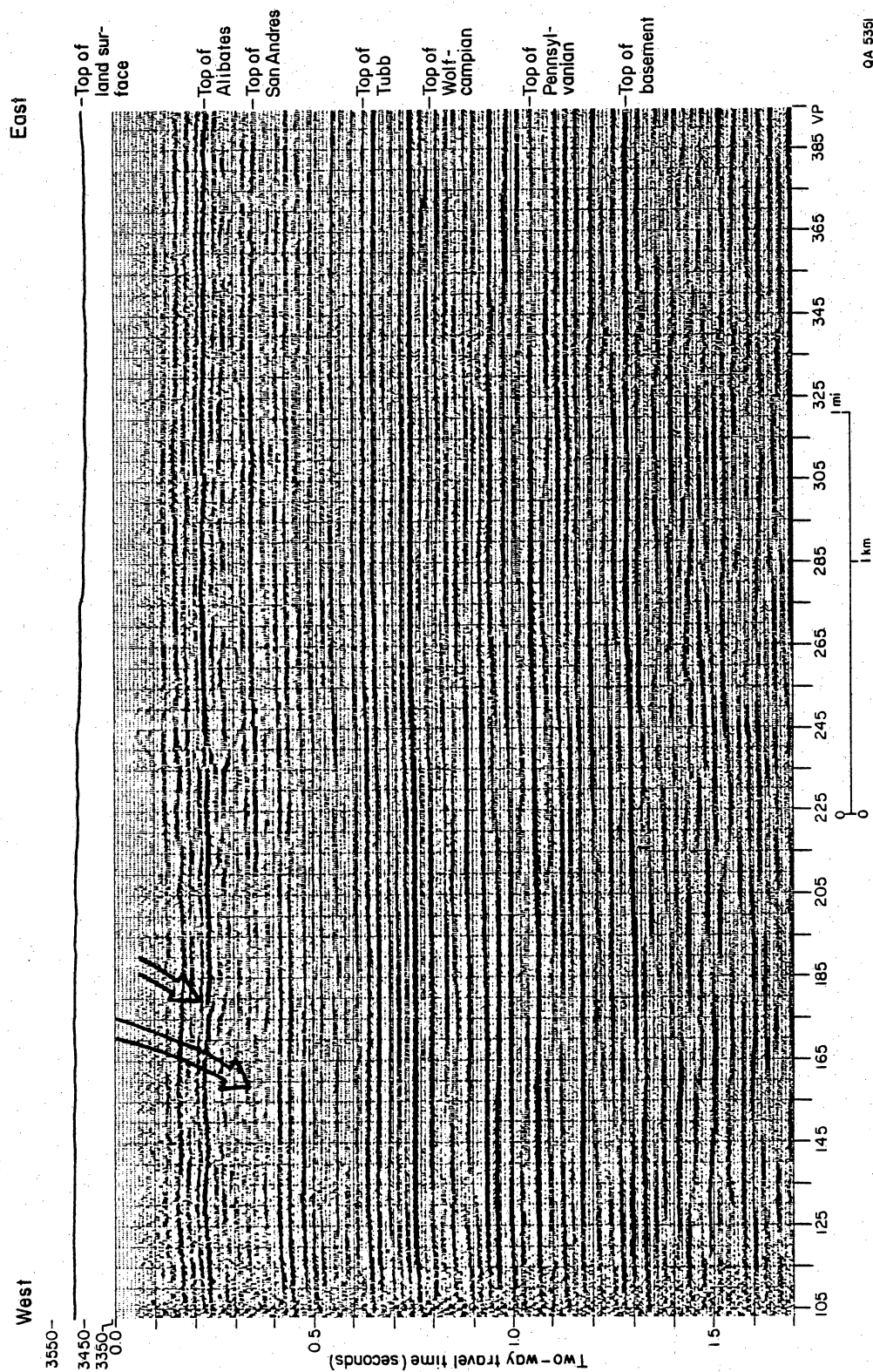


Figure 6. Portion of line Stone and Webster Engineering Corporation H-2 in northern Swisher County. Salt dissolution may have been responsible for disruption of the Alibates and loss of top-of-San Andres reflector (arrows). Location given in figure 2.

Table 1. List of DOE test wells.

<u>Well number</u>	<u>Well name</u>	<u>County</u>	<u>Velocity data*</u>
1	DOE/Gruy Federal Rex White No. 1	Randall	ISL
2	Stone and Webster Engineering Corp. Mansfield No. 1	Oldham	ISL
3	Stone and Webster Engineering Corp. Sawyer No. 1	Donley	ISL
4	DOE/Gruy Federal Grabbe No. 1	Swisher	ISL, SS
5	Stone and Webster Engineering Corp. Detten No. 1	Deaf Smith	ISL, SS
6	Stone and Webster Engineering Corp. G. Friemel No. 1	Deaf Smith	ISL, SS
7	Stone and Webster Engineering Corp. Harman No. 1	Swisher	ISL, SS, VS
8	Stone and Webster Engineering Corp. Holtzclaw No. 1	Randall	ISL, SS, VS
9	Stone and Webster Engineering Corp. J. Friemel No. 1	Deaf Smith	ISL, SS, VS, VSP
10	Stone and Webster Engineering Corp. Zeeck No. 1	Swisher	ISL, SS, VS, VSP

\*Velocity data

ISL Integrated sonic log

SS Synthetic seismogram (geogram)

VS Velocity survey

VSP Vertical seismic profile

## EVIDENCE OF BASIN AND RANGE-AGE DEFORMATION IN THE TEXAS PANHANDLE

Roy T. Budnik

*Anomalous thickening of the Ogallala Formation (Neogene) in the Carson County basin appears to be related to Basin and Range-age extension to the west. Late Paleozoic, Mesozoic, and Neogene sediments thicken into the basin. Structure maps on pre- and post-salt units are similar. The Carson County basin probably formed as a result of renewed strike-slip motion along preexisting faults.*

A major extensional event in the Neogene formed the Basin and Range province in the Western United States. Related deformation in Colorado, central New Mexico, Texas, and Mexico produced a series of north-south-trending fault-bounded structures that define the Rio Grande Rift (fig. 7; Eaton, 1980). Extension, in part along preexisting faults, controlled the position of the rift (Kelley, 1979). Axial grabens along the Rio Grande Rift are filled with as much as 13,000 ft (4,000 m) of alluvial and lacustrine deposits of the Santa Fe Formation (fig. 7; Kelley, 1977). These sediments accumulated during the period of highest rates of extension 12 to 2 mya (Chapin and Seager, 1975). Coeval (11 to 2 mya; Schultz, 1977; Stormer, 1972) alluvial and eolian deposits (the Ogallala Formation) were shed eastward as a thin apron across what is now the High Plains (fig. 7; Baldwin and Muehlberger, 1959). In the Texas Panhandle, the Ogallala Formation is generally less than 300 ft (100 m) thick (fig. 2; Seni, 1980). Locally, for example in the Carson basin, the Ogallala is in excess of 800 ft (250 m) thick (fig. 8).

The Carson basin (Rogatz, 1939) is part of the Whittenburg Trough, which lies along the south side of the Amarillo Uplift (fig. 9; Soderstrom, 1968). The trough and adjoining uplifts formed in the Early Pennsylvanian, probably as a result of strike-slip motion on preexisting faults (Kluth and Coney, 1981), and influenced depositional patterns throughout the Pennsylvanian and Early Permian (McGookey, 1981; Budnik and Smith, 1982; McGookey and Goldstein, 1982). Depositional patterns in Middle and Upper Permian strata are difficult to determine, as the San Andres Formation and younger units have been extensively modified by Cenozoic salt dissolution in the vicinity of the Amarillo Uplift

(Gustavson and others, 1980b). In Carson County, salt is present in these units over the structural high bounding the Carson basin on the south but is absent elsewhere in the county (fig. 10). Within the area where the salt is absent, the remaining non-salt part of the interval is thickest in the basin and thins over the Amarillo Uplift (fig. 10), indicating that the uplift influenced depositional patterns during the Middle and Late Permian. Triassic strata (Dockum Group) are preserved in the Carson basin but are absent over the uplifts surrounding it (fig. 11). The Ogallala Formation is thickest in the Carson basin and thins over the remainder of the area, including the deepest part of the Whittenburg Trough (fig. 8).

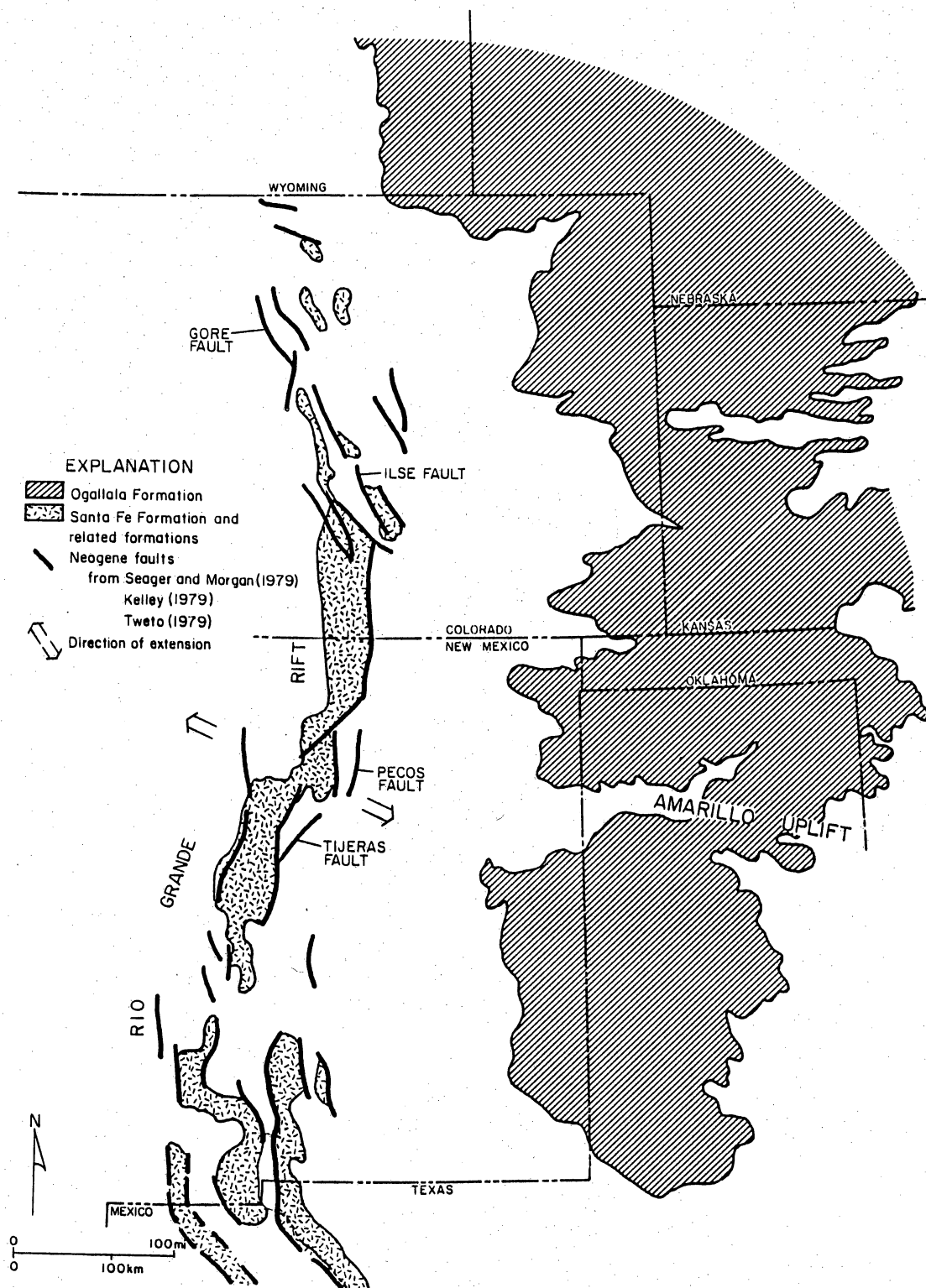
Structure developed on the base of the Ogallala Formation is not solely a dissolution phenomenon. Dissolution has removed Middle and Upper Permian salt from all but the southwestern part of the county (fig. 10); salt is present in Lower Permian units throughout the county. Salt in the Middle and Upper Permian may have been thicker in the Carson basin, as suggested by the thickening of the non-salt part of the interval, but there is no evidence to indicate that there was enough salt present to account for the entire greater thickness of the Ogallala in the basin. Similarity of structure maps of both post-salt (base of Ogallala and top of Alibates; fig. 12a and b) and pre-salt units (Tubb, Wolfcamp, and top of basement; fig. 13a, b, and c) indicates a similar structural history for both. A proprietary seismic reflection line across the eastern extension of the Carson basin confirms the presence of a graben in the pre-salt units (fig. 13); reflections from higher units were not recorded during the survey. Location of the anomalous thickening of the Ogallala Formation in the Carson basin coincides with thickening in the pre- and post-salt units (figs. 11, 12, and 14). Similarity of the isopach of the Ogallala Formation and the structure on the base of the Ogallala and all underlying units indicates basement control during deposition.

To the west, in Potter County, several hundred feet of coarse sandstone and conglomerate (the Potter Formation; Patton, 1923) accumulated in the Whittenburg Trough

during initial Ogallala deposition. Ogallala sediments that fill the Carson basin may be of a similar nature. The pattern of deposition in the Ogallala Formation throughout the Texas Panhandle reflects the influence of basement structure. The Ogallala is thickest in the Anadarko, Dalhart, and Palo Duro Basins and thins over the Amarillo Uplift, the Bravo Dome, and the Cimarron Arch (fig. 8). Major channels, in general, follow structural lows (fig. 15).

Contemporaneity of the Ogallala and Santa Fe Formations suggests that deformation in the Carson basin occurred at the same time as Basin and Range extension to the west. The Amarillo Uplift is perpendicular to the Rio Grande Rift and parallel to the direction of extension in the rift (fig. 7). This orientation is such that the stress field that produced extension in the rift may have produced strike-slip motion along the uplift. Geometry of the Tertiary part of the Carson basin is consistent with that of other pull-apart basins around the world (fig. 16), suggesting, but not proving, a similar origin.

Neogene Basin and Range extension, which deformed a large part of the Western United States, appears to have subtly affected the Texas Panhandle. The syntectonic Ogallala Formation reflects the influence of basement structure, most notably along the Amarillo Uplift, during deposition. The Ogallala Formation has been broadly folded over the top of the John Ray Dome and other structures that lie along the northern edge of the Whittenburg Trough (fig. 17), suggesting continued deformation after the end of Ogallala deposition. Present seismicity (fig. 18) indicates that faults bounding the Carson basin may still be active.



QA 5350

Figure 7. Distribution of syntectonic Neogene sediments of the High Plains and Rio Grande Rift (Robinson, 1972; Scott, 1975; Weeks and Gutentag, 1981). Faults from Tweto (1979) and Kelley (1979).

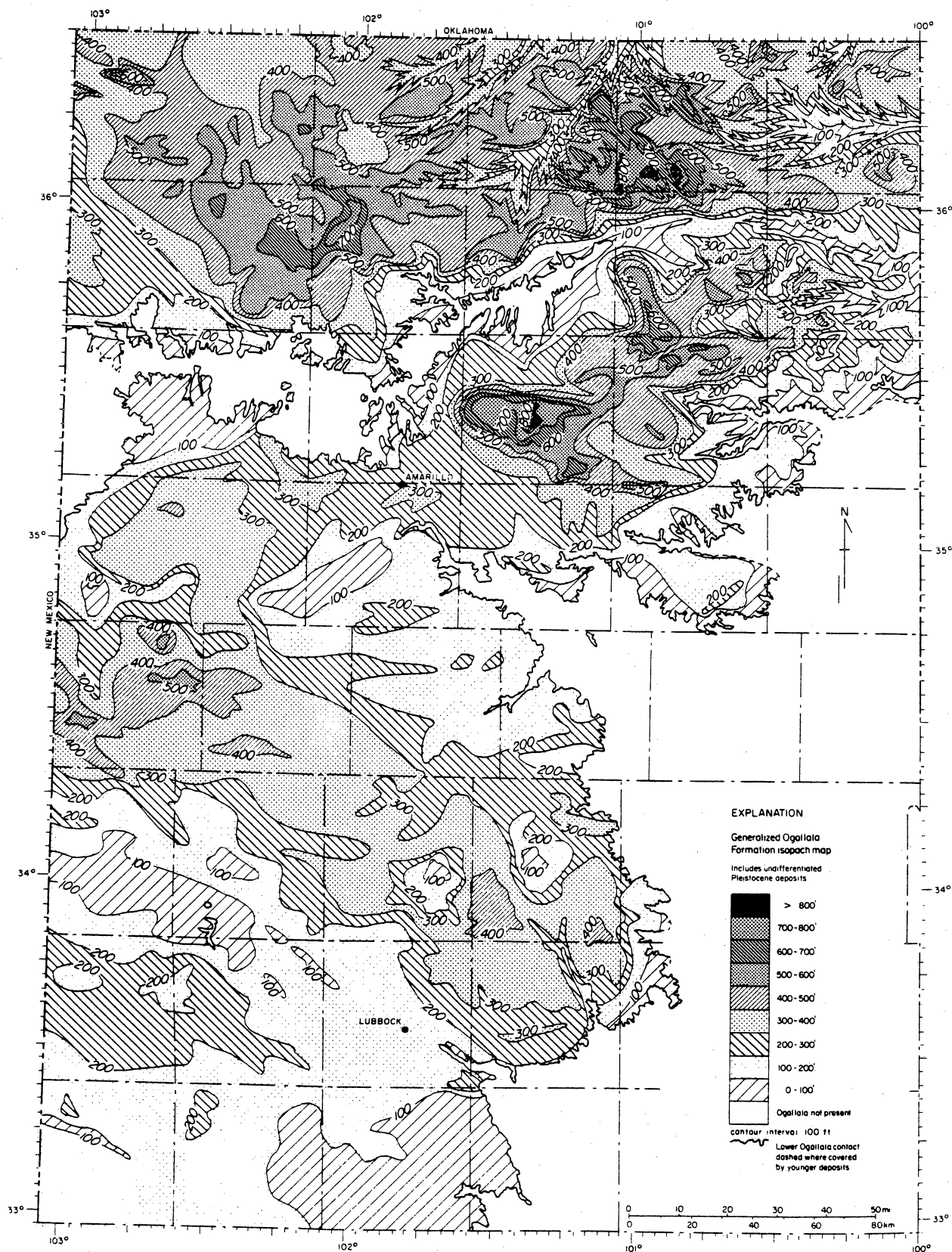


Figure 8. Isopach map, Ogallala Formation (Seni, 1980). The Ogallala thickens into the major basins and thins over the intervening uplifts.



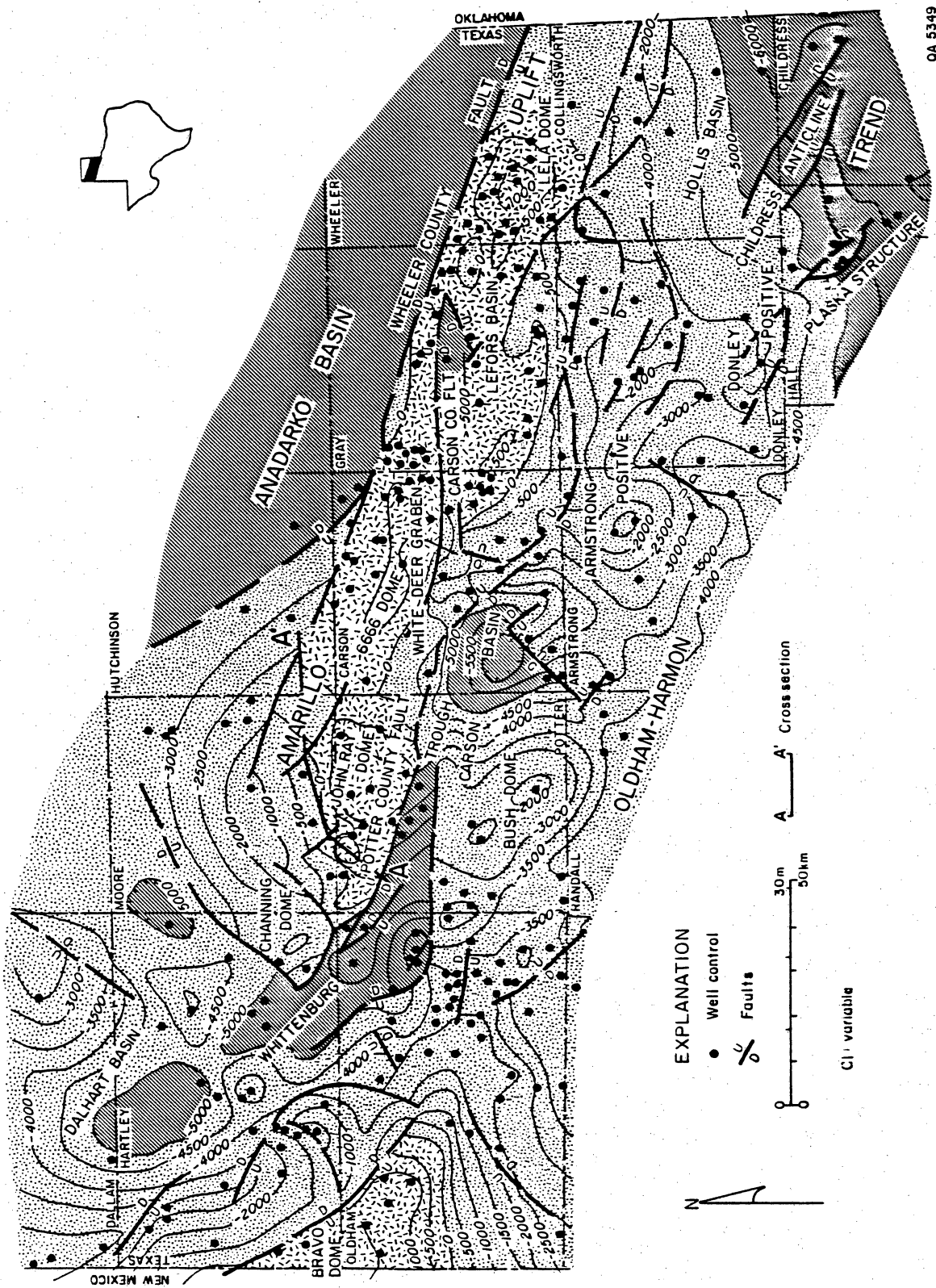


Figure 9. Structure-contour map on top of basement, Whittenburg trough and flanking uplifts.

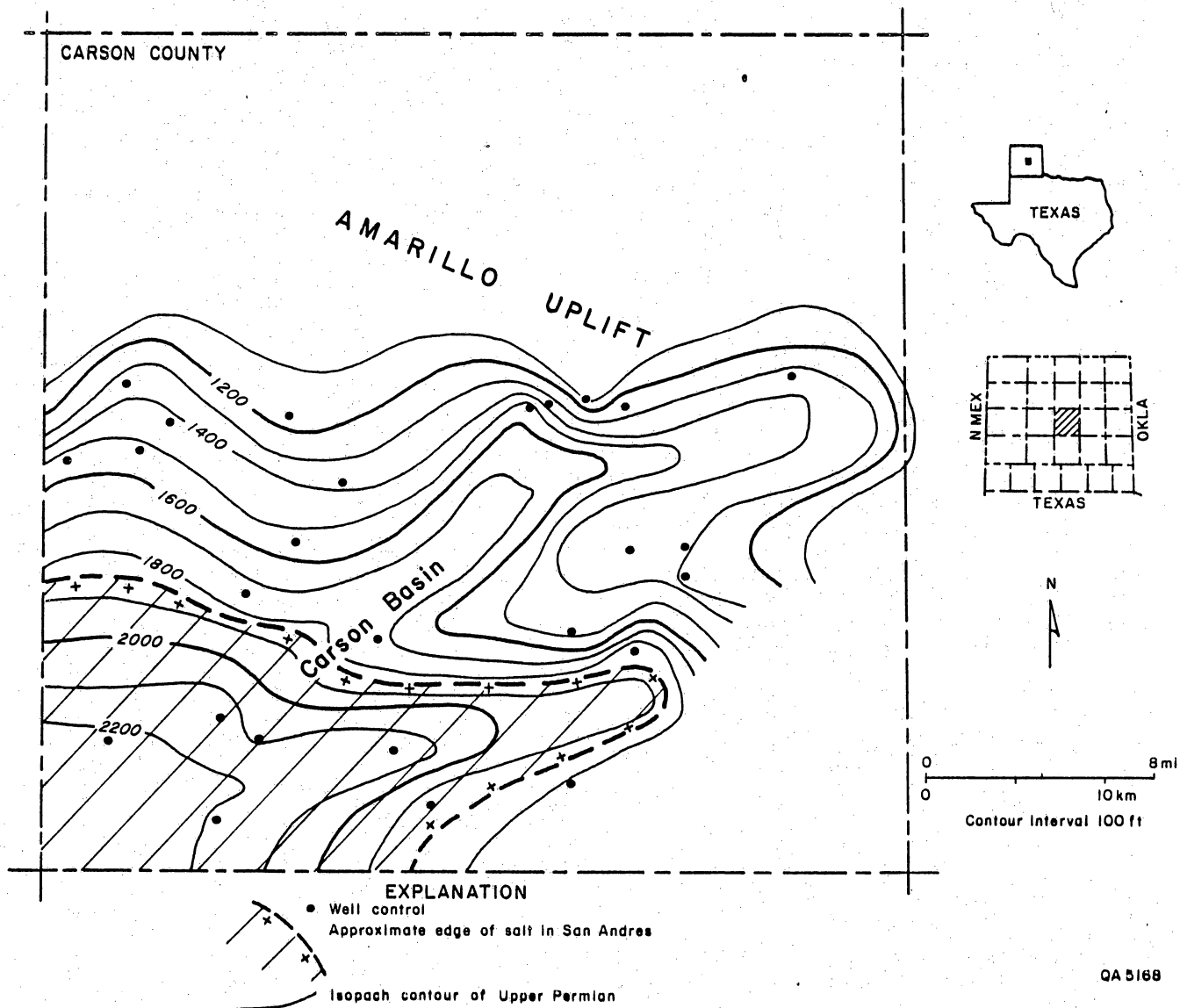


Figure 10. Distribution of salt and isopach of Middle and Upper Permian strata, Carson basin. Salt present in diagonally ruled area.

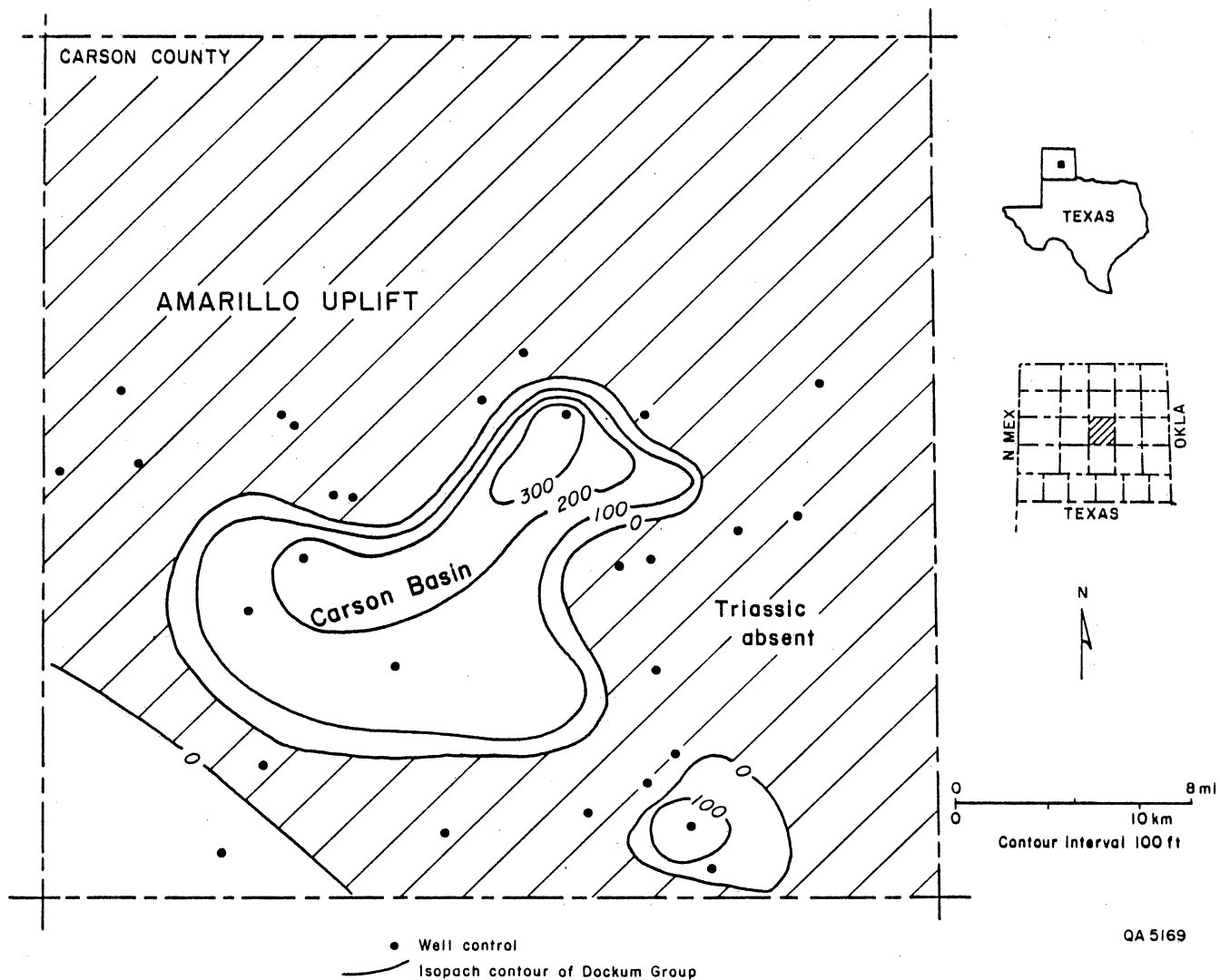


Figure 11. Isopach map of the Dockum Group (Triassic) in the Carson basin.

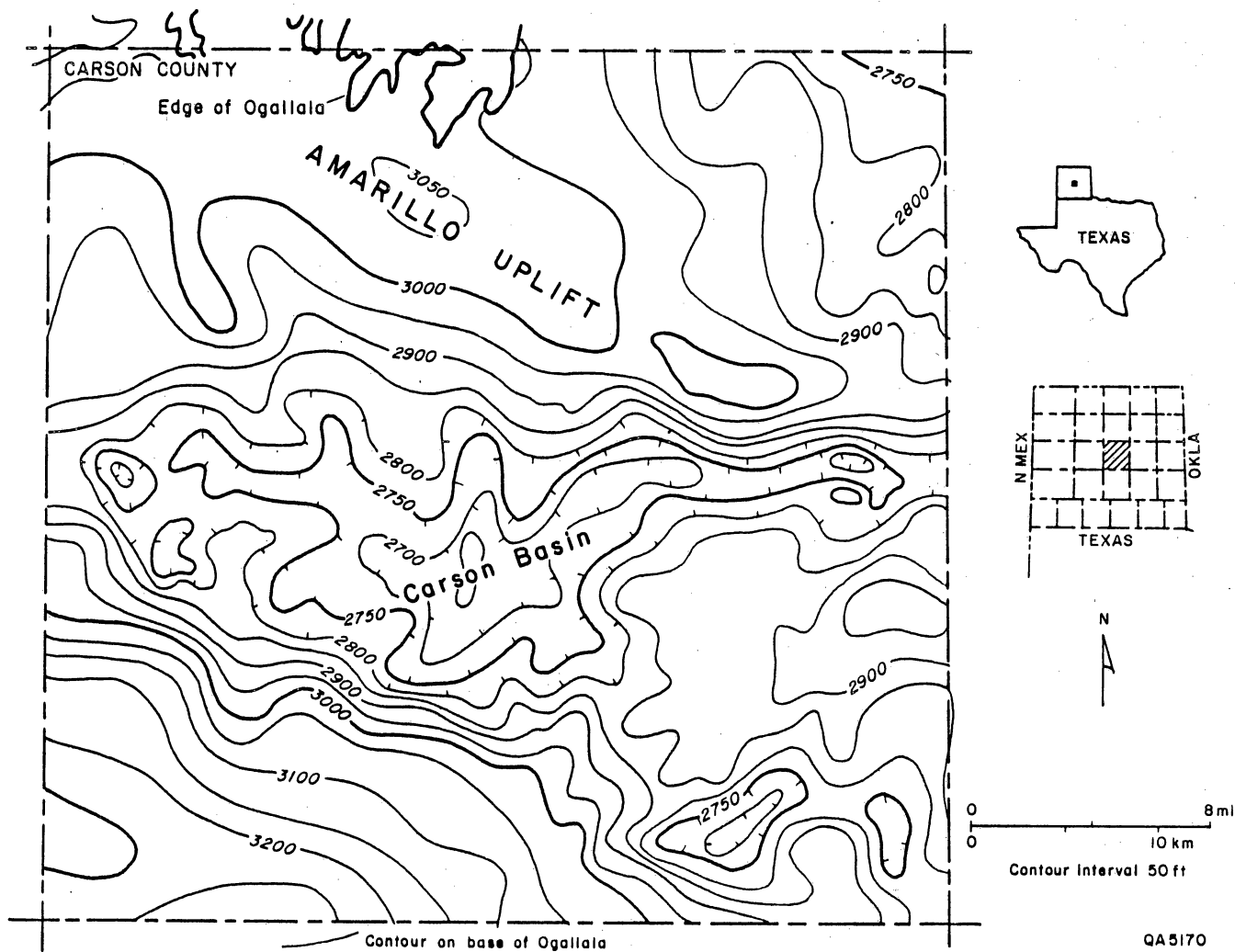


Figure 12a. Structure map of base of the Ogallala Formation, Carson basin (Knowles and others, 1982).

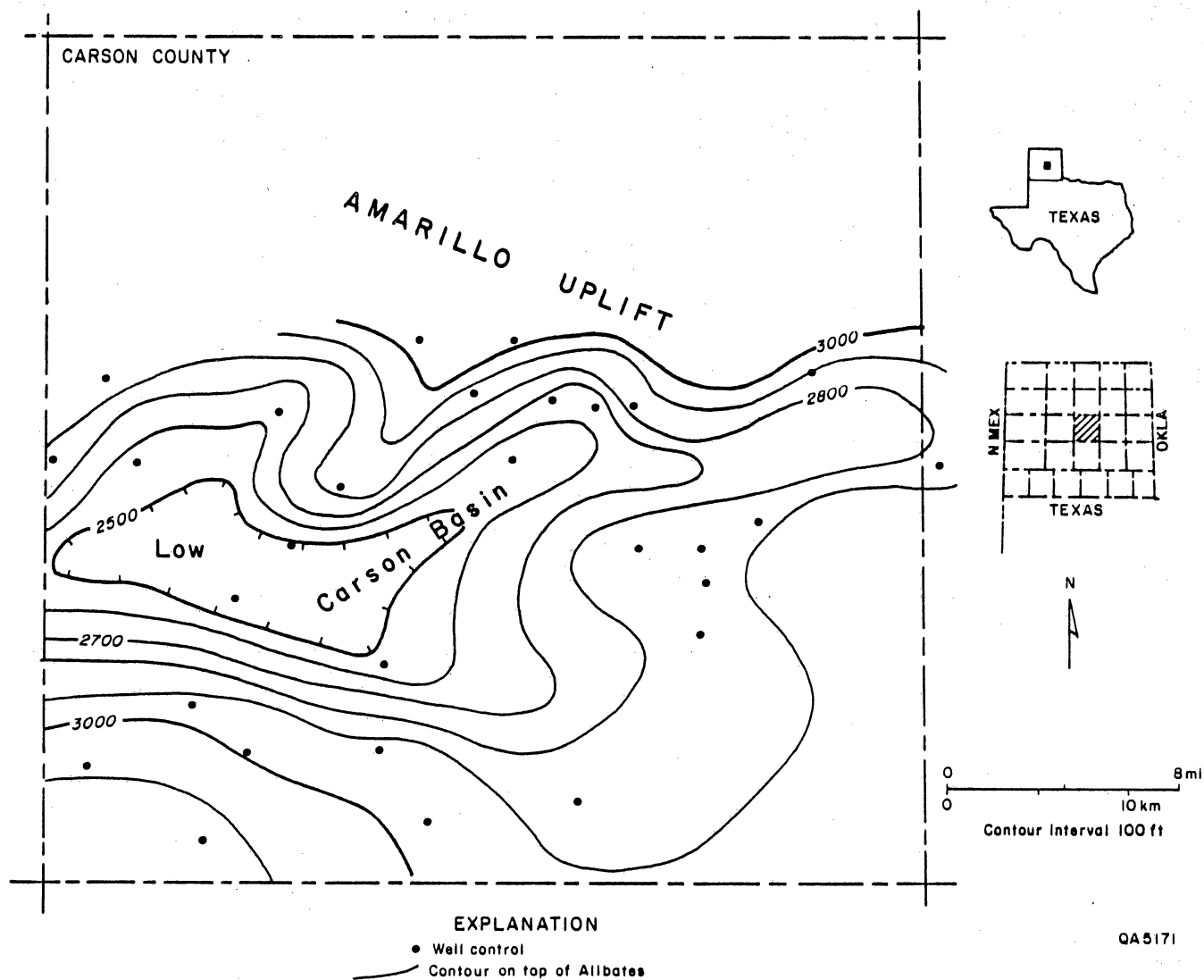


Figure 12b. Structure map of top of the Alibates Formation, Carson basin.

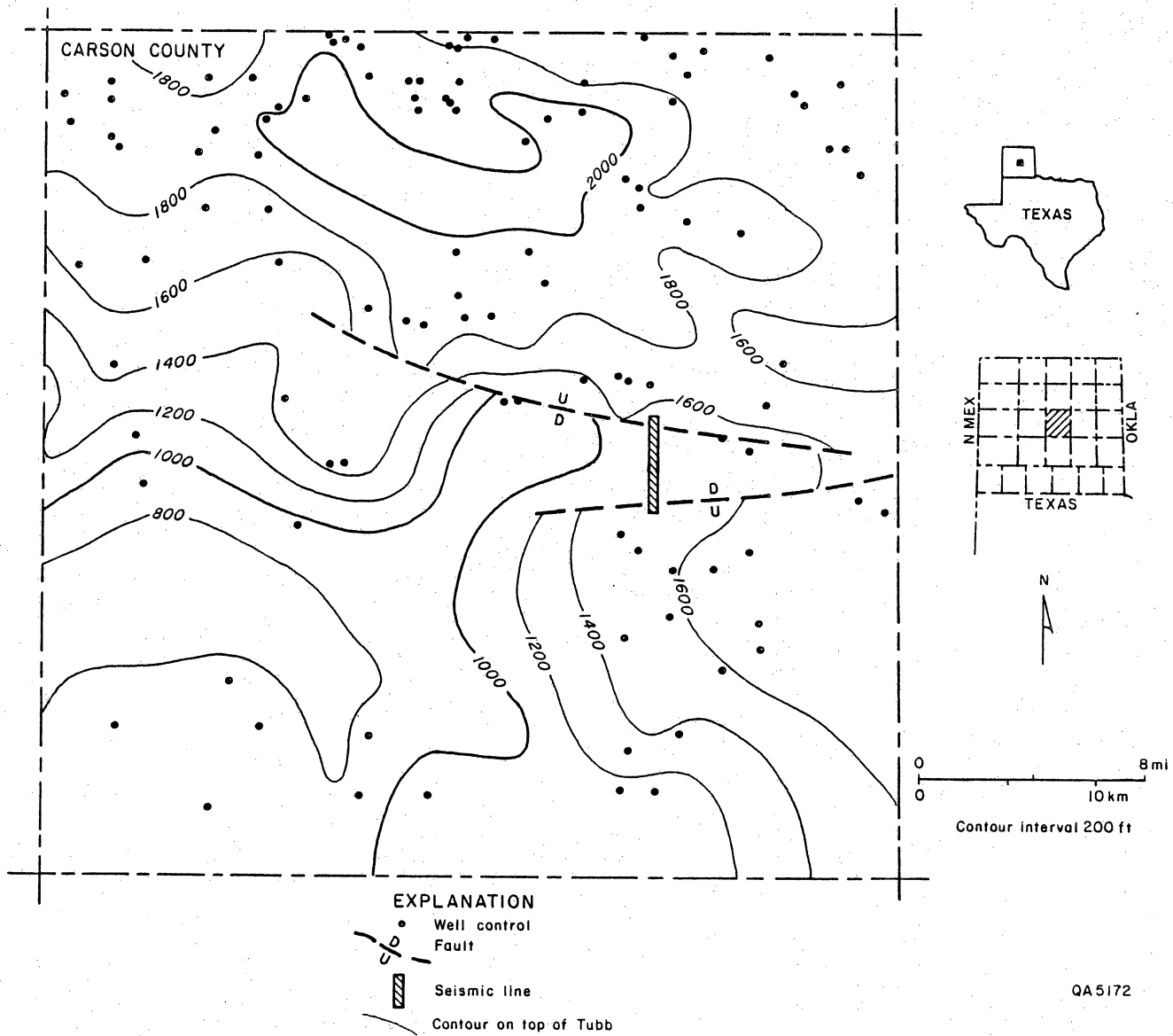


Figure 13a. Structure map of top of the Tubb Formation, Carson basin.

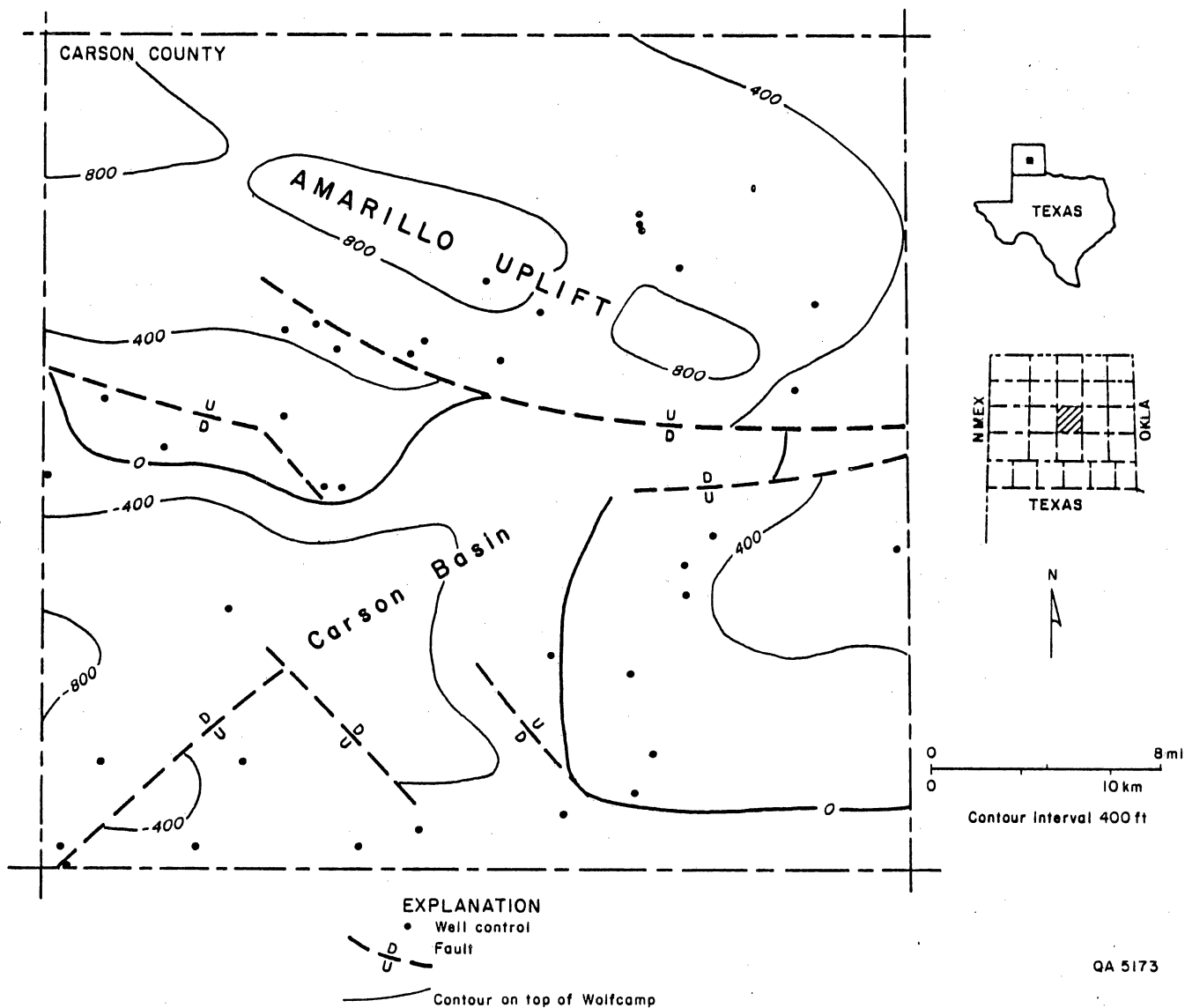


Figure 13b. Structure map of top of Wolfcamp, Carson basin.

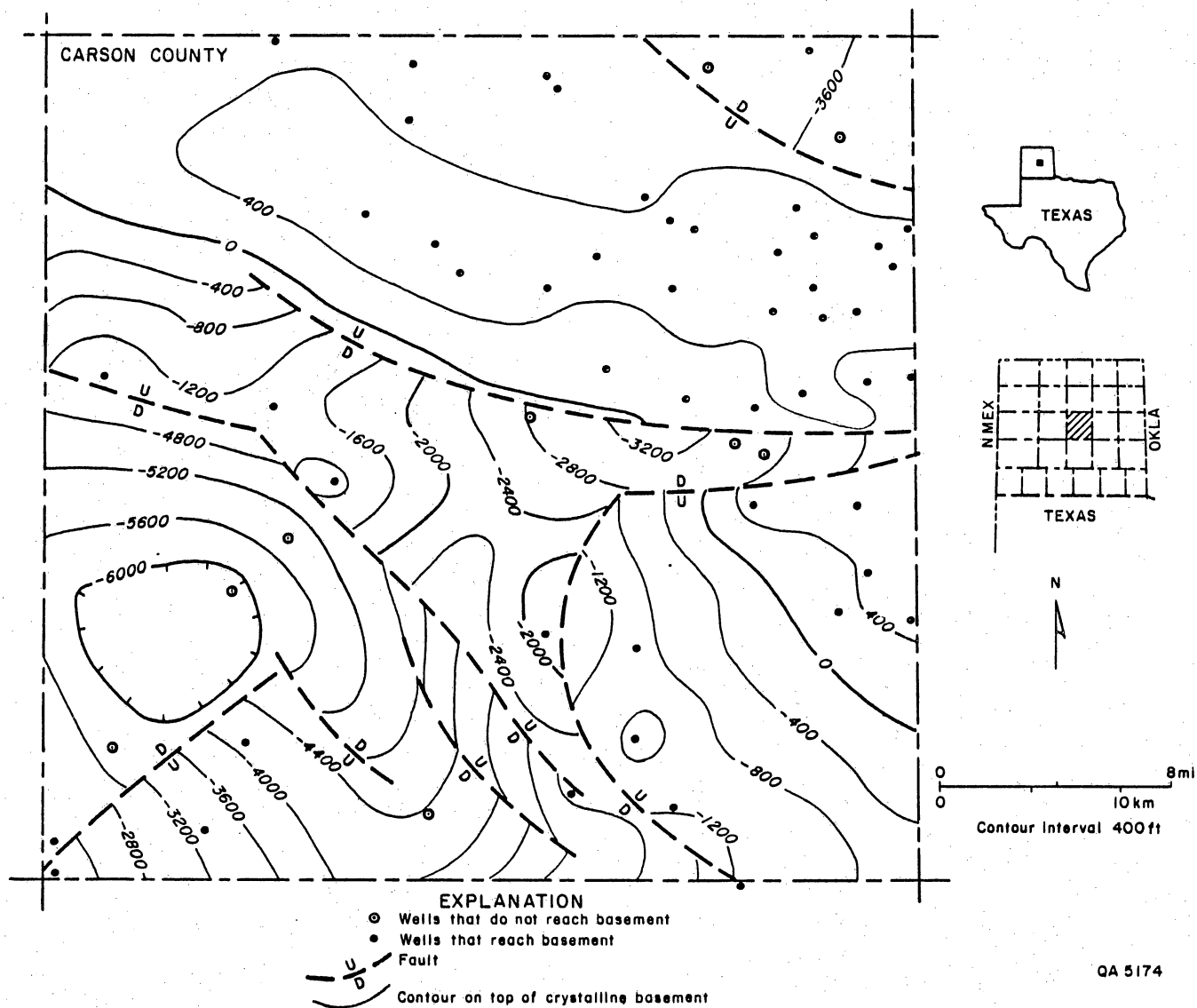


Figure 13c. Structure map of top of basement, Carson basin. Dashed contours indicate minimum depth based on wells that penetrated granite wash but did not reach basement.



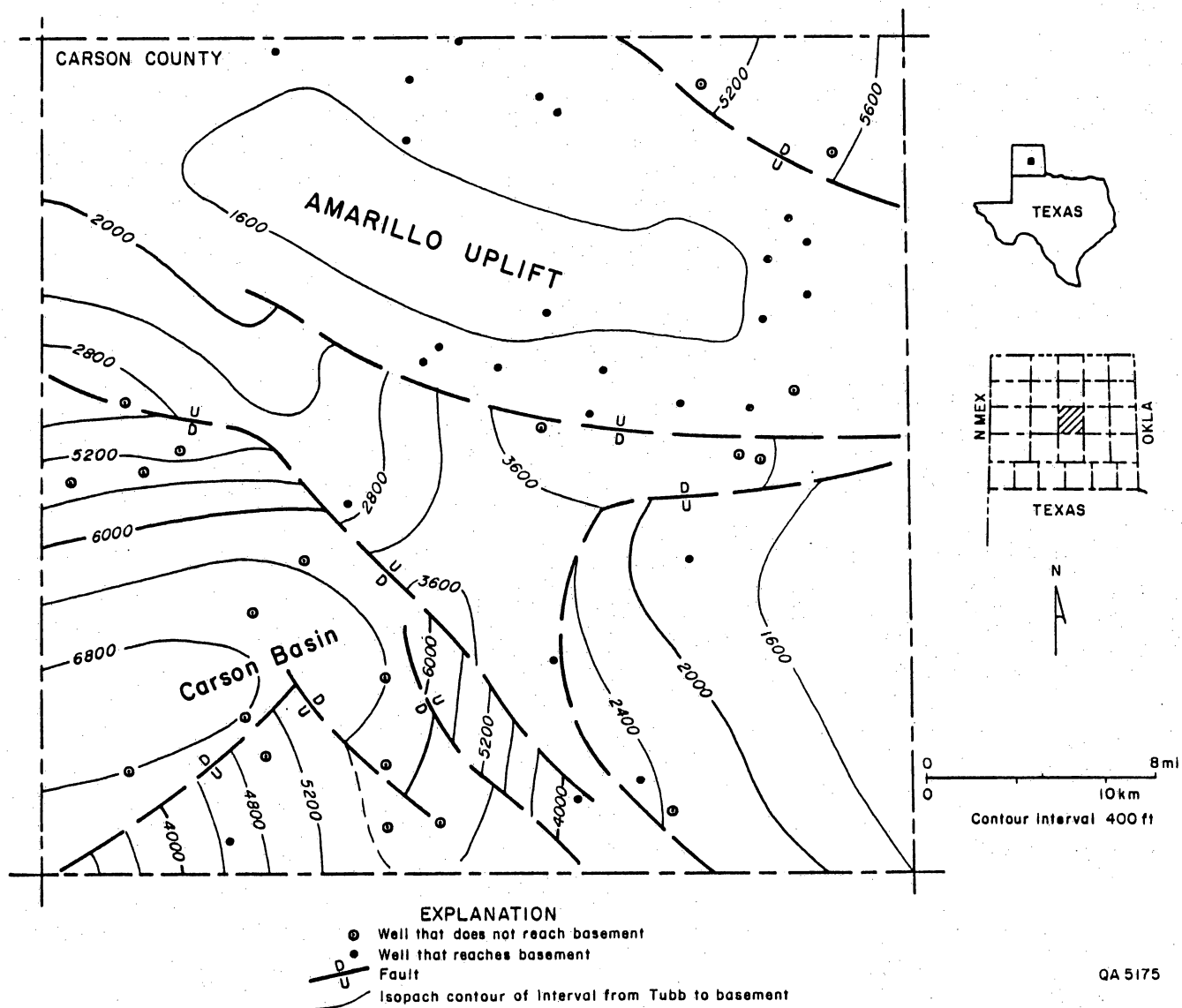


Figure 14. Isopach map of the Pennsylvanian and Lower Permian (top of Tubb to top of basement), Carson basin. Dashed contours indicate minimum thickness based on wells that penetrated granite wash but did not reach basement.

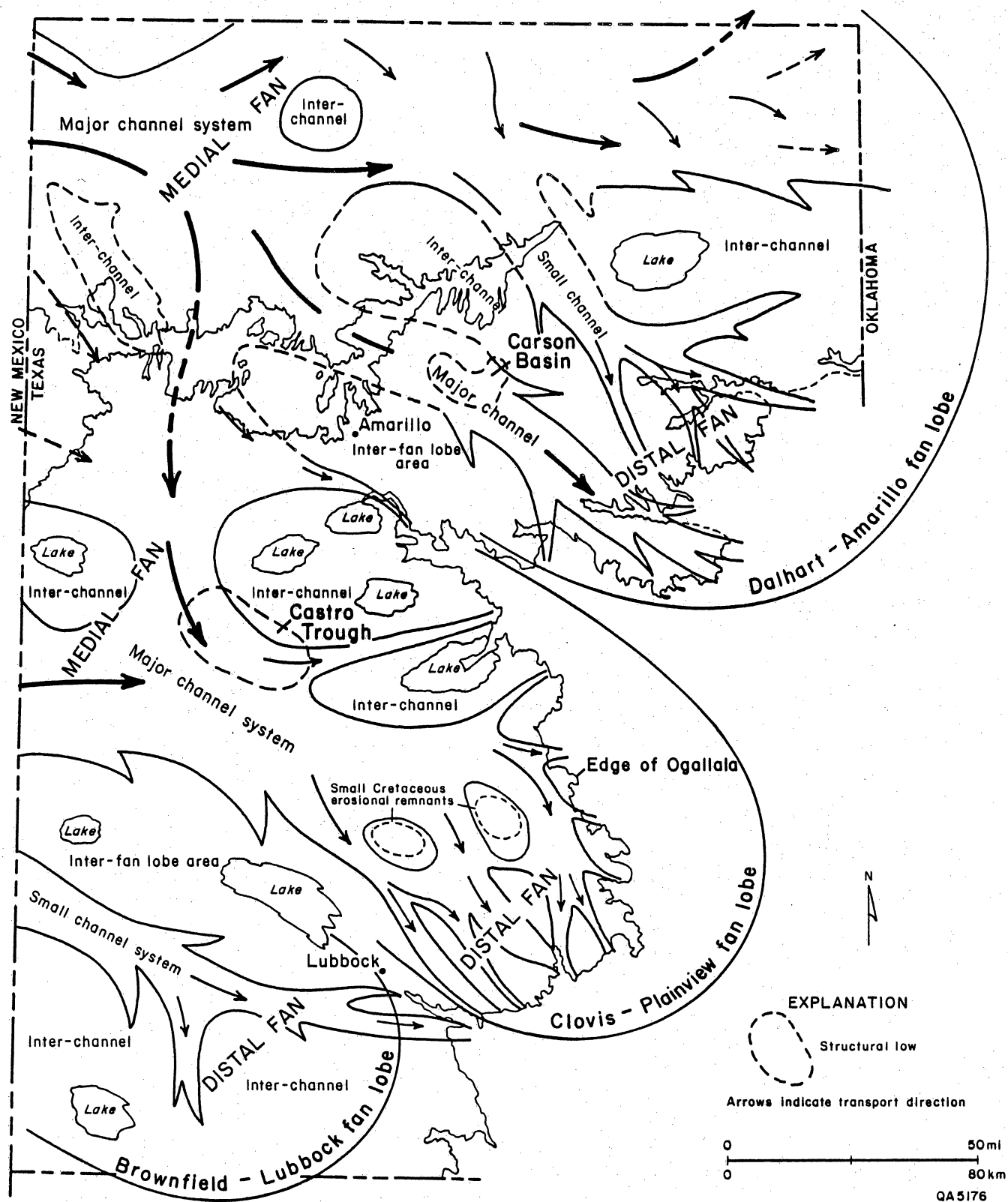


Figure 15. Schematic illustration of Ogallala depositional facies and sediment dispersal systems (Seni, 1980).

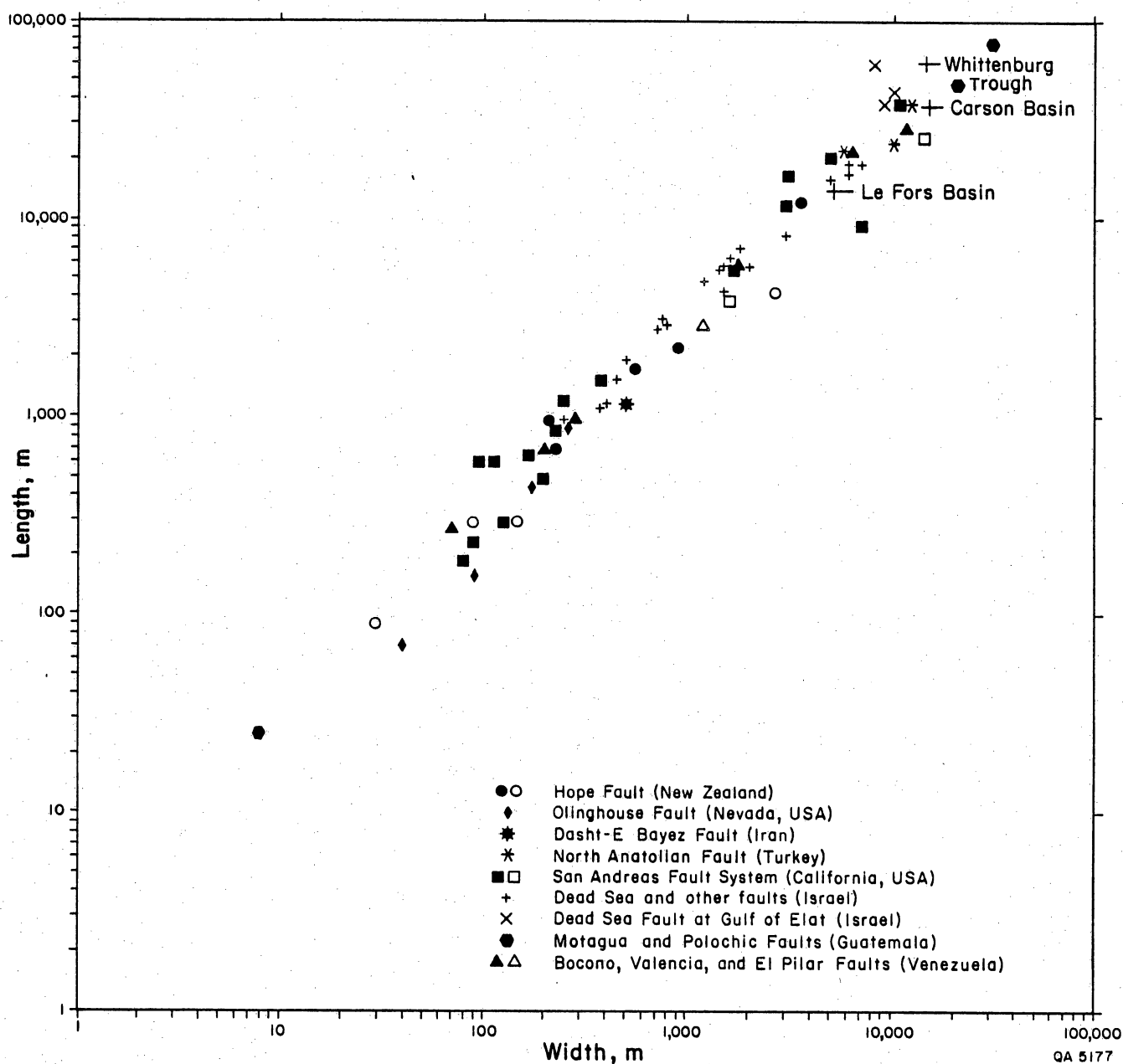


Figure 16. Log length versus log width for 70 pull-apart basins or rhomb grabens and horsts associated with major strike-slip faults of the world (Aydin and Nur, 1982). The Neogene Carson basin is plotted as is the Pennsylvanian LeFors basin shown in figure 9. The length to width ratios of both basins are consistent with those of other basins postulated to have formed along strike-slip fault zones.

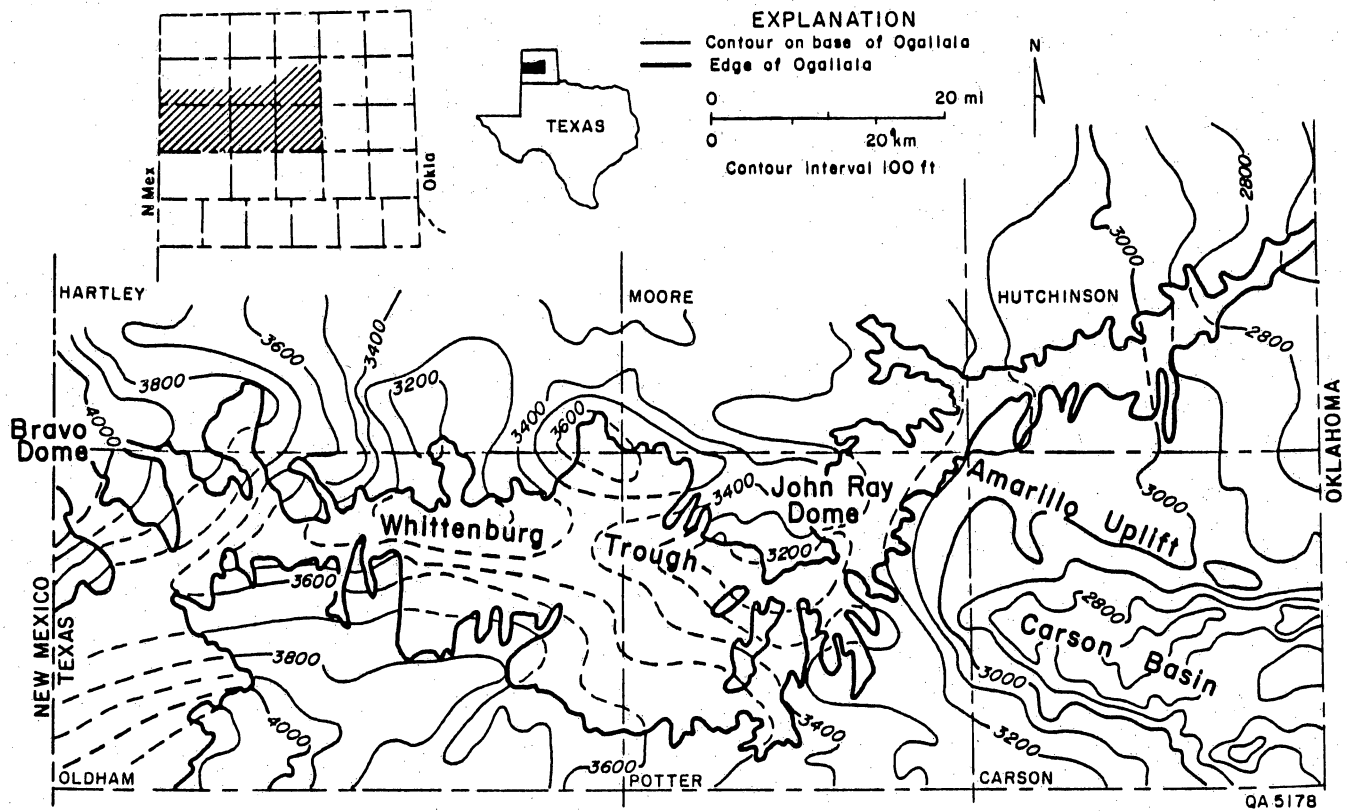


Figure 17. Structure-contour map on the base of the Ogallala Formation at the western end of the Amarillo Uplift. The Ogallala has been broadly folded over basement uplifts. From Knowles and others (1982). Contours dashed where projected.

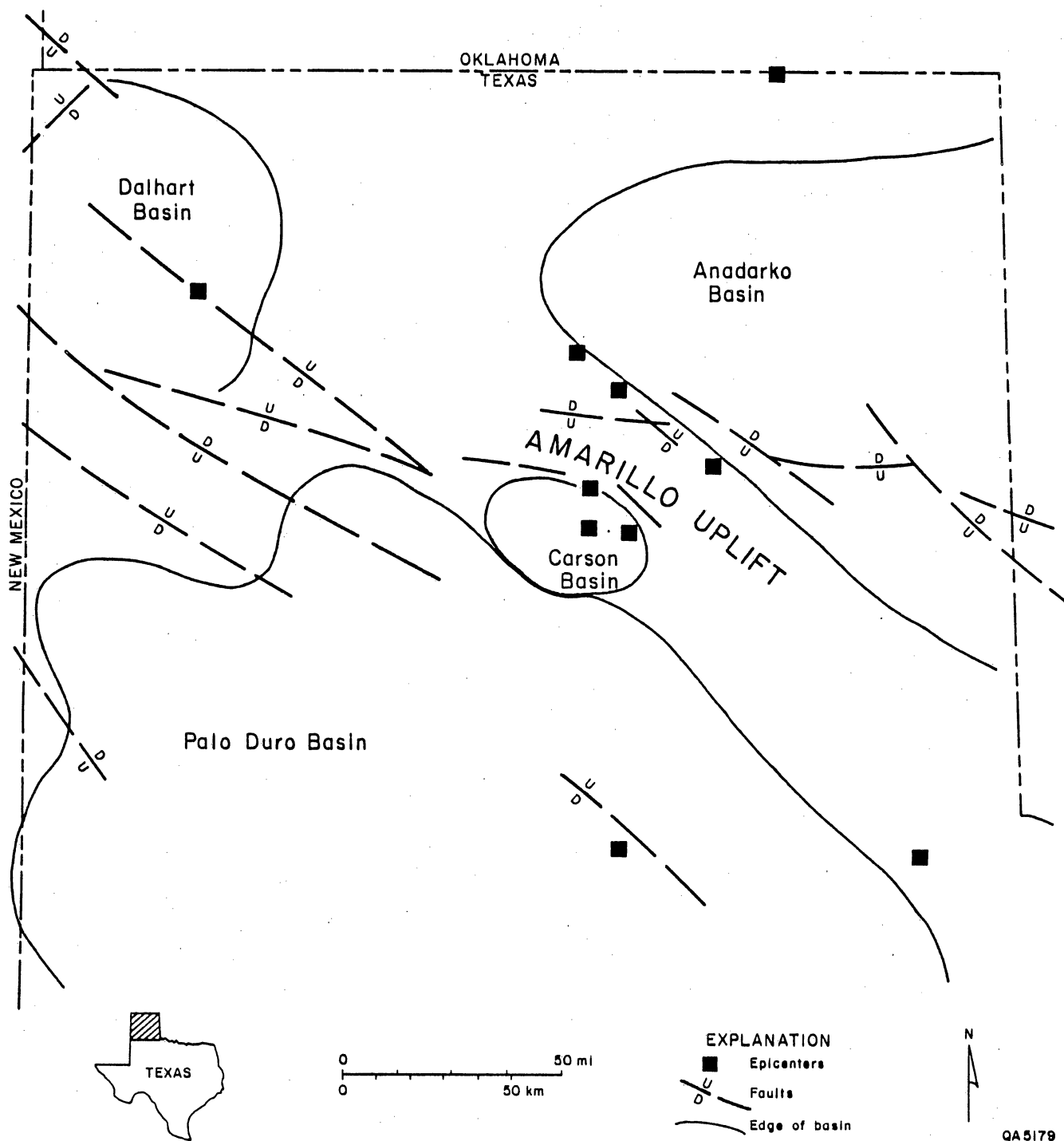


Figure 18. Seismicity in the Texas Panhandle (from Reagor and others, 1982).

## OCCURRENCE OF CLASTIC DIKES IN THE TEXAS PANHANDLE

Edward W. Collins

*Clastic dikes cut strata throughout the Texas Panhandle, western Oklahoma Panhandle, and eastern New Mexico. The dikes appear to have been formed from the filling of fractures or fissures from above. Subsidence caused by evaporite dissolution is the most likely mechanism by which horizontal strain and extension opened the fractures or fissures.*

Clastic dikes are among the brittle deformational features observed in outcrop in Randall, Potter, Moore, Oldham, Hartley, and Hall Counties of the Texas Panhandle, as well as at localities in the Oklahoma Panhandle and in eastern and northeastern New Mexico. These clastic dikes usually range in thickness from about 15 cm to 3 mm, although one dike measured in northeastern New Mexico is 1.5 m thick. In the Texas Panhandle poor exposures prevent tracing the vertical and lateral extent of most of the dikes. Almost all of the dikes cut upper Triassic strata although clastic dikes have also been observed in the Pliocene Rita Blanca Formation in Hartley County and in Pleistocene deposits in Hall County.

The mechanics of dike emplacement are difficult to determine unless the dikes can be traced in outcrop to source beds. The composition of a dike usually cannot indicate a definite source bed because Triassic, Tertiary, and Quaternary sediments have similar lithologies.

The dikes appear to have been formed by filling from above of fractures or fissures. At Buffalo Lake in western Randall County, dikes from the overlying Tertiary Ogallala source beds cut Triassic Dockum sediments. Where a dike termination can be observed with depth, the dike thins and pinches out. The trends of these dikes are very similar to fracture orientations measured at this location (fig. 19). Dikes throughout the Texas Panhandle and eastern New Mexico also appear to be due to fracture filling (fig. 19). Subsidence is the most likely mechanism by which horizontal strain and extension opened the fractures or fissures. In the Texas Panhandle, geomorphic features such as recent fissures, sinkholes, collapse basins, and breccia-filled chimneys have been attributed to

subsidence processes caused by evaporite dissolution (Gustavson and others, 1982). Subsidence created by differential compaction is another mechanism that can develop fissures (Jachens and Holzer, 1982), although in the Texas Panhandle evaporite dissolution is the most likely cause of subsidence.

Most of the clastic dikes in the Texas Panhandle were emplaced during the Cenozoic. Dikes cutting Triassic sediments at one locality in Palo Duro Canyon State Park, however, appear to have originated from a siltstone unit within the Dockum Group and are probably Triassic in age. The predominant dike trend at this locality is the same as the joint trends (fig. 19).

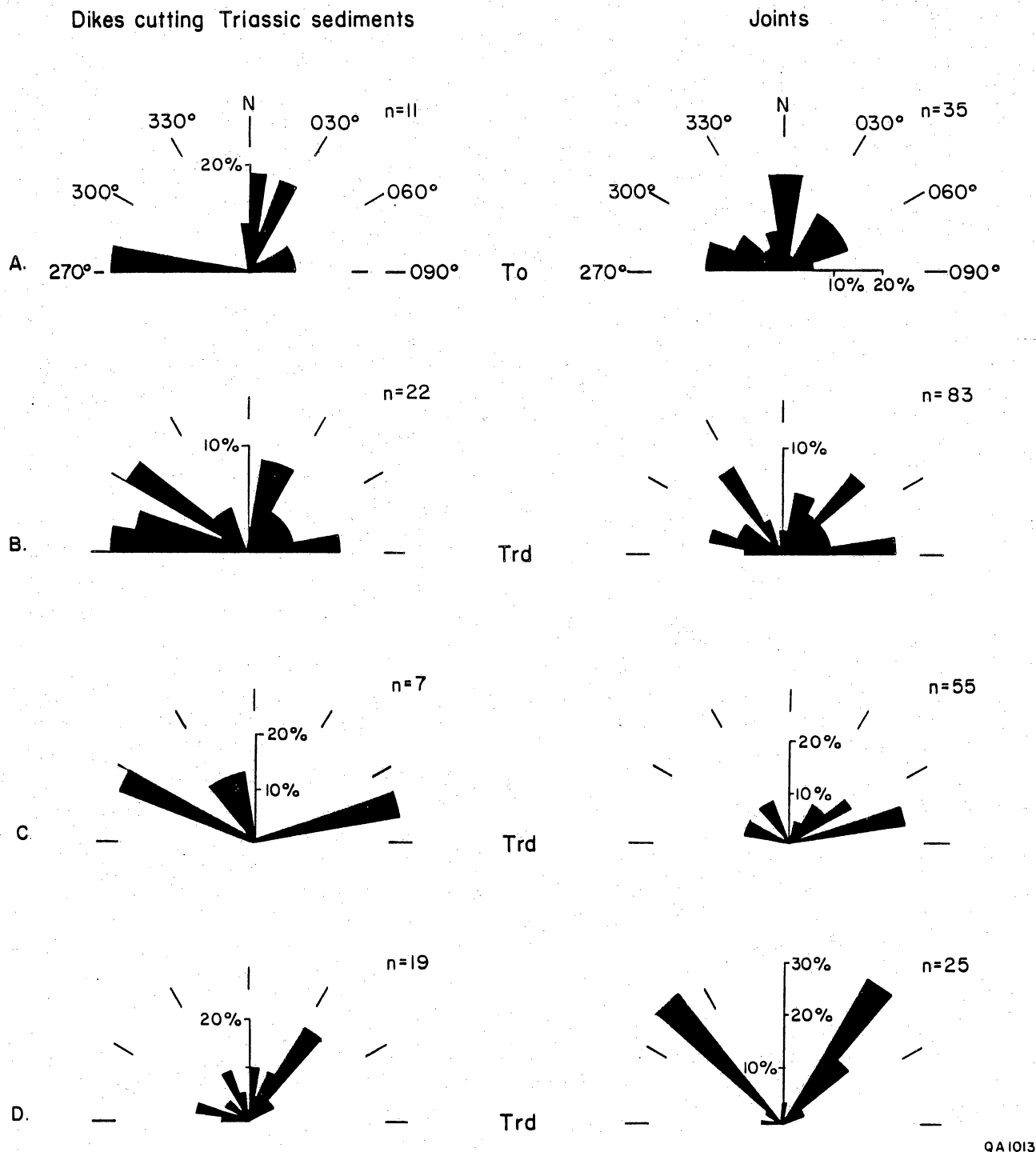


Figure 19. Comparison of clastic dikes and joint orientations in the Texas Panhandle and eastern New Mexico. Data were collected from the following localities: (A) near Buffalo Lake dam, western Randall County, Texas; (B) U.S. Highway 385 at the southern edge of the Canadian River Valley, eastern Oldham County, Texas; (C) New Mexico State Highway 93 at the western caprock escarpment, Quay County, eastern New Mexico; and (D) 1.8 km north of Lighthouse Peak at Palo Duro Canyon State Park, eastern Randall County, Texas. The clastic dikes cut Triassic Dockum Group sediments, and the joints were measured in Triassic Dockum Group (Trd) and Tertiary Ogallala Formation (To) strata. The joint data from the Buffalo Lake locality (A) are from Finley and Gustavson (1981, p. 25).



## GEOMETRY AND ORIGIN OF SYNCLINAL DEPRESSIONS AT CAPROCK CANYONS STATE PARK, BRISCOE COUNTY, TEXAS

Edward W. Collins

*Folding of Permian strata above a salt-dissolution zone has been identified in Caprock Canyons State Park, Texas Panhandle. Synclinal depressions have been mapped in the area, and the association between the structural basins, joints, and veins suggests that systematic regional joints that predate dissolution collapse have influenced salt dissolution.*

Synclinal depressions have been mapped in upper Permian strata at Caprock Canyons State Park, Briscoe County. This area is within a regional salt-dissolution zone (Gustavson and others, 1982; Gustavson and others, 1980b). It has been suggested that systematic joints that predate dissolution collapse could have acted as preferred pathways for fluid movement and caused low-amplitude folding (Collins, 1983a, b; Goldstein, 1982). Detailed structural mapping has defined the geometry of the synclinal depressions and has shown the relationship between the structural basins and vein-filled joints.

Three types of gypsum veins are present (Goldstein and Collins, 1984; Goldstein, 1982): veins that are nearly vertical, veins that parallel bedding, and veins that cut the bedding at 30 to 60 degrees. Where the veins intersect, vertical veins are everywhere cut by inclined veins and nearly everywhere cut by horizontal veins. The gypsum fibers in the vertical veins are horizontal, indicating that these veins formed by horizontal extension. The vertical gypsum veins mineralized in systematic joints that predate dissolution collapse (Goldstein, 1982, p. 27). The mineral fibers of the inclined and horizontal veins are vertical, indicating that mineralization occurred during vertical extension. These vein-filled fractures developed during dissolution collapse of the strata (Goldstein, 1982, p. 27).

The style of folding exhibited at Caprock Canyons State Park is best described as chaotic. Gentle folds cause the beds to dip usually less than 15 degrees. Synclinal depressions or basins that have been mapped in the area vary in shape from elongate to circular. These basins are up to 1.5 km in length. The synclinal depressions are composed of conical synclines and anticlines that gently plunge as much as 10 degrees toward the

center of the basin (fig. 20). The amplitude of these folds is usually less than 10 to 15 m. Rim anticlines or "domes" may also occur around the periphery of the basins, commonly separating two basins. Smaller scale folding also exists, and although the folding may be associated with the development of the larger synclinal depressions, some of the smaller folds are probably due to expansion associated with the conversion of anhydrite to gypsum.

A close association exists among the joints, veins, and structural basins. Within a specific basin the most significant trend of the near-vertical veins is the same as the basin axis, and even though the inclined veins strike in all directions, the dominant strike direction is the same as the orientation of the basin (fig. 21a and b). Systematic joints that predated dissolution collapse probably provided pathways for fluid migration and enhanced salt dissolution. Collapse of strata occurred within zones of enhanced dissolution and developed synclinal depressions and nonsystematic joints.

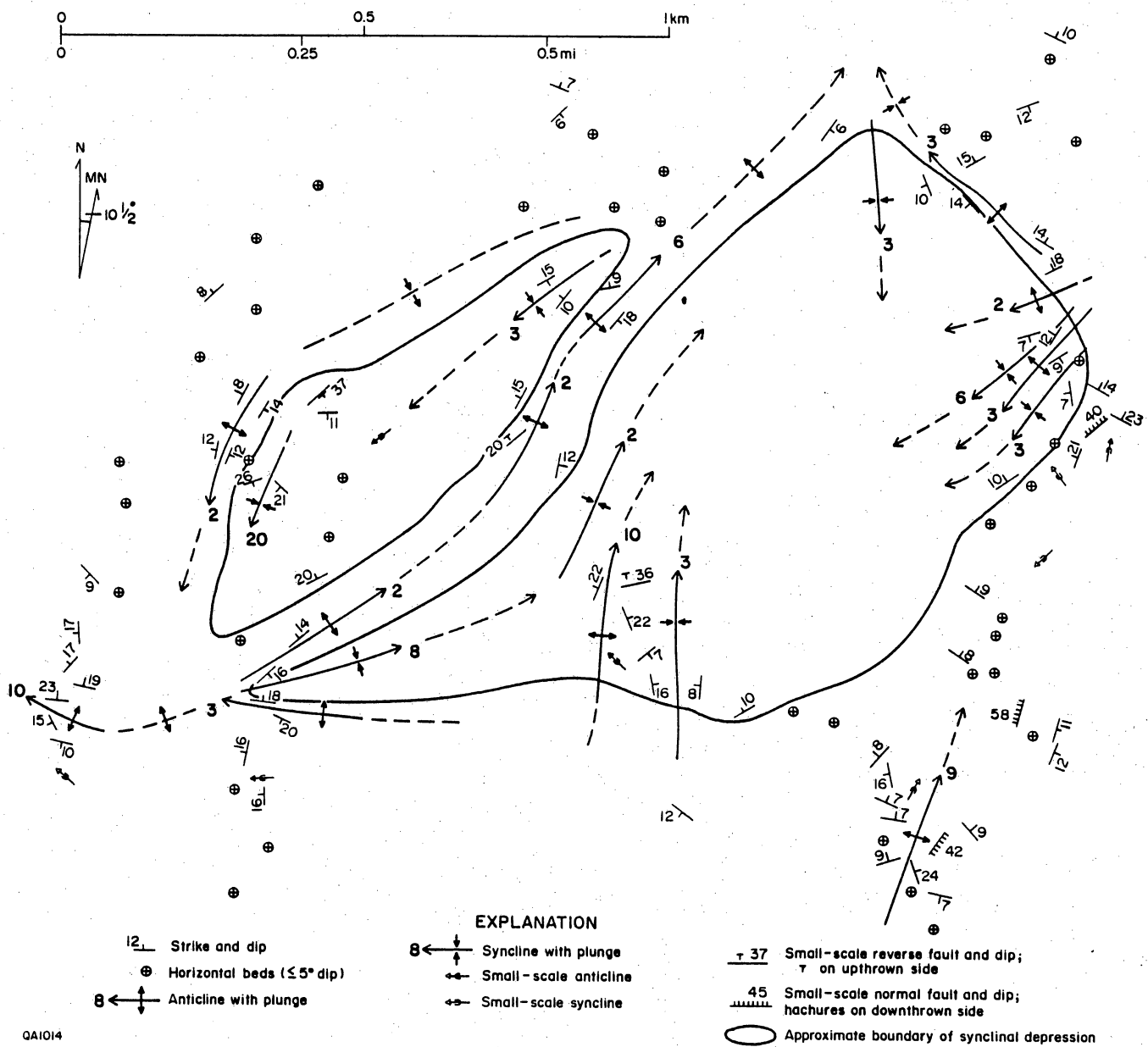


Figure 20. Structure map exhibiting the geometry of folds at Caprock Canyons State Park, Briscoe County. The major synclinal axes of these two basins trend northeast (040-050). The mapped area is located 1.5 km north of Lake Theo.

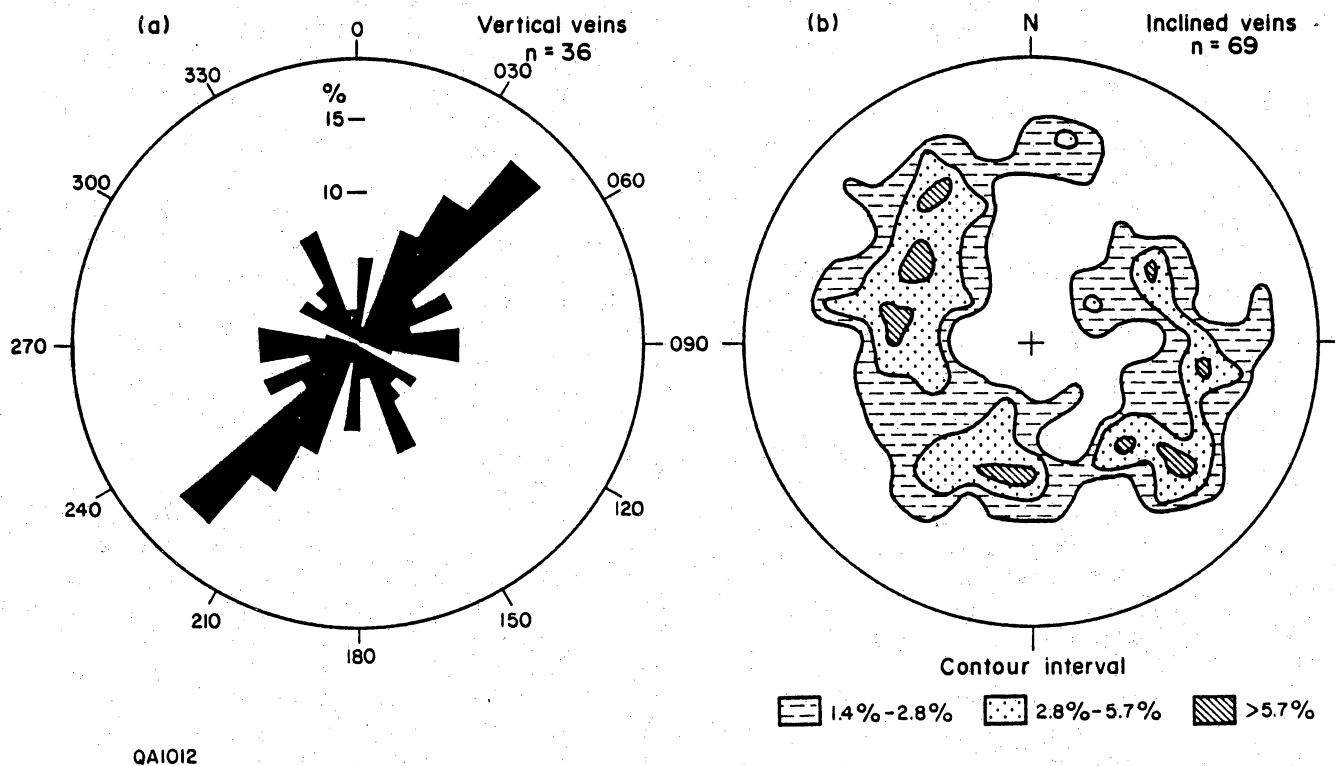


Figure 21. (a) Rose diagram exhibiting trends of vertical gypsum veins for map area in fig. 20. The vertical veins represent gypsum mineralization in regional, systematic joints that predate dissolution-collapse. (b) Schmidt net plot (lower hemisphere) of poles to inclined veins for map area in fig. 20. The inclined veins represent gypsum mineralization in nonsystematic joints that occurred from dissolution collapse.

## MISSISSIPPIAN CONODONT BIOSTRATIGRAPHY IN THE PALO DURO BASIN AREA

Stephen C. Ruppel

*Conodont faunas were recovered from four wells in the Palo Duro Basin area. Correlation of these faunas with well-established zonations elsewhere in the midcontinent suggests that early Mississippian (Osage) deposition was restricted to the area of the Anadarko Basin axis and that subsequently (during the Meramecian) deposition spread throughout the area as seas transgressed southwestward across the Texas Panhandle.*

The Mississippian System of North America is subdivided into four series, which are, from youngest to oldest, Kinderhook, Osage, Meramec, and Chester (Dott, 1941; Cheney and others, 1945). Although proper correlation of these units requires biostratigraphic or chronostratigraphic control, in the midcontinent region, especially in the subsurface where paleontologic data are generally lacking, these units have been extended primarily by lithologic similarity. Biostratigraphic studies in Kansas (Thompson and Goebel, 1969) have supported the time-stratigraphic accuracy of these correlations and suggested that Mississippian lithologies are synchronous throughout large areas of the midcontinent. A necessary corollary of this assumption is the idea that depositional conditions were relatively uniform during the Mississippian over widespread geographic areas. Recent biostratigraphic studies of the Mississippian rocks in the Palo Duro Basin based on conodonts, however, do not support this model.

Three Mississippian series are commonly recognized in the Palo Duro Basin (fig. 22) on the basis of lithologic correlation from Kansas and Oklahoma (Cunningham, 1969). Conodonts have been recovered from "Osage" and "Meramec" rocks in cores from four wells in the Texas Panhandle area (fig. 23). Specimens recovered from the upper part of the Chappel Formation (correlative with the "Meramec" of the Palo Duro Basin) in the Hardeman Basin (Hardeman County; tables 2 and 3) are representative of the Apatognathus scalenus -Cavusgnathus Zone of Collinson and others (1962, 1971) and of the Cavusgnathus Zone of Dutro and others (1979) and Sandburg (1979). This indicates at least a middle to late Meramecian age for these rocks, which is generally consistent with previous

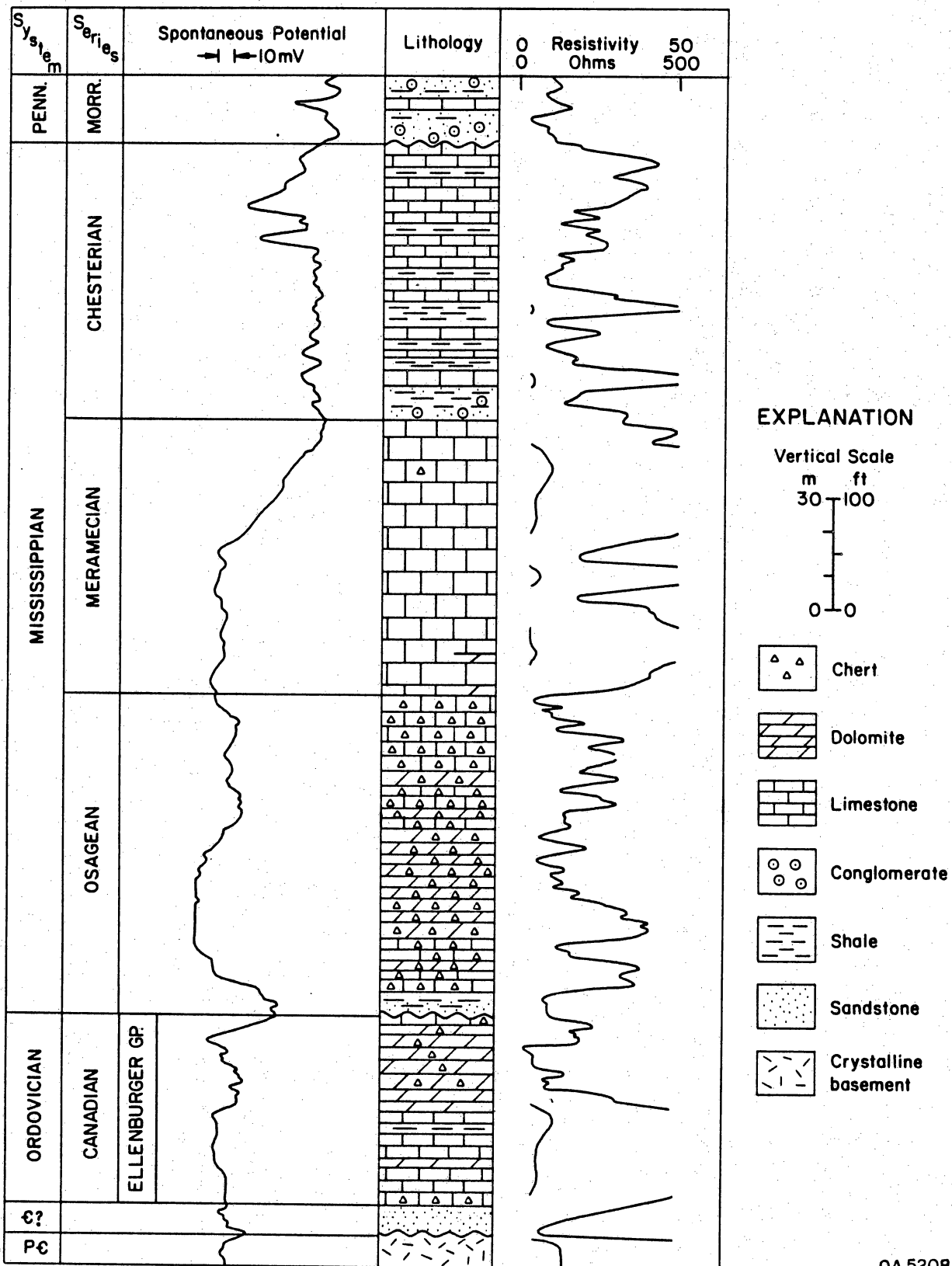
interpretations that the Chappel contains an upper Meramec part and a lower Osage part (Mapel and others, 1979). However, the presence of these middle to late Meramecian conodonts near the base of the upper Chappel suggests that the lower Chappel (correlative with the "Osage") is younger than previously assumed.

Conodonts were recovered from 12 samples in core from Childress County (fig. 23) representing both the "Meramec" and the "Osage" (correlative with the upper and lower parts of the Chappel, respectively, in the Hardeman Basin). Conodonts obtained from the "Meramec" (table 4) are essentially the same as those recovered from the Hardeman Basin cores. The fauna recovered from the lower ("Osage") Mississippian in Childress County (table 4) differs slightly (it contains Taphrognathus as well as Cavusgnathus) but nevertheless also implies a middle Meramecian age (Collinson and others, 1971; Dutro and others, 1979). This indicates that rocks of Osage age are either absent in the area or represented by a thin layer (about 40 ft [12 m] of Mississippian at the base of the Childress County well was not cored). Correlations between this well and those in the Hardeman Basin based on lithologies and conodont faunas suggest that most of the Chappel Lower and Middle Mississippian section in the area is of Meramecian age (fig. 24).

Because of Pennsylvanian erosion, only the lower ("Osage") part of the Mississippian section is present in northern Donley County. Conodont samples were taken from 36 ft (11 m) of core taken in the upper part of the section (fig. 24). Faunas obtained in this well (table 5) represent the Taphrognathus Zone of Dutro and others (1979) and Sandburg (1979) and are thus significantly older than any of the others studied. Because this zone spans the Osage-Meramec boundary, it is impossible to accurately date these rocks. However, the abundance of Taphrognathus favors a Meramec age (Collinson and others, 1971). The presence of 200 ft (61 m) of Mississippian section below the studied interval suggests that Osagean rocks are the oldest known Mississippian rocks of the area (fig. 24).

The conodont faunas indicate that the earliest Mississippian deposition in the southern Panhandle area began in the northern part of the Palo Duro Basin (Donley

County). Although local sediment accumulation may have begun in the Hardeman Basin during the Osagean, major deposition in the area did not commence until the Meramecian. On the basis of these relationships it appears that the Palo Duro and Hardeman Basins were flooded (transgressed) progressively from north to south. This is consistent with thicknesses and lithologies of supposed early Mississippian rocks in the Anadarko Basin. As was true through much of the Paleozoic, the Anadarko Basin was a site of relatively greater subsidence than surrounding areas. Therefore it would be expected that the earliest Mississippian deposition would be in the basin and along its margins. The relatively old Mississippian deposits in Donley County may represent the southern margin of the Anadarko Basin during the Osagean.



QA 5208

Figure 22. Conventional subdivision of Mississippian rocks in the Palo Duro Basin (after Cunningham, 1969). Possible Kinderhook deposits (not shown) occur sporadically at the base. Amerada Petroleum Corporation Lafayette Hughes Trustee No. 1, Hall County, Texas (BEG No. 18).



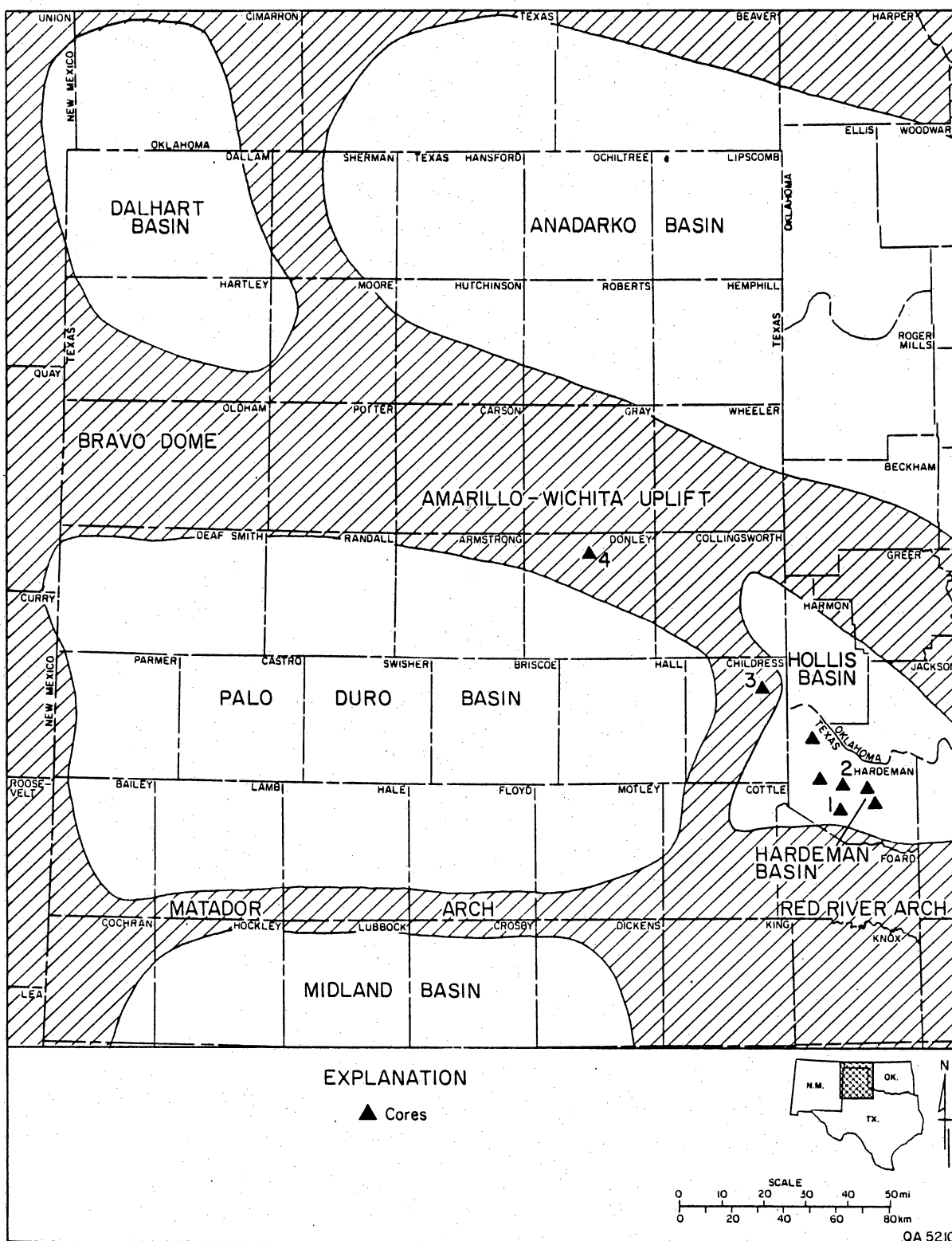


Figure 23. Map of the Texas Panhandle showing the location of the Palo Duro and Hardeman Basins and four cored wells discussed in this report. Donley 3: Service Drilling Company Kathleen C. Griffin No. 1; Childress 10: Wes-Tex, Kewanee, and Coastal States Gas Producing Co. JA Steve Owens No. 1; Hardeman 42: Sun Oil Co. Quanah Townsite Unit No. 1; Hardeman 44: Standard Oil Co. of Texas Coffee No. 1.

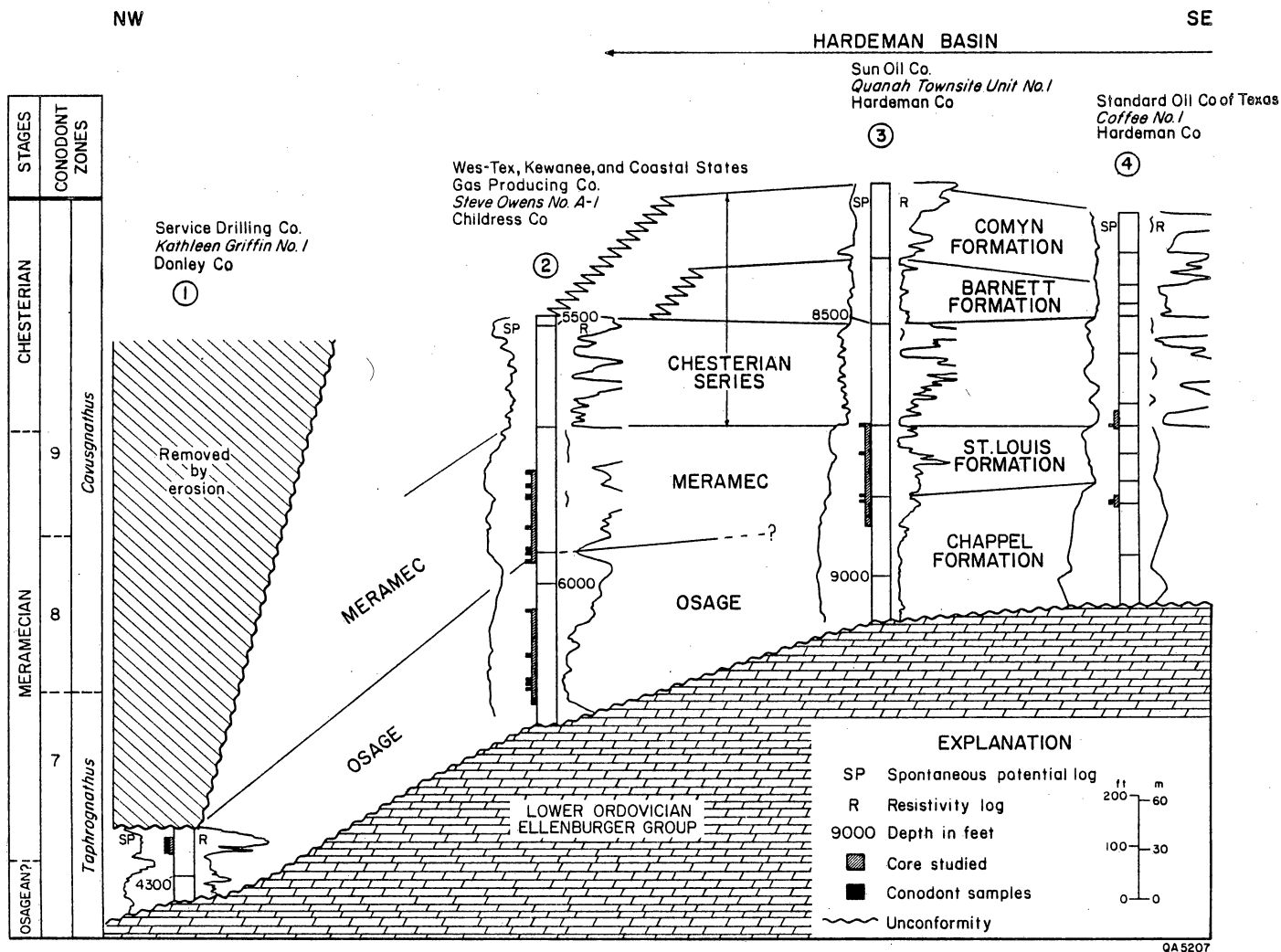


Figure 24. Probable correlation of four wells from which conodonts were recovered. No horizontal scale. Wells and line of section are shown in figure 23.

Table 2. Conodonts recovered from Core 1, Hardeman County  
(Standard Oil Co. of Texas, Coffee No. 1).

Upper Chappel Formation

Apatognathus sp.

Cavusgnathus charactus

Cavusgnathus convexus

Cavusgnathus unicornis

Cavusgnathus sp.

Gnathodus bilineatus

Gnathodus commutatus commutatus

Gnathodus texanus

Hindeodella sp.

Ligonodina levis

Ligonodina sp.

Lonchodina sp.

Lonchodus sp.

Neoprioniodus tulensis

Neoprioniodus spp.

Spathognathodus crisulus

Spathognathodus scitulus

Spathognathodus spp.

Table 3. Conodonts recovered from Core 2, Hardeman County  
(Sun Oil Co., Quanah Townsite Unit No. 1).

Upper Chappel Formation

Apatognathus sp.

Cavusgnathus charactus

Cavusgnathus convexus

Cavusgnathus unicornis

Cavusgnathus spp.

Gnathodus texanus

Hibbardella spp.

Hindeodella spp.

Ligonodina levis

Ligonodina tenuis

Ligonodina spp.

Lonchodus sp.

Neoprioniodus loxus

Neoprioniodus tulensis

Neoprioniodus spp.

Ozarkodina curvata

Ozarkodina spp.

Spathognathodus campbelli

Spathognathodus cristulus

Spathognathodus scitulus

Spathognathodus spiculus

Spathognathodus spp.

Table 4. Conodonts recovered from Core 3, Childress County (Wes-Tex, Kewanee, and Coastal States Gas Producing Company, Steve Owens No. 1-A).

"Meramec" Series

Cavusgnathus regularis  
Cavusgnathus unicornis  
Cavusgnathus spp.  
Hindeodella spp.  
Ligonodina levis  
Ligonodina spp.  
Neoprioniodus tulensis  
Taphrognathus varians  
Taphrognathus-Cavusgnathus transition

"Osage" Series

Apatognathus sp.  
Cavusgnathus charactus  
Cavusgnathus convexus  
Cavusgnathus regularis  
Cavusgnathus unicornis  
Cavusgnathus spp.  
Gnathodus texanus  
Hindeodella spp.  
Ligonodina tenuis  
Ligonodina spp.  
Lonchodus spp.  
Neoprioniodus loxus  
Neoprioniodus tulensis  
Neoprioniodus spp.  
Ozarkodina spp.  
Spathognathodus scitulus  
Taphrognathus varians  
Taphrognathus-Cavusgnathus transition  
 New genus

Table 5. Conodonts recovered from Core 4, Donley County  
(Service Drilling Co., Kathleen C. Griffin No. 1).

"Osage" Series

Apatognathus spp.

Gnathodus texanus

Hibbardella spp.

Hindeodella spp.

Ligonodina spp.

Neoprioniodus spp.

Ozarkodina spp.

Taphrognathus varians

## PRE-PENNSYLVANIAN CARBONATES AS POTENTIAL HYDROCARBON SOURCE ROCKS, PALO DURO AND DALHART BASINS, TEXAS

Stephen C. Ruppel

*Analysis of organic matter content and thermal maturation of Mississippian and Lower Ordovician carbonates in the Palo Duro and Dalhart Basins indicates that these rocks may have acted as petroleum source rocks. Their source rock potential is far less, however, than equivalent rocks in the oil-producing Hardeman Basin to the east.*

Although no petroleum production has been established in the pre-Pennsylvanian rocks of the Palo Duro and Dalhart Basins, numerous shows in these rocks (figs. 25 and 26) indicate that hydrocarbons have been generated in the area. To determine the likelihood of hydrocarbon accumulation in the pre-Pennsylvanian sequence it is important to ascertain the extent of potential source rocks. Dutton (1980a, b; Dutton and others, 1982) has recently characterized the source rock potential of the area by studying the organic matter content of shaly rocks throughout the stratigraphic section. Because shales are essentially absent from the Mississippian and Ordovician (Ellenburger Group) carbonates that constitute the pre-Pennsylvanian part of the section, Dutton's work concentrated on Pennsylvanian and Permian rocks. Although shales are often considered to have the highest potential as source rocks, recent studies have illustrated that carbonate rocks may have petroleum potentials equal to shales containing twice as much organic matter. Shales normally must have a minimum of 0.5 percent total organic carbon (TOC) to produce commercial quantities of hydrocarbons (Tissot and Welte, 1978), whereas carbonates, because they contain higher percentages of liptinic organic matter, may be effective sources with as little as 0.12 percent TOC (GeoChem Laboratories, 1980).

To determine source rock potential of the pre-Pennsylvanian carbonates, analyses of TOC were conducted at selected carbonate intervals in 52 wells in the Palo Duro and Dalhart Basins. Samples from five additional wells in the Hardeman Basin were analyzed for comparative purposes (figs. 27 and 28). A total of 101 samples were analyzed, 74 from cuttings, 27 from core (table 6). To avoid possible contamination from Pennsylvanian shale

cavings, all cuttings were carefully picked to remove shale fragments. Because the type of organic matter present is at least as important as the amount, determinations of organic matter type were made for 15 wells (table 7); usable vitrinite reflectance ( $R_o$ ) values (useful for determining thermal maturity) were obtained for 9 of these wells (table 7).

The average TOC value for all pre-Pennsylvanian samples analyzed in the Palo Duro and Dalhart Basins is 0.107 percent. This is lower than the average values for carbonates reported elsewhere (about 0.2 percent TOC; see Tissot and Welte, 1978; Hunt, 1979) and is also below the minimum usually given for carbonate source rocks. Total organic carbon values from the Mississippian "Osage," however, although variable, are generally higher than those from other pre-Pennsylvanian units; 41 percent of the "Osage" samples exhibit TOC values greater than 0.12 percent, and 16 percent are higher than 0.20 percent TOC (fig. 29). Thus some "Osage" rocks probably have sufficient organic matter to produce hydrocarbons. The Mississippian "Meramec" and the Ordovician Ellenburger Group have the lowest TOC contents and are not likely source rocks (table 6, fig. 29). Insufficient TOC values were obtained from the Mississippian "Chester" to characterize its source rock potential. Total organic carbon values from the Hardeman Basin are generally higher although they exhibit greater variability (table 6, fig. 29). The highest values (0.726 percent, 0.934 percent TOC) were obtained from calcareous shales and shaly carbonates (Barnett Formation), although a relatively pure limestone (Chappel Formation) measured 0.668 percent TOC.

The organic matter that comprises the pre-Pennsylvanian carbonates is primarily sapropelic (containing mostly algal and amorphous material, spores and pollen); the greater the amount of sapropel, the greater the potential hydrocarbon generation (Hunt, 1979). Samples from the "Osage" contain an average of 68 percent sapropel (32 percent vitrinite and inertinite). Other pre-Pennsylvanian units average about 50 percent (table 7). The "Osage" thus also appears to have the greater potential for hydrocarbon production on the basis of organic matter type.



Even if a potential source rock contains adequate kinds and amount of organic matter, it cannot generate hydrocarbons unless it has reached a minimum state of thermal maturity. Both vitrinite reflectance ( $R_o$ ) and kerogen color (table 7) have been used to interpret the degree of thermal maturity of the pre-Pennsylvanian sequence in the area. A vitrinite reflectance of about 0.5 percent  $R_o$  is commonly accepted as indicative of the minimum level of maturation necessary for major oil generation (Tissot and Welte, 1978). On the basis of reflectance values obtained in the Palo Duro and Dalhart Basins, this degree of maturity is reached at about 7,500 ft (fig. 30). Pre-Pennsylvanian deposits lie at depths equal to or greater than 7,500 ft throughout most of the central and southern parts of the Palo Duro Basin. Kerogen color studies (expressed in terms of Thermal Alteration Index [TAI]) tend to support the conclusion that most pre-Pennsylvanian units in the Palo Duro and Dalhart Basins are at or near the minimum level of maturation necessary for hydrocarbon production. Most (75 percent) of the samples studied are classed as immature-mature; the remainder (25 percent) are mature (Schwab, 1977).

Although most indicators suggest that the pre-Pennsylvanian carbonates in the Palo Duro and Dalhart Basins have reached the threshold of hydrocarbon generation, equivalent rocks in the Hardeman Basin to the east, which are currently producing hydrocarbons, are considerably more mature. Kerogen color studies indicate that all three samples examined are fully mature (table 7). Independent studies of conodonts support this conclusion. Mississippian conodonts are progressively darker in color from the eastern Palo Duro Basin into the Hardeman Basin (table 8), indicating a higher degree of thermal maturity (Epstein and others, 1977). Finally, although only two samples were studied, vitrinite reflectance indicates the presence of much more mature rocks in the Hardeman Basin (fig. 30).

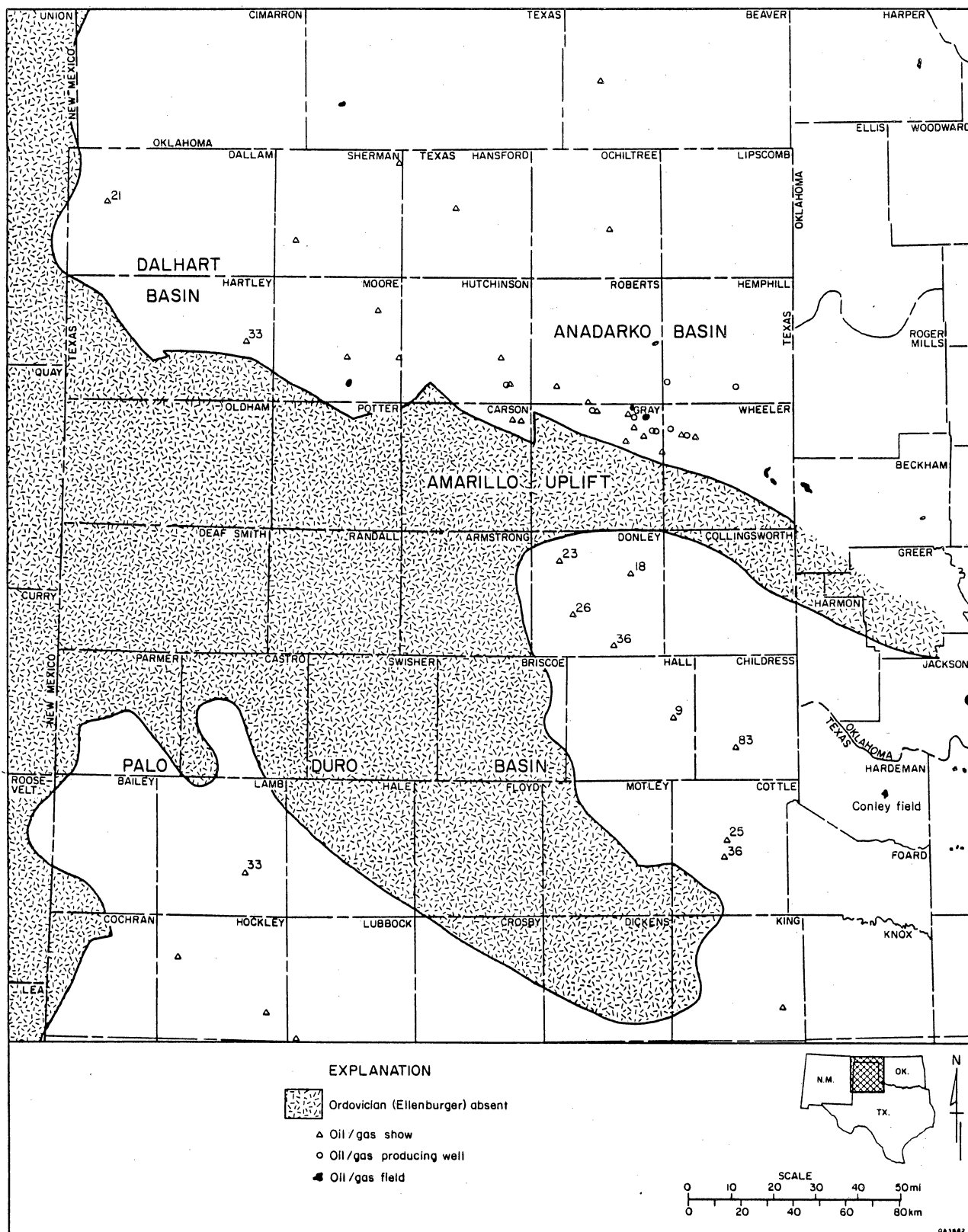


Figure 25. Reported hydrocarbon shows, discoveries, and fields in the Ellenburger Group (Ordovician) in the Texas Panhandle. Note: data plotted for the Anadarko Basin are based on limited information.

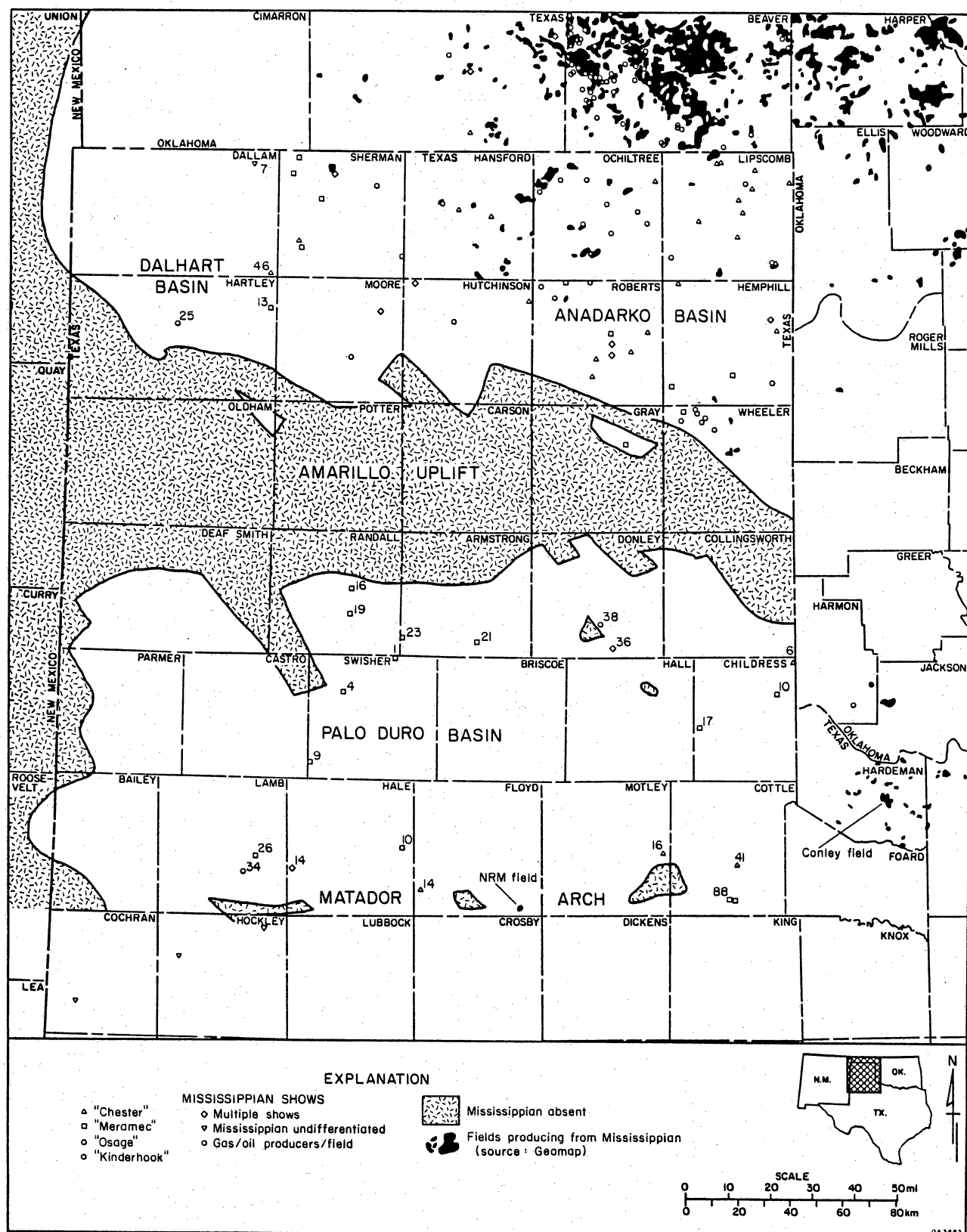


Figure 26. Reported hydrocarbon shows, discoveries, and fields in the Mississippian rocks of the Texas Panhandle. Note: data plotted in the Anadarko Basin are based on limited information.

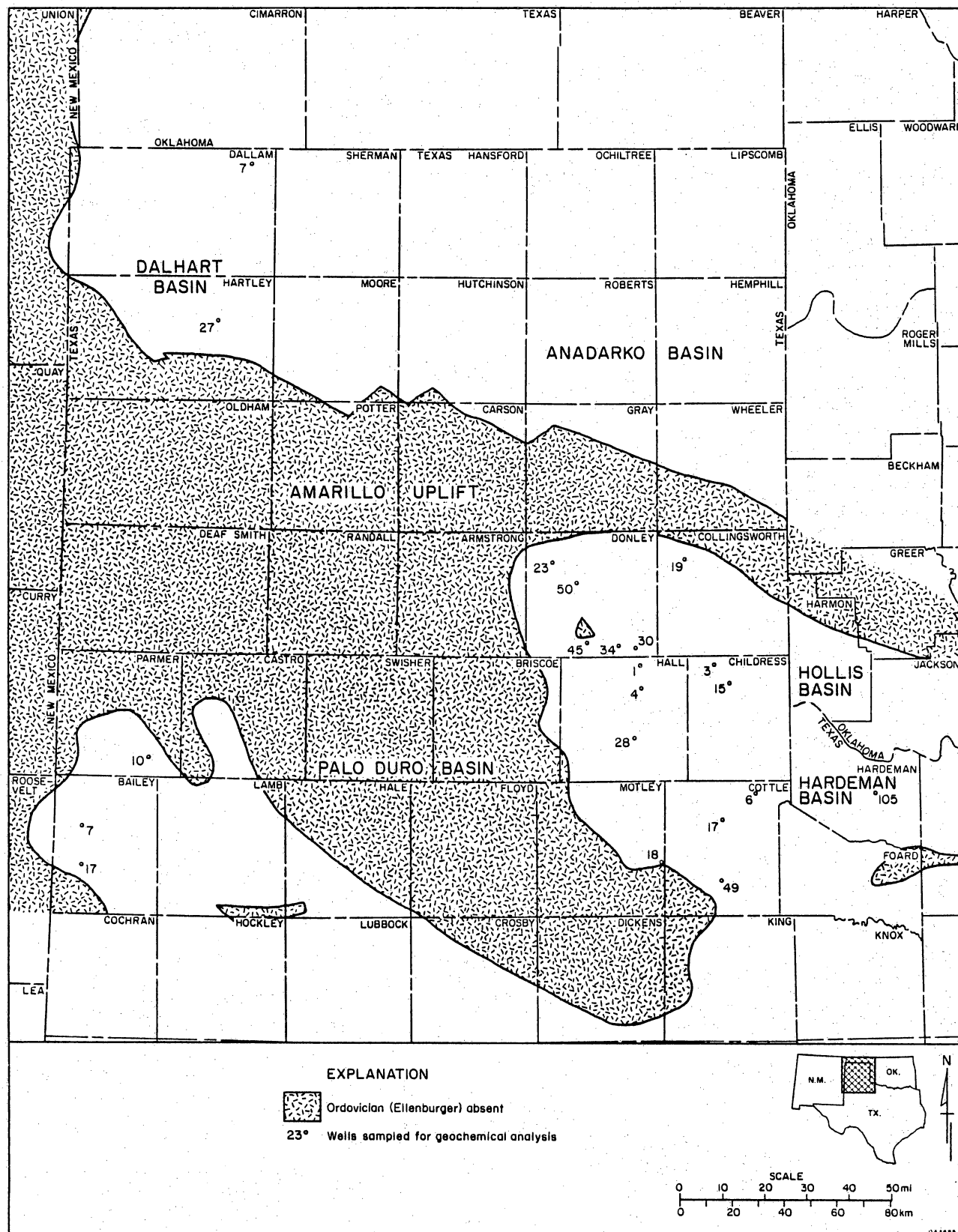
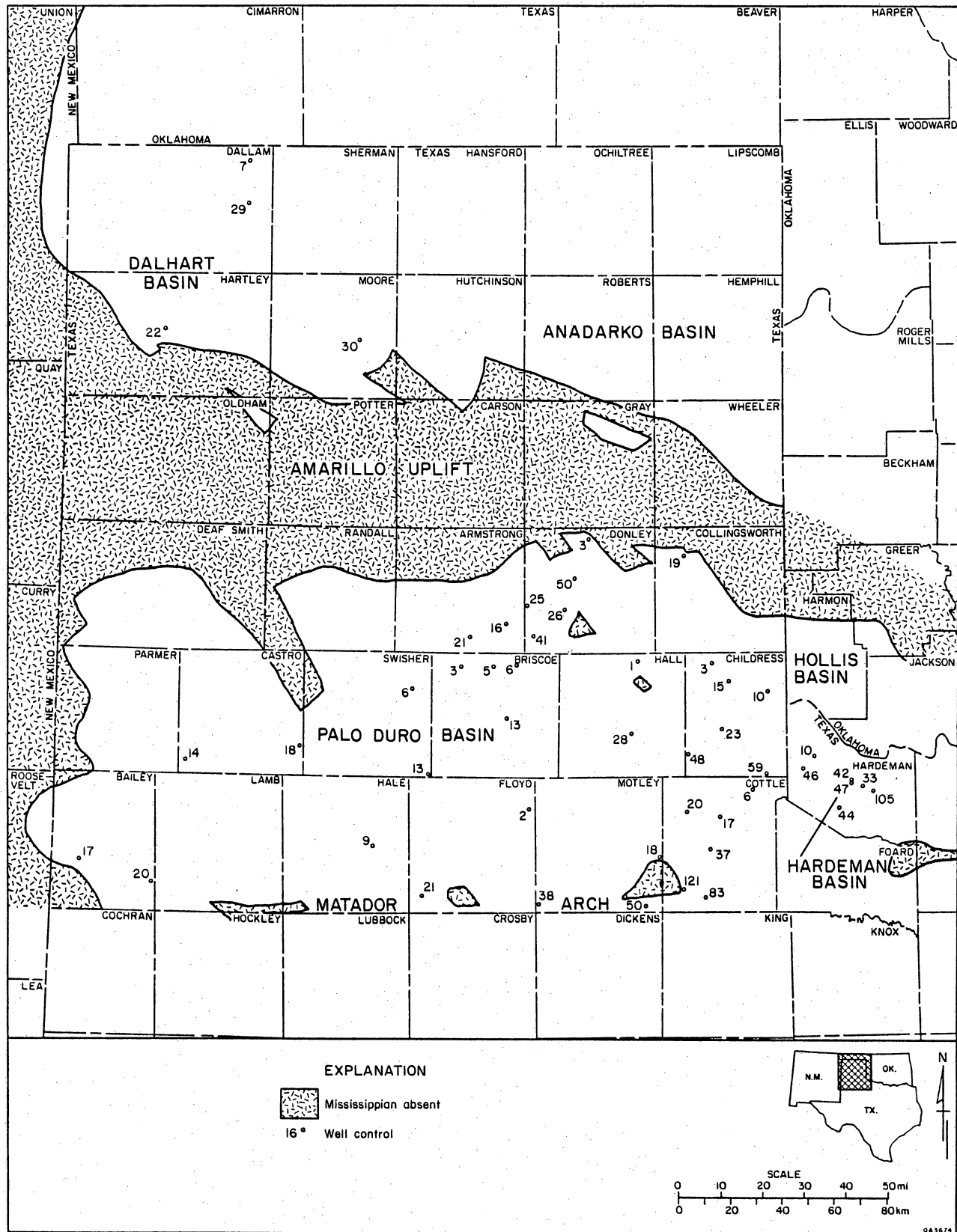
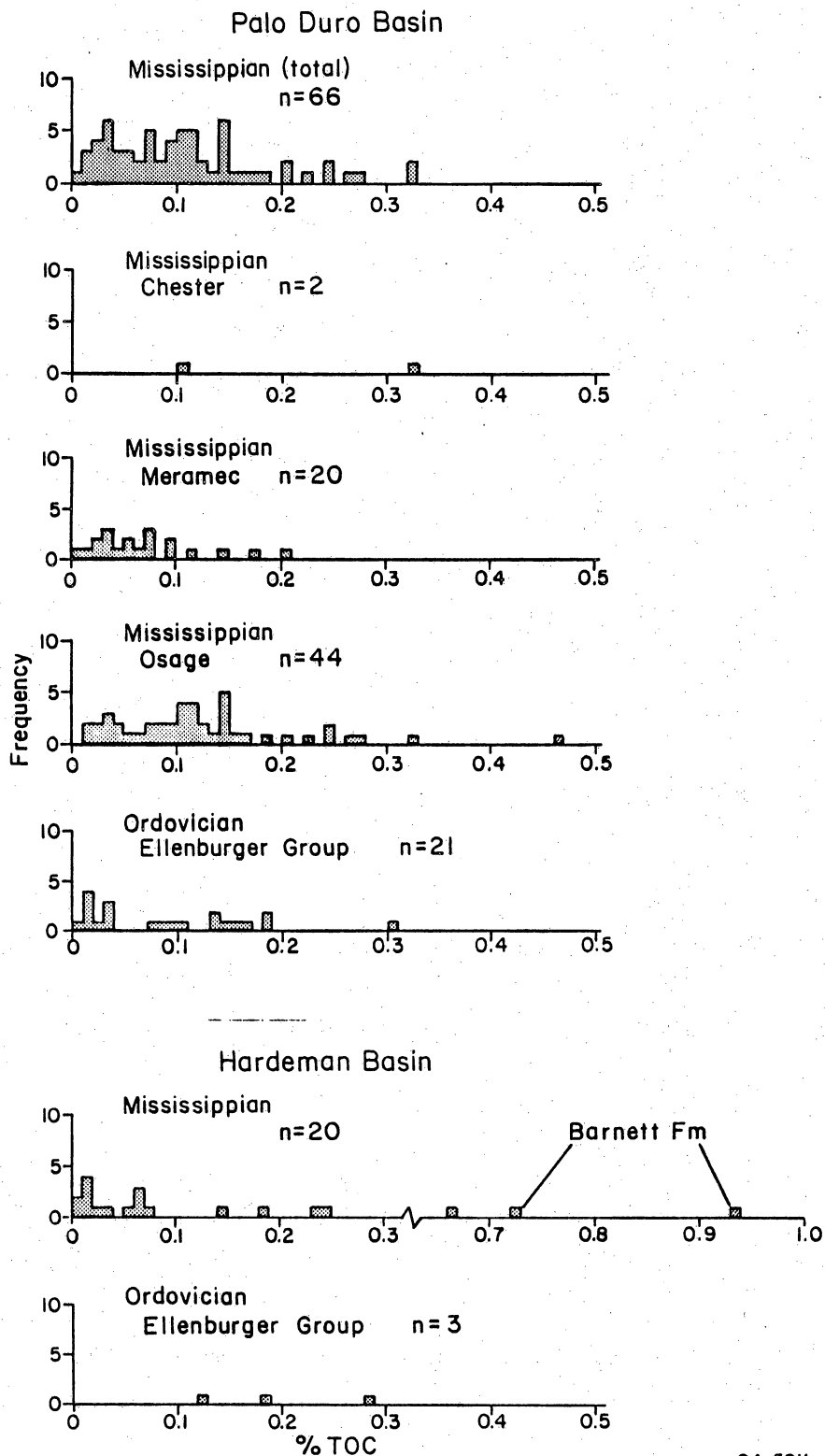


Figure 27. Distribution of Ordovician (Ellenburger Group) deposits and wells in the Texas Panhandle area that were sampled for total organic carbon.





QA 5211

**Figure 29.** Frequency distribution of total organic carbon abundance in pre-Pennsylvanian carbonates from the Palo Duro, Dalhart, and Hardeman Basins.

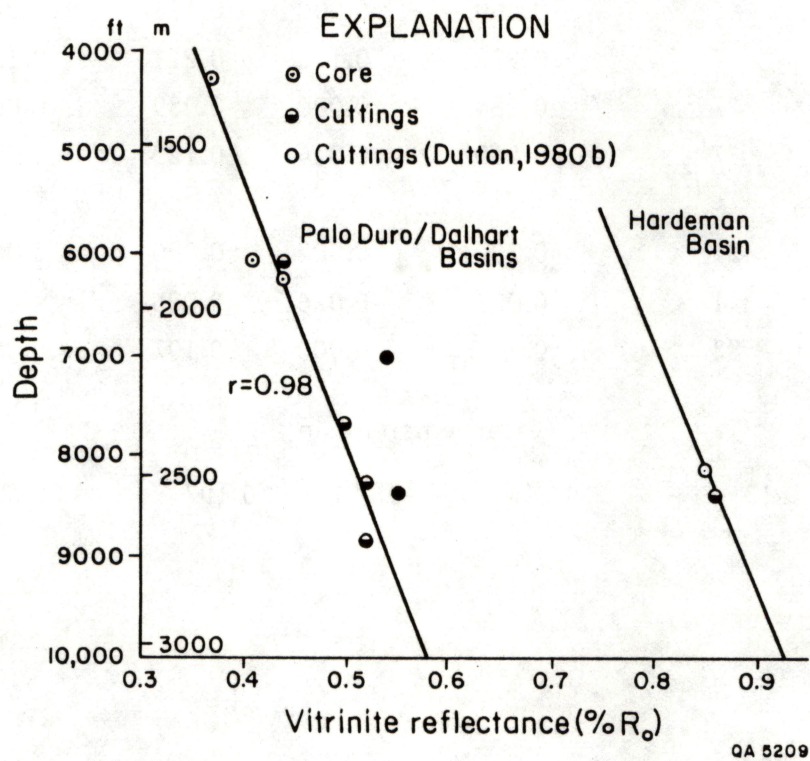


Figure 30. Plot of vitrinite reflectance with depth for the Palo Duro, Dalhart, and Hardeman Basins.

Table 6. Total organic carbon.

	Number of	% Total organic carbon				(TOC)
<u>Unit</u>	<u>analyses</u>	<u>High</u>	<u>Low</u>	<u>Mean</u>	<u>Std.dev.</u>	<u>Median</u>
Palo Duro and Dalhart Basins						
Mississippian	66	0.460	0.000	0.111	0.088	0.096
Chester	2	0.322	0.100	0.211	0.157	----
Meramec	27	0.264	0.000	0.089	0.067	0.076
Osage	37	0.460	0.014	0.123	0.094	0.104
Lower Ordovician						
(Ellenburger)	21	0.306	0.002	0.090	0.080	0.080
Cambrian?	1	0.026	0.026	0.026	----	----
Totals	88	0.460	0.000	0.107	0.086	0.094
Hardeman Basin						
Mississippian	13	0.934	0.002	0.197	0.355	0.142



Table 7. Kerogen analysis.

Well	County	Depth (feet)	Unit/Lithology	R <sub>o</sub> (%)	TAI	Sapropel (%) algal-amorphous exinite	Humus (%) vitrinite inertinite
Hassie Hunt Trust Estate Owens No. 1	Briscoe	8280-8300	"Osage" Dolomite	0.52	3.00	71	29
Wes-Tex, Kewanee, and Coastal States Gas Producing Co. Owens No. A-1	Childress	6069	"Osage" Limestone	0.41	2.85	81	19
Wes-Tex, Kewanee, and Coastal States Gas Producing Co. Owens No. A-1	Childress	6228	"Osage" Limestone	0.44	3.00	82	18
Meeker and Gupton Carroll No. 1	Cottle	7680-7710	"Osage" Limestone	0.50	3.00	76	24
Humble Oil and Refining Co. Sheldon No. 1	Dallam	5230-5260	"Osage" Limestone	---	3.00	55	45
Humble Oil and Refining Co. Belo No. 1	Dallam	6050-6090	"Osage" Shaly Dolomite	0.44	3.00	45	55
Service Drilling Co. Griffin No. 1	Donley	4260	"Meramec" Sandy Limestone	0.37	2.85	61	39
H. L. Hunt Ritchie No. 5	Donley	6390-6420	"Osage" Limestone	---	3.43	72	28
Sun Oil Co. Smith No. 1	Hardeman	8390-8400	Barnett Shale/Limestone	0.86	3.33	50	50
Standard Oil Co. of Texas Coffee No. 1	Hardeman	8143	Chappel Shale/Limestone	0.85	3.33	50	50
Sun Oil Co. Thompson No. 1	Hardeman	8110-8120	Barnett Shale/Limestone	---	3.33	50	50
Shamrock Oil Co. Taylor No. 2	Moore	5850-5870	"Osage" Shaly Limestone	---	3.00	70	30
Humble Oil and Refining Co. Matador Land and Cattle No. 2-H	Motley	7700-7770	"Osage" Shaly Limestone	---	3.43	56	44
Sinclair Oil & Gas Co. Savage No. 1	Swisher	9310-9340	"Meramec" Limestone	---	3.50	50	50
DATA FROM DUTTON (1980B)							
W. J. Weaver Adair No. 1	Briscoe	8310-8390	"Chester" Limestone	0.55	3.00	50	50
W. J. Weaver Adair No. 1	Briscoe	8810-8890	"Osage" Limestone	0.52	3.00	61	39
Baria and Werner et al., Mayes No. 1	Cottle	7060-7140	"Chester" Limestone	0.54	3.00	85	15

Table 8. Conodont color trends: Palo Duro and Hardeman Basins.

<u>Well</u>	Conodont Color Alteration Index (%)					
	<u>1.0</u>	<u>1.5</u>	<u>2.0</u>	<u>3.0</u>	<u>4.0</u>	<u>5.0</u>
<u>Northern Palo Duro Basin</u>						
Core 4, Donley County (4226 ft-4260 ft)	---	87	13	---	---	---
<u>Eastern Palo Duro/Western Hardeman Basin</u>						
Core 3, Childress County (5780 ft-6195 ft)	---	44	55	0.5	0.5	---
<u>Hardeman Basin</u>						
Core 2, Hardeman County (8142 ft-8144 ft)	---	---	23	67	10	---
Core 1, Hardeman 42 (8700 ft-8703 ft)	---	---	10	55	30	5

## REGIONAL CORRELATION AND CYCLICITY OF THE SAN ANDRES FORMATION (PERMIAN, GUADALUPIAN), PALO DURO BASIN, TEXAS PANHANDLE

Michael A. Fracasso

*Systematic variations in the completeness of cycles and the vertical distribution of thin sheet siltstones in the San Andres Formation allow a subdivision into informal lower, middle, and upper genetic units. The fundamental mode of cyclicity is the same throughout, but the rate of cyclic oscillation differs in each of the units. These differences may reflect changes in structural control, frequency of eustatic sea-level change, or both.*

Small-scale cyclicity within the San Andres Formation in the Palo Duro Basin has been previously documented (Presley, 1979a, 1979b, 1980, 1981) and has led to an informal two-fold stratigraphic division into a lower unit in which cycles are pronounced (informally designated as cycles 1-5) and an upper unit in which cycles are much less marked (Presley, 1979b). Recent detailed studies of correlation within the San Andres reveal that cyclicity is a vertically pervasive feature and that cycles can be correlated throughout the entire formation within the present-day structural limits of the Palo Duro Basin (fig. 31). Systematic variations in the completeness of cycles and the vertical distribution of thin siliciclastic sheet siltstones allow further subdivision of the San Andres into informal lower, middle, and upper genetic units.

An idealized San Andres cycle, based on examination of continuous cored intervals (Hovorka, 1983a), is an asymmetric carbonate-evaporite vertical sequence that reflects upward-increasing salinity. The base of each cycle is defined by a dissolution surface and overlying detrital insoluble residue that truncate the evaporitic upper unit of the cycle below. Overlying the insoluble residue are, in sequence, carbonate, anhydrite, and halite (fig. 32; cycle 4). The relatively thick, complete cycles of the lower San Andres (informally designated as cycles 1-5) are commonly more complex, exhibiting frequent minor fluctuations in salinity that are superimposed on the primary episode of increasing salinity that produced the generalized vertical sequence of lithologies (fig. 32; lower cycle 3, top lower cycle 4).

Siliciclastic beds of two main types are represented by sharp peaks to the right of the low salt/anhydrite baseline on gamma-ray logs that reflect an abrupt rise in API values. These high API gamma-ray peaks were correlated with cores and distinguished by analysis of core samples. The first type of siliciclastic bed is a detrital insoluble residue that characteristically forms the base of a cycle of increasing salinity. An influx of low-salinity water, possibly reflecting marine transgression, caused dissolution of the upper exposed portion of the halite of the preceding cycle and concentrated its disseminated clastic component. The second type of siliciclastic bed represents a clastic progradation across the evaporite facies tract and may or may not have been associated with a major episode of brine freshening. Both types of siliciclastic bed can be readily distinguished in core by their internal petrologic characteristics as well as their position in vertical facies sequences (Hovorka, this volume, "Cyclicality in the San Andres Formation").

One key to the correlation and recognition of cyclicality in the San Andres Formation is the identification of the largely siliciclastic detrital insoluble residue that defines the base of each cycle. Insoluble residues that define the bases of the complete, relatively thick cycles of the lower San Andres (lower cycles 2, 3, and 4) produce characteristic asymmetric signatures on gamma-ray logs (fig. 32). The log pattern displays, from the base upward, a high API basal peak, representing the siliciclastic insoluble residue, that is sharply set off from the low-API anhydrite-halite baseline below and is topped by a gradual shift back toward the low baseline.

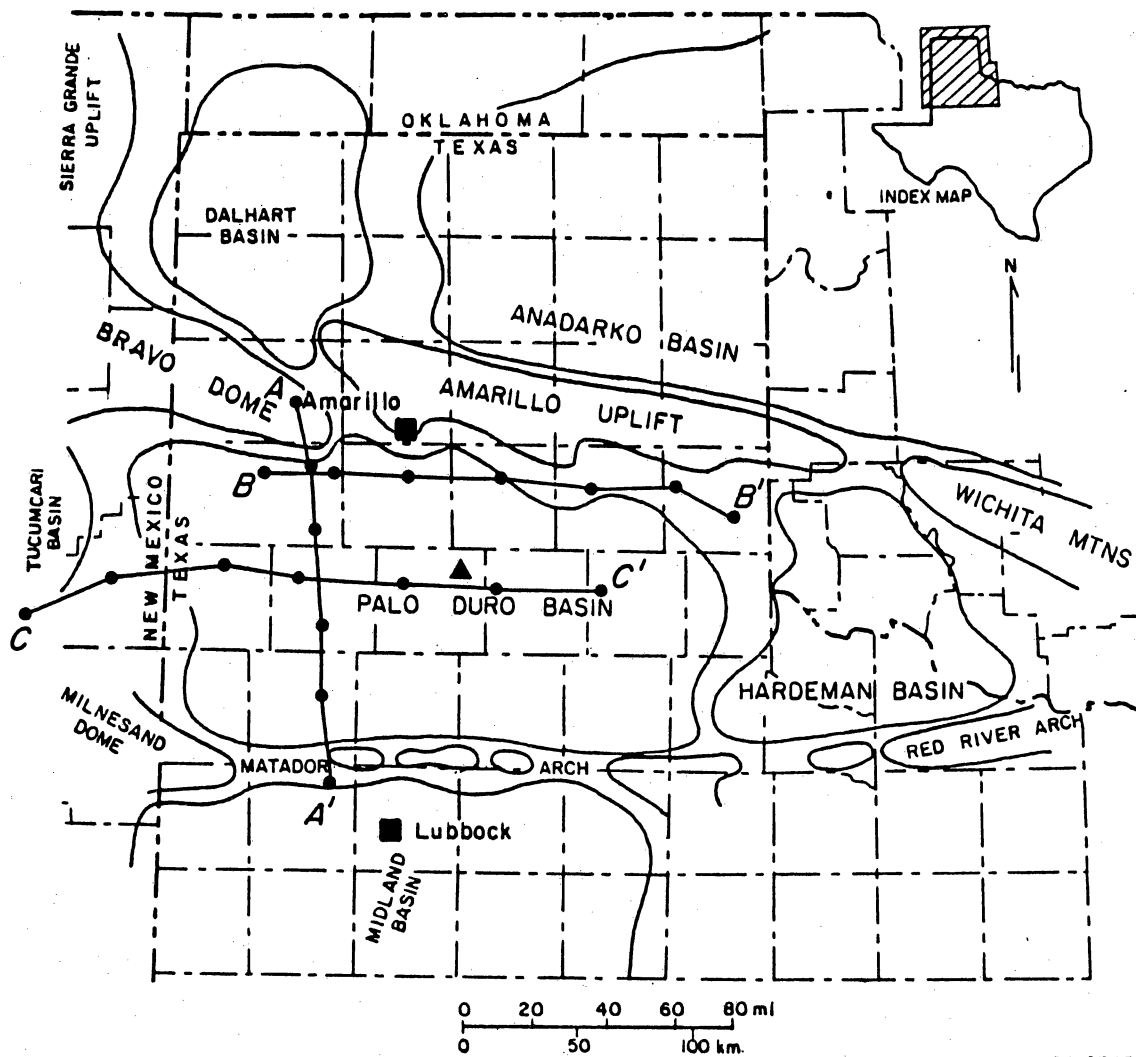
The insoluble residue-carbonate couplet of the thin cycles characteristic of the middle and upper San Andres (couplet thickness ranges from approximately 2 to 18 ft) produces a single sharp, high-API gamma peak that cannot be differentiated from the gamma peaks produced by progradational siliciclastic beds (see figs. 33, 34, and 35; interval above "base middle cycle 1"). Recognition and correlation of such abbreviated cycle bases and primary clastic beds on a regional scale require their absolute identification in core samples and extrapolation to correlative gamma peaks in other wells.

The regional continuity of cycle bases and systematic differences in the vertical distribution of both completeness and thickness of cycles permit recognition of three discrete genetic packages that are best differentiated in the basin center (figs. 31, 33, and 34). The San Andres in the Palo Duro Basin may accordingly be divided into informal lower, middle, and upper units. The lower San Andres genetic package corresponds to the previously recognized lower San Andres division and includes the previously designated cycles 1-5 (figs. 31, 33, 34, and 35). These relatively thick cycles possess a complete vertical facies sequence from the basal insoluble residue to the upper halite. Cycles 2-5 together comprise slightly more than half of the total thickness of the San Andres Formation in the Palo Duro Basin center. The existence of relatively thick carbonates at the bases of these cycles implies prolonged episodes of open circulation and near-normal marine salinity at moderate water depths, probably a minimum of several meters. Such conditions would most likely exist during times of relatively rapid basin subsidence that kept pace with high carbonate production during transgressive events.

The newly recognized middle San Andres genetic unit corresponds to the largely anhydritic lower half of the previously recognized upper San Andres (figs. 33, 34, and 35; interval above base of middle cycle 1 and below base of upper cycle 1). Cycles of the middle San Andres are thin and incomplete compared with those of the lower San Andres. Halite facies at the tops of cycles are not preserved. However, their former existence is inferred from the insoluble residues that define the bases of the abbreviated siliciclastic-carbonate-anhydrite vertical facies sequences. Thus, the lower and middle San Andres genetic units exhibit a common fundamental cyclic pattern of vertical facies sequences. Therefore, the thin, abbreviated cycles of the middle San Andres suggest a change in the tempo, rather than the mode of cyclic depositional style. This change in tempo may have been caused by a lowering of the basin subsidence rate, an increase in the frequency of eustatic sea-level change, or both.

The newly recognized upper San Andres genetic unit corresponds to the halite-bearing top portion of the previously recognized upper San Andres division, above the  $\pi$ -marker bed (figs. 33, 34, and 35; interval between base of upper cycle 1 and below base of Queen-Grayburg sequence). Cycles of the upper San Andres are characterized by thin basal carbonate-anhydrite units very similar to those of the middle San Andres, yet the halite facies in the upper portions of the cycles are also preserved. Moreover, prominent and relatively thick progradational red beds are interspersed throughout the upper San Andres interval (figs. 33, 34, and 35). Again, the fundamental mode of cyclicity appears to be the same as that of the lower and middle San Andres, but the tempo differs from both. A pronounced asymmetry in the rate of eustatic sea-level oscillations relative to those of the lower and middle San Andres, superimposed on a relatively constant regional basin subsidence rate, might produce such cycles. Alternatively, fluctuating regional basin subsidence rates, relative to those of the lower and middle San Andres, superimposed on symmetric rates of eustatic sea-level oscillation, could produce the same effect.

The marked increase in thickness and frequency of primary depositional red beds in the upper San Andres interval appears to be genetically unrelated to San Andres cyclicity. These clastic interbeds are lithologically very similar to the overlying Queen-Grayburg red bed sequence (S. D. Hovorka, personal communication, 1983) and are probably each minor pulses that preface the major Queen-Grayburg progradation. This clastic influx may represent a reactivation of tectonism in the source area or a change in the regional clastic dispersal pattern.



QA 6545

▲ DOE - Gruy Federal Grabbe No.1

Figure 31. Palo Duro Basin and surrounding structural elements, Texas Panhandle (after Nicholson, 1960). A-A', B-B' and C-C' are the locations of correlation sections through the San Andres Formation that are illustrated as figures 33, 34, and 35, respectively.

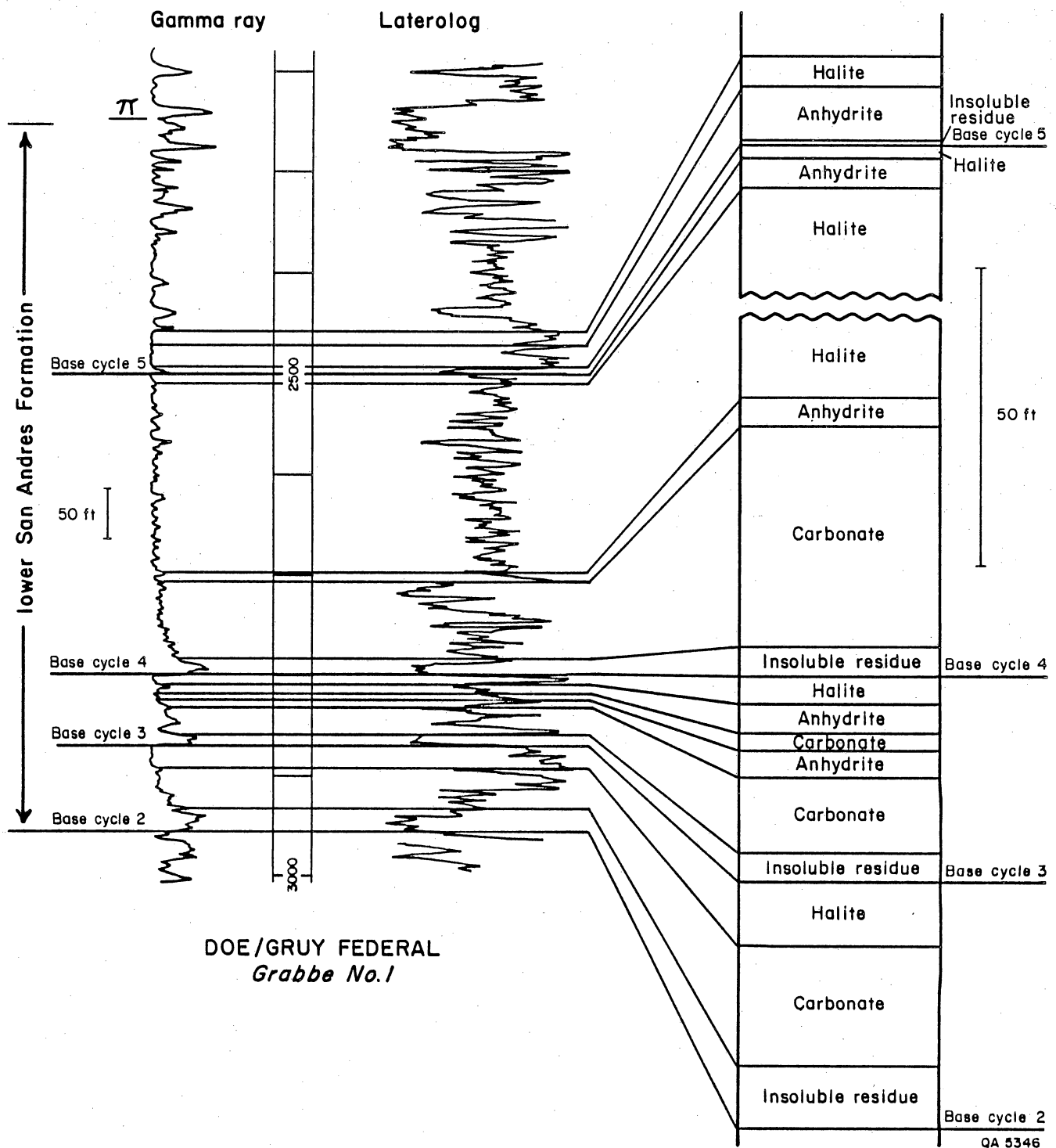


Figure 32. Geophysical log pattern and lithology of lower San Andres Formation cycles 2, 3, and 4. Lithology is from examination of continuous cored interval, DOE-Gruy Federal Grabbe No. 1, Swisher County, Texas Panhandle. Cycle 4 displays the idealized cyclic facies sequence, whereas cycle 3 exhibits a more complex salinity fluctuation as shown by the interbedded anhydrite and carbonate units. See figure 31 for well location.



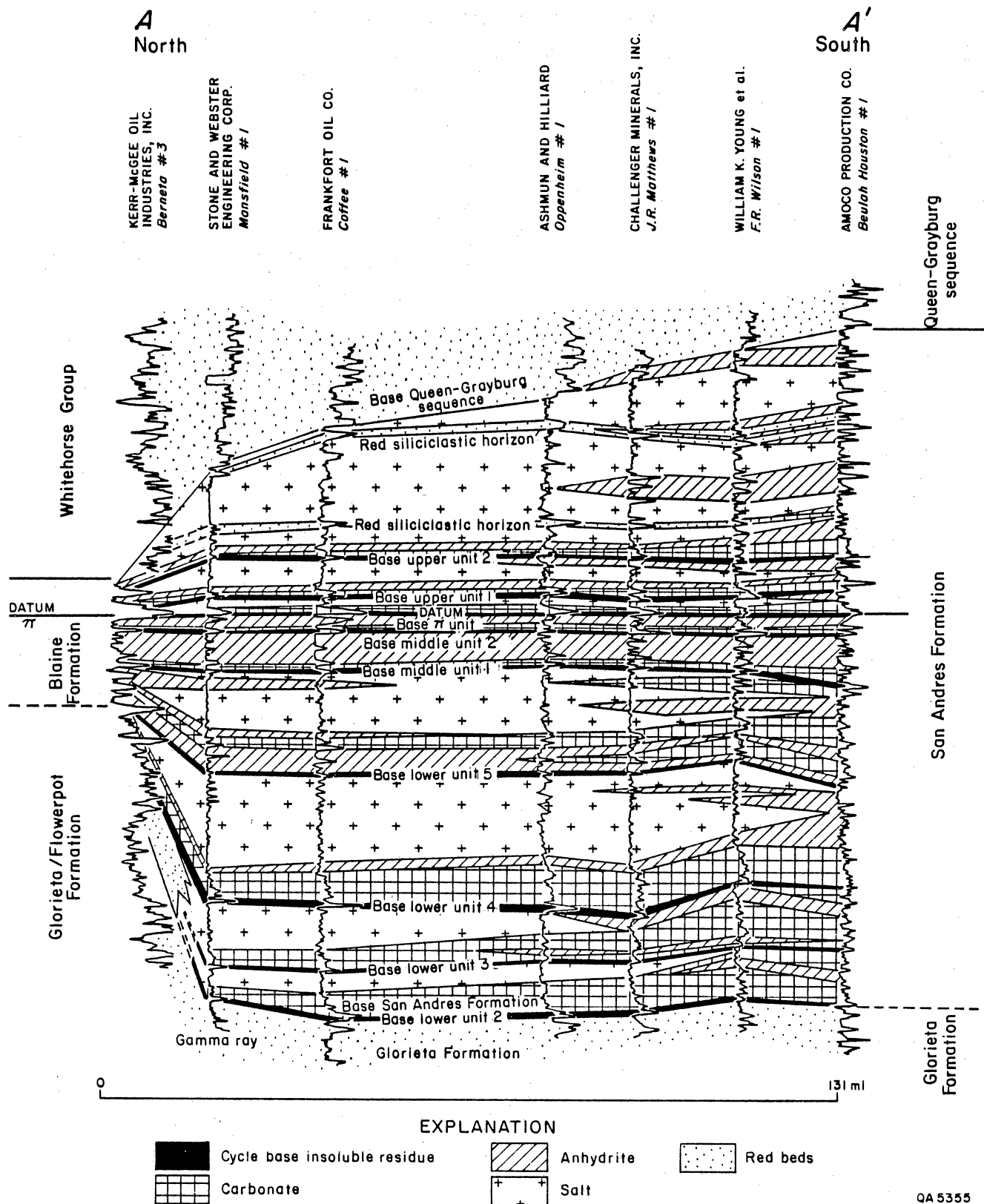


Figure 33. Correlation section A-A', San Andres Formation, Dalhart and Palo Duro Basins and northern shelf of the Midland Basin, Texas Panhandle. Illustrated wells are not proportionately spaced, although absolute distance between the two endpoints is accurate. Thirty-three wells were originally used to establish the illustrated correlations, and the average well spacing was 3.96 mi. Not all regionally correlative horizons have been labeled.

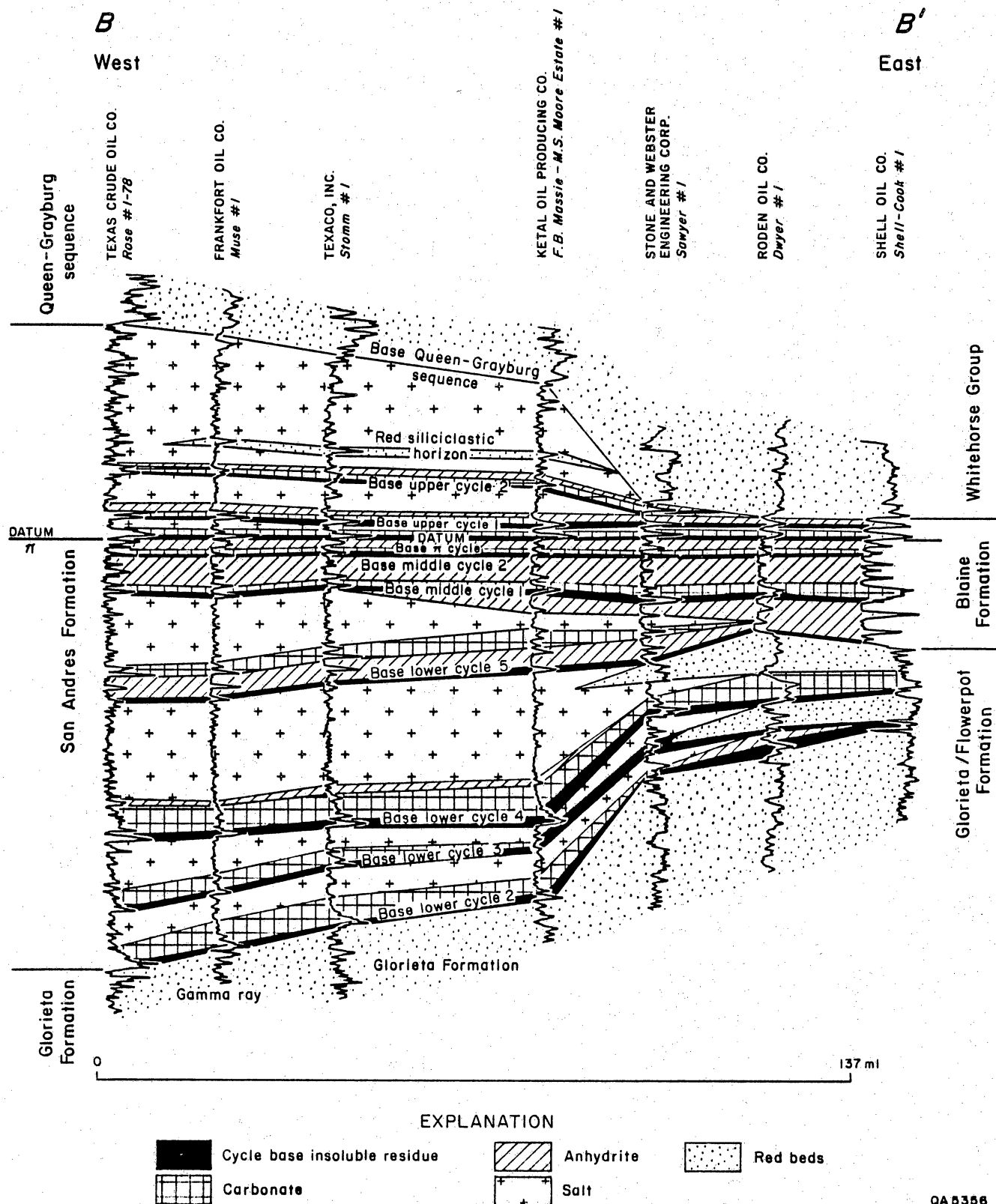


Figure 34. Correlation section B-B', San Andres Formation, western to eastern Palo Duro Basin, Texas Panhandle. Illustrated wells are not proportionately spaced, although absolute distance between the two endpoints is accurate. Eighteen wells were originally used to establish the illustrated correlations, and the average well spacing was 7.6 mi. Not all regionally correlative horizons have been labeled.

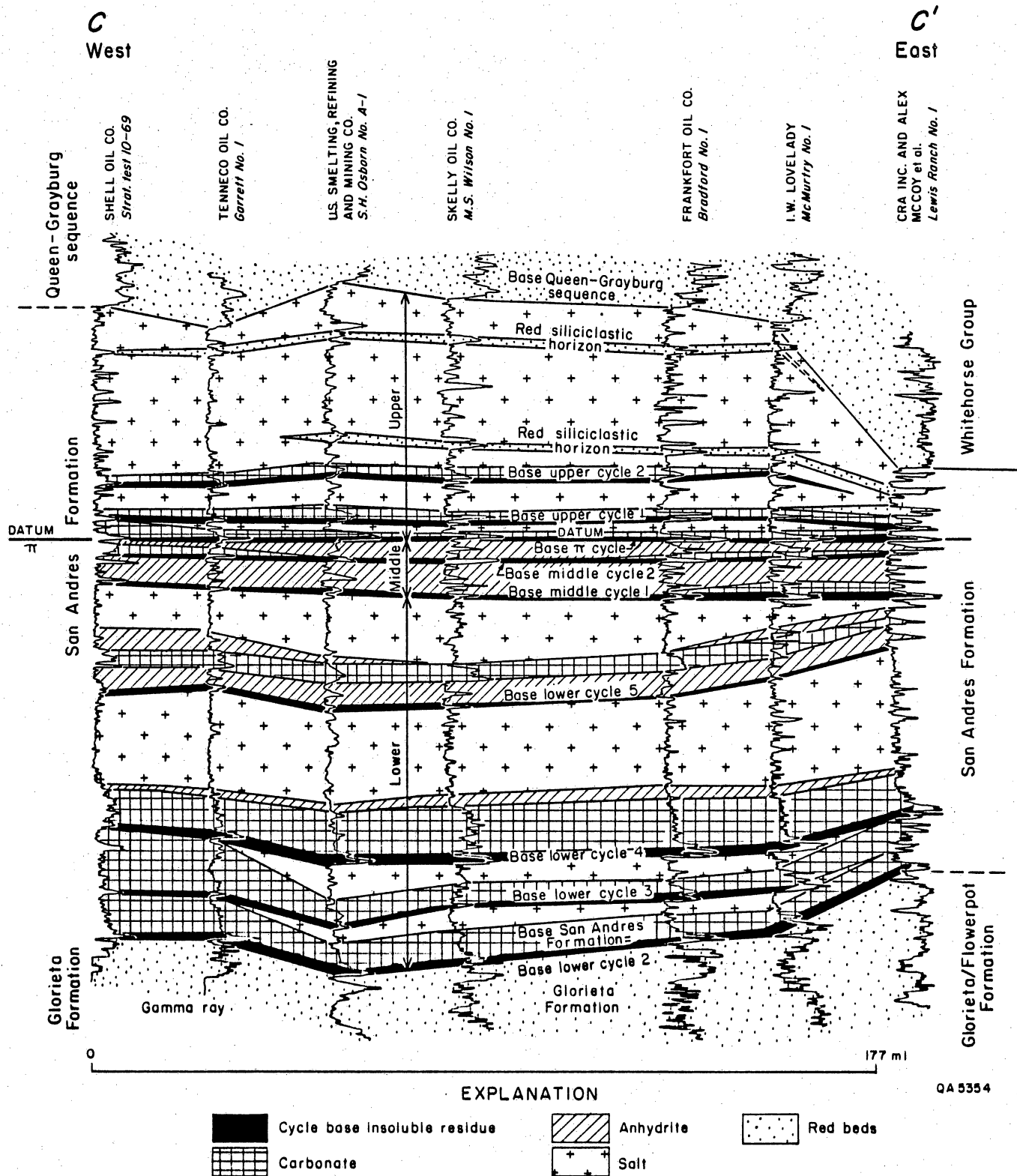


Figure 35. Correlation section C-C', San Andres Formation, Tucumcari Basin to eastern Palo Duro Basin, New Mexico and Texas Panhandle. Illustrated wells are not proportionately spaced, although absolute distance between the two endpoints is accurate. Twenty-four wells were originally used to establish the illustrated correlations, and the average well spacing was 7.37 mi. Not all regionally correlative horizons have been labeled.

## LATE PERMIAN VOLCANIC ASH BEDS IN THE QUARTERMASTER-DEWEY LAKE FORMATIONS, TEXAS PANHANDLE

Allan Kolker and Michael A. Fracasso

*The age of the Quartermaster and Dewey Lake Formations of the Permian Basin has generally been considered to be Late Permian; however, the possibility of an early to middle Triassic age has also been suggested. The discovery of volcanic ash beds in these formations in the Palo Duro Basin, radiometrically dated as Late Permian, establishes the age of these units with greater precision.*

The lithologically correlative Quartermaster (Texas and Oklahoma Panhandle outcrops), Dewey Lake (Panhandle and Midland Basin subsurface), and Pierce Canyon (Delaware Basin outcrop and subsurface) Formations (location B, fig. 36) are progradational continental red-bed sequences that represent the culmination of a regional, cyclic trend of marine regression from the Permian Basin that began in the early to middle Permian (King, 1942). The age of these units is questionable because they are unfossiliferous.

The underlying and conformable Rustler Formation in the Delaware Basin and Alibates sequence in the Palo Duro Basin contain carbonate and evaporite beds that represent the last transgression of the Permian sea. Late Permian (Ochoan) impoverished and poorly preserved invertebrate faunas have been reported from both units (Baker, 1915; Roth and others, 1941; Dunbar and others, 1960). The overlying Dockum Group is widely regarded as Late Triassic in age, largely on the basis of continental biostratigraphic zonation. The Quartermaster, Dewey Lake, and Pierce Canyon Formations are usually regarded as Ochoan in age because of their apparent genetic/lithologic continuity with the underlying conformable Ochoan sequence (King, 1942; Miller, 1966). Their contact with the overlying Dockum Group has been described as both unconformable and conformable. The possibility of a locally conformable relation with overlying Late Triassic strata has been the main basis for consideration of an early to middle Triassic age for at least part of the Quartermaster-Dewey Lake-Pierce Canyon sequence. For the most part, the question of time conformity may have been confused with the geometric property of stratal

concordance, and the Dockum and underlying units may be locally concordant but nonetheless unconformable throughout their areal extent.

Two volcanic ash beds have recently been discovered in the Quartermaster (outcrop) and Dewey Lake (subsurface) Formations in the Palo Duro Basin. The lower ash bed, which ranges in stratigraphic position from 13 to 66 ft above the top of the Alibates unit, has been dated by the K-Ar method at  $251 \pm 4$  and  $261 \pm 9$  m.y. Both values are well in the range of Late Permian ages. The upper ash bed has not been dated. The contact between the Dockum and Quartermaster-Dewey Lake unit varies from concordant to discordant at the locations of ash sample sites and measured sections (figs. 36, 37, and 38); the level of the lowest Dockum biota has not been determined at these sites.

Stratigraphic sections in the Quartermaster and Dewey Lake Formations were measured and sampled at several outcrop and subsurface sites (continuous cored sequences) in the Palo Duro Basin (figs. 36, 37, and 38) to document the areal distribution and stratigraphic position of the ash beds. Illustrated lithologies were determined by the greater-than-50-percent lithology in each 2-ft interval of the original measured sections. For example, a 2-ft-thick sequence of 60 percent massive mudstone and 40 percent 1- to 2-inch-thick very fine sandstone interbeds was illustrated as 2 ft of mudstone. The top of the Alibates unit was used as a lower datum wherever possible, and sections were measured either to the base of the Dockum Group or to a thick, massive cliff-forming sandstone commonly present in the uppermost Quartermaster just below the Dockum.

The Dewey Lake sequence was not examined in detail in the DOE-Gruy Federal Rex White No. 1 core (location A, fig. 36), but the presence of both upper and lower ash beds is noted. The lower ash bed there is situated approximately 18 ft above the top of the Alibates. The lower ash bed was identified in all sections, but the upper ash bed was located only in Caprock Canyons State Park and in the DOE-Gruy Federal Grabbe No. 1 and Rex White No. 1 cores. This may be a function of differential thickness rather than a real difference in areal distribution. The lower ash bed is commonly several inches thick

(1/8- to 8-inch observed range) and weathers to a prominent pink-white, whereas the upper ash has a maximum observed thickness of only 1 inch and weathers to a light purple to maroon, providing less contrast against the surrounding brick-red Quartermaster-Dewey Lake sediments.

The lower ash bed is visibly cross-laminated in both outcrop and core samples (fig. 39 a, b). Its apparently wide areal distribution and blanket-like geometry seem to preclude deposition in restricted channels. The primary structures thus imply syndepositional reworking by gentle bottom currents. The upper ash bed is sporadically distributed and displays no internal primary structures in outcrop or core. It is present as a concentration of millimeter-scale intraclasts dispersed in a 2-inch-thick intraclastic zone in the Grabbe No. 1 core, implying reworking subsequent to partial induration.

Mineralogy and texture of the lower ash bed are the same in each sampled occurrence, including Palo Duro Canyon State Park, lower Palo Duro Canyon, Caprock Canyons State Park, and the Swisher County No. 1 Grabbe core (fig. 40). Each sample contains varying amounts of subhedral to euhedral phenocrysts in a well-crystallized clay matrix having no distinct outlines of relict shards (fig. 39c). Locally, the orientation of clay grains is highly random and may be inherited from devitrified shards. Common phenocrysts include sanidine, quartz, biotite, and minor amounts of apatite, zircon, and Fe-Ti oxide. A large proportion of sanidine grains are hollow, possibly a diagenetic feature (fig. 39d). Some quartz grains are embayed. The presence of euhedral biotite and apatite indicates that transport has been minimal. The upper ash at Caprock Canyons State Park contains plagioclase in addition to sanidine and has a larger proportion of phenocrysts to matrix than the lower ash beds. Phenocrysts are coarser grained, and hollow sanidine is less common in the upper ash.

The matrix of each lower ash bed sample consists of nonexpansive clay having a 10 Å basal spacing, probably illite (fig. 40). A minor amount of expansive clay (smectite) is present in sample PD-2 (Palo Duro Canyon) and was probably derived from alteration of

illite. The upper ash at Caprock Canyons (sample 072982) contains only expansive clay (smectite) having basal spacings of 15.5 Å when air dried and 17.1 Å when glycolated, which collapse to 9.8 Å upon heating to 550°C for 2 hours.

K-Ar age determinations on biotite in ash beds at Caprock Canyons State Park (two determinations) and in the Swisher County No. 1 Grabbe core give Late Permian ages ranging from  $261 \pm 9$  to  $251 \pm 4$  m.y. (table 9). All ages are within the range of overlap of experimental errors. K-Ar ages of  $251 \pm 4$  and  $257 \pm 9$  m.y. were determined by different labs for two splits of a 785-mg concentrate of biotite from Caprock Canyons. Only 110 mg of biotite was separated from tuffaceous material in the No. 1 Grabbe core. Sample size was limited by the lower overall biotite concentration and limited volume of core available for processing. Duplicate analyses of K-Ar<sup>40</sup> were performed on this material, but the second Ar<sup>40</sup> analysis is considered less reliable because of a malfunction in an induction furnace used to reduce contamination by atmospheric Ar<sup>40</sup>. The proportion of radiogenic Ar<sup>40</sup> to atmospheric Ar<sup>40</sup> is only 0.178 in this analysis compared with 0.718 to 0.850 for previous determinations. Because of the small sample size, no biotite concentrate was left to repeat the second Ar<sup>40</sup> analysis for S-915. Using the first Ar<sup>40</sup> determination gives an age of  $261 \pm 9$  m.y., as reported in table 9; an age of  $271 \pm 9$  m.y. is obtained if an average of the two Ar<sup>40</sup> analyses is used.

The presence of hollow sanidine in the Pierce Canyon red beds and elsewhere in the Dewey Lake Formation has been noted by Miller (1955, 1966). Local concentrations of apatite, biotite in excess of muscovite, and embayed euhedral quartz were also recognized in the Pierce Canyon Formation. Overall, the grain size of sanidine in samples from the Palo Duro Basin ( $\bar{x} = 0.095$  mm) appears to be less than that observed in the Pierce Canyon red beds (0.13 mm), suggesting that the Delaware Basin is closer to the source area. Some variation in grain size may be due to changes in wind velocity during transport (Williams and others, 1954).

The consistent stratigraphic position, similarity in mineralogy and texture, and agreement (within experimental error) of K-Ar ages indicate that the "lower" ash bed observed in all the localities is correlative and represents a unique event. Correlation of the "upper" ash bed(s) is more difficult to ascertain because of their reduced thickness and sporadic exposure.



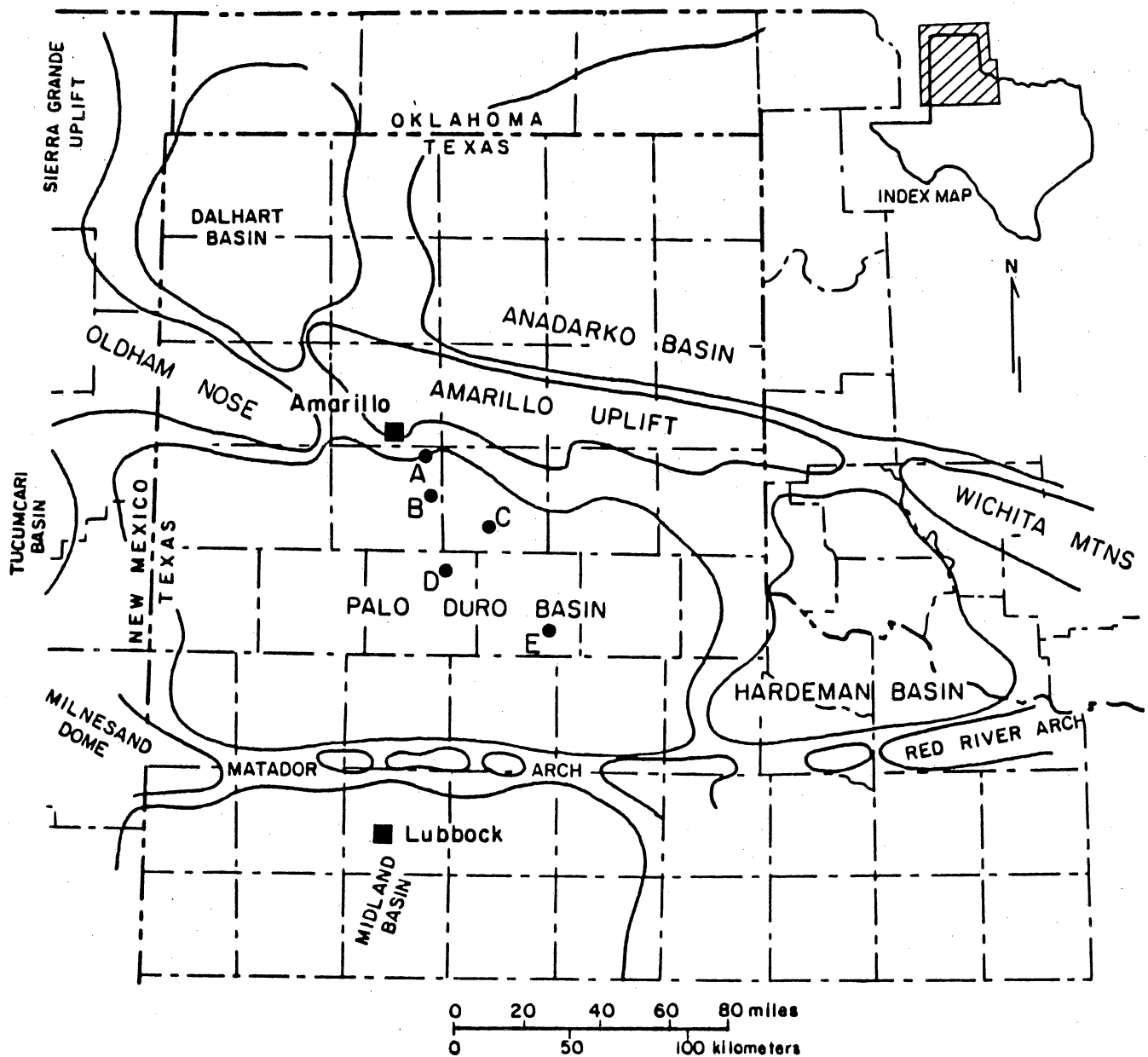


Figure 36. Structural elements in the Texas Panhandle region (after Nicholson, 1960) and locations of measured sections and volcanic ash beds in the Quartermaster and Dewey Lake Formations. (A) DOE-Gruy Federal Rex H. White No. 1; (B) Palo Duro Canyon State Park, section K-3-83; (C) Texas Highway 207/117 crossing Palo Duro Canyon, section K-4-83; (D) DOE-Gruy Federal Grabbe No. 1; (E) Caprock Canyons State Park, sections K-1-83, K-2-83, and K-5-83.

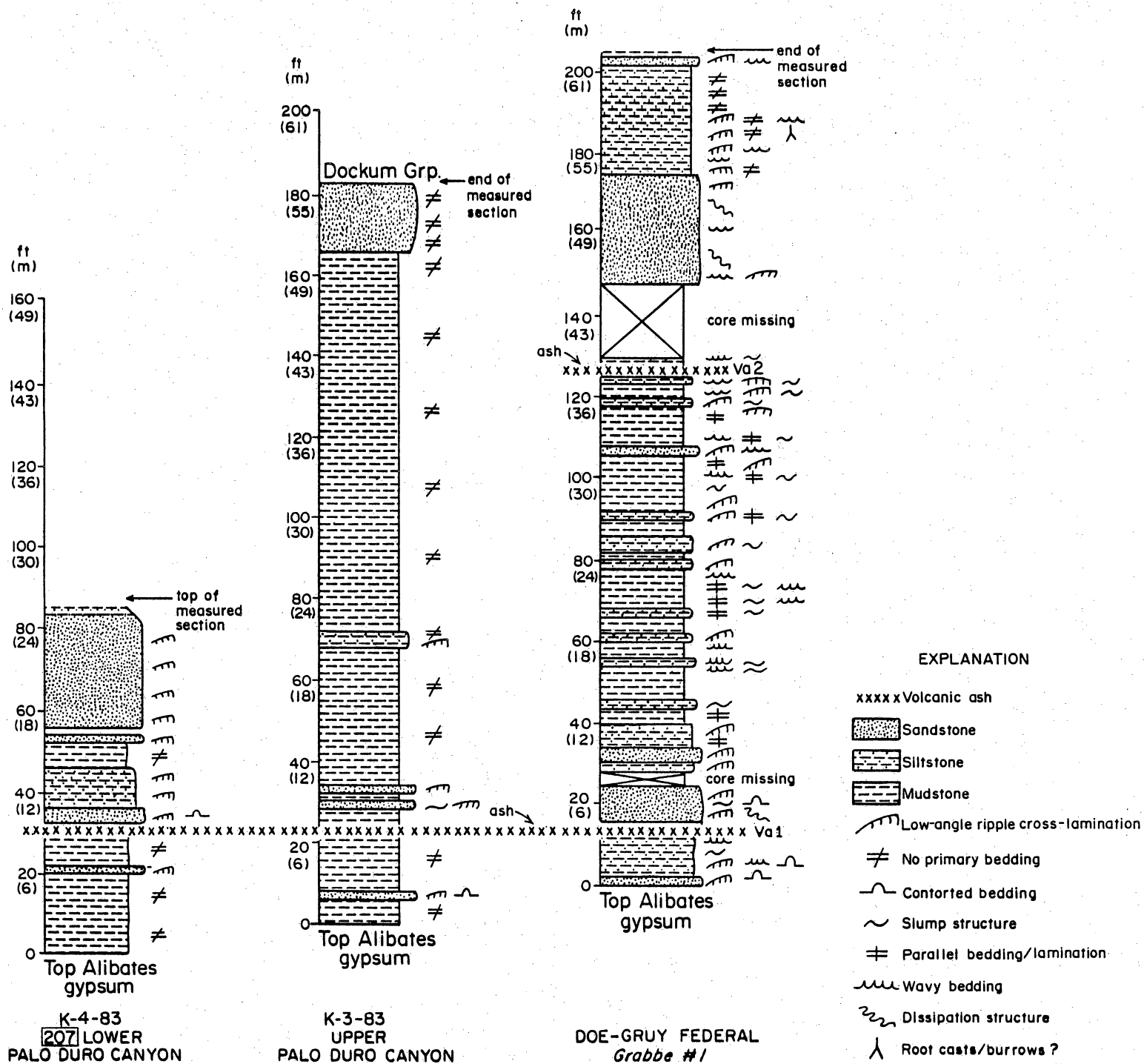


Figure 37. Measured sections K-4-83, K-3-83, and DOE-Gruy Federal Grabbe No. 1, Quartermaster and Dewey Lake Formations, Texas Panhandle. See figure 36 for locations.

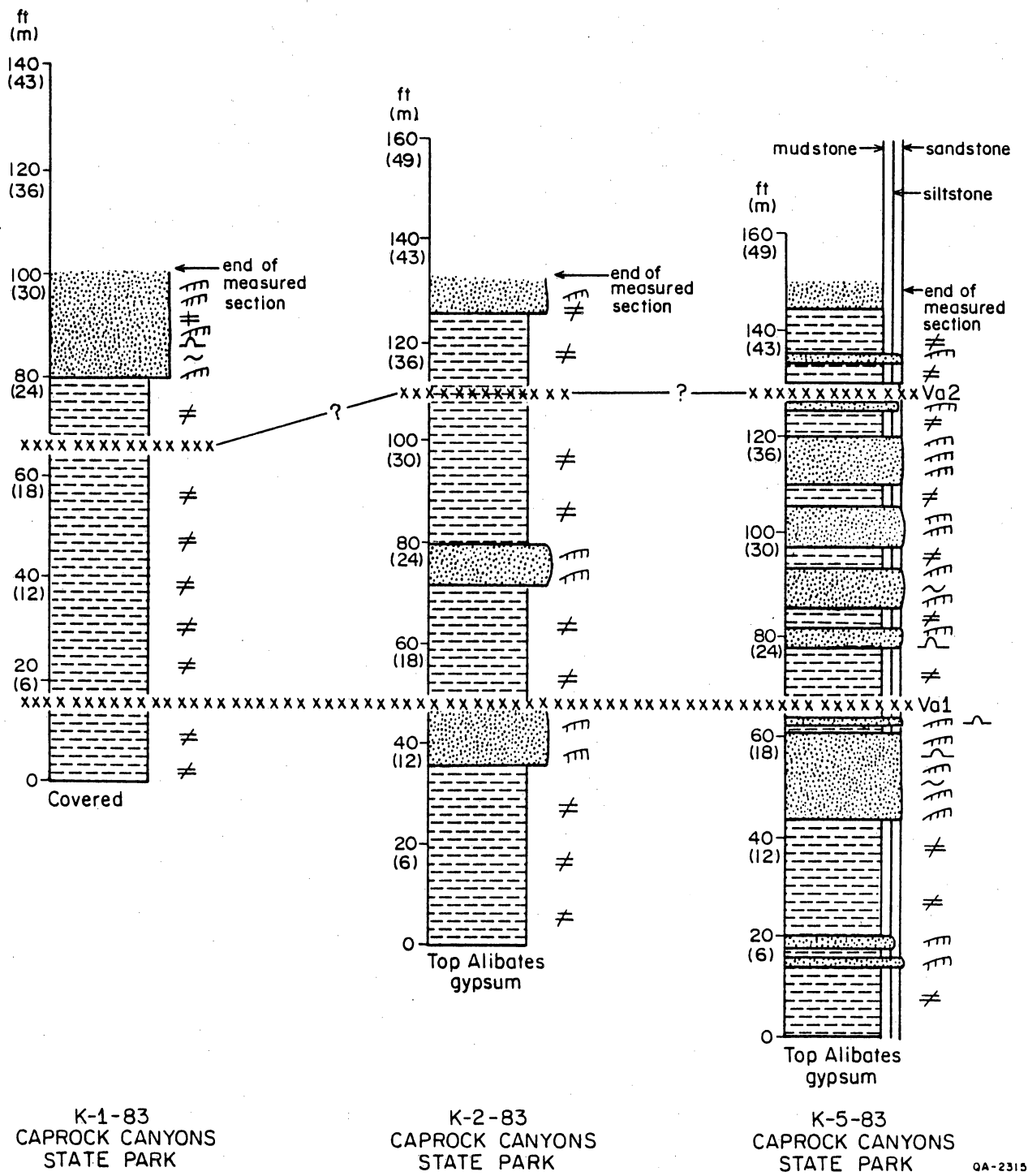
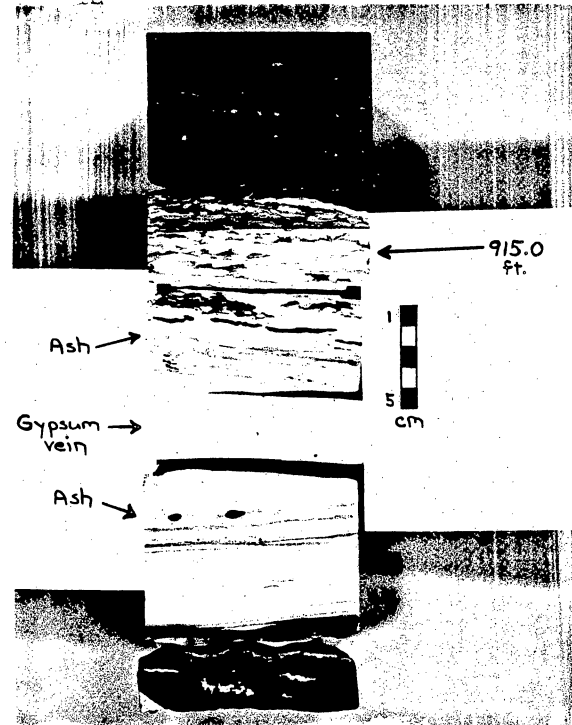


Figure 38. Measured sections K-1-83, K-2-83, and K-5-83, Quartermaster Formation, Texas Panhandle. See figure 36 for locations.



a



b



c



d

Figure 39. Lower volcanic ash bed of the Permian Quartermaster and Dewey Lake Formations, Texas Panhandle. (a) Ripple cross-lamination, outcrop sample, Caprock Canyons State Park. (b) Ripple cross-lamination, core sample, DOE-Gruy Federal Grabbe No. 1. (c) Photomicrograph of subhedral to euhedral phenocrysts in crystalline clay matrix; no relict shard outlines. (d) Photomicrograph of hollow sanidine grains, possibly diagenetic in origin.

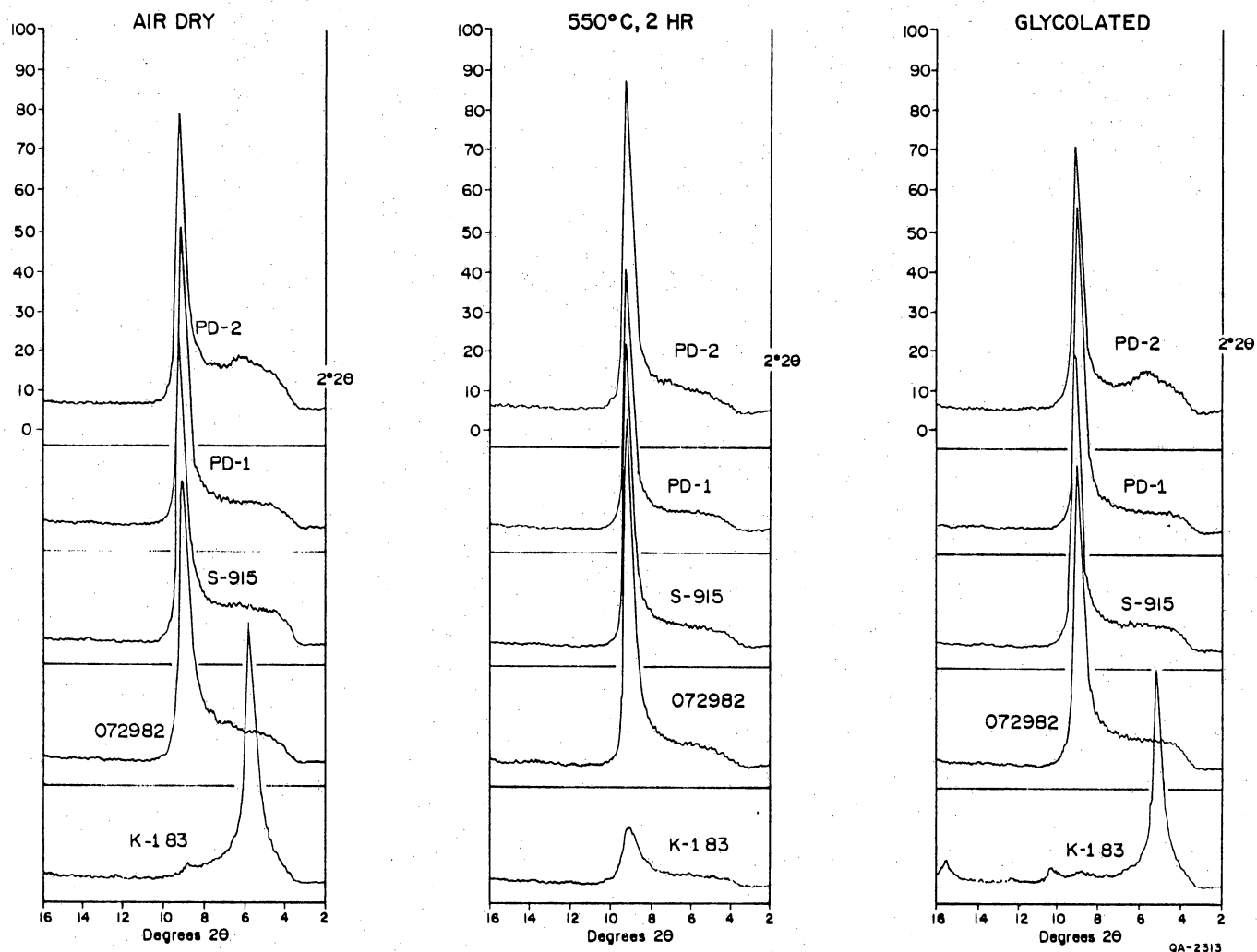


Figure 40. Clay mineral X-ray diffraction analysis of lower volcanic ash bed, Quarter-master and Dewey Lake Formations, Texas Panhandle; Palo Duro Canyon State Park (PD-2), lower Palo Duro Canyon (PD-1), Swisher County Grabbe No. 1 core (S-915), Caprock Canyons State Park (072982), and Caprock Canyons State Park (K-1-83).

Table 9. K-Ar ages and geochemical data from biotite in volcanic ash beds, Quartermaster and Dewey Lake Formations, Texas Panhandle.

Sample 072982, Caprock Canyons State Park, Briscoe County, Texas (34°24'52"N, 101°5'51"W)

Sample weight	590 mg	195 mg
%K	7.434 7.383	7.409 (avg.) 7.542
Ar <sup>40</sup> *	0.1438 0.1402	0.1420 ppm (avg.) 0.1406 ppm
Ar <sup>40</sup> *	0.823	79%
Total Ar <sup>40</sup>	0.850	
Age	257 ± 9 m.y.	251 ± 4 m. y.
Laboratory	Krueger Geochron Labs, Cambridge, MA	The University of Texas at Austin, Department of Geological Sciences (F. W. McDowell, analyst)

Sample S-915, DOE-Gruy Federal Grabbe No. 1 Core, Swisher County, Texas (34°39'44"N, 101°37'55"W)

		Microprobe analysis average of 10 analyses on 5 grains, weight percent		Ions per 24 (O,OH,F)	
Sample weight	110 mg				
%K	7.329 7.393	7.361 (avg.)	SiO <sub>2</sub> 38.77	Si	5.844
			TiO <sub>2</sub> 3.84	Ti	0.436
			Al <sub>2</sub> O <sub>3</sub> 13.15	Al	2.337
Ar <sup>40</sup> *	0.1435		FeO <sup>b</sup> 13.99	Fe	1.765
	0.1552 <sup>a</sup>		MgO 14.44	Mg	3.243
			Na <sub>2</sub> O 0.47	Na	0.139
			K <sub>2</sub> O 8.90 (K=7.39%)	K	1.711
Ar <sup>40</sup> *	0.718		OH <sup>c</sup> 3.97	OH	2.000
Total Ar <sup>40</sup>	0.178 <sup>a</sup>		Total 97.53	Total	17.475
Age	261 ± 9 m.y.				
Laboratory	Krueger Geochron Labs, Cambridge, MA				

Ar<sup>40</sup>\* = radiogenic Ar<sup>40</sup>

a - incomplete sample decontamination

b - total Fe as FeO

c - calculated

\*\* - see text

Constants used:

$\lambda_g = 4.963 \times 10^{-10}/\text{yr}$

$\lambda_e = 0.581 \times 10^{-10}/\text{yr}$

$K^{40}/K = 1.167 \times 10^{-4}$

## PRELIMINARY STRATIGRAPHIC CORRELATIONS AND STRUCTURAL IMPLICATIONS OF THE DOCKUM GROUP, PALO DURO BASIN, TEXAS

David A. Johns

*Preliminary stratigraphic correlations in the Late Triassic Dockum Group indicate the present geometry of the basin reflects Triassic and later tectonic events. Cross sections show regional and local thickening of sandstone units due to tectonism contemporaneous with deposition. Well core and cross sections illustrate the variable erosional contacts at the base of the Dockum in the basin.*

Previous studies of Dockum Group strata have focused primarily on outcrop interpretation (Seni, 1978; Boone, 1979; McGowen and others, 1979, 1980; Seni and others, 1980), whereas subsurface studies have not been as extensive, particularly in the Palo Duro Basin (McGowen and others, 1980; Granata, 1981). Since these studies were completed, additional well control has become available, particularly from the drilling and coring operations of the West Texas Waste Isolation Project.

The Late Triassic Dockum Group conformably and disconformably overlies the Permian Dewey Lake Formation. It is disconformably overlain by Cretaceous strata in the southern part of the basin and is separated from the overlying Ogallala Formation in the central and northern portion of the basin by an angular unconformity (fig. 41). Two cross sections constructed across the basin (figs. 42, 43, and 44) show that the upper erosional contact with the Ogallala is easily identified and locally cuts deeply into Dockum strata. Where present, Cretaceous rocks are commonly difficult to identify using available geophysical logs because their gamma-ray response is similar to that of Triassic rocks (fig. 45). The basal Triassic contact is also not readily detected, possibly because the lower Dockum rocks are composed of reworked Permian sediments (Page and Adams, 1940). Four Department of Energy wells cored the Permian-Triassic boundary interval, providing an excellent opportunity to visually identify the contact on the basis of criteria applied at outcrops and to note its corresponding geophysical log response. Such procedures allow a higher degree of confidence in subsurface correlations and permit more accurate regional stratigraphic analysis that combines the use of subsurface and outcrop data.

The Palo Duro Basin is a broad syncline gently plunging to the south-southeast (figs. 43 and 44). The base of the Dockum, although locally disconformable owing to erosion (McGowen and others, 1979), is structurally concordant with the underlying Permian strata. These units have been warped into a syncline and illustrate that the present geometry of the basin, largely a relict late Paleozoic structure, also reflects Triassic and later structural changes. However, there is some evidence of development during early Dockum deposition. A west-to-east cross section (fig. 43) across the basin shows that the basal sandstone package is roughly uniform in thickness, thus indicating no areas of preferred sand deposition. The north-to-south section (fig. 44) shows that the basal sandstone package is thicker in the middle of the present-day basin and thins over the Matador Arch. This suggests that the arch was a positive structural element during sandstone deposition. Evidence of differential subsidence within the basin can be inferred from figure 43, which shows the nonsandstone section between the basal and middle Dockum sandstone packages thinning to the east. This eastward thinning is probably due to two factors: (1) nondeposition in the east because of greater subsidence in the western part of the basin and (2) erosion of the nonsandstone section by headward-eroding streams during a period of low lake level (McGowen and others, 1979). Differential subsidence could cause a relative lowering of base level. It is possible that the high-stand/low-stand cycles of deposition noted by McGowen and others (1979) could be due to both climatic variations and structural activity.

Depositional styles of Triassic strata contrast with those of Permian strata. The Permian evaporite environments were replaced by lacustrine and fluvial-deltaic environments, possibly resulting from climatic changes and reactivation of older structural elements due to the opening of the Gulf of Mexico (McGowen and others, 1979). Although the fluvial-deltaic deposits in the Dockum generally lack vertical and horizontal continuity, some sandstone packages, particularly in the basal package, can be traced laterally for miles and can be used to illustrate effects of Triassic tectonic activity. For example, in



Lamb County (fig. 44) the basal sandstones thicken southward into a structural low (well no. 67), suggesting a structure contemporaneous with deposition. This structural low could have originated from either tectonic activity or dissolution in the underlying Salado salt section. The cross section shows that thickness of Salado salt in well no. 67 is about 80 ft less than that of well no. 58. Because this amount is also the difference in thickness of the basal Dockum sandstone package, a logical conclusion would be that dissolution of salt occurred contemporaneously with sandstone deposition. The cross section, however, shows that about 250 ft is offset on the top of the Alibates Formation (fig. 44), of which 80 ft can be attributed to salt dissolution. The remaining 170 ft of offset is readily explained by faulting. Because reactivation of old structural elements is thought to have initiated Dockum deposition, it is more likely that faulting occurred first, possibly creating permeable conduits along which ground water could have flowed to the salt beds.

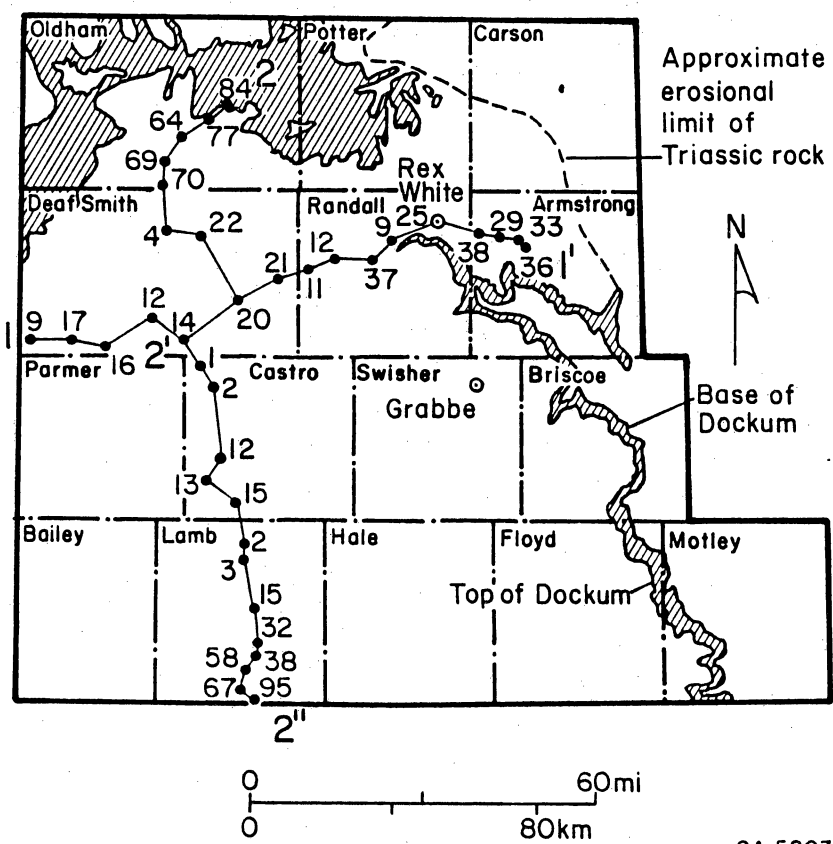
Seni (1978) noted the erosional nature of the lower Dockum contact in Palo Duro Canyon State Park. Analysis of core from the DOE-Gruy Federal Rex White No. 1 well (Randall County No. 25), located near the park, also displays a pronounced erosional boundary (fig. 45). Delineation of this contact is very important because the coarse siltstone at the top of the Dewey Lake Formation appears to be widespread in the basin and is difficult to differentiate from the basal Dockum sandstones on older, less sensitive gamma-ray logs.

In the Tule Canyon area, in western Briscoe and eastern Swisher Counties, Boone (1979) noted a gradational contact at the base of the Dockum. Analysis of core from the nearby DOE-Gruy Federal Grabbe No. 1 well (Swisher No. 17), although inconclusive because of recovery problems, suggests that the contact lies at the base of a fine-grained sandstone (fig. 45) that, judging from gamma-ray log character, appears to have a sharp lower boundary similar to that in the Rex White well. This discrepancy between outcrop and core may be due to local channeling at the base of the Dockum, thus emphasizing the highly variable character of the pre-Dockum surface.

SYSTEM	SERIES	GROUP	FORMATION	GENERAL LITHOLOGY AND DEPOSITIONAL SETTING
QUATERNARY	HOLOCENE		Alluvium, dune sand, playa	
	PLEISTOCENE		Tahoka "cover sands" Tule/ "playa" Blanco	Lacustrine clastics and windblown deposits
TERTIARY	NEOGENE		Ogallala	Fluvial and lacustrine clastics
CRETACEOUS			undifferentiated	Marine shales and limestone
TRIASSIC		DOCKUM		Fluvial-deltaic and lacustrine clastics
UPPER PERMIAN	OCHOAN		Dewey Lake	Bedded salt, anhydrite, red beds, and peritidal dolomite
			Alibates	
	ARTESIA		Salado/Tansill	
			Yates	
			Seven Rivers	
			Queen/Grayburg	
			San Andres	

QA 5202

Figure 41. Stratigraphic column and general lithology of the Palo Duro Basin. From Budnik and Smith (1982).



QA 5203

Figure 42. Outcrop of Dockum Group and locations of cross sections in the Palo Duro Basin.

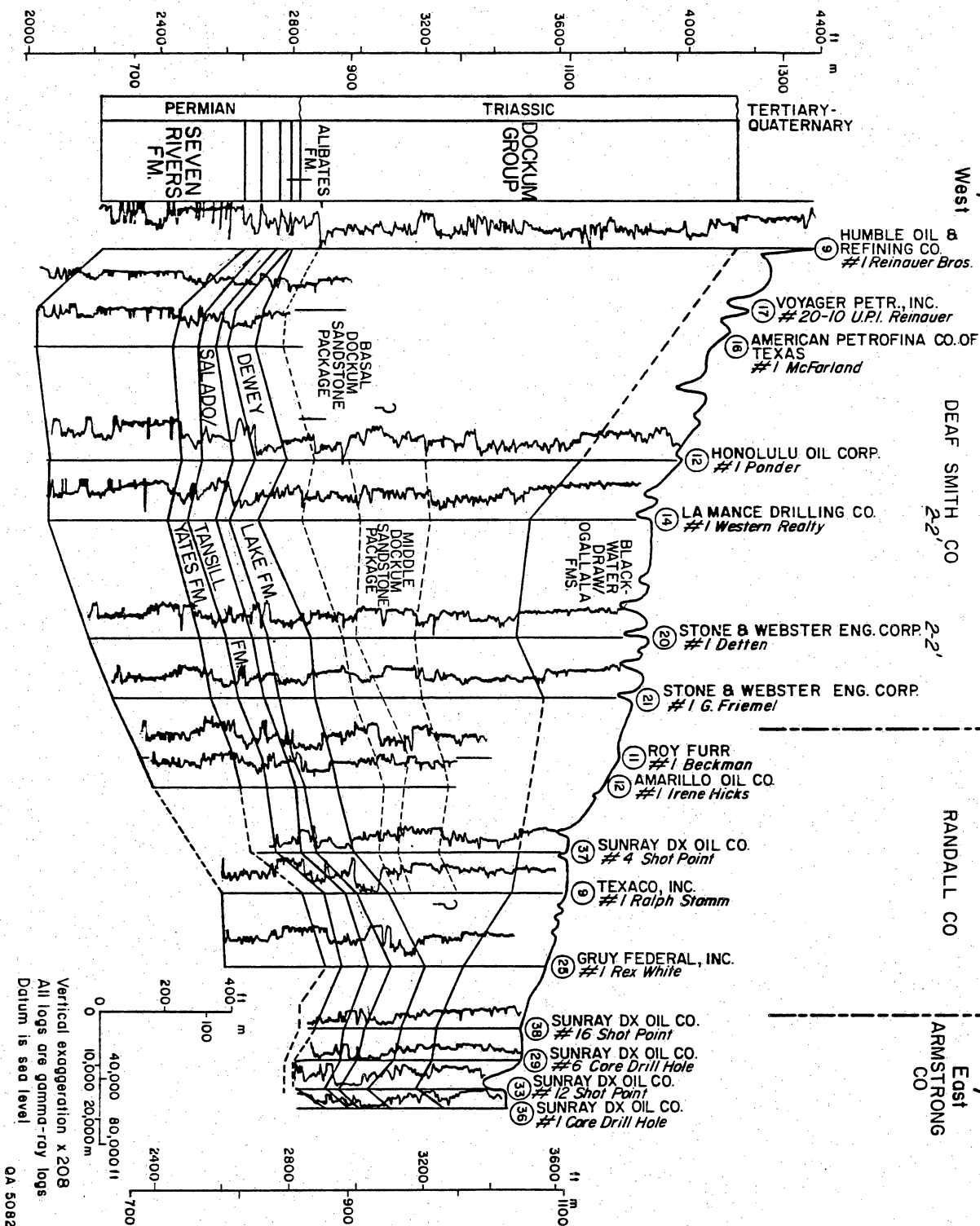


Figure 43. West-east regional cross section 1-1' of post-Queen-Grayburg Formations. See Figure 42 for line of section.

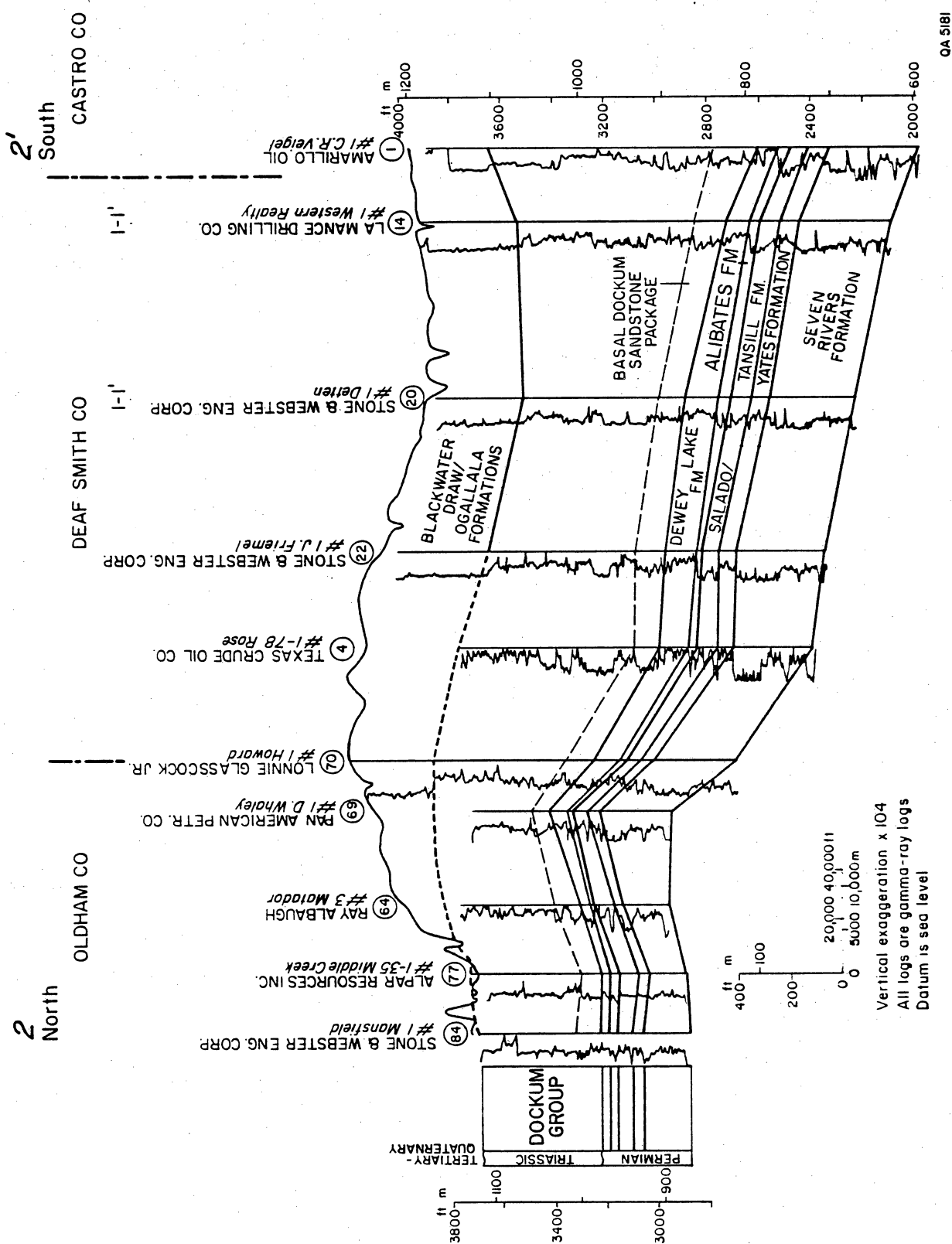


Figure 44. North-south regional cross section 2-2" of post-Queen-Grayburg Formations. See figure 42 for line of section.

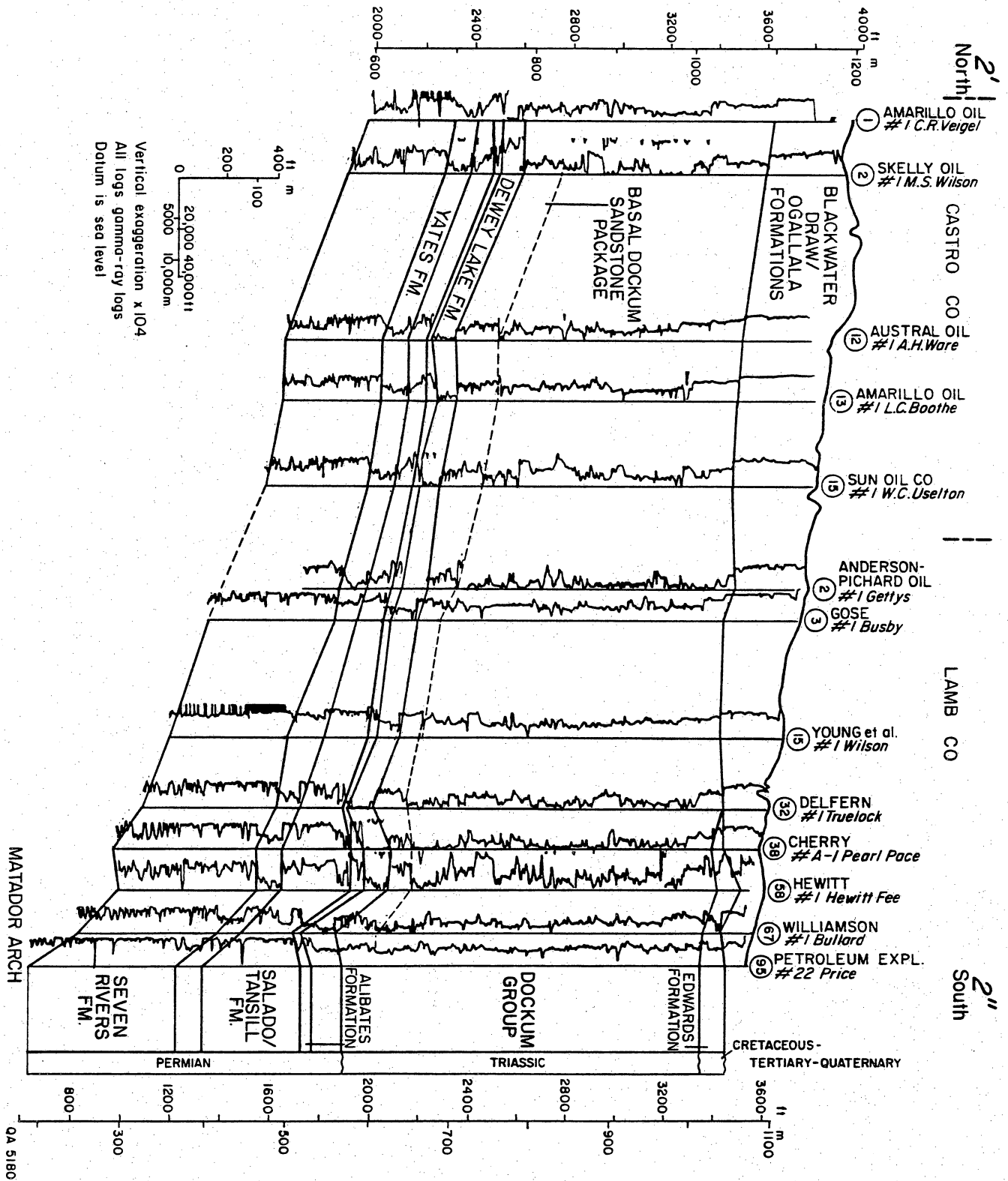
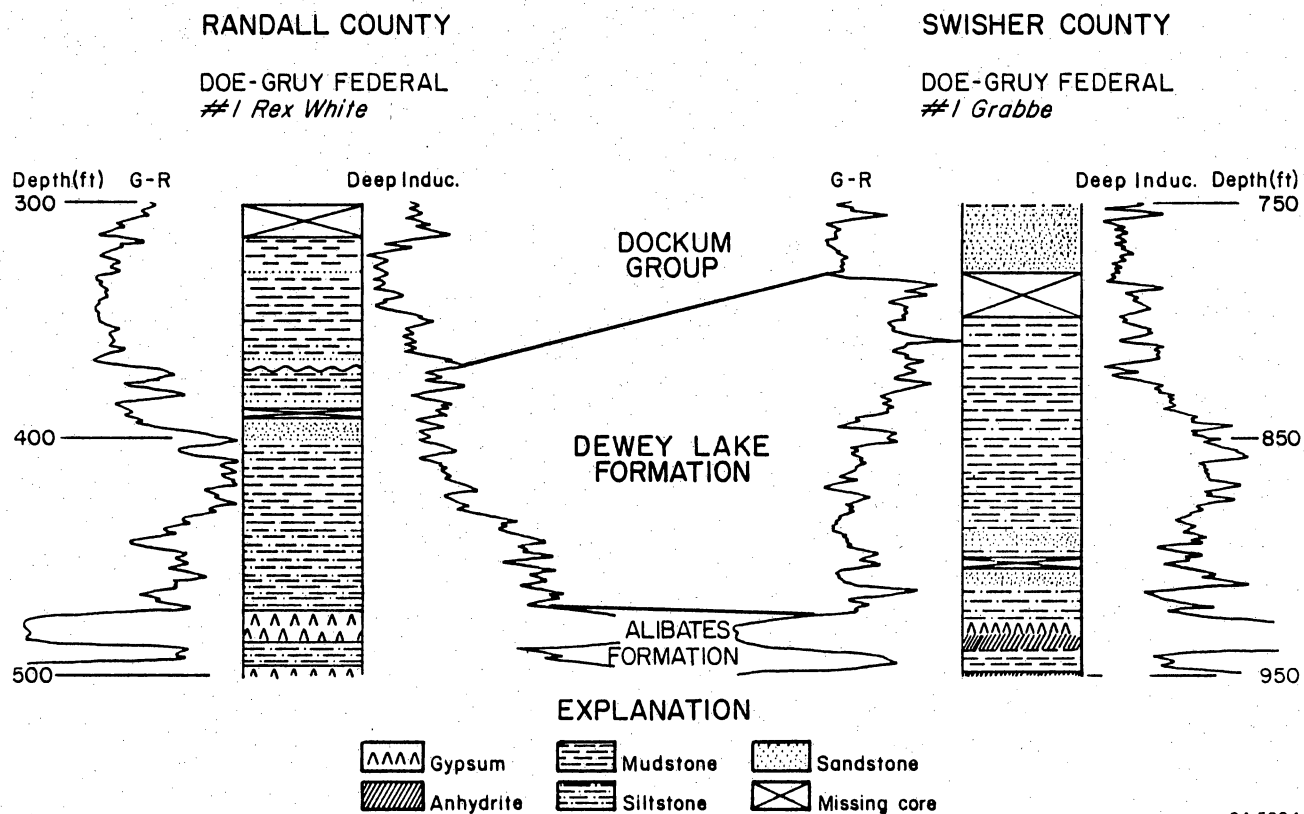


Figure 44. Continued.



**Figure 45. Core description of the Dewey Lake Formation and Dockum Group correlated with geophysical well log patterns, Rex White No. 1 (Randall No. 25) and Grabbe No. 1 (Swisher No. 17).**

LITHOSTRATIGRAPHIC SECTIONS: STONE AND WEBSTER ENGINEERING CORPORATION HARMAN NO. 1 AND ZEECK NO. 1, SWISHER COUNTY, TEXAS

Susan D. Hovorka, Sterling Thomas, Barbara A. Luneau, and Stephen C. Ruppel

*Cores from two new wells, the Stone and Webster Engineering Corporation Harman No. 1 and the Stone and Webster Engineering Corporation Zeeck No. 1, have allowed further examination of the stratigraphic column in Swisher County, including the base of the dissolution zone and top of salt and the San Andres Formation. In addition, the Zeeck No. 1 core contains parts of the Wichita and Wolfcamp shallow-water carbonates and Pennsylvanian starved basin deposits.*

The Stone and Webster Engineering Corporation (SWEC) Harman No. 1 well in northwestern Swisher County was completed to 5,052 ft total depth; 1,475 ft were cored. The SWEC Zeeck No. 1 well in central Swisher County was completed to 7,645 ft, and 2,083 ft were cored. The stratigraphy and lithology of these wells are illustrated in plates I and II (in pocket), which include a suite of geophysical logs, stratigraphy, a generalized lithologic log, and a graph of percent halite of the cored intervals of each well. This paper describes the lithologies present in these cores, emphasizing features that have contributed new insight into depositional and diagenetic processes of these rocks.

Stone and Webster Engineering Corporation Harman No. 1

The upper cored interval from the Harman No. 1 well (1,072 to 1,302 ft) contains the lower half of the Alibates Formation, the Salado-Tansill Formation, the Yates Formation, and the top of the Seven Rivers Formation. Insoluble residues of this interval left after dissolution of bedded halite in the Salado-Tansill Formation are less abundant than this interval in other cores (Hovorka, this volume, "Evidence of Halite Dissolution in Core from beneath the Southern High Plains, Texas"). The Yates Formation is thicker and is composed of a higher percentage of very fine sandstone, compared with the same interval in the other cores.

The uppermost halite in the Harman No. 1 core (1,196 to 1,260 ft, Yates Formation) occurs as isolated halite crystals corroded and rimmed with a thick layer of multifaceted



dolomite or anhydrite (fig. 46). The top of the uppermost halite bed occurs in the Seven Rivers Formation at 1,264 ft; horizontal veins filled with halite occur above and below this unit (fig. 47). Such veins have not been identified within the salt section and, therefore, are tentatively interpreted as being related to mobilization of halite during dissolution. Preserved halite in the interval cored contains no primary structures, which is interpreted as being due to moderate recrystallization within the Permian depositional environment, under present conditions or at some time in between.

The lower cored interval includes most of the San Andres Formation, from the base of unit 2 carbonate to the top of the formation, and 155 ft of the overlying Queen-Grayburg Formation. The new informal division of the San Andres into cyclic genetic units (Fracasso, this volume) is used here. Interesting features observed in this core include well developed grainstone sequences in the unit 4 limestone, many of which fine upward (fig. 48). Many of the grains are skeletal fragments or coated grains. Also present are large productid brachiopods, possible phylloid algal fragments, and mollusk fragments, some with preserved skeletal fabric. The top of the unit 4 carbonate is dolomite with anhydrite nodules and contains oncolite grainstone and possible mud cracks, evidence of subaerial exposure (fig. 49). The unit 4 anhydrite is unusually thick and colored dark by the large amount of admixed mudstone. Good examples of anhydrite fabrics are present within the San Andres. Single anhydrite crystals greater than 20 cm tall with well-preserved fine growth laminae are present at 2,145 to 2,147 ft (fig. 50). Large pseudomorphs after gypsum are also present at 2,626 and 2,648 ft. Irregular bedding surfaces with pseudomorphs after gypsum crystals radiating outward, rather than upward, can be seen at 2,168 ft and 2,561 to 2,564 ft (fig. 51).

Dominant lithologies in the overlying Queen-Grayburg Formation are very fine and fine sandstone with dissipation structures (Ahlbrandt and Fryberger, 1981) (fig. 52) and lag deposits of polished medium sand forming a bimodal texture indicative of eolian origin. The contact between the Queen-Grayburg sandstone and the underlying San Andres halite is

marked by 10 ft of mudstone characterized by deformed flaser bedding in the upper part and displacive halite crystals and wavy anhydrite beds in the lower part.

#### Stone and Webster Engineering Corporation Zeeck No. 1

The upper cored interval of the Zeeck No. 1 well includes the lower part of the Alibates and the upper part of the Seven Rivers Formations. Contorted structures in the Alibates are tentatively attributed to an early episode of diagenesis, possibly accompanied by dissolution and collapse (Hovorka, this volume, "Evidence of Halite Dissolution..."). The upper part of the Salado-Tansill is mudstone with a minor amount of gypsum and anhydrite. It exhibits abundant slickensided joints in mudstone, high-amplitude wavy lamination in thin anhydrite beds, and mudstone-anhydrite breccias. These features are interpreted as being due to dissolution of halite (Hovorka, this volume, "Evidence of Halite Dissolution..."). The uppermost occurrence of halite in this core is at 1,101 ft in the Salado-Tansill Formation in the form of vertical white halite-filled veins partially replaced by anhydrite (fig. 53). Because of their similarity to vertical halite-filled fractures common within the halite section, these veins are tentatively interpreted as relict early diagenetic fractures. Beds surrounding the uppermost halite-filled fractures are mudstone-anhydrite insoluble residues, indicating that smaller halite crystals have been dissolved from this interval. In the 15 ft below the uppermost halite, halite occurs as corroded, partially anhydrite-replaced crystals and as cement in a clean sandstone bed. Below 1,117 ft, halite occurs as typical mudstone-halite. A few fractures in mudstone-halite at 1,123 ft, some magnesite nodules at 1,129 ft (fig. 59), and unusually coarse halite crystals at 1,140 to 1,143 ft are interpreted as possible evidence of recrystallization due to the penetration of ground water into this interval (fig. 54-55; Hovorka, this volume).

The lower cored interval includes the top of the unit 2 halite and overlying San Andres Formation and 120 ft of the Queen-Grayburg Formation. Notable features of the

San Andres Formation include plant fragments in the unit 3 carbonate (3,082 ft and dolomite intraclast beds with scoured bases (storm scour channels, fig. 56) stratigraphically equivalent to the unit 4 anhydrite in other cores. The unit 4 anhydrite in the Zeeck well is less than 1 ft thick. The upper part of an anhydrite bed within unit 4 halite (2,814 ft) contains red-brown mudstone in horizontal and vertical pockets, possibly due to microkarst in the gypsum precursor to anhydrite (fig. 57). An anhydrite bed deformed by collapse into a small karst pit in halite is present at 2,244 ft in unit 5.

Good examples of chevron structures in halite are present at 2,773 to 2,778 ft (large flawed chevrons with even zonation) and at 2,656 (chevrons oriented with coigns pointing sideways as well as upward), 2,859, and 2,848 ft (chevrons truncated by mudstone beds). Examples of recrystallized halite at the tops of cycles are present at 2,827 (beneath anhydrite bed within unit 4 halite), 2,736 (top unit 4), and 2,565 ft (top of incomplete cycle in middle San Andres).

Three intervals cored below the halite section are the lower part of the Wichita Formation and top of the Wolfcamp, an interval of Wolfcamp basinal shales, and an interval of Pennsylvanian basinal shales. The Pennsylvanian sequence (7,300 to 7,370 ft) is composed of dark claystone containing abundant beds of very fine sandstone and coarse siltstone with starved-ripple lamination. Sparse, compacted horizontal burrows, normal and reverse graded beds, and intervals with abundant pyritized plant fragments are present. Identification of this interval as Pennsylvanian is based on regional correlation of geophysical logs. The Wolfcamp basinal facies (6,058 to 5,909.8 ft) is composed of dark, calcareous claystone and argillaceous limestone. Compacted burrows, whole and fragmented brachiopods, and plant fragments are common. A carbonized impression identified as Caulurpa sp. found at 5,969.2 ft has been preserved at the Texas Memorial Museum.

The upper cored interval (5,309 to 5,780 ft) has 228 ft of dark, variably calcareous claystone with sparse brachiopods and foraminifers. Two carbonate units are present in this interval: crinoid-brachiopod mudstone coarsening to packstone at 5,701 to 5,727 ft and

fossiliferous packstone and wackestone containing abundant oncolites at 5,604 to 5,642 ft. The upper carbonate unit has been partially dolomitized, and some grains have been replaced or cemented by anhydrite. Skeletal carbonates of the Wolfcamp shelf facies begin abruptly at 5,552 ft, where they are burrowed and cross-laminated grainstones and packstones (fig. 58) containing ooids and coated grains. Porous, sucrosic dolomite occurs between 5,470 and 5,510 ft. The gradational contact between the Wolfcamp and the Wichita Formation is marked by upward decrease in grain size and allochem diversity. Abrupt vertical changes between oncolite grainstone, algal lamination, small stromatolites at 5,429 ft, and ripped-up organic material at 5,441 ft suggest that these sediments may have accumulated in intertidal and supratidal environments. Much of the partial dolomitization of carbonates in the Wolfcamp-Wichita transitional interval is tentatively interpreted as diagenetic rather than syndepositional because the dolomite is sucrosic and its distribution is not facies controlled. Anhydrite is present only as replacive masses. The contact between the Wolfcamp and Wichita Formations is placed at 5,452 ft on the basis of regional correlations, but Wolfcamp-like coarse grainstone occurs as high as 5,392 to 5,398 ft, and large amounts of nodular anhydrite are not present below 5,370 ft, indicating that hypersaline Wichita conditions in this area were established gradually. The Wichita in the upper part of the cored interval is composed of alternating dolomitized, fine, coated grain grainstone and packstone, dolomitized carbonate mudstone, nodular anhydrite mosaic, and minor siliciclastic mudstone and claystone, similar to Wichita rocks in the SWEC Sawyer No. 1 core.



Figure 46. Uppermost occurrence of halite in Stone and Webster Engineering Corporation Harman No. 1 core composed of corroded halite crystals (H) rimmed with anhydrite and dolomite (A), Yates Formation, 1,198 ft.

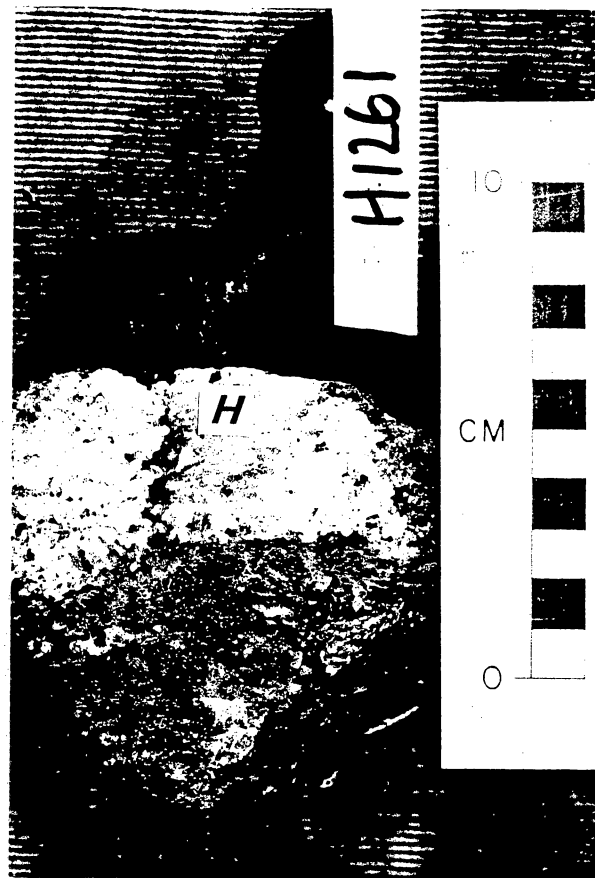


Figure 47. Halite-filled vein (H), interpreted as possible evidence of local reprecipitation of halite associated with regional dissolution. Stone and Webster Harman No. 1 core, Seven Rivers Formation, 1,261 ft.

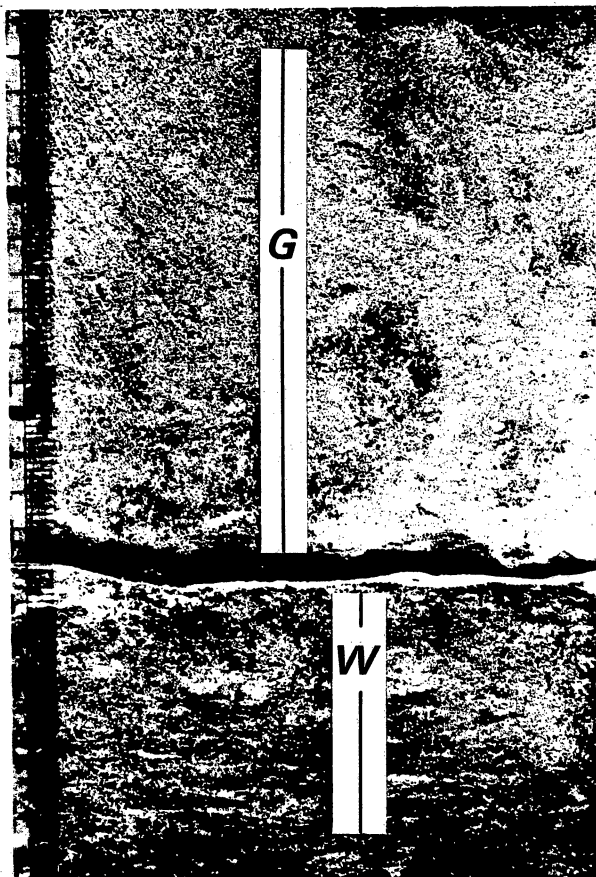


Figure 48. Typical limestone of unit 4 of the San Andres Formation, showing the burrowed coarse grainstone (G) at the base of one upward-fining sequence overlying the fine wackestone (W) at the top of the underlying sequence. Stone and Webster Engineering Corporation Harman No. 1 core, 2,862 ft, core width 10 cm.



Figure 49. Possible supratidal dolomite at the top of San Andres unit 4 showing thin bedding, oncolite grainstone, and possible desiccation crack. Stone and Webster Engineering Corporation Harman No. 1 core, 2,834 ft, core width 10 cm.

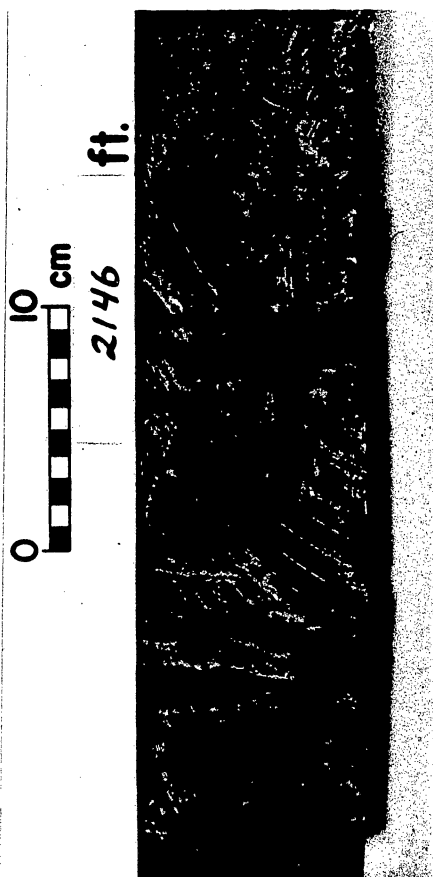


Figure 50. Tall, finely banded halite and anhydrite pseudomorphs after bottom-nucleated gypsum crystals. San Andres Formation, Stone and Webster Engineering Corporation Harman No. 1, 2,146 ft.

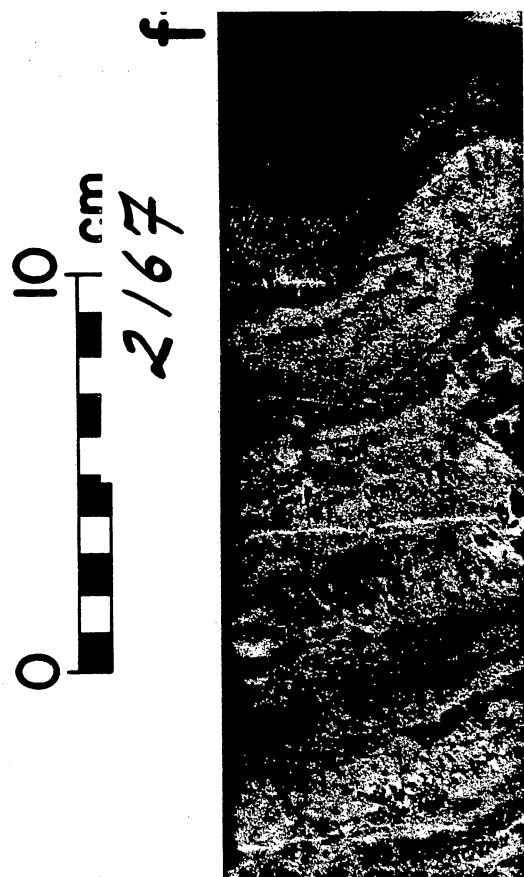


Figure 51. Pseudomorphs after gypsum crystals radiating outward from an irregular bedding surface. San Andres Formation, Stone and Webster Engineering Corporation Harman No. 1, 2,167 ft.

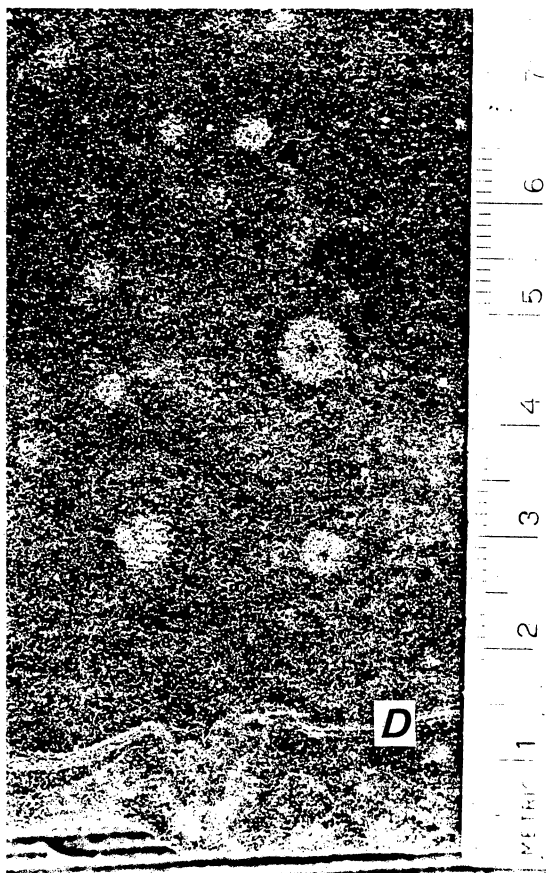


Figure 52. Typical fine sandstone with irregular, millimeter-thick clay concentrations called dissipation structures (D) in the Queen-Grayburg Formations, Stone and Webster Engineering Corporation Harman No. 1 core, 1,934 ft.

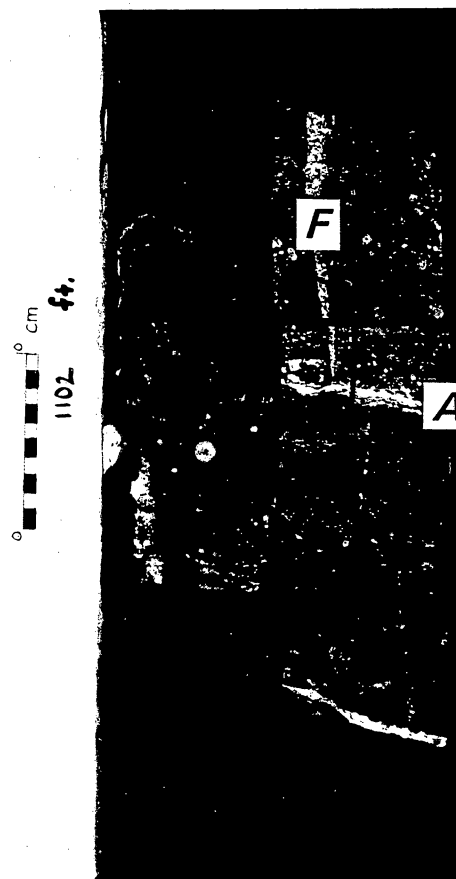


Figure 53. Halite-filled vertical fractures (F) separated by thin horizontal partings of anhydrite (A) in the uppermost occurrence of halite in the Stone and Webster Engineering Corporation Zeeck No. 1 core, Salado-Tansill Formations, 1,102 ft.





Figure 54. Unusual magnesite nodules indicating the probable penetration of diagenetic waters into the halite of the Salado-Tansill Formations, Stone and Webster Engineering Corporation Zeeck No. 1 core, 1,129 ft.



Figure 55. Extremely coarse crystals in Salado-Tansill halite indicating the penetration of ground water deeper than the interval in which dissolution occurred. Stone and Webster Engineering Corporation Zeeck No. 1, 1,143 ft.

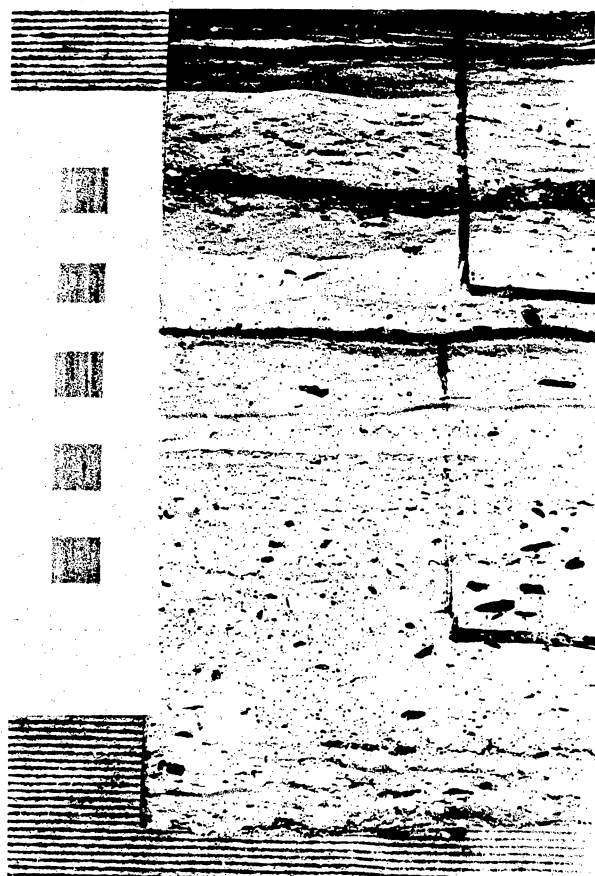


Figure 56. Oncolite grainstone at the top of unit 4 carbonate, Stone and Webster Engineering Corporation Zeeck No. 1 core, 2,918 ft.

0 10 cm  
→ 22814.5 ft.



Figure 57. Possible karst pits in an anhydrite bed within the unit 4 halite filled with mudstone and halite. Stone and Webster Engineering Corporation Zeeck No. 1 core, 2,814.5 ft.

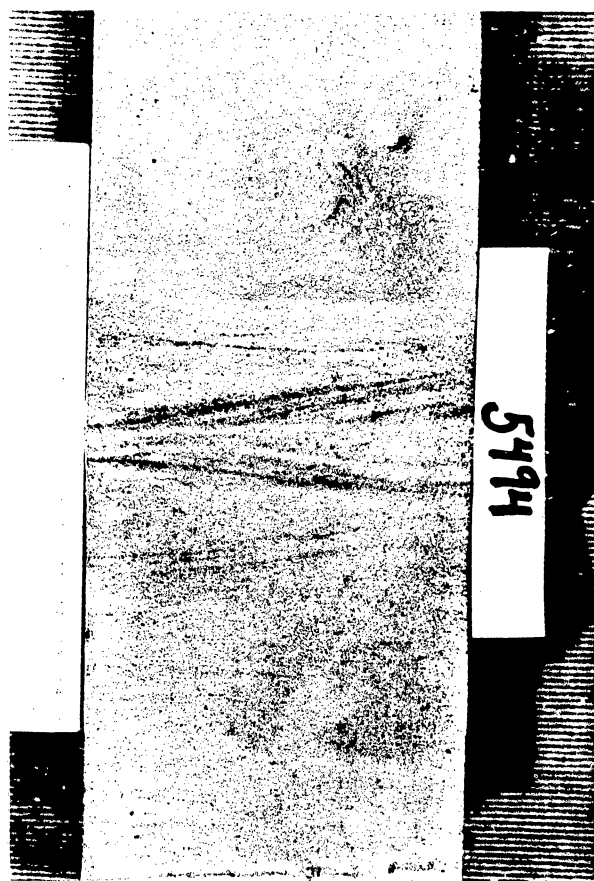


Figure 58. Cross-laminated carbonate grainstone in the Wolfcamp, Stone and Webster Engineering Corporation Zeeck No. 1, 5,494 ft.

## CORRELATION OF CLEAN, MUDDY, AND ANHYDRITIC ZONES IN HALITE, SAN ANDRES FORMATION UNITS 4 AND 5, DEAF SMITH COUNTY, TEXAS

Susan D. Hovorka, Barbara A. Luneau, and Sterling Thomas

*Detailed logging of cores from three DOE stratigraphic test wells in Deaf Smith County has established a basis for correlation of zones of mudstone beds, clean halite, and anhydritic halite within the halite rock of units 4 and 5 of the San Andres Formation.*

The results of previous studies of the thick halite rock intervals in the San Andres Formation are difficult to interpret. Handford (1981) studied bromide content of halite, a trace constituent useful for interpreting the composition of the brine from which the halite formed, and found no apparent trend in the San Andres unit 4 halite. Ruppel and Ramondetta (1982) mapped the salt quality (mudstone content) of the San Andres units 4 and 5 on the basis of gamma-ray log response. Trends shown on the salt quality maps are spotty and difficult to interpret.

Recurring sequences within the halite units of the San Andres Formation have been observed during logging of seven new DOE cores. Detailed logging using a variety of visual logging techniques has identified 1- to 3-m-thick zones that are traceable between the three Deaf Smith wells (figs. 59 and 60). Logging techniques used are (1) visually estimating volume percent composition, (2) mapping sedimentary structures, (3) identifying dominant salt type on the basis of textural classification of halite (Hovorka, this volume, "Textural Classification of Salt with Genetic Significance"), and (4) mapping the location, composition, and thickness of all interbeds or partings of any thickness within halite.

Figure 59 illustrates two thin anhydrite beds from the unit 5 halite. These beds are correlatable in three wells. Comparison between the cores shows the continuity of thin units over tens of kilometers; it also documents the presence of facies variations. For example, the thicker lower anhydrite bed in the J. Friemel (2,430 ft) and Detten (2,436 ft) cores overlies several thin mudstone partings, but in G. Friemel at about 2,295 ft no mudstone is present below the anhydrite, but three partings are present above it.

Figure 60 shows one of a number of sequences in unit 4 of clean, slightly anhydritic salt with well-preserved primary fabric overlain by abundant mudstone beds and zones of chaotic mudstone-halite rock. Individual mudstone and anhydrite partings are not correlatable between wells, but zones in which partings are concentrated can be correlated.

This kind of correlation is possible through all of units 4 and 5 in Deaf Smith County, and preliminary logging suggests that in Swisher County similar zones are correlatable. The most difficult zone to correlate is the upper 10 ft of halite in each cycle.

A depositional model for the origin of these zones is based on study of sedimentary structures and bromide composition (Fisher and Hovorka, this volume). Clean, anhydritic halite with abundant primary fabric such as shown in the lower part of figure 60 was deposited in shallow, regionally extensive brine pools. Continued connection with the marine environment allowed episodic influx of marine-derived brines. These brines (1) slightly corroded the halite on the floor of the pools and (2) precipitated a minor amount of anhydrite before (3) evaporating sufficiently to continue to precipitate halite. If more complete connection with the marine environment were established, probably because of an increase in water depth, the resultant salinity decrease might lead to an episode of anhydrite deposition, as illustrated by the two beds depicted in figure 59. The mudstone beds represent episodes of influx of clastics into the basin. Most of the mudstone beds overlie 1- to 30-cm-thick layers of halite that has been corroded, pitted by karst processes and recrystallized, suggesting that mudstone deposition occurred when the halite was sub-aerially exposed. Mudstone beds were probably deposited when input of brine was shut off, causing the flat to become dry.

That these zones, reflecting subtle variations in the halite environment, can be correlated from well to well indicates that the factors controlling facies in the halite affected large areas. Halite was deposited not in isolated brine pools but, like the underlying carbonate and sulfate parts of the cycle, in a shallow but extensive water body.

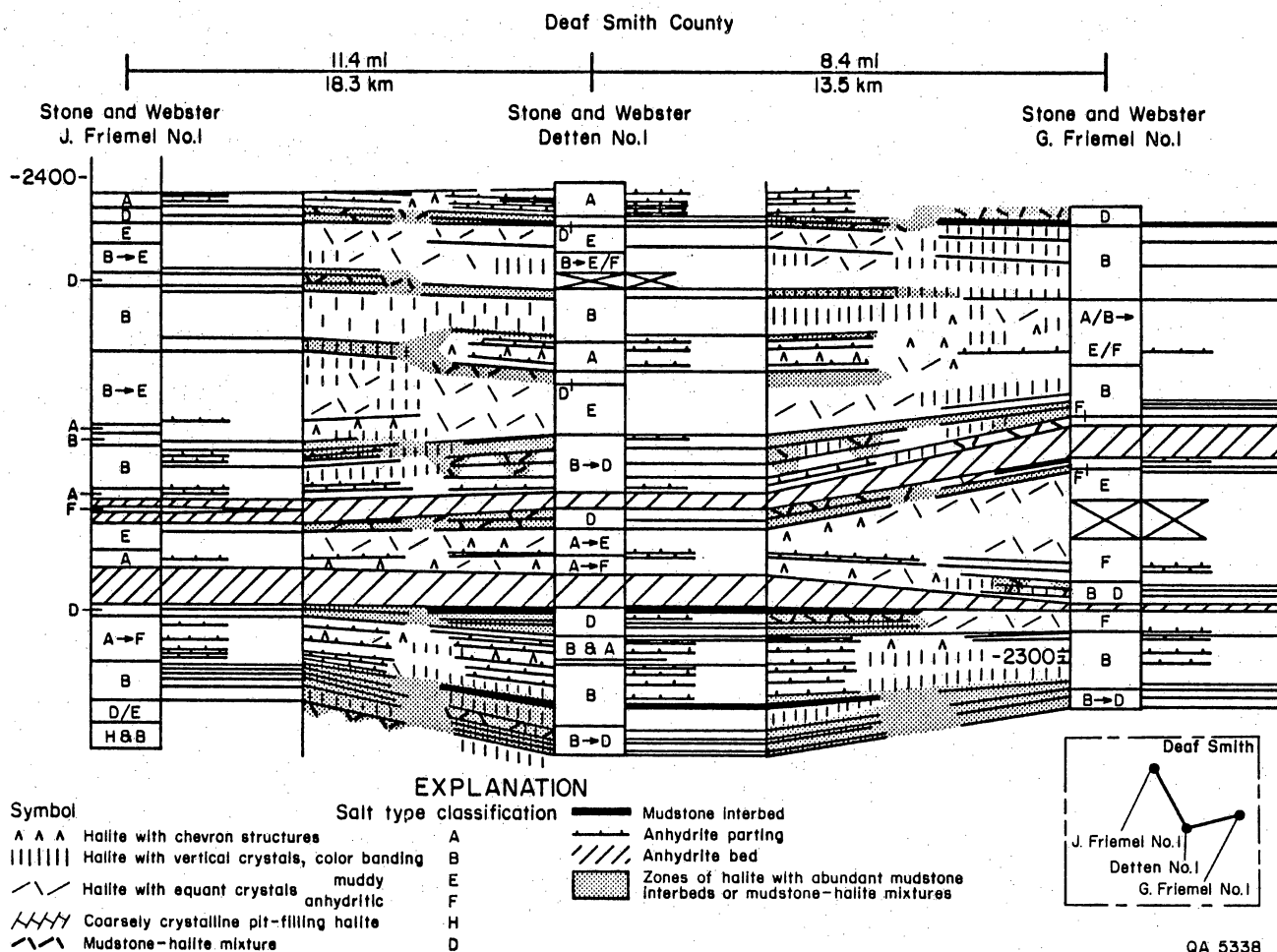


Figure 59. Example of detailed logs of Stone and Webster Engineering Corporation J. Friemel No. 1, Detten No. 1, and G. Friemel No. 1 cores, San Andres Formation unit 5, showing correlation of two thin anhydrite beds.

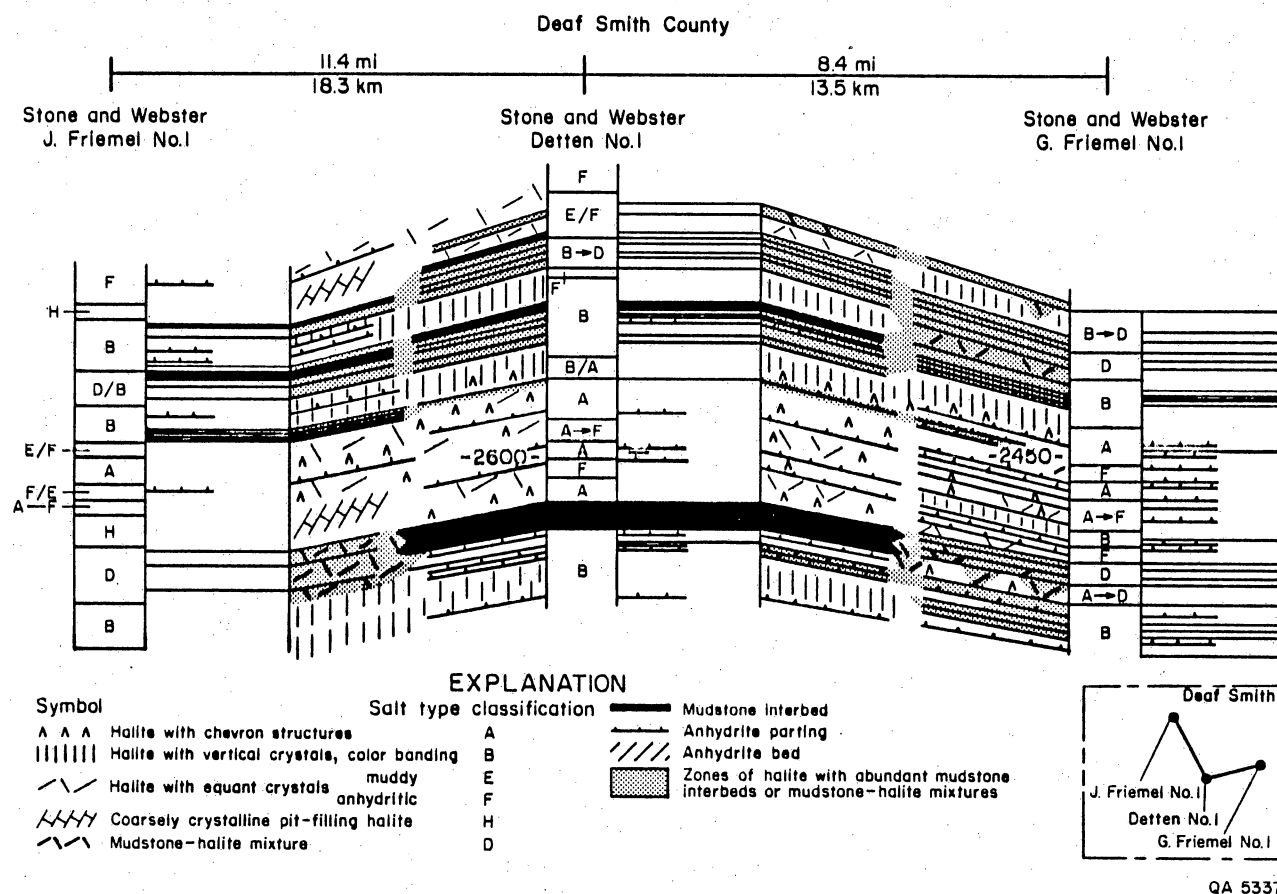


Figure 60. Example of detailed logs of Stone and Webster Engineering Corporation, J. Friemel No. 1, Detten No. 1, and G. Friemel No. 1 cores, San Andres Formation unit 4, showing correlation of zones of anhydritic halite with primary fabric and the overlying zone of muddy halite with many mudstone interbeds.

## EVIDENCE OF HALITE DISSOLUTION IN CORE FROM BENEATH THE SOUTHERN HIGH PLAINS, TEXAS

Susan D. Hovorka

*Cores from seven of the stratigraphic test wells drilled by DOE in the northern Palo Duro Basin have been examined. All of the cores contain evidence that halite once existed above its present uppermost occurrence. Dissolution beneath the Southern High Plains appears to have been a slow, noncatastrophic process in which rapid collapse did not occur. Two stages of diagenesis, probably accompanying two episodes of halite dissolution, can be identified.*

Features formed during dissolution of thick sequences of bedded halite in the San Andres Formation beneath the Rolling Plains physiographic province were examined in the Stone and Webster Engineering Corporation (SWEC) Sawyer No. 1 core from Donley County, Texas (Hovorka, 1983c). A related but different suite of dissolution zone features that result from dissolution of stratigraphically higher bedded halite beneath the Southern High Plains was identified in cores from seven DOE stratigraphic test wells (fig. 61):

- (1) wavy-laminated anhydrite-gypsum-multifaceted dolomite: insoluble residue from the dissolution of relatively clean, anhydritic halite beds (fig. 62);
- (2) mudstone-anhydrite-gypsum-multifaceted dolomite: insoluble residue from dissolution of chaotic mudstone-halite rock (figs. 63 and 64);
- (3) fractured mudstone with slickensided surfaces: a result of collapse of beds overlying areas of halite dissolution (fig. 65);
- (4) horizontal and high-angle fibrous gypsum-filled veins, opened during collapse as underlying halite was removed (fig. 66);
- (5) hydration of anhydrite to gypsum under the influence of penetrating ground waters (fig. 67);
- (6) recrystallization of anhydrite to a coarser grain size, probably due to interaction with invading ground water (fig. 68); and
- (7) recrystallization of halite to coarse grain size, probably also due to interaction with invading ground water (fig. 69).



The evidence that these features are related to dissolution is

- (1) the features are confined to the part of the stratigraphic section above or intertonguing with the uppermost halite; and
- (2) the features are restricted to stratigraphic intervals that contain salt in other areas.

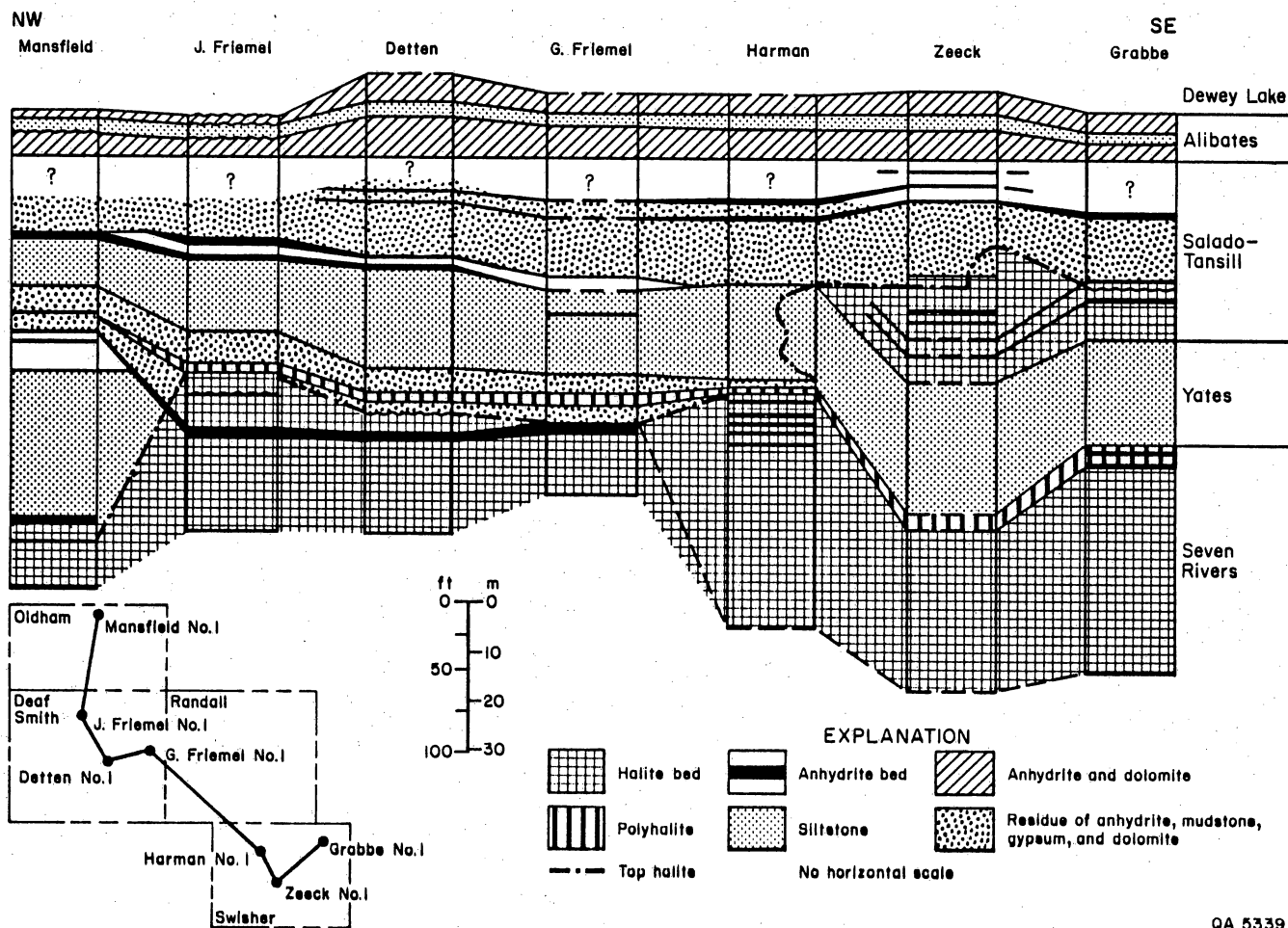
Some evidence of the timing of dissolution can be gained from examination of the core. Most of the dissolution at the top of the salt section is identified as occurring in the burial rather than the depositional environment, therefore occurring in post-Permian or latest Permian time. Multifaceted dolomite is abundant in residues. This dolomite is a late diagenetic product not present in residues formed in the depositional environment (Hovorka, 1983b, c) and therefore indicates a late timing of dissolution. Halite has been dissolved from all depositional environments from the most evaporitic to the most terrestrial, indicating dissolution did not occur in the Permian depositional environment. The top of halite occurs in a different stratigraphic position in each well (fig. 61), and its removal due to dissolution crosscuts facies boundaries.

Comparison of the seven cores from the Southern High Plains and the SWEC Sawyer No. 1 core from the Rolling Plains east of the Caprock Escarpment shows that (1) less halite has been dissolved from the High Plains because of penetration of dissolving waters to stratigraphically shallower intervals, (2) cavern formation and collapses producing breccias have not been identified in the High Plains but are commonly observed in the Rolling Plains both at the surface (Simpkins and others, 1981) and in core, and (3) anhydrite has been less extensively hydrated to gypsum in the High Plains cores, perhaps because the lower permeability of enclosing sediments decreased the availability of fresh waters. Dissolution of bedded halite is clearly an active process in the Rolling Plains. The processes of dissolution in the Southern High Plains appear to be sluggish, and the current rate of dissolution is not apparent from core studies. However, there is no evidence of post-dissolution diagenesis, which suggests that dissolution may be an ongoing rather than a

relict process. Specific examples of apparently ongoing dissolution are open pores left after the removal of halite and before the precipitation of gypsum (fig. 70) and euhedral gypsum replacing anhydrite (fig. 71).

An early stage of diagenesis and probable accompanying dissolution is recognized by precipitation of calcite and replacement of sulfates by carbonates (figs. 72, 73, and 74). This type of diagenesis is confined to the uppermost stratigraphic units--the Dewey Lake, Alibates, and top of the Salado-Tansill Formations--and does not occur in the crosscutting, therefore younger, areas of dissolution. Precipitation of carbonates occurred in a geochemical regime different from the present one, and because of its restriction to uppermost stratigraphic horizons, probably formed before development of the present basin geometry and topography. The Alibates Formation is microfaulted and folded at many intervals in core; this is tentatively attributed to removal of halite cement from carbonate and anhydrite and collapse of the resulting dolomite silt ooze when underlying halite was removed (fig. 75). Similar deformation of carbonate after removal of halite cement has been observed in the SWEC Sawyer No. 1 core, which recovered some intervals of soft dolomite silt ooze. Siltstone casts of halite hopper crystals in the Dewey Lake Formation were observed in outcrop by Kolker and Fracasso (verbal communication), and deformed intraclastic texture attributed to churning of sediment during growth and removal of displacive halite in the depositional environment has been observed throughout the formation.

The early calcite-precipitating waters probably caused dissolution of halite from the Dewey Lake, Alibates, and top of Salado-Tansill Formations at some time or times during the latest Permian or Mesozoic. A change in environment causing locally deeper, apparently slow but still ongoing dissolution produced the suite of most recent features observed in all cores.



QA 5339

Figure 61. Stratigraphic sections comparing features present in the dissolution zone of seven DOE stratigraphic test wells from the Palo Duro Basin. All of these wells but the Mansfield No. 1 were drilled on the Southern High Plains, an area where dissolution of halite has been considered to be minimal.

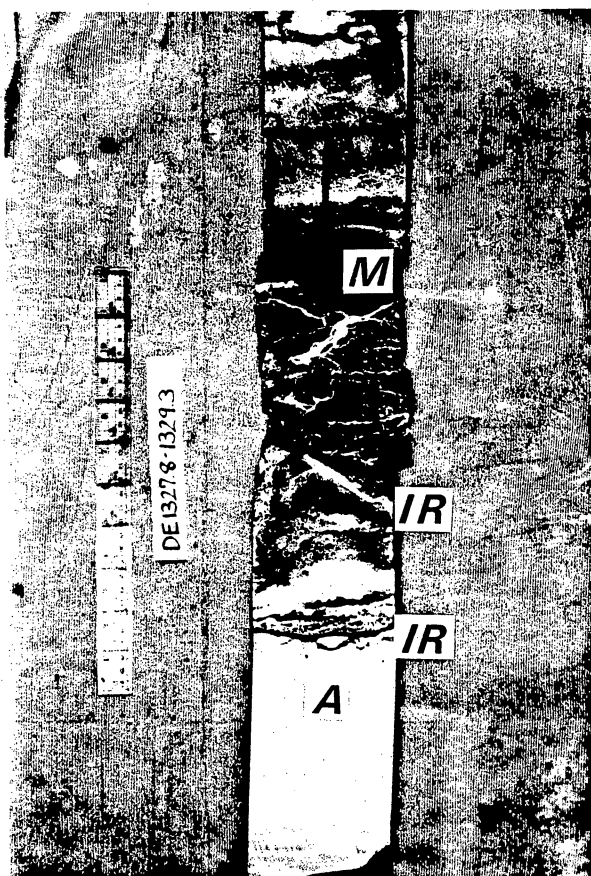


Figure 62. Typical fabrics in the dissolution zone, Seven Rivers Formation, Stone and Webster Engineering Corporation Detten No. 1 core, 1,327.8 to 1,329.3 ft. Anhydrite (A) at the base of the core is overlain by an insoluble residue of anhydrite, gypsum, and multi-faceted dolomite with characteristic wavy lamination (IR). Mudstone (M) has been fractured, and some fractures are filled with gypsum cement. Anhydrite at the top is coarse (CA) and may have originated as an insoluble residue or by recrystallization of an anhydrite bed.

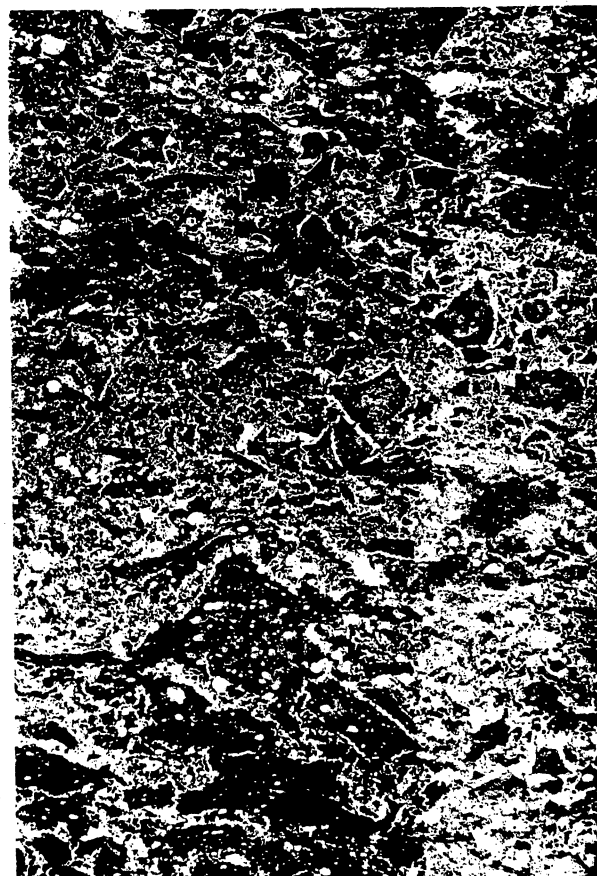


Figure 63. Insoluble residue breccia of mudstone, anhydrite, gypsum, and multi-faceted dolomite in core, DOE-Gruy Federal Rex White No. 1, 613 ft, Salado-Tansill Formations, width about 8 cm.

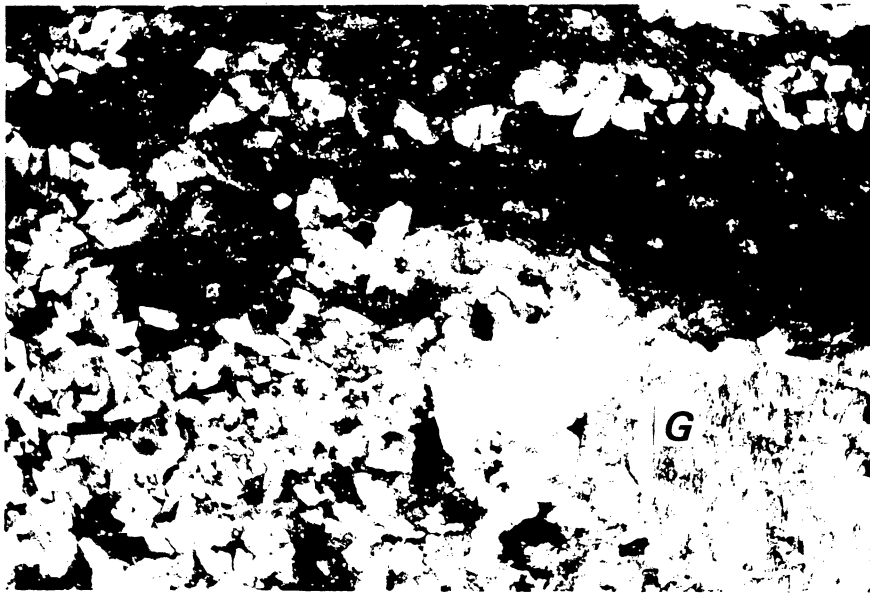


Figure 64. Photomicrograph of insoluble residue of mudstone, anhydrite, gypsum, and multifaceted dolomite. Euhedral crystals are multifaceted dolomite, mudstone is dark, gypsum (G) has a fibrous texture. Stone and Webster Engineering Corporation Mansfield No.1 core, 608.4 ft, crossed nicols, width 3.25 mm, Seven Rivers Formation.



Figure 65. Slickensided surfaces of fractures, some coated with gypsum vein fillings. Same mudstone core as shown in figure 62, Stone and Webster Engineering Corporation Detten No. 1 core, 1,328.5 ft, Seven Rivers Formation.



Figure 66. Fibrous gypsum-filled veins, Salado-Tansill Formations, DOE-Gruy Federal Rex White No. 1 core, 528 ft.

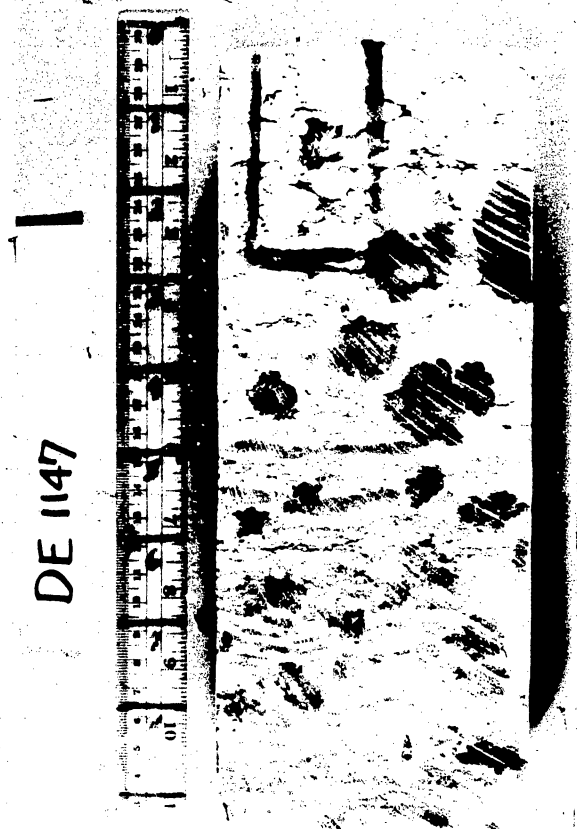


Figure 67. Nodular anhydrite hydrated to gypsum in isolated spherical patches (dark areas); Stone and Webster Engineering Corporation Detten No. 1 core, 1,147 ft, Alibates Formation.



Figure 68. Photomicrograph of spherulitic, coarsely crystalline anhydrite in the dissolution zone, DOE-Gruy Federal Grabbe No. 1 core, 1,040.9 ft, Salado-Tansill Formations, crossed nicols, width 7.7 mm.



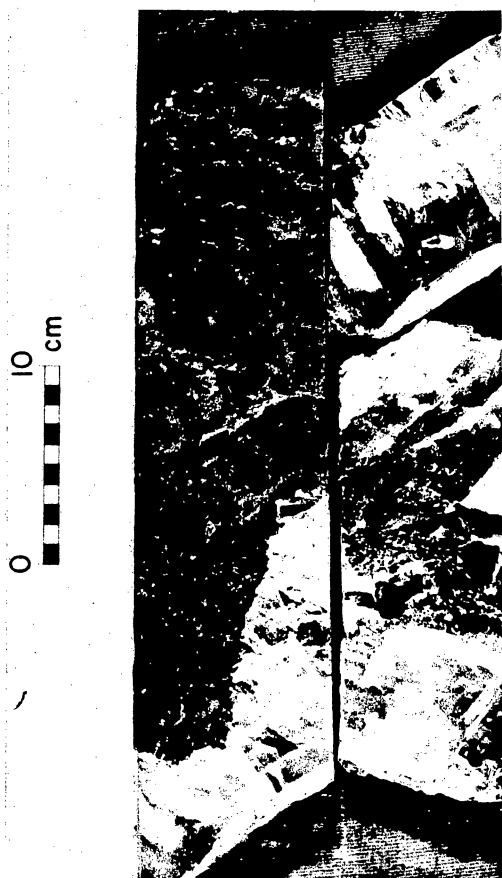


Figure 69. Coarsely crystalline halite texture characteristic of the uppermost halite preserved. The planar surfaces at the broken ends of core are along cleavage through single halite crystals, Seven Rivers Formation, DOE-Gruy Federal Grabbe No. 1 core, 1,164 to 1,168.8 ft.

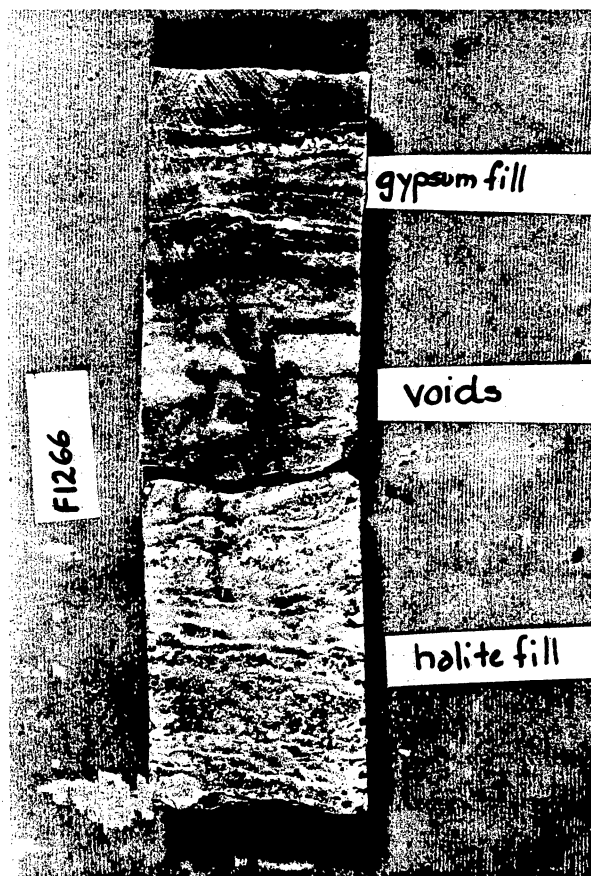


Figure 70. Dissolution zone at 1,263 to 1,266 ft in the Stone and Webster Engineering Corporation G. Friemel No. 1 core at the base of the Seven Rivers Formation. Halite remains in pockets in anhydrite in the lower part of the core. In the middle of the core, halite has been dissolved and the pockets are open voids. In the upper part of the core, the pores have been filled with gypsum. Halite in the middle of the core appears to have been dissolved more recently than that in the upper part because gypsum has not yet had time to fill the voids, suggesting dissolution may be an ongoing process in this area. Core is 10 cm wide.



Figure 71. Euhedral gypsum replacing fine anhydrite mosaic. The anhydrite is an insoluble residue from Permian or more recent dissolution of halite. The faces of the gypsum crystal indicate that it is the most recent replacing phase, probably the result of penetration by ground waters 327 ft into the halite section. Upper San Andres Formation, Stone and Webster Engineering Corporation Mansfield No. 1 core, 1,153.5 ft.

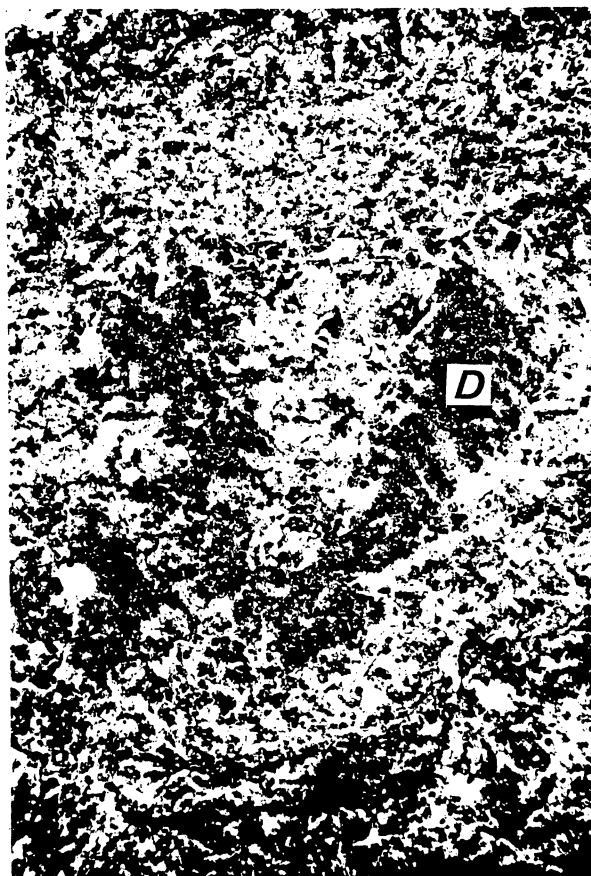


Figure 72. Replacement of gypsum crystals by anhedral dolomite (D) in anhydrite matrix in the Alibates Formation, DOE-Gruy Federal Grabbe No. 1 core, 958.9 ft, width 7.7 mm, crossed nicols. This type of replacement has been observed only in the Alibates Formation.

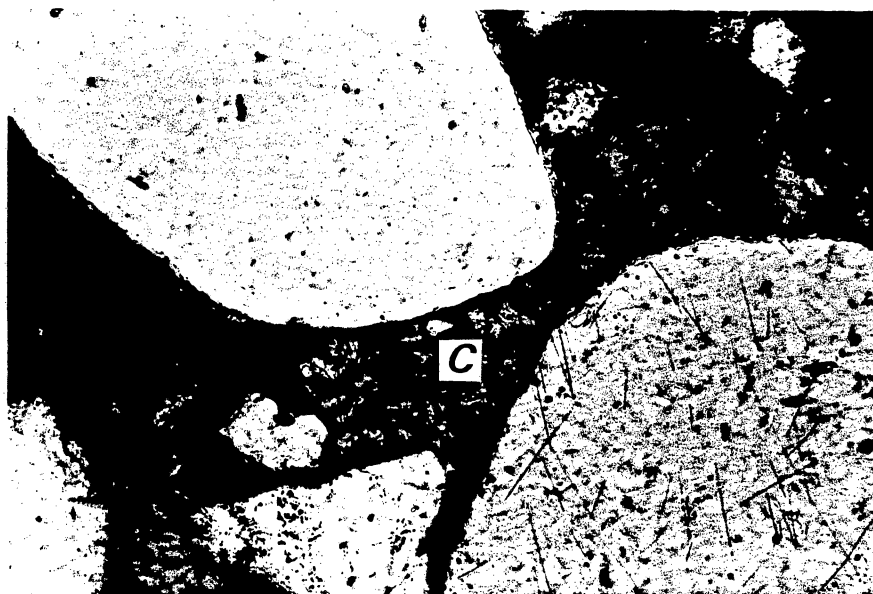


Figure 73. Calcite cement (C) in bimodal eolian sandstone, Dewey Lake Formation, DOE-Gruy Federal Grabbe No. 1 core, 740.9 ft, width 0.85 mm, crossed nicols. Calcite-cemented sandstone is observed only in the Dewey Lake Formation because of early removal of halite cement.



Figure 74. Calcite (white) replacing coarse euhedral gypsum crystals in mudstone. The coarse crystals are unlike any found in the younger dissolution zone or in the unaltered salt section and are interpreted to have formed during an early dissolution event. Invading ground water first mobilized sulfate and reprecipitated it as coarse gypsum crystals, which were then replaced by calcite. Stone and Webster Engineering Corporation Mansfield No. 1, 585.0 ft, width 7.7 mm, plane light, Salado-Tansill Formations.



Figure 75. Microfaulting and folding typical of the Alibates Formation, Stone and Webster Engineering Corporation Harman No. 1 core, 1,096 ft.

## TEXTURAL CLASSIFICATION OF SALT WITH GENETIC SIGNIFICANCE

Susan D. Hovorka

*A classification of halite based on crystal size, crystal shape, amount and composition of impurities, distribution of fluid inclusions, and characteristic sedimentary structures has been developed from examination of cores of Upper Permian bedded salt from the Palo Duro Basin. Eight classes are characterized by a variety of fabrics, from those that originated as primary brine-pool precipitates to those that formed during diagenesis.*

Analysis of nine cores through Permian bedded halite in the Palo Duro Basin has required development of a classification of halite textures. Most of the halite studied in detail has been from the San Andres Formation units 4 and 5, although similar fabrics occur in the selected intervals from other parts of the Permian section examined. Halite is classified on the basis of examination of slabbed core; however, geochemical and petrographic studies have aided in the development of this classification.

The fabrics used to classify halite and the resulting eight classes are shown in table 10. Each halite type is identified by a letter symbol, used for measured sections and geochemical data, and a type name. Typical crystal size, shape, composition and location of impurities, and fluid inclusion distribution are given for each type. The associated halite types, a summary of identifying characteristics, and a sketch of typical fabric are shown. The first five classes (chevron halite rock; color-banded, vertically oriented halite rock; chaotic mudstone-halite rock; equant muddy halite rock; and equant anhydritic halite rock) are fabrics arranged, left to right, from those showing the most primary fabrics to those showing the most altered fabrics. The remaining three classes of halite (displacive halite, cavity-filling halite cement, and fibrous fracture-filling halite cement) are fabrics produced by halite introduced into sediments during diagenesis.

Chevron halite rock (type A) is characterized by abundant minute (less than 50-micron) fluid inclusions. Variation in the density and size of the inclusions defines relict growth faces of the crystals (chevron structures), showing that the crystals grew upward as a crust on the brine-pool floor (fig. 76). Most crystals are elongated vertically

as a result of competition for space. Truncation surfaces formed by lowered salinity, probably during addition of marine-derived brine not yet evaporated to halite saturation, are visible as and anhydrite partings (figs. 77 and 78). Anhydrite in partings as well as between crystals is the most common impurity in chevron halite, typically 1 to 5 percent of the rock, and in combination with the abundant fluid inclusions imparts a conspicuous white color to the rock.

The fabric of chevron halite in almost all examples has been disturbed by recrystallization along grain boundaries and by formation of karst pipes and pits. Karst pits are several centimeters wide and 10 cm to as much as 2 m deep and can be recognized as areas where primary fabrics have been dissolved and the cavity filled with coarse, clear halite cement and/or concentrations of siliciclastic mudstone (figs. 79 and 80). The floors of pits are blanketed with anhydrite or mudstone left as a residue when the halite was dissolved. Pipes are narrow (1-cm-wide), anastomosing, vertical flaws in the halite where halite was recrystallized or dissolved, presumably along fractures that have now been healed. Pits and pipes appear to have been superimposed on brine-pool fabrics during episodes when the brine-pool dried up and the halite was exposed to corrosion by meteoric water. Many but not all pits and pipes can be traced upward to mudstone beds that are thought to have been deposited on the surface during the formation of pits and pipes.

Color-banded, vertically oriented halite rock (type B) resembles chevron halite rock in the abundance of anhydritic partings and the vertical elongation of the crystals, but the minute fluid inclusions and the chevrons they define are absent. Dark color due to trace amounts of clay and organic material is typical. Variations in the intensity of the color define bedding (color banded) (figs. 80 and 81). Vertically oriented crystals, anhydrite partings, and color bands are commonly associated but occur separately in a few intervals. Color-banded, vertically oriented halite rock, like chevron halite rock originated as a brine-pool precipitate. The difference in fabric is due to as-yet-unidentified subtly

different environmental conditions. Color-banded, vertically oriented halite rock contains abundant pits and pipes.

Chaotic mudstone-halite rock (type D) is composed of masses of siliciclastic mudstone between relatively coarse, euhedral to anhedral halite crystals (figs. 81 and 82). No bedding is preserved, and the origin of this fabric is in many examples enigmatic. A model for formation of chaotic mudstone-halite rock has been developed on the basis of examination of intervals in which some texture is preserved. The parent material was color-banded, vertically oriented or chevron halite rock. Extensive alteration during prolonged exposure resulted in destruction of most primary fabric by the formation of pits and pipes and recrystallization of halite. Mudstone accumulation was favored by several factors: (1) The dry condition of the flat prevented precipitation of halite, but input of fine siliciclastic material, probably fallout from duststorms, continued in this environment. (2) The dry condition of the flat favored transportation of siliciclastics by fluvial and sheetwash processes. (3) Impurities in the halite were concentrated at the surface and on pit floors as halite dissolved. Any or all of these processes result in accumulation of mudstone at the surface and within pits. A second process contributing to the development of chaotic disrupted fabric in chaotic mudstone-halite rock is displacive growth of halite crystals within the sediment. This halite precipitated when halite-bearing waters of either marine or meteoric origin were evaporated from the flat. Repetition of the sequence of pipe and pit formation followed by precipitation of displacive halite produces the chaotic fabric characteristic of chaotic mudstone-halite rock.

Equant muddy halite rock (type E) is a catch-all class for halite with no identifiable primary fabric and no evidence of the kind of intense alteration that has affected chaotic mudstone-halite rock. A minor amount (1 to 10 percent) of mudstone is present, but it is not concentrated in pits or in beds (fig. 83). The origin of this fabric is not clear, and possibly not all intervals identified as equant muddy halite rock have the same origin. This fabric, under certain conditions, formed from color-banded, vertically oriented halite that



recrystallized under the influence of waters penetrating along grain boundaries or along now-obscure fractures. In other circumstances, a minor amount of claystone or gypsum deposited with halite may have released enough water during diagenesis to recrystallize halite. Some halite may have been deposited without fabrics recognized as primary, and would, therefore, fall into this class even though it had never undergone recrystallization.

Equant anhydritic halite rock (type F) is the equivalent of equant muddy halite rock without mudstone or with mudstone concentrated in scattered spots. Much of it appears to have formed as a result of recrystallization of chevron halite rock. A few scattered intervals have a salmon-pink color, suggesting that the invading waters may have altered a few percent gypsum or anhydrite to polyhalite. The mineralogy of these intervals has not been determined by petrography or geochemistry.

Displacive halite (type G), in contrast to the halite rock types discussed previously, is a minor element in other lithologies. Displacive halite is a common constituent in mudstone and siltstone beds, especially those associated with halite rock. Displacive halite also occurs in anhydrite beds within, beneath, or overlying halite rocks, and in a few locations is found within carbonate rocks close to halite. Displacive halite forms cubes, slightly skeletal crystals (hopper crystals), and extremely skeletal crystals (fig. 84).

Cavity-filling halite cement (type H) is most abundant as a filling in karst pits. In these locations the crystals can be extremely coarse, in many examples larger than the 10 cm core width (fig. 85). In some examples, the presence of a pit is deduced from the presence of an interval of very coarse halite. The cavity-filling halite cement is typically clear, clean halite with large fluid and vapor-filled inclusions. Impurities associated with the halite are the insoluble residue that typically defines the pit floor and anhydrite and mudstone that fell into the pit as cement was precipitating. Halite cement is abundant in other lithologies, especially sandstone and carbonate grainstones.

Fibrous fracture-filling halite cement (type I) is common throughout the halite section, especially in mudstone interbeds within halite rock. It also occurs within fractures

in carbonate rocks and dark anhydritic mudstone beds at the base of cycles (fig. 86). Halite-filled fractures do not occur in anhydrite beds, apparently because any fractures that developed were healed by anhydrite. The fibrous fracture-filling halite is very similar in appearance in all lithologies. It characteristically has a deep-orange color. All fractures are vertically oriented and most do not appear to widen upward toward paleosurfaces, indicating that they are formed in the subsurface. A few examples examined in thin section are tentatively thought to have formed later than most diagenetic features such as multifaceted dolomite and anhydrite but before precipitation of these phases ceased. Fibrous halite precipitation, therefore, occurred as one of the last early diagenetic process.



Figure 76. Minute fluid inclusions concentrated along relict growth faces of bottom-nucleated halite crystals defining chevron structures. Thin section, width 7.7 mm, plane light, from the San Andres Formation, unit 5 at 1,377 ft in the Stone and Webster Engineering Corporation Mansfield No. 1 core.

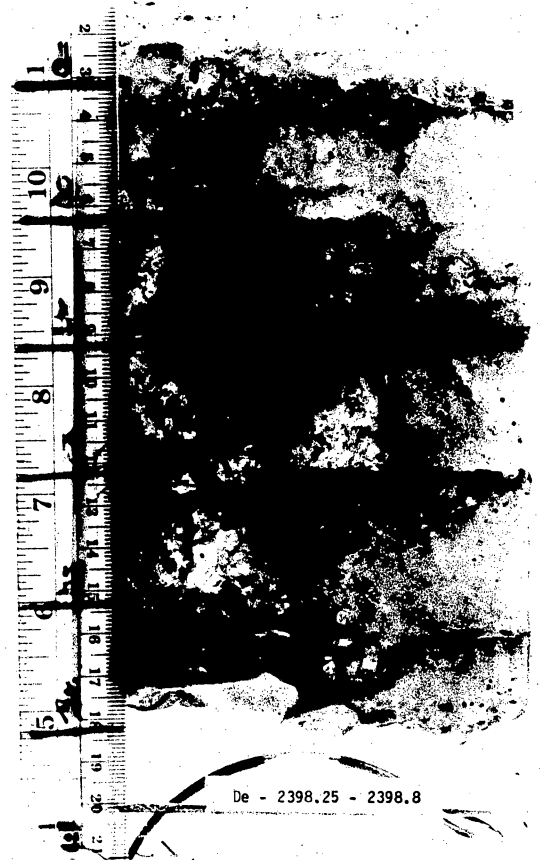


Figure 77. Typical chevron halite rock from unit 5 of the San Andres Formation, Stone and Webster Engineering Corporation Detten No. 1 core, 2,398.2 ft. Note the white color of the halite due to abundant fluid inclusions. Darker bands are truncation surfaces marked by anhydrite.



Figure 78. Photomicrograph of chevron halite truncated by a corrosion surface above which anhydrite (A) has been deposited. Width 3.25 mm, plane light, from unit 5 of the San Andres Formation, depth 1,438.0 ft, Stone and Webster Engineering Corporation Mansfield No. 1 core.



Figure 79. Dark pit filled with coarse, muddy halite and formed by dissolution, introduction of mudstone, and recrystallization of primary chevron halite rock along a vertical fracture. Top of core shown is a mudstone bed that may have been at the sediment surface during development of karst. The upper 12 cm of the core is chaotic mudstone-halite (M) formed by diagenetic alteration of halite rock during exposure. Core is from unit 4 of the San Andres Formation, Stone and Webster Engineering Corporation G. Friemel No. 1, depth 2,531 to 2,539 ft.

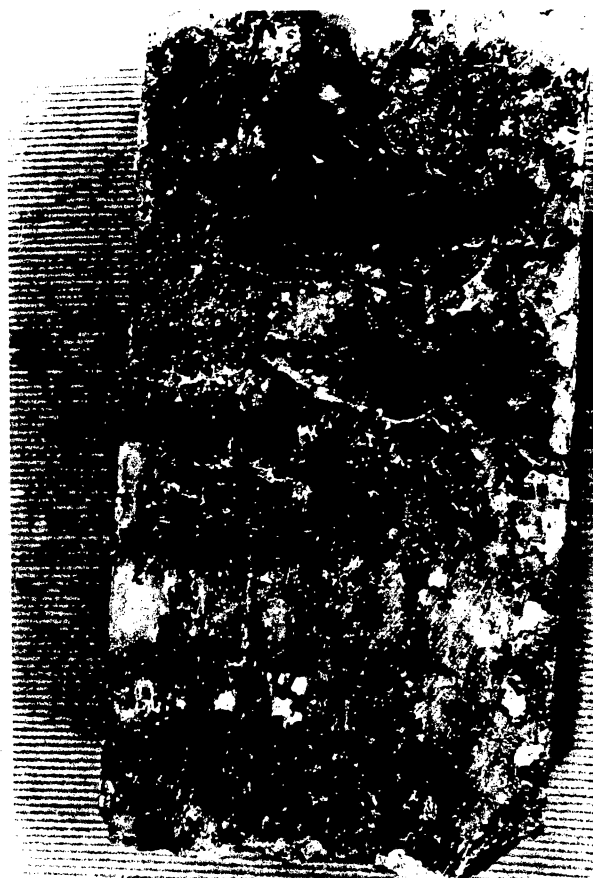


Figure 80. Pit filled with coarse cavity-filling halite cement in color-banded, vertically oriented halite host. Pit is outlined. Core is 10 cm wide, from unit 4 of the San Andres Formation, Stone and Webster Engineering Corporation G. Friemel No. 1, depth 2,580 ft.

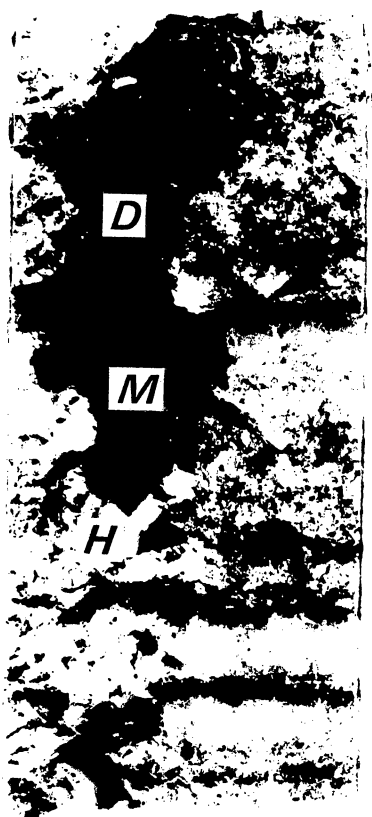


Figure 81. Pit in color-banded, vertically oriented halite filled with, in succession, (1) halite cement (H), (2) siliciclastic mudstone (M), and (3) displacive halite cubes (D). Core is from the upper San Andres Formation, Stone and Webster Engineering Corporation Zeeck No. 1 well, depth 2,039.4 ft.

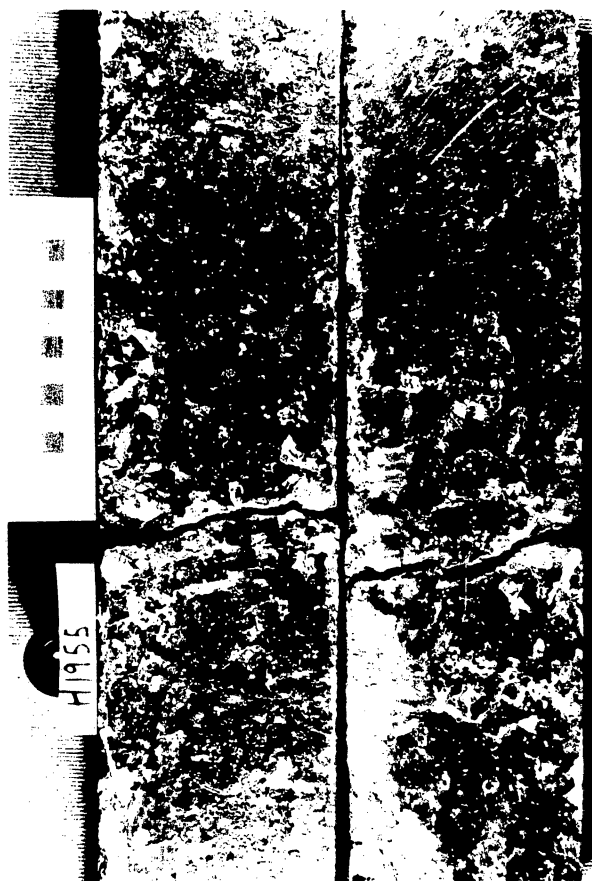


Figure 82. Typical chaotic mudstone-halite rock in which primary fabric has been destroyed. Core from the upper San Andres Formation, Stone and Webster Engineering Corporation Harman No. 1 well, depth 1,955 ft.



Figure 83. Recrystallized muddy halite rock from a halite interval within the Queen-Grayburg Formations. The recrystallization is intense in this rock, probably because of interaction with meteoric water either in the depositional environment or when this interval was penetrated by ground waters. Core from Stone and Webster Engineering Corporation Zeeck No. 1, depth 1,909.0 ft.



Figure 84. Displacive halite cubes in mudstone beds, unit 5, San Andres Formation, Stone and Webster Engineering Corporation Mansfield No. 1 core, depth 1,494 ft.



STONE & WEBSTER  
#1-MANSFIELD

0 10 cm  
1276 ft.



Figure 85. Cavity-filling halite cement forms very coarse crystals (H) in a pit in color-banded halite rock. The floor of the pit is draped with anhydrite-mudstone insoluble residue (IR). Core from unit 4, San Andres Formation in the Stone and Webster Engineering Corporation Mansfield No. 1 well, 1,276 ft.

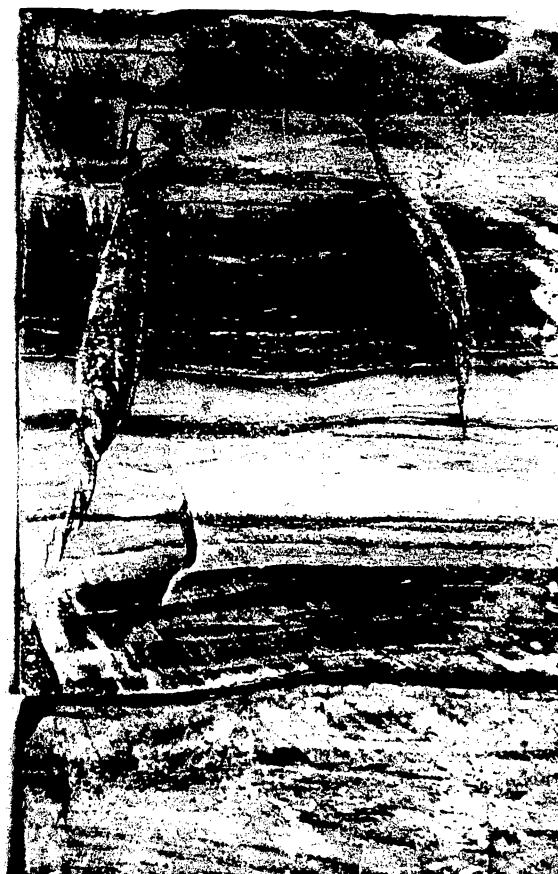


Figure 86. Fibrous halite fracture-fill in carbonate mudstone of unit 4, San Andres Formation, Stone and Webster Engineering Corporation Mansfield No. 1 core, depth 1,930.5 to 1,933.5 ft.

Table 10. Textural classification of halite with genetic significance.

Symbol	A	B	D	E	F	G	H	I
halite type	chevron halite rock	color-banded, vertically oriented halite rock	chaotic mudstone-halite rock	equant muddy halite rock	equant anhydritic halite rock	displacive halite in other sediments	cavity-filling halite cement	fibrous fracture-filling halite cement
halite crystal size	0.5-5 cm tall	0.5-5 cm tall	0.3-3 cm	1-5 cm	1-5 cm	0.5-3 cm	1-20+ cm	0.3-1 cm
halite crystal shape	subvertical mosaic; L:W = 3:2 to 4:1	subvertical mosaic; L:W = 3:2 to 4:1	equant anhedral to euhedral crystals	equant mosaic	equant mosaic	euhedral cubes or hopper shapes	equant mosaic	fibrous
composition	anhydrite common; mudstone possible	anhydrite, mudstone, organic	mudstone, minor anhydrite	mudstone, minor anhydrite	anhydrite	mudstone; also dolomite, anhydrite	cavity-filling halite is clean but is associated with mudstone and anhydrite insoluble residues	trace of hematite present as coloring agent, otherwise pure halite
percentage	1-5%	1-5%	10-50%	1-10%	1-25%	50-99%		
location	anhydrite on grain boundaries, partings, mudstone only in pipe fills	within and between grains, along partings, in pipes	in masses between halite crystals, some also within grains	within grains, minor between grains	along partings, grain boundaries	matrix for halite		
fluid inclusions	abundant, small, define relict growth facies	varied	few	varied	varied	few	large and abundant	?
associated with halite types	F along crystal boundaries and pipes, H and/or D in pipes	F & E, H and/or D in pipes	mudstone beds typically includes remnant B halite	may contain remnant A, B, possible H	may contain remnant A, B, possible H	non-halite rocks	all halite types	in non-halite rocks
identifying characteristics	minute fluid inclusions along relict halite growth faces	bedding and/or vertical orientation of crystals	10-50% mudstone in intercrystalline masses, chaotic texture	halite colored red brown or black by 1-10% impurities, no fabric, no bedding	halite with 1-25% anhydrite, no fabric, no bedding	euhedral to subhedral halite crystals in sediments	exceptionally coarse clear crystals, fill cavity in other salt type	fibrous halite in fracture, many examples red colored
sketch								

## CYCLICITY IN THE SAN ANDRES FORMATION

Susan D. Hovorka

*Partial and complete regressive sequences, composed of a basal dark mudstone, limestone, dolomite, nodular anhydrite, bedded anhydrite, and halite, occur throughout most of the San Andres Formation. Even subtle variations in sediment character can be recognized over large distances within the Palo Duro Basin. The continuity of these units reflects the extremely flat topography of the area during deposition and implies that throughout the area studied similar sediments were forming contemporaneously.*

Reconnaissance work in the Palo Duro Basin identified five cycles in the lower San Andres Formation on the basis of interpretation of geophysical log response (Presley, 1979b). Examination of parts of nine cores drilled in the northern part of the Palo Duro Basin has improved understanding of the nature of these cycles. Fracasso (this volume) has traced cycles throughout the Palo Duro Basin and into adjacent areas.

A typical cycle is composed of a basal anhydritic dark mudstone, skeletal limestone, dolomite, nodular anhydrite, bedded anhydrite, and halite. This sequence forms as the result of gradually increasing salinity of the depositing water body (fig. 87).

Basal anhydritic dark mudstone accumulated during transgression as marine waters dissolved the halite of the underlying cycle and red mudstone and anhydrite interbeds within the halite remained as a residue. The upper part of some mudstone beds is ripple laminated, or fissile and organic-rich, and represents sediments deposited during transgression (fig. 88). The dark color of the mudstone is characteristic and reflects pyrite and organic material.

The carbonate part of the cycle is composed of a limestone overlain by dolomite. Facies variations within the limestone are due to migration of high-energy bar sediments across lower energy interbar sediments (fig. 89). The dolomite in the upper part of the carbonate cycle was deposited during initiation of hypersaline conditions. Skeletal grains are sparse or absent and rippled ooid or coated grain grainstone and carbonate mudstone drapes are the most typical sediments.

The anhydrite part of the cycle displays a consistent, well-formed sequence (fig. 90). The contact between anhydrite and dolomite is gradational. Anhydrite nodules are found in the upper few tens of centimeters of the dolomite. Nodular anhydrite mosaic with and without internodular dolomite makes up the lower part of the anhydrite unit, whereas bedded anhydrite with halite or anhydrite pseudomorphs after gypsum constitutes the upper part. Near the top of the anhydrite, halite replaces not only large gypsum crystals but also much of the sulfate matrix, leaving the remaining anhydrite as coarser felted blades in halite cement.

Halite rock with anhydrite and mudstone interbeds and disseminated impurities forms the upper part of each cycle. The halite part of the cycle does not show a well-developed sequence in textures or geochemical profiles but is composed of 1- to 4-m-thick sequences of muddy and anhydritic halite (Hovorka, this volume, "Correlation of Clean, Muddy, and Anhydritic Zones in Halite...").

Cycles in the San Andres Formation differ from the idealized cycle in four ways: (1) The initiating transgression may not bring normal marine water into the study area, so the lower units of the idealized cycle may not be deposited; therefore, the cycle may begin with dolomite, nodular anhydrite, or bedded anhydrite above a thin residue; (2) The cycle may be aborted by another transgression before halite deposition is reached, causing the upper units of the ideal cycle to be missing; (3) The halite at the top of the cycle may be completely removed during the transgression at the base of the next cycle; and (4) The cycle may be interrupted at any stage by introduction of clastics. San Andres unit 5 is a composite of three incomplete cycles (fig. 91). The first cycle was initiated by a transgression that lowered the salinity only to anhydrite saturation and produced a thin residue. The transgression initiated the second cycle, which deposited ripple laminated dolomite and nodular and bedded anhydrite with halite pseudomorphs after gypsum. The third transgression wavered between dolomite and nodular anhydrite deposition before producing bedded anhydrite with pseudomorphs after gypsum, and finally, halite. The

anhydrite bed within the halite might represent the updip pinch-out of a fourth cycle. The lower two cycles probably deposited some halite that was removed by the next transgression. Evidence of the former presence of halite is (1) the presence of fabric similar to that characteristic of the contact between the anhydrite and overlying halite, (2) the influence of halite-saturated brines on the diagenesis of the anhydrite, notably the halite pseudomorphs after gypsum, and (3) the presence of dark anhydritic mudstone insoluble residue (fig. 92).

Subtle variations in the sequence of salinity-controlled facies can be correlated across the northern Palo Duro Basin study area (fig. 93). The occurrence of subtle changes across all the cores indicates that, although the water depths were very shallow, sediments in the study area were deposited from a continuous, extensive water body. The westernmost core, Stone and Webster Engineering Corporation Mansfield No. 1, shows a pattern of cyclicity similar to other wells, but the facies present in some cycles differ from the facies present in the equivalent cycles in other wells. The facies differ both by being deposited from water of nearly normal marine salinity (burrowed dolomite rather than anhydrite at 1,140 to 1,150 ft, halite removed at 1,229 ft) and by being deposited by more hypersaline water (deposition and/or preservation of a thicker halite unit at 1,152 to 1,180 ft). The Mansfield well is located in a structurally complex area near the western end of the Amarillo Uplift, where variable subsidence may have influenced sedimentation. Comparison of lithology and structures of additional cycles in more cores will improve understanding of the controls on continuity and variation of facies in the Palo Duro Basin.

# TYPICAL SAN ANDRES CYCLE

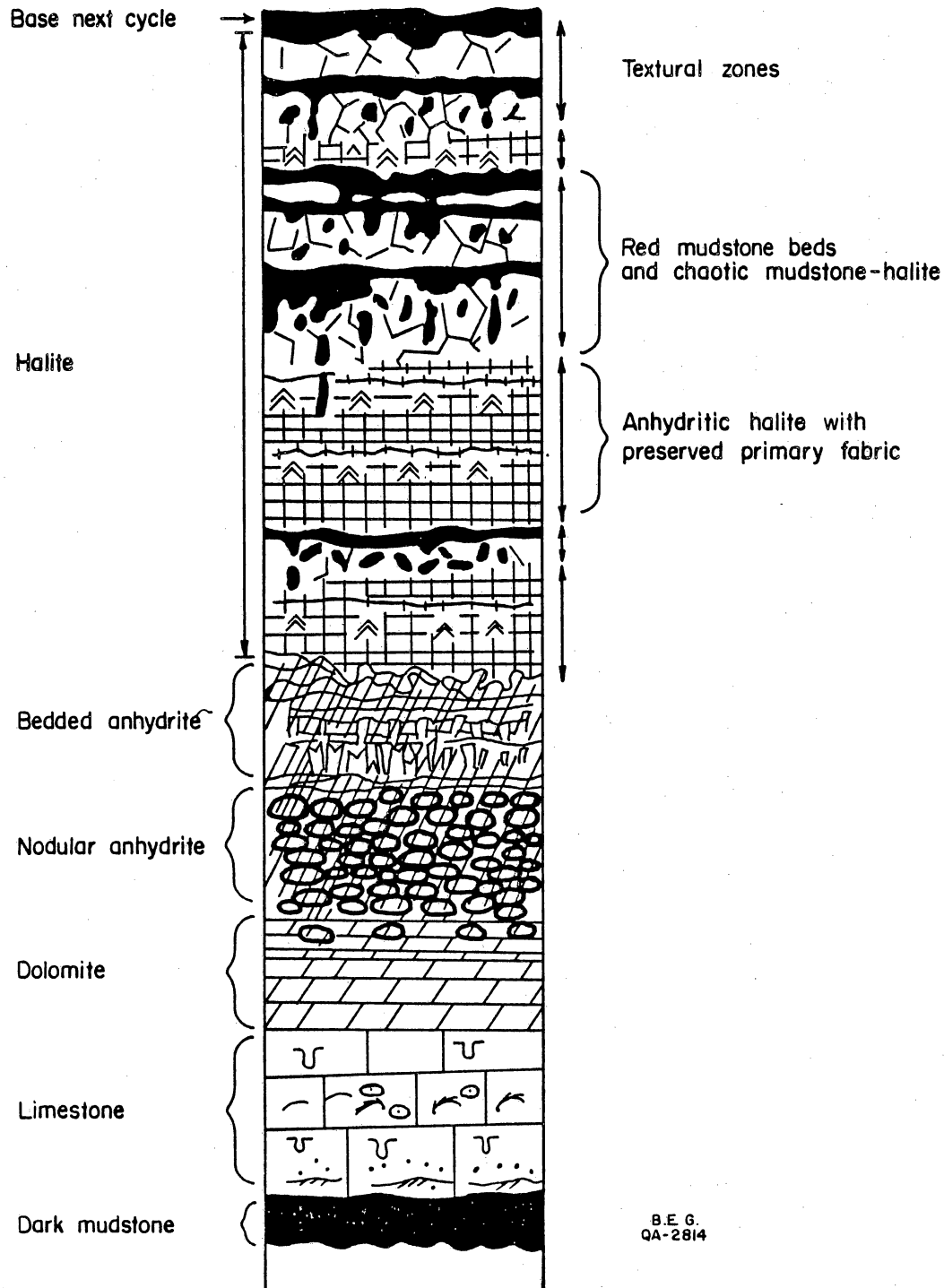


Figure 87. Idealized San Andres cycle showing sequence of lithologies and sedimentary structures that would result from an uninterrupted increase in salinity.



Figure 88. Dark mudstone at the base of a cycle. The lower part is strongly disrupted mudstone with light patches of anhydrite that accumulated as a residue of the insoluble components left as their halite host was dissolved during transgression. The upper 4 cm of the core piece is finely ripple-laminated and originated either by input of additional clastics or by reworking of the top of the residue. Stone and Webster Engineering Corporation Detten No. 1 core, depth 2,288 ft, upper San Andres Formation.

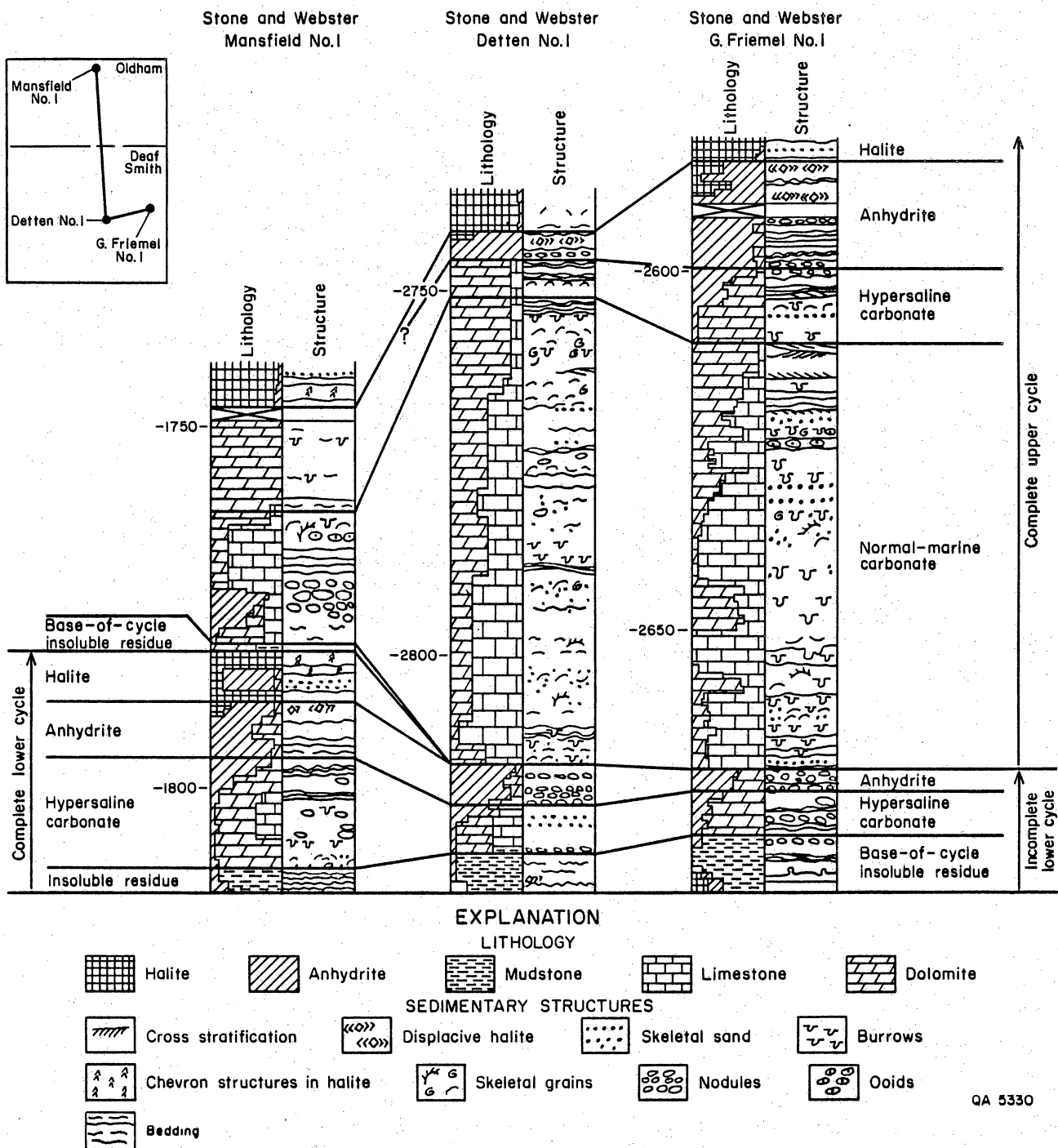


Figure 89. Correlation of San Andres Formation unit 4 carbonate showing that facies in the marine-limestone part of the interval are the result of variations in the energy of the depositional environment. Increasing salinity is an important control on facies only at the top of the carbonate sequence. The base of the carbonate is an incomplete cycle exhibiting the effects of increasing salinity and is tentatively correlated with halite deposition in the Stone and Webster Engineering Corporation Mansfield No. 1 core.



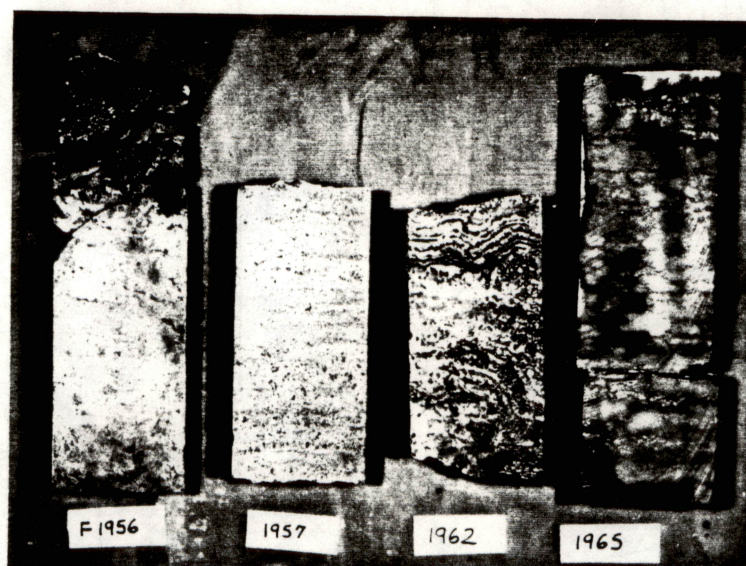


Figure 90. Examples of sequence of lithologies in the anhydrite part of the cycle. The vertical sequence (shown from left to right) is (1) nodular anhydrite with internodular dolomite at the base, (2) bedded anhydrite, (3) bedded anhydrite with halite pseudomorphs after gypsum, and (4) top of the anhydrite unit and base of the overlying halite, where anhydrite fabric has been extensively altered during diagenesis by halite-saturated water. Examples from Stone and Webster Engineering Corporation G. Friemel No. 1, upper San Andres Formations, depths 1,967.5, 1,962, 1,957, and 1,956 ft, core width 10 cm.

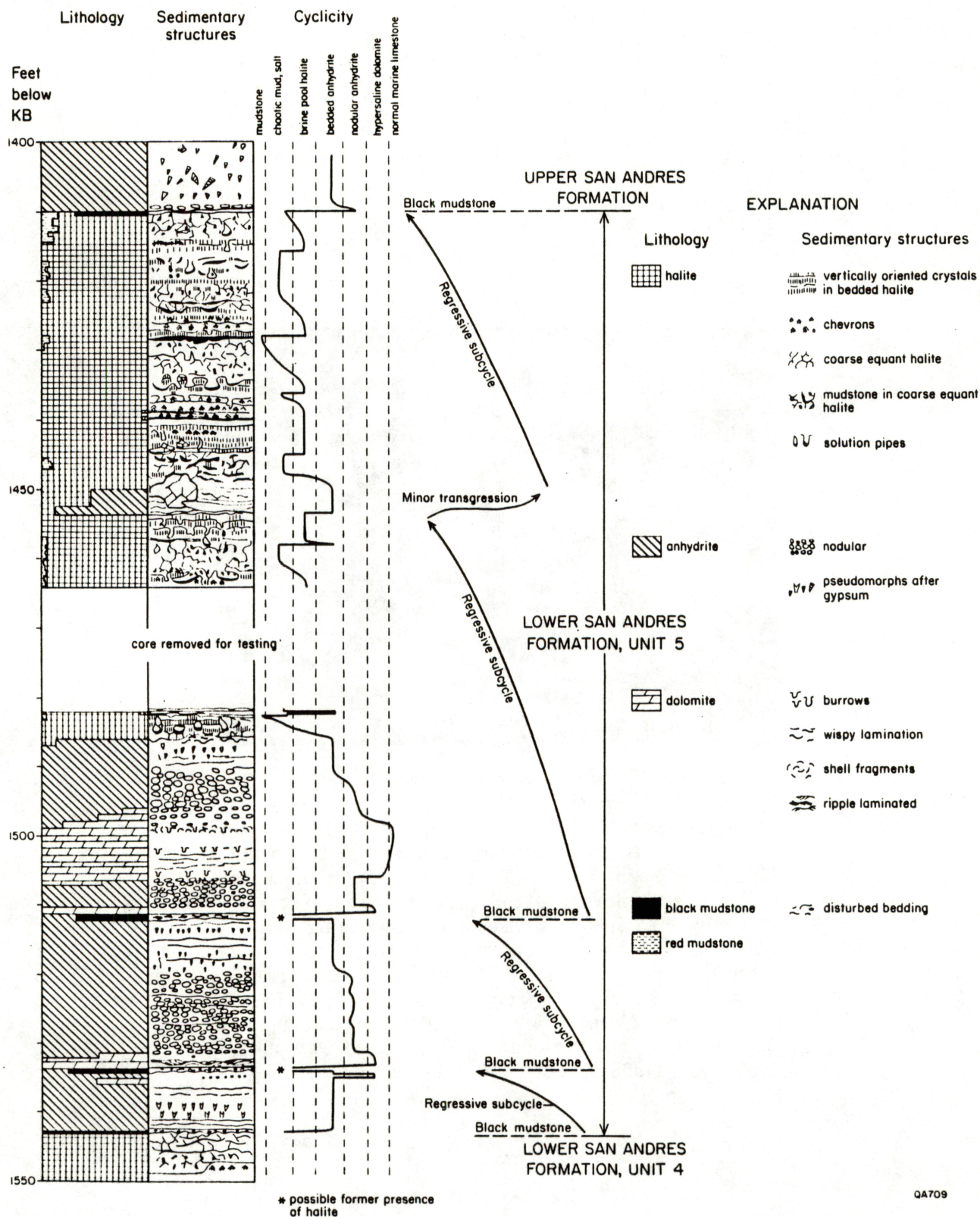


Figure 91. Cyclicity in San Andres unit 5, Stone and Webster Engineering Corporation Mansfield No. 1 core. The unit 5 is a composite of three incomplete cycles, each initiated by a transgression that dissolved any halite deposited by the previous cycle. The anhydrite-depositing minor transgression within the halite part of the upper cycle did not dissolve enough halite to form a residue.





Figure 92. An incomplete cycle in the upper San Andres Formation Stone and Webster Engineering Corporation Detten No. 1 core, depth 2,357 ft. Mudstone insoluble residue in the top 10 cm of the core (M) formed by accumulation of insoluble components when halite was removed by the transgression that initiated the next cycle. Other evidence that halite was initially deposited is the abundant halite pseudomorphs after gypsum in the lower part of the core (H), indicating halite-saturated waters were important in earliest diagenesis, and the area of disturbed fabric at the top of the core (D) where removal of halite has altered fabrics like those seen in figure 90 at the anhydrite-halite contact.

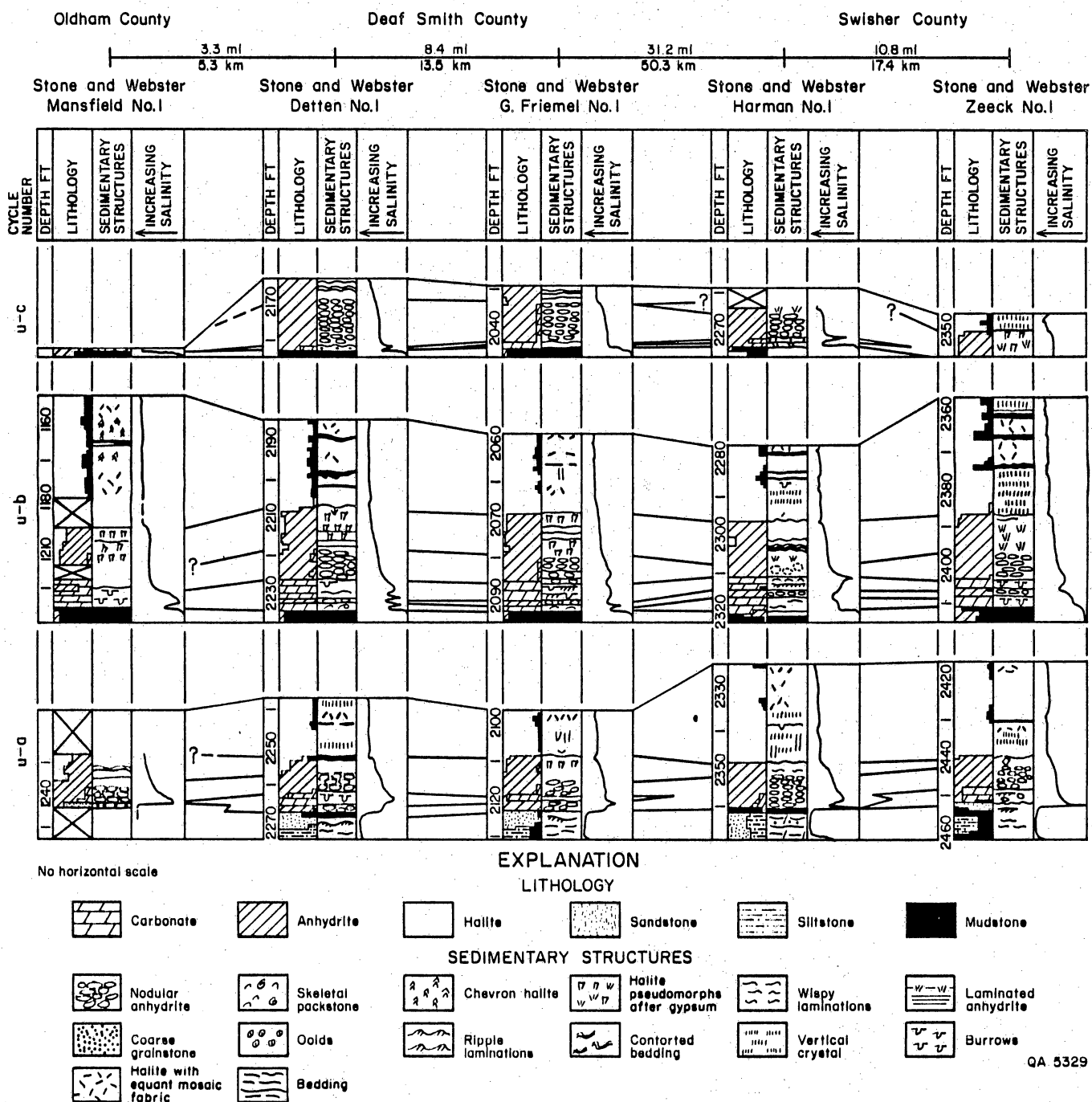


Figure 93. Correlation of three thin cycles in the upper San Andres Formation across the northern Palo Duro Basin, showing the continuity of subtle variations in the nature of cyclicity. The sandstone bed that truncates the lowest cycle shown is the regional "pi" marker bed.

# GEOCHEMICAL AND TEXTURAL EVIDENCE OF PRIMARY AND ALTERED HALITE, PERMIAN SAN ANDRES FORMATION, PALO DURO BASIN, TEXAS

R. Stephen Fisher and Susan D. Hovorka

*Thick-bedded halite units of the San Andres Formation precipitated in shallow but regionally extensive brine pools that were frequently and episodically flooded and subaerially exposed. Previously unrecognized 1- to 6-ft-thick subcycles within salt units are characterized by primary textures and bromide contents of about 70 ppm at the base, altered textures and variable bromide concentrations near the top, and a thin mudstone cap containing halite veins having high bromide contents (as much as 342 ppm).*

Bromide (Br) content of halite has been used as an indicator of geochemical conditions prevalent when halite was precipitated (Holser, 1979). Sea water is the dominant reservoir of Br in sedimentary environments, and the distribution coefficient of Br in halite is such that the first crystals formed from evaporating sea water will contain approximately 65 ppm Br. With continued evaporative concentration of the brine, the Br content of halite will increase to about 250 ppm at the onset of sylvite precipitation. Dissolution in a halite-undersaturated solution and subsequent concentration-precipitation will result in halite with Br concentrations lower than 65 ppm (Holser, 1979).

Classic thick halite deposits typically have depth-versus-Br profiles in which Br concentrations change smoothly across vertical distances of 100 ft or more (fig. 94). The well-developed regressive sequence of lithologies characteristic of the San Andres Formation (black mudstone-limestone-dolomite-nodular anhydrite-bedded anhydrite-halite) suggests that a similar sequence of systematically changing brine composition should be reflected in the Br content of San Andres halite. However, such orderly profiles are absent (Handford, 1981; Fisher and Kreitler, 1983; figs. 95, 96, and 97), which suggests frequent short-term fluctuations in geochemical conditions rather than an overall trend of continued evaporative concentration of a large volume of brine for a long period of time.

Textural and geochemical evidence indicates that halite precipitation occurred in shallow but regionally extensive brine pools that were episodically flooded and subaerially exposed. Within individual halite units, 1- to 6-ft-thick subcycles resulting from frequent,

brief interruptions of halite precipitation have been recognized from textural characteristics. These subcycles contain primary textures (chevrons and vertical crystals) at the base, altered and disrupted textures (chaotic mud-salt mixtures, replacive, displacive, cavity-fill, and recrystallization features) near the top, and a thin mudstone cap, commonly containing red, fracture-filling halite veins (fig. 98). Halite having primary chevron-shaped growth bands defined by fluid inclusions has Br concentrations ranging from 55 to 82 ppm (average 70 ppm), indicating that evaporative concentration did not proceed much beyond the point of initial halite saturation because of continual communication with the marine environment. Episodic influx of less saline brine resulted in dissolution of a minor amount of halite and precipitation of a thin anhydrite layer on the corroded surface (fig. 99). Continued evaporation brought the brine pool back to halite saturation, and halite precipitation resumed. Cessation of continued influx of marine-derived brine resulted either in further evaporative concentration of the brine or in partial dissolution and recrystallization of halite in contact with fresh water. Highly variable Br concentrations (28 to 163 ppm) in the upper part of the subcycle resulted. Interruption of halite deposition permitted a thin mudstone bed to accumulate at the top of the cycle, a product of sheetwash and eolian transport of terrigenous clastic material. Halite that fills shrinkage cracks in these mudstone layers has Br concentrations as high as 342 ppm, recording precipitation from the most highly concentrated brine.

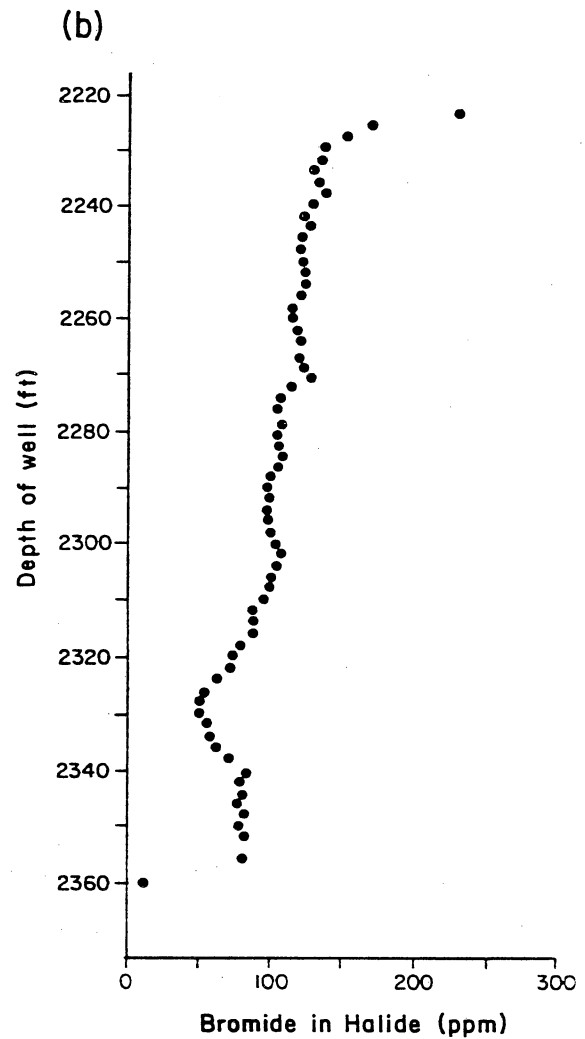
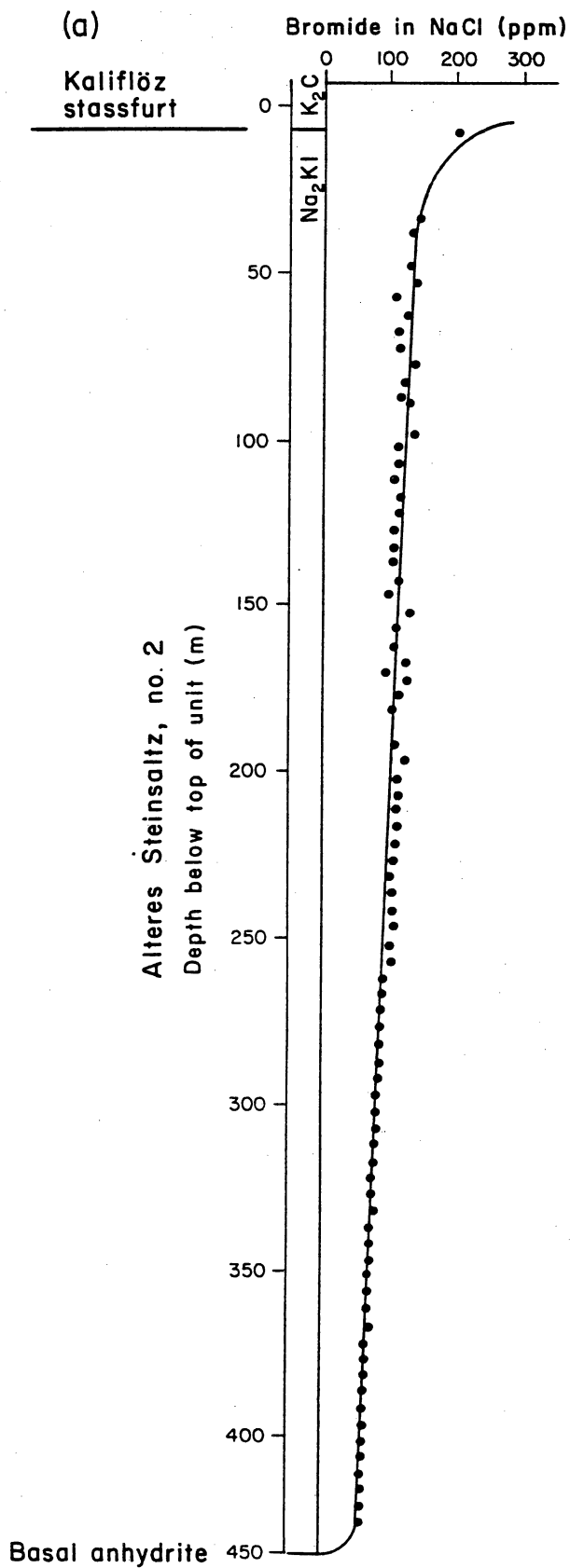


Figure 94. Typical bromide-versus-depth profiles: (a) Permian Zechstein unit 2 (Stassfurt Series), Aschersleben, Germany (DDR) and (b) Salt unit 3, Paradox Formation, Grand County, Utah.

QA5212

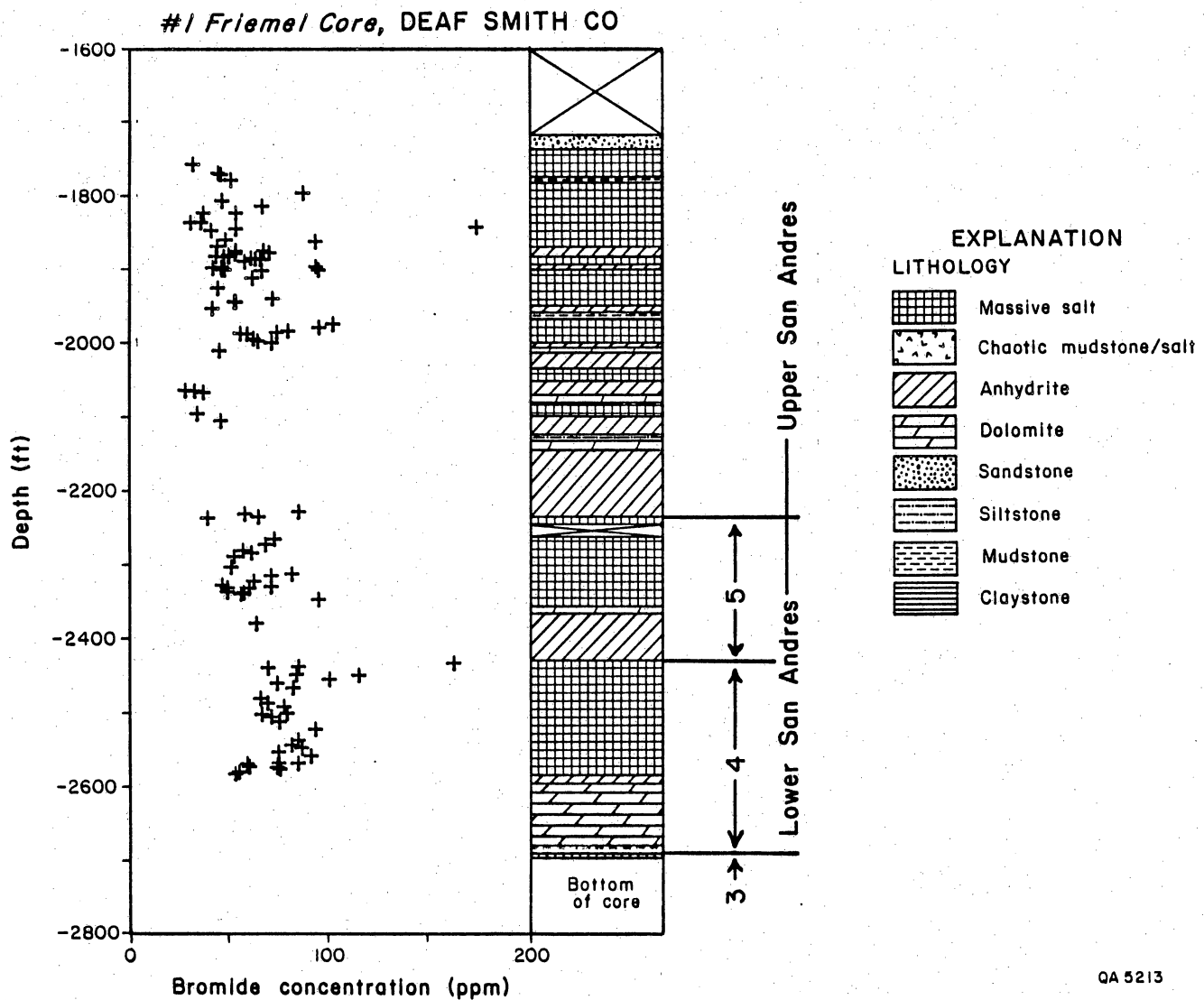


Figure 95. Bromide versus depth, San Andres Formation, Stone and Webster Engineering Corporation G. Friemel No. 1.



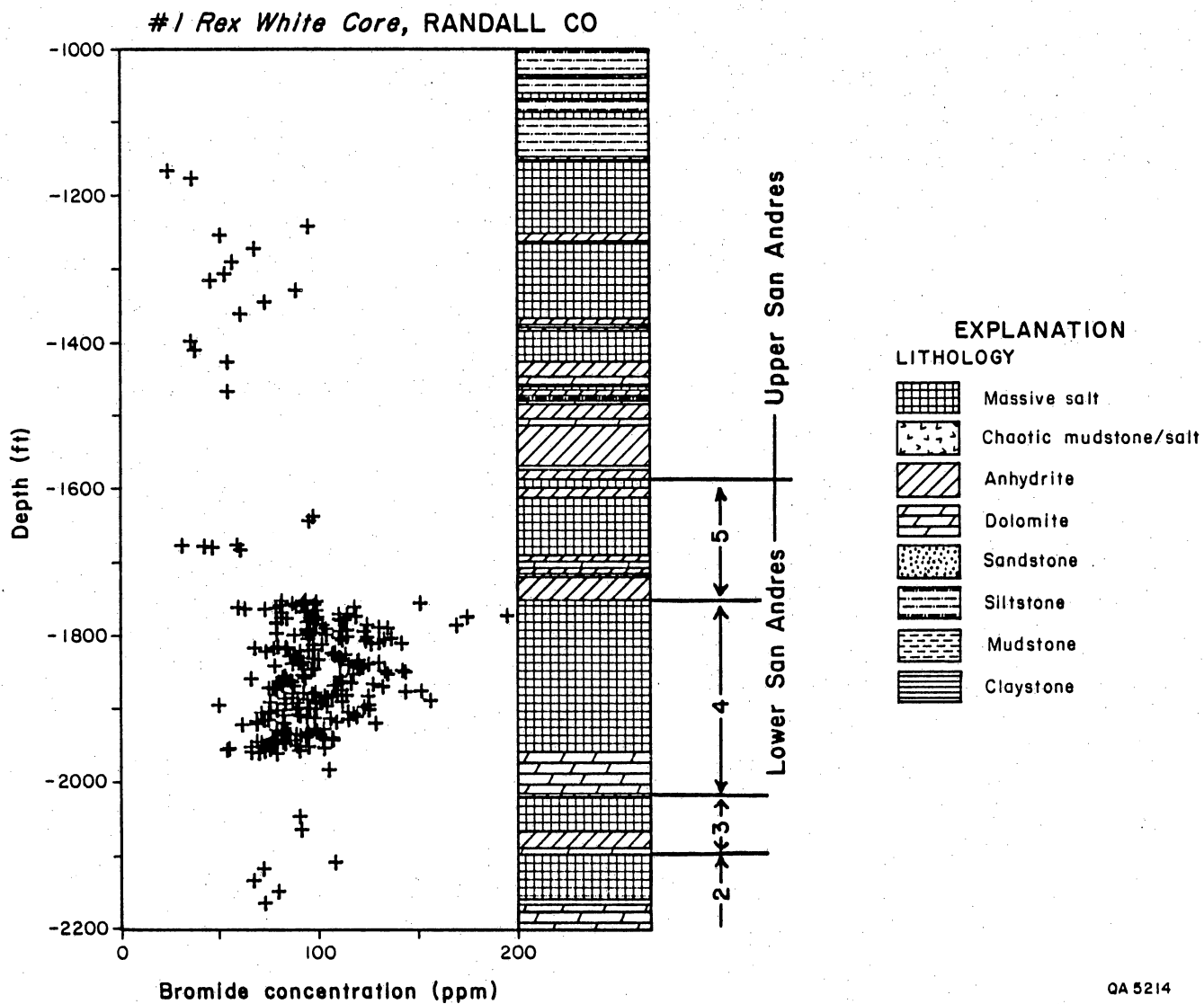


Figure 96. Bromide versus depth, San Andres Formation, DOE-Gruy Federal Rex White No. 1.

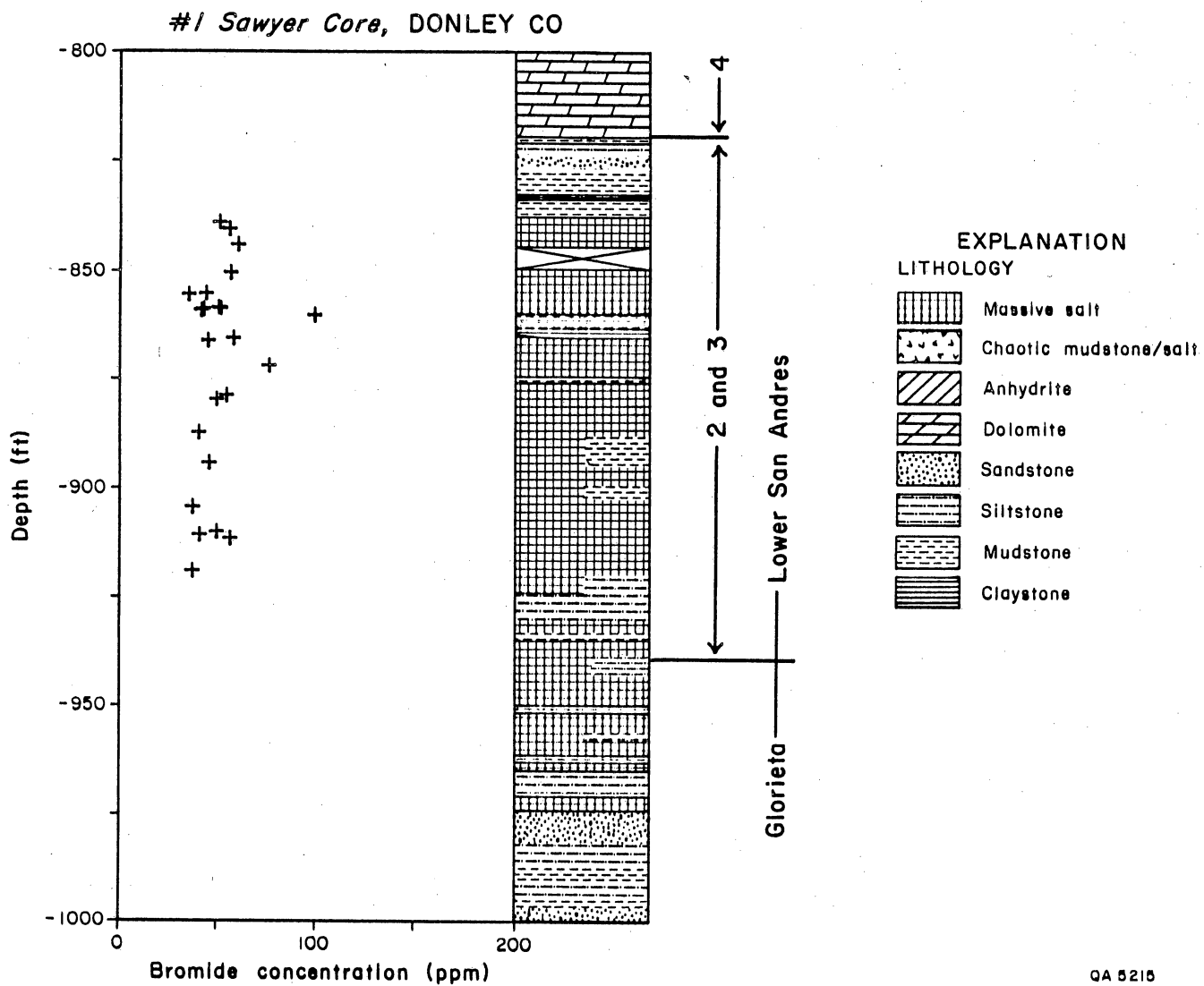


Figure 97. Bromide versus depth, San Andres Formation, Stone and Webster Engineering Corporation Sawyer No. 1.



Figure 98. Typical subcycle, Stone and Webster Engineering Corporation Detten No. 1 core.

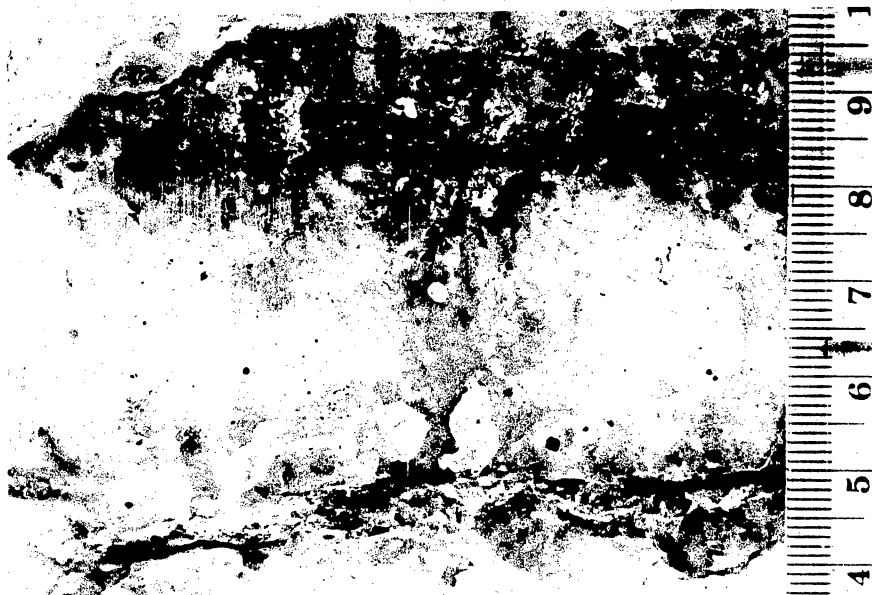


Figure 99. Type "B" halite with anhydritic bands, Stone and Webster Engineering Corporation Detten No. 1 core.

## CLAY MINERAL ASSEMBLAGES IN EVAPORITE HOST ROCKS, PALO DURO BASIN, TEXAS

R. Stephen Fisher

*Clay minerals in clastic rocks, dolomite, anhydrite, and halite in the Palo Duro Basin consist of detrital illite and chlorite, and diagenetic, mixed-layered, chlorite-vermiculite, chlorite-smectite, chlorite-swelling chlorite, and saponite. Illite dominates the detrital suite; the relative occurrence of mixed-layered clays is sensitive to geochemical conditions in the diagenetic environment.*

The abundance, type, and distribution of clay minerals in the Palo Duro Basin are significant both as controls on radionuclide transport and retardation and as indicators of the geologic history of the region. Clays commonly have a net-negative lattice charge, a capacity for expansion and contraction in response to wetting and drying, and a large surface area/volume ratio. The high cation-exchange capacity of clays, and thus their ability to retard radionuclide migration, is favorable for nuclear waste repository siting, whereas their expanding and contracting behavior and consequent physical instability is a disadvantage. Clastic layers, even if initially halite-cemented, are likely to be the preferred pathways for movement of halite-undersaturated fluids in an evaporite sequence consisting of dolomite, anhydrite, and halite, and clay minerals will be the most effective barrier to the transport of radioactive cations within the clastic units. Furthermore, the capacity of clay minerals to undergo changes in chemical composition or structure in response to the conditions of the depositional and subsurface environment enables their use as indicators of paleochemical conditions.

Palmer (1981) and Bassett and Palmer (1981) reported the clay mineral assemblage found in various lithologies from the DOE-Gruy Federal Rex White No. 1 and Grabbe No. 1 wells; the dominant clays found were chlorite-vermiculite, chlorite-smectite, chlorite-swelling chlorite mixed-layer phases, and discrete illite and chlorite (fig. 100). The cation exchange capacity and expansive nature of these clays are known, and the behavior of interlayered mixtures is predictable (Carroll, 1969; Weaver and Pollard, 1973). During the past year additional samples were analyzed, and X-ray diffraction patterns were inter-

preted and clay minerals identified according to criteria used by Bassett and Palmer (1981). These latest samples are the clay-sized methanol-insoluble fraction of salt samples selected for water-content analysis.

Figure 101 presents relative occurrences of clay minerals for three sample groups: (1) nonhalite rocks more than 10 ft (vertically) from bedded salt, (2) nonhalite rocks interbedded with salt, and (3) the insoluble residue of salt rocks. Chlorite-vermiculite occurs only in the clay fraction of rocks associated with salt; it is present in minor amounts in clastic rocks and dolomite interbedded with salt and is common in salt rocks (fig. 101). These observations, based partially on discussions in Palmer (1981), are interpreted as follows. The detrital clay assemblage in the Palo Duro Basin consists of discrete illite, chlorite, and mixed-layer illite-smectite. The progressive increase in chlorite-vermiculite occurrence from salt-free to salt-associated to salt-dominated environments (fig. 101) reflects the effects of clay diagenesis in increasingly magnesium-enriched environments. See figure 102 for the effect of evaporative concentration on the composition of the residual brine; see Bassett (1959), Weaver and Pollard (1973), Douglas (1977), and Palmer (1981) for the effect of a high-magnesium environment on clay diagenesis.

The current conceptual model of clay diagenesis, illustrated in figure 103, is now being tested. If clay mineral assemblages can be demonstrated to be a function of diagenesis in a high-magnesium environment, determining clay mineralogy will complement the use of bromide content of salt as an indicator of the extent of evaporative concentration of sea water in halite-precipitating environments. In addition, the mineralogical and chemical composition of clays may be used to determine areas of paleodissolution of salt beds, that is, regions where salt was initially present and has since been removed in solution.

a	SERIES	FORMATION	SAMPLE DEPTH (ft)	LITHOLOGY						CLAY MINERALOGY																																																																																																																																																																																																																																																																																																																																																																																																																																																																																																																																																																																																																																																																																																																																																																																																																																																																																																																																																																																																																																																																																																																																																																																																																																																																																																																																																																																																																																																																																																																																																																																																																																																																																																														
				Clastics	Dolomite	Halite				Illite	Chlorite-smectite	Chlorite-vermiculite	Chlorite-swelling chlorite	Chlorite																																																																																																																																																																																																																																																																																																																																																																																																																																																																																																																																																																																																																																																																																																																																																																																																																																																																																																																																																																																																																																																																																																																																																																																																																																																																																																																																																																																																																																																																																																																																																																																																																																																																																																										
						Present	< 10 ft	None																																																																																																																																																																																																																																																																																																																																																																																																																																																																																																																																																																																																																																																																																																																																																																																																																																																																																																																																																																																																																																																																																																																																																																																																																																																																																																																																																																																																																																																																																																																																																																																																																																																																																																																
GUADALUPE	SEVEN RIVERS	lower	823	•																																																																																																																																																																																																																																																																																																																																																																																																																																																																																																																																																																																																																																																																																																																																																																																																																																																																																																																																																																																																																																																																																																																																																																																																																																																																																																																																																																																																																																																																																																																																																																																																																																																																																																																				</

QA 5221

SERIES	FORMATION	SAMPLE DEPTH (ft)	LITHOLOGY					CLAY MINERALOGY					
			Clastics	Dolomite	Halite			Illite	Chlorite-smectite	Chlorite-vermiculite	Chlorite-swelling chlorite	Chlorite	
					present	< 10 ft	No halite						
GUADALUPE	OCHOA	Salado	1042	●			●		●			●	
	Yates	1096	●				●		●			●	
	Upper Seven Rivers	1183	●						●				
		1311	●				●						
		1352	●				●					●	
		1383	●				●					●	
	L. Seven Rivers	1419	●				●					●	
		1450	●				●					●	
	Queen/Grayburg	1588	●				●			●			
		1687	●									●	
		1746	●				●					●	
		1814	●							●			
	Upper San Andres	1976	●				●					●	
		2087	●	●			●			●			
		2201	●	●			●					●	
		2241	●							●			
	Lower San Andres	2340	●	●			●			●			
		2458	●				●				●		
		2601	●	●			●			●			
		2786	●	●								●	
		2861	●	●			●			●			
		2940	●	●						●			
LEONARD	Glorieta	3003	●				●		●				
		3118	●				●					●	
		3228	●				●			●			
		3284	●				●						●
	Upper Clear Fork	3460	●				●			●			
		3547	●	●			●				●		
		3608	●	●			●						
		3654	●	●								●	
	Tubb	3820	●	●					●				
		3872	●	●					●				●
		3943	●	●					●				●
		4007	●				●						●
	L. Clear Fork	4074	●				●					●	
		4191	●							●			

QA 5221

Figure 100. Host-rock lithology and clay mineralogy of samples from (a) DOE-Gruy Federal Rex White No. 1 core and (b) DOE-Gruy Federal Grabbe No. 1 core.

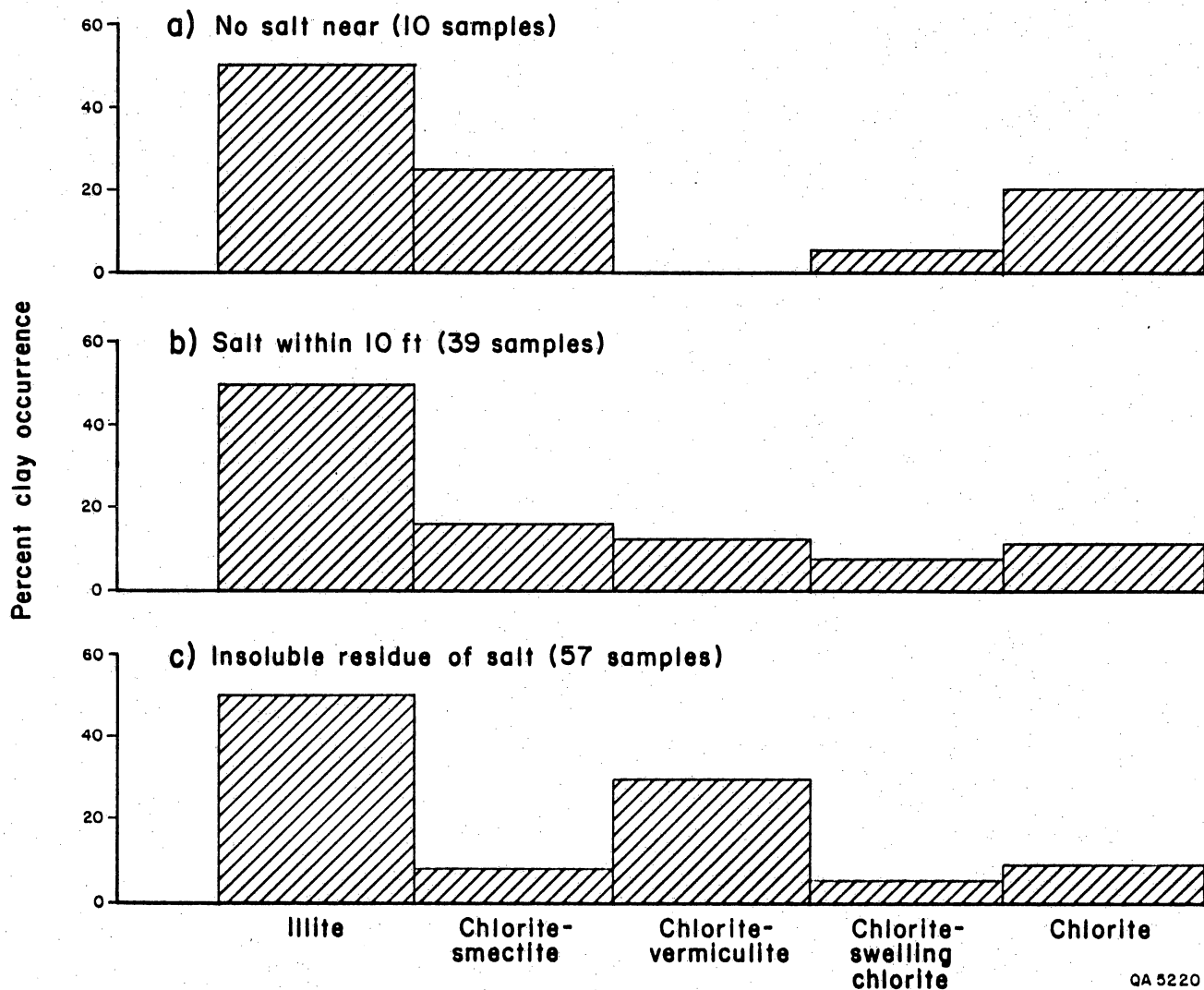


Figure 101. Histograms showing relative occurrence of clay minerals on three groups of samples: (a) no salt within 10 ft of sample, (b) nonsalt samples within 10 vertical feet of bedded salt, and (c) insoluble residue within salt rocks.



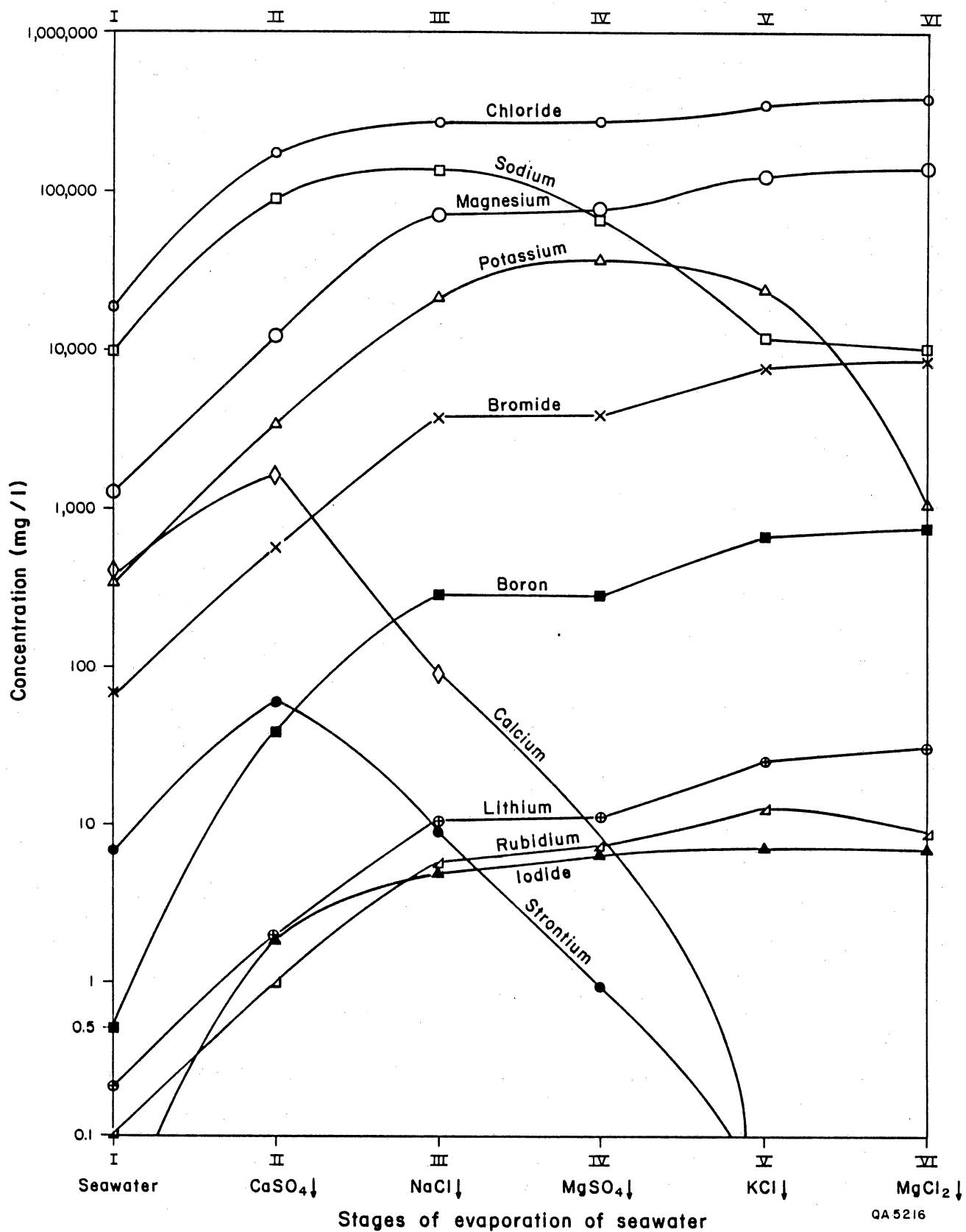


Figure 102. Changes in concentrations of major ions during evaporation of average modern seawater.

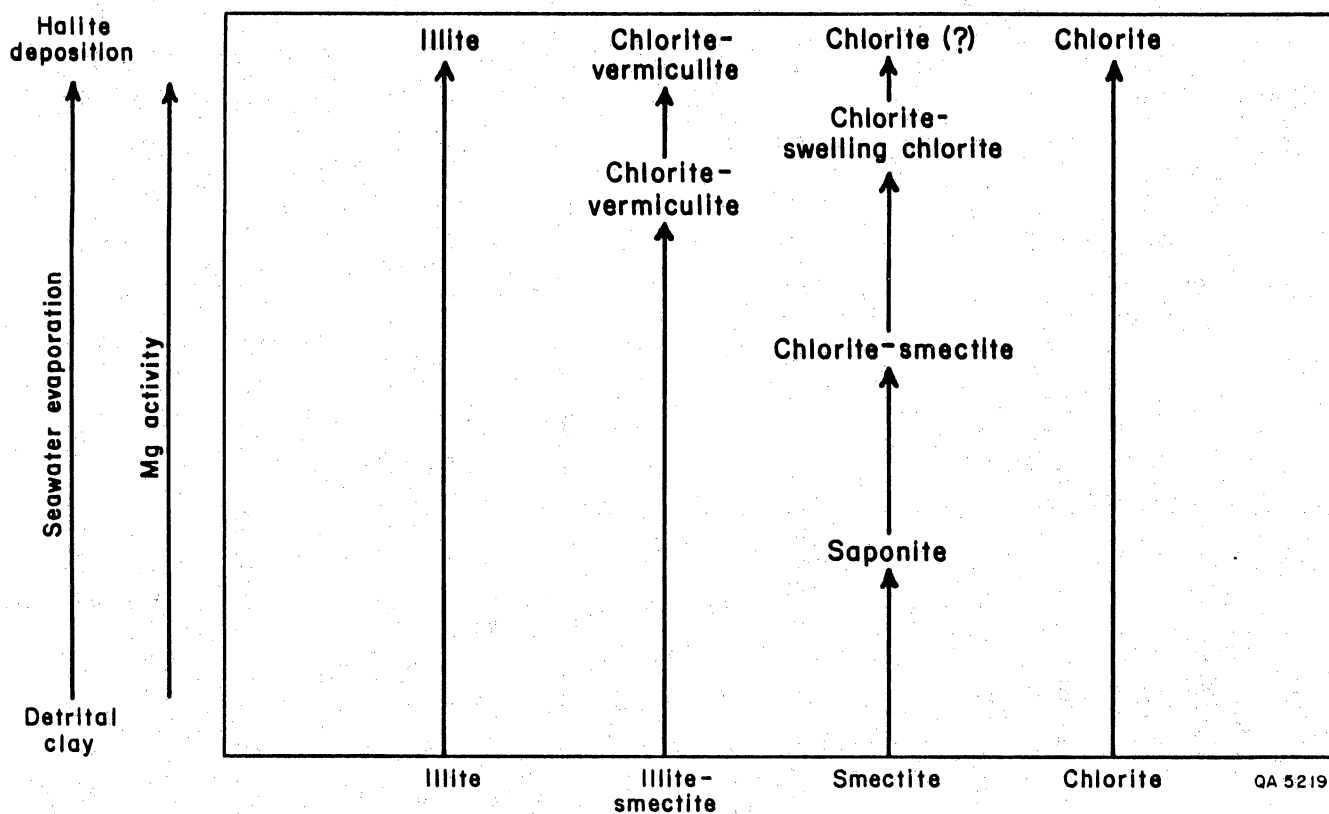


Figure 103. Conceptual model of clay diagenesis in environments of increasing magnesium activity.

# PETROLOGY AND DEPOSITIONAL ENVIRONMENTS OF POST-WICHITA/PRE-DOCKUM SILICICLASTIC ROCKS (LEONARDIAN-OCHOAN), PALO DURO BASIN

Allan Kolker, Susan D. Hovorka, Douglas A. McGookey, and H. Seay Nance

*Middle to Upper Permian post-Wichita Leonardian through Ochoan siliciclastic sediments in the Palo Duro Basin were primarily deposited in eolian dune, eolian flat, intermittent stream channel, wind-tidal(?) flat, shallow normal marine to hypersaline shelf, halite-influenced flat, and low-salinity pond environments. Source areas were probably granitic and medium-grade metamorphic terrains to the west and northwest of the Palo Duro Basin.*

## Objectives

Objectives of this report are to describe the textural and compositional characteristics of siliciclastic rocks whose component sediments were deposited in a variety of related environments during Leonardian, Guadalupian, and Ochoan stages in Palo Duro Basin.

## Methods

Forty-seven samples were collected and disaggregated from core recovered from DOE-Gruy Federal Grabbe No. 1, DOE-Gruy Federal Rex White No. 1, Stone and Webster Engineering Corporation Mansfield No. 1, and SWEC Sawyer No. 1. Textural characteristics of the sand fraction (2 to 64 mm) were determined by use of a Rapid Sediment Analyzer (Nelson, 1976) and of the mud fraction (64 to 0.5 mm) by Coulter TAIL Electronic Fine Particles Counter (Shideler, 1976). Statistical textural parameters were reduced according to Folk (1974). Compositional summaries were based on petrographic interpretation of 33 of these samples in which 100 to 300 points per sample were counted. Heavy mineral separates were prepared for sand and silt grain sizes, and the relative abundance of heavy mineral species was estimated.

Post-Wichita Middle to Upper Permian clastic rocks in the Palo Duro Basin are remarkably similar in grain size, mineralogy, and sedimentary structures. These rocks consist largely of subangular to subrounded coarse silt and very fine sand mixed with a

lesser amount of terrigenous clay. Siliciclastic material coarser than fine sand occurs only as lags of well-rounded grains in a subangular to subrounded matrix of finer material. Clastic rocks in the Glorieta and Queen/Grayburg Formations are generally coarser than the remainder of the section and include several intervals of clean, very fine to fine sandstone.

Preliminary analysis of sedimentary structures and vertical facies sequences in Department of Energy cores permits interpretation of seven environments in which terrigenous clastic sediments were deposited: (1) eolian dune, (2) eolian flat, (3) intermittent stream channel, (4) wind-tidal(?) flat, (5) shallow normal marine to hypersaline shelf, (6) halite-influenced flat, and (7) low-salinity pond.

#### Eolian Dunes

Sediments deposited in the eolian dune environment are characterized by packages 6 inches to 3 ft thick of high-angle (20 to 35 degrees) crossbedded fine sandstone. Good sorting, the presence of bimodal lags in some beds, and possible toe structures of sand-flow deposits are further evidence of an eolian origin (Presley and McGillis, 1982).

#### Eolian Flats

Sediments deposited in the eolian flats are characterized by poorly defined ripple cross-lamination and thin discontinuous layers of clay matrix (dissipation structures of Ahlbrandt and Fryberger, 1981). Petrography and grain-size analyses show that many examples of eolian flats are also bimodal.

#### Intermittent Streams

Intermittent stream channel deposits contain thick sequences of climbing ripples and may include ripples and small scour features associated with eolian sediments. Lenticular and flaser bedding are thought to be produced in a wind(?) or tidal(?) flat environment

where alternation of currents deposits rippled sand and silt and slack water deposits clay drapes. The position of this environment in the facies tract is not clear.

#### Shallow Shelf

Clastics deposited in shallow marine to hypersaline shelf environments are identified by their stratigraphic position beneath dolomitized skeletal or oolitic grainstones or anhydrite beds. Extremely thin (1- to 2-mm-thick) lenses of siltstone and very fine sandstone are typical of these environments.

#### Halite-Influenced Flats

Halite-influenced flats are characterized by flaser and lenticular bedding that has been disturbed or destroyed by crystallization of displacive halite within the sediment, alternating with dissolution of halite and collapse. These processes probably result from encroachment of halite-saturated water, followed by leaching of halite due to minor fluctuations in the position of halite-saturated brine pools.

#### Low-Salinity Ponds

Sediments in low-salinity ponds are commonly laminated and have thick clay drapes, fluid escape structures, load casts, and other features resulting from soft sediment deformation. No evidence of the former presence of halite was observed.

All the various samples are positively (fine) skewed in texture (table 11). Grain-size parameters of the halite-influenced flats are most consistent. These samples have the most pronounced truncation of the coarse fraction, contain the largest proportion of clay-sized material, and are consequently the most poorly sorted (fig. 104a). None of the samples from halite-influenced flats have a bimodal grain-size distribution, whereas more than half of the samples from the eolian flats have some bimodality (fig. 104). Samples of the eolian flats contain less clay and are better sorted than the halite-influenced flats.

The eolian flats have the greatest range in skewness values, partly owing to offset of the fine-skewed trend by the addition of varying amounts of medium sand as a subordinate mode (figs. 104b and 105). Grain-size parameters of fluvial samples vary the most overall, but the ranges in values are only slightly greater than those for the eolian flats (table 11; fig. 104c).

Mineralogy typical of the entire section includes "plutonic" quartz, feldspar (orthoclase > microcline > plagioclase), micas (muscovite, chlorite, and biotite in subequal proportions), clay matrix or pseudomatrix, and framework carbonate grains commonly having euhedral overgrowths on rounded cores (fig. 105). Feldspar grains are largely unaltered. Identified rock fragments include composite (metamorphic) quartz, chert, aphanocrystalline carbonate rock fragments, and hematitic clay and mud clasts. In the siliciclastic rocks sampled for this study, halite is the dominant cement where it has not been removed by dissolution.

Quartz:feldspar:rock fragment (Q:F:R) ratios of all 33 samples analyzed petrographically scatter around a composition of quartz-rich lithic arkose (fig. 106). The average Q:F:R is 72.1:19.2:9.7. Some variation in ratios is due to the local occurrence of clay and mud clasts, counted as sedimentary rock fragments, and the introduction of medium quartz sand to fine-grained feldspathic sediments.

Although Q:F:R values overlap considerably for different formations, samples above the base of the San Andres Formation tend to have less quartz and more rock fragments than samples below the San Andres (Hovorka and others, 1982). Most of this difference may be due to the Upper and Lower Seven Rivers and Yates Formations, which were found to have the lowest average quartz contents, on the basis of only seven samples (fig. 106). Using a t test, the difference in  $Q/F + R$  above and below the base of the San Andres Formation was found to be significant at the 91 percent confidence level, on the basis of 33 total samples (Nie and others, 1975). The difference in F/R is not statistically significant, which may be due to the small number of samples.

Heavy mineral concentrates were prepared for all 47 samples, and a consistent suite of minerals was found to be present in the entire section. The most abundant heavy minerals are opaque Fe-Ti oxides and their alteration products, including "leucoxene" after ilmenite and hematite (now goethite?) after magnetite. Common nonopaque heavy minerals include at least two types of zircon, green, brown, and minor blue tourmaline garnet, rutile, and staurolite. Rutile is the least abundant of the common heavy minerals. Garnet and staurolite have the greatest variation in proportions, probably because of selective preservation rather than original compositional differences. If present, apatite would not have survived acid treatment during sample disaggregation. The presence of staurolite was confirmed for three samples by examining energy-dispersive spectra. Both garnet and staurolite have idiomorphic surface features attributed to euhedral diagenetic overgrowth (Simpson, 1976) or chemical etching (Bramlette, 1929; Rahmani, 1973; Gravenor and Leavitt, 1981).

The limited and consistent range in grain size of Middle to Upper Permian clastic rocks suggests a common history of sediment sorting prior to deposition in a variety of environments in the Palo Duro Basin. The positive skewness values and bimodal sands are consistent with eolian transport but are not singularly diagnostic (Folk, 1966, 1971; Friedman, 1979; Ahlbrandt, 1979; McLaren, 1981). A broad area of eolian environment was present to the west and northwest of the Palo Duro Basin during late Glorieta time (Presley and McGillis, 1982).

The predominance of quartz grains having straight extinction characteristic of plutonic rocks coupled with abundant K-feldspar suggests a largely granitic source terrain (Folk, 1974). The presence of staurolite and metamorphic rock fragments indicates a lesser contribution by at least medium grade (amphibolite facies) metamorphic rocks. Positive areas surrounding the Palo Duro Basin that were exposed during the Middle to Upper Permian include the Marathon-Ouachita fold and thrust belt to the east and southeast, the Wichita-Arbuckle Uplift to the northeast and east, and the Pedernal and Uncompahgre

Uplifts to the west and northwest. With the exception of the Ouachita foldbelt, granitic rocks were being eroded from each of these areas during the Middle to Upper Permian. Staurolite-grade metamorphic rocks were absent in exposed portions of the Ouachita foldbelt (Flawn and others, 1961; Nicholas and Rosendal, 1975). In the Wichita province, basement country rocks are generally low grade, except in the vicinity of intrusive bodies. The rocks were covered by clastic sediments during the Early Permian (Wolfcampian) (Powell and Fischer, 1976; Powell and others, 1980). Positive areas to the west and northwest of the Palo Duro Basin contain granitic and pelitic rocks regionally metamorphosed at the amphibolite facies and thus appear to have the most likely overall composition for source areas (Gonzalez and Woodward, 1973; Grambling, 1979; Nielsen and Scott, 1979; Tweto, 1980). Staurolite is particularly abundant in parts of the Sangre de Cristo range (Rinconada Formation) of New Mexico (Miller and others, 1963; Barrett and Kirschner, 1979).



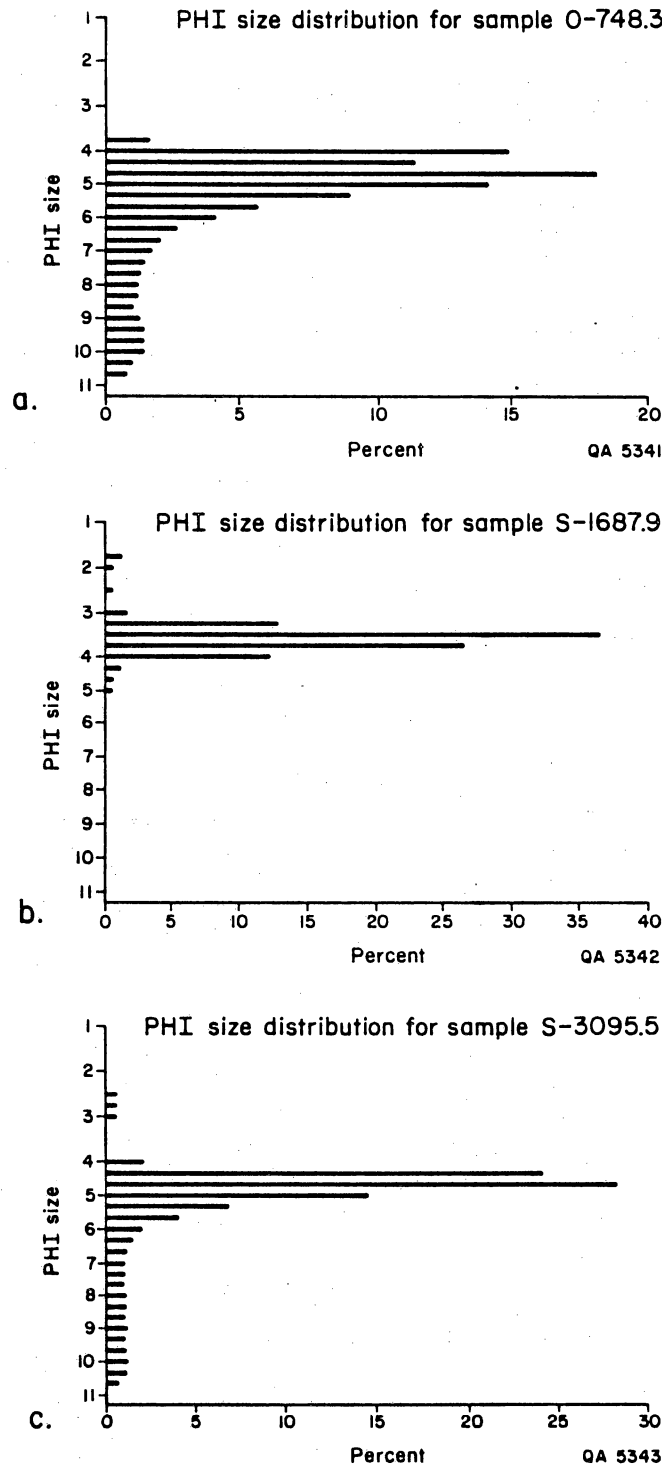


Figure 104. Representative grain size frequency distributions of (a) sample 0-748.3, lower Seven Rivers Formation, halite-influenced flat facies, Stone and Webster Engineering Corporation Mansfield No. 1 core, (b) sample S-1687.9, Queen-Grayburg Formations, eolian flat facies, DOE-Gruy Federal Grabbe No. 1 core, and (c) sample S-3095.5, Glorieta Formation, channel facies in flats, DOE-Gruy Federal Grabbe No. 1 core.

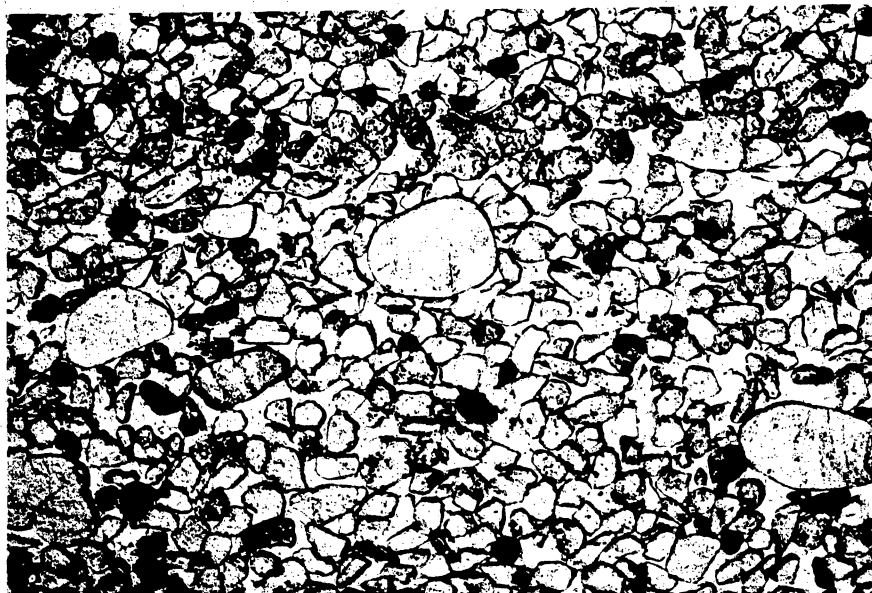


Figure 105. Bimodal very fine to medium sublitharenite. Note fresh appearance of all grains, including 7 percent orthoclase, 1 percent microcline, and 1 percent plagioclase; good sorting in fine sand and good rounding in medium sand. Stone and Webster Engineering Corporation Mansfield No. 1 core, 928.8 ft, Queen-Grayburg Formations, width 3.25 mm, plane light.

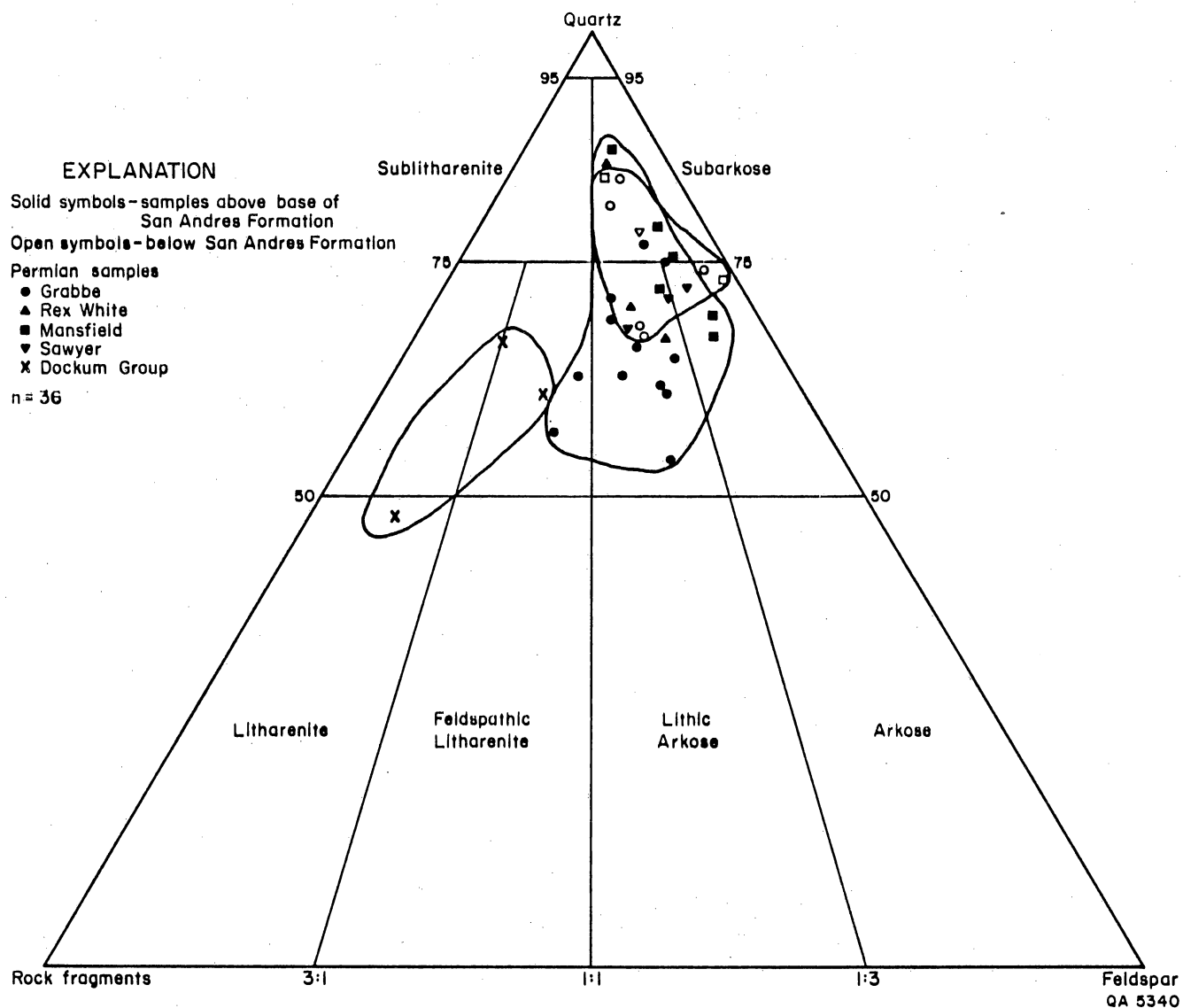


Figure 106. Quartz:feldspar:rock fragment (Q:F:R) ratios for 33 Permian samples and 3 Dockum Group samples.

Table 11. Grain-size parameters and inferred depositional facies for representative samples of  
Tubb through Dockum, Grabbe No. 1 core.

Formation	Sample	Mean (phi)	Sorting (phi)	Skewness	Inferred facies
Dewey Lake(?)	S-740.9	4.90	2.13	0.27	channel
Dewey Lake	S-895.3	5.96	1.70	0.57	channel
Salado/Tansill	S-1026.0	4.96	1.20	0.43	halite-influenced flat
Yates	S-1096.5	3.51	1.02	0.16	eolian flat
Upper Seven Rivers	S-1178.0	4.20	1.21	0.68	eolian flat
Upper Seven Rivers	S-1310.3	3.74	0.88	0.62	eolian flat
Lower Seven Rivers	S-1403.0	4.04	0.79	0.55	eolian flat
Lower Seven Rivers	S-1501.0	3.95	0.79	0.58	wind-tidal/eolian flat
Lower Seven Rivers	S-1547.8	3.96	0.70	0.45	eolian flat
Queen-Grayburg	S-1613.0	3.80	0.71	0.48	eolian flat
Queen-Grayburg	S-1687.9	3.48	0.40	0.04	eolian flat
Queen-Grayburg	S-1717.0	3.36	0.43	0.19	fluvial or tidal(?) channel
Queen-Grayburg	S-1829.0	3.67	1.18	0.77	eolian flat
Upper San Andres	S-2241.4	4.78	1.40	0.66	halite-influenced flat
Glorieta	S-2980.6	5.05	1.30	0.52	eolian flat
Glorieta	S-3095.5	4.93	1.26	0.69	channel
Glorieta	S-3143.4	4.61	0.91	0.59	channel
Glorieta	S-3314.0	4.55	1.05	0.44	eolian flat(?)
Clear Fork	S-3407.2	5.07	1.11	0.43	channel(?)
Clear Fork	S-3655.2	5.36	1.12	0.46	halite-influenced flat
Tubb	S-3859.0	2.78	0.50	0.31	channel flat
Tubb	S-4013.8	5.17	1.46	0.60	eolian flat(?)

## THERMAL MATURITY OF SOME SOURCE ROCKS IN THE PALO DURO BASIN

Shirley P. Dutton

*Vitrinite reflectance of samples from Swisher and Oldham Counties indicates that hydrogen-rich kerogen should be mature at depths below about 6,800 ft (2,070 m). Pyrolysis data support the interpretation that Pennsylvanian basinal shales in Swisher County reached the oil-generation zone.*

Geochemical analyses of cores and cuttings from the Stone and Webster Engineering Corporation Zeeck No. 1 well, Swisher County, and the Mansfield No. 1 well, Oldham County, were used to measure the quality and thermal maturity of potential source rocks in these areas of the Palo Duro Basin. Total organic carbon (TOC) content of Pennsylvanian basinal shales is generally greater than 0.5 percent, indicating that they are fair to good hydrocarbon source rocks (table 12). Permian shales (Wolfcampian and Leonardian) tend to have lower TOC content (table 12). The organic matter in both Pennsylvanian and Permian shales consists of amorphous material (fine-particulate), woody debris (vitrinite), plant tissue, coaly debris (inerts), and spores and pollen.

Thermal maturity was assessed by vitrinite reflectance ( $R_o$ ) and pyrolysis. An  $R_o$  of 0.5 percent is considered to be the beginning of the oil-generation zone for hydrogen-rich organic matter by the lab that performed most of the analyses (Lab 1). Plots of vitrinite reflectance versus depth indicate that shales below about 6,100 ft (1,860 m) in the Mansfield No. 1 well have reached 0.5 percent  $R_o$  (fig. 107a). Shales in the Zeeck No. 1 well were analyzed for vitrinite reflectance by two laboratories, and the  $R_o$  values they reported for equivalent samples were significantly different (table 12). Differences in  $R_o$  measurements could be caused by microscope calibration differences or by differences between operators in the type of vitrinite grains they chose to measure. Two different regression lines were calculated for vitrinite reflectance versus depth--one that uses only data from Lab 1 and another that uses data from Lab 2 (fig. 107b). Lab 2 uses an  $R_o$  value of 0.6 percent as the boundary between immature and mature hydrogen-rich kerogen. The line for Lab 1 data indicates that a vitrinite reflectance of 0.5 percent is reached at a

depth of 6,800 ft (2,070 m); the regression line using only Lab 2 data reaches 0.6 percent  $R_o$  at 6,650 ft (2,030 m). Thus, there is agreement between the different labs on the depth of the oil-generating zone for hydrogen-rich kerogen despite considerable difference in measured  $R_o$  values.

Pyrolysis was performed as another method to determine the thermal maturity of Wolfcampian and Pennsylvanian shales from the Zeeck No. 1 well (table 13). The results suggest that the Pennsylvanian shales from about 7,300 ft (2,225 m) have reached the oil-generation zone (fig. 108). The Wolfcampian shales are probably immature, but they have anomalously high  $S_1$  values (fig. 108). The pyrolysis and vitrinite reflectance data indicate that hydrogen-rich kerogen below about 6,800 ft (2,070 m) probably is thermally mature.

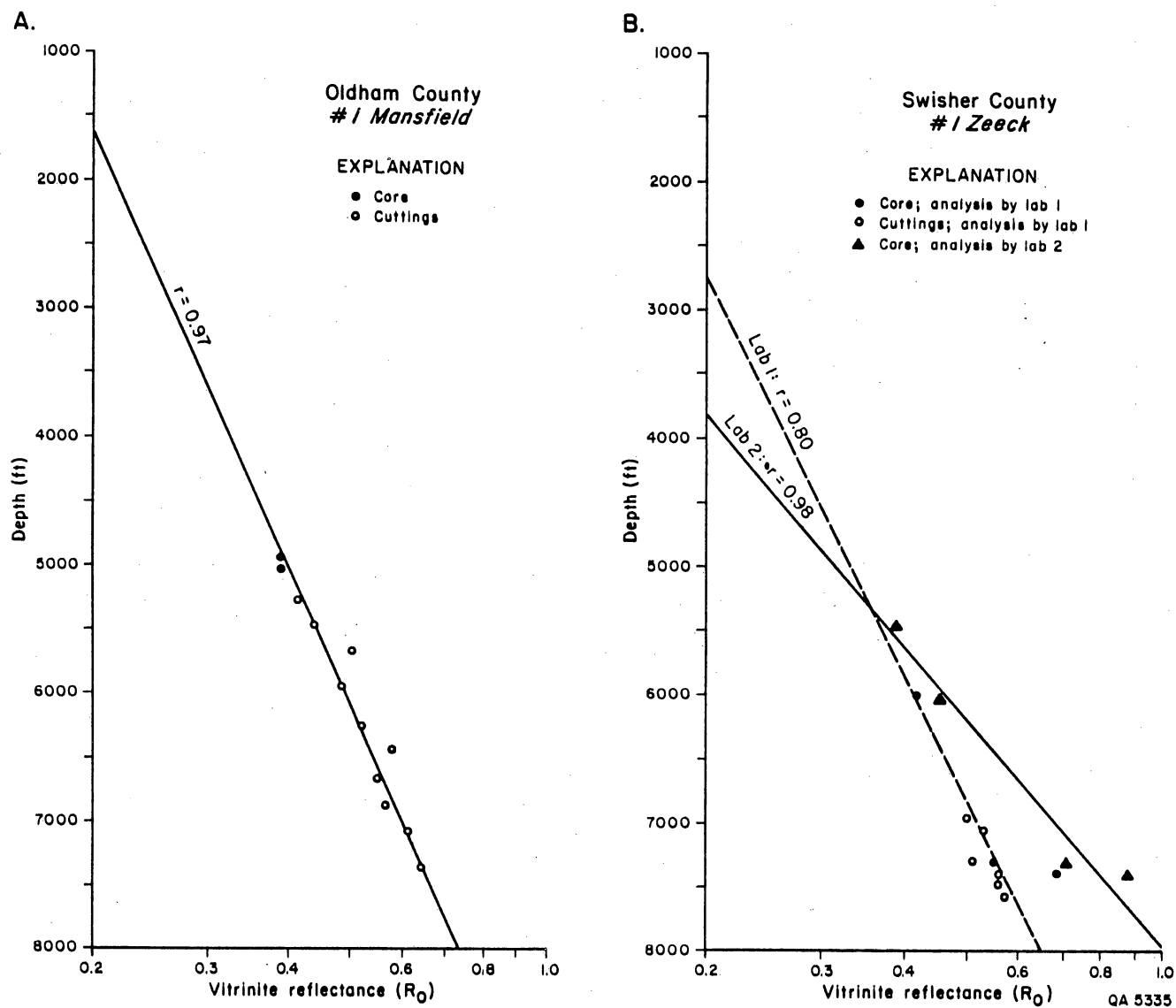


Figure 107. Trend of vitrinite reflectance with depth for two wells in the Palo Duro Basin.

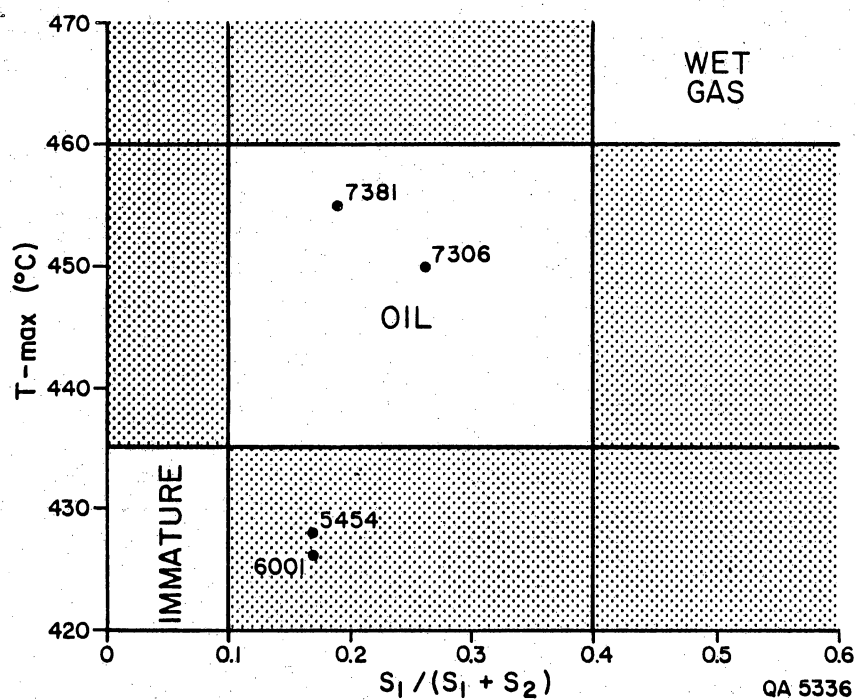


Figure 108. Plot of pyrolysis T-max (°C) against the ratio  $S_1 / (S_1 + S_2)$  defining the oil-generation zone (GeoChem Laboratories, 1980). See table 13 for a definition of T°C Max and  $S_1 / (S_1 + S_2)$ . Pennsylvanian shales from Swisher County plot in the oil zone, but Wolfcampian shales are probably immature.



Table 12. Total organic carbon (TOC) content and vitrinite reflectance ( $R_o$ ) of wells in Oldham and Swisher Counties, Palo Duro Basin.

Stone and Webster Mansfield No. 1 Oldham County			Stone and Webster Zeeck No. 1 Swisher County			
Depth (ft)	TOC (%)	$R_o$ (%)	Depth (ft)	TOC (%)	$R_o$ (%)	
					Lab 1	Lab 2
4,118 (c)	0.96	-	5,454 (c)	0.43	-	0.39
4,120 (4,080-4,160)	0.00	-	5,566 (c)	0.13	-	-
4,394 (c)	0.09	-	5,649 (c)	0.16	-	-
4,400 (4,360-4,440)	0.12	-	5,753 (c)	0.19	-	-
			5,918 (c)	0.14	-	-
4,640 (4,600-4,680)	0.00	-	6,001 (c)	0.45	0.42	0.45
4,960 (4,920-4,995)	0.57	-	6,950 (6,910-6,990)	1.31	0.50	-
4,962 (c)	0.99	0.39	7,050 (7,010-7,090)	1.82	0.53	-
4,995 (c)	0.55	0.39				
5,080 (5,040-5,120)	0.48	-				
5,280 (5,240-5,320)	1.07	0.41	7,280 (7,240-7,320)	1.04	0.51	-
5,480 (5,440-5,520)	0.93	0.44	7,306 (c)	0.71	0.55	0.71
5,680 (5,640-5,720)	1.01	0.50	7,380 (7,340-7,420)	1.00	0.56	-
5,940 (5,900-5,980)	1.65	0.48	7,381 (c)	0.63	0.69	0.88
6,240 (6,200-6,280)	1.73	0.52	7,480 (7,440-7,520)	0.93	0.56	-
6,440 (6,400-6,480)	1.61	0.57	7,580 (7,540-7,620)	0.86	0.57	-
6,680 (6,640-6,720)	1.44	0.55				
6,890 (6,850-6,930)	1.29	0.56				
7,090 (7,050-7,130)	1.94	0.61				
7,375 (7,350-7,400)	0.88	0.64				

Leonardian

Wolfcampian

Pennsylvanian

Wolfcampian

Pennsylvanian

(c) denotes core sample. Other samples are cuttings from the depth range indicated.

Table 13. Results of pyrolysis of samples from Stone and Webster Zeeck No. 1 well, Swisher County.

Depth (ft)	Tmax (°C)	S1 (mg/g)	S2 (mg/g)	S3 (mg/g)	Production index	TOC (wt. %)	Hydrogen index	Oxygen index
5,454	428	0.05	0.26	0.26	0.16	0.43	60	60
6,001	426	0.05	0.25	1.08	0.17	0.45	55	240
7,306	450	0.10	0.29	1.65	0.26	0.71	40	232
7,381	455	0.05	0.22	1.01	0.19	0.62	35	162

Tmax = Temperature index, °C

S1 = Free hydrocarbons, mg HC/g of rock

S2 = Residual hydrocarbon potential (mg HC/g of rock)

S3 = CO<sub>2</sub> produced from kerogen pyrolysis (mg CO<sub>2</sub>/g of rock)

Production index = S1/(S1 + S2)

TOC = Total organic carbon, wt. %

Hydrogen index = mg HC/g organic carbon

Oxygen index = mg CO<sub>2</sub>/g organic carbon

## OIL FIELDS IN THE NORTHWESTERN PALO DURO BASIN

Shirley P. Dutton

*Pennsylvanian granite wash and carbonates are important oil reservoirs in the northwestern Palo Duro Basin. Fields are primarily controlled by structure, and traps are provided by simple or faulted anticlines.*

Although most of the Palo Duro Basin does not produce oil, several fields have been discovered in the northwestern part of the basin. Discoveries have been made in Pennsylvanian granite wash and carbonates (table 14) in east-central Oldham and western Potter Counties (fig. 109). This paper summarizes the publicly available information about those fields based on hearing files and annual reports of the Railroad Commission of Texas. Information about granite wash is available from core samples that were recovered from the Stone and Webster Engineering Corporation J. Friemel No. 1 well in Deaf Smith County, 12 m (19 km) south of Vega (fig. 109).

Calculations of oil in place indicate that the largest fields in Oldham County initially contained about 10 million barrels of oil (table 14). The amount of oil that ultimately can be recovered is less. An estimated 1,560,000 barrels of oil are recoverable from Hryhor field, assuming a 17-percent recovery factor (Railroad Commission of Texas, 1982). Cumulative oil production from these 12 fields was 6,078,283 barrels by January 1, 1983 (table 14).

Traps in the fields are mainly provided by simple or faulted anticlines. A map submitted to the Railroad Commission of Texas indicates that Sundance, Hryhor, and Lambert fields, three of the largest fields in the area, are located on adjacent fault-bounded anticlines (fig. 110). Manarte (Granite Wash, Upper) field is formed by a combination structural and stratigraphic trap. Oil is trapped on the eastern side of the field by granite-wash pinch-out at the margin of a north-south-trending channel (Railroad Commission of Texas, 1969). On the other three sides of the field oil is trapped by a southwest-plunging anticline.

Granite wash is the most important reservoir facies in the northwestern Palo Duro Basin (table 14). The samples of granite wash from the J. Friemel well are probably similar to, but older than, the productive granite wash in Oldham County. The grain size of the samples varies from granular, very coarse sandstone to sandy pebble conglomerate. The samples are poorly to moderately sorted, with subangular grains. The framework grains are mainly quartz, feldspar, and micrographic granite fragments, so the sandstones are classified as arkoses (Folk, 1974). Abundant micrographic granite indicates that the source area was the Bravo Dome in western Oldham County (Flawn, 1956).

Porosity in the Deaf Smith granite wash was measured by porosimeter as 16.1 to 17.9 percent. Porosity measured in thin sections ranged from 12.0 to 17.5 percent. The difference is probably caused by microporosity within clay cements and elsewhere that cannot be seen in thin section but can be measured by a porosimeter. Both primary porosity and secondary porosity, which formed by dissolution of framework grains, are present. The porosity has been somewhat reduced by the precipitation of quartz overgrowths, ankerite, and kaolinite.

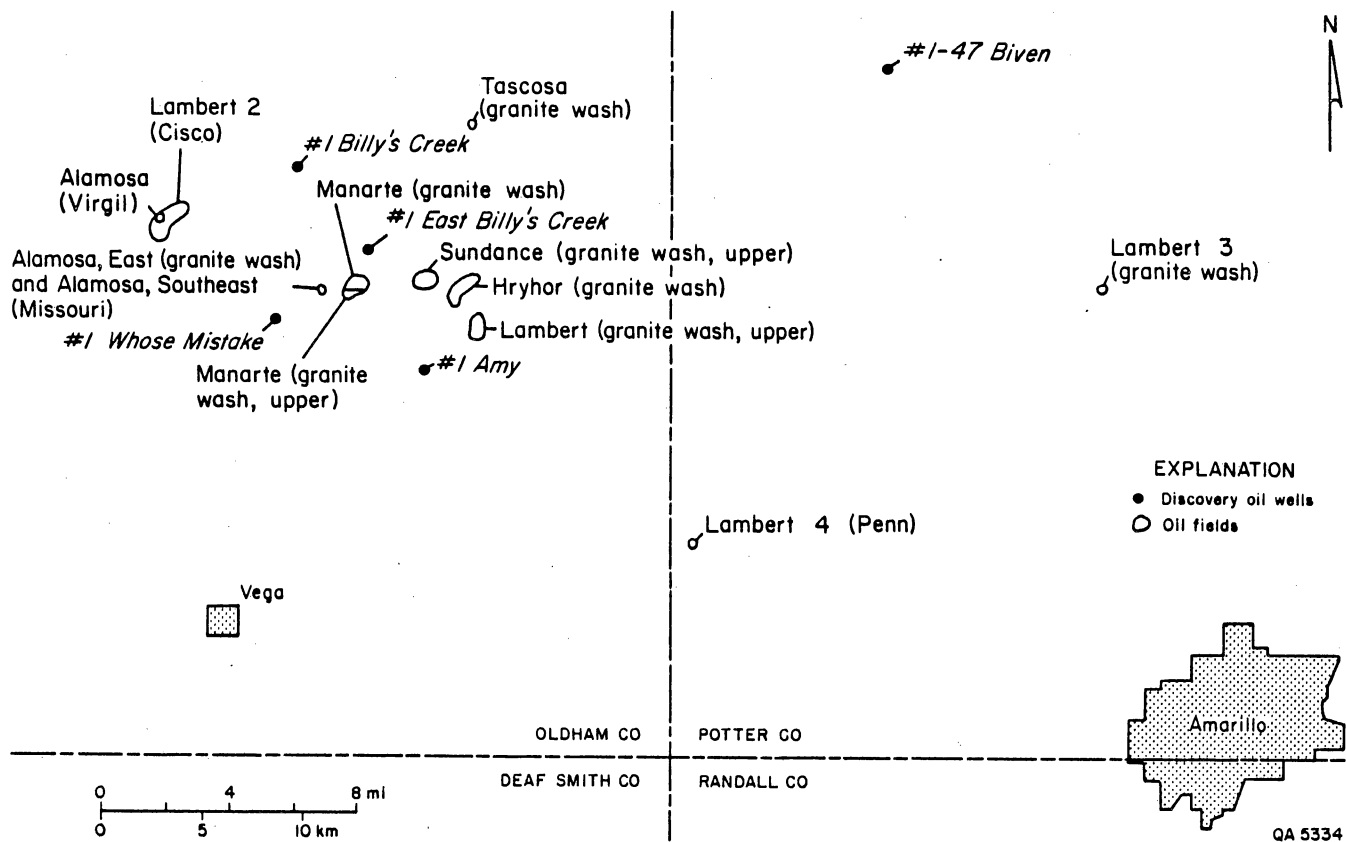


Figure 109. Location of oil fields in Oldham and western Potter Counties. Reservoirs in these fields are Pennsylvanian granite wash or carbonate.

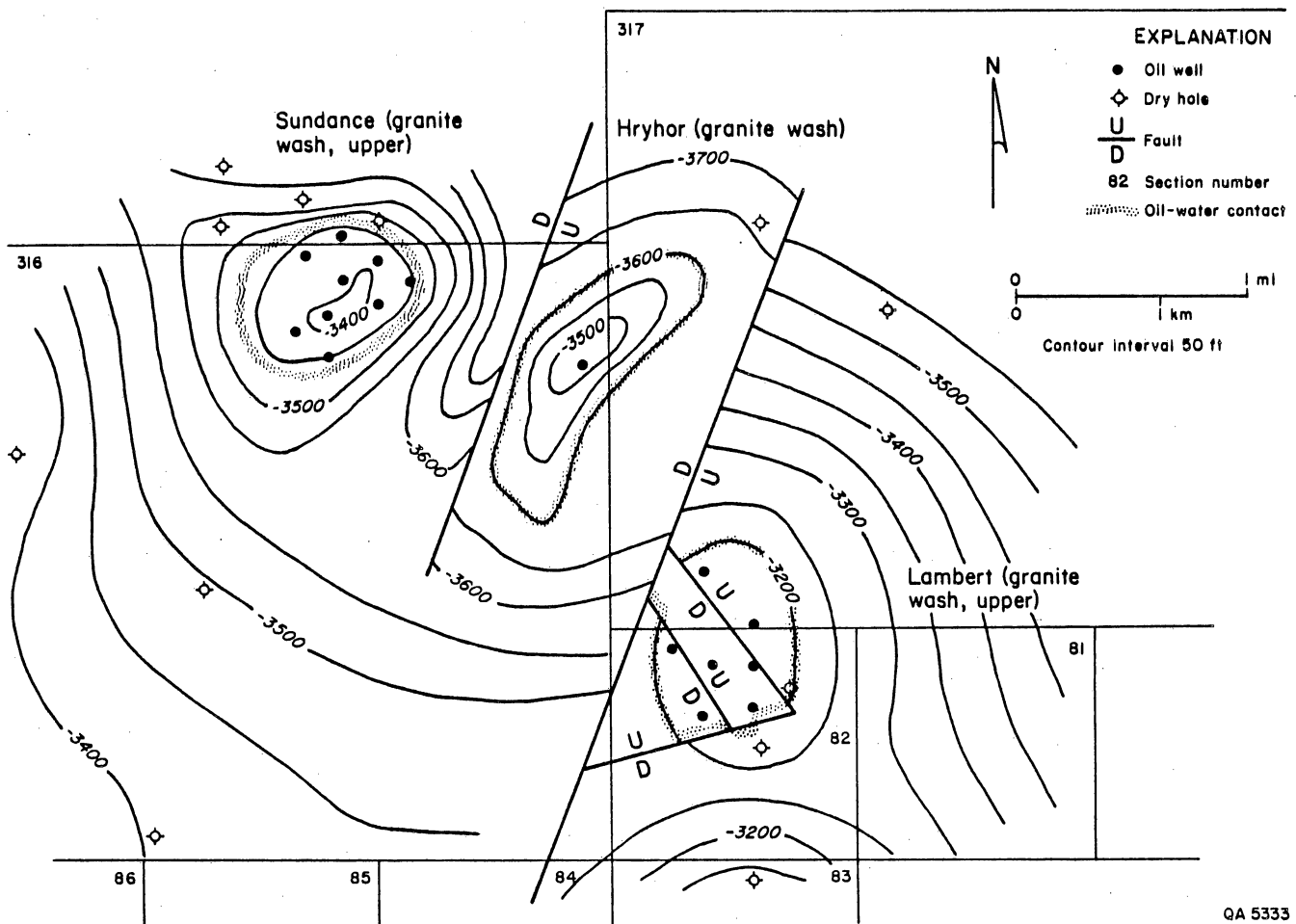


Figure 110. Structure-contour map on top of the upper granite wash, the reservoir for Lambert, Hryhor, and Sundance fields (Railroad Commission of Texas, 1982). See figure 109 for location.

Table 14. Oil fields in the northwestern Palo Duro Basin.

<u>Field name</u>	<u>Discovery date</u>	<u>Depth (ft)</u>	<u>Reservoir</u>	<u>Drive mechanism</u>	<u>API gravity</u>	<u>Porosity (%)</u>
Alamosa (Virgil)	5/57	6,101	Lower Virgilian limestone	--	40.0	--
Alamosa, East (Granite wash)	9/57	7,116	Missourian granite wash	--	43.3	--
Alamosa, Southeast (Missouri)	7/59	6,664	Missourian dolomite	--	36.6	--
Hryhor (Granite wash)	3/82	7,156	Granite wash	Dissolved gas and possible water drive	43.2	18
Lambert (Granite wash, upper)	1/79	6,786	Missourian granite wash	Water drive	42.6	13
Lambert 2 (Cisco)	10/79	6,110	Virgilian algal limestone	Dissolved gas drive	42.0	4.5
Lambert 3 (Granite wash)	7/80	5,720	Granite wash	--	36.0	--
Lambert 4 (Penn)	2/81	5,942	Pennsylvanian sandstone	--	42.8	--
Manarte (Granite wash)	3/69	7,093	Granite wash	Water drive	39.7	17
Manarte (Granite wash, upper)	7/69	6,542	Granite wash	Water drive	40.4	11
Sundance (Granite wash, upper)	8/81	7,058	Granite wash	Dissolved gas and possible water drive	42.7	10
Tascosa (Granite wash)	1/58	8,524	Missourian granite wash	--	43.0	--
<u>1983 Discoveries</u>						
Baker & Taylor 1 Billy's Creek		7,895	Granite wash (upper)		45.6	
Baker & Taylor 1 East Billy's Creek		9,956	Lower Missourian granite wash		43.2	
Baker & Taylor 1 Whose Mistake		6,526	Missourian granite wash		41.8	
Shell 1-47 Bivens		8,890			43.0	
Baker & Taylor 1 Amy		6,368	Missourian granite wash		42.2	

Table 14 (cont.)

Permeability (md)	Average net pay (ft)	Interstitial water saturation (%)	Productive acres	Estimated oil in place (bbl)*	Total 1982 production		Cumulative oil production to 1-1-83 (bbl)
					Gas (Mcf)	Crude oil (bbl)	
--	--	--	--	--	0	0	58,270
--	--	--	--	--	0	0	97,195
--	--	--	--	--	0	0	48,277
--	15	42	320	3,887,689	34,864	405,508	405,508
48	68	40	320	13,167,498	68,453	329,606	1,375,980
8	25	45	400	1,920,105	27,566	119,358	333,492
--	--	--	--	--	26	671	11,989
--	--	--	--	--	20,817	1,675	5,485
60	36	43	400	10,825,203	2,723	6,794	491,349
60	41	32	440	10,468,583	8,052	209,141	2,719,706
668	20	25	320	3,723,840	44,634	487,987	526,830
--	--	--	--	--	0	0	4,202
					Total		6,078,283
							744 bbl/day
							216 bbl/day
							53 bbl/day
							93 bbl/day
							32 bbl/day

\*Estimated oil in place =  $7758 \frac{\text{bbl}}{\text{acre-ft}} \times \text{Productive acres} \times \text{Average net pay} \times \text{Porosity} \times (1 - \text{water saturation})$



# COMPARISON OF NEUTRON-DENSITY AND NEUTRON-SONIC CROSSPLOTING METHODS IN DETERMINING LITHOLOGY AND POROSITY IN WOLFCAMP CARBONATES

Robert D. Conti

*The neutron-density crossplotting methods are superior to neutron-sonic methods for making quantitative carbonate-lithology and porosity determinations in Wolfcamp deep-basin aquifers. This is because the former method more precisely detects secondary porosity and, consequently, more accurately identifies lithology.*

Two crossplotting methods were used to derive relative percentages of dolomite and limestone in the predominantly carbonate sequences of the Palo Duro Basin Wolfcamp strata. Neutron porosity ( $\phi_n$ ), density porosity ( $\phi_\rho$ ), and interval transit time ( $\Delta t$ ) values were read and recorded from Schlumberger's Compensated Neutron-Formation Density Log, Compensated Neutron-Litho-Density Log, and Borehole Compensated Sonic Log in intervals of "known pure" carbonate lithologies as identified by macroscopic core analysis and recorded in detailed core logs (vertical scale: 1 inch = 100 ft) (Ruppel and Hovorka, 1983a, b; in pocket). Each porosity log is a recording of unique physical properties of the rocks, so that by simultaneous analysis of two logs, "their separate responses to different minerals allow a quantitative distinction of both mineral composition and pore volume" (Borneman and Doveton, 1983). Crossplotted porosity-log responses (Burke and others, 1969) employ values read from neutron, density, or sonic logs that reflect lithology, fluid content, and porosity so that porosity values can be calculated in intervals of simple-matrix (that is, monomineral) lithology (Schlumberger, 1972). Wolfcamp strata, however, consist mostly of complex lithologies, necessitating simultaneous analysis of two porosity logs.

Wolfcamp core was recovered from U.S. Department of Energy (DOE) test holes in Donley County, Stone and Webster Engineering Corporation (SWEC) Sawyer No. 1 (3,082-3,924 ft); Oldham County, SWEC Mansfield No. 1 (4,502-4,990 ft); and Swisher County, SWEC Zeeck No. 1 (5,472-5,618 ft).

Lithologic logs of Wolfcamp core from three DOE test holes in the Texas Panhandle were examined for intervals of 100 percent limestone and 100 percent dolomite. After the depths of each interval were recorded, depth-equivalent neutron-porosity, density-porosity, and interval-transit-time values were read from the Schlumberger porosity logs and plotted onto Schlumberger charts CP-1d and CP-2b (Schlumberger, 1979) for neutron-density analyses (figs. 111 and 112) and neutron-sonic analyses (figs. 113 and 114), respectively.

A comparison of crossplotting methods (figs. 111 and 113) for pure-dolomite intervals shows that data cluster more closely to the dolomite line in the neutron-density plot (fig. 111) than they do in the neutron-sonic plot (fig. 113), indicating the neutron-density method yields a more accurate discernment of dolomite. The neutron-density plot (fig. 111) also shows higher maximum porosity values than the neutron-sonic plot (fig. 113). For example, in the neutron-density plot (fig. 111), maximum porosity in the SWEC Sawyer No. 1 well equals 0.27. In the neutron-sonic plot, maximum dolomite porosity in the Sawyer No. 1 well equals 0.21. In the neutron-sonic plot, maximum dolomite porosity in the SWEC Mansfield No. 1 and Zeeck No. 1 wells equals 0.21 by neutron-density plotting (fig. 111) and 0.19 and 0.17, respectively, by neutron-sonic plotting (fig. 113). Lower maximum porosities in figure 113 probably result from the sonic log's inability to detect secondary porosity (Burke and others, 1969; Schlumberger, 1972; Fertl, 1981; MacCary, 1983).

Comparison of neutron-density (fig. 112) and neutron-sonic (fig. 114) crossplotting methods for limestone also indicates that when the former technique is used, limestone data cluster more closely to the limestone line than when the latter technique is used. Again, this indicates a more accurate differentiation of lithology through neutron-density crossplotting. As in the previous dolomite example, the neutron-density technique yields higher maximum porosities than the neutron-sonic method. For example, maximum neutron-density porosity in the SWEC Sawyer No. 1 limestone (fig. 112) equals 0.30. Neutron-sonic (fig. 114) maximum limestone porosity in the Sawyer No. 1 well equals 0.25.

Neutron-density maximum porosities in the SWEC Mansfield No. 1 and Zeeck No. 1 wells equal 0.28 and 0.22, respectively (fig. 112), whereas they equal 0.19 and 0.17, respectively, for the same wells in the neutron-sonic plot (fig. 114). Again, maximum porosities identified in the neutron-sonic plot are probably lower because the sonic log does not detect secondary porosity (Burke and others, 1969; Schlumberger, 1972; Fertl, 1981; MacCary, 1983).

Comparison of lithologic determinations derived from two standard crossplotting methods in Wolfcamp dolomite and limestone shows consistently greater variation in lithologic identity resulting from neutron-sonic crossplotting. This is especially true for the 100-percent limestone intervals studied. Pure-limestone neutron-sonic responses identify silica, anhydrite, and salt, in addition to widely varying ratios of limestone/dolomite (fig. 114). Pure-limestone neutron-density responses in figure 112, however, only indicate limestone/dolomite and limestone/silica permutations. The presence of silica in the neutron-density plot almost always coincides with chalcedony replacement of fossil fragments or the presence of chert grains, as indicated in core logs (Ruppel and Hovorka, 1983a, b; in pocket).

This study of crossplotted porosity-log responses in the Palo Duro Basin Wolfcamp carbonate intervals shows that neutron-density crossplotting is superior to neutron-sonic crossplotting in deriving quantitative estimates of (binary-mineral) lithology ratios and porosity values. This initial finding from Wolfcamp-specific studies supports use of the more generally preferred neutron-density logs for analysis of lithology and for evaluation of porosity in predominantly carbonate sequences (Raymer and Biggs, 1963; Schlumberger, 1972; MacFadzean, 1973; Fertl, 1981; MacCary, 1983).

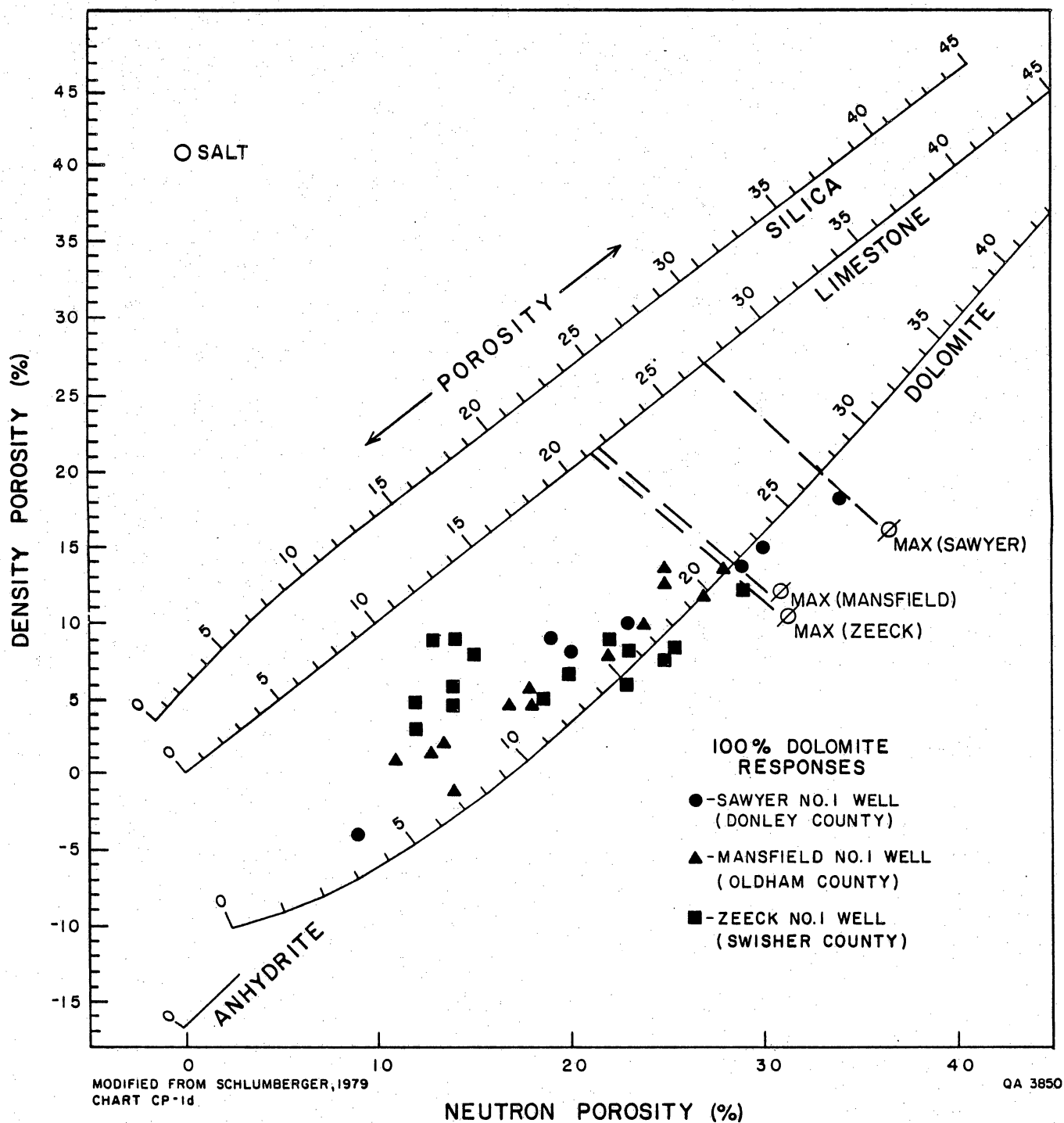


Figure 111. Neutron-porosity values plotted against the density-porosity values for "pure" dolomite. The data cluster more closely to the dolomite line than they do in the neutron-sonic plot for the same intervals (fig. 113). Maximum porosities in the Stone and Webster Engineering Corporation Sawyer No. 1, Stone and Webster Engineering Corporation Mansfield No. 1 and Stone and Webster Engineering Corporation Zeeck No. 1 wells equal 0.27, 0.21, and 0.21, respectively. Generally the maximum porosities shown in figure 113 are lower for each of the three wells.

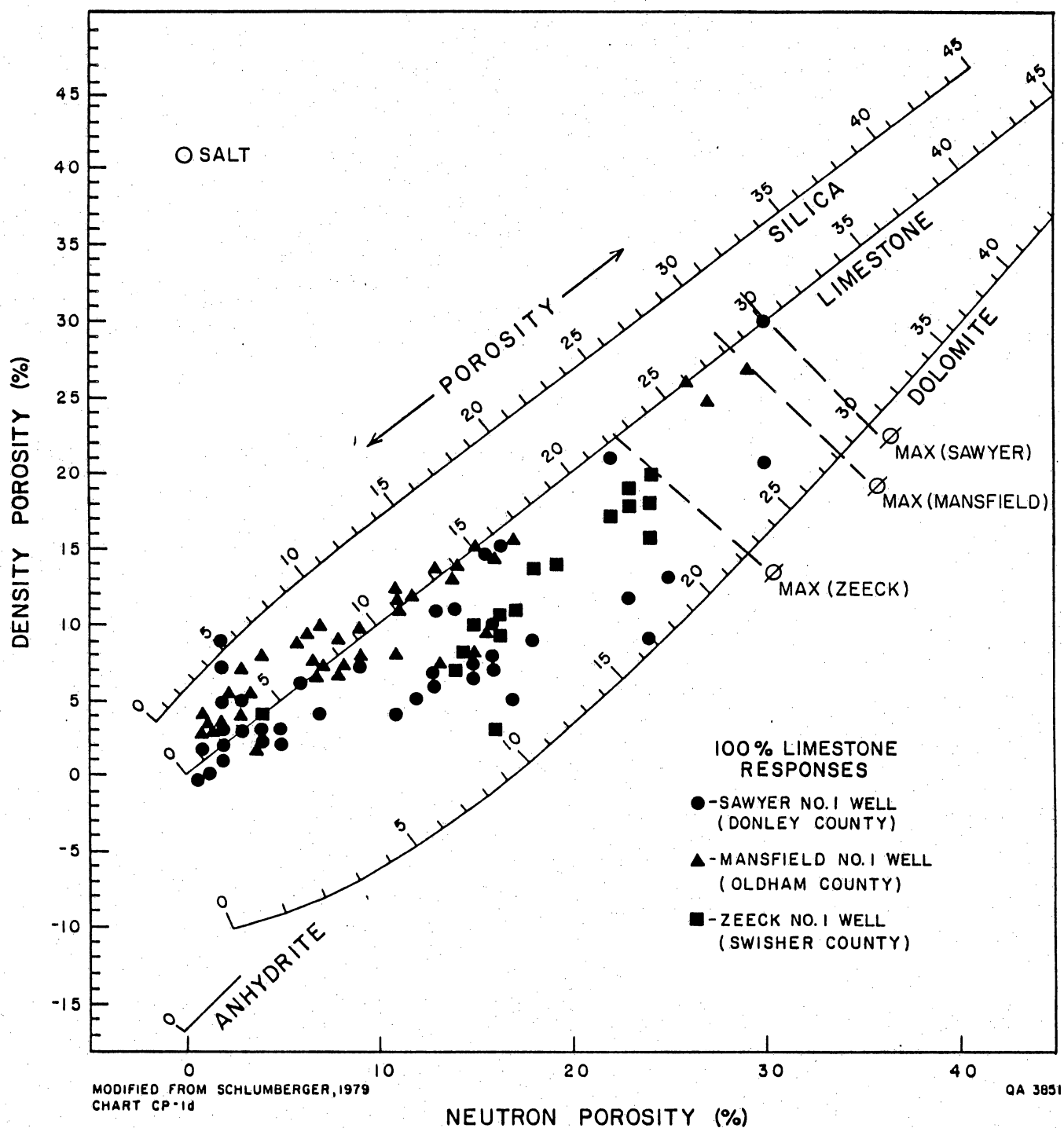


Figure 112. Neutron-porosity values plotted against the density-porosity values for "pure" limestone. The data cluster more closely to the limestone line than they do in the neutron-sonic plot for the same intervals (figure 114). Maximum porosities in the Stone and Webster Engineering Corporation Sawyer No. 1, Stone and Webster Engineering Corporation Mansfield No. 1 and Stone and Webster Engineering Corporation Zeeck No. 1 wells equal 0.30, 0.28, and 0.22, respectively. The maximum porosities shown in figure 114 are lower for each of the three wells.

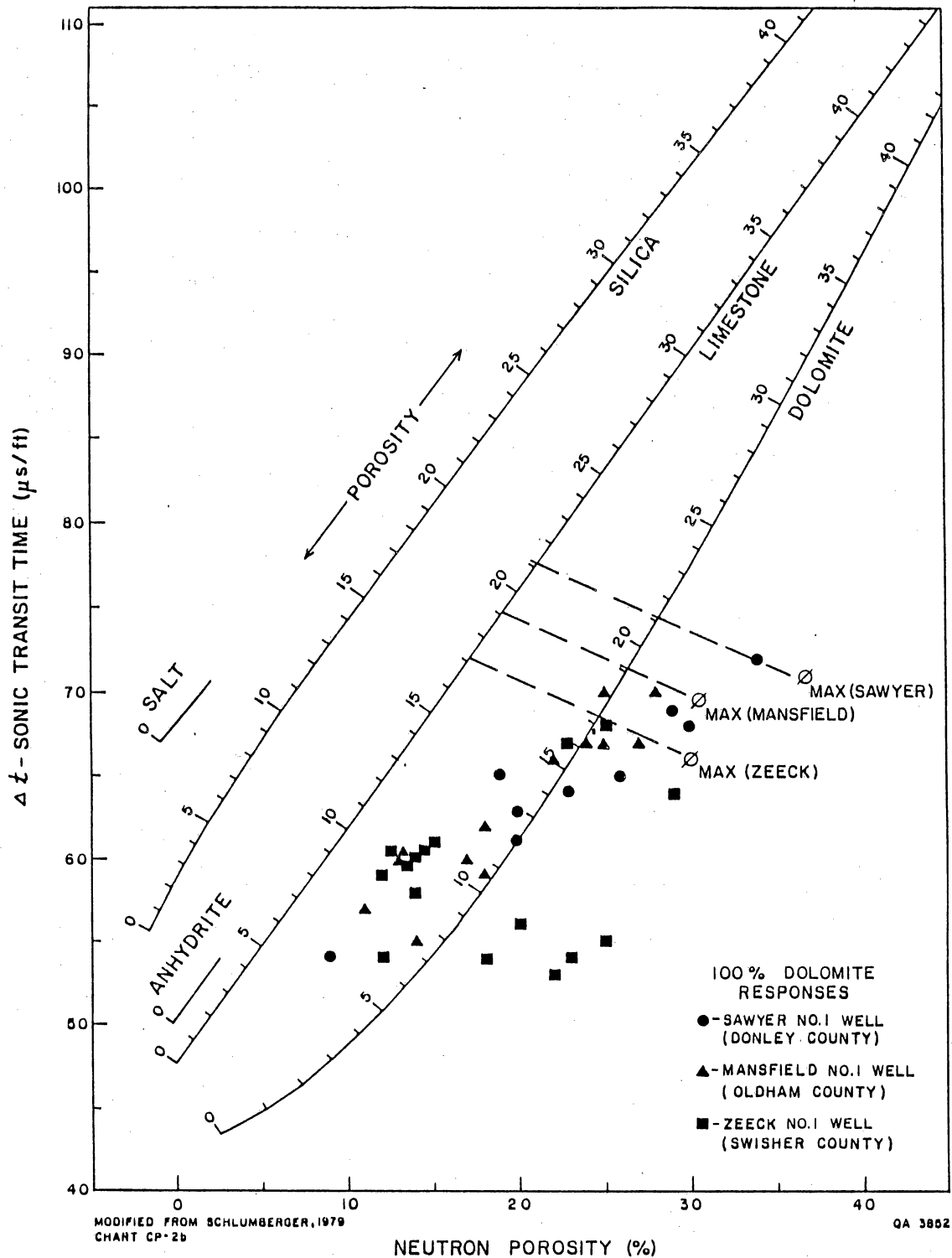


Figure 113. Neutron-porosity values plotted against the sonic-transit-time values for pure dolomite. The data cluster more closely to the dolomite line in figure 111 than they do in this plot for the same intervals, indicating inferior lithology resolution by neutron-sonic crossplotting. Maximum porosities in the Stone and Webster Engineering Corporation Sawyer No. 1, Stone and Webster Engineering Corporation Mansfield No. 1 and Stone and Webster Engineering Corporation Zeeck No. 1 wells equal 0.21, 0.91, and 0.17, which are all lower than the maximum porosities shown in figure 111. Maximum porosities are probably lower because the sonic log does not detect secondary and vuggy porosity.

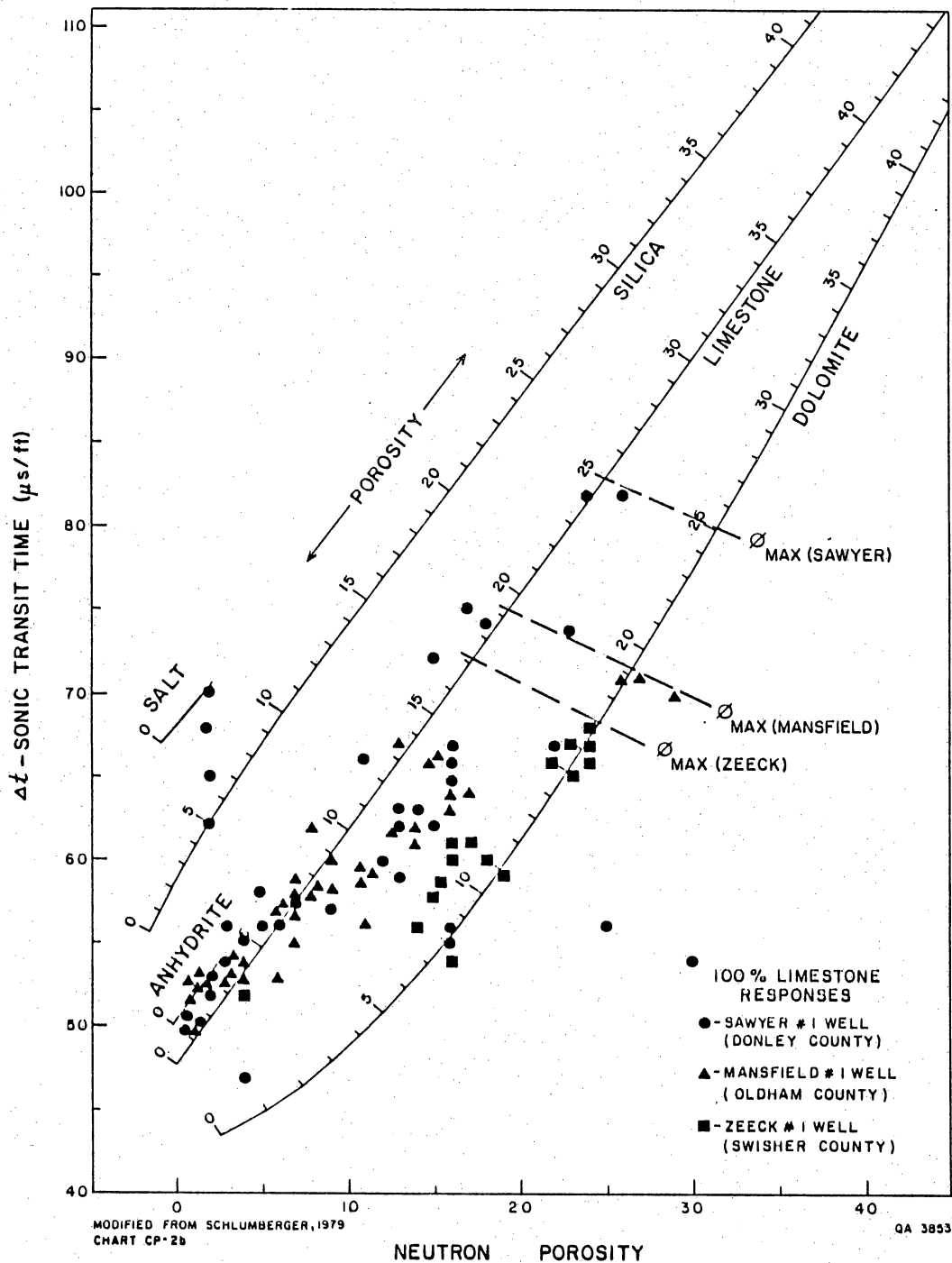


Figure 114. Neutron-porosity values plotted against the sonic-transit-time values for "pure" limestone. The data cluster more closely to the limestone line in figure 112 than they do in this plot for the same intervals, indicating inferior lithology resolution by neutron-sonic crossplotting. Maximum porosities in the Stone and Webster Engineering Corporation Sawyer No. 1, Stone and Webster Engineering Corporation Mansfield No. 1, and Stone and Webster Engineering Corporation Zeeck No. 1 wells equal 0.25, 0.19, and 0.17, respectively, which are all lower than the maximum porosities shown in figure 112. Porosities are probably lower because the sonic log does not detect secondary and vuggy porosity.

## HYDROGEOLOGIC TESTING OF THE SAN ANDRES FORMATION IN THE PALO DURO BASIN, TEXAS PANHANDLE

Alan R. Dutton

*Hydrogeologic tests support predictions, based on a regional study, of hydrogeologic characteristics of the unit-4 carbonate unit of the San Andres Formation in the Palo Duro Basin. The hydraulic-head gradient across the Palo Duro Basin is to the southeast, and the average permeability, 0.038 md, is very small. Salinity of formation water exceeds 330 g/L. Isotopic shifts in deuterium and oxygen are required to produce the isotopic composition of San Andres water,  $\delta D = -15\text{‰}$  and  $\delta^{18}O = 2\text{‰}$  (SMOW), from meteoric recharge water.*

Thick salt deposits in the San Andres Formation in the Palo Duro Basin are being considered as a medium for a high-level nuclear waste repository. However, information on the movement and composition of ground water in the carbonate rocks that underlie the salt deposits in the San Andres Formation is very limited. Therefore, hydrogeologic characteristics of the lower San Andres carbonate units were predicted with more plentiful data from the regions surrounding the Palo Duro Basin (Dutton, 1983; Orr and Dutton, 1983). Results of hydrogeologic tests in the San Andres verify those predictions.

Regional study of hydraulic head suggested that, although the San Andres Formation in the Palo Duro Basin is part of the Evaporite aquitard (Bassett and Bentley, 1983), lateral movement of ground water is possible in the carbonate units of the lower San Andres (Dutton, 1983; Orr and Dutton, 1983). Ground water in the Palo Duro Basin should flow to the southeast with an average flow velocity as small as 2.4 cm/1000 yr (assuming permeability of 0.038 md, hydraulic conductivity of  $10^{-4.65}$  m/day, and hydraulic-head gradient of 0.003).

Results of six drill-stem tests in the unit-4 carbonate of the San Andres Formation have a geometric mean of 0.038 md and a range of 0.2 md; the standard deviation of the logarithm (base 10) of measured permeability is 0.526 md (table 15). No clear pattern of variation in permeability with geographic location, lithology, or diagenesis is apparent (fig. 115). However, there is a southeastward decrease in hydraulic head from the J. Friemel No. 1 well to the Zeeck No. 1 well (table 15). The southeast gradient is



consistent with the prediction for the Palo Duro Basin that was based on earlier, more limited data (Orr and Dutton, 1983).

A fresh-water head, assuming water weight of 0.433 psi/ft, and a salt-water head, assuming water weight of 0.515 psi/ft, are given in table 15 for each test location. Equivalent fresh-water heads have been calculated for various formations in the Palo Duro and other basins (Bond, 1972; Bassett and Bentley, 1983; Orr and Dutton, 1983) because actual density of water at each test site may be unknown. Fresh-water head values for the San Andres Formation are considered unreasonable because they are greater than the potentiometric surface of the upper, post-Permian clastic aquifer and about equal to ground-level elevation (table 15). Brine is known to be in the San Andres unit-4 carbonate, and the values of salt-water head agree well with results of modeling of ground-water flow in the Palo Duro Basin (Senger and Fogg, this volume).

As meteoric water moves into the Palo Duro Basin from recharge areas in New Mexico, it dissolves halite and anhydrite and approaches saturation with respect to these minerals (Dutton, 1983). Preliminary samples of ground water from the unit-4 carbonate unit at the Zeeck No. 1 well in Swisher County have a total content of dissolved solids in excess of 330,000 mg/L; the water is calculated by the computer program SOLMNEQ (Kharaka and Barnes, 1973) to be undersaturated with respect to halite by roughly 0.3 orders of magnitude. With estimated values of  $\delta D = -15 \text{ ‰}$  and  $\delta^{18}O = 2 \pm 1 \text{ ‰}$  (SMOW), the isotopic composition of the San Andres water from the Zeeck No. 1 well lies in a trend off the meteoric water line among waters from granite-wash sandstones and Wolfcamp carbonate rocks in the Palo Duro Basin (Kreitler and others, 1985). The  $\delta D$  of the San Andres water is unlike  $\delta D$  of shallow ground water either in East-Central New Mexico or across the Texas Panhandle (see Senger, Richter, and Kreitler, this volume). Isotopic shifts in both deuterium and oxygen are required to produce the isotopic composition of San Andres water from meteoric water.

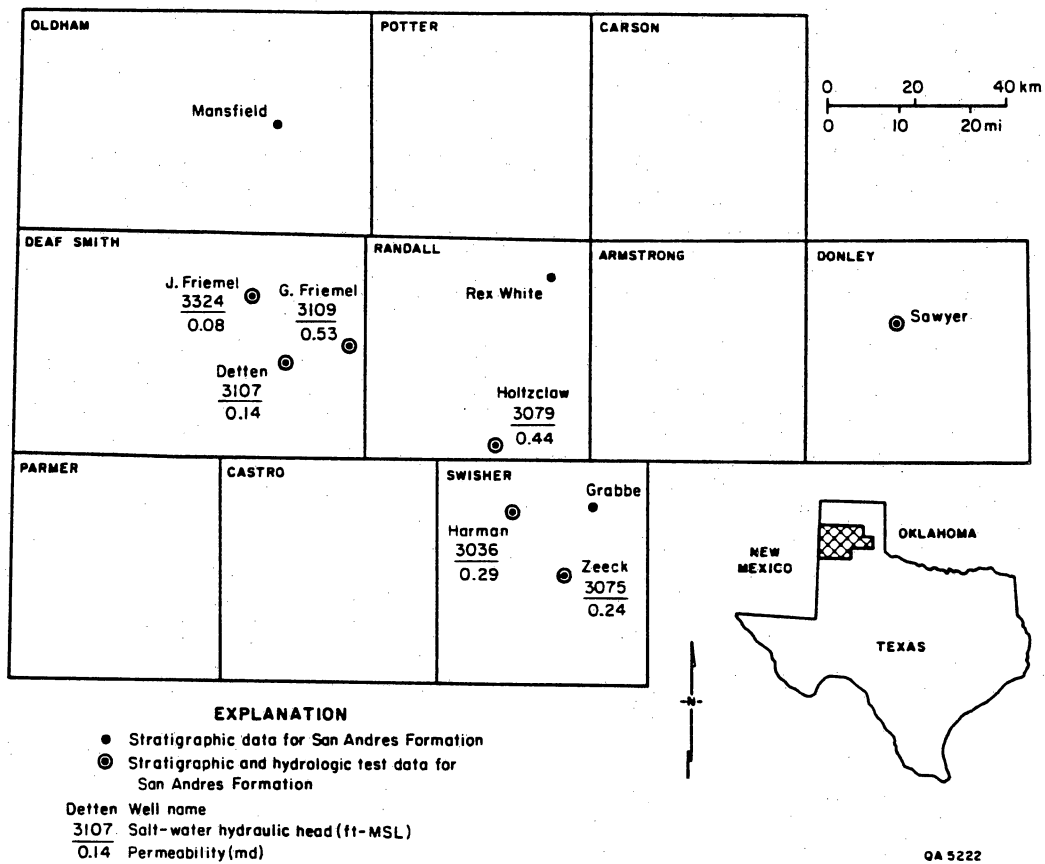


Figure 115. Locations of drill-stem tests in the San Andres Formation with values of salt-water head and permeability.

Table 15. San Andres hydrologic data from Palo Duro Basin test wells.

Test well name	Permeability (md)	Ground-level elevation (ft)	Upper aquifer head (ft)	San Andres head (ft)	Wolfcamp aquifer head (ft)
			1	2	3
J. Friemel No. 1	0.013	4025	37,755	3701	3304
Detten No. 1	0.024	3855	3700	3685	3262
G. Friemel No. 1	0.11	3817	3675	3458	3099
Holtzclaw No. 1	0.01	3622	3425	3583	3156
Harman No. 1	0.041	3532	3380	3533	3050
Zeeck No. 1	0.219	3411	3325	3206	2746
					2289*
					2075
					2050
					2000
					2200
					2338*

1. Data for 1974-1975 from Texas Department of Water Resources (1984).
2. Pressure head calculation based on water weight of 0.433 psi/ft.
3. Pressure head calculation based on water weight of 0.515 psi/ft.
4. \*indicates results of drill-stem tests; otherwise values are interpolated from preliminary map of Wolfcamp aquifer hydraulic head.

## WATER SAMPLING AND HYDROLOGIC TESTING IN THE SALT-DISSOLUTION ZONE OF THE TEXAS PANHANDLE

Alan R. Dutton

*Test wells have been constructed in the Palo Duro Basin to provide data on the hydrogeology of the salt-dissolution zone. The bases of the test zones are within 7 to 49 ft of the upper surface of bedded salt. The test zone in three of the four wells was drilled with an air-mist foam to reduce the extent of contamination of the strata to be tested. Hydrologic tests and chemical analyses of water samples are carried out to determine the source of ground water that dissolves the salt, and the rate and timing of the salt-dissolution processes.*

The zone of salt dissolution in the Palo Duro Basin is being tested to determine the hydrogeology, timing, and rate of salt-dissolution processes. Stone and Webster Engineering Corporation Sawyer No. 2 near Clarendon in Donley County, Mansfield No. 2 near Vega in Oldham County, Detten No. 2 near Hereford in Deaf Smith County, and Harman #1 north of Tulia in Swisher County are being used in these tests (fig. 116). Interpretations are based on data from chemical analyses of water samples and from tests of hydrologic properties of the dissolution zone. The scope of field activities is to obtain and analyze uncontaminated samples of ground water from the test zones and to conduct drawdown and recovery tests of hydrologic parameters.

### Stratigraphy of Salt-Dissolution Zone

The broad zone of salt dissolution that encompasses the Texas Panhandle lies to the west under the Pecos River valley, to the north under the Canadian River valley, and to the east below the Rolling Plains (Gustavson and others, 1980, 1981c). The elevation and location of the deepest zone of salt dissolution varies across the Panhandle (figs. 117 and 118). Toward the center of the basin, the position of the uppermost salt bed climbs higher in the stratigraphic section. At the Sawyer No. 2 well, the uppermost salt is in the lower San Andres Formation (fig. 119). At the Mansfield, Detten, and Harman wells, the highest salt lies in the Seven Rivers Formation (figs. 120, 121, and 122).

## Design and Construction of Test Wells

The test wells are designed to obtain samples of water involved in the dissolution of salt. Test zone bases are within 7 to 49 feet of the upper surface of bedded salt (figs. 119 through 122). The test intervals include the strata considered most likely to transmit water through the dissolution zone on the basis of study of core and electric logs. Thiocyanate ( $\text{SCN}^-$ ) tracer was to be used in the drilling fluid to indicate the degree of contamination of the ground water.

The Sawyer No. 2, Mansfield No. 2, and Detten No. 2 test wells are offset by 100 to 200 ft from deeper hydrostratigraphic test wells that had been completed as part of studies on nuclear waste isolation feasibility. The approach to constructing these three wells generally was to drill to the top of the test zone, make geophysical-log surveys, and case the wellbore. The test zone itself was then drilled or cored with an air-mist foam to reduce the volume of drilling fluid that could contaminate the strata. After total depth was reached, ground water was produced from the test zone for several hours by forcing compressed air through the drillpipe and out at the test zone. The Sawyer and Mansfield wells yielded about 50 to 80 gallons per minute with this production method. The Detten No. 2 well did not yield water by this technique. No other well development or stimulation was done.

Unlike the three offset wells, the Harman No. 1 well was originally drilled to 3,041 ft below land surface using salt-based mud (10.4 pounds gallon weight). It was converted for use as a dissolution-zone test well by placing a cement plug in the borehole below the zone of interest, leaving a 148-ft interval between the base of casing and the top of the plug. Therefore, the test zone at the Harman well is much more contaminated with drilling fluid than are the zones at the other three sites.

Further details of well construction are reported by Stone and Webster Engineering Corporation (1983).

## Testing and Sampling Procedures

The general approach being used at each well is to conduct tests to determine hydrologic properties while pumping to remove ground water that might be contaminated with drilling fluid. A submersible turbine is used at the Sawyer and Mansfield wells where transmissivity is fairly high. At the Detten and Harman wells, where transmissivity is rather low, water is bailed from the well. The concentration of thiocyanate tracer is monitored to document the removal of drilling contaminants. The produced water is stored on-site and hauled away for subsurface disposal.

Once the concentration of tracer indicates that cleanup is complete, sampling of ground water for chemical analysis takes place. Determinations are made of temperature, pH, Eh, calcium, sodium, magnesium, potassium, strontium, iron, sulfate, sulfide, bicarbonate, chloride, bromide, iodide, and the isotopes of deuterium ( $H^2$ ), oxygen-18, sulfur-34, carbon-13 and carbon-14, chloride-36, and iodide-129. Sampling techniques vary according to the specific constituent or parameter being measured.

## Preliminary Results

The concentration of thiocyanate tracer several months after well construction but before the start of tests was essentially 0 ppm at the Sawyer and Mansfield wells and about 30 ppm at the Detten and Harman wells. Natural movement of ground water in the dissolution zone was great enough to partly (70 percent) or entirely flush the small amount of drilling contamination away from the test well. At the date of this report, no conclusive results have been found from tests at the Detten and Harman wells.

Ground water from the Sawyer No. 2 well is saline with total concentration of dissolved solids of 94,924 mg/L. The water is about 1.6 orders of magnitude undersaturated with respect to halite. Ground water at the Mansfield No. 2 well is also saline with total concentration of dissolved solids of 67,537 mg/L. This water is undersaturated with

respect to halite by about two orders of magnitude. Clearly, the saline water in the stratigraphic intervals being tested at these two wells is derived from the dissolution of salt by percolating ground water.

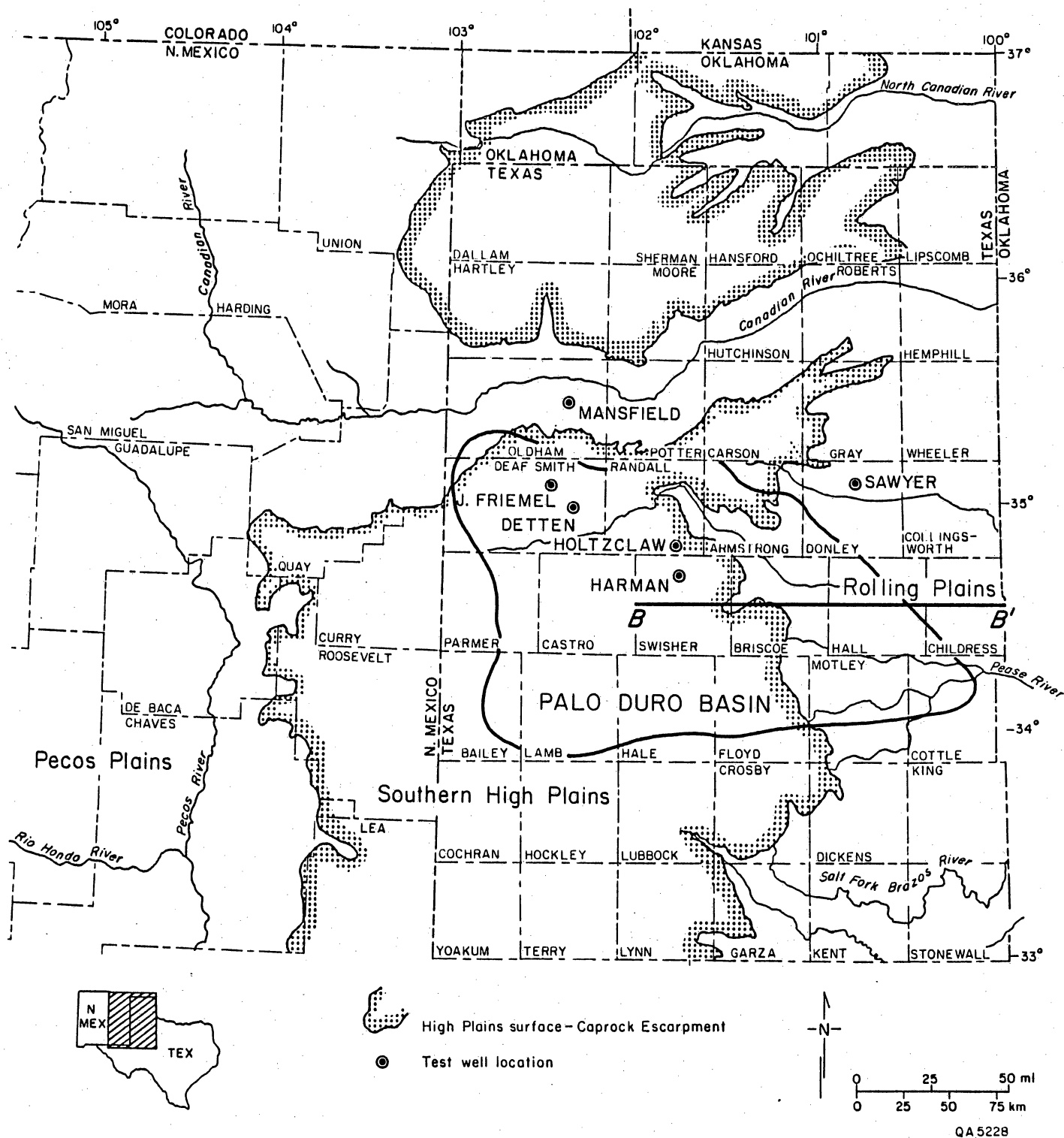


Figure 116. Locations of hydrochemical test wells in the salt-dissolution zone in the Texas Panhandle.



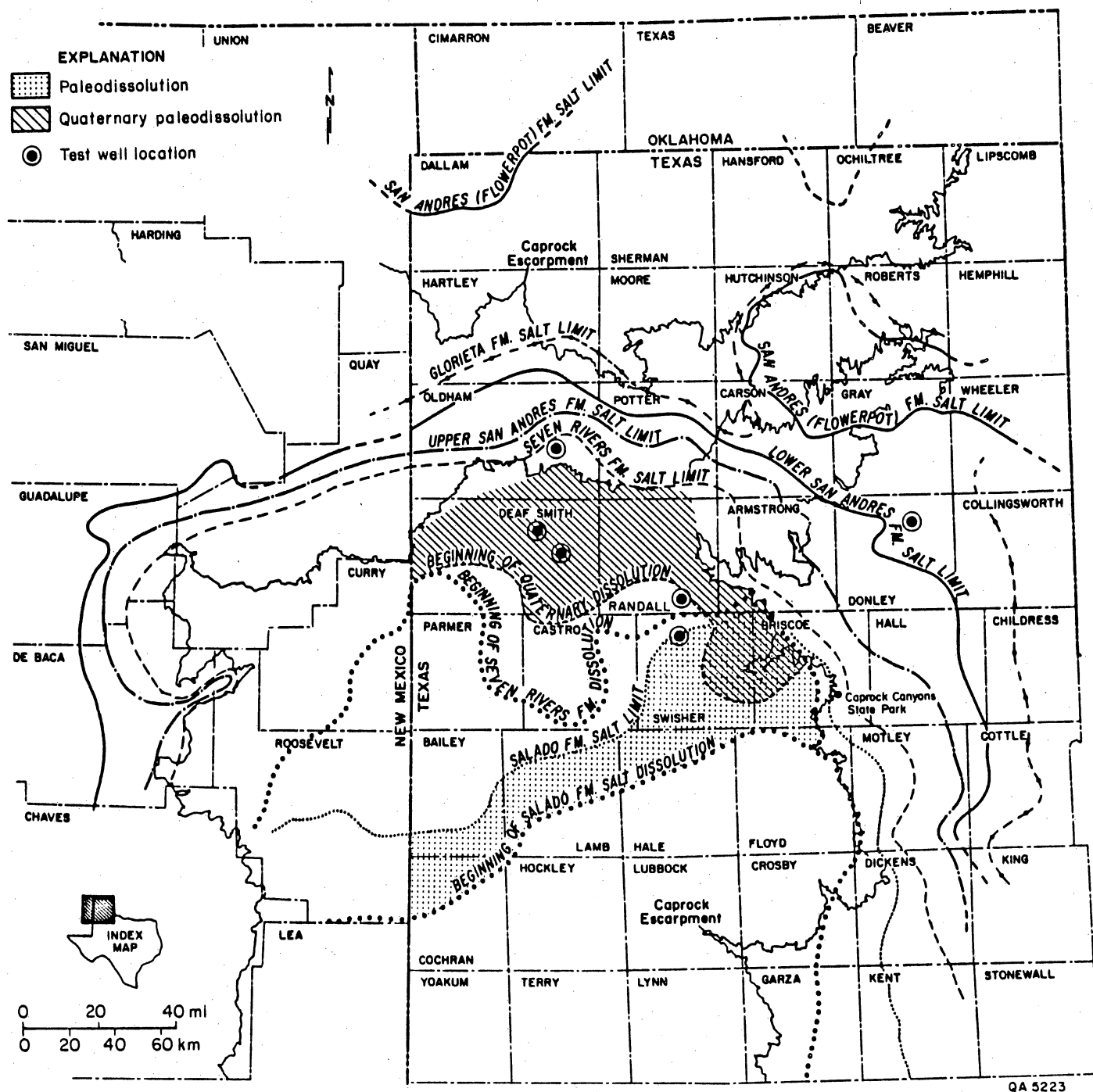


Figure 117. Salt-dissolution zones, Texas Panhandle and eastern New Mexico. Except for the Seven Rivers and Salado Formations, where both the beginning of salt dissolution and the limit of salt are shown, the limit of salt for the younger formation marks the approximate beginning of salt dissolution for the next older formation (from Gustavson, 1982).

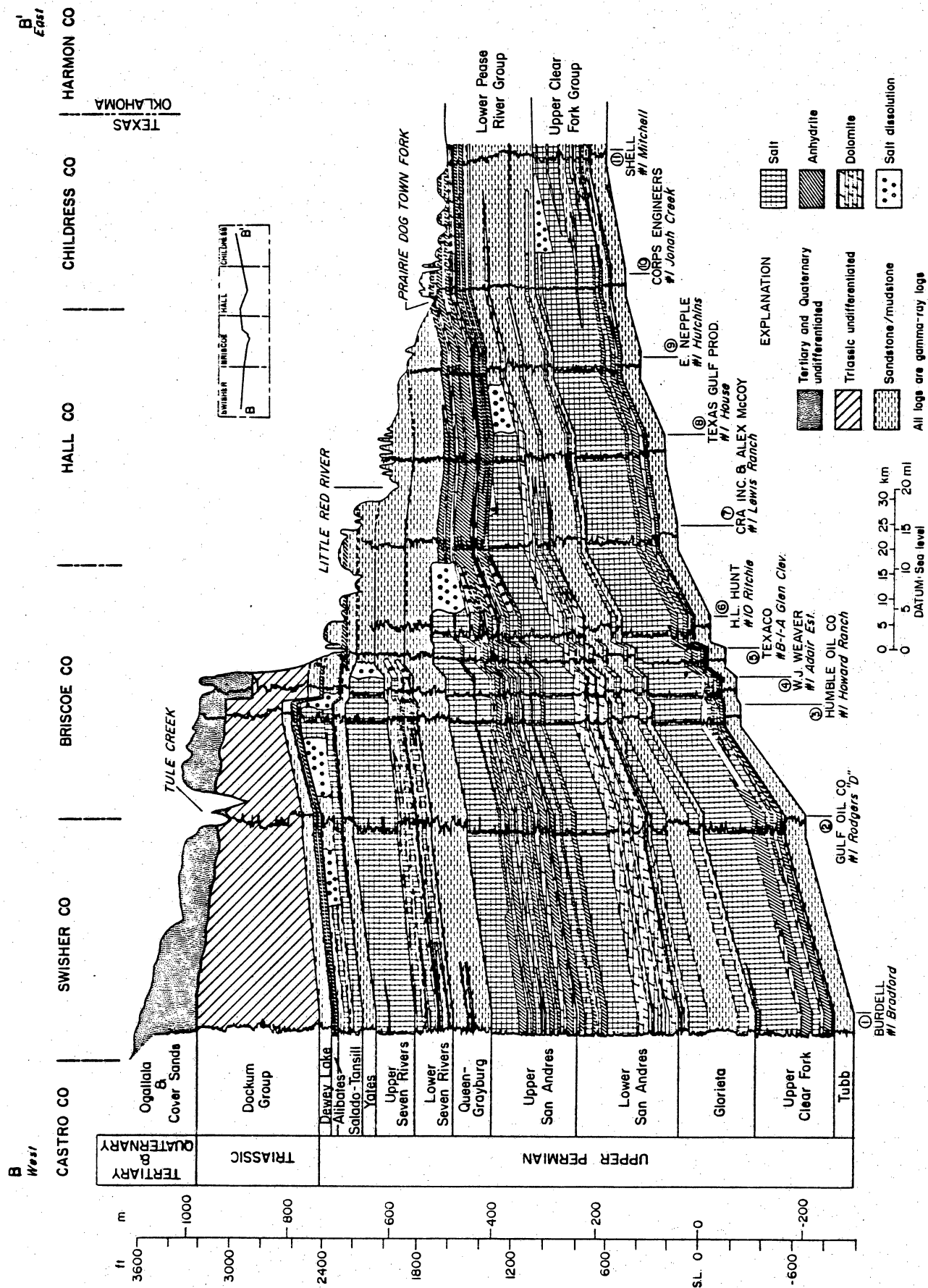


Figure 118. Major zones of salt dissolution underlying the eastern margin of the Southern High Plains. Line of west-to-east cross section is shown in figure 116 (from Gustavson and others, 1980).

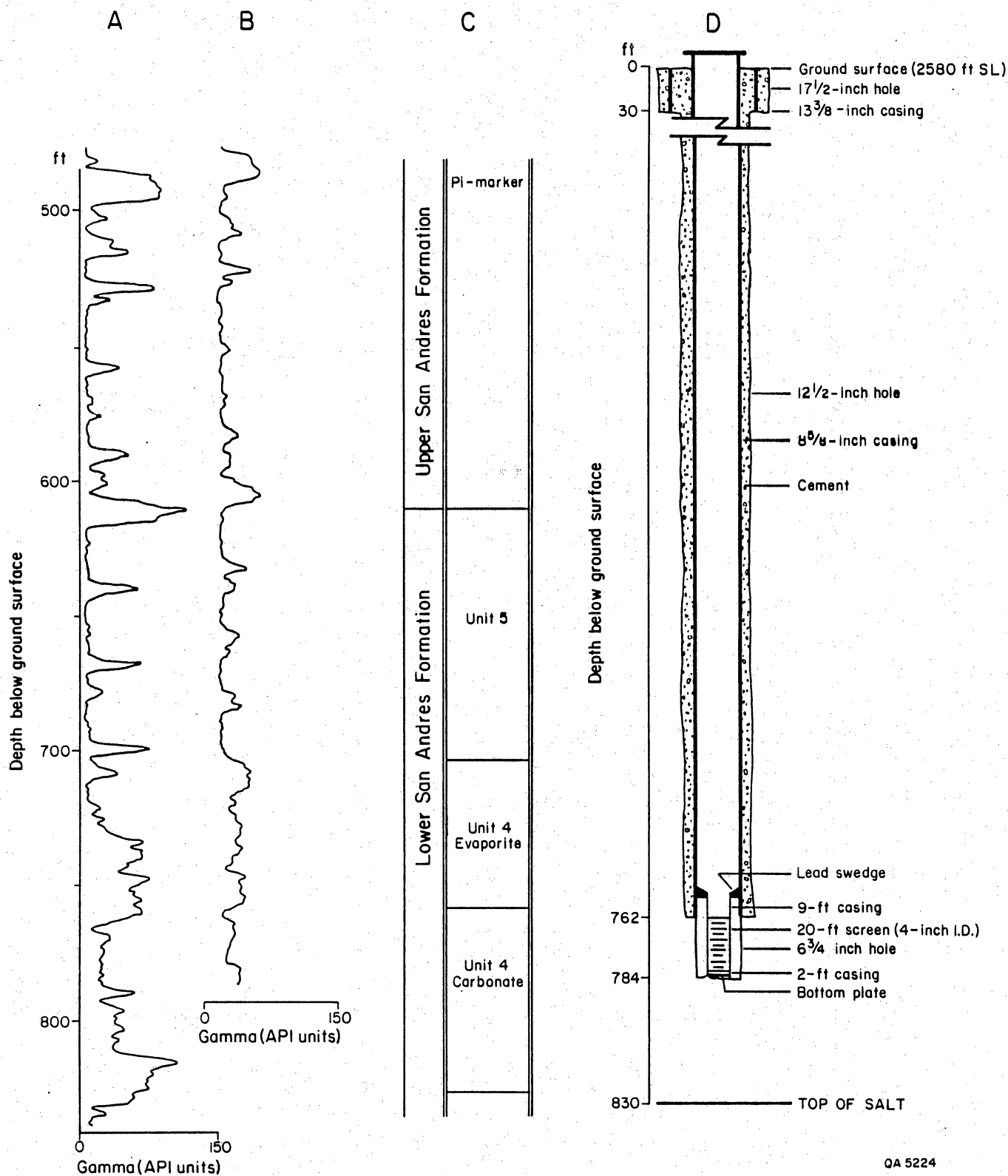
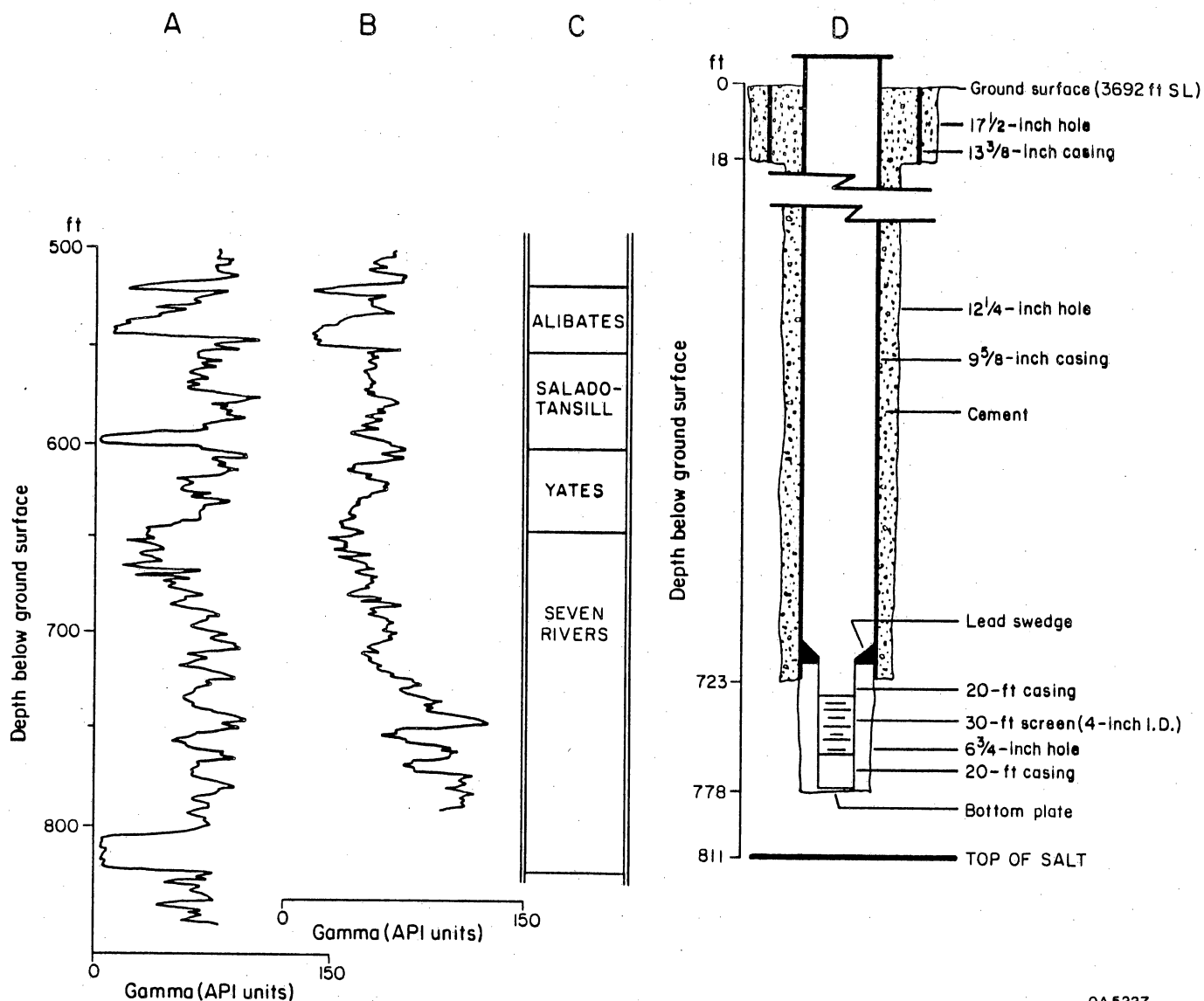
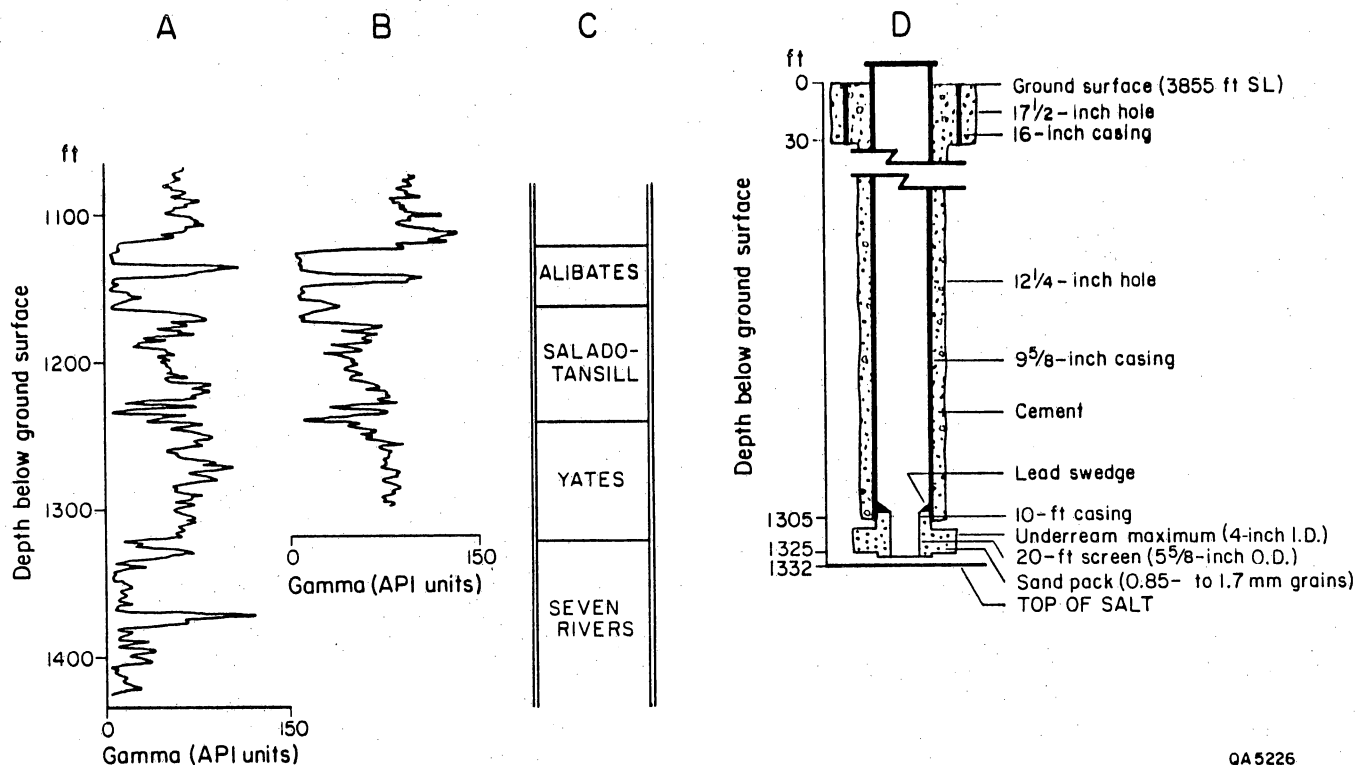


Figure 119. Stratigraphy and construction of the Stone and Webster Engineering Corporation Sawyer No. 2 hydrochemical test well. (A) Gamma-ray log in the Stone and Webster Engineering Corporation Sawyer No. 1 well. (B) Gamma-ray log in Stone and Webster Engineering Corporation Sawyer No. 2 well. (C) Stratigraphic setting of test zone. (D) As-built drawing of the test well (modified from Stone and Webster Engineering Corp., 1983).



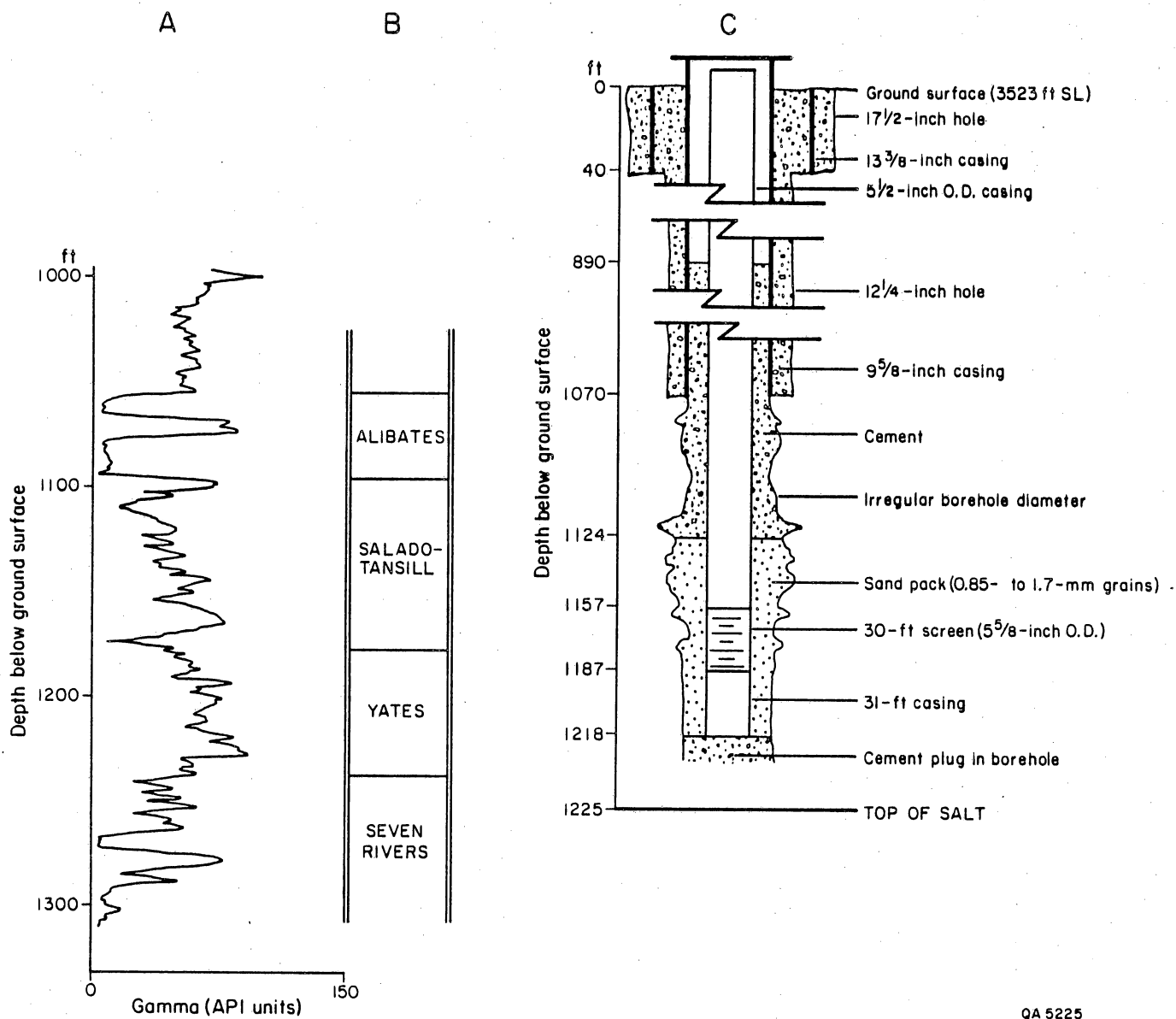
QA 5227

Figure 120. Stratigraphy and construction of the Stone and Webster Engineering Corporation Mansfield No. 2 hydrochemical test well. (A) Gamma-ray log in the Stone and Webster Engineering Corporation Mansfield No. 1 well. (B) Gamma-ray log in Stone and Webster Engineering Corporation Mansfield No. 2 well. (C) Stratigraphic setting of the test zone. (D) As-built drawing of the test well (modified from Stone and Webster Engineering Corp., 1983).



QA5226

**Figure 121. Stratigraphy and construction of the Stone and Webster Engineering Corporation Detten No. 2 hydrochemical test well. (A) Gamma-ray log in the Stone and Webster Engineering Corporation Detten No. 1 well. (B) Gamma-ray log in the Stone and Webster Engineering Corporation Detten No. 2 well. (C) Stratigraphic setting of the test zone. (D) As-built drawing of the test well (modified from Stone and Webster Engineering Corp., 1983).**



QA 5225

Figure 122. Stratigraphy and construction of the Stone and Webster Engineering Corporation Harman No. 1 hydrochemical test well. (A) Gamma-ray log in the test well. (B) Stratigraphic setting of the test zone. (C) As-built drawing of the test well (modified from Stone and Webster Engineering Corp., 1983).

## POTENTIOMETRIC SURFACE OF THE UPPER PENNSYLVANIAN AQUIFER, TEXAS PANHANDLE

D. Anderson Smith

*An objective geostatistical method was used to map distribution of hydraulic heads measured in upper Pennsylvanian rocks of the Palo Duro Basin and surrounding areas. Geostatistical analysis was applied to describe data variation. Kriging was then used to estimate head values on the basis of data with minimum estimate variance. Derived estimates were contoured using CPS 1.*

Pennsylvanian drill-stem-test (DST) data from 3,797 wells in the Palo Duro, Anadarko, Dalhart, Hardeman, and Midland Basins and parts of New Mexico west of the Palo Duro Basin were studied. Data were differentiated for the upper and lower Pennsylvanian. The upper sequence includes the Canyon and Cisco Groups, and the lower includes the Bend and Strawn Groups. Maximum thickness of the Pennsylvanian section is 2,000 ft in the center of the Palo Duro Basin and 7,600 ft in the center of the Anadarko Basin and thins onto uplifts exposed during the Pennsylvanian Period. The upper Pennsylvanian sequence thins onto the uplifts and ranges in maximum thickness from 1,500 ft in the center of the Palo Duro Basin to 5,000 ft in the center of the Anadarko Basin.

This upper and lower Pennsylvanian subdivision was based on a vertical change in facies noted by Dutton and others (1982). Dutton reported that the lower Pennsylvanian sequence is composed of terrigenous clastics and thin interbedded limestones with thick limestone buildups common in the upper sequence. Because of this vertical change in facies, mapping each sequence separately produces a more realistic representation of the head distribution in the Pennsylvanian.

The Petroleum Information (PI) data base of the upper Pennsylvanian consisted of DST pressures from 1,799 wells. Using the criterion of a gradient greater than 0.3 psi/ft, 776 pressures were initially considered reliable. Gradient is defined as the shut-in pressure divided by depth. Two hundred seventy-five head values were deleted from this data base because they were either significantly lower or higher than nearby head values. Eleven

values derived from either DOE wells or from actual DST charts were added to the data base. These additions resulted in a final data file of 512 head measurements.

Kriging was selected as a statistical method of objectively estimating the hydraulic head values because it provides an estimate of the value, calculates the estimate in such a way that the estimation variance is minimized, and provides values for the estimation variance that can be mapped as a measure of confidence of the head values. This mapping technique was used previously to map the potentiometric surface of the Wolfcamp aquifer (Smith and others, 1983).

Variograms of the upper Pennsylvanian head data for the entire data set and for subareas of the study area were generated. Geostatistical analysis showed that there was no single structure that could model the entire region, but that separate regions of the study area could be modeled by different variograms. Separate spherical variograms were calculated for the Anadarko Basin (fig. 123) and for the Palo Duro Basin (fig. 124).

The variogram parameters from the Palo Duro Basin variogram are

range of influence (a): 26,000 m

random variance (nugget  $C_0$ ): 31,000 ft<sup>2</sup>

spatial variance (C): 40,500 ft<sup>2</sup>

total variance (sill  $C + C_0$ ): 71,500 ft<sup>2</sup>

In the Palo Duro Basin variogram model the random variance is slightly smaller than the spatial variance, indicating that kriging can account for more than half of the total variation in the data. The average kriging block variance is 21,604 ft<sup>2</sup>, which is comparable to the nugget, or random, variance.

The variogram parameters from the Anadarko Basin variogram are

range of influence (a): 20,000 m

random variance (nugget  $C_0$ ): 195,000 ft<sup>2</sup>

spatial variance (C): 125,000 ft<sup>2</sup>

total variance (sill  $C + C_0$ ): 320,000 ft<sup>2</sup>



In the Anadarko Basin variogram model the random variance is larger than the spatial variance. This indicates that random variance dominates the data base and that, although kriging will give valid block estimates, kriging accounts for less than half of the total variation. The average krige block variance is  $69,248 \text{ ft}^2$ , squared which is much smaller than the nugget or random variance.

The variation in the Anadarko Basin model is more than four times as large as the variation in the Palo Duro Basin model. The larger variation in the Anadarko Basin model may be due to the pressures in the basin being universally affected by oil and gas production.

Each region was then kriged using the variogram parameters from its respective variogram and the data in its respective area. In much of the Palo Duro Basin the data distribution was too scarce to allow a krige block to be estimated. In these areas, those raw data values considered to be of best quality were included with the krige block estimates to form the contoured data base (Orr and Dutton, 1983). The krige block estimates and selected raw data values were then contoured using CPS-1, a Radian Corporation contouring package.

The upper Pennsylvanian potentiometric surface map implies a general east to northeast component of flow across the Palo Duro Basin (fig. 125). Further east the inferred flow direction is more to the southeast. Hydraulic heads in the Anadarko Basin are highest in the central deepest parts of the basin. Flow is inferred to be to the southeast and east along the Amarillo Uplift and to the north and northwest out of the basin. Our map of the potentiometric surface of the upper Pennsylvanian aquifer shows a similar trend to that of the potentiometric surface of the Wolfcamp aquifer, but we infer a more west-east component of flow across the Palo Duro Basin. The head values and gradients are similar, suggesting that the Wolfcamp and upper Pennsylvanian may act as a single hydrologic unit.

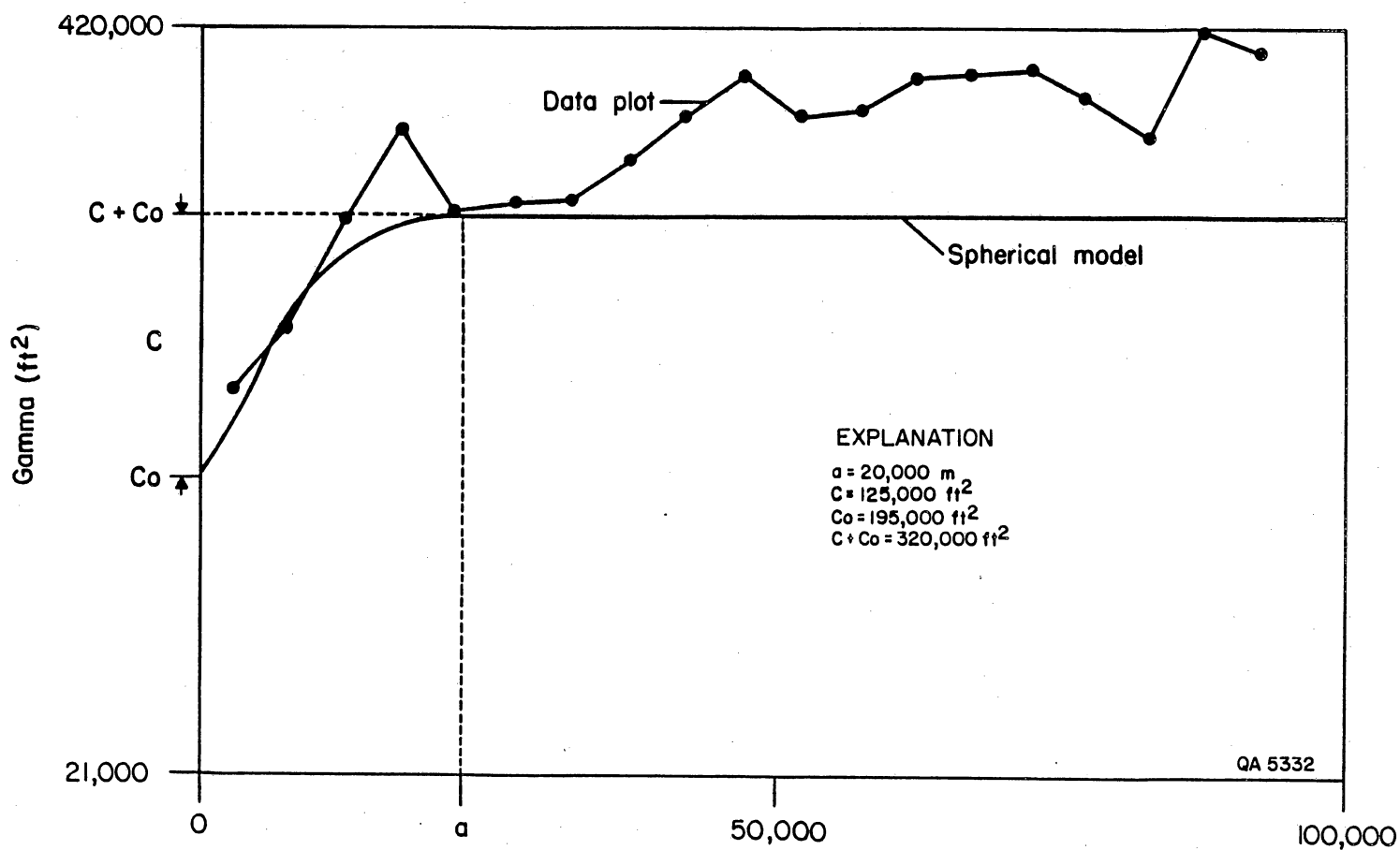


Figure 123. Semi-variogram of upper Pennsylvanian equivalent fresh-water heads calculated from drill-stem-test shut-in pressures in the Anadarko Basin, Texas Panhandle and Oklahoma.

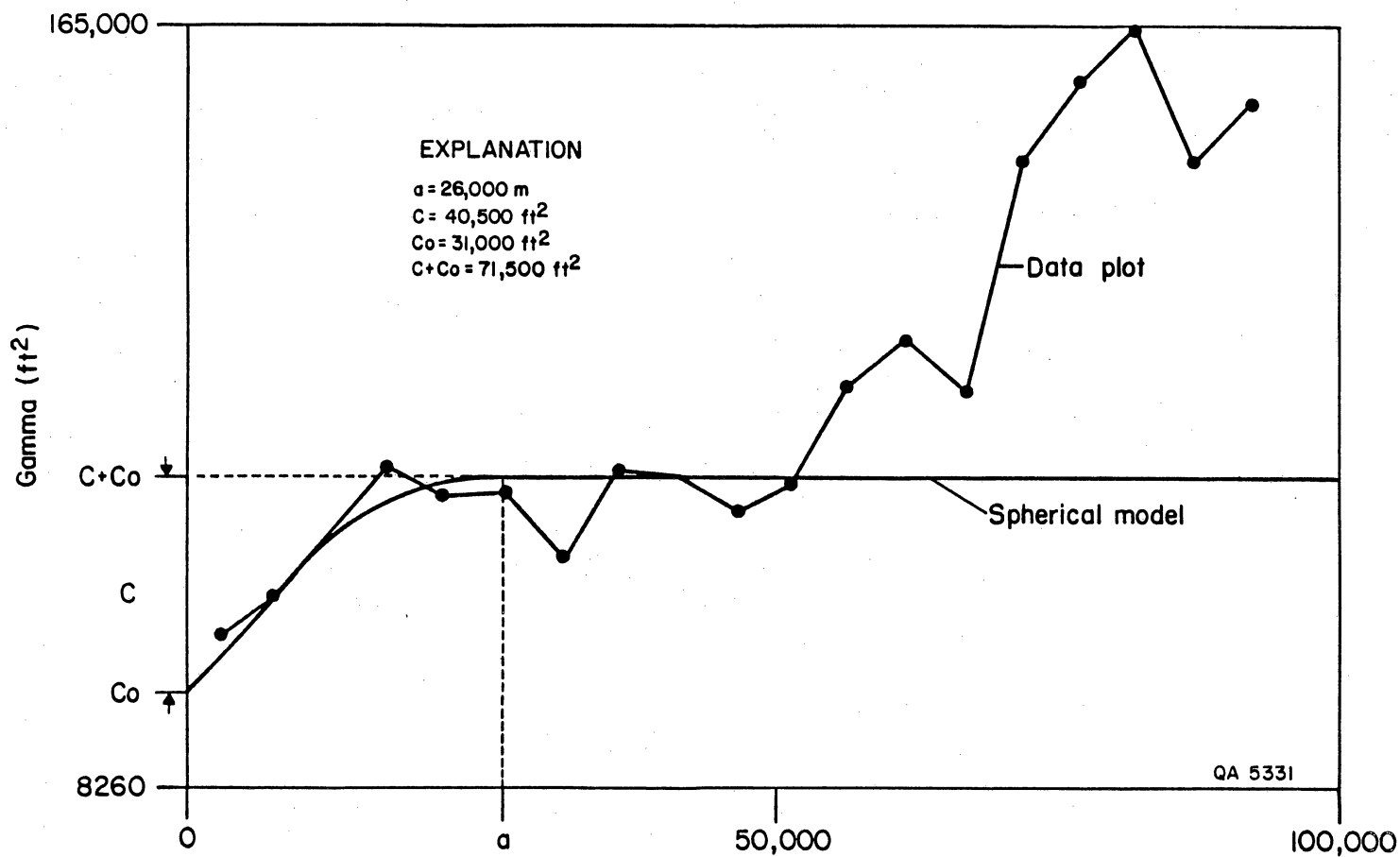


Figure 124. Semi-variogram of upper Pennsylvanian equivalent fresh-water heads calculated from drill-stem-test shut-in pressures in the Palo Duro and Midland Basins, Texas Panhandle, Oklahoma, and New Mexico.

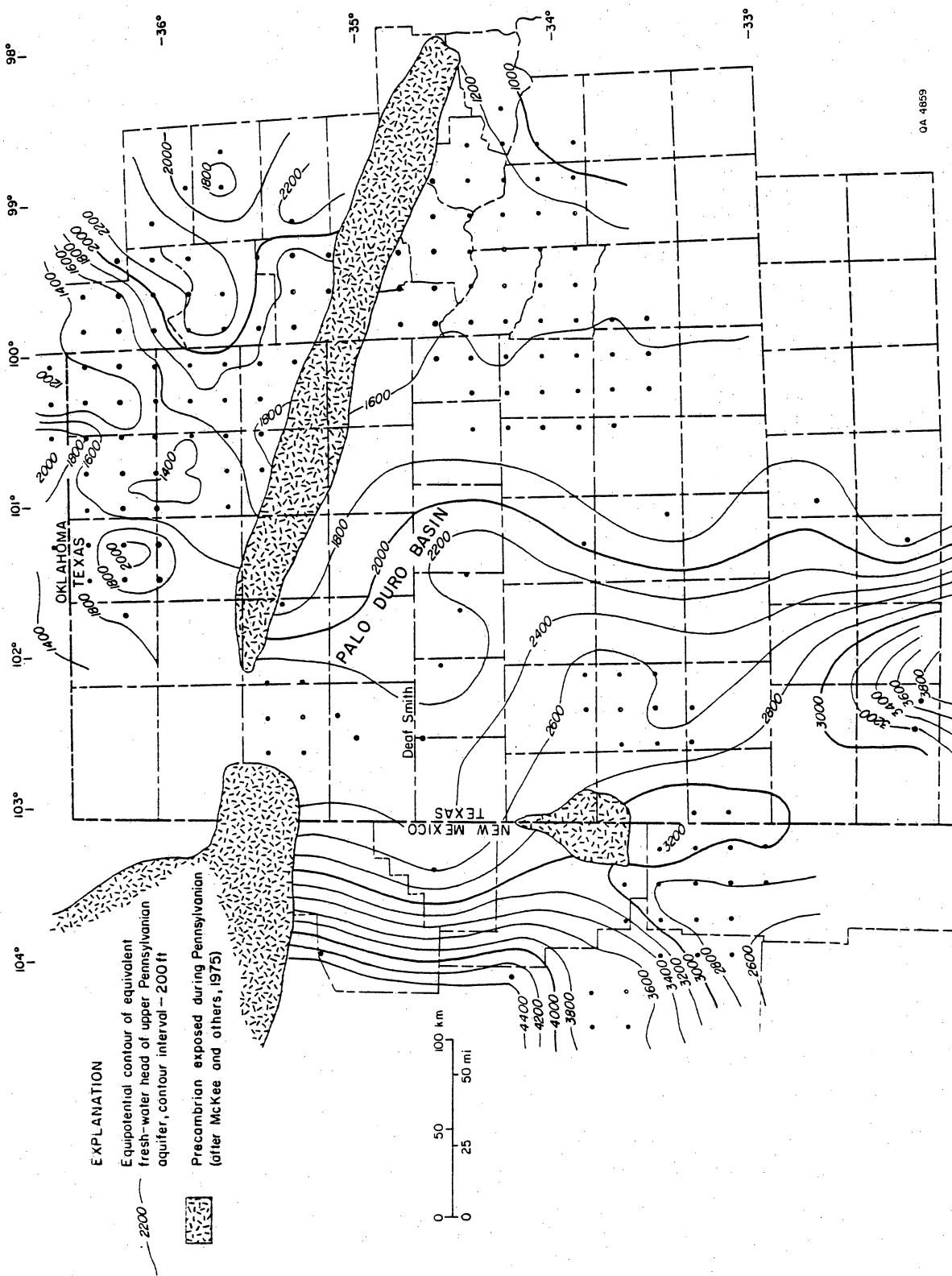


Figure 125. Potentiometric surface map of equivalent fresh-water heads calculated from drill-stem-test shut-in pressures in upper Pennsylvanian strata in the Texas Panhandle, Oklahoma, and New Mexico.

## INTERPRETATION OF PRESSURE-DEPTH DATA FROM CONFINED AQUIFERS

Elizabeth D. Orr and Charles W. Kreitler

*The quality, quantity, and distribution of available data, and variability in the potentiometric surface, aquifer structure, and surface topography determine the reliability of pressure-depth plots for hydrologic interpretation in confined regional aquifers.*

Pressure-depth plots are a relatively new tool for characterizing regional groundwater flow. The reliability and accuracy of these plots have not, however, been addressed in any published research. The purpose of this investigation is (1) to identify and document easily neglected factors that impede accurate interpretation of pressure-depth plots, and (2) to suggest a method whereby pressure-depth plots can be more reliably used for hydrologic interpretation.

Whereas a potentiometric surface indicates regional horizontal flow directions, pressure-depth data can indicate whether flow within the aquifer has an upward or downward component (Tóth, 1978, 1979). Potential for vertical flow is best indicated by plotting two or more pressure-depth measurements from each of several closely spaced wells: an upward component of flow is indicated when the slope of the pressure-depth regression line is greater than hydrostatic (no flow or horizontal flow conditions), and a downward component is indicated when the slope is less than hydrostatic (fig. 126a). The intersection of the regression line on the depth axis indicates depth to the potentiometric surface (fig. 126b).

One factor that impedes accurate interpretation of pressure-depth plots is limited data. Available data, usually obtained from drill-stem tests (DST's) in petroleum exploration wells, may be of questionable quality and exhibit anomalous features (fig. 127).

Pressure-depth plots may also vary and exhibit scatter because they reflect changes in the hydrologic configuration of the regional aquifer, specifically variations in the potentiometric surface, the geologic structure of the aquifer, and the surface topography (fig. 128). In large areas that are relatively homogeneous with respect to surface

topography, structure, and the potentiometric surface, a plot of pressure-depth data from several wells will reflect the same conditions as in individual wells (fig. 128a--no flow). However, if any of the three hydrogeologic factors vary significantly, the regression line through pressure-depth data from several wells will be different in slope and intercept than a regression line through data from an individual well. Figure 128b is a model for parallel flow up the inclined Deep-Basin Brine aquifer from Lamb County to Potter County in Palo Duro Basin. The northeasterly direction of flow is inferred from the potentiometric surface of the average Deep-Basin Brine aquifer (Wirojanagud and others, 1986). A regression line through computed data for five widely spaced wells indicates underpressured conditions and a strong potential for upward flow within the aquifer. However, the pressure-depth data from each individual well indicates a very minor upward component of flow that is undetectable on a pressure-depth or head-depth plot. The upward flow component indicated by the regression line through all the data grossly exaggerates the true component of upward flow indicated by a single well. The intercept on the depth axis erroneously indicates a depth to the water table that is deeper than the maximum possible in this hydrogeologic setting. A similar problem occurs where there is horizontal flow with increasing topography, as shown in figure 128c. The pressure-depth plot, however, would indicate an erroneous upward component of flow.

In some cases, closely spaced data that look accurate can be, in fact, misleading. Figure 128d reflects parallel flow in a direction of decreasing topography and increasing aquifer elevation. Computed data for individual wells correctly indicate a slight upward component of flow. However, the regression line through all the data indicates a downward flow component and depth to water at land surface.

Because there is rarely enough accurate DST data from any one well to compare with trends indicated by all data within a specific area, it is important to identify the effects of the hydrogeologic setting before drawing conclusions from pressure-depth plots.

Accurate interpretation is hindered further because DST data are not uniformly or even randomly distributed. Oil and gas exploration wells target particular stratigraphic units and areas. In the southeastern part of Palo Duro Basin, most DST's in the hydrologically connected Deep-Basin Brine aquifer are from Pennsylvanian carbonates. In the northwestern part, most DST's are from Granite Wash deposits and Wolfcampian carbonates. The slopes and intercepts of pressure-depth regression lines may vary considerably depending on how the available DST data are distributed.

In summary, accurate interpretation of pressure-depth plots is best facilitated by having sufficient high-quality, uniformly distributed DST data from small areas having minimum variation in the potentiometric surface, the aquifer structure, and the surface topography. When analyzing less than ideal data, it is important to first understand the possible effects that a varying hydrogeologic setting and uneven data distribution may have on plotted pressure-depth configurations. A suggested method is first to compute pressure-depth data for a given hydrogeologic setting assuming parallel flow, and then to compare the plotted results with the field data (fig. 129). Significant differences in the regression lines of the plots would indicate real potential for vertical flow. Similarities in the regression lines would suggest no potential for vertical flow: the slopes of the regression lines, even if different from hydrostatic, may be an effect of the hydrogeologic setting or data distribution and not the hydrologic conditions within the confined aquifer.

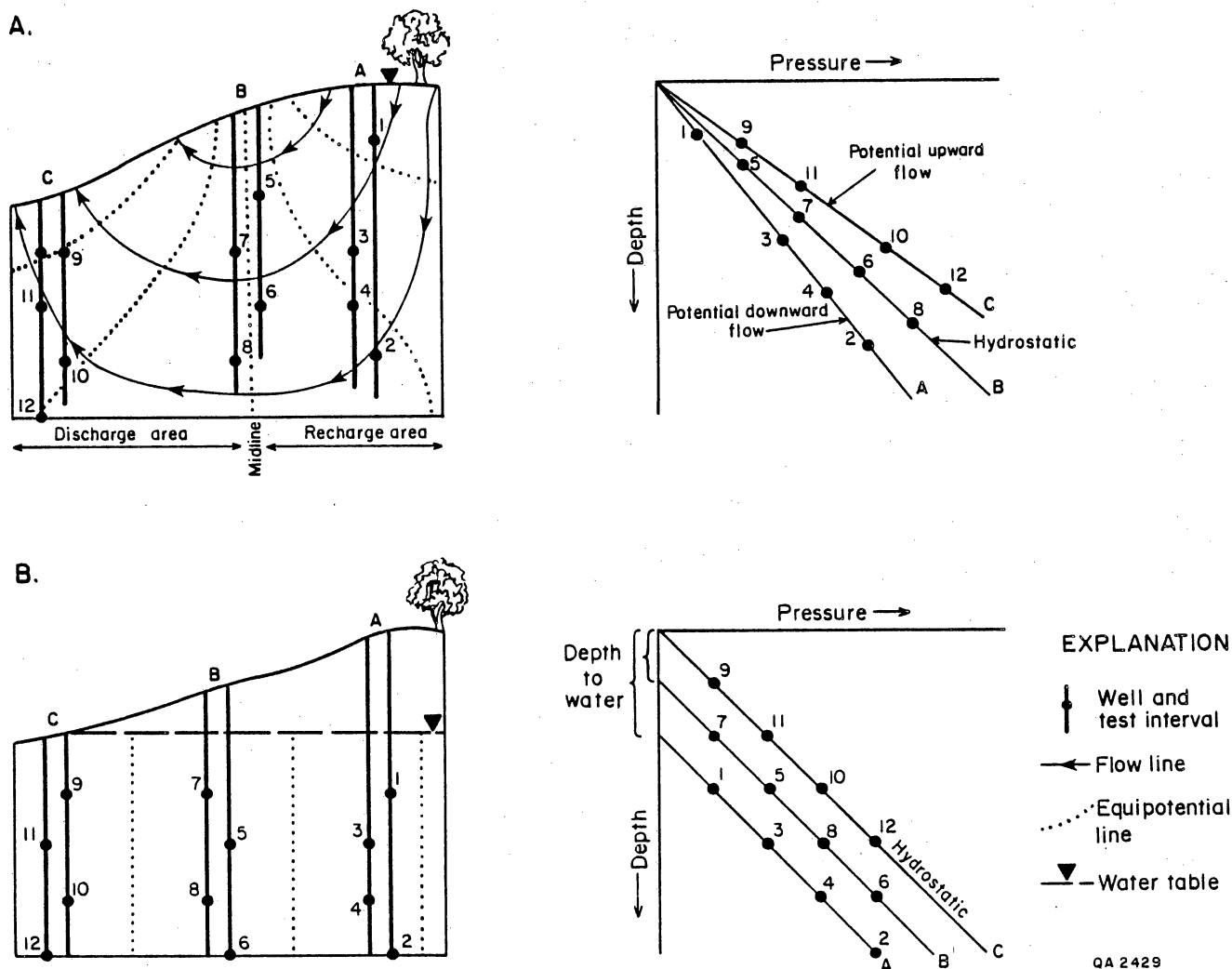


Figure 126. Flow patterns and pressure-depth relationships for (A) a simple unconfined drainage basin, and (B) a confined hydrostatic aquifer. Varying slopes of plotted pressure-depth data in A indicate regions of potential upward and downward flow. Offsets in plotted pressure-depth data in the subhydrostatic region in B are a result of variations in the surface topography.



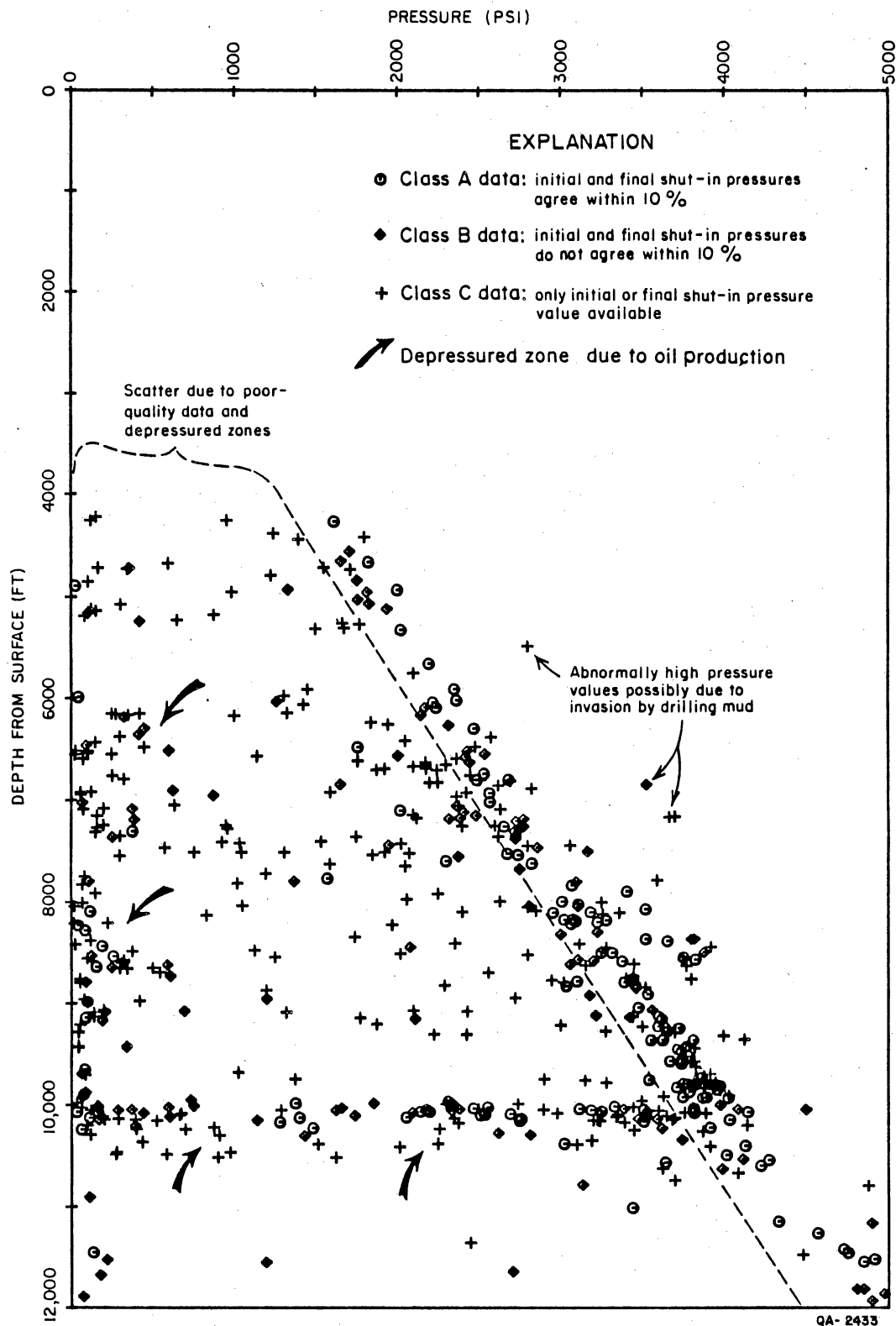
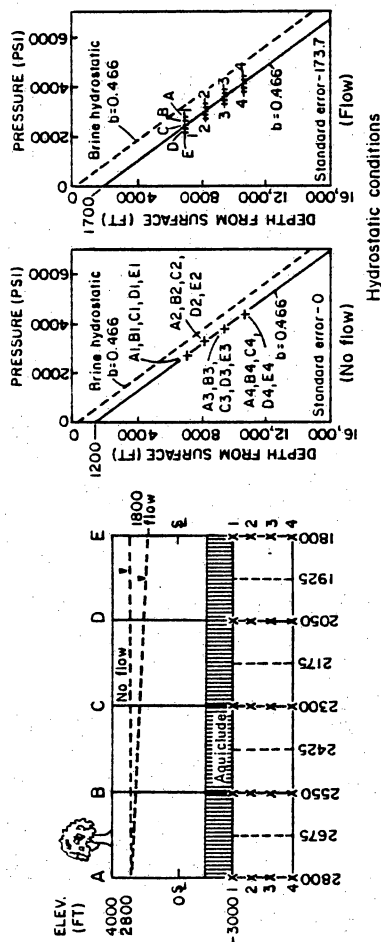


Figure 127. Plot of pressure-depth drill-stem-test data in Hockley County showing (1) high scatter due to mixed quality data, (2) depressed zones due to high oil and gas production, and (3) abnormally high pressure values possibly due to drilling mud invasion.

# FLAT SURFACE TOPOGRAPHY

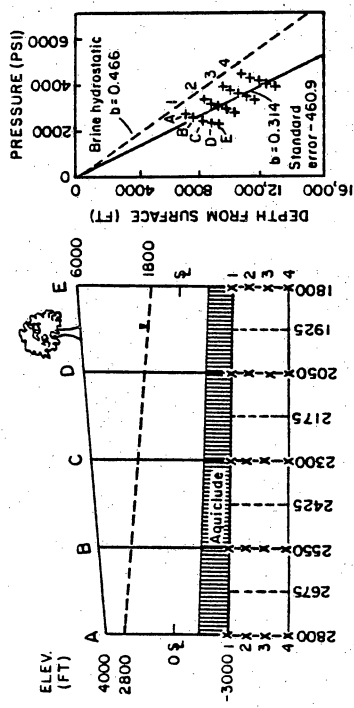
HORIZONTAL AQUIFER STRUCTURE

A



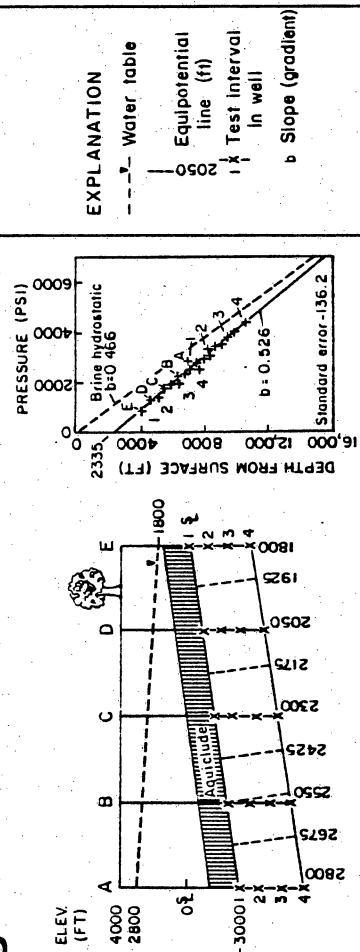
# VARYING SURFACE TOPOGRAPHY

C



VARYING AQUIFER STRUCTURE

B



D

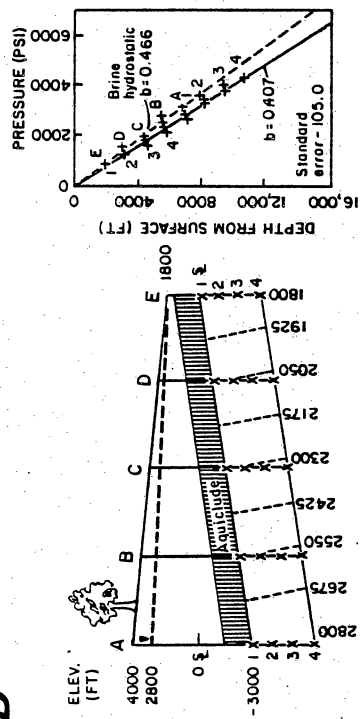


Figure 128. Variations in configurations of plotted pressure-depth data due to changes in surface topography, aquifer structure, and the potentiometric surface. Plotted data were modeled for five wells over 140 mi assuming parallel flow or no flow within a confined aquifer: (A) no variations in hydrogeologic setting, (B) parallel flow up an inclined aquifer, (C) parallel flow up an inclined aquifer in a direction of increasing topography, and (D) parallel flow up an inclined aquifer in a direction of decreasing topography. Slopes of regression lines that are greater or less than that estimated for brine hydrostatic conditions (0.466) may exaggerate or erroneously depict the true potential for vertical flow. Intersections of the regression lines on the depth axis may inaccurately depict the depth to the potentiometric surface.

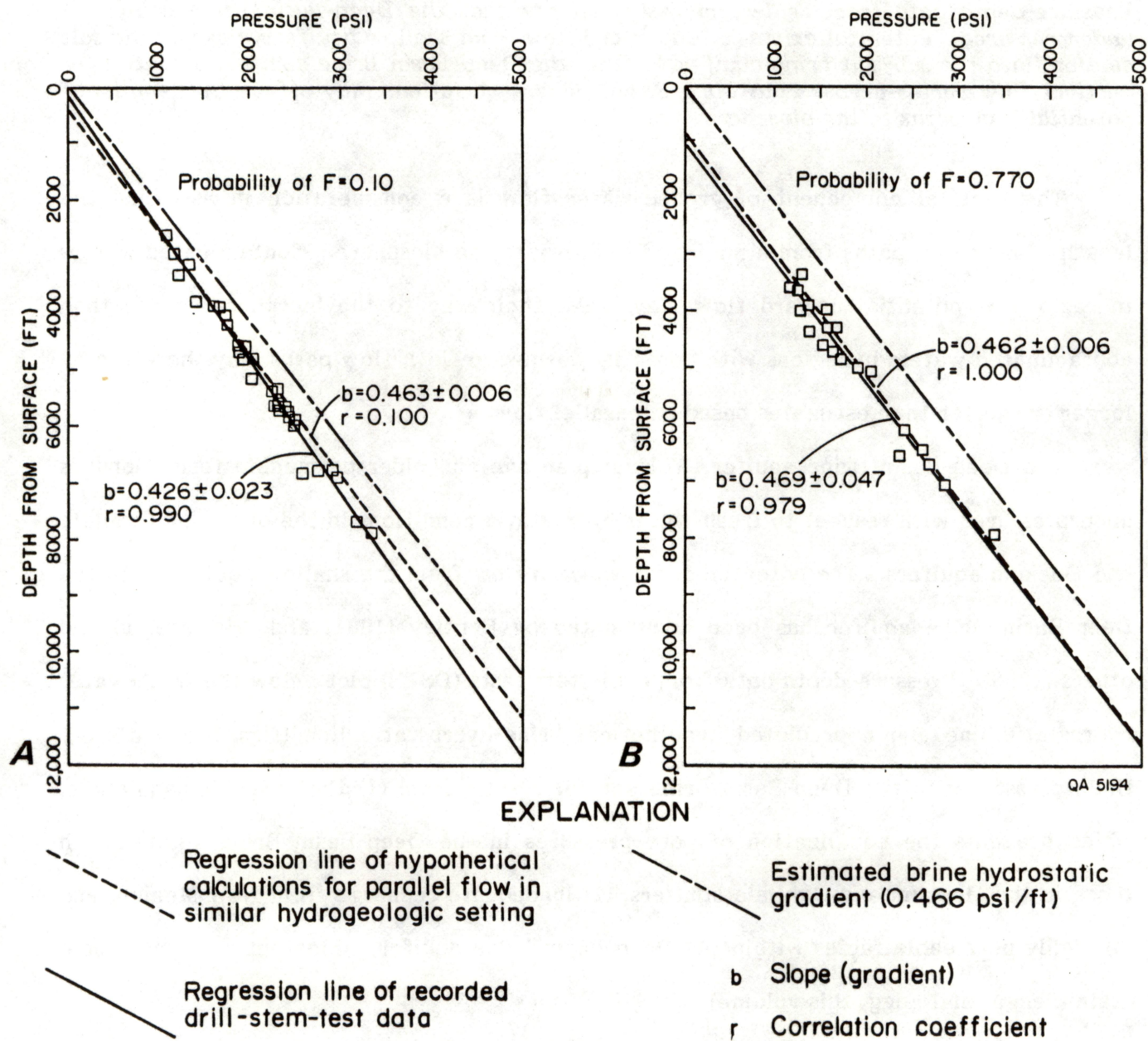


Figure 129. Comparisons of drill-stem-test data and modeled pressure-depth data for the confined Deep-Basin Brine aquifer in areas east of the Caprock Escarpment: (A) eastern Motley County, north to southwestern Donley County. The slope of modeled data (0.469), (B) Childress, Cottle, and northeastern King Counties.

## VERTICAL COMPONENTS OF GROUND-WATER FLOW IN THE PALO DURO BASIN

Elizabeth D. Orr and Charles W. Kreitler

*Pressure-depth data from drill-stem tests indicate that the Deep-Basin Brine aquifer is underpressured. Potential exists for downward flow from shallow aquifers, through the salt section, into the sub-salt brine aquifer. Within the Deep-Basin Brine aquifer, potential for vertical flow varies across Palo Duro Basin. These variations may affect the lengths of potential flow paths to the biosphere.*

The vertical component of ground-water flow is a consideration in assessing the length of potential paths from a nuclear repository to the biosphere. Contaminated waters in regions of potential upward flow may make their way to the biosphere sooner than contaminated waters in regions with potential downward flow; flow paths may therefore be longer or shorter than estimates based on parallel flow.

The Deep-Basin Brine aquifer (Wolfcampian age and older permeable formations) is underpressured with respect to fresh-water hydrostatic conditions in the overlying Ogallala and Dockum aquifers. The potential for downward flow from the shallow aquifers into the Deep-Basin Brine aquifer has been documented by Bentley (1981) and Wirojanagud and others (1986). Pressure-depth data from drill-stem tests (DST's) plot below the fresh-water hydrostatic line and a predicted hypothetical brine-hydrostatic line (figs. 130 and 131). Underpressuring in the Deep-Basin Brine aquifer results from (1) the evaporite aquiclude, which prevents the equalization of pore pressures in the Deep-Basin Brine aquifer with those in the Dockum and Ogallala aquifers, (2) inadequate recharge from New Mexico, and (3) highly permeable facies within the Deep-Basin Brine aquifer, which act as a hydrologic drain (Senger and Fogg, this volume).

The potential for vertical flow within the Deep-Basin Brine aquifer was investigated by analyzing pressure-depth relationships across the basin. The 446 data points in figure 131 are a sample of DST data from 276 petroleum exploration wells (fig. 130). The pressure values used were the larger of either the initial or final shut-in pressures; of

these, only that data with gradients (pressure/depth) greater than or equal to 0.2 were considered valid.

Pressure-depth plots were constructed for small areas arbitrarily delineated by contours of surface elevation and the elevation of the top of the Wolfcamp (fig. 130). The contour intervals are not equal but were chosen (1) to facilitate the most even data distribution possible and (2) to display the most distinct trends in the plotted pressure-depth data. Each area is relatively homogeneous with respect to the depth to the Deep-Basin Brine aquifer; effects of variations in topography, aquifer structure, and the potentiometric surface could therefore be minimized on pressure-depth plots.

Statistical test of regression lines indicated that data from certain areas could be grouped and plotted together (figs. 132 and 133). The slopes and intercepts of plots in figures 132 and 133 vary from area to area, indicating that the high scatter in figure 131 may in part be a result of superimposed pressure-depth relationships from different regions. These variations may also indicate varying potential for vertical flow. However, some of these variations may be the result of the hydrogeologic setting and data distribution. Consequently, modeled data were computed for each area assuming parallel flow in a similar hydrogeologic system (Orr and Kreitler, this volume, "Interpretation of Pressure-Depth Data from Confined Aquifers"). Tests indicating statistically different slopes of the regression lines of DST data and computed data imply a potential for vertical flow.

Of the seven areas in figure 132, four areas, C, D, E, and G, have pressure-depth gradients that are less than the computed gradients for parallel flow in the same hydrogeologic setting, indicating potential downward cross-formational flow. Data from the Stone and Webster Engineering Corporation Sawyer No. 1 and Zeeck No. 1 test wells support this conclusion: calculated head values decrease with depth. (Data in area E are very sparse and scattered; interpretations based on these data may be questionable.)

No statistically significant differences were found between the slopes of the regression lines of DST and computed data in areas B and F; parallel flow within the aquifer is implied. Pressure-depth data in area B show a high degree of scatter, and much of the data are of poor quality. The scatter may be due to the effects of high oil and gas production in the area. Conclusions based on these data should be considered tentative.

The slope of the pressure-depth regression line in area A (0.479) is greater than that of modeled data for parallel flow in the same setting (0.442), implying potential upward flow. The slopes of the regression lines for DST data and modeled data, however, are statistically different with only 86 percent confidence. Therefore, part of the high gradient may be attributable to parallel flow up the inclined aquifer. However, test data from the Mansfield No. 1 well support the conclusion of potential upward cross-formational flow. Calculated heads for Pennsylvanian intervals are 300 to 400 ft higher than heads in the overlying Wolfcampian intervals.

Figure 134 summarizes the potential vertical components of ground-water flow in the Deep-Basin Brine aquifer based on the interpretation of pressure-depth data. Accuracy of this map is limited because (1) the boundaries in figure 134, especially in sparse data regions, are not absolute, and (2) interpretations based on poor quality data associated with oil production may be imprecise. The following assumptions must also be noted: (1) the potentiometric surfaces on which flow directions are based are accurate; (2) the estimate of density for the Deep-Basin Brine aquifer is correct (density and temperature do not vary vertically or horizontally within the deep basin); and (3) the model hydrogeologic settings for which data were calculated are true reflections of the hydrogeologic conditions of each area. Changes in these assumptions would naturally alter interpretations of the hydrogeology and pressure-depth relationships.

Hydrogeologic causes for the observed patterns of vertical flow are not readily apparent. Because of the low permeability of the salt section, the effect of flow through the salt section (on pressure-depth configurations) may be negligible compared with the

effect of varying permeabilities within the Deep-Basin Brine aquifer. On a regional scale, water in the Deep-Basin Brine aquifer moves roughly parallel within the structure of the basin. Local permeability variations may cause vertical deflections of ground water into more permeable facies.

Potential downward flow in areas E and G may be related to higher permeabilities in Pennsylvanian granite-wash and fan-delta deposits. In Donley County, faults through the Permian and Pennsylvanian systems may provide pathways for downward ground-water flow. Potential downward flow in areas C and D may be a result of inadequate recharge to the highly permeable lower Pennsylvanian granite-wash deposits. Thick dolomitic shelf-margin systems that cut through basin systems may provide pathways for ground-water flow from above. Deep-basin brines in area A flow toward the flanks of the Amarillo Uplift where thick deposits of granite wash occur. Further upward cross-formational flow may occur along faults in the area. Areas B and D, which appear to reflect hydrostatic conditions of parallel flow, coincide approximately with the salt-dissolution zone. Faulting and collapse resulting from salt dissolution may increase the vertical permeability, thereby decreasing the vertical hydraulic gradient. Heads could equilibrate to some degree, and pressure-depth data would appear more hydrostatic. In these areas, there may actually be vertical components of flow within the Deep-Basin Brine aquifer, as well as increased downward flow through the salt section.

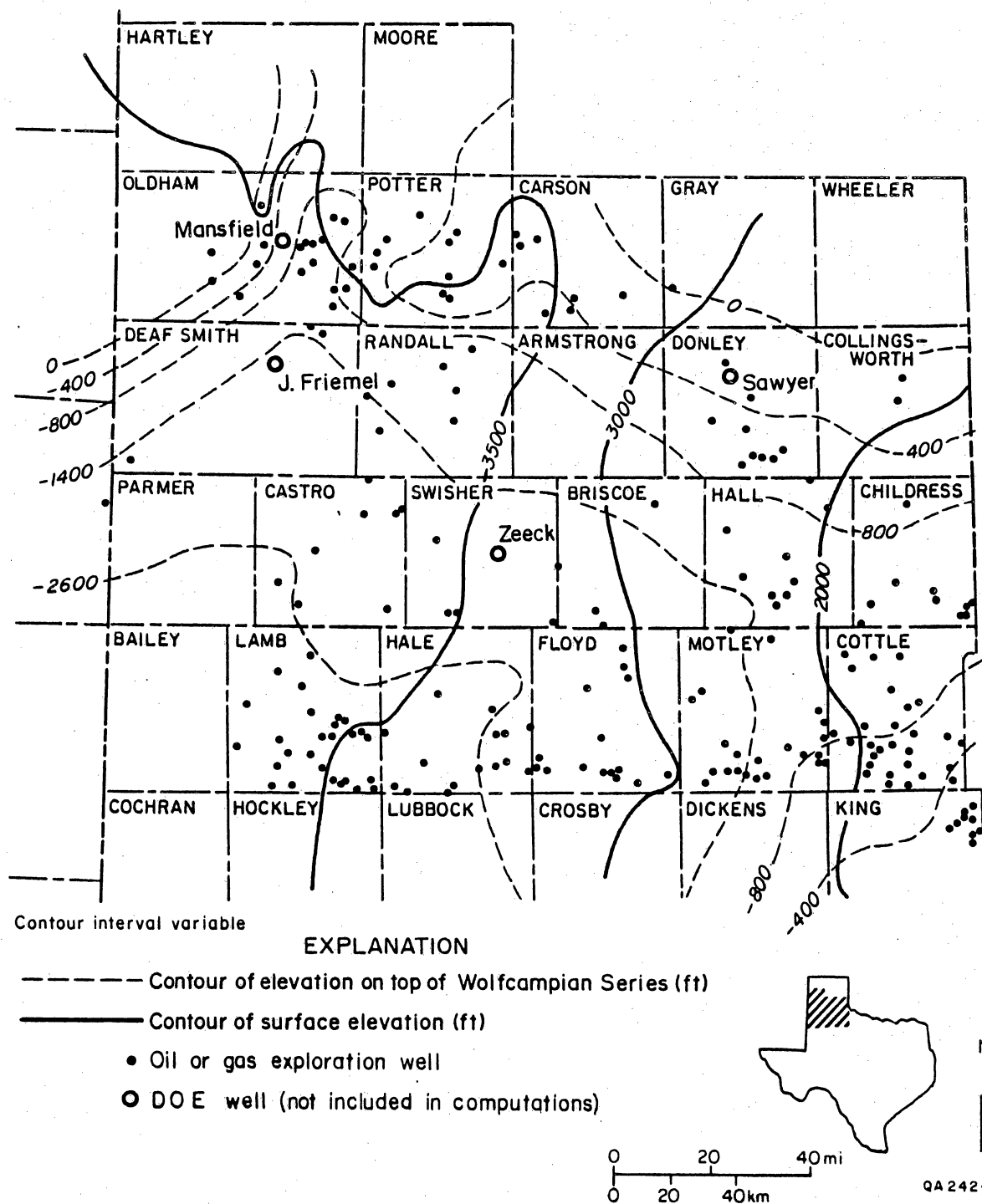


Figure 130. Location of selected drill-stem tests in wells in the Deep-Basin Brine aquifer. Contours of surface elevation and the elevation of the top of Wolfcampian strata (Handford, written communication) delineate relatively homogeneous hydrogeologic areas.



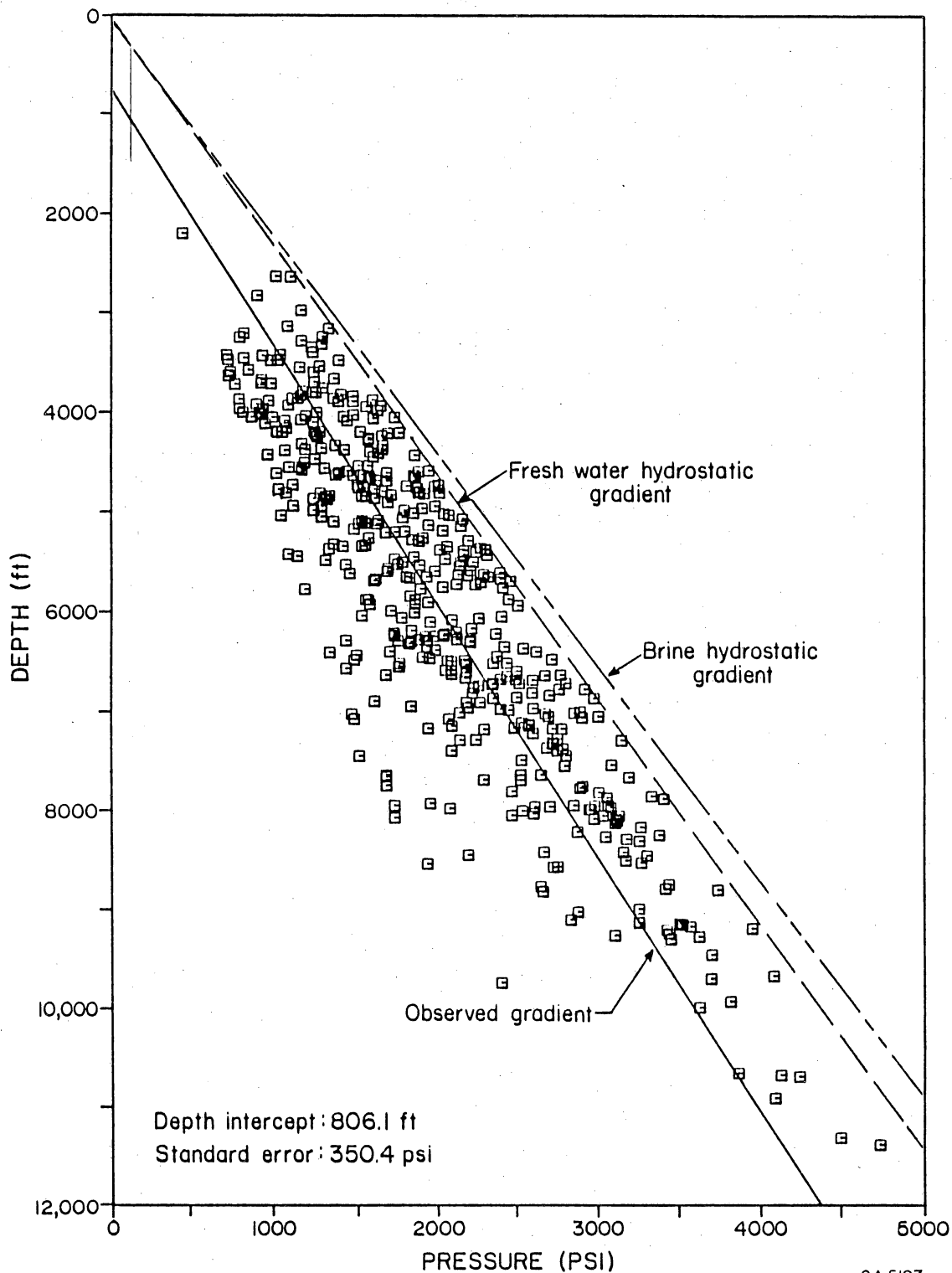


Figure 131. Reported shut-in pressure versus depth from selected wells in the Deep-Basin Brine aquifer (Wolfcampian and older aquifers), Palo Duro Basin. Hydrostatic gradient of fresh water (0.433 psi/ft) approximates conditions in shallow Ogallala and Dockum aquifers. Estimated hydrostatic gradient of deep-basin brines (0.466 psi/ft) approximates conditions in the Deep-Basin Brine aquifer. Location of wells displayed in figure 130.

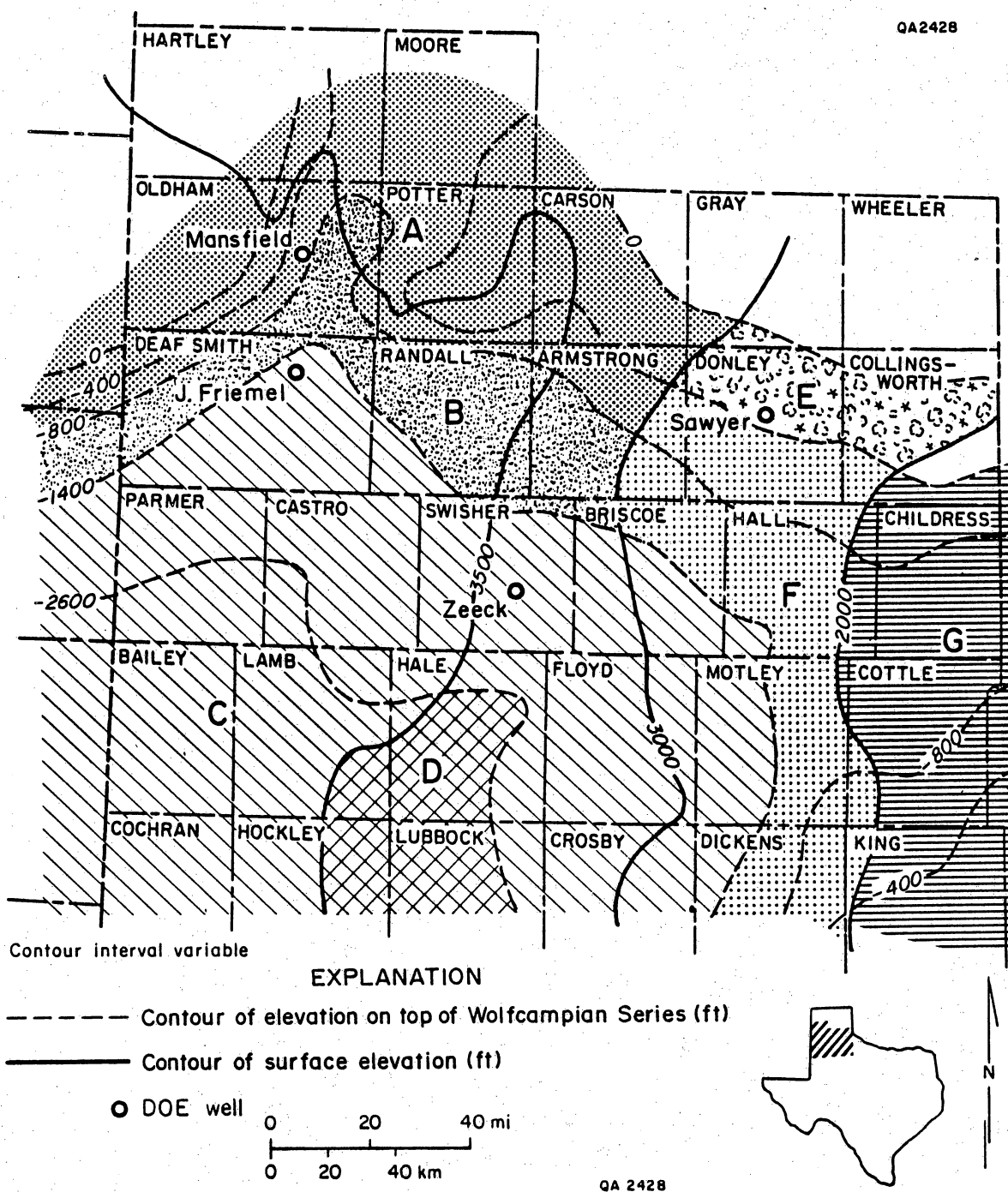


Figure 132. Areas in Palo Duro Basin having similar pressure-depth relationships.

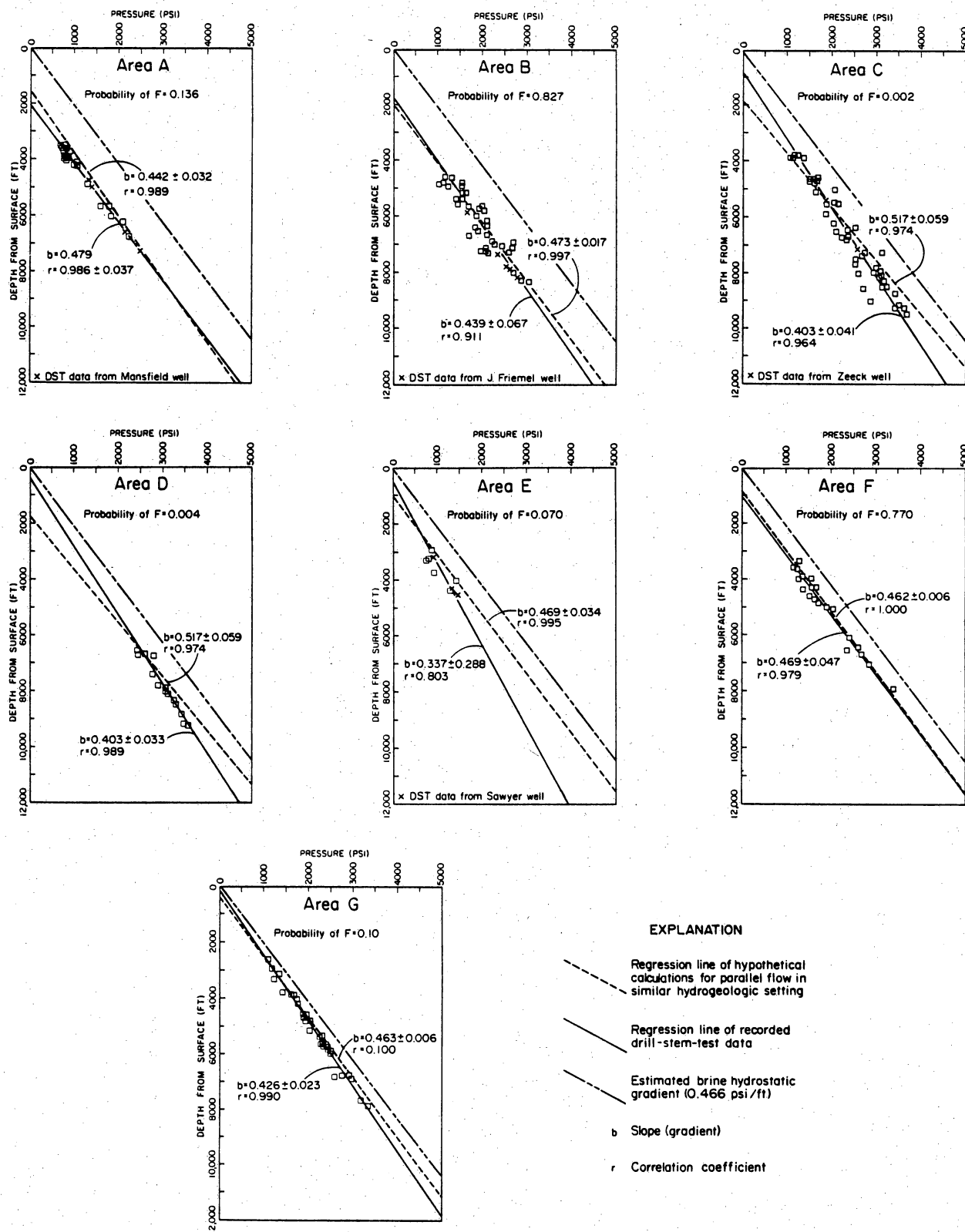


Figure 133. Pressure-depth plots for homogeneous regions of the Deep-Basin Brine aquifer. Significant differences (indicated by the probability of F statistic) between regression lines of plotted pressure-depth data and regression lines of computed data for parallel flow in similar hydrogeologic settings indicate potential for vertical flow within the Deep-Basin Brine aquifer.

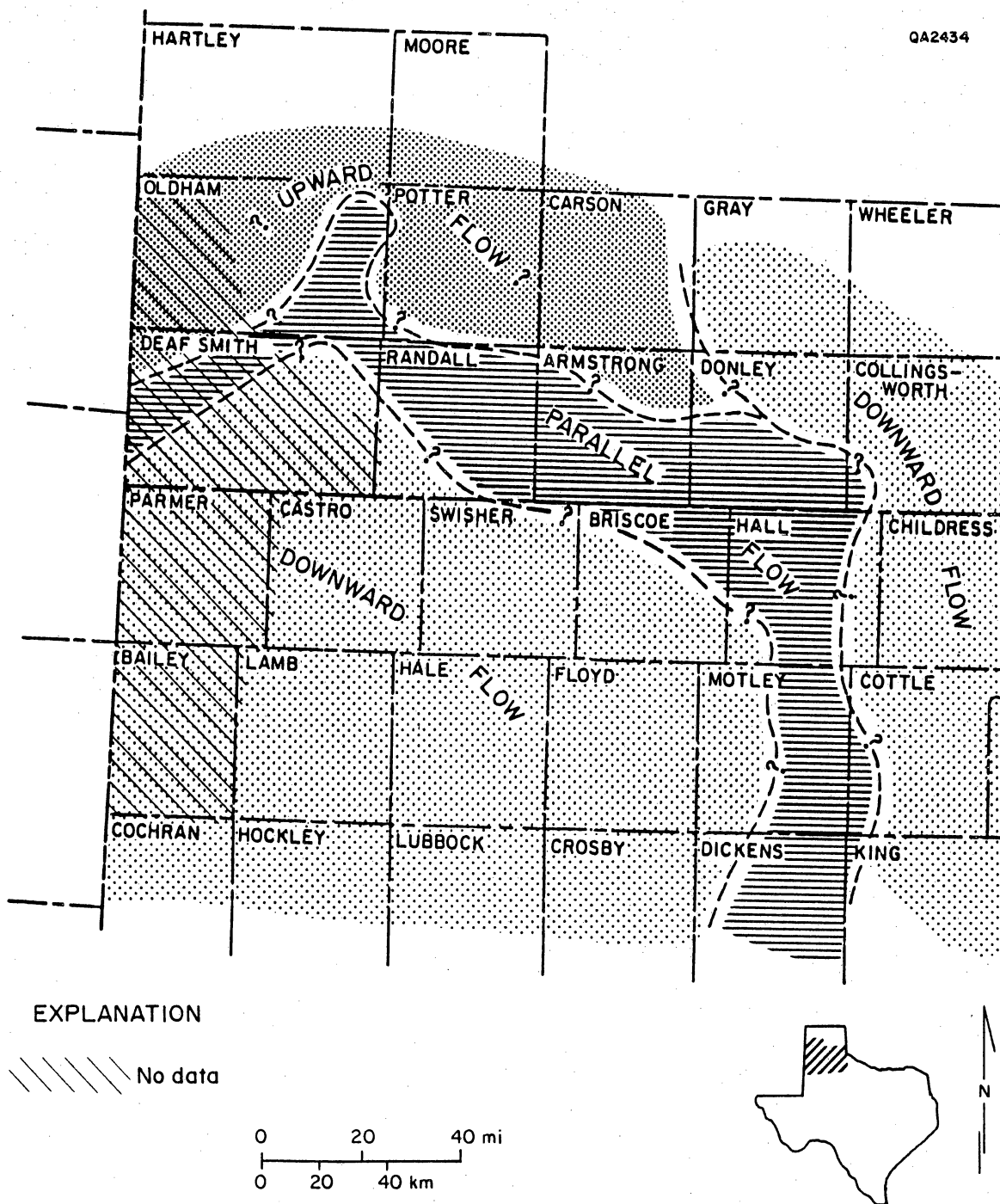


Figure 134. Regions in Palo Duro Basin having potential vertical components of groundwater flow in the Deep-Basin Brine aquifer. Interpretation is based on comparisons of observed pressure-depth relationships and computed pressure-depth data for parallel flow in similar hydrogeologic settings (figure 132).

## NUMERICAL MODELING OF THE WOLFCAMP AQUIFER, PALO DURO BASIN

Prakob Wirojanagud, Charles W. Kreitler, and D. Anderson Smith

*Ground waters in the Wolfcamp aquifer flow to the northeast toward the semi-impermeable, granitic Amarillo Uplift. The Wolfcamp potentiometric surface can be reasonably simulated only when permeability of the granite wash that flanks the uplift is about 260 md. The best simulation results indicate a travel time across the basin from 1.2 to 2.0 m.y. Total discharge through the Wolfcamp aquifer is about 680,000 m<sup>3</sup>/yr.*

A conceptual hydrogeologic model of the Palo Duro Basin, Texas Panhandle, is subdivided into three hydrogeologic units: the shallow Ogallala and Dockum aquifers, the Permian Evaporite aquitard, and the deep, confined, underpressured Permian and Pennsylvanian brine aquifer. The relatively low permeability Evaporite aquitard separates the flow regime into two distinctly different flow systems: the upper unconfined aquifer (Ogallala-Dockum) and the Deep-Basin Brine aquifer. Both aquifer systems are extensive; thus, flows are essentially horizontal. Results of pressure-depth analysis of fluids in the deep-brine aquifer indicating uniformity of heads (Bentley, 1981; Orr and Kreitler, 1985) suggest that the whole deep-brine aquifer is interconnected, probably by depositional thinning of the shale aquitards or by faults and fractures.

The Wolfcamp Formation is the shallowest permeable unit beneath the thick Permian evaporite section in the deep-basin system. It is composed of carbonates, shales, and arkosic sand and gravels (granite wash) with effective average permeability values of 8.9, 0.0001, and 8.6 md, respectively. A potentiometric head map of the Wolfcamp aquifer derived from the measured head data indicates a regional flow direction from southwest to northeast across the basin and from west to east along the Matador Arch (fig. 135). This anomalous hydrologic condition (flow toward a low-transmissivity barrier) may result from the presence of highly permeable granite-wash deposits that flank the uplift and function as a "hydrologic sink."

A two-dimensional, vertical-averaging, finite-element model, which incorporates the different lithologies and their different permeabilities as well as leakage through the

overlying Evaporite aquitard, has been used to simulate the observed potentiometric surface of the Wolfcamp aquifer. The Palo Duro Basin study area was divided into a finite-element mesh of 120 discrete elements having 405 nodes to accommodate the heterogeneities of the system. The physically complex flow system has, therefore, been represented by a numerical model whose behavior is governed by the boundary conditions, the aquifer's properties (transmissivity and vertically integrated porosity), and the amounts of leakage. Leakage depends on the permeabilities and thicknesses of the Evaporite aquitard as well as on the heads in the overlying unconfined aquifer.

Investigations using numerical simulations indicate that the conditions that best simulate the Wolfcamp potentiometric surface are modified permeability values of 260 md for the granite wash (in contrast with the average value of 8.6 md), 50 md for the highly porous carbonate (fig. 136), and 0.00008 md for the Evaporite aquitard, as well as a combination of specified head conditions (in the western part) and no-flow conditions (in the eastern part) along the Amarillo Uplift (fig. 137). One pore-volume of water in the Wolfcamp aquifer within the Palo Duro Basin is about  $7.9 \times 10^{11} \text{ m}^3$ , and it takes about 1.2 to 2.0 m.y. for ground water to flow across the basin (fig. 138). The amounts of discharge through the western part of the northern boundary and the eastern boundary are about 280,000 and 400,000  $\text{m}^3/\text{yr}$ , respectively. Contours of head difference between the upper unconfined aquifer and the Wolfcamp aquifer (fig. 138) show a higher potential for downward leakage in the northwestern area; leakage declines toward the eastern and southeastern parts of the basin.

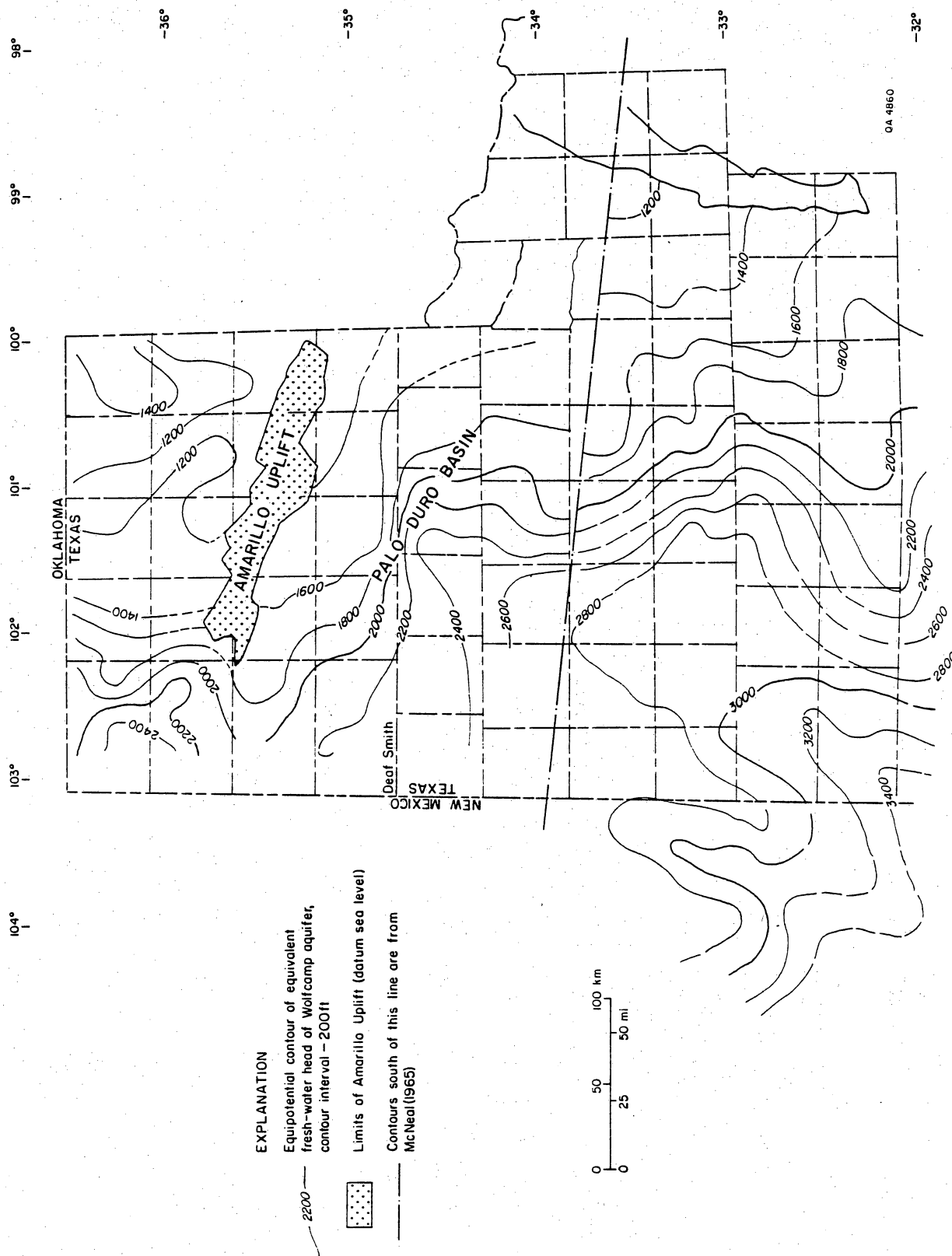


Figure 135. Transmissivity distribution of the best Wolfcampian aquifer simulation based on permeability values of 260 md for granite wash, 8.9 md for carbonates, 50 md for highly porous carbonates, and 0.0001 md for shale. Transmissivity value at a given point is computed as summation of products of permeability and thickness (in  $m^2/day$ ).

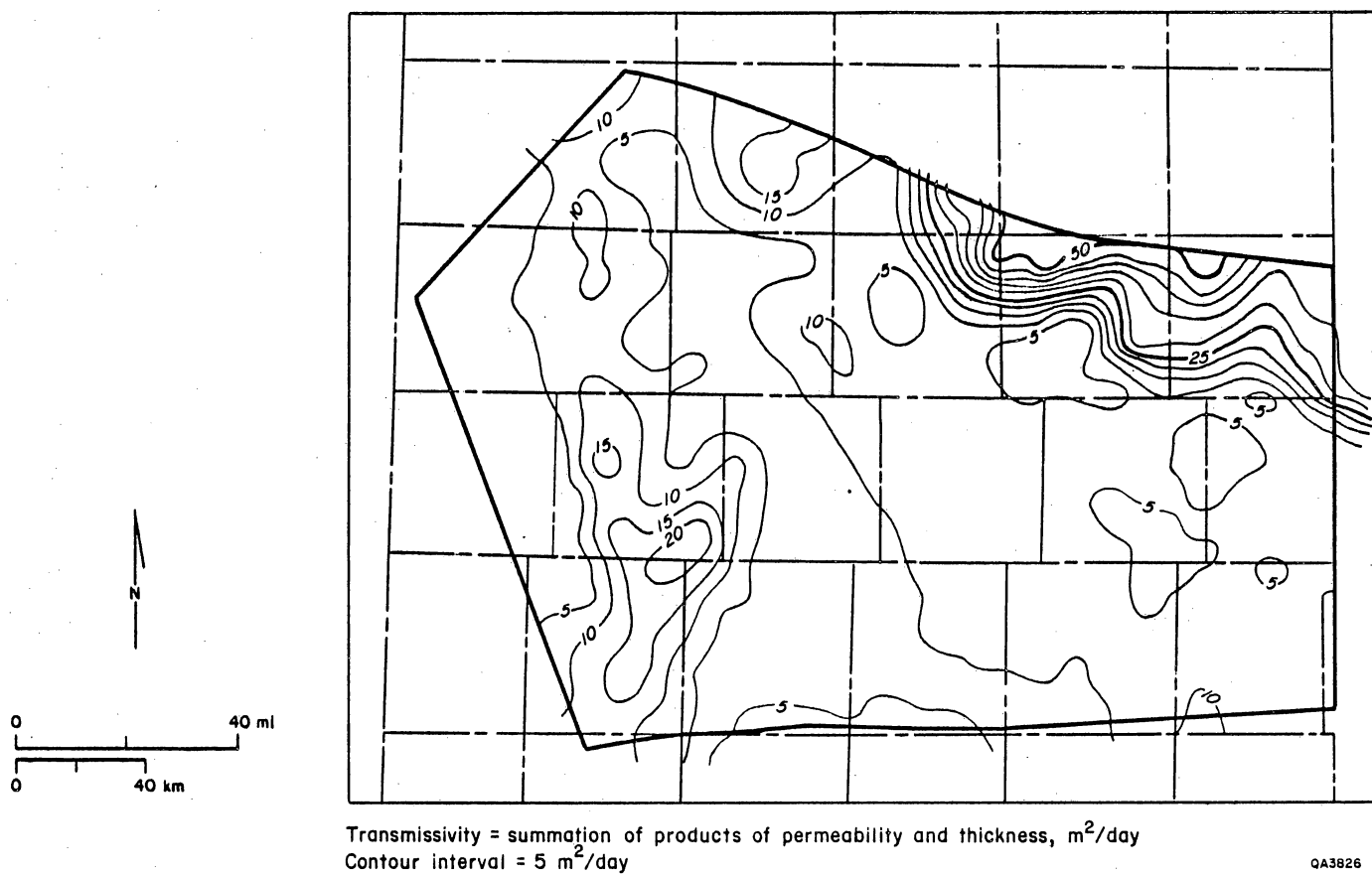


Figure 136. Computed head distribution from the best Wolfcampian aquifer simulation (fig. 135). Values of head along the specified-head boundaries are according to the observed Wolfcamp head map. The model assumes a permeability value of 0.00008 md for the Evaporite aquitard.



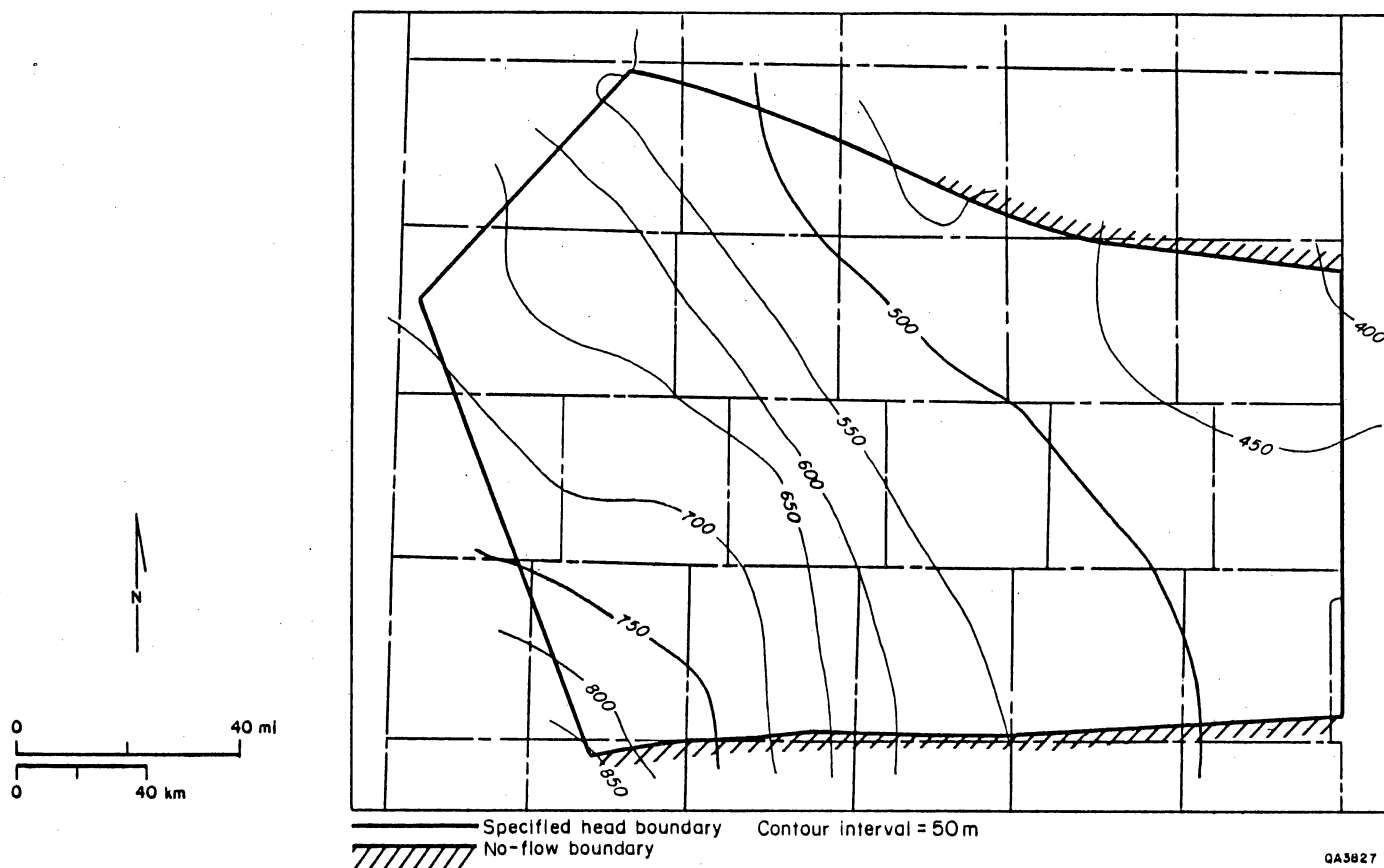


Figure 137. Streamlines and travel times from the best Wolfcampian aquifer simulation (fig. 135) based on porosity values of 0.14 for granite wash, 0.08 for carbonates, 0.10 for highly porous carbonates, and 0.05 for shale. Travel-time interval between marks along streamlines is 400,000 yr.

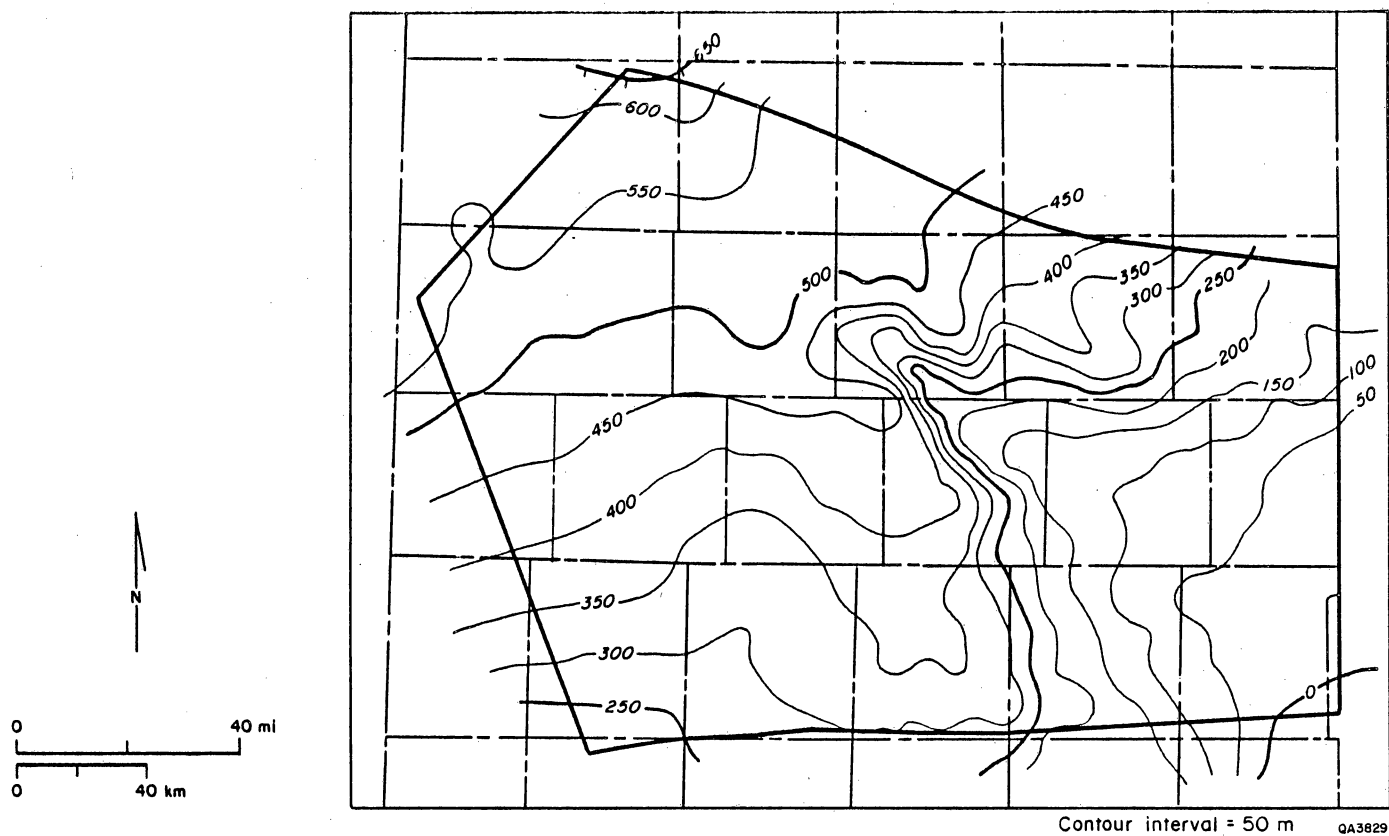


Figure 138. Potential for leakage from the upper unconfined aquifer down to the Deep-Basin Brine aquifer through the Evaporite aquitard, computed as head difference between the upper unconfined aquifer and the Wolfcamp aquifer. Negative values indicate potential for upward flow through the aquitard.

## MODELING OF VERTICAL GROUND-WATER FLOW IN THE PALO DURO BASIN: A PROGRESS REPORT

Rainer K. Senger and Graham E. Fogg

*The cross-sectional ground-water flow model was used to simulate streamlines in addition to hydraulic heads along a cross section through the Palo Duro Basin. The computed streamlines show that most of the ground-water flow is concentrated in the shallow aquifers, whereas only a small fraction of the total flow ( $0.047 \text{ m}^3/\text{day}$ ) is passing through the Deep-Basin Brine aquifer. The small flow rates in the deep system can be attributed to (1) its relative isolation from the shallow, relatively steep hydraulic gradients, and (2) discharge of ground water at the Pecos River that would otherwise recharge the deeper aquifer.*

The regional ground-water flow model of a cross section through the Palo Duro Basin (fig. 139; modified from Senger and Fogg, 1983) was improved by computing ground-water streamlines and by using new data on recharge rates to the Ogallala aquifer and hydraulic conductivity of the different hydrologic units. The computed streamlines show ground-water flow patterns and fluxes that were difficult, if not impossible, to discern from the previously published contour maps of computed hydraulic heads, owing to anisotropic hydraulic conductivity values and extreme vertical exaggeration of the cross-sectional model. Streamlines were generated by solving for the stream functions,  $\psi$ , in the equation:

$$\frac{\partial}{\partial x} \left( \frac{1}{K_z} \frac{\partial \psi}{\partial x} \right) + \frac{\partial}{\partial z} \left( \frac{1}{K_x} \frac{\partial \psi}{\partial z} \right) = 0 \quad (1)$$

where  $K_x$  and  $K_z$  are horizontal and vertical hydraulic conductivity, respectively. Equation (1) is of the same form as the steady-state ground-water flow equation; thus, the same numerical algorithm used to solve for hydraulic head (FREESURF; Neuman and Witherspoon, 1970) was used to solve for the stream function  $\psi$ . Boundary conditions for the streamline solution consisted of prescribed stream function  $\psi$  (Dirichlet boundary conditions) along the lower boundary of the mesh and prescribed stream-function gradient,  $\nabla \psi$  (Neuman boundary conditions) along the upper surface of the mesh. For further details concerning boundary conditions and the derivation of equation (1) refer to Fogg and Senger (1985).

Information about average recharge to the Ogallala aquifer in the Texas Panhandle (Knowles and others, 1982) was used to assign prescribed flux boundary conditions to the High Plains surface (fig. 139). In the previous study (Senger and Fogg, 1983), fluxes along the High Plains surface obtained with prescribed head boundary conditions produced a highly erratic recharge-discharge pattern with a net annual recharge to the aquifer of about 0.18 inches (0.45 cm). The new prescribed flux boundary conditions represent recharge to the Ogallala aquifer ranging from 0.048 inches (0.145 cm) to 0.250 inches (0.625 cm), as was reported in Knowles and others (1982). The remaining nodes along the upper surface and the eastern boundary of the mesh still have prescribed head boundary conditions.

Pressure-depth data from Jackson County, Oklahoma, located approximately at the eastern edge of the model, support the previously assumed hydrostatic conditions along the eastern boundary. Hydraulic conductivity values of the shallow Ogallala and Dockum aquifers (8.0 and 0.8 m/day, respectively) were based on pumping test data reported in Myers (1969). The new prescribed flux-boundary conditions require reduced hydraulic conductivity of both Ogallala and Dockum at the western High Plains to simulate the observed hydraulic heads in those two aquifers. Anisotropic conditions in the shallow aquifer system were approximated by assuming a reduced vertical hydraulic conductivity with  $K_x/K_z = 10$  (table 16).

Permeabilities in the Deep-Basin Brine aquifer were assumed to be anisotropic with  $K_x/K_z = 100$ . The permeability value of 1.36 md, assigned to the Permian/Pennsylvanian shelf carbonates (table 16), represents a weighted arithmetic average of different carbonate strata within the Deep-Basin Brine aquifer (Wirojanagud and others, 1986).

Recent results from a field-pumping test of granite-wash deposits within the Deep-Basin Brine aquifer (Stone and Webster Engineering Company J. Friemel No. 1 well, Deaf Smith County) yielded permeability values of 10 to 400 md with an average of 140 md (equivalent to a hydraulic conductivity of 0.16 m/day). This is substantially larger than the geometric mean of 8.6 md based on data from drill-stem tests, pumping tests, and compiled

information from the Texas Department of Water Resources (Wirojanagud and others, 1986). The higher permeability values obtained from the recent tests are considered more typical of proximal granite-wash lithology. Accordingly, granite wash in the western part of the cross section was assigned a hydraulic conductivity value of about 0.01 m/day, whereas granite wash east of the Caprock Escarpment was assumed to have higher hydraulic conductivity of about 0.12 m/day, which resulted in reasonable hydraulic head distribution in the deep section.

Information on permeabilities of the Permian/Pennsylvanian formations in New Mexico is very limited. Previously assigned values (Senger and Fogg, 1983), taken from Freeze and Cherry (1979), represent average hydraulic conductivities of about  $8.2 \times 10^{-2}$  m/day for comparable geologic material (table 16). The assumed permeabilities of the westernmost hydrologic units were supported by the computed discharge of  $1.35 \text{ m}^3/\text{day}$  at the Pecos River, which agrees reasonably well with inferred discharge based on streamflow measurements of about  $1.30 \text{ m}^3/\text{day}$  in the area (Mower and others, 1964).

Despite the adjustments in the model, computed hydraulic heads (fig. 140) show the same general flow regime in the basin as in the previous study (Senger and Fogg, 1983): (1) a shallow flow system governed primarily by topography and (2) a deeper flow regime recharging in New Mexico and separated from the shallow system by the thick evaporite section in the center of the cross section, which helps maintain underpressured conditions beneath the evaporite section.

The plot of streamlines (fig. 141) shows in detail the shallow and deep ground-water flow system. Flow rates in the two systems are so drastically different that two different streamtube intervals had to be used (a streamtube is bounded by streamlines). Each streamtube in the shallow section (shaded pattern) carries  $0.2 \text{ m}^3/\text{day}$ , whereas each streamtube in the deep section carries only  $0.01 \text{ m}^3/\text{day}$ . As a result, the total modeled flow rates through the shallow and deep sections are about  $4.43 \text{ m}^3/\text{day}$  and  $0.047 \text{ m}^3/\text{day}$ ,

respectively. Specific discharge rates of ground-water flow may be obtained by dividing the flow rate in a streamtube by its width. In addition, pore-fluid velocity is given by dividing specific discharge by porosity. The model gives values of specific discharge for the deep sections in the range of  $10^{-4}$  to  $8 \times 10^{-6}$  m/day. Maximum ground-water flow velocity in the shallow (Ogallala) aquifer is about  $1.5 \times 10^{-1}$  m/day, based on a value of specific discharge of  $2 \times 10^{-2}$  m/day, and assuming a porosity in the Ogallala of 16 percent (Knowles and others, 1982). In the Deep-Basin Brine aquifer, the model indicates maximum ground-water flow velocities in the shelf carbonates and proximal granite wash of  $1.1 \times 10^{-4}$  m/day and  $4.4 \times 10^{-4}$  m/day, respectively, assuming average porosities of 8 percent and 23 percent, respectively (Wirojanagud and others, 1986). The ground-water travel times through the Deep-Basin Brine aquifer from the westernmost recharge area in New Mexico to the eastern boundary in Oklahoma are in the range of 1.2 to 4.0 m.y., depending on streamtube and average porosity.

Leakage through the evaporite section as computed by the model is only about  $6 \times 10^{-8}$  m/day. Nevertheless, because of its vast area, the evaporite section contributes by vertical leakage about  $0.0125 \text{ m}^3/\text{day}$ , or 27 percent of the water passing through the Deep-Basin Brine aquifer. Additional simulations are being made with different permeability values for the evaporite section to estimate a range of possible leakage rates.

The very slow flow rates computed by the model in the deep system are attributed to the relatively low permeability in the central part of the Deep-Basin Brine aquifer and its separation from the relatively steep hydraulic gradients of the shallow aquifer system by the Evaporite aquitard. In addition, the Pecos River serves as a discharge area for ground water that would otherwise recharge to the deeper aquifer. Additional simulations are planned in which the effect of the Pecos River on the overall ground-water flow pattern will be investigated by eliminating the topographic effect of the Pecos valley in the finite-element mesh and comparing the computed head and streamline distribution with the ones in this study.

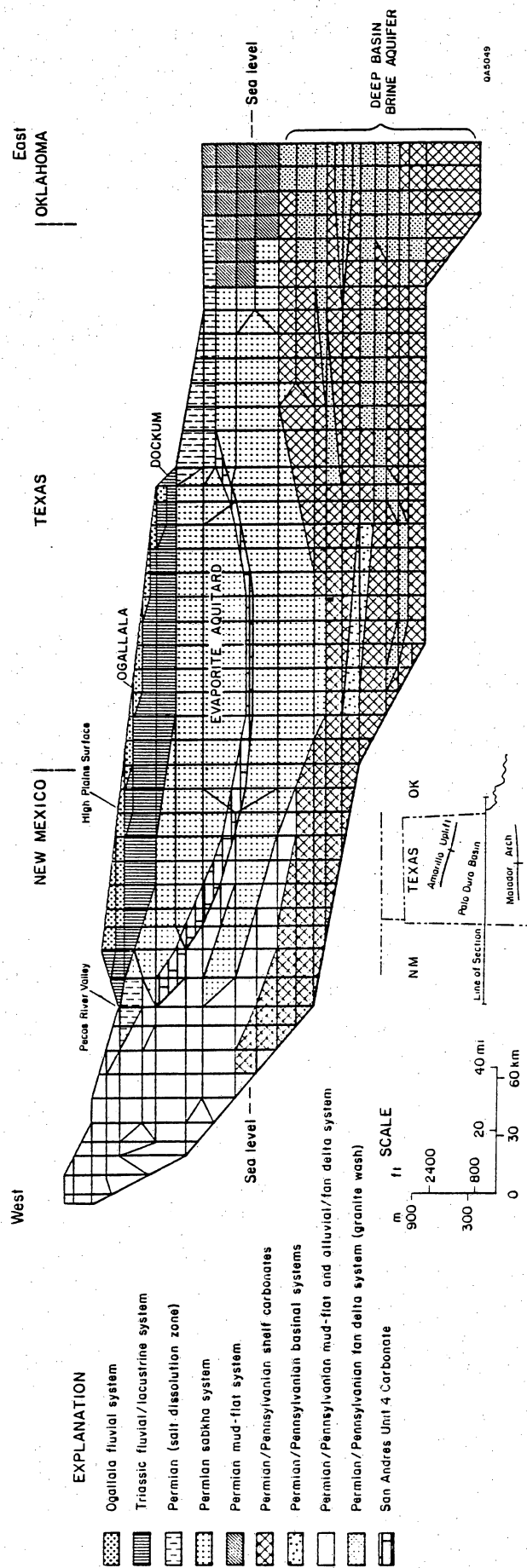


Figure 139. Finite-element mesh representing the major hydrologic units. Each element is assigned a hydraulic conductivity value according to the different simulations. The upper surface of the mesh is represented with prescribed head boundary conditions and prescribed flux boundary condition (High Plains surface) and reflect the water table conditions. Heads are assumed to be uniform with depth along the eastern boundary. The lower surface of the mesh is a no-flow boundary that corresponds to the contact between the Deep-Basin Brine aquifer and basement rock.

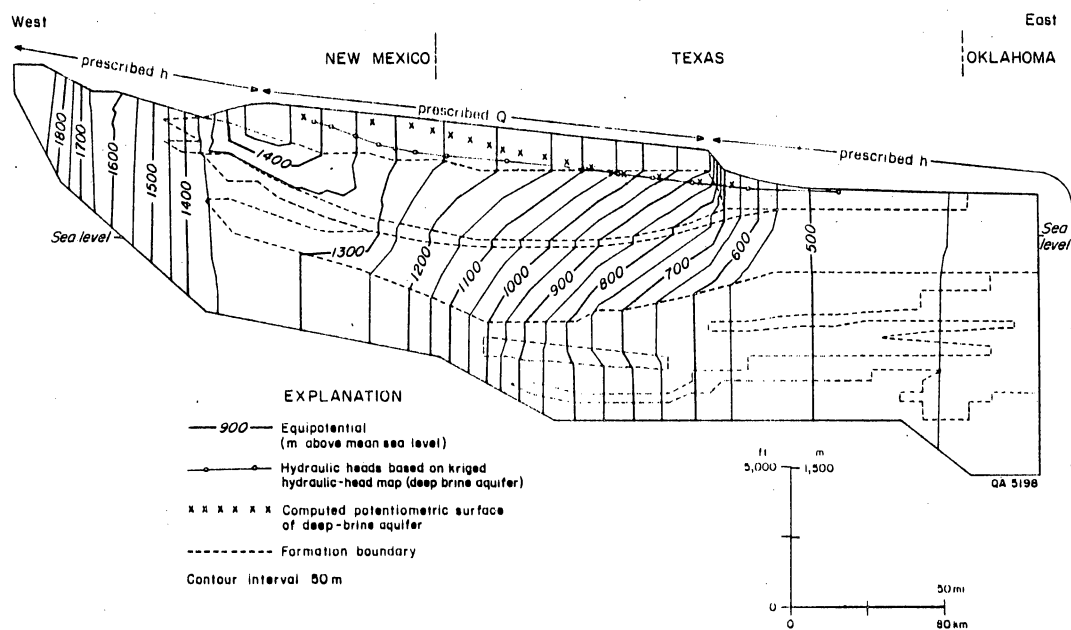


Figure 140. Computed hydraulic head distribution. Subhydrostatic pressure conditions occur beneath the evaporite section.



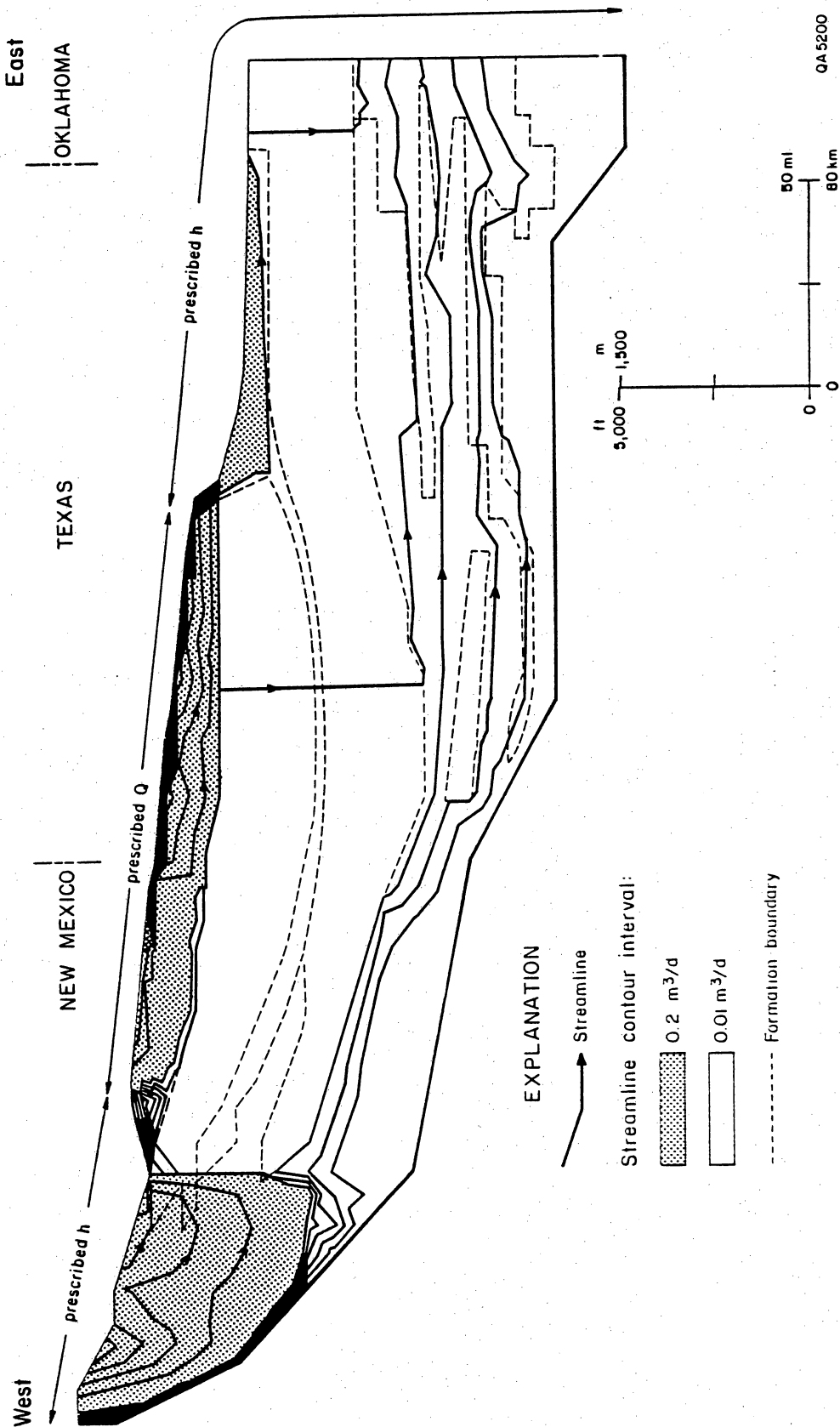


Figure 141. Computed streamline distribution. Highest flow rates are in the shallow system, whereas only a very small fraction (0.04 m<sup>3</sup>/day) goes through the Deep-Basin Brine aquifer.

Table 16. Hydraulic conductivity of the major hydrologic units, Texas Panhandle.

<u>Hydrologic unit</u>	<u>Hydraulic conductivity (m/day)</u>	
	<u>Horizontal</u>	<u>Vertical</u>
1. Ogallala fluvial system <sup>1</sup>	$8.0 \times 10^0$	$8.0 \times 10^{-1}$
2. Triassic fluvial/lacustrine system <sup>1</sup>	$8.0 \times 10^{-1}$	$8.0 \times 10^{-2}$
3. Permian (salt dissolution zone) <sup>2</sup>	$8.2 \times 10^{-2}$	$8.2 \times 10^{-4}$
4. Permian sabkha system <sup>3</sup>	$3.2 \times 10^{-7}$	$3.2 \times 10^{-7}$
5. Permian mud-flat system <sup>4</sup>	$8.2 \times 10^{-5}$	$8.2 \times 10^{-5}$
6. Permian/Pennsylvanian shelf carbonates <sup>3</sup>	$1.36 \times 10^{-2}$	$1.36 \times 10^{-4}$
7. Permian/Pennsylvanian basinal systems <sup>3</sup>	$1.1 \times 10^{-7}$	$1.1 \times 10^{-7}$
8. Permian/Pennsylvanian mud-flat and alluvial/fan delta system <sup>4</sup>	$8.2 \times 10^{-2}$	$8.2 \times 10^{-4}$
9. Permian/Pennsylvanian fan delta system (distal granite wash) <sup>3</sup>	$1.0 \times 10^{-2}$	$1.0 \times 10^{-4}$
10. Permian/Pennsylvanian fan delta system (proximal granite wash) <sup>5</sup>	$1.2 \times 10^{-1}$	$1.2 \times 10^{-3}$
11. San Andres unit 4 carbonate <sup>6</sup>	$1.2 \times 10^{-4}$	$1.2 \times 10^{-4}$

Sources of data:

<sup>1</sup>After Myers (1969); assumed  $K_X/K_Z = 10$ .

<sup>2</sup>U.S. Geological Survey open-file data; assumed  $K_X/K_Z = 100$ .

<sup>3</sup>After Wirojanagud and others (1986).

<sup>4</sup>Typical value of geologic material (Freeze and Cherry, 1979).

<sup>5</sup>See text.

<sup>6</sup>After Dutton and Orr (1985).

## GEOCHEMICAL CHARACTERISTICS OF SALT SPRING AND SHALLOW SUBSURFACE BRINES IN THE ROLLING PLAINS OF TEXAS AND SOUTHWESTERN OKLAHOMA

Bernd C. Richter and Charles W. Kreitler

*Chemical and isotopic analyses of brines from salt springs and the shallow subsurface in the Rolling Plains allow differentiation between (1) salt-spring and subsurface brines resulting from the dissolution of halite by local meteoric ground water, (2) salt-spring and subsurface brines resulting from the mixing of halite-dissolution brine with deep-basin brine, and (3) subsurface brines resulting from discharge of deep-basin brines. The geographic distribution of these different brine types correlates well with numerical modeling of ground-water flow within the area.*

Numerous salt-emission areas occur within the outcrop of Permian rocks in the Rolling Plains of Texas and southwest Oklahoma on the eastern flanks of the Palo Duro and Midland Basins (fig. 142). Brine of the sodium chloride type is discharged in springs and seeps and underlies the area at relatively shallow depths. The source of the salinity is considered to be either evaporite dissolution by shallow meteoric ground water in a local flow system or discharge of deep-basin brine in a regional flow system.

Ground water in the Palo Duro Basin basically flows through two major aquifer systems (Bassett and Bentley, 1983): (1) a shallow one, which receives recharge within the High and Rolling Plains and is responsible for halite dissolution along the salt-dissolution zone in the east (Gustavson and others, 1980), and (2) a deep one, which receives recharge in eastern New Mexico and traverses the High Plains below the Permian salt section. Flow direction in general is from recharge areas in the west to discharge areas in the east. Discharge of the shallow system within the study area is known to occur. Discharge of the deep system may occur within the study area or just to the east of it, but this is, as yet, undocumented. On the basis of Br/Cl ratios and isotopic composition, Kreitler and Bassett (1983) concluded that salt-spring brines in the northern part of the study area resulted from the dissolution of halite by meteoric ground water.

Additional samples from salt springs and test holes, especially from areas to the south, as well as deep-basin brines from the Palo Duro and Midland Basins, have been included to study further the source of salinity. Chemical and isotopic compositions, molar

sodium to chloride ratios (mNa/mCl) and bromide to chloride (Br/Cl) weight ratios are shown in tables 17 through 19.

Brines derived from dissolution of halite by fresh ground water commonly have mNa/mCl ratios close to 1 and Br/Cl weight ratios less than  $4 \times 10^{-4}$ , whereas deep-basin brines show values of less than 1 and greater than  $25 \times 10^{-4}$ , respectively (Whittemore and others, 1981). On the basis of these ratios, three brine types can be distinguished within the study area, that is, halite-dissolution brine (Group A, table 17), deep-basin brine (Group C, table 19), and mixtures of A and C (Group B, table 18) (fig. 143). Ratios of other chemical constituents (Ca/Cl, Mg/Cl, K/Cl, I/Cl) support this grouping. Brines from Group A show the lowest values for these ratios, except Na/Cl, as expected from halite dissolution by fresh ground water. Group A brines dominate in the northern and western parts of the area and include most of the salt springs (fig. 142).

Chemical constituents of brines from Group C plot close to typical oil-field brines in the Palo Duro and Midland Basins, except that the Mg/Cl ratio is unusually high. Discharge of deep-basin brine is thought to account for this brine type. Group C brines are restricted to test-hole samples and occur at the North Croton Creek and Croton/Dove/Haystack Creek areas and in one sample from the Elm Fork site in Harmon County, Oklahoma (fig. 142). An anomalous brine, which plots close to Group C brines, in the shallow subsurface just east of Cottle County was described by Johnson (1979). This suggests deep-basinal discharge in the easternmost and southeastern parts of the Rolling Plains (Hardeman Basin and Eastern Shelf).

Group B samples from springs and test holes exhibit compositions between halite-dissolution and deep-basin brines, suggesting mixing of these two end members. Ratios of chemical constituents show them to plot closer to Group A than Group C brines, indicating the dominance of halite-dissolution components in Group B. The geographic distribution of Group B (fig. 142) supports the concept of mixing of Groups A and C.

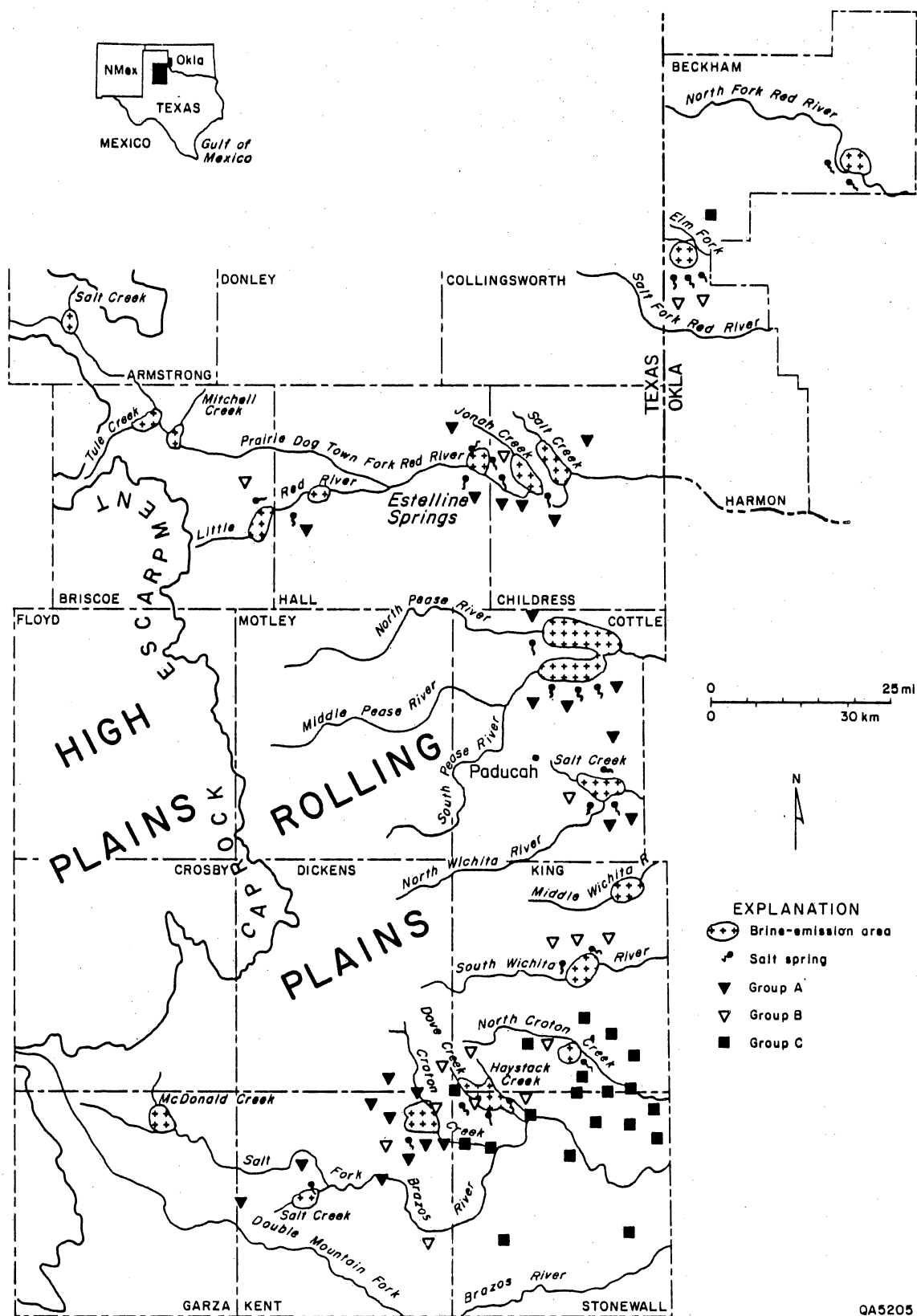
A plot of Br/Cl ratios versus depth for four salt-emission areas shows deep-basin brine at relatively shallow depths in the southern part of the Rolling Plains. Brine is nearest to land surface in the North Croton Creek area (figs. 142 and 144). Brines indicating deep-basin discharge have not been found in test holes at Jonah/Salt Creek (maximum depth 315 ft) and Middle Pease River (maximum depth 130 ft), whereas they were found at 25 ft below land surface at North Croton Creek.

The  $\delta^{18}\text{O}$  and  $\delta\text{D}$  values of most of the salt springs (Group A) compare well with values of shallow, fresh ground water in the area, suggesting a meteoric origin for the saline waters (fig. 145; Kreitler and Bassett, 1983; Senger and others, this volume). Test-hole samples from the North Croton Creek area (Group C), which plot on a line with deep-basin brine at high Cl concentrations and meteoric water at low Cl concentrations as its end members, indicate mixing of a deep-basin brine with local meteoric ground water. This is also reflected in the significant enrichment of  $\delta^{18}\text{O}$  and Cl with depth for individual test holes in this area.

Comparison of potentiometric fresh-water heads of the Wolfcamp aquifer with heads of the unconfined aquifer supports the geochemical findings (fig. 146). Heads of the brine aquifer are below unconfined heads in the north, but above or near to them in the south. A computer-generated head-difference map for the Wolfcamp and unconfined aquifers shows this trend; head differences generally decrease east of the escarpment and approach zero in southeastern Cottle County, Texas (Wirojanagud and others, this volume).

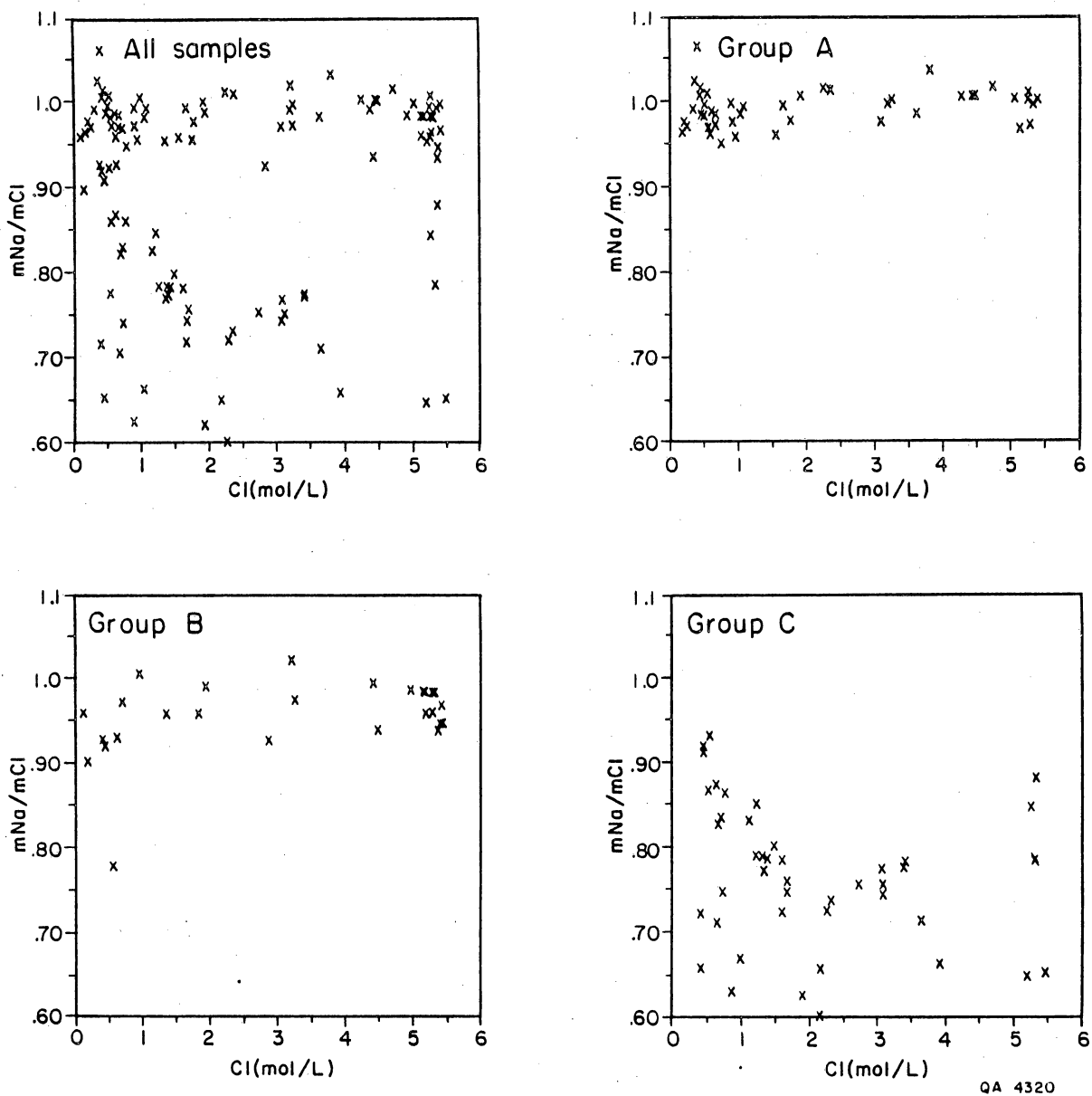
Most salt springs do not show deep-basin characteristics. Few salt springs suggest mixtures of halite-dissolution brine with small amounts of deep-basin brine. The dominance of halite-dissolution brines may mask any deep-basin characteristics in some of the samples, especially where mixing with local fresh water near the discharge site dilutes the samples to relatively low salinity. The source of the deep-basin brine is not known. It may be the Midland Basin rather than the Palo Duro Basin, as indicated by the geographic distribution of Group C brines and the potentiometric surface of the deep-basin Wolfcamp

aquifer. Chemical analyses from deeper test holes, particularly for the northern part, would be of great value in determining the depth to deep-basin brine for the entire study area.



QA5205

Figure 142. Location of salt-emission areas and the geographic distribution of samples belonging to Groups A, B, and C. Group designation was decided on the basis of chemical constituents, primarily the  $mNa/mCl$  and  $Br/Cl$  ratios.



QA 4320

Figure 143. Plots of  $mNa/mCl$  ratios versus  $mCl$ . High  $mNa/mCl$  ratios in Groups A and B indicate halite dissolution. Low  $mNa/mCl$  ratios in Group C indicate a deep-basin origin.



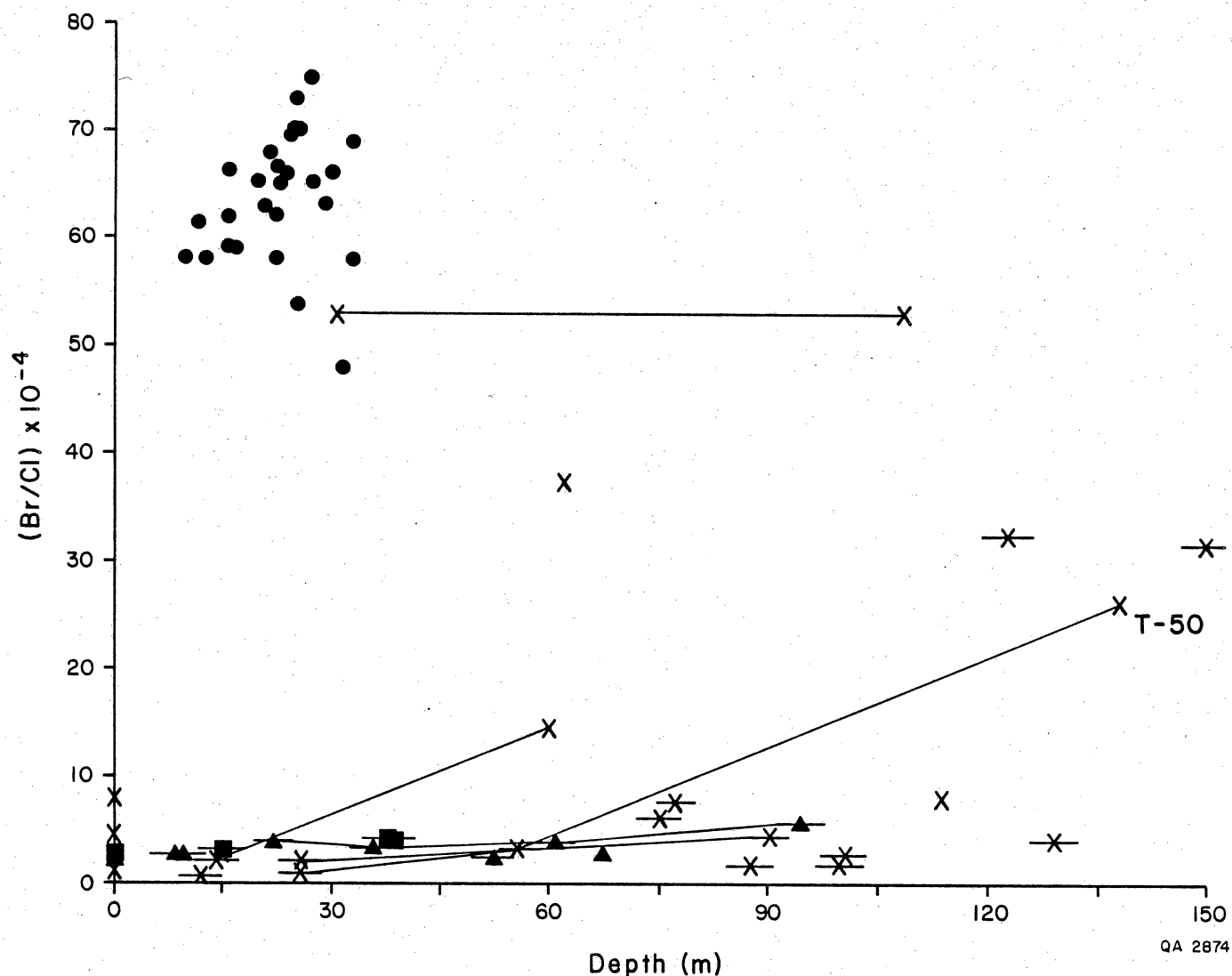


Figure 144. Plot of Br/Cl weight ratio versus depth for four brine-emission areas (locations shown in fig. 142). Low Br/Cl ratios in samples from Jonah Creek and Middle Pease River suggest halite dissolution to account for the brines. Low and high Br/Cl ratios at Croton/Dove /Haystack Creeks indicate halite-dissolution brine underlain by deep-basin brine at this locality. Uniformly high Br/Cl ratios in samples from North Croton Creek indicate deep-basin brine close to land surface in the southeastern Rolling Plains.

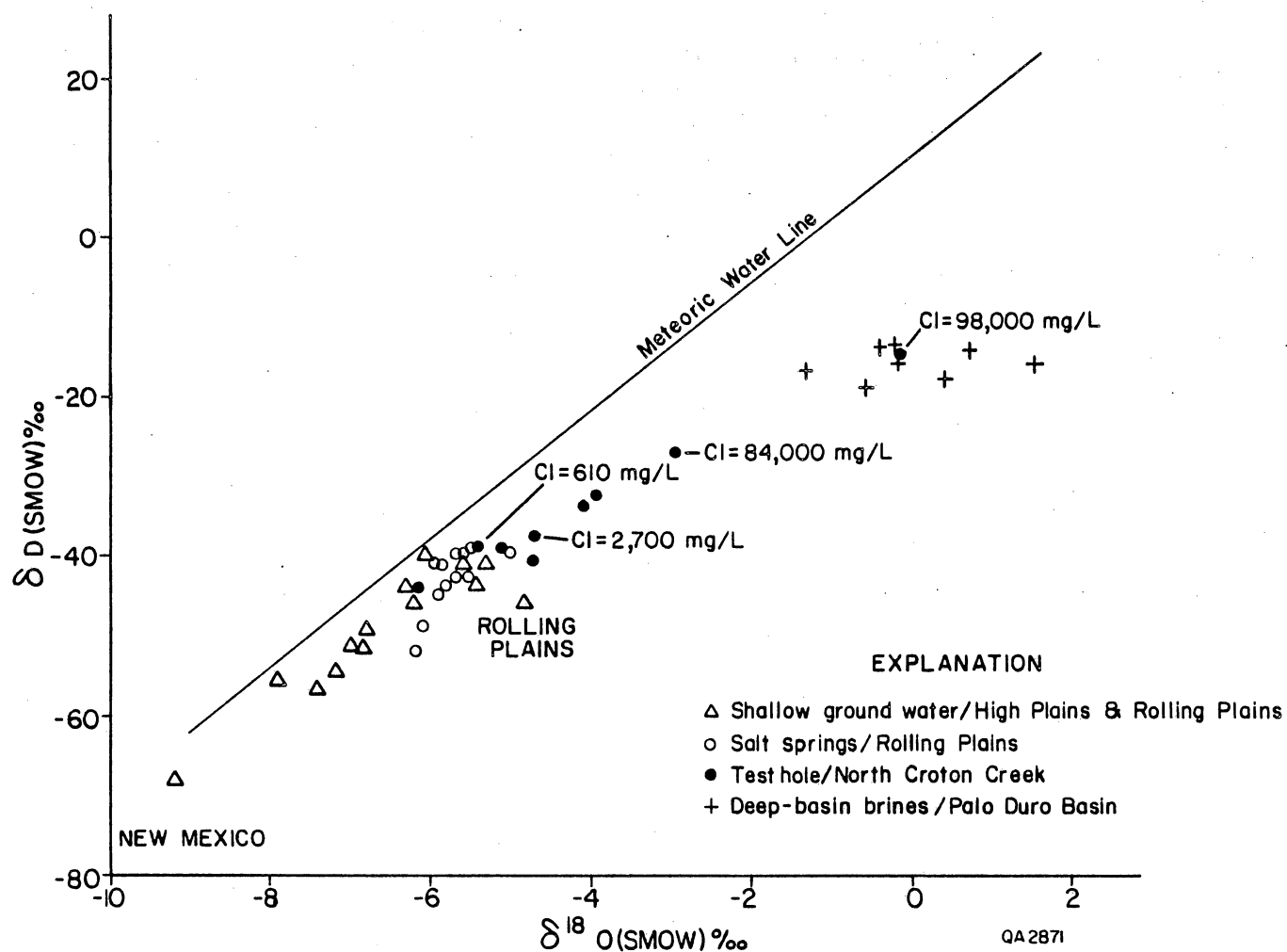


Figure 145. Plot of  $\delta D$  versus  $\delta^{18}O$  for (1) shallow, fresh ground water from municipal wells in New Mexico and the Texas Panhandle (Senger and others, this volume), (2) salt springs in the Rolling Plains, (3) test hole samples from the North Croton Creek area, and (4) deep-basin brines from the Palo Duro Basin.

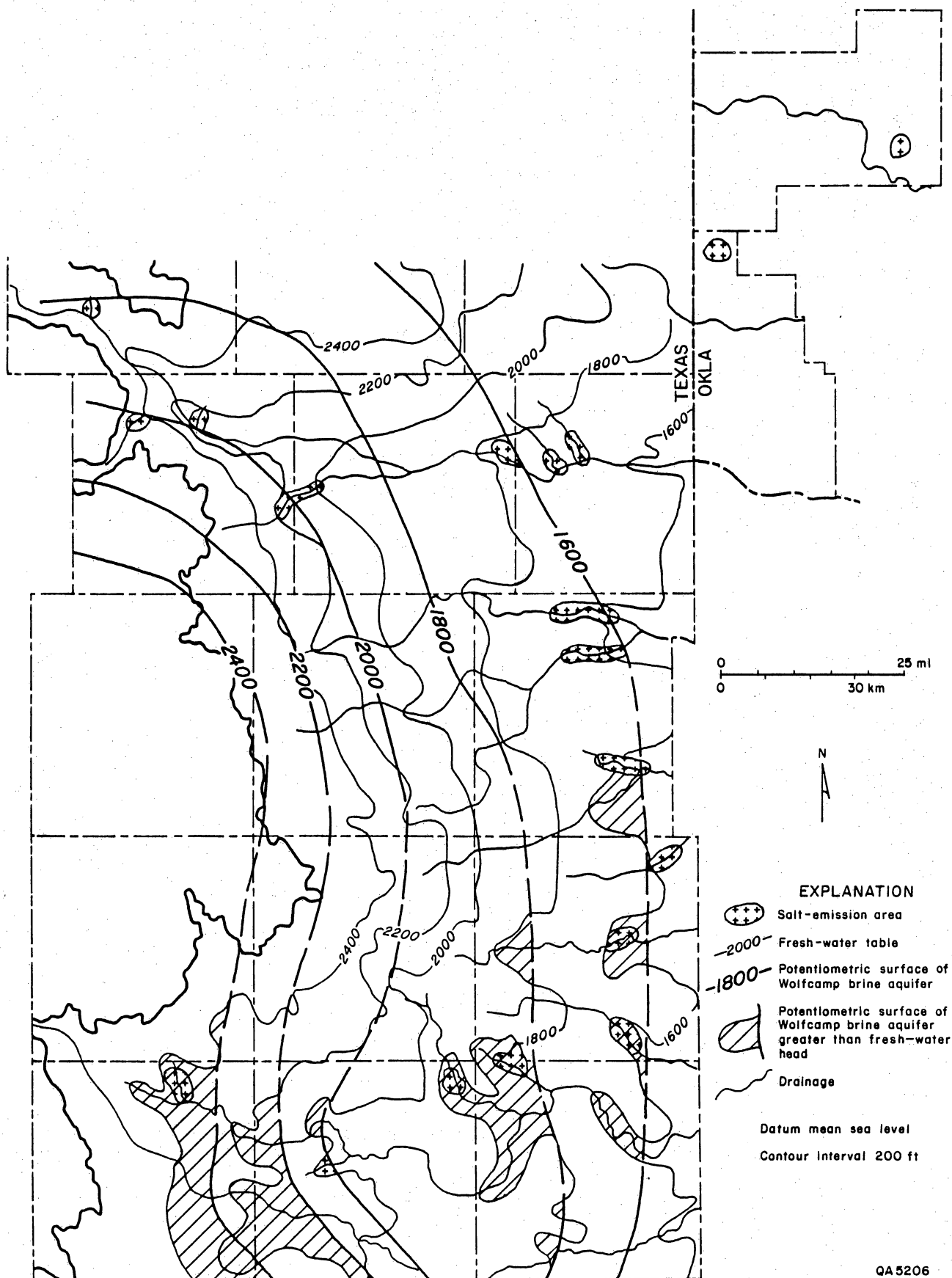


Figure 146. Hypothetical potentiometric-surface map of the Wolfcamp aquifer compared with fresh-water table. The Wolfcamp map is compiled from the potentiometric-surface maps of McNeal (1965) and Smith and others (1983).

Table 17. Chemical and isotopic analyses of Group A brines.

County	Sample no.	Date collected	Sample type and depth (ft)	Temp. (°F)	pH	Na	K	Ca	Mg	HCO <sub>3</sub>	SO <sub>4</sub>	Cl	Br	mNa/mCl	Br/Cl x 10 <sup>-4</sup>	δ <sup>18</sup> O (‰, SMOW)	δD
Hall	1	6-17-69	Spring	-	7.50	5,230	22	1,010	306	196	3,350	8,250	-	0.98	-	-	-
"	3a	4-01-80	"	53	8.00	23,166	57.2	1,835	341	124	4,805	32,225	6.3	1.11	1.95	-4.7	-
"	3b	10-29-69	"	-	6.60	13,100	78	1,350	548	100	4,520	20,800	-	0.97	-	-	-
"	3c	10-29-69	"	-	6.80	8,775	35	905	1,156	408	6,700	13,200	-	1.02	-	-	-
Childress	4a	3-28-83	"	71	7.52	25,100	35	1,440	295	111	4,750	38,995	9.98	0.99	2.56	-	-
"	4b	3-28-83	"	68	7.30	14,730	28.7	1,304	245	150	4,000	23,400	5.96	0.97	2.55	-	-
"	5	3-24-59	"	-	7.60	5,990	-	1,030	213	110	2,860	9,500	-	0.97	-	-	-
Cottle	8	6-14-83	"	76	8.55	7,630	10.9	1,050	230	99	3,450	11,860	3.30	0.99	2.78	-	-
"	9a	3-29-83	"	78	8.19	12,340	19.3	1,270	194	104	3,940	19,320	6.08	0.98	3.15	-	-
"	9b	3-29-83	"	75	8.10	13,860	19	1,270	223	121	3,960	21,624	6.72	0.99	3.11	-4.97	-40
"	9c	3-29-83	"	72	7.50	11,800	18.7	1,250	178	121	3,750	18,257	5.53	0.98	3.03	-5.83	-41
"	10a	3-29-83	"	71	7.31	12,430	22.1	1,230	243	130	3,960	19,497	6.17	0.98	3.16	-5.90	-45
"	10d	4-02-80	"	65	7.40	9,790	30.5	1,165	238	138	3,431	14,210	4.00	1.06	2.81	-	-
"	11a	3-30-83	"	63	7.30	7,380	16.8	979	196	170	3,160	11,465	4.43	0.99	3.86	-	-
"	11b	3-30-83	"	70	7.40	3,910	11	782	156	164	2,410	6,253	2.39	0.96	3.82	-5.56	-39
"	11c	3-30-83	"	70	7.51	3,350	10	748	149	173	2,150	5,384	2.11	0.96	3.92	-5.64	-40
Kent	17	11-02-82	"	70	7.30	39,900	87.9	1,750	608	43	5,540	63,000	11	0.98	1.75	-6.11	-49
"	18	11-01-82	"	70	6.90	103,000	281	667	1,200	27	6,710	158,000	26.8	1.01	1.70	-5.79	-44
Childress	19	5-06-81	Well	48.3-100.3	8.40	12,740	36.4	1,380	290	175	4,050	19,450	7.50	1.01	3.86	-	-
"	20	5-16-81	"	127.0-132.5	8.10	23,890	46.2	1,650	360	114	4,810	37,400	13.00	0.98	3.48	-	-
"	21	8-16-74	"	150-224.8	-	44,550	114	2,430	154	-	5,220	68,480	17.30	1.00	2.53	-	-
"	22	6-11-81	"	22.1-44.5	-	20,660	34.9	1,700	397	-	4,710	32,720	9.30	0.97	2.84	-	-
"	23	8-13-74	"	165-185	-	34,850	55.4	1,910	562	-	5,220	55,960	13.70	0.96	2.45	-	-
"	24	10-14-81	"	32-47.8	-	16,970	35.3	1,570	372	-	4,500	27,550	7.70	0.95	2.79	-	-
"	25	10-14-81	"	116-135	-	13,360	33.2	1,310	303	-	4,110	21,400	5.50	0.96	2.57	-	-
"	26	10-07-81	"	20-28.3	-	21,420	39.5	1,660	380	-	5,010	34,460	9.30	0.96	2.70	-	-
Cottle	27	3-25-81	"	86-173	7.50	10,541	26.5	1,291	255	165	3,650	16,000	6.50	1.02	4.06	-4.74	-
"	28	3-19-81	"	103.1-151.5	66	10,439	20.6	1,292	249	127	4,040	16,000	7.00	1.01	4.37	-	-
"	29	3-07-79	Spring	-	-	15,010	25	1,550	322	-	4,440	23,480	6.80	1.06	2.90	-	-
"	30	4-07-81	Well	49.8-52.8	-	11,010	23.4	1,300	272	-	3,990	17,190	5.70	0.99	3.32	-	-
Kent	31	8-30-64	"	173-400	6.90	20,676	72.7	1,496	349	66.5	4,073	32,000	5.70	1.00	1.78	-	-
"	32	9-14-64	"	307-357	70.5	52,590	153.8	1,294	621	58	5,084	79,970	13.10	1.01	1.64	-	-
"	33	7-16-64	"	0-175	70	91,044	169.2	769	428	32	6,837	135,820	19.60	1.03	1.44	-	-
"	34	8-03-64	"	44-53	-	55,400	91	913	415	39	5,397	84,470	17.50	1.01	2.07	-	-
"	35	10-06-64	"	519.5-602	-	122,604	183	1,382	522	26	4,375	189,916	21.60	1.00	1.14	-	-
"	36	2-16-65	"	100	6.10	98,952	280	1,343	1,390	46	6,938	151,962	21.2	1.00	1.40	-	-
"	37	2-16-65	"	300	6.00	116,620	264	1,020	1,254	43	6,344	179,694	35.00	1.00	1.95	-	-
"	38	8-26-64	"	100-400	71	111,085	283	1,225	521	68	6,632	168,454	25.90	1.02	1.54	-	-
"	39	9-02-64	"	2-190	71	82,525	290	1,669	1,048	86	6,252	129,160	27.40	0.98	2.12	-	-
"	40	9-01-64	"	0-93	71	38,734	104	1,626	466	46	5,575	60,027	11.80	0.99	1.97	-	-
"	41	2-02-65	"	360	6.40	74,687	209	1,393	996	54	7,617	115,342	19.4	1.00	1.68	-	-
"	42	2-02-65	"	460	5.90	118,244	225	982	1,469	48	1,918	188,000	9.30	0.97	4.9	-	-
"	43	9-27-64	"	401.5-525	68	103,460	285	1,283	843	96	6,391	158,895	27.10	1.00	1.71	-	-
"	44	5-25-65	"	500	70	122,808	95	1,079	265	32.5	5,659	187,824	11.90	1.01	1.63	-	-
"	45	10-21-64	"	424-603	71	73,060	79.8	1,439	288	77	4,139	113,524	10.00	0.99	1.88	-	-
"	46	10-20-64	"	260-410	71	121,200	158	2,136	398	12	2,964	187,200	48.00	1.00	2.56	-	-
"	47	10-08-64	"	340	70	114,050	144	2,171	480	15	3,257	182,530	-	0.96	-	-	-
"	48	3-25-66	"	206-299	65	124,836	1,794	925	1,163	38	7,211	192,708	26.70	1.00	1.39	-	-

- not analyzed

# from Stevens (1974)

+ from Brune (1981)

++ from Popkin (1973)

\* from Kreftler and Bassett (1983)

S. Ar

samps

types of

brines.

Table 18. Chemical and isotopic analyses of Group B brines.

County	Sample no.	Date collected	Sample type and depth (ft)	Temp. (°F)	pH	Na	K	Ca	Mg	HCO <sub>3</sub>	SO <sub>4</sub>	Cl	Br	mNa/mCl	Br/Cl x 10 <sup>-4</sup>	δ <sup>18</sup> O (‰, SMOW)	δD
Hall	2	1-22-69	Spring	-	7.40	10,000	33	2,400	750	182	2,780	19,800	-	0.78	-	-	-
Harmon	6a	9-01-82	"	-	6.70	116,000	219	1,050	1,600	71.8	3,570	187,000	92.2	0.96	4.93	-5.63	-43
"	6b	9-01-82	"	-	6.55	115,000	118	1,130	1,630	43.7	3,550	185,000	89.6	0.96	4.84	-5.51	-43
Beckham	7	9-01-82	"	70	7.50	39,900	134	2,120	1,050	118	4,870	64,200	52.6	0.96	8.19	-6.17	-52
Cottle	10b	3-29-83	"	70	7.30	8,630	20.2	996	198	140	3,430	14,357	5.2	0.93	3.62	-	-
King	12a	-	"	80	6.80	15,480	36	1,414	307	131	3,829	24,560	14.00	0.97	5.70	-	-
"	12b	3-31-83	"	71	7.38	3,350	15	903	202	127	2,820	5,732	5.19	0.90	9.05	-	-
"	12c	11-03-82	"	64.5	7.30	2,290	15.2	822	204	126	2,720	3,680	5.46	0.96	14.84	-5.97	-41
"	13	12-03-66	"	-	7.00	30,000	126	1,330	764	116	3,470	48,300	-	0.96	-	-	-
"	14	11-02-82	"	68	7.10	75,400	102	2,040	651	36	4,340	114,000	36.9	1.02	3.24	-5.65	-40
"	15	6-14-83	"	69	7.30	23,070	36.2	1,720	335	78	5,040	35,380	16.2	1.01	4.58	-	-
Stonewall	16	6-14-83	"	72	6.70	100,700	277	2,350	1,770	25	4,200	156,400	13	0.99	8.31	-	-
Childress	49	6-19-81	Well	197-249	68	112,000	220	1,950	750	71.6	2,670	175,100	70	0.99	4.00	-	-
"	50	6-18-81	"	249-300	68	73,300	227	2,250	770	79.3	3,000	116,000	65	0.97	5.60	-	-
"	51	9-02-81	"	25.7-37.0	-	9,310	18.3	1,390	295	-	3,840	15,590	4.2	0.92	2.69	-	-
Stonewall	52	5-27-65	"	360	6.90	61,150	374	2,100	1,580	36	4,270	102,000	-	0.92	-	-	-
"	53	9-21-64	"	297-560	-	44,300	119	2,120	482	204	5,300	69,000	30	0.99	4.35	-	-
"	54	10-09-64	"	213-300	68	120,000	477	2,875	1,450	69	3,785	188,000	145	0.98	7.71	-	-
"	55	3-07-66	"	276-491	69	117,300	377	3,640	1,180	34	2,018	191,000	153.4	0.95	8.03	-	-
"	56	6-30-67	"	0-80	70	96,760	407	2,300	1,730	25	3,545	159,100	9.9	0.94	.62	-	-
Kent	57	2-18-65	"	185	6.00	116,523	276	1,416	1,000	30	4,900	182,700	59.3	0.98	3.25	-	-
"	58	10-19-64	"	201-300	68	116,570	226	3,080	852	82	2,368	187,240	122	0.96	6.52	-	-
"	59	2-17-65	"	200	6.30	117,320	514	3,309	2,194	102	2,170	191,500	235	0.94	12.27	-	-
"	60	9-01-64	"	295-489	73	119,900	357	1,882	1,098	56	3,429	188,243	86.3	0.98	4.58	-	-
"	61	9-30-64	"	366-495	70	115,920	518	2,460	4,272	38	2,640	190,800	179	0.94	9.38	-	-
"	62	3-24-66	"	329-415	68	116,640	359	2,628	975	8	2,760	182,400	102	0.99	5.59	-	-
"	63	6-20-63	"	29	-	13,583	77	1,675	555	104	3,951	22,535	-	0.93	-	-	-
King	64	3-02-66	"	170-374	66	120,680	762	1,885	1,522	94	3,322	192,072	269.4	0.97	14.03	-	-

- not analyzed

# from Stevens (1974)

++ from Popkin (1973)

\* from Kreitler and Bassett (1983)

\*\* sample obtained from U.S. Army Corps of Engineers, Tulsa

Table 19. Chemical and isotopic analyses of Group C brines.

County	Sample no.	Date collected	Sample type and depth (ft)	Temp. (°F)	mg/l										Br/Cl x 10 <sup>-4</sup>	δ <sup>18</sup> O (‰, SMOW)	δD
					pH	Na	K	Ca	Mg	HCO <sub>3</sub>	SO <sub>4</sub>	Cl	Br	mNa/mCl			
King	65	5-15-79	Well	82	66	7.30	12,000	220	1,100	930	140	5,700	20,000	140	0.93	70.00	-
	66	5-08-79	"	80	69	6.40	60,000	1,300	3,400	7,200	190	1,300	130,000	860	0.71	66.15	-3
	67	5-15-79	"	52	68	7.20	7,000	170	1,500	900	100	3,000	15,000	100	0.72	66.67	-
	68	5-15-79	"	70	67	6.60	38,000	200	1,400	8,500	30	6,700	81,000	510	0.72	62.96	-3.9
	69	5-15-79	"	97	66	7.00	26,000	100	1,400	4,400	92	7,100	51,000	320	0.79	62.75	-4.6
	70	5-15-79	"	80	68	6.70	30,000	380	1,300	5,100	110	9,100	61,000	420	0.76	68.85	-
	71	5-16-79	"	59	66	6.70	25,000	410	2,000	4,300	74	5,000	49,000	290	0.79	69.18	-4.9
	72	5-16-79	"	38	69	6.80	14,000	320	1,000	3,200	82	8,900	26,000	160	0.83	51.54	-
	73	5-16-79	"	52	67	6.80	23,000	130	420	6,400	100	15,000	45,000	280	0.79	62.22	-6.8
	74	5-17-79	"	85	68	6.50	55,000	950	3,100	7,000	260	3,800	110,000	770	0.77	70.00	+1
"	75	5-17-79	"	110	69	6.20	97,000	1,500	2,400	12,000	160	2,900	190,000	1,100	0.79	57.90	-
	76	5-08-79	"	94	69	6.60	28,000	750	3,900	5,800	160	1,300	69,000	610	0.63	88.41	-1.9
	77	5-08-79	"	90	67	6.90	13,000	320	4,700	1,700	100	830	32,000	240	0.63	75.00	-
	78	5-09-79	"	75	69	6.80	16,000	390	3,200	3,000	180	1,900	37,000	230	0.67	62.16	-1.9
	79	5-15-79	"	65	67	6.50	28,000	150	2,200	3,900	200	4,900	54,000	350	0.80	64.81	-
	80	5-15-79	"	100	67	6.50	48,000	730	2,400	7,000	150	5,000	98,000	650	0.76	66.33	-14
	81	5-16-79	"	75	67	6.40	29,000	710	2,100	5,200	190	5,200	60,000	400	0.75	66.67	-
	82	5-16-79	"	109	67	6.40	53,000	960	3,300	8,400	170	3,900	110,000	760	0.74	69.09	-7
	83	5-16-79	"	65	68	6.10	60,000	1,200	2,100	15,000	54	3,000	140,000	920	0.66	65.71	-
	84	5-16-79	"	72	69	7.00	6,800	230	1,800	1,200	250	2,700	16,000	110	0.66	68.75	-4.3
"	85	5-18-79	"	90	67	6.40	30,000	390	10,000	4,300	80	1,500	77,000	500	0.60	64.94	-
	86	5-08-79	"	117	69	7.00	11,000	310	3,700	1,100	74	1,900	24,000	200	0.71	83.33	-6.9
	87	5-09-79	"	84	68	6.80	33,000	44	3,000	6,800	180	2,900	78,000	570	0.65	73.08	-5
Stonewall	88	5-11-79	"	32	64	7.10	9,500	160	970	900	64	4,500	16,000	94	0.92	58.75	-
	89	5-10-79	"	86	67	7.20	10,000	150	460	1,000	110	2,800	17,000	91	0.91	53.53	-
	90	5-11-79	"	42	63	6.90	24,000	290	1,700	2,900	60	5,000	48,000	280	0.77	58.33	-3.9
	91	5-10-79	"	76	64	7.00	13,000	240	960	1,500	100	6,100	23,000	150	0.87	65.22	-
	92	5-10-79	"	52	64	7.00	13,000	280	370	3,800	72	5,000	27,000	160	0.74	59.26	-5.2
	93	5-10-79	"	105	68	7.00	22,000	260	1,600	1,900	110	5,200	41,000	200	0.83	48.78	-4.08
	94	5-09-79	"	74	70	6.40	40,000	820	3,800	5,500	230	15	84,000	490	0.73	58.33	-2.93
	95	5-27-65	"	170	-	6.50	103,200	825	11,070	3,700	32	687	188,000	-	0.85	-	-27
	96	2-18-65	"	365	-	5.30	78,045	628	23,716	8,809	14	245	185,130	994.6	0.65	53.72	-
	97	2-18-65	"	100	-	5.80	82,600	716	24,034	9,100	18	3,733	195,000	1,034	0.65	53.03	-
"	98	5-27-65	"	400	-	4.40	61,240	774	10,415	2,853	-	1,211	122,000	-	0.77	-	-
	99	5-27-65	"	600	-	4.00	61,860	807	10,220	2,990	-	1,212	122,400	-	0.78	-	-
	100	10-12-64	"	382-625	70	7.00	13,200	243	2,680	423	29	2,600	24,700	77.30	0.82	31.30	-
	101	10-14-64	"	318-503	70	6.30	15,613	164	2,740	640	44	3,120	28,000	91	0.86	32.50	-
	102	5-27-65	"	350	71	3.40	54,300	662	5,100	6,530	-	2,300	111,000	-	0.75	-	-
	103	10-15-64	"	255-361	67	5.40	24,200	332	3,053	1,590	6	3,750	44,000	166	0.85	37.73	-
	104	3-01-66	"	198-397	69	5.20	29,700	555	2,700	3,200	10	4,300	58,500	213.6	0.78	36.51	-
	105	3-06-66	"	260-370	69	5.00	25,000	400	2,300	3,470	8.5	4,740	49,500	161	0.78	32.53	-
	106	3-04-66	"	296-475	67	6.30	11,200	130	1,060	2,000	30	7,080	20,000	83.40	0.86	41.70	-
	Kent	107	2-18-65	"	463	-	5.70	108,840	788	9,600	2,400	48.5	6,254	190,284	500.5	0.88	26.30
Harmon	108	10-25-80	"	11.9-558	-	-	27,360	154	8,020	1,860	-	1,830	58,560	335	0.72	57.21	-

- not analyzed

\* from Stevens (1974)

\*\* sample obtained from U.S. Army Corps of Engineers, Tulsa

† analysis obtained from USGS, Austin

## ISOTOPIC COMPOSITION OF SHALLOW GROUND WATER IN EASTERN NEW MEXICO AND THE TEXAS PANHANDLE

Rainer K. Senger, Bernd C. Richter, and Charles W. Kreitler

*The hydrogen ( $\delta D$ ) and oxygen ( $\delta^{18}O$ ) isotopic composition of shallow ground waters indicates typical meteoric water;  $\delta D$  and  $\delta^{18}O$  values range from  $-82\text{ ‰}$  to  $-41\text{ ‰}$  and  $-11.46\text{ ‰}$  to  $-5.36\text{ ‰}$ , respectively, showing a general increase toward the east. The isotopic enrichment of the ground water toward the east reflects the general decrease in altitude and the relatively heavy isotopic composition of precipitation in the Gulf Coast area. The isotopic composition of ground water from the Dockum Formation in Swisher County suggests an origin further to the west at higher elevations and the absence of significant mixing with isotopically heavier Ogallala water.*

Ground-water samples from 15 municipal wells were collected along a 300-mi traverse from the Manzano Mountains in New Mexico to the west, across the High Plains and Rolling Plains, to approximately the Texas-Oklahoma state line in the east (fig. 147). Hydrogen and oxygen isotopes in shallow ground water commonly reflect the isotopic composition of precipitation, thus allowing the distinction of ground waters in different areas.

Location and isotopic composition of the water samples, reported in the conventional delta notation, are given in table 20. The range of  $\delta D$  values falls well within the expected range of meteoric water in this area (fig. 148) as reported by Lawrence and Taylor (1972). Accordingly, the  $\delta D$  and  $\delta^{18}O$  values show a general decrease from east to west (fig. 147, table 20). This isotopic depletion reflects the general increase in elevation and the dominance of isotopically heavy precipitation in the eastern part, which originates predominantly in the Gulf of Mexico.

The isotopically lightest ground water was found at highest elevations near the Manzano Mountains in New Mexico, as shown by the ground-water sample from Mountainair city well (elevation 6,545 ft) with  $\delta D$  and  $\delta^{18}O$  values of  $-82\text{ ‰}$  and  $-11.46\text{ ‰}$ , respectively. Similar values are reported from the Roswell Basin farther to the south in Chaves County (south of DeBaca County), indicating recharge from the mountain massifs to the west (Hoy and Gross, 1982). Near the Pecos River, shallow ground water from the alluvium near the town of Santa Rosa (elevation 4,600 ft) shows  $\delta D$  and  $\delta^{18}O$  values of

-55 ‰ and -7.30 ‰, respectively, reflecting the isotopic composition of meteoric water at that altitude (Hoy and Gross, 1982). In contrast, a deep ground-water sample from Santa Rosa City well no. 3 shows significantly lighter isotopes, indicating that recharge to the confined San Andres Formation occurs farther to the west at higher elevations.

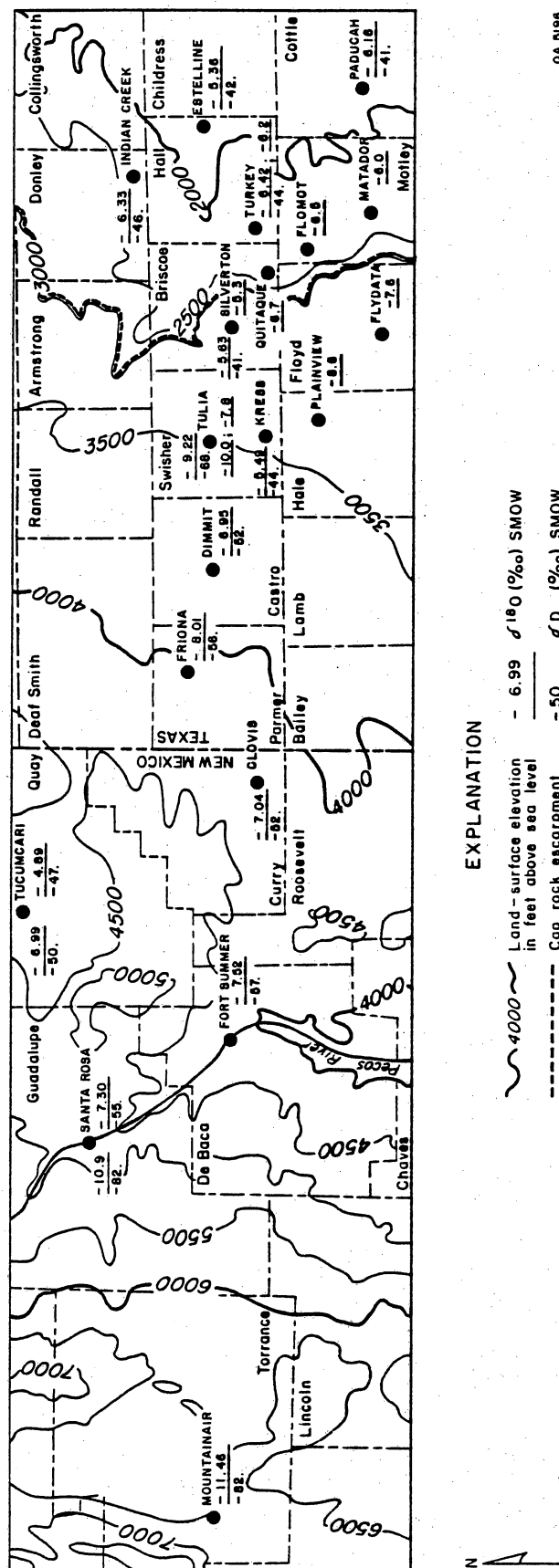
Along the High Plains, the isotopic composition of ground waters generally decreases from west to east, reflecting the overall topography. A water sample from Tulia, Swisher County, however, shows unusually low  $\delta D$  and  $\delta^{18}O$  values of -68 ‰ and -9.22 ‰, respectively, for this particular area. A similar isotopic composition was found in a water sample from the deeper Dockum Formation ( $\delta^{18}O = -10$  ‰), whereas a water sample from the Ogallala Formation yielded a  $\delta^{18}O$  value of -7.8 ‰. The difference in isotopic composition suggests that deeper ground water in the Dockum Formation with low  $\delta^{18}O$  values originates farther to the west at higher elevations and that ground waters of both formations do not mix significantly.

Shallow ground water east of the Caprock Escarpment generally has the highest values of oxygen and hydrogen isotopes. Kreitler and Bassett (1983) reported similar  $\delta^{18}O$  values of shallow ground water but lower  $\delta D$  values. The hydrogen isotope analysis, however, has been stated as being erroneous (Kreitler and Bassett, 1983).

A plot of  $\delta^{18}O$  and  $\delta D$  (fig. 149) shows that the data from shallow ground water fall close to the meteoric water line (the isotopic composition of nearly all meteoric waters plots on this trend). Minor isotopic enrichment of the ground water is probably due to evaporation and other isotopic modifications occurring during recharge.

The isotopic composition of most of the saline spring waters in the Rolling Plains of the Palo Duro Basin is similar to that of the local meteoric ground water (Richter and Kreitler, this volume). Thus, the data presented here characterizing the isotopic range of shallow ground water helps to support the meteoric origin of water from saline springs as reported previously by Kreitler and Bassett (1983) and Richter and Kreitler (this volume).





QA 5196

Figure 147. Sampling locations of municipal wells in New Mexico and the Texas Panhandle. The upper number and lower number show the  $\delta^{18}\text{O}$  and  $\delta\text{D}$  isotopic compositions, respectively.

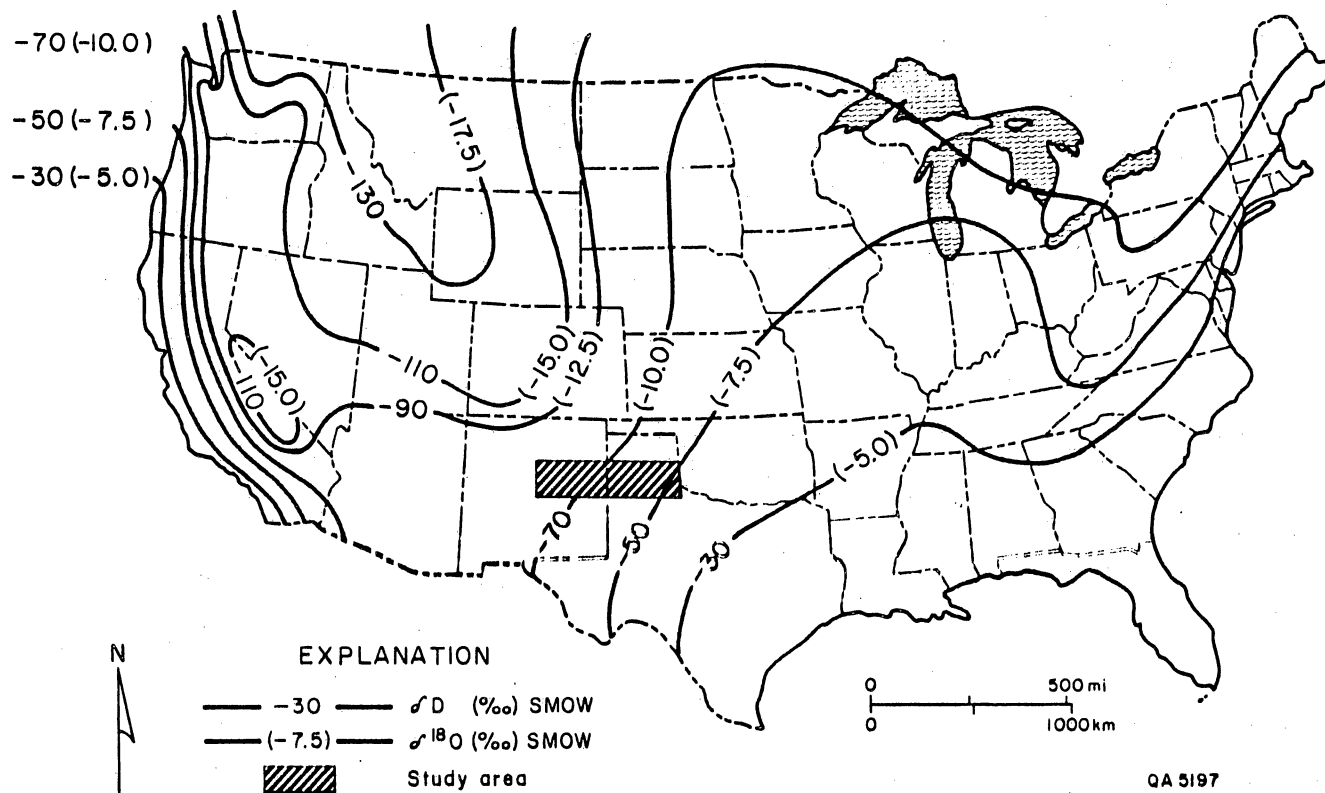


Figure 148. Map of the United States, showing the approximate contours of  $\delta D$  and  $\delta^{18}O$  (in parentheses) of present-day meteoric water (after Lawrence and Taylor, 1972).

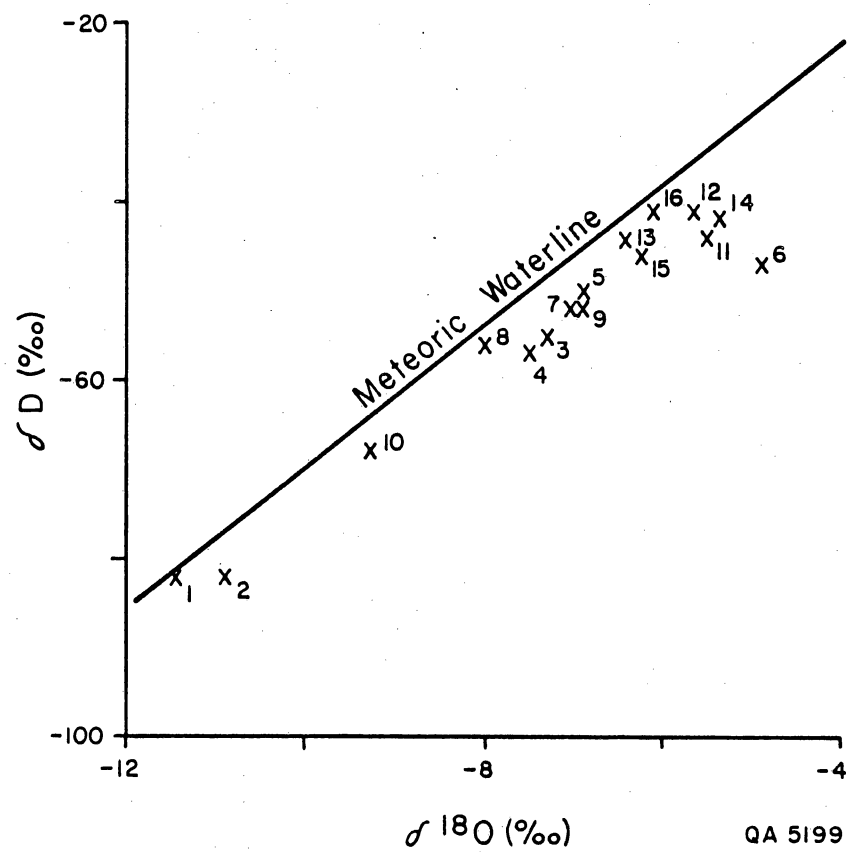


Figure 149. Plot of  $\delta^{18}\text{O}$  and  $\delta\text{D}$  for shallow ground water from municipal wells in New Mexico and the Texas Panhandle.

Table 20.  $\delta^{18}\text{O}$  and  $\delta\text{D}$  for selected water wells in New Mexico and Texas Panhandle.

Sample location of municipal wells	Formation	Depth (ft)	$\delta^{18}\text{O}$ (‰)	$\delta\text{D}$ (‰)
1. Mountainair	Yeso	215	-11.46	-82
2. Santa Rosa No. 3	San Andres	620	-10.89	-82
3. Santa Rosa	Alluvium	62	-7.30	-55
4. Fort Sumner	?	201	-7.52	-57
5. Tucumcari No. 12	Dockum	330	-6.96	-50
6. Tucumcari No. 10	Dockum	310	-4.89	-47
7. Clovis No. 29	Ogallala	360	-7.04	-52
8. Friona No. 9	Ogallala	310	-8.01	-56
9. Dimmit No. 1	Ogallala	375	-6.95	-52
10. Tulia No. 1	Dockum	816	-9.22	-68
11. Kress	Ogallala	300	-5.49	-44
12. Silvertown	Ogallala	200	-5.63	-41
13. Turkey	Permian/Alluvium	174	-6.42	-44
14. Estelline	Permian/Alluvium	62	-5.36	-42
15. India Creek	Permian/Alluvium	20	-6.33	-46
16. Paducah	Permian/Alluvium	260	-6.16	-41
17. Tulia No. 14	Dockum	816	-10.0	
18. Tulia No. 7	Ogallala	200?	-7.8	
19. Silvertown	Ogallala	181	-5.3	
20. Plainview No. 14	Ogallala (Base)	325+	-8.6	
21. Floydada	Ogallala (Base)	312+	-7.6	
*22. Quitaque	Permian/Alluvium	192	-6.5	
*23. Quitaque	Permian/Alluvium	?	-6.8/-6.9	
*24. Turkey	Permian/Alluvium	110	-5.3/-6.2	
*25. Flomot	Permian/Alluvium	?	-6.1/-6.7	
*26. Matador	Permian/Alluvium	293	-6.0	

\*Kreitler and Bassett (1983)

+Base of Ogallala Formation

## A REVIEW OF RESEARCH ON BOREHOLE SEALING AND ITS APPLICATION TO A PROPOSED REPOSITORY IN THE PALO DURO BASIN

William W. Simpkins

*Much research on borehole sealing has been done since the initial problems with the proposed Lyons site. Most emphasis has been placed on laboratory development and testing of grout plugs. The Bell Canyon Test at the WIPP site is the only major in situ test to date. Information from that test suggests that flow rates in boreholes in the Palo Duro Basin will be greater as a result of the steeper hydraulic gradient there than at WIPP.*

### Historical Perspective

The perception that abandoned boreholes might be a problem in the siting of a waste repository began with the proposed repository site at Lyons, Kansas. The National Academy of Sciences (NAS) recommended a study of abandoned boreholes in the immediate vicinity (NAS, Committee on Radioactive Waste Management, 1970). Twenty-nine oil and gas wells were found within 1 mi of the site boundaries, and ten of those wells were within 660 ft of the actual site (Culler, 1971). Hambleton (1972) compared the site to a "piece of Swiss cheese" because of the potential for fluid circulation along boreholes down to and away from the repository level. Some wells penetrated the Arbuckle Group rocks whose potentiometric surface is above the repository level. Hydrologic investigations documented a downward hydraulic gradient at one borehole that was contourable on the potentiometric surface map (Angino and Hambleton, 1971).

After abandonment of the Lyons option in 1972, site screening identified the Waste Isolation Pilot Plant (WIPP) site in southeastern New Mexico. The site had a very low well density, the closest well being 2 mi away. Sandia Laboratories initiated the materials development program for borehole plugs at the WIPP site in 1975. Funding of the overall program was given to the Office of Nuclear Waste Isolation (ONWI) in 1977.

A comprehensive review of the borehole sealing program was completed in 1979 by D'Appolonia Consulting Engineers, Inc. (ONWI, 1979). Topics of investigation included (1) evaluation of existing materials and techniques; (2) hydrothermal transport; (3) plugging

with earth materials; (4) in situ instrumentation; (5) cement grouting; and (6) salt-dissolution modeling.

### Salt-Dissolution Studies

Studies on salt dissolution around boreholes have been a major focus of the sealing program because of the earlier decisions naming salt as the most desirable host medium for high-level nuclear waste. Theoretical models of the dissolution process were first constructed by T. N. Dixon at the University of Texas and continued by A. L. Podio and R. M. Knapp from 1974 to 1979. Using both theoretically and physically based models, Knapp and Podio (1979) concluded that (1) a one-dimensional model appears adequate for representing salt transport in a vertical wellbore, (2) a wellbore will provide an avenue for brine transport from an upper salt unit to a lower permeable unit, (3) convection flow but not dissolution can be physically modeled, and (4) the brine transport process can be reasonably approximated using finite-difference methods.

Field studies of salt dissolution around abandoned boreholes concerned potential subsidence (Walters, 1975, 1978; Fader, 1975). The former concluded that such dissolution was an uncommon process in the oil fields of Kansas; whereas, Fader (1975) concluded that deterioration of the casing and cement in boreholes was common and that salt dissolution was a common process. He calculated the amount of salt removed to cause land subsidence and estimated the flow rates needed to accomplish the dissolution. Flow estimates range from 5 to 24 gallons per minute.

### Development and Testing of Grouts

Design and testing of grout for borehole plugs has continued (Buck and others, 1981; Wakeley and others, 1981; Sarkar and others, 1982; Roy and Grutzeck, 1982). Materials development for the grouts has been the responsibility of Pennsylvania State University (Penn State) and the U.S. Army Corps of Engineers Waterways Experiment Station (WES).

Specific grouts for a bedded salt repository are discussed in Roy and others (1982). Scale model testing of grouts has recently been done by Terra Tek (J. Gould, personal communication, 1983).

The Borehole Plugging Program (BHP) at Sandia Laboratories has conducted the only major in situ test of grout in an open borehole. The Bell Canyon Test was designed to evaluate the Penn State and WES grouts and investigate the installation of a "typical plug" in anhydrite (Christensen and Peterson, 1981). A well was drilled to the Bell Canyon Formation aquifer (4,534 ft), and an 8-inch diameter (20-cm), 6-ft-long (2-m) plug was installed in the overlying Castille Formation (anhydrite) at 4,495 ft (1,370 m). The Bell Canyon aquifer has a shut-in pressure of 12.4 MPa (1,800 psi) and a production capacity of  $10^4$  gallons per day (38,000 liters/day). Borehole plug performance was assessed using pressure-buildup tests, shut-in tests and tracer-transit-time tests. The grout plug reduced flow up the borehole from the Bell Canyon aquifer to 0.2 gallons per day (0.6 liters/day). Permeabilities (k) of the plugs were in the range of 50 microdarcys, and porosities were about 1.5 percent. The Bell Canyon Test indicated that grouts may be effective borehole sealants if the physical properties are matched with the local rock. A fresh-water grout mix was shown to be the most effective.

Intera Environmental Consultants (1981) used the results of the Bell Canyon Test for a consequence assessment model of the WIPP site. They discussed three scenarios of inter-aquifer communication: (1) the U-tube scenario of one aquifer connected by two wells through a repository, (2) flow between two aquifers along a single borehole, and (3) both cases where multiple boreholes exist. The concept of hydraulic conductance (HC) is defined for the borehole plug as

$$HC = \frac{k A}{L} \text{ where } A = \text{cross-sectional area of the plug} \\ \text{and } L = \text{length of the plug}$$

Hydraulic conductance is somewhat analogous to the transmissivity of a horizontal aquifer of hydraulic conductivity (K) and thickness (b). Units of HC are in millidarcy-feet. In

general, for the WIPP site, maximum flow rates between aquifers are achieved up to about 100 md-ft, after which point the transmissivity of the aquifer is the main control on flow. A typical Bell Canyon Plug with  $HC = 2.91 \times 10^{-3}$  md-ft would limit flow between the Bell Canyon and Rustler aquifers to less than  $10^{-3}$  ft<sup>3</sup>/day.

#### Application to the Palo Duro Basin

Hydraulic head data from the Palo Duro Basin indicate that any flow in an open borehole connecting the Ogallala-Dockum aquifer and the Wolfcamp aquifer would be downward throughout the proposed locations in Deaf Smith and Swisher Counties. Flow rates (Q) down a hypothetical borehole can be calculated by the equation

$$Q = HC \text{ (pg/u)} H1 - H2$$

where (H1-H2) = the difference in hydraulic head between aquifers

Using (H1-H2) values of 525 m (Deaf Smith) and 400 m (Swisher) and  $HC = 2.91 \times 10^{-3}$  md-ft,  $Q = 2.58 \times 10^{-4}$  m<sup>3</sup>/day ( $9.27 \times 10^{-3}$  ft<sup>3</sup>/day) for Deaf Smith and  $Q = 2.97 \times 10^{-4}$  m<sup>3</sup>/day ( $7.08 \times 10^{-3}$  ft<sup>3</sup>/day) for Swisher. These flow rates are higher than those at WIPP because of the steeper hydraulic head gradient between aquifers in the Palo Duro Basin. The U-tube scenario of Intera Environmental Consultants (1981) is less likely to occur because of the shallow gradient in the Ogallala-Dockum aquifer. However, the consequences of contamination are much greater because of the importance of the aquifer to agriculture in the region.

Salt dissolution around abandoned boreholes has not been formally recognized in the Palo Duro Basin. Baumgardner and others (1982) documented the development of a large sinkhole in Winkler County in the heavily drilled Midland Basin in which dissolution may have been related to a borehole. Speculation as to the impact of dissolution in a borehole and communication between aquifers in the Palo Duro Basin must be tempered with the apparent scarcity of boreholes in the locations of interest. County maps as of 1977 show only 12 wells in the Deaf Smith location (plus 2 DOE) and 8 wells in the Swisher location



(plus 3 DOE). Their density is much less than the worst case projections of the Intera Environmental Consultants (1981) report of 1 well per 40 acres. The continued interest of oil companies and stratigraphic and hydrologic investigations associated with repository siting will increase the chance for interaquifer communication. Currently, wells are plugged only in accordance with the State of Texas regulations that provide only for the protection of fresh-water aquifers and formations bearing mineral resources.

## WATER CONTENT OF BEDDED SALT, PALO DURO BASIN, TEXAS

R. Stephen Fisher

*A standardized procedure of soxhlet extraction in anhydrous methanol and Karl Fischer titration has been established for the analysis of water content in salt. Values determined on more than 100 Palo Duro Basin salt samples range from <0.2 to >5 weight percent. Clay-rich salts typically contain an order of magnitude more water than samples with dolomite, anhydrite, or no impurities.*

The total amount and distribution of fluid in bedded salts are important controls on the suitability of the strata for high-level nuclear waste isolation. Both the physical strength of salt and the reactivity of host rock with waste-cannister or backfill material are adversely affected by high water content. Furthermore, the local geochemical environment surrounding a waste repository will be largely determined by the amount and composition of mobile water in the salt units.

The distribution of fluid in host salt determines its mobility in the subsurface environment. Water present in some hydrous minerals may never be released under expected repository conditions. Water along mineral surfaces or in fractures will move in response to the local hydrologic gradient, whereas fluid inclusions will move in response to the imposed thermal gradient.

The amount of water measured in a salt sample depends not only on the amount of each type of water present but also on the sample selection, sample preparation, and analytical techniques employed. Distributions of fluid inclusions and impurities in salt are generally very inhomogeneous. Small samples are less likely to yield representative values than larger ones, and crushed samples will typically yield low water-content values because of the rupture of fluid inclusions, increase in surface area, and subsequent loss of both intergranular and intragranular water. Measurements of weight loss on heating may produce values that are either too low, if heating is not sufficient to break all fluid inclusions, or too high, if organic matter is oxidized and the water of all hydrous minerals is released (see Bassett and Roedder, 1981).

More than 100 salt samples have been analyzed by a standardized procedure at the BEG. The halite fraction of large (200 to 500-g) samples is dissolved in anhydrous methanol; water content of the methanol is then measured by Karl Fischer titration and calculated as weight percent of the total sample. This method detects all intergranular water and the water of fluid inclusions in halite; it does not measure the included fluids in minerals other than halite or the bound water in hydrous minerals. The amount and mineralogy of the insoluble residue also is determined, permitting a calculation of the water of mineral hydration.

Samples were selected from the available core to represent a variety of salt types and depositional environments. Mean water content for all samples is 0.8 weight percent; however, this value is strongly influenced by the high water content of clay-rich samples. Mean water content of clay-free salt samples is approximately 0.4 weight percent. The amount of clay present in salt and the amount of associated intergranular water are therefore important parameters that must be established early in the waste repository site selection and evaluation process.

Future work will establish methods to distinguish the different forms of water in the various salt types and to determine their relative mobilities.

## HYDROGEOCHEMISTRY OF SUB-SALT BRINES FROM THE SAWYER, MANSFIELD, AND ZEECK WELLS, PALO DURO BASIN, TEXAS

R. Stephen Fisher

*Brines from aquifers below the San Andres Formation at three sites in the Texas Panhandle are highly saline Na-Cl brines that are capable of dissolving both halite and anhydrite. Although there are not yet sufficient data for detailed evaluation of the chemical evolution of fluids along flow paths within specific units, results of analyses to date suggest that cross-formational mixing of brines may be significant.*

Previous reports regarding the hydrogeochemistry of sub-salt hydrologic units in the Palo Duro Basin have been based on data obtained from petroleum companies, petroleum information services, and other sources of published data (Bassett and Bentley, 1983; Bureau of Economic Geology, 1983a, b; Bureau of Economic Geology, 1982). The major ionic compositions of brines from the deep-basin aquifers in the Palo Duro Basin are described by Bassett and Bentley (1983). They also discuss the limits on the usefulness of their data base because of changes that occur in fluid composition during sample collection and storage. This status report presents analyses of deep-basin brines that were sampled and analyzed specifically for the West Texas Waste Isolation Project from the Sawyer, Mansfield, and Zeeck wells.

As of June 1983, brine analyses have been completed for 10 intervals in 3 wells. Figure 150 shows the location of these wells and additional wells that will be completed and sampled in the future. A map of the potentiometric surface indicates that the direction of regional ground-water flow in the Wolfcamp is to the northeast (fig. 150). Flow directions in units below the Wolfcamp are not well known but are probably similar to those in the Wolfcamp (Bassett and Bentley, 1983). The Wolfcamp potentiometric surface shows that flow is generally from the Zeeck site to the Sawyer site; the Mansfield well is on a different flow path. At this time there are not enough wells and samples, nor are specific flow paths sufficiently well known to permit evaluation of brine compositional differences parallel or perpendicular to flow direction within any single hydrologic unit.

The major ionic compositions of formation fluids are summarized in table 21. The brines contain from 141 to 243 g/L total dissolved solids and have ionic strengths between 2.7 and 4.7 and densities ranging from 1.09 to 1.14 g/cm<sup>3</sup>. The dominant ions are sodium and chloride; minor, but important, amounts of calcium and magnesium are also present (figs. 151 and 152). Because of the high ionic strengths of these brines, ionic complexing will be significant and may control the solubility and mobility of radionuclides.

The capacity of the deep-basin brines for reaction with the host rock is an important criterion in the evaluation of the geochemical stability of the basin. Given the age of the basin and the flow rates computed from hydrologic data, the brines would be expected to be in chemical equilibrium with the host rock (Bassett and Bentley, 1983). Preliminary evaluation of the saturation states of the brines reported in table 21 indicates that these brines are capable of dissolving halite and anhydrite. The reaction state of the brines with respect to silicate minerals cannot be evaluated at this time because of the lack of suitable thermodynamic data.

Dissolution of halite is the most reasonable source of the chlorinity and salinity of the deep-basin brines. For the most part, this dissolution probably occurred earlier in the flow history, nearer a recharge area to the west. Brines from the Mansfield well, however, appear to have derived much of their total dissolved solids content by downward movement through overlying evaporite units, as indicated by  $\delta^{18}\text{O}$  and  $\delta\text{D}$  compositions only slightly modified from meteoric values, high Na and Cl concentrations, and anomalously high Cl/Br ratios (table 21, and Bureau of Economic Geology, 1983a).

Brines that have simply dissolved halite should have Na/Cl ratios near the value of halite (0.65, by weight) if no other reactions have occurred and if all sodium and chloride were provided by halite. The Na/Cl ratios of brines from the Sawyer, Zeeck, and Mansfield wells range from 0.43 to 0.58 (table 21). The depletion of sodium relative to chloride may be attributed to ion exchange reactions and albitization of feldspar, although mineralogic data to test this hypothesis are not yet available. The departure of the Na/Cl ratio of Palo

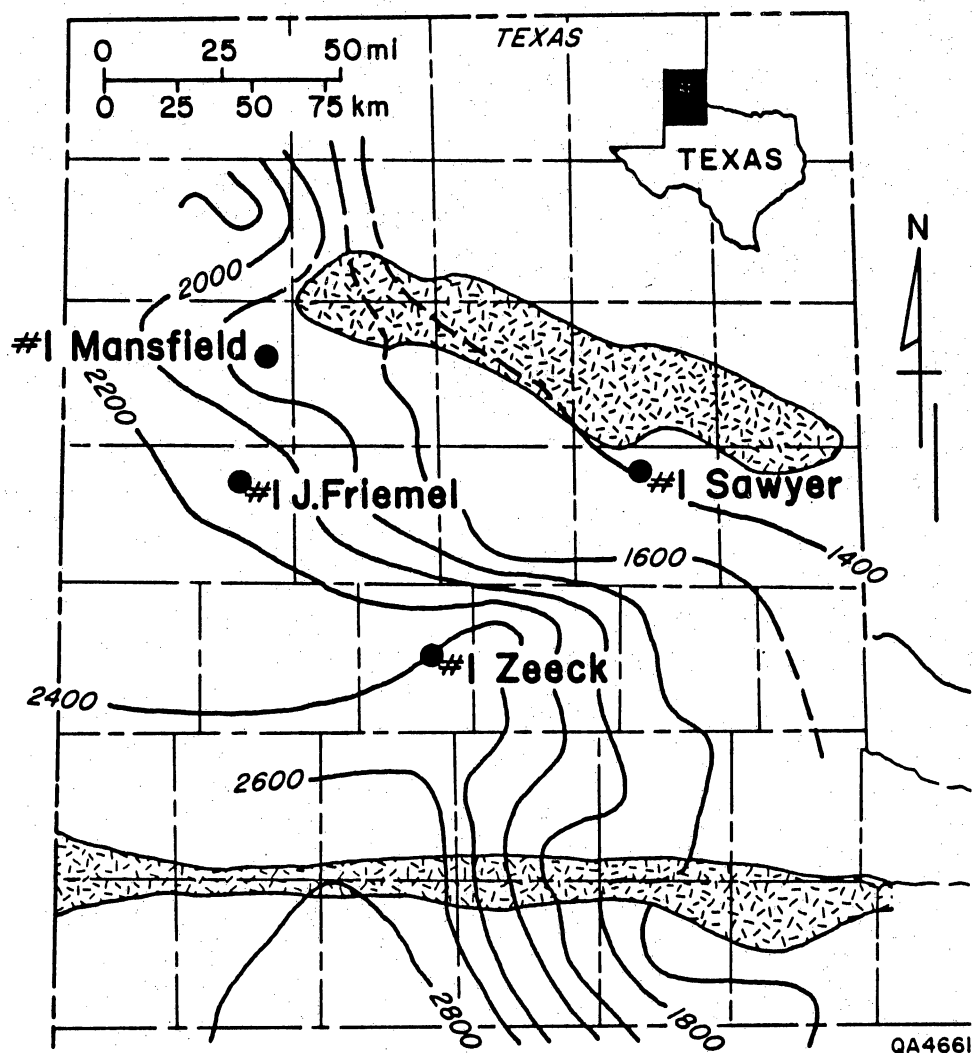
Duro brines from 0.65 is one indicator of the extent of reaction or modification of the fluid subsequent to halite dissolution.

Sodium/chloride ratios of Wolfcamp brines at the Zeeck site are greater than those at the Sawyer site, which could be interpreted as indicating that as fluids move along a flow path from Zeeck to Sawyer, sodium is progressively removed by any of several possible reactions. However, brines from the Wolfcamp at the Sawyer site are considerably less saline than Wolfcamp brine at the Zeeck site (table 21). To derive the Sawyer Wolfcamp brine from that at the Zeeck site, approximately 26,000 mg Na/L and 34,000 mg Cl/L must be removed from a brine already undersaturated with respect to halite. These changes are probably the result of cross-formational mixing of fluids rather than the product of reactions and processes within the Wolfcamp carbonate aquifer. Sub-Wolfcamp brines at the Sawyer site are more saline than the Zeeck Wolfcamp fluid; mixing these waters will not produce the Sawyer Wolfcamp brine. Preliminary data indicate that the San Andres fluid at the Sawyer site contains about 95,000 mg/L total dissolved solids (Dutton, 1985); cross-formational mixing of this brine with Wolfcamp fluid could produce the Wolfcamp brine observed.

At this time, the only hydrogeologic unit sampled in several locations is the Wolfcamp. Stratigraphic and geologic information indicate that the lithology of the unit is relatively homogeneous, and flow directions are generally well known (Bassett and Bentley, 1983; Bureau of Economic Geology, 1983b). Where two zones of the Wolfcamp can be sampled at the same site, the brine compositions are essentially identical (table 21, Wolfcamp zones at Mansfield and Zeeck sites). However, significant differences exist between the chemical and isotopic compositions of Wolfcamp fluids at the different sites; the nature of Wolfcamp brine at a given position in the basin cannot be predicted from analyses of Wolfcamp brines elsewhere in the basin, even for the relatively simple Na-Cl system. An important component of cross-formational flow is indicated for the Wolfcamp and must be considered probably for other hydrogeologic units as well.

Future work will include collection and analysis of brines from additional wells. These data, together with refined hydraulic-head and fluid-flow models, will allow a more detailed evaluation of compositional variations within specific units throughout the basin. Computer programs designed for evaluation of mineral-fluid reaction states of brines, and for simulation of mass transport will be used to provide a better understanding of the hydrogeochemical environment of deep-basin brines and aquifers.

# POTENTIOMETRIC SURFACE WOLFCAMP AQUIFER



## EXPLANATION

Equipotential contour of equivalent fresh water head :  
feet above sea level

General fluid flow path



Positive basement feature



D.O.E. well-cored through Wolfcamp

Figure 150. Potentiometric-surface map of the Wolfcampian carbonate aquifer, Texas Panhandle. This map includes changes incorporated into the potentiometric surface on the basis of data received prior to February 28, 1983.



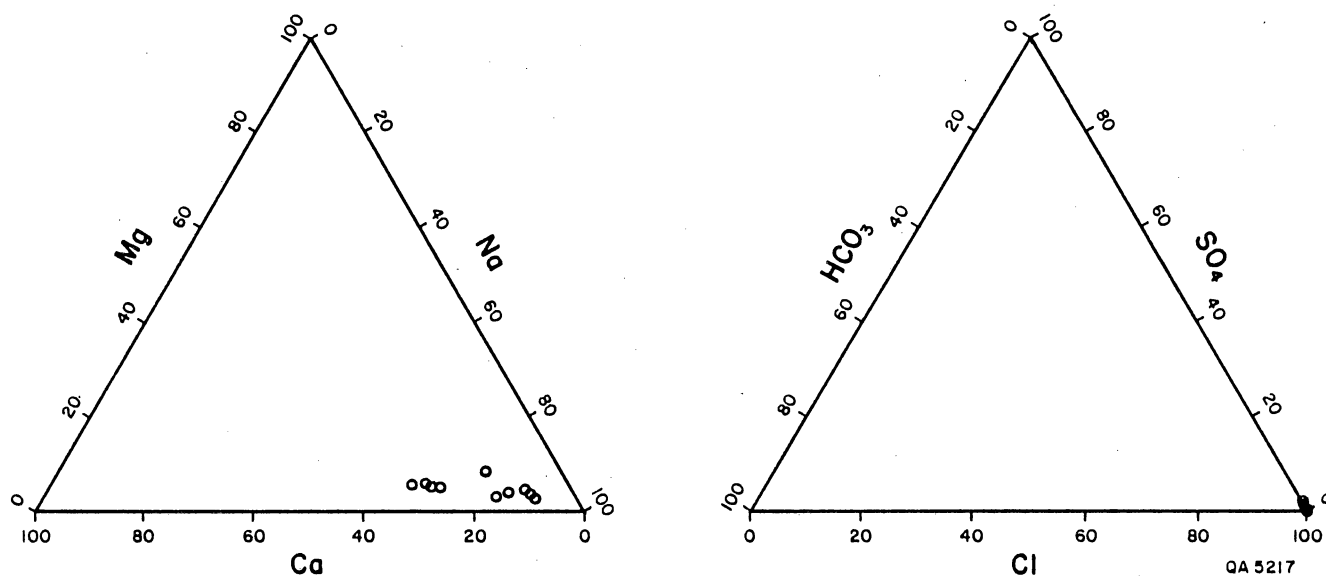
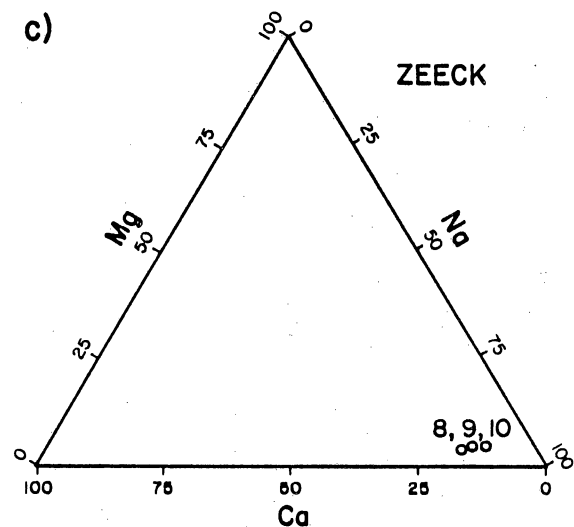
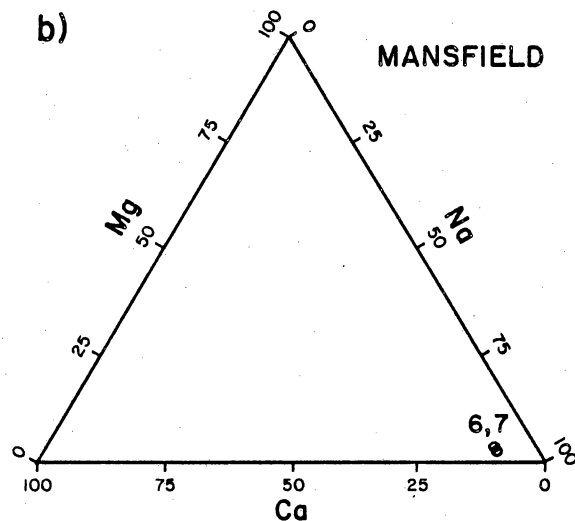
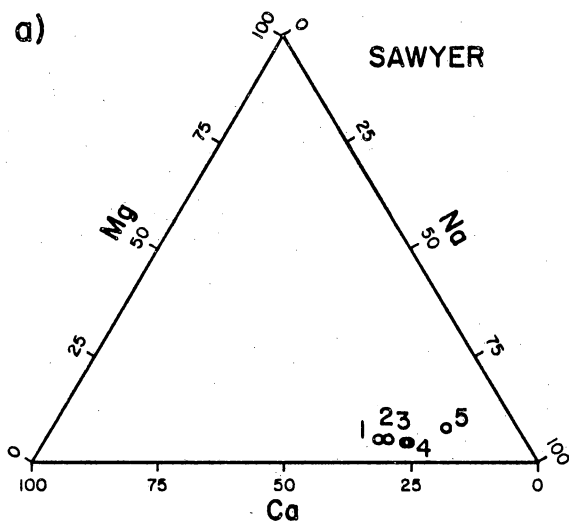


Figure 151. Summary Piper diagrams showing the cationic and anionic compositions of the 10 deep-basin brine samples collected from DOE test wells. The compositions of individual samples can be identified in figure 152.



1. Sawyer zone 1, Ellenburger
2. Sawyer zone 2, Upper Ellenburger
3. Sawyer zone 3, Mississippian carbonate
4. Sawyer zone 4, Pennsylvanian granite wash
5. Sawyer zone 5, Permian Wolfcamp
6. Mansfield zone 1, Permian Wolfcamp
7. Mansfield zone 2, Permian Wolfcamp
8. Zeeck zone 1, Pennsylvanian carbonate
9. Zeeck zone 2, Permian Wolfcamp
10. Zeeck zone 3, Permian Wolfcamp

QA 5218

Figure 152. Piper diagrams showing the cationic compositions of the 10 water samples analyzed from DOE hydrologic test wells. Triangle a contains values from the Sawyer No. 1 well. Triangle b contains values from the Stone and Webster Engineering Corporation Mansfield No. 1 well. Triangle c contains values from the Stone and Webster Engineering Corporation Zeeck No. 1 well.

Table 21. Chemical compositions of brine samples collected from DOE test wells. Analyses performed at the Mineral Studies Laboratory, UTBEG (except for isotope analyses, which were performed by Global Geochemistry Corporation). All but one sample were collected at the surface; the Zeeck zone 2 sample was collected downhole (concentrations in mg/L).

Well zone	Sawyer No. 1 1-Ellenburger	2-Upper Ellenburger	3-Mississippian Carbonate	4-Penn Granite Wash	5-Permian Wolfcamp
depth tested (ft)	4,716-4,746	4,604-4,640	4,500-4,535	4,258-4,342	3,172-3,189
downhole temp (°C)	39++ 5.35	39++ 7.5	39++ 5.4	39++ 4.4	35 6.1
pH (field)	-	-	+229	+244	+20
Eh (mv)	22,900	21,600	19,400	18,300	6,760
Ca	2,600	2,810	2,310	2,180	2,490
Mg	60,200	64,000	61,000	63,400	43,450
Na	459	420	337	332	118
K	139,000	133,000	132,000	136,000	86,300
Cl	169	230	237	336	2,010
SO <sub>4</sub>	560	40.2	106	26*	144
HCO <sub>3</sub> (field)	17	<0.2	5.8	9.6	10.4
SiO <sub>2</sub>	78	25	17	34	17
I	534	490	554	511	330
Br	3.2	2.4	1.0	.72	.05
Ba	190	23	29	41	6.4
Fe	3.6	2.6	2.6	2.4	9.63
Li	40	14	16	18	.239
Mn	660	710	574	563	113
Sr	2.6	4.0	.49	.29	.091
Zn	2.4	3.6	1.8	1.6	3.2
F	227,000	223,000	216,000	221,000	141,000
TDS	260	271	238	266	262
Cl/Br	.43	.48	.52	.47	.50
Na/Cl	-1.73	-.83	-.61	-1.19 & -.75	+.72
δ <sup>18</sup> O	-27	-13	-18.5	-15	-23
δD	+5.14	-2.25	+3.42	+.12 & -.06 & +.14	+1.83
δ <sup>13</sup> C (PDB)	-	-	+12.86	+13.77 & +13.63 & +13.95	+10.37
δ <sup>34</sup> S (CDT)					

\*lab value

++estimated from bottom-hole temperature

Table 21 (cont.)

Well zone	Mansfield No. 1		1-Pennsylvanian Carbonate	Zeeck No. 1	
	1-Permian Wolfcamp	2-Permian Wolfcamp		2-Permian Wolfcamp+	3-Permian Wolfcamp
depth tested (ft)	4,818-4,890	4,514-4,638	7,140-7,230	5,605-5,640	5,474-5,540
downhole temp (°C)	38	41	56	42	41
pH (field)	5.6	4.8	5.8	6.7*	6.25
Eh (mv)	-30	-153	+375	-	-
Ca	5,960	6,020	11,900	8,130	6,240
Mg	1,320	1,600	1,550	1,700	1,820
Na	78,400	76,100	76,350	66,100	69,300
K	369	380	197	318	339
Cl	138,000	131,000	151,500	118,000	120,000
SO <sub>4</sub>	1,220	1,320	81.1	866	1,650
HCO <sub>3</sub> (field)	131	161	30.9*	156*	45.6
SiO <sub>2</sub>	6.79	8.53	8.87	-	8.40
I	2.32	4.31	55.9	33.1	35.3
Br	107	118	805	546	512
Ba	.023	.126	4.1	1.54	.01
Fe	3.74	13.3	31.8	-	5.29
Li	6.87	11.6	4.18	-	7.58
Mn	.207	.310	.626	-	.083
Sr	99.5	89.9	1,380	271	110
Zn	.059	.380	.053	-	.40
F	2.6	2.6	.74	-	3.0
TDS	226,000	217,000	243,000	196,000	200,000
Cl/Br	1,290	1,110	188	216	234
Na/Cl	.57	.58	.50	.56	.58
δ <sup>18</sup> O	-5.78	-5.12	+5.73	+1.5**	+2.17
δD	-43	-42	-14	-16.5 & -15.6**	-23
δ <sup>13</sup> C (PDB)	+2.63	+1.83	+3.31	-	+2.76
δ <sup>34</sup> S (CDT)	+17.35	+16.6 & +16.51	+12.58	-	+13.3

\*lab value

\*\*analyses from the University of Arizona

+tracer level high, indicating contamination of sample by drilling fluid

## STRUCTURAL CONTROL OF PHYSIOGRAPHY, GEOMORPHIC PROCESSES, AND LITHOFACIES, TEXAS PANHANDLE

Thomas C. Gustavson and Roy T. Budnik

*The vertical juxtaposition of structure, lithofacies, dissolution, and physiographic features, ranging in age from Paleozoic to Plio-Pleistocene, suggests control by the same structural elements in the central western part of the Texas Panhandle.*

Basement faults in the Texas Panhandle primarily strike northwest; a secondary system strikes northeast (fig. 153). The structural axis or deepest part of the Palo Duro Basin strikes northwest through Castro County and Deaf Smith County. A secondary structural low associated with northeast-trending faults is in eastern Deaf Smith County and northwestern Randall County.

Patterns of Paleozoic lithofacies suggest that thickness and lateral extent were controlled by differential movement of fault blocks during deposition. Several units thicken over the structural low that trends northeast to southwest in Deaf Smith County, including Lower Pennsylvanian limestones (Dutton, 1980a), Wolfcampian carbonates (Handford, 1979), the Clear Fork Formation (Presley and McGillis, 1982), Glorieta Formation clastics (Presley and McGillis, 1982), San Andres Formation salts (Presley, 1981), and the Alibates Formation (McGillis and Presley, 1981) (fig. 154).

Fractures, interpreted from geophysical logs, have preferred northeasterly and northwesterly orientations in eastern Deaf Smith County (Gustavson and Budnik, 1985) (fig. 154). Examination of core from the same wells confirmed the presence of fractures throughout the stratigraphic column. Fractures were nearly vertical and may be mineralized.

Salt in the Seven Rivers Formation thins along the same trend that the Alibates Formation and other units thicken along, but is offset to the southeast (fig. 155). The Seven Rivers Formation has undergone extensive dissolution in eastern Deaf Smith County, according to Gustavson and Finley (1985) and McGookey and others (1985). The northeast-trending zone of thin salt in eastern Deaf Smith County may have resulted from accelerated dissolution owing to preferred ground-water flow along northeast-trending fractures.

A series of closed basins within a regional paleotopographic low is expressed on the mid-Tertiary erosion surface (fig. 156). The northeast-trending paleotopographic grain of this area parallels the basement structural grain and observed fracture trends (figs. 153 and 154). This suggests that Tertiary topography, developed on Dockum Group strata, was fracture controlled. The closed basins on the mid-Tertiary erosion surface contain sediments of the Miocene-Pliocene Ogallala Formation; all are thought to have formed as a result of dissolution and collapse during Ogallala sedimentation.

Tierra Blanca Creek and Frio Draw trend northeast through Deaf Smith and Randall Counties (fig. 157). These streams, and the wide topographic low that they occupy, overlie the mid-Tertiary paleotopographic low (fig. 156), the Seven Rivers salt thin (fig. 155), the Alibates Formation thick (fig. 154), and the basement structural low (fig. 153). Furthermore, Frio Draw and Tierra Blanca Creek parallel northeast fracture trends in Parmer, southeast Deaf Smith, and Randall Counties. These relations suggest that the topographic development of this area has also been structurally influenced.

Fine-grained sediments, interpreted to be lacustrine deposits, accumulated in a basin east of Hereford, Texas, during the late Pliocene (Norton, 1954) and in a basin at Canyon, Texas, during the late Pleistocene (Frye and Leonard, 1963; Schultz, personal communication, 1981). These basins, which overlie the zone of thin Seven Rivers salt, may have formed as a result of differential subsidence owing to dissolution of salt in much the same way that the closed basins are thought to have formed during Ogallala deposition.

Present-day regional topographic contours strike northeast through most of the study area. Contours are offset to the northwest approximately 30 km (20 mi) along the trend of thin salt (fig. 155), paleotopographic lows (fig. 156), and Frio Draw-Tierra Blanca Creek (fig. 157). The vertical juxtaposition of salts thinned by dissolution, Tertiary subsidence basins, and surface topographic lows along a northeast trend suggests that dissolution and subsidence contributed to the physiographic evolution of Randall and eastern Deaf Smith Counties during the late Pliocene and Pleistocene.

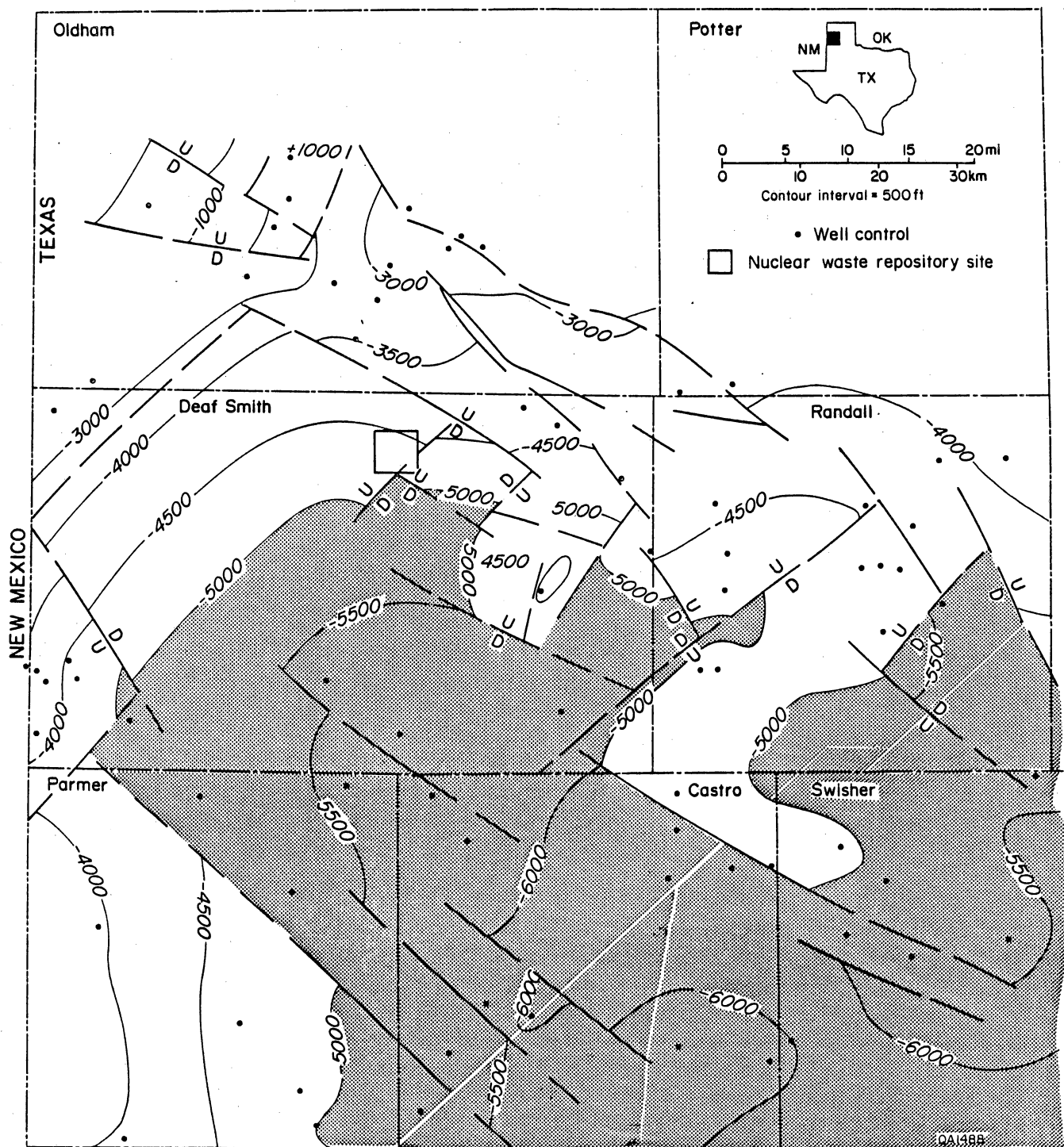


Figure 153. Basement structure map of the northern part of the Palo Duro Basin, Texas Panhandle. Most faults in the Texas Panhandle strike northwest; a secondary system strikes northeast. Basement structure in eastern Deaf Smith County is interpreted from both well logs and seismic-reflection data. Basement >5,000 ft below sea level is shaded.

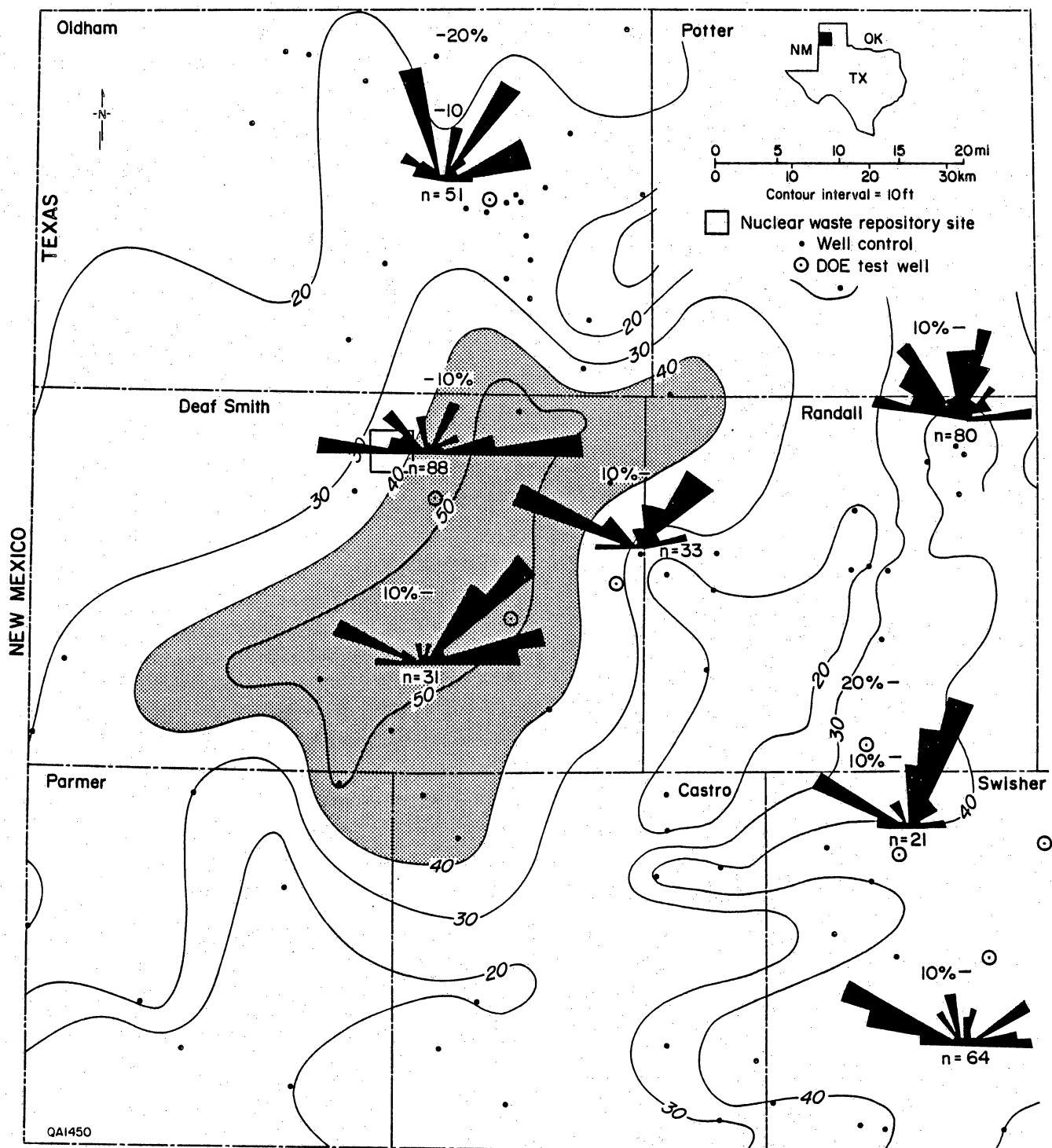


Figure 154. Isopach map of the Upper Permian Alibates Formation (McGillis and Presley, 1981). The Alibates Formation thickens over basement structural lows and thins over basement structural highs (compare figs. 153 and 154). Thickness >40 ft is shaded. In eastern Deaf Smith County preferred fracture orientations are northwest and northeast. Fractures are interpreted from Schlumberger, Inc., Fracture Identification Logs.



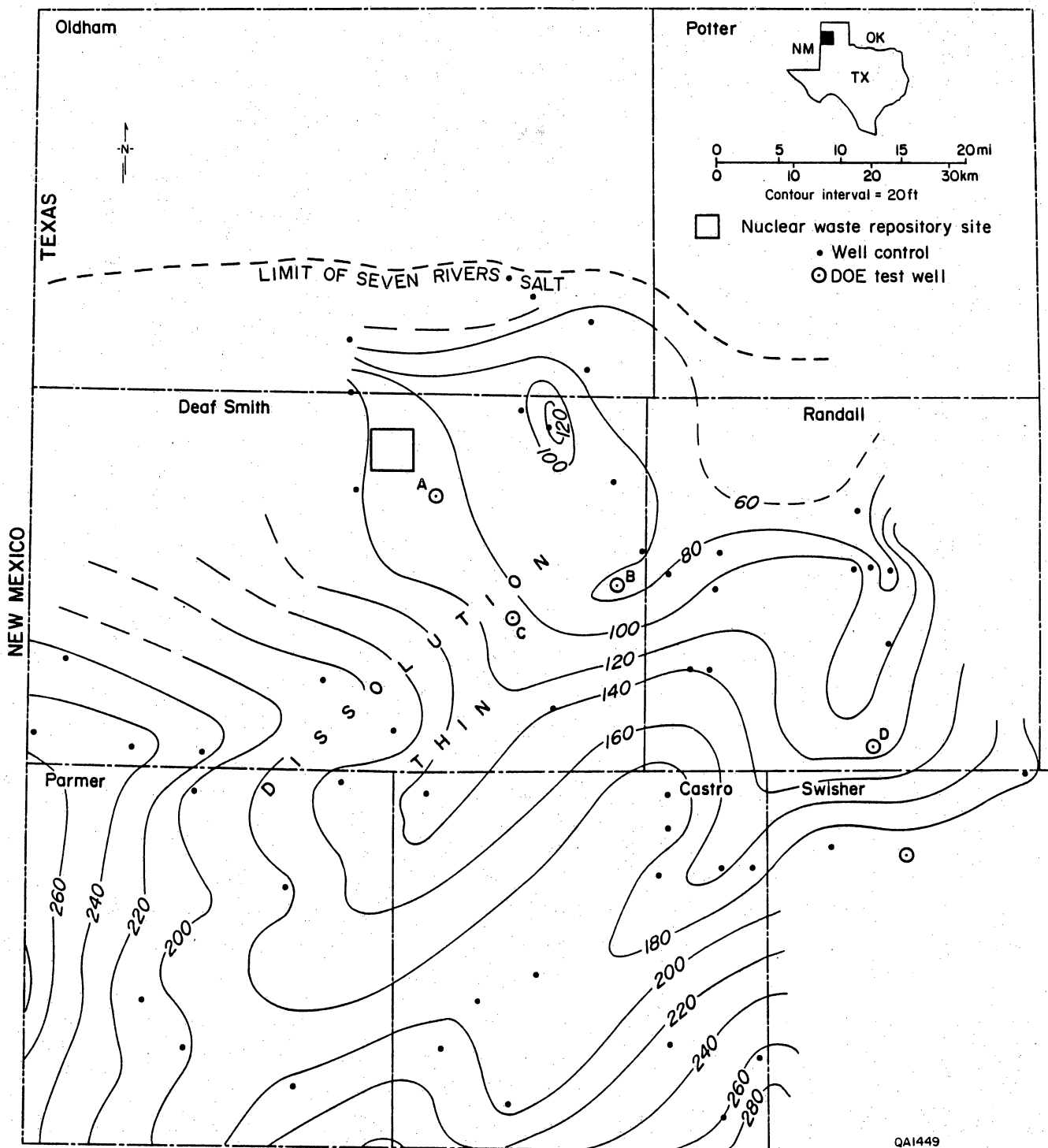


Figure 155. Net-salt map of the Upper Permian Seven Rivers Formation. The northeast trend of thinning of the uppermost salt in this part of the Palo Duro Basin parallels local northeast fracture trends and northeast-trending basement faults. Thinning in this case is attributed to salt dissolution. Collapse breccias and other evidence of dissolution were observed in cores from Stone and Webster Engineering Corporation J. Friemel No. 1 (A), G. Friemel No. 1 (B), Detten No. 1 (C), and Holtzclaw No. 1 (D).

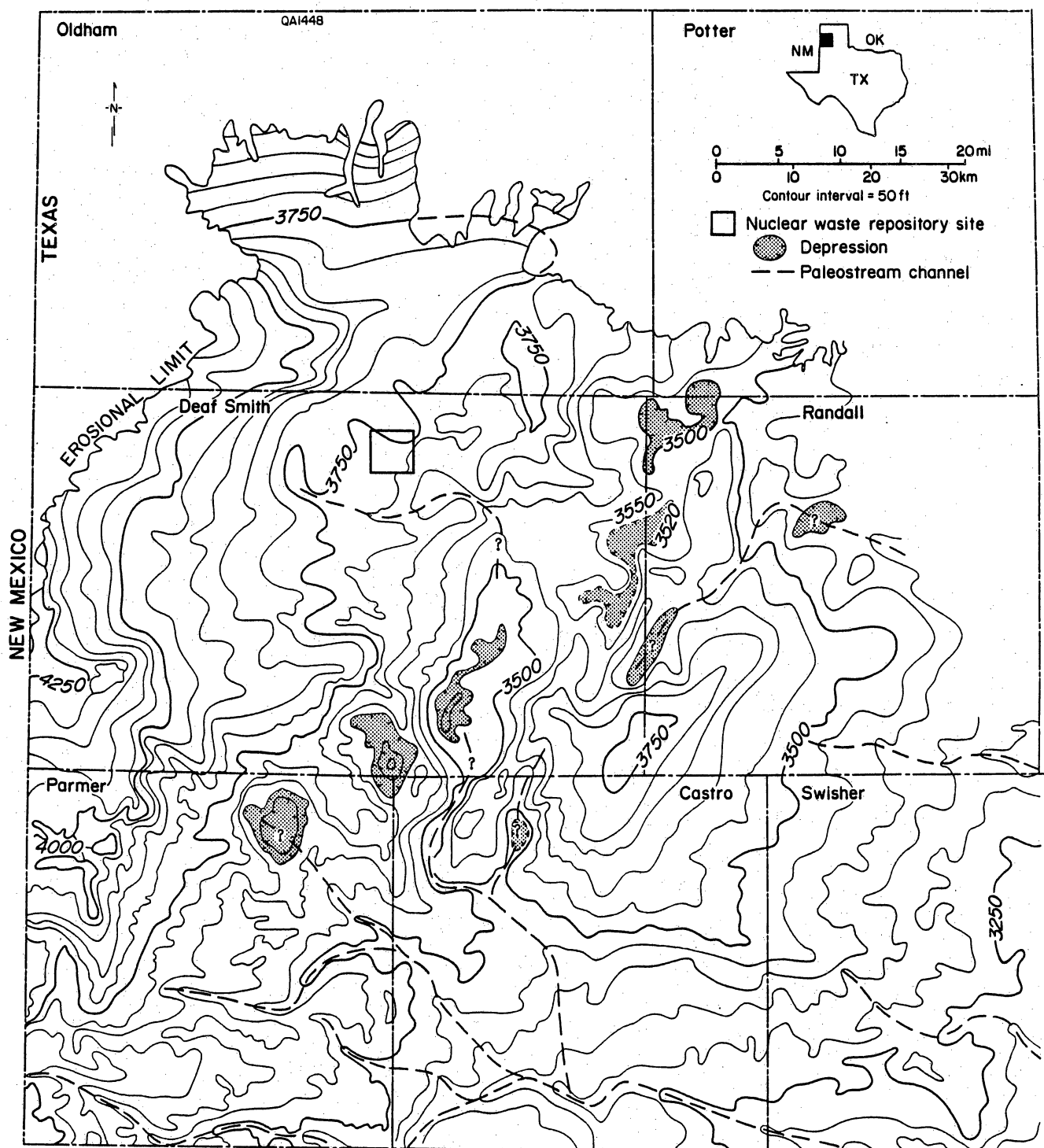


Figure 156. Structure-contour map on the base of the Ogallala Formation is essentially a paleotopographic map on the middle Tertiary erosional surface. A series of paleotopographic lows and closed depressions on the middle Tertiary erosional surface overlie the northeast structure and dissolution-collapse trends. Paleotopographic lows probably result from both stream erosion and collapse following dissolution (after Knowles and others, 1982).

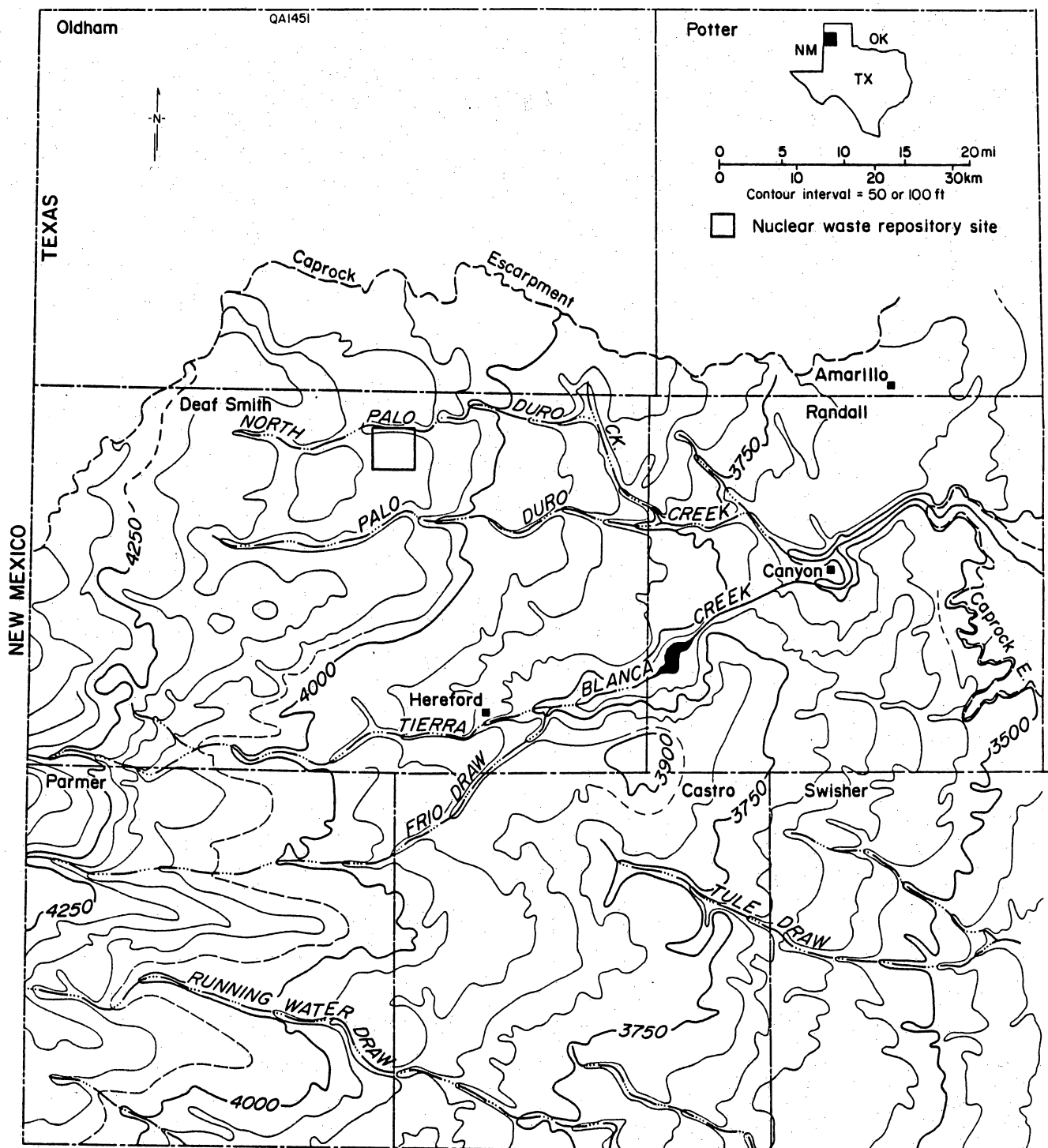


Figure 157. Present-day topographic map of a part of the Southern High Plains of the Texas Panhandle. Regional topographic slope on the Southern High Plains is to the southeast at approximately 2 m/km (10.6 ft/mi). Streams drain to the southeast with the exception of Tierra Blanca Creek, Palo Duro Creek, and their tributaries, which drain to the east and northeast.

## STRATIGRAPHY OF AN EXTENSIVE QUATERNARY SEDIMENTARY SEQUENCE-- BRISCOE, FLOYD, HALL, AND MOTLEY COUNTIES, TEXAS

S. Christopher Caran and Robert W. Baumgardner, Jr.

*Quaternary deposits as much as 250 ft (76 m) thick cover an area of more than 3,000 mi<sup>2</sup> (7,800 km<sup>2</sup>) on the western Rolling Plains of Texas. The genetic stratigraphy of this sedimentary sequence is complex, reflecting paleoclimatic and paleoenvironmental changes throughout the late Pleistocene and Holocene Epochs. Deposition also appears to have been structurally controlled in part, and the deposits are faulted and downwarped locally.*

A thick wedge of late Pleistocene and Holocene sediment borders the Eastern Caprock Escarpment for approximately 150 mi (240 km) (fig. 158). These deposits extend eastward from the escarpment for 20 to 30 mi (32 to 50 km) across the western Rolling Plains. They overlie an irregular erosional unconformity on Triassic and Upper Permian (Ochoan and Guadalupian) strata. Intensive investigations (more than 400 field sites and well logs examined) in four counties and reconnaissance surveys in an additional six counties (fig. 158) provide evidence applicable to the stratigraphic interpretation of these deposits. Figure 159 illustrates a representative section through the Quaternary strata at a water well and nearby outcrop in southeastern Briscoe County (fig. 158, site 1). Deposits here are 178 ft (54.3 m) thick and include all major genetic components of the regional Quaternary sequence. Thicknesses of these components vary across the area, as shown in figure 160, but their aggregate thickness exceeds 250 ft (76 m) locally (Texas Department of Water Resources, Austin, unpublished water-well logs).

The Quaternary sequence consists of three principal genetic components. The basal component (unit 7 of the well log, fig. 159) is an upward-fining fluvial deposit. In the representative section (fig. 159) this component is 55 ft (16.8 m) thick, but thicknesses approach 100 ft (30 m) elsewhere (fig. 160). Where comparable deposits crop out they are characterized by large-scale crossbedding and imbrication. There is little evidence of pedogenic alteration of these strata. Unit 7 is a very poorly sorted sandy gravel and gravelly sand varying from coarse sand to pebbles, cobbles, and rare boulders. Much of this material consists of reworked lithoclastic sediment shed off the Eastern Caprock

Escarpment. Lithoclasts of caliche derived from the Miocene/Pliocene Ogallala Formation are particularly abundant. The character of this sediment and its provenance along the escarpment are indicative of deposition within alluvial fans that coalesced to form a bajada. Eventually, individual drainage systems became differentiated so that the bajada sequence was overlain by a series of deposits of broad, braided streams or alluvial plains. Gravels and sands of the alluvial fans lie unconformably on the Permian and Triassic subcrop across most of the region.

At a few sites, but not in the section at the water well of figure 159, the basal component is underlain by a thin (less than 35 ft [10 m]), discontinuous bed of silty clay or sandy silt (fig. 160). These argillaceous sediments probably were derived essentially in place from the weathering of Permian bedrock (generally a siltstone, shale, or fine sandstone). Loading caused local deformation of this Quaternary regolith, producing an enfolded, invasive flame structure in at least one locality. At most sites this stratum, if originally present, was stripped during or prior to emplacement of the alluvial-fan sequence.

Overlying the coarse basal sand and gravel at many sites are lacustrine deposits (unit 6 of the well log, fig. 159) consisting of calcareous, well-sorted, silty or fine sandy clay. In the water well, strata representing this component are 9 ft (2.7 m) thick, but correlative deposits exceed thicknesses of 40 ft (12 m) elsewhere (fig. 160). The planar bedded clay is organic-rich (sapropelic) locally and almost everywhere fossiliferous, containing abundant, mostly complete, well-preserved remains of pelecypods, gastropods, and ostracodes. Horizontal laminae are disrupted by burrows and traces of roots. Where similar lacustrine deposits are exposed, the individual strata can be traced for tens of feet (several meters), but the beds or lenses composing these laminae are laterally discontinuous and generally bounded by silty sands. However, lacustrine deposits dominate the middle part of the Quaternary section throughout the study area and appear to reflect the availability of abundant moisture at a time when the influx of coarse sediment was

reduced. The cause of this diminished clastic sedimentation may be related to reduced erosion along the Caprock Escarpment or entrapment of the coarse detritus farther west. At many localities structural deformation occurred prior to, during, and soon after deposition of the lacustrine deposits (Baumgardner and Caran, this report). Subsidence may have isolated some areas from through-going drainage, thereby preventing deposition of coarse clastic material.

The upper part of the Quaternary sequence, above the principal lacustrine deposits, is a complex of fluvial and eolian sediment interrupted by pedogenic horizons (units 1 through 5 of the well log, and the entire measured section, fig. 159). In the representative section at the water well these deposits probably are 114 ft (34.8 m) thick, although the uppermost 25 ft (7.6 m) of sediment were not sampled when the well was drilled (fig. 159). Strata presumed to be comparable to those of the missing, near-surface interval are exposed 1 mi (1.6 km) west-southwest of the well. The section measured at this exposure can be extrapolated to the well site to complete the representative section (fig. 159).

Sediment composing the upper component is calcareous, moderately well to very poorly sorted, gravelly and silty sand and sandy clayey silt. Eolian winnowing probably concentrated the coarse fraction of some beds, whereas illuviation increased the argillic content of others. Still other beds are calcic soil horizons or zones of phreatic diagenesis. The unit as a whole consists of stacked sets or cycles of upward-fining strata indicative of waning channel-flow, overbank deposition, and eolian redistribution of sediment. These cycles were supplanted vertically by eolian deposits over much of the area. Within the section are several thick paleosols with well-developed pedogenic profiles. These soils were produced during extended periods of slow accretion of fine sediment, only occasionally punctuated by an influx of colluvium or overbank deposits. Locally thin limnic deposits are found as well (fig. 159, inset). The climate had become drier and warmer after accumulation of the principal lacustrine deposits of the middle part of the sequence.

Drainage was confined to increasingly stable channels, culminating in the modern drainage network.

The stratigraphic sequence summarized in figures 159 and 160 is consistent with sections measured throughout the study area, although some sections are incomplete owing to erosion, or attenuated over local prominences on the irregular subcrop. The sequence appears to have accumulated very rapidly. The upper and middle components have been dated by radiocarbon analysis (samples from 18 localities throughout the region: Caran and Baumgardner, 1985), but the age of the basal component appears to exceed the range of finite radiocarbon dating. Both the finite and infinite dates are internally consistent, although there are gaps in the record for which no absolute chronology has yet been established. Oldest dates are from the site where Dalquest (1964) described a rich, vertebrate fauna (Quitaque Local Fauna) near Quitaque Creek in northwestern Motley County (fig. 158, site 2). The fossils lie within the upper part of a basal gravel immediately beneath lacustrine deposits. Shells of fresh-water mussels associated with the vertebrate remains were dated radiometrically, providing a  $^{14}\text{C}$ -age of  $31,400 \pm 3,200$  to 5,600 yr (Dalquest, 1964, p. 505). The use of molluscan shells for radiocarbon dating has been shown to be problematic because mollusks can incorporate older carbon from carbonate minerals or aqueous solution, or younger carbon can be introduced after burial (Keith and Anderson, 1963). In the current study organic humates from the base of the lacustrine deposits at this site were dated and found to be greater than 38,000 yr old (Caran and Baumgardner, 1985, table 1). The oldest finite date is from higher in a correlative lacustrine section nearby; that date is  $23,255 \pm 2,335$  yr b.p. (Caran and Baumgardner, 1985, table 1). Correlation of lacustrine or other deposits at widely separated localities does not necessarily imply synchrony. However, dates obtained from samples collected at most exposures of the upper and middle components generally agree and are consistent with those reported by Johnson and others (1982) and Caran and Neck (this report) from the Lake Theo archeological site, southeastern Briscoe County (fig. 158, site 3), where Folsom and

Plainview artifacts have been discovered in association with the remains of extinct Bison antiquus. This agreement indicates the composite Quaternary section, as summarized in figure 160, is representative of these deposits throughout the western Rolling Plains. The regional stratigraphy appears to be tied to paleoclimatic and paleoenvironmental changes for which there is a reasonably good chronology (Caran and McGookey, 1983).

Quaternary deposits on the Rolling Plains form one of the most extensive, late Quaternary sequences of nonglacial, continental sedimentation in the central United States. Investigation of this sequence will provide important data concerning the paleoclimatology and geomorphic history of the entire region. Deformation of these deposits and possible structural enhancement of deposition (Baumgardner and Caran, this report) signal the existence of actively subsiding karstic basins with regional distribution. Subsidence at a rate sufficient to produce marked, local thickening of the alluvium has forced adjustment of local base level and probably increased rates of incision. Because the deposits clearly postdate the local retreat of the Caprock Escarpment, their age may be a key to understanding the rate of escarpment recession under the varied climatic conditions of the late Quaternary Period.



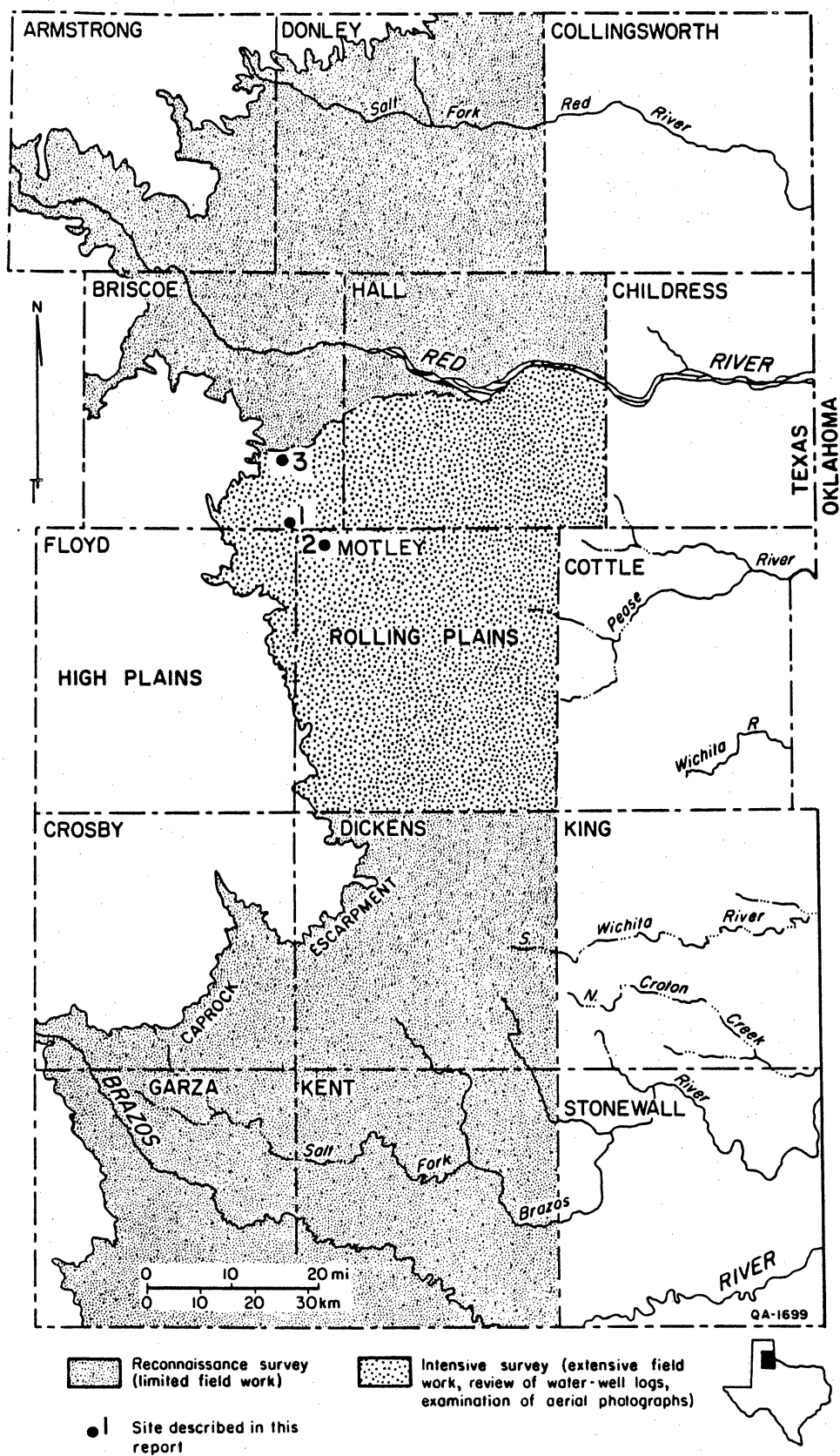
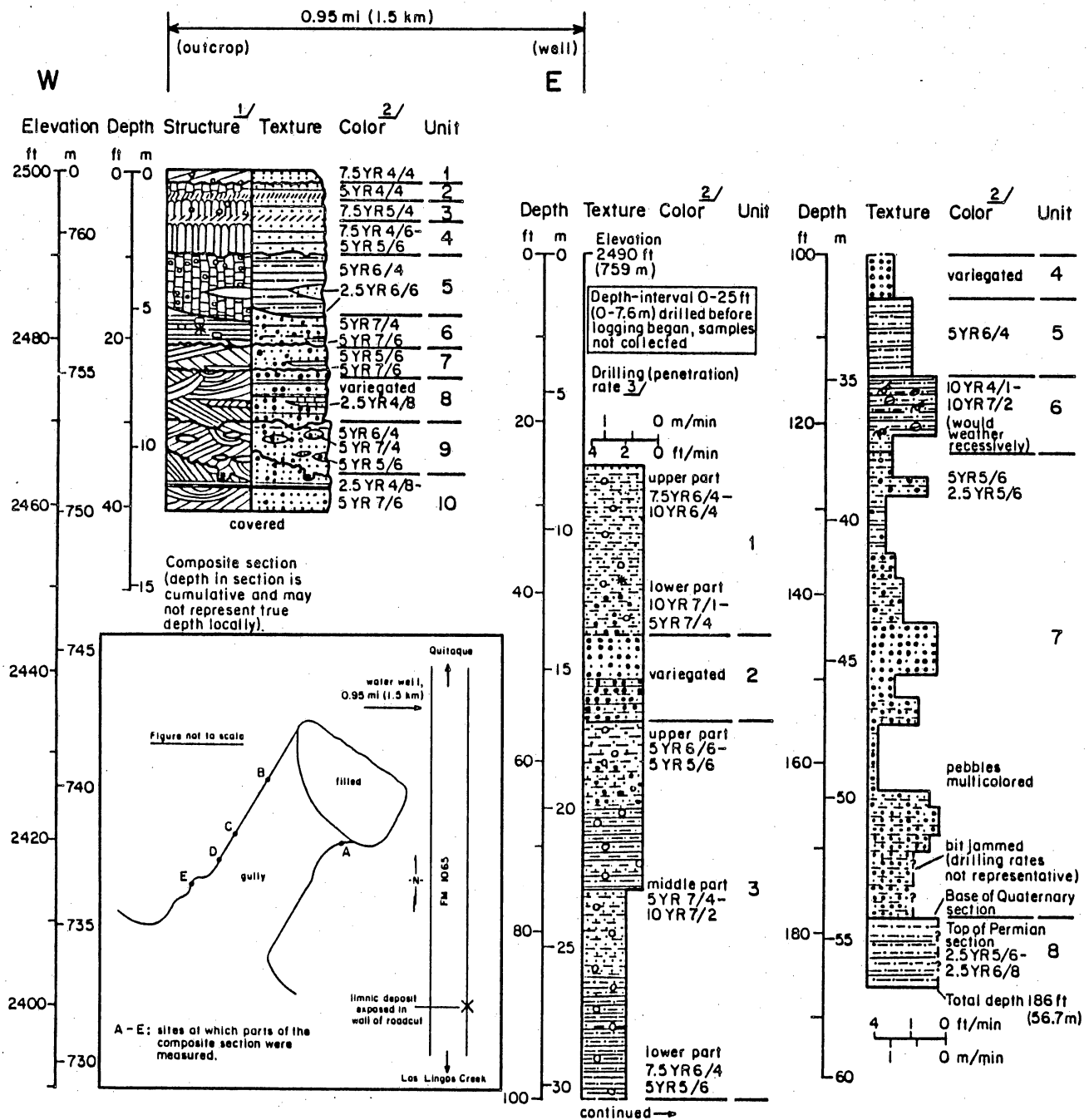


Figure 158. Area of investigation, western Rolling Plains of Texas. Localities discussed in this report are noted.



- <sup>1/</sup> Sedimentary, compactional, and pedogenic structures and fossils.
- <sup>2/</sup> Munsell color, determined on fresh, dry surface.
- <sup>3/</sup> In general, drilling rate is inversely related to hardness of rock. Graph of changes in drilling rate with depth is comparable to weathering profile, except where noted.

QA4452

Figure 159a. Representative sections through late Quaternary deposits of the western Rolling Plains. The outcrop is 4 mi (6.4 km) south of Quitaque, Briscoe County, Texas, immediately west of State Highway 1065. The water well is 1 mi (1.6 km) east-southeast of this location.

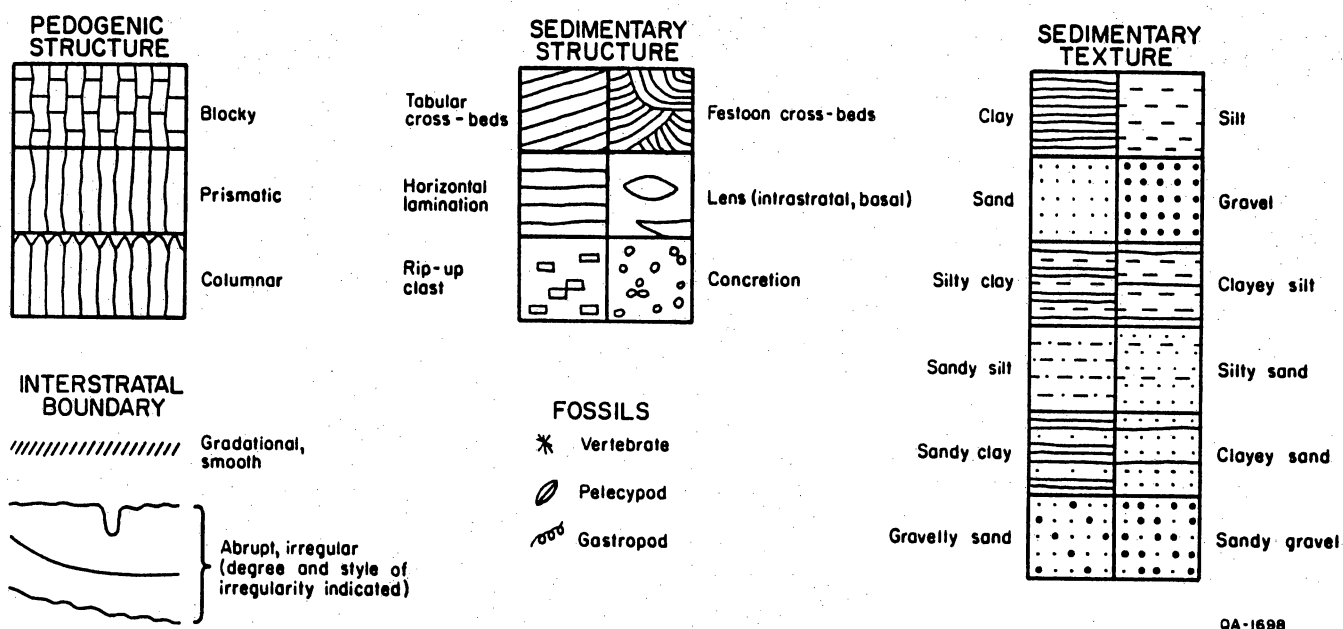


Figure 159b. Explanation of symbols used in the figure illustrating these sections. [Note: The sections were described and sampled by the authors. Selected samples have been placed in storage at the Bureau of Economic Geology, Austin, Texas.]

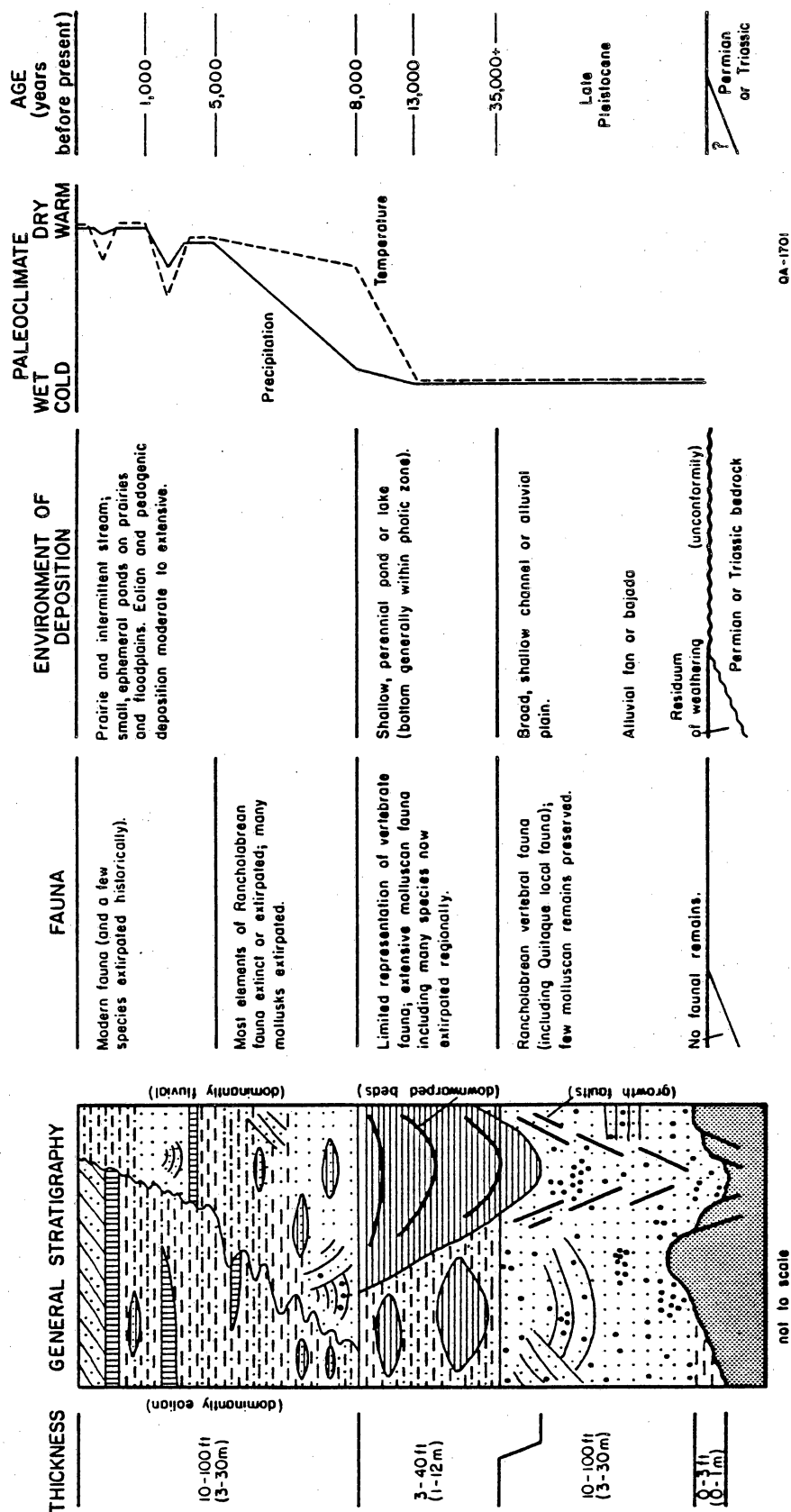


Figure 160. Generalized composite section and paleoenvironmental interpretation of late Quaternary deposits, western Rolling Plains. Explanation of symbols in figure 159. Principal genetic units are labeled.

## QUATERNARY FAULTING IN SOUTHEASTERN BRISCOE COUNTY, TEXAS

Robert W. Baumgardner, Jr., and S. Christopher Caran

*Downwarped and penecontemporaneously faulted beds of late Quaternary terrigenous sediment are well exposed in southeastern Briscoe County, Texas. Deformation was probably caused by subsidence of the Permian subcrop owing to dissolution of bedded salt at depth. Fluvial sands and gravels and lacustrine clays fill a subsidence basin, producing a locally thickened Quaternary section. A well-developed paleosol above lacustrine deposits was tilted and laterally truncated prior to modern eolian deposition at the site.*

Active, recently active, and inactive subsidence features are common in the western Rolling Plains of Texas. Most of these features are small, karstic sinkholes up to 330 ft (100 m) in diameter and subsidence basins a few miles long. Gustavson and others (1982) investigated more than 400 of these features (dolines) in Hall and Briscoe Counties, Texas. These structures formed and are forming as a result of dissolution of Upper Permian (Ochoan and Guadalupian) evaporites, particularly halite, at depths of 650 to 1,000 ft (200 to 300 m) (Gustavson and others, 1982; McGookey and others, 1985).

A similar pattern of karstic subsidence produced features of comparable size throughout late Pleistocene and Holocene time. During this interval, subsidence may have been more widespread than it is today because of the wetter climate and presumably greater rates of infiltration and transmissibility of ground water in the late Pleistocene (Caran and McGookey, 1983). The moist climate of the late Pleistocene converted sinkholes and subsidence basins to pluvial ponds and lakes, the largest of which probably also received phreatic discharge. Limnic and lacustrine deposits occupy a stratigraphically consistent position in the Quaternary section of the western Rolling Plains. At one site these deposits are more than 30 ft (9.1 m) thick and show evidence of structurally enhanced deposition.

This site, a steep-walled gully 47 ft (14.4 m) deep in southeastern Briscoe County (fig. 161), provides excellent exposure of structurally deformed lacustrine deposits. The laterally continuous beds of laminated, calcareous clay are moderately sapropelic and contain abundant unworn shells of aquatic and riparian mollusks. These sediments were

deposited in the low-energy environment of a shallow lake. The beds and individual laminae originally were horizontal, but those on the southern flank now dip 11 to 16 degrees to the northwest with a strike of N55°E (fig. 162). Beds of lacustrine sediment elsewhere at the site also dip toward the center of the basin but at a lesser angle. An overlying bed, probably a paleosol, also dips into the basin but much less steeply. In addition, lacustrine beds low in the exposed section contain numerous small penecontemporaneous faults and clay-filled fractures.

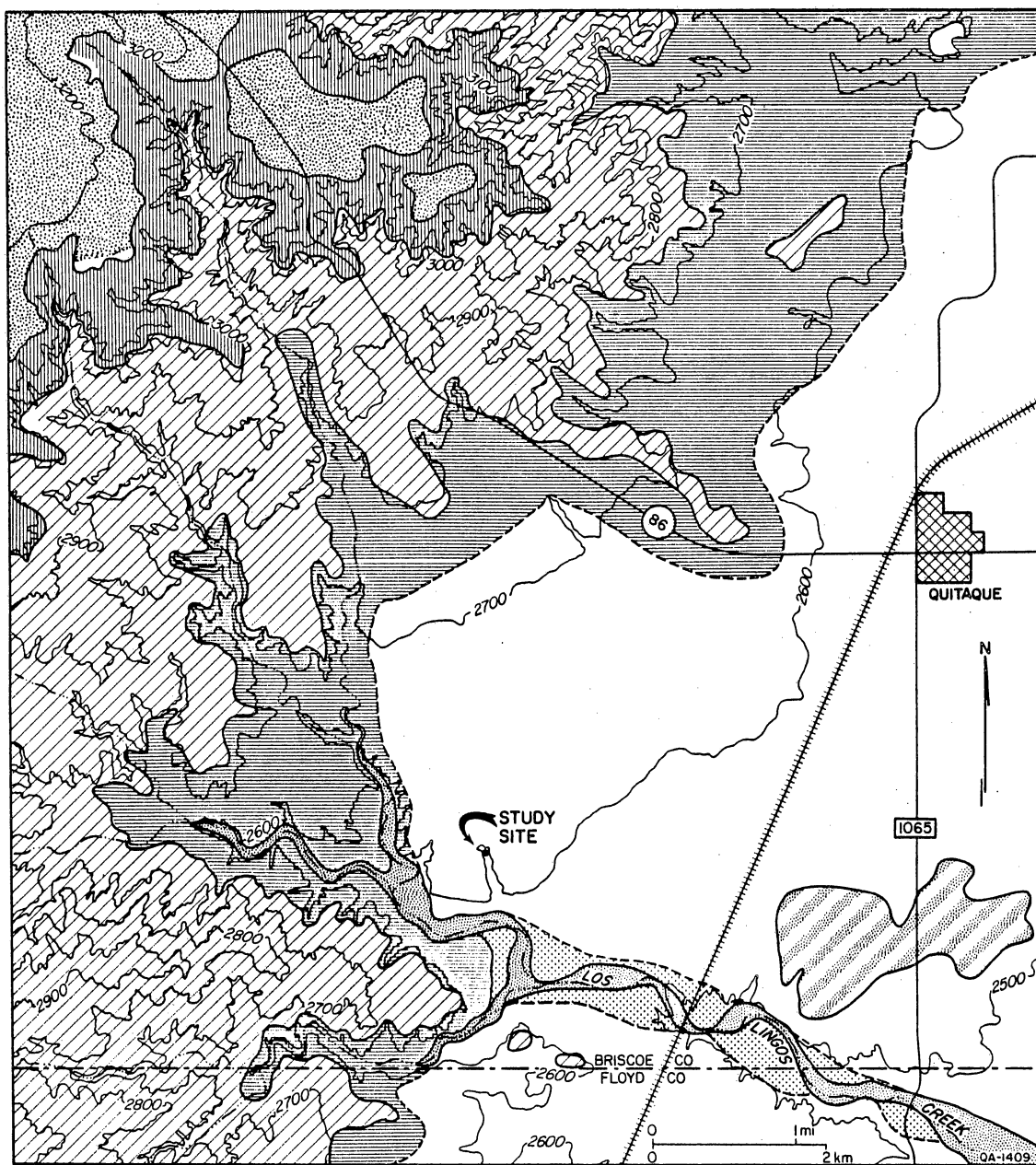
South of and stratigraphically below the tilted lacustrine sediments are crossbedded fluvial sands and gravels exposed in the walls of the gully. Joints and normal faults are common in these sediments in a zone about 66 ft (20 m) wide. Total vertical offset across this zone of deformation is several meters. The normal faults have two principal trends, N90°E, 66°N, and N65°E, 62°SE. These and other antithetic sets form small grabens. Some beds in downthrown blocks thicken markedly across faults, whereas others simply are offset. Vertical displacement measured along one fault plane is 3.9 inches (10 cm) (fig. 163). The amount of displacement decreases to zero about 6.6 ft (2 m) higher in the section at this location, indicating that movement along part of the fault was penecontemporaneous with deposition of the sediments.

The fault shown in figure 163 created fracture porosity, thereby allowing preferential movement of solute-rich ground water. Adjacent to the fault plane, beds below the conspicuous layer of gravel are more highly cemented, whereas beds above the gravel are more thoroughly stained with iron oxides than are strata farther from the fault.

The combination of (1) laminated lacustrine sediments dipping at a relatively steep angle, capped with (2) a nearly conformable but less steeply dipping paleosol, and (3) underlying beds of penecontemporaneously faulted sand and gravel indicates that structural disturbance and subsidence occurred before, during, and after formation and infilling of the lake. The location of this site is several miles closer to the Caprock Escarpment (fig. 161) than are the dolines studied by Gustavson and others (1982) but is

still within the zone of salt dissolution along the margin of the Southern High Plains (Gustavson and others, 1981c).

This example illustrates that recent structural deformation near the Caprock Escarpment has faulted Quaternary sediments and altered the near-surface ground-water regime in those sediments. Under slightly different circumstances, this type of structural disturbance could lower local base levels and enhance or initiate incision. Subsidence and faulting also provide permeable pathways for infiltrating ground water. Over an extended period these processes could be expected to affect the rate of retreat of the Caprock Escarpment. Investigation of the thick sequence of Quaternary sediments along the flank of the escarpment may provide a realistic assessment of the rates at which these processes have occurred under varying conditions of climate. The rate of escarpment retreat toward the interior of the Southern High Plains is an important factor to consider when examining potential sites there for a high-level nuclear waste repository.



(after Barnes and Eifler, 1968)

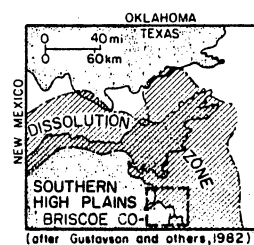
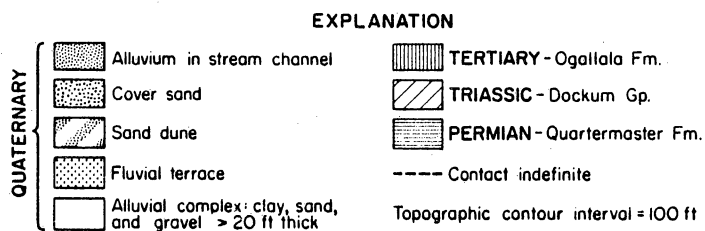


Figure 161. Location of tilted lacustrine deposits and faulted sand and gravel deposits in southeastern Briscoe County, Texas. Distance from structurally disturbed sediments to the foot of the Caprock Escarpment varies from 1.3 to 2.9 mi (2.1 to 4.6 km).





Figure 162. Tilted Quaternary sediments. Lower contact of calcareous gray clay (arrow) dips  $11^{\circ}$  to  $16^{\circ}$  NW, with a strike of  $N55^{\circ}E$ . North is to the left. For location of this site, see figure 161.



Figure 163. Fault in Quaternary sediments. Downthrown to the left, vertical displacement is 3.9 inches (10 cm). Scour along fault plane at base of gravel layer suggests movement preceded deposition of gravel. Antithetic faults in sand above gravel layer in downthrown block indicate that the fault has been active since deposition of sand. Fault orientation is  $N90^{\circ}E, 66^{\circ}N$ . Scale bar is numbered in 3.9-inch (10-cm) increments.

## LONG-TERM RATES OF DENUDATION BASED ON HYPSONETRIC ANALYSIS OF DRAINAGE BASINS AND UNDERLYING SALT BEDS, TEXAS PANHANDLE

Robert W. Baumgardner, Jr.

*Hypsometric analysis of representative drainage basins indicates that even when effects of salt dissolution are removed from long-term estimates of denudation, present rates of denudation are considerably higher than estimated rates for periods longer than 100,000 yr.*

Because the purpose of the study was to determine the effect of geomorphic processes on a potential nuclear repository site in the Southern High Plains, five basins each having headwaters along the margin of the Southern High Plains were chosen for study. Future headward development of the basins would reduce the distance between the actively eroding edge of the plains and the potential repository site, thereby posing a potential threat to repository integrity that should be described and understood.

The hypsometric integral of a drainage basin is the percentage of rock volume remaining within the drainage divides between the highest and lowest elevations in the basin (Strahler, 1952). The method used in this study to determine hypsometric integral was described by Haan and Johnson (1966). The original volume of material within five drainage basin areas (fig. 164) was estimated by projecting the present-day surface of the Southern High Plains across the basins using the current slope and direction (10 ft/mi; S45E) and calculating the hypsometric integral for that synthetic topographic surface. Because the present surface of the Southern High Plains probably has been lowered by denudation since basin formation began, this method gives a conservative estimate of original basin volume. The volume of material in each basin was calculated as follows:

$$V_b = A_b \times H_b \times HI$$

where  $V_b$  = basin volume in  $\text{mi}^3$

$A_b$  = basin area in  $\text{mi}^2$

$H_b$  = basin relief in mi

HI = hypsometric integral

When the hypsometric integral for the pre-erosion surface is used, the original basin volume is derived. This is the amount of material originally in place above the elevation of the present-day basin mouth and within the present-day drainage divides. When the present-day hypsometric integral is used, the present basin volume is derived. This is the amount of material still in place after basin development to the present condition. The difference between these two volumes is the amount of material removed since erosion of the High Plains surface and retreat of the Caprock Escarpment began within the present drainage divides of each basin (table 22). Dividing the volume of material removed by basin area yields the average amount of surface lowering in the basin.

Long-term estimates of denudation were obtained by separating surface lowering caused by erosion from surface lowering caused by evaporite dissolution and subsidence. Thickness of dissolved salt was derived by dividing volume of dissolved salt by basin area. Volume of dissolved salt was computed by hypsometric analysis of isopach maps of salt-bearing formations that underlie each basin or of isopach maps of total dissolved salt (table 23). The average thickness of salt dissolved below each basin was subtracted from the average decrease in elevation in the basin. Then, the average surface lowering caused by erosion was divided by the estimated age of the basin. Basin age was calculated for three basins by dividing the length of the basin by the estimated rate of retreat of the Caprock Escarpment and the Ogallala Formation, which forms the headwaters of those three basins (Gustavson and Finley, 1985; Gustavson and others, 1981b).

Two assumptions affect the numbers in table 23: (1) that salt dissolution below the drainage basins occurred after the Caprock Escarpment began to retreat and (2) that collapse of the rocks overlying the salt did not significantly change their volume. Recent studies show that the dissolution zones are concentric to the Caprock Escarpment around the Southern High Plains (Gustavson and others, 1981b). Furthermore, only the two uppermost salt-bearing formations--Salado and Seven Rivers--have dissolution fronts beneath the High Plains surface where there is a prominent escarpment. These data

suggest that the positions of the dissolution fronts are synergistically related to the position of the Caprock Escarpment. Dissolution of salt near the escarpment may enhance scarp retreat by increasing local stream and topographic gradients, leading to increased sediment removal. At the same time, scarp retreat may enhance salt dissolution by removing overburden that separates the salt from shallow ground water.

With regard to the second assumption, that collapse of rocks did not change their volume, it is likely that brecciation during collapse increased the volume occupied by the rocks overlying the salt beds. However, data are not available from these basins to make consistent estimations of the amount of volume change. Therefore, the amount of surface lowering due to salt dissolution and subsidence is assumed to be equal to the average thickness of dissolved salt. As a result, the amount of surface lowering due to erosion (denudation) is conservatively estimated in all basins.

Average rates of denudation derived by the method described here range from a low of 4.1 inches/1,000 yr (10.4 cm/1,000 yr) to a high of 20.6 inches/1,000 yr (52.3 cm/1,000 yr) (table 23). These rates are somewhat higher than Schumm's (1963) estimated denudation rates of 2.4 to 8.8 inches/1,000 yr (6 to 22 cm/1,000 yr) for basins of 31 mi<sup>2</sup> (80 km<sup>2</sup>) area and rates of 1.2 to 4.0 inches/1,000 yr (3 to 10 cm/1,000 yr) for basins of 1,500 mi<sup>2</sup> (3,900 km<sup>2</sup>) area. On the other hand, these rates are lower than values of denudation for the Rolling Plains of Texas based on reservoir sedimentation rates, sheet erosion rates, and suspended sediment analyses, which range from 4 inches/1,000 yr (10 cm/1,000 yr) to 118 inches/1,000 yr (297 cm/1,000 yr) (Gustavson and others, 1981a). The latter comparison indicates that present rates of denudation are considerably higher than longer term rates based on estimates for time periods longer than 100,000 yr. These higher, present-day rates may be the result of present climatic conditions or land use practices, or both.

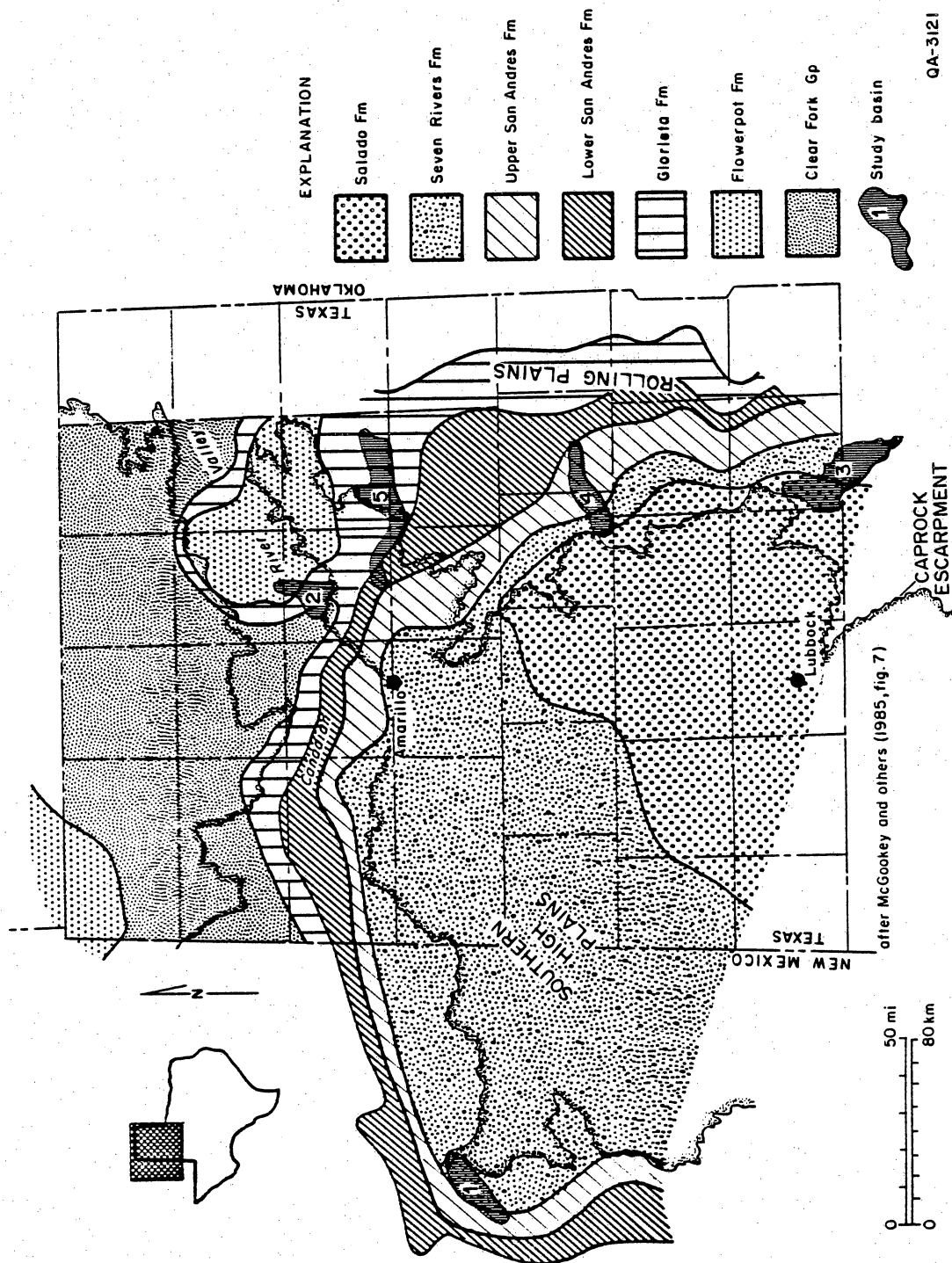


Figure 164. Dissolution fronts in Permian salt-bearing formations, Texas Panhandle and northeast New Mexico. Dissolution fronts are approximately parallel to the Caprock Escarpment around the Southern High Plains. Most salt beds are still intact beneath the Southern High Plains. All study basins are within the zones of salt dissolution: (1) Alamogordo Creek, (2) Dixon Creek, (3) Duck Creek, (4) Little Red River, (5) McClellan Creek. After McGookey and others, 1985.

Table 22. Hypsometric integrals for five representative basins and volume of material removed from each since basin development began. Original hypsometric integrals were calculated from projection of the High Plains surface across each basin.

Name of drainage basin	Basin area (mi <sup>2</sup> )	$\frac{\text{Hypsometric integral}}{\text{Original}}$	$\frac{\text{Present}}{\text{Present}}$	$\frac{\text{Basin volume (mi}^3\text{)}}{\text{Original}}$	$\frac{\text{Present}}{\text{Present}}$	Volume removed (mi <sup>3</sup> )	Average surface lowering (ft)
Alamogordo	183	0.89	0.41	41.9	18.2	23.7	680
Dixon	148	0.91	0.59	22.5	13.4	9.1	325
Duck	318	0.86	0.45	55.9	29.3	26.6	440
Little Red	185	0.93	0.29	44.4	13.8	30.6	870
McClellan	298	0.78	0.55	43.6	30.7	12.9	230

Table 23. Erosion and salt dissolution for representative drainage basins. Denudation rates were not calculated for Dixon or McClellan Creeks because of uncertain ages of those basins.

Name of drainage Basin	Average surface lowering (ft)	Average thickness of dissolved salt (ft)	Average surface lowering by erosion (ft)	Basin age (yr)	Average denudation rate (in/1,000 yr)
Alamogordo	680	260	420	> 600,000	< 8.4
Dixon	325	-	-	-	-
Duck	440	260	180	322,000-532,000	4.1-6.7
Little Red	870	370	500	290,000-479,000	12.5-20.6
McClellan	230	-	-	-	-



## STATISTICAL ANALYSIS OF EROSION PIN MEASUREMENTS: DESCRIPTION OF EROSION AND DEPOSITION

William W. Simpkins

*Statistical analysis of 3,770 erosion pin measurements indicates significant differences and variability both within and between monitoring stations. The data are normally distributed around a mean value of -0.14 cm. Field investigators have confirmed the existence of differing levels of pin activity consistent with the magnitude/frequency concepts implied by the normal distribution. Analyses also suggest that increasing the length of the data record or measurement interval may not affect the frequency distribution of the data or their validity.*

Erosion pins continue to be monitored at six erosion and climate monitoring stations in the Texas Panhandle (for location, see Machenberg, this volume). Approximately 3,770 measurements were taken for 492 erosion pins during a 2- to 4-yr period through December 1982. Finley and Howard (1981) previously reported some preliminary erosion estimates and statistical relationships. Simpkins and others (1982) discussed erosion rates calculated for a 2-yr period of record and speculated on controls on erosion. Continuation of that analysis showed very low correlations ( $r$ ) between predictor variables (such as percent vegetal cover, slope angle, and soil characteristics) and erosion/deposition. The lack of significant correlations may be related to the frequency distribution of erosion and deposition values.

Two measurements are taken during each measurement time: a pin-to-ground distance (top of pin to ground) and a pin-to-washer distance (top of pin to top of washer). Early measurements utilized various other distances that may in part account for the variability in earlier parts of the record. All distances are measured in centimeters and estimated to the nearest millimeter. Pins are measured at 6-mo intervals; some pins in remote areas are measured at 1-yr intervals. Measurements are also made after periods of heavy rainfall to document effects of runoff. Because pins were emplaced at different levels by the initial researchers, it is more useful to compare the between-time differences: DG (pin-to-ground difference) and DW (pin-to-washer difference). Histograms for DG and DW are shown in figures 165 and 166. Both curves adhere to the normal

distribution, with  $\bar{X} = -0.14$  and  $\bar{X} = -0.10$ , respectively. The leptokurtic (peaked) distribution is expected because large samples ( $N = 3279$ ) tend to decrease the standard deviation and reflect the distribution of the population (Blalock, 1972). The DW distribution is somewhat more leptokurtic (peaked) than the DG distribution because of the nature of the measurement. During deposition, the washer should remain in place ( $DW = 0$ ), whereas the pin-to-ground distance should decrease. During erosion, hoodoos or pedestals are often formed underneath the washer; hence the washer remains stationary ( $DW = 0$ ), whereas DG increases. A linear regression computed for DG and DW measurements shows a significant correlation ( $\alpha = 0.001$ ) with  $r = 0.66$ . However, because DG measurements are somewhat more responsive to processes of erosion and deposition, we will focus on them here. The relationship of DG and DW values has been investigated using the computer program SPRINT (Surface Process Interpreter), and results are given in Simpkins and Gustavson (1985).

Statistics (DG) for 2 to 4 yr of record ( $N = 3,279$ ) at each erosion monitoring station are given in table 24. Stations at Caprock Canyons State Park (West), Muleshoe National Wildlife Refuge (NWR), Lake Meredith National Recreation Area (NRA), and Palo Duro Canyon State Park reflect the erosion trend of the entire sample. Only the Buffalo Lake NWR and Caprock Canyons State Park (East) stations show mean deposition. Analysis of variance indicates that the overall means at each station are significantly different ( $p < 0.001$ ). Two-tailed T-tests also indicate that most of the means of each individual station are significantly different, particularly those stations showing deposition versus those showing erosion. The large variance (and standard deviation) at the Muleshoe station is probably responsible for the close correlations between erosion and predictor variables discussed by Simpkins and others (1982).

Geomorphic processes of erosion and deposition are conceptually and physically different. At this scale, however, it is important to recognize that numerous small DG values lie along both sides of the mean of zero. These pins may in effect be cancelling

each other out (fig. 165). Large DG values (both erosion and deposition) make up a much smaller percentage of the sample population. A higher level of erosion or deposition activity takes place at those specific sites. These two groups illustrate the geomorphic concepts of magnitude and frequency: Group 1 contains low-magnitude, high-frequency events that probably do the least work, and Group 2 contains high-magnitude, low-frequency events that cause the most erosion or deposition. Dissimilar geologic processes of erosion and deposition are thus related in terms of their geomorphic "activity" through time, without contradicting statistical assumptions or resorting to log transformations of the variables. Leopold and others (1966) also recognized this and reported rates as overall net, net deposition, and net erosion.

Field investigations tend to confirm the hypothesis that certain pins in different microenvironments show more activity (erosion or deposition) through time than others. Erosion pins were photographed during July and August 1983 to better identify these activity relationships. Examples of relatively inactive and active pins are shown in figures 167 and 168, along with a chart showing their erosion or deposition (DG values) over the study period. Typically, sites with high erosion or deposition activity (frequently  $> \pm 1$  standard deviation from the mean) have well-defined, stable rills or gullies cutting around or through the pin, or lie on steep, unvegetated slopes where the full force of sheetwash can focus on the pin. Sites of low activity are usually found on shallow, highly vegetated, alluvial slopes not subjected to appreciable rill or gully development. Vegetation, slope angle, rainfall, and soil characteristics may, to an uncertain extent, determine where the stable drainages form. The randomness in small-scale drainage network development introduces some random variability within the erosion pin data record.

The preceding discussion has focused on all 6-mo to 1-yr DG values for the period of record. One original assumption of this study was that variability (noise) would be damped over a long period of record and that erosion rates calculated at a later date could be

considered more accurate than rates calculated after only a few months of data collection (Finley and Gustavson, 1980).

Investigators elsewhere have recognized some problems in the early part of the record due to pin emplacement and subsequent soil disturbance. Emmett (1965) suggested a 1-yr waiting period before measurement, whereas Haigh (1977) suggested that 3 mo is sufficient. We tested the validity of Haigh's hypothesis for our data using two analysis of variance techniques. First, the DG values from individual stations were compared through time, the date of deployment serving as Time 1 (table 25). Only the first six measurement periods were selected because of the varied length of the data records and need to keep a large N value for significance testing. A slight statistical difference exists between the variances ( $s^2$ ) for only the first two measurement periods. A repeated-measures analysis of variance (one factor with a two-factor mixed design; Bruning and Kintz, 1977) was employed to look at relationships (variance) within and between stations through the same measurement periods (table 26). The results demonstrate three important relationships:

- (1) The time series behavior of erosion and deposition (DG values) is not equivalent among the stations ( $p < 0.001$ ).
- (2) Erosion and deposition (DG values) are significantly different ( $p < 0.001$ ) between places at any particular measurement time (relative to emplacement).
- (3) Erosion and deposition (DG values) are significantly affected by the previous history of the erosion pin at that site ( $p < 0.001$ ).

Relationship (2) is expected because the measurement times are not equal throughout the record. Relationship (1) confirms the first analysis of variance that suggested a significant difference in certain early parts of the data record. Relationship (3) strengthens the previous hypothesis (inferred from the normal distribution) that certain erosion pins may be consistently active or inactive in relation to their particular microtopographic setting. These two analyses may provide some basis for excluding the early part of the data record. However, the early variability may be due in part to the use of several different

measurement systems in the early part of the investigation. Overall, the analyses suggest that the number of and interval between pin measurements have little effect in altering the frequency distribution or statistical validity of DG values. Under the assumption that most DG values belong to the same statistical population, longer intervals between measurements or a shorter data record could be employed without compromising the validity of the data. However, longer data records are necessary to observe high-magnitude, low-frequency events. These rates are most critical for waste isolation studies and are addressed in the following article (Simpkins, this volume).

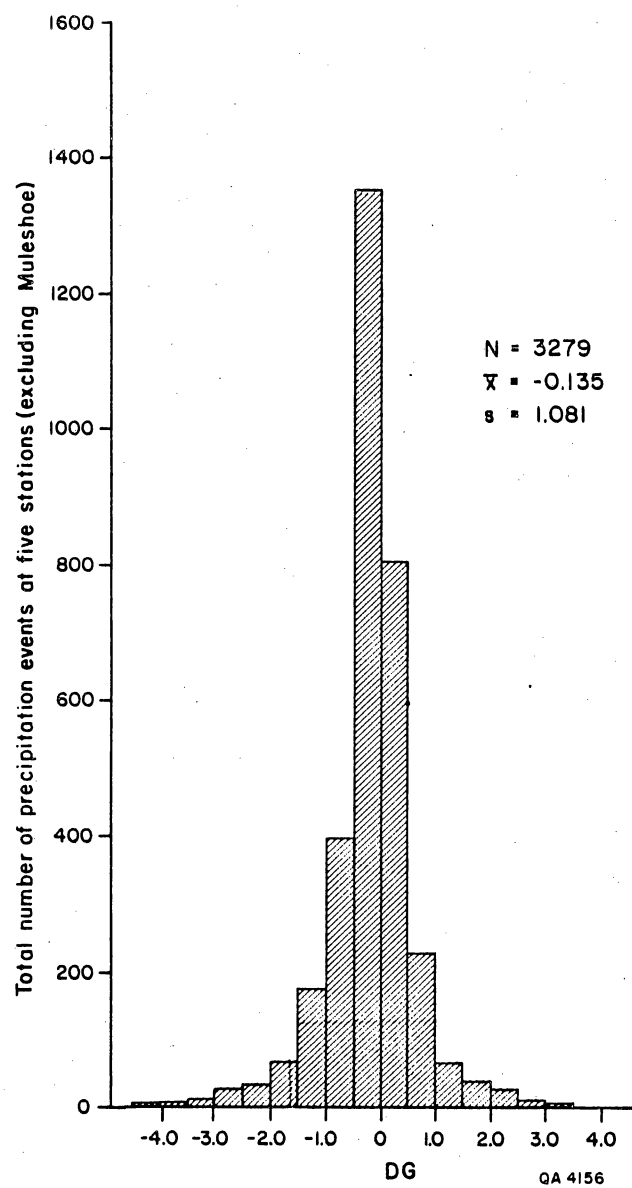


Figure 165. Histogram of DG values for the study period. Values are in centimeters.

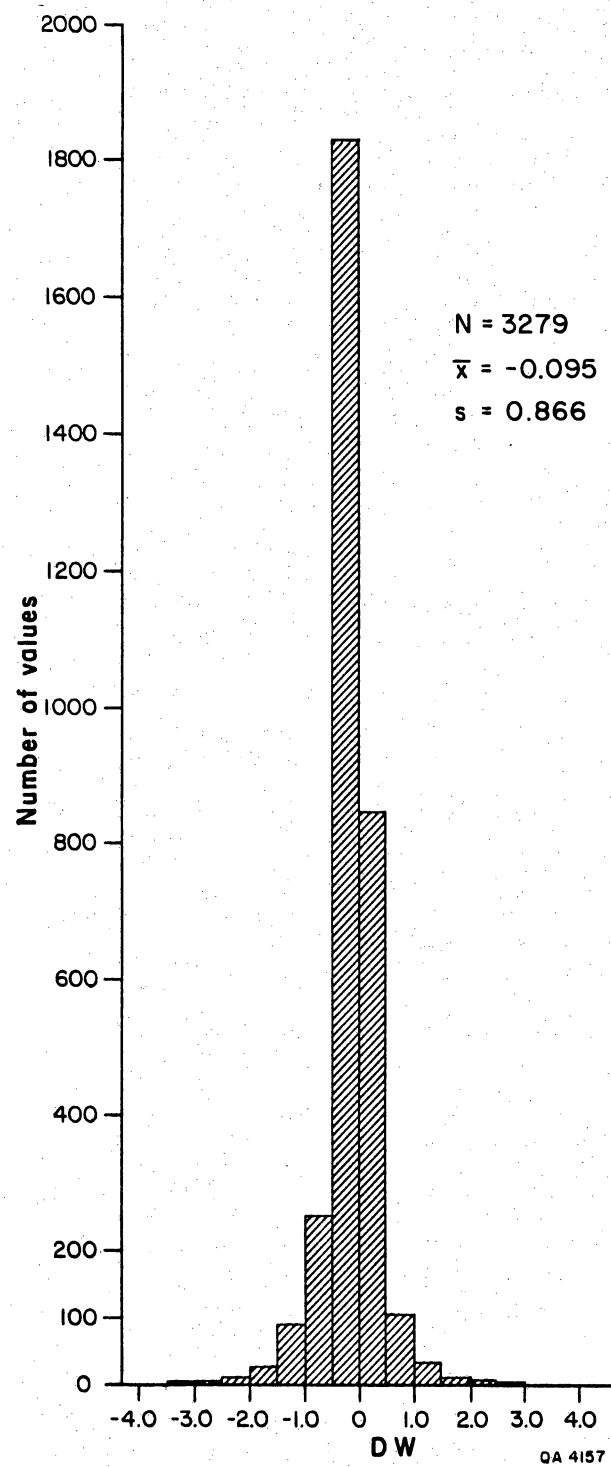
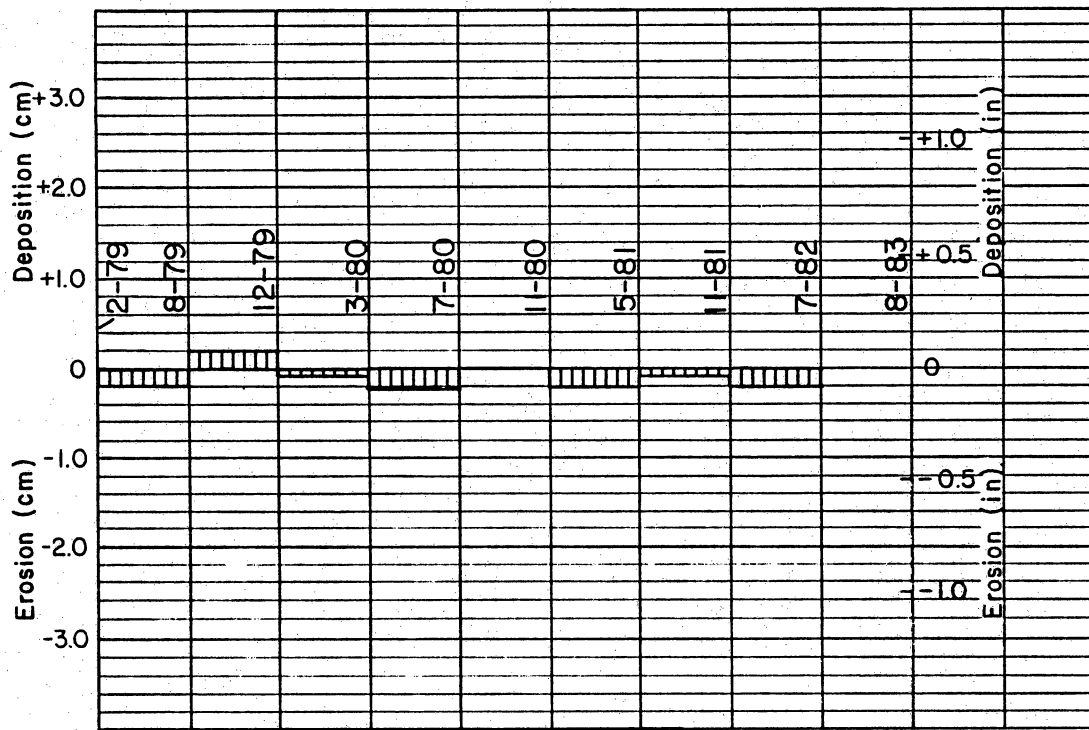
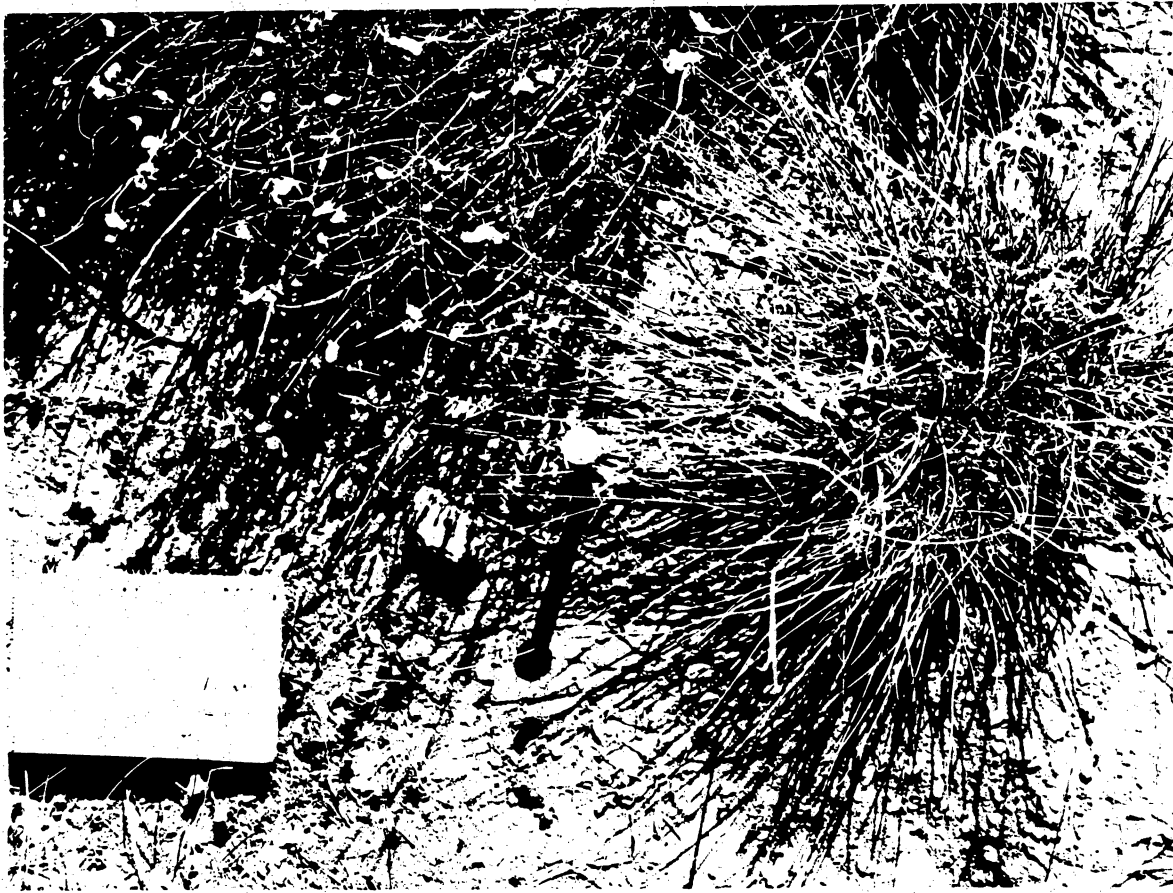


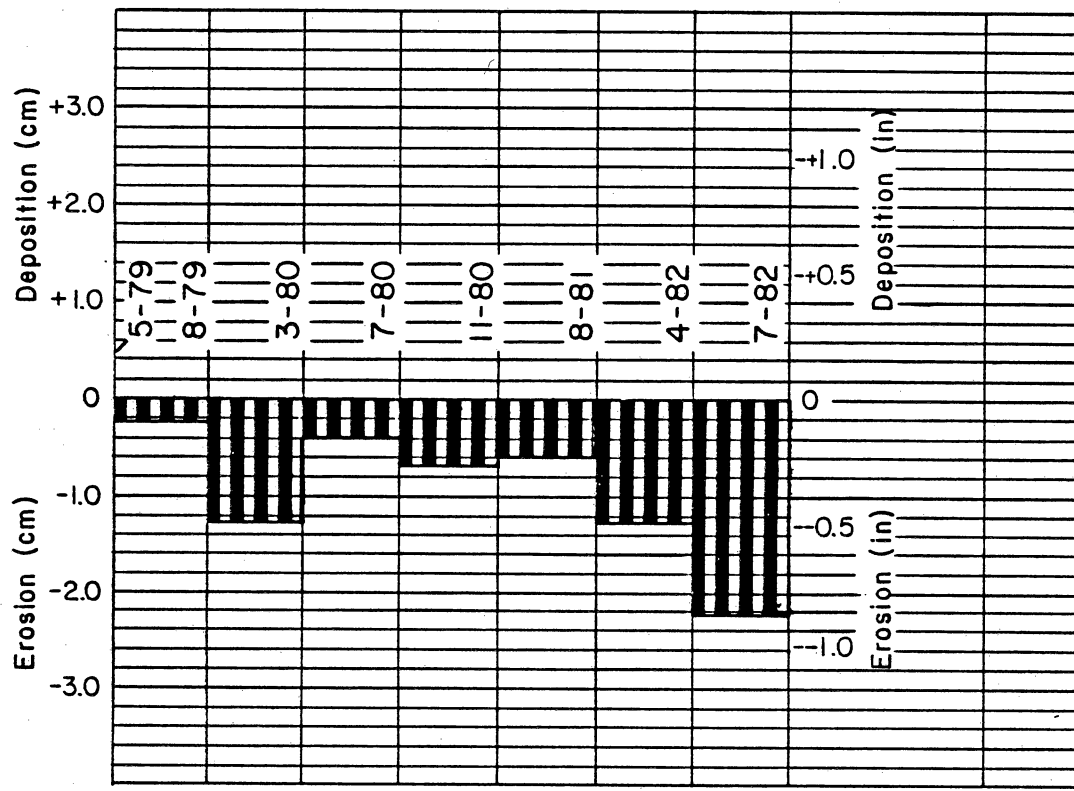
Figure 166. Histogram of DW values for the study period. Values are in centimeters.



QA4160

Figure 167. Photograph of an erosion pin (QUP1) that showed very little activity during the study period. Table 27 shows record of DG values (cm).





QA4159

Figure 168. Photograph of an erosion pin (CCS8) that showed a great amount of activity during the study period. Note position of pin relative to the microchannel system around it. Table 27 shows record of DG values (cm).

Table 24. DG statistics on six erosion monitoring stations in the Texas Panhandle.

	Buffalo Lake NWR	Caprock Canyons State Park (West)	Lake Meredith NRA	Muleshoe NWR	Palo Duro Canyon State Park	Caprock Canyons State Park (East)	All stations
Mean	0.08	0.19	-0.11	-0.16	-0.28	0.04	-0.14
Variance	0.96	0.86	0.56	2.78	1.12	0.44	1.17
Standard deviation	0.98	0.93	0.75	1.67	1.06	0.66	1.08
Standard error	0.05	0.04	0.03	0.07	0.04	0.05	0.02
Minimum (erosion)	-10.0	-8.5	-3.1	-14.5	-6.7	-4.80	-14.5
Maximum (deposition)	+7.2	+5.8	+5.5	+8.2	+5.3	+2.3	+8.20
Number of measurement differences (DG)	416	646	886	566	613	152	3,279

Table 25. Statistics on stations from measurement periods 1 to 6. Note that the only statistically significant differences in variances occur during the first two measurement periods. See text for interpretation. DG values in cm.

Measurement time	Stations											Significance
	Buffalo Lake NWR	Caprock Canyons State Park (West)		Lake Meredith NRA		Muleshoe NWR	Palo Duro Canyon State Park		Caprock Canyons State Park (East)		All stations	
1	$\bar{X}$	0.19	-0.39	-0.26	-1.02	-0.33	0.12	-0.37	p < 0.00			
	s	0.64	0.72	0.83	3.02	0.87	0.28	1.53				
2	$\bar{X}$	0.02	-0.34	-0.09	-0.02	-0.62	-0.02	-0.23	p < 0.00			
	s	0.83	1.08	0.67	0.52	1.06	0.39	0.87				
3	$\bar{X}$	0.04	-0.15	-0.12	-0.26	-0.26	-0.37	-0.17	n.s.			
	s	0.81	0.62	0.48	1.80	0.86	1.72	0.98				
4	$\bar{X}$	-0.07	-0.08	-0.14	-0.37	-0.03	-0.24	0.01	n.s.			
	s	1.52	0.50	0.60	1.15	1.04	0.48	0.93				
5	$\bar{X}$	-0.06	0.11	-0.11	-0.32	-0.37	-0.02	-0.13	n.s.			
	s	0.94	0.73	0.78	1.70	1.43	0.56	1.11				
6	$\bar{X}$	0.34	-0.21	-0.12	0.14	-0.24	0.32	-0.05	n.s.			
	s	1.00	1.21	0.94	0.79	1.35	0.60	1.09				

Table 26. Repeated-measures analysis of variance (after Bruning and Kintz, 1977). The variances of all categories are significantly different ( $p < 0.001$ ). See text for interpretation.

Source	Sum of squares	D.F.	Calculated F value	Significance
Mean	32.27372	1	55.59	$p < 0.001$
Station	46.49273	21	3.81	$p < 0.001$
Error	225.27810	388		
Time	17.26155	5	4.38	$p < 0.001$
T x S	235.43964	105	2.85	$p < 0.001$
Error	1528.49901	1940		

## STATISTICAL ANALYSIS OF EROSION PIN MEASUREMENTS: CALCULATION AND PROJECTION OF EROSION AND DEPOSITION RATES

William W. Simpkins

*A statistical study of erosion and deposition rates for the period 1978-1982 indicates that although mean net erosion has increased during this interval, the mean rate at which it proceeds has effectively decreased. A probabilistic approach to rate projection provides an alternative to linear extrapolations of rates into the future. Geomorphic thresholds may be important in any rate calculation.*

A major emphasis in geomorphic studies of the Texas Panhandle is the calculation of modern erosion and denudation rates. Numerous approaches have been used (Gustavson and others, 1981a; Finley and Howard, 1981; Finley and Baumgardner, 1981; Simpkins and Baumgardner, 1982). A similarity exists between the rates calculated at different scales and time intervals (Gustavson and others, 1981a). A summary of erosion pin studies by Haigh (1977) indicates that for climates similar to those in our study area those published rates are within an order of magnitude of the 2-yr rates presented by Simpkins and others (1982). Simpkins (previous article, this volume) discusses methods of summarizing erosion and deposition using the means of the total sampling distribution (following Leopold and others, 1966).

Data are presented in table 27 for both raw erosion and deposition amounts (table 27a) and rates (table 27b). In most cases, the process of erosion (-) is preferred to deposition (+). This trend is a reflection of our sample bias toward sites with active erosion (-).

Simpkins (previous article, this volume) discusses the implication of record length on variability and validity of data. He concludes that increasing the length between measurement periods or the length of the total data record does not have a major effect on the distribution of pin-to-ground difference (DG) values. However, the effect of time is apparent on DG values summed within specified time intervals. Pin-to-ground difference (DG) values summed for 1-, 2-, and 3-yr intervals are shown in table 28. Erosion appears to be more prevalent as the number of summed measurements increases. This may indicate

that many of the negative DG values tend to be repeated at a site, rather than alternating between erosion and deposition and moving the mean toward zero. Another explanation is that time has allowed some of the lower frequency, higher magnitude values to emerge and dominate the statistic.

Analysis of variance indicates that all the means ( $\bar{X}$ ) are significantly different ( $p < 0.001$ ) within each year class. The increase in variance (and standard deviation) from year one to three suggests repetition erosion or deposition events from one measurement time to the next, causing the normal curve to flatten (become platykurtic). These concepts are consistent with relationship (3) presented in the repeated-measures analysis of variance (Simpkins, previous article, this volume).

In contrast to the effect of time on DG summed values, calculated annual erosion and deposition rates appear to decrease as the record length increases (table 29). In addition, if all DG values are taken and rates calculated through their appropriate time period, the rates are for the most part the highest (more positive or negative) of all mean rates reported (table 29). This phenomenon can be related to the normal distribution of the sample. Because large-magnitude events at a site occur infrequently a longer period of record will incorporate some of these values along with those of greater frequency. But because of their lower frequency, the high values cannot offset the increased value of the denominator (time); hence, erosion rates effectively decrease. There is no indication that the systems involved are moving toward an equilibrium between erosion and deposition, although the short-term sediment storage phenomenon observed by Finley and Gustavson (1982) could be offsetting the erosion. The decrease in rates could also be due to higher variability (that is, more anomalous large values) in the early part of the data record (Simpkins, previous article, this volume). Nevertheless, rate calculations seem strongly influenced by the length of the data record.

Calculation and presentation of erosion by amounts (Haigh, 1977) and by per annum rates (Leopold and others, 1966) generally involve only determining a mean rate. Difficulty

arises with subsequent extrapolation of that rate because important high-magnitude events are subdued. The normal distribution of the sample may provide an alternative to linear extrapolation techniques. Figure 169 is a standardized normal curve showing the areas under the curve associated with different standard deviations ( $\sigma$ ) from the mean ( $\mu$ ). Each frequency distribution from our study is converted to this standard curve by the use of Z-scores. Areas associated with Z-scores are determined by use of a standardized table (Blalock, 1972). The probability distribution of the DG values for each station can best be visualized by plotting the areas (under the normal curve) on probability paper (fig. 170). At each DG (ordinate) value, the corresponding percent (abscissa) is the percentage of DG values less than or equal to the DG (ordinate) value specified. For example, in figure 170, for all stations only 22.5 percent of the values recorded have DG values less than or equal to -1.0 cm. At the Muleshoe NWR station (fig. 170), about 31 percent of the DG values are less than or equal to -1.0 cm. Comparison of each station indicates a different probability of any particular erosion or deposition event during approximately a 6-mo time interval between measurements.

Construction of recurrence intervals would be the next usual step in the extrapolation of these data. Plotting formulas such as Gumbels extreme value distribution and time series analysis are not recommended, however, for data series covering less than 10 yr (Viessman and others, 1977). The data also do not conform to a continuous data series model, as is usually true for daily weather or stream-discharge data. It is possible, however, to extract probability values from other published data series and, in a relative sense, compare them with the probabilities discussed here. A study of a 10-yr storm event at the Buffalo Lake NWR station (Finley and Gustavson, 1982) is used as an example. On May 26, 1978, thunderstorms that occurred near Canyon, Texas, dumped 71 mm (2.4 in) of rain on the nearby climate monitoring station at the Buffalo Lake NWR. The rainfall was concentrated in a period of 3 hr with a maximum 30-min intensity of 64 mm/hr (2.3 in/hr). A recurrence interval of 10 yr ( $p = 0.10$ ) was calculated for that storm (Finley and

Gustavson, 1982). Erosion was visible at all scales within the tributary canyons to Tierra Blanca Creek. Mean values of erosion from pins (erosion only) of different slope classes ranged from -1.45 to -3.06 cm, with individual values ranging from 0.0 to -6.2 cm. The original records indicate that very few pins showed evidence of deposition during the storm (< 10 percent of total). The overall mean net erosion rate was approximately -1.68 cm with a fairly wide scatter (S.D. = 1.78). Utilizing the probability plot in figure 170b and assuming a direct relationship of rainfall and erosion on the sample, a 10-yr event ( $p = 0.10$ ) would yield DG values  $\leq -1.60$  (erosion) or DG values  $\geq +1.32$  (deposition) at the Buffalo Lake NWR station. The DG value of -1.60 cm is compatible with the mean and range of those DG values published for the 10-yr storm. However, the high values of erosion (-6.2 cm) generated by that storm have a very low probability ( $p < 10.5$ ) of occurring at Buffalo Lake (fig. 170b). Overall, the range of DG values for the storm are at the extreme end of the 3-yr frequency distribution.

One explanation for this discrepancy is that the statistics and frequency distribution derived from the 3-yr data at Buffalo Lake represent a short-term portion (sample) of a long-term record (population). Over the long term, the record should show more high erosion values clustering around a new mean. This seems unlikely given the nature of the data base (Simpkins, previous article, this volume). A more likely explanation is that the DG values generated by the 10-yr storm represent either a different population or a very small subpopulation of the 3-yr distribution. Although this was a 10-yr storm event, the frequency of intense thunderstorms in the region is such that higher values of erosion due to these storms should be more common. This event stands alone in its ability to erode and transport sediment. The effect of the 1978 event on the erosion pins was "catastrophic" and probably reflects the crossing of some critical geomorphic threshold.

To test this hypothesis of the critical threshold, a storm of similar magnitude and intensity was chosen for direct comparison. The storm occurred at Buffalo Lake on September 17-18, 1981, and was of a similar magnitude and intensity. Mean values of



erosion (using slope classes of Finley and Gustavson [1982]) ranged from -0.38 to -2.16 cm, with individual values ranging from -0.1 cm to -2.95 cm. The overall mean of -0.06 cm is more in line with the 3-yr statistic. The 3-yr period between the two major storms seems to have resulted in a more expected effect on the erosion pins. Because it appears possible for low-frequency storms to generate values within the prescribed distribution, it follows that the response of erosion pins to the 1978 storm was the result of crossing a geomorphic threshold. The particular combination of factors responsible for this response has obviously not been present since that 1978 event. Such a threshold could be influenced by the season (spring vs. summer), the amount of material available for transport, and antecedent moisture conditions. The difficulty in identifying geomorphic thresholds of this type is supported by Campbell and Honsaker (1982).

In conclusion, a probabilistic approach to predicting erosion and deposition from erosion pins is useful unless the system is totally threshold controlled. If this is true, new populations of values can be generated in the future, rendering the linear extrapolations of present erosion rates useless. Longer periods of record are no doubt needed to sample all the possible populations. Studies of probability and frequency relationships in erosion and deposition rates should continue in FY 84.

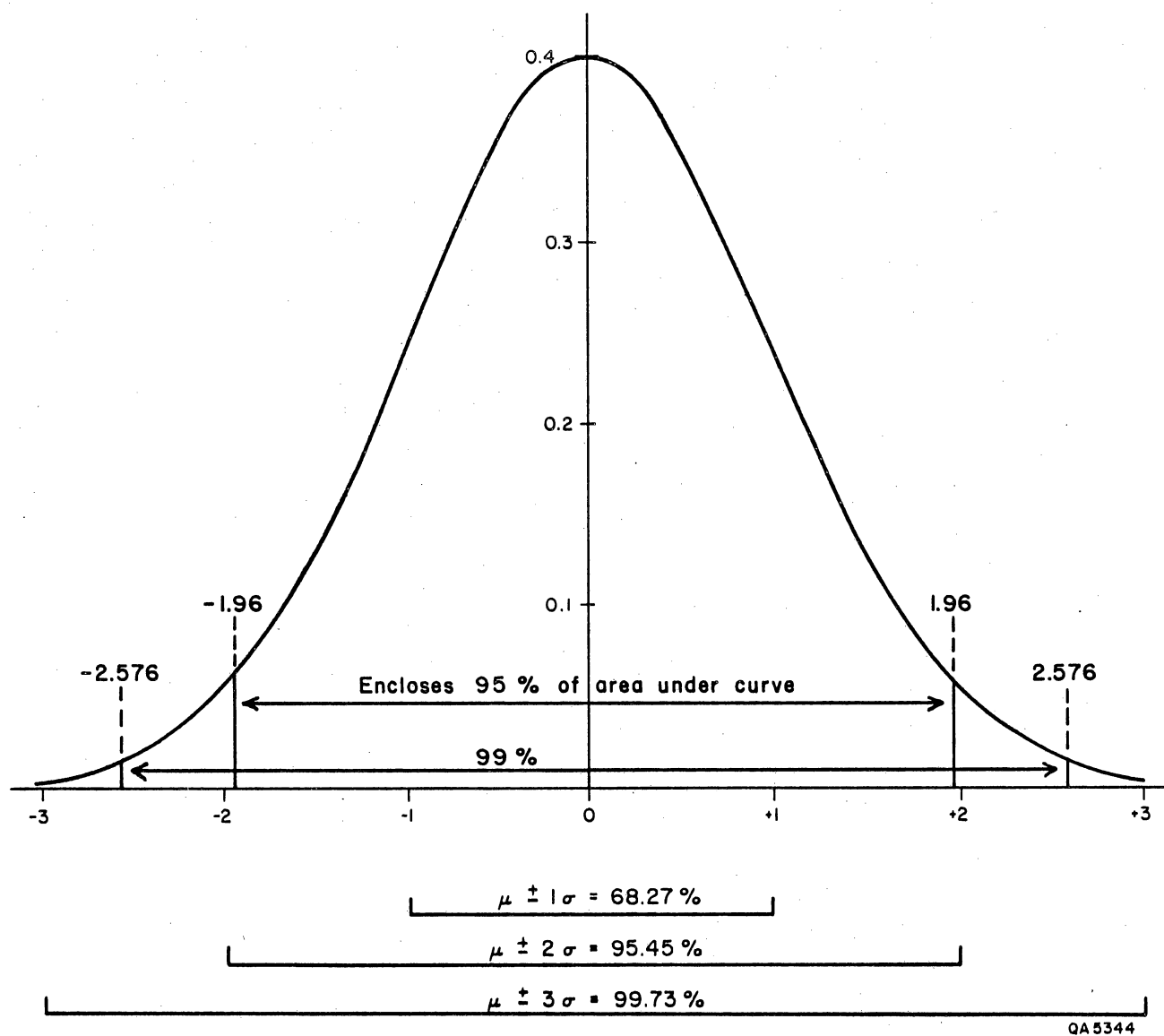


Figure 169. The standardized normal curve showing areas associated with common parameters ( $\sigma$ ,  $\mu$ ). Drawing adapted from Till (1974).

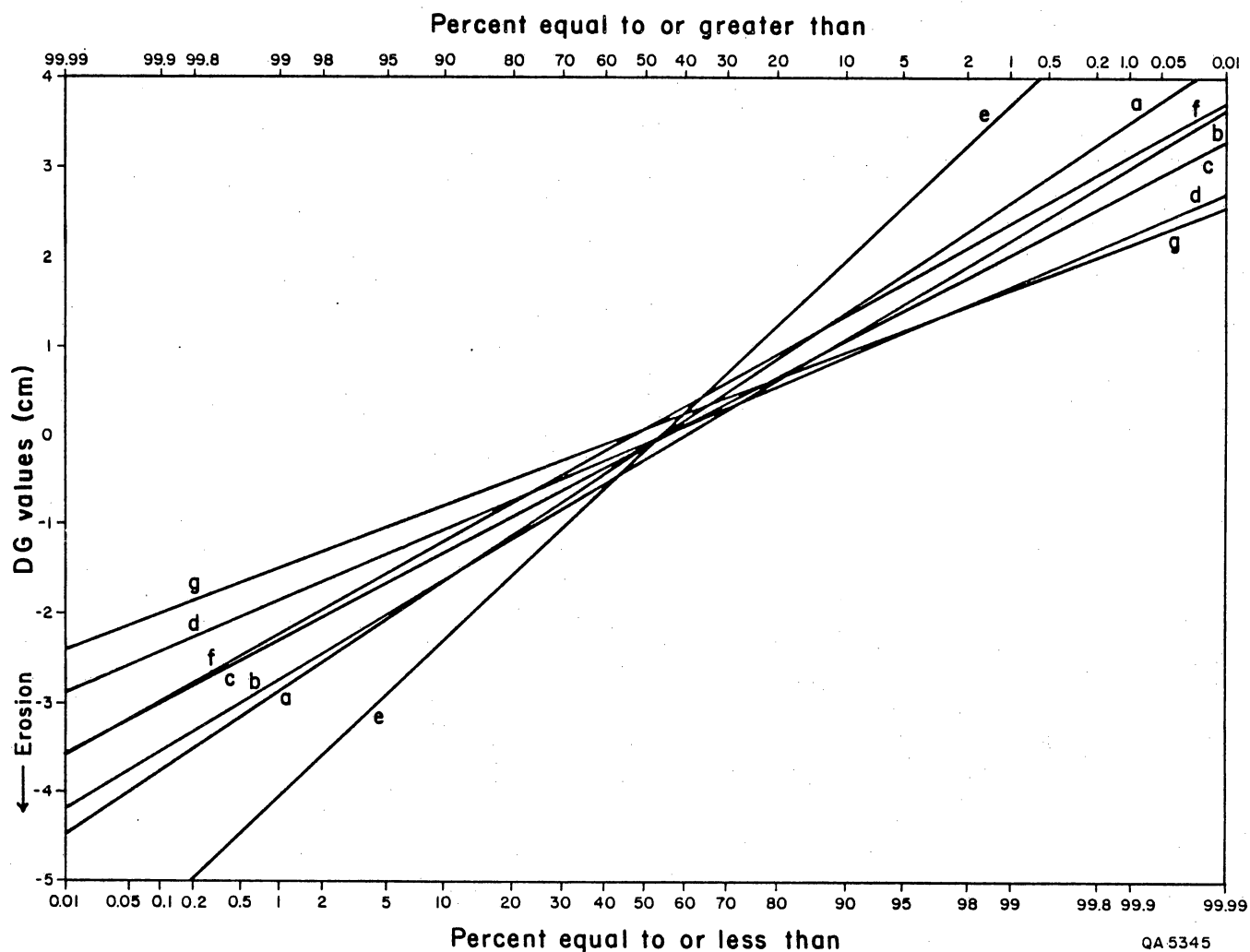


Figure 170. Probability plots of erosion pin data. (a) All stations combined; (b) Buffalo Lake National Wildlife Refuge; (c) Caprock Canyons State Park (West); (d) Lake Meredith National Recreation Area; (e) Muleshoe National Wildlife Refuge; (f) Palo Duro Canyon State Park; (g) Caprock Canyons State Park (East). Slopes of the lines differ in accordance with the area underneath sections of the normal curve.

Table 27a. Statistics of pin-to-ground difference (DG) separated into erosion or deposition and then combined into an overall statistic.

		Buffalo Lake NWR	Caprock Canyons State Park (West)	Lake Meredith NRA	Muleshoe NWR	Palo Duro Canyon State Park	Caprock Canyons State Park (East)
Erosion	$\bar{X}$	-0.58	-0.71	-0.58	-1.01	-0.94	-0.44
	S.D.	0.94	0.82	0.55	1.92	0.98	0.72
Deposition	$\bar{X}$	0.65	0.55	0.50	0.80	0.64	0.40
	S.D.	0.91	-0.58	0.70	1.13	0.79	0.43
Overall	$\bar{X}$	0.08	-0.19	-0.11	-0.16	-0.28	0.04
	S.D.	0.98	0.93	0.75	1.67	1.06	0.66

Table 27b. Cumulative 3-yr (DG) statistics separated into erosion or deposition and combined into an overall statistic.

		Buffalo Lake NWR	Caprock Canyons State Park (West)	Lake Meredith NRA	Muleshoe NWR	Palo Duro Canyon State Park	Caprock Canyons State Park (East)
Erosion	$\bar{X}$	-0.33	-0.77	-0.48	-0.45	-0.79	-0.11
	S.D.	-0.48	-0.57	0.51	0.43	0.63	0.07
Deposition	$\bar{X}$	0.66	0.49	0.42	0.29	0.44	0.42
	S.D.	0.89	0.39	0.34	0.29	0.48	0.47
Overall	$\bar{X}$	0.20	-0.40	-0.28	-0.13	-0.61	0.21
	S.D.	0.87	0.77	0.61	0.52	0.74	0.44

Table 28. Comparison of DG (row amounts) statistics after 1, 2, and 3 yr of record.  
An increase in  $\bar{X}$  towards more erosion is indicated at most stations.

		Buffalo Lake NWR	Caprock Canyons State Park (West)	Lake Meredith NRA	Muleshoe NWR	Palo Duro Canyon State Park	Caprock Canyons State Park (East)	Total stations
1 yr	$\bar{X}$	0.24	-0.88	-0.44	-0.61	-0.98	-0.27	-0.58
	S.D.	1.07	1.16	0.87	1.92	1.16	1.14	1.30
2 yr	$\bar{X}$	0.12	-0.91	-0.62	-0.51	-1.19	-0.04	-0.66
	S.D.	2.05	1.54	1.23	1.96	1.45	1.07	1.67
3 yr	$\bar{X}$	0.61	-1.33	-0.83	-0.40	-1.82	0.61	-0.80
	S.D.	2.62	2.53	1.84	1.62	2.21	1.28	2.28

Table 29. Comparison of DG rate statistics after 1, 2, and 3 yr of record.  
A general decrease in  $\bar{X}$  is indicated at most stations.

		Buffalo Lake NWR	Caprock Canyons State Park (West)	Lake Meredith NRA	Muleshoe NWR	Palo Duro Canyon State Park	Caprock Canyons State Park (East)	Total stations
1 yr	$\bar{X}$	0.21	-0.72	-0.40	-0.39	-0.83	-0.28	-0.47
	S.D.	0.92	0.95	0.88	1.53	0.99	1.10	1.09
2 yr	$\bar{X}$	0.06	-0.46	-0.28	-0.23	-0.63	-0.02	-0.33
	S.D.	1.02	0.78	0.55	0.10	0.78	0.63	0.85
3 yr	$\bar{X}$	0.21	-0.40	-0.28	-0.13	-0.61	0.21	-0.26
	S.D.	0.87	0.77	0.61	0.52	0.74	0.44	0.74
All rates (6-month intervals)	$\bar{X}$	0.31	-0.88	-0.55	-0.60	-1.23	0.06	-0.61
	S.D.	1.86	1.54	1.35	2.01	1.74	0.10	1.71

## MODERN EOLIAN PROCESSES ON THE SOUTHERN HIGH PLAINS AND ADJACENT AREAS

Marcie D. Machenberg and S. Christopher Caran

*Eolian processes have substantially modified the landscape on the Southern High Plains within historic time. The maximum inferred rate of deflation was 18.9 mm/yr at a site in Bailey County, Texas, a region of loose, sandy soils and frequent, seasonal dust storms. At least locally, agricultural practices have accelerated natural rates of erosion and deposition by winds.*

An extensive cover of windblown sand and silt mantles the gently sloping surface of the Southern High Plains. Deflation and eolian deposition were among the dominant geomorphic processes affecting this region throughout most of Plio/Pleistocene and Holocene time. Historically, human activities have amplified the importance of wind action by disrupting the natural vegetative cover, thereby exposing the unconsolidated sediments.

Agriculture, particularly dry-land cultivation, has been the principal form of land use in the area since at least the early 1900's (Webb, 1931). Effects of tilling practices on deflation are shown in figure 171. The cultivated field on the right (east) is approximately 0.8 m lower than the range site on the left (west). The long, narrow field was cleared and brought into cultivation probably in the 1920's (C. D. Tunnell, personal communication, 1983). Its furrows run north to south, along the field's long axis. The orientation of these furrows parallels the dominant winds, thereby maximizing local deflation. During the winter and early spring, some of the strongest winds are from the north, whereas the prevailing wind direction is southerly at other times of the year (Bomar, 1983). Other factors that enhance the erosional impact of winds include antecedent dry conditions and frost heaving. Both are seasonal effects that increase the susceptibility of soils to removal during frequent spring dust storms. After becoming entrained, soil aggregates from this field and others like it are transported from their source and redeposited as a broad sheet of eolian sediment.

In Bailey County, sandy soils and periods of extended drought combine to create conditions highly favorable for deflation. This region and adjacent eastern New Mexico have been identified as major sources of sediment entrained by dust storms during the spring (Kessler and others, 1978; McCauley and others, 1981) (fig. 172). Rates of enhanced deflation through historic time were inferred from examination of exposed concrete foundations of abandoned buildings in the area (figs. 173 and 174). The ages of five structures showing evidence of deflation around their bases were determined from unpublished records, and average annual rates of deflation were calculated (table 30). The highest rate was 18.9 mm/yr. McCauley and others (1981) reported that in February 1977 plowed fields in eastern New Mexico were locally eroded to depths of more than 1 m during a single dust storm. However, an extreme event of this kind is probably offset by seasonal deposition, perhaps within a short time. In contrast, the mean rates shown in table 1 represent relatively long term, net losses.

To evaluate the relative significance of deflation observed in the Bailey County area, rates there were compared with measurements of erosion at heavily denuded sites elsewhere. Because few representative rates of prolonged deflation at other sites have been reported, data regarding denudation caused by both fluvial and eolian erosion were compared with the maximum deflation measured during the current study. Extrapolation of this rate, to 18.9 m/1000 yr, helps put this figure in perspective. The millennial rate is almost 50 percent greater than the maximum rate of erosion recorded in a small drainage basin in the Loess Hills of Iowa (Federal Interagency River Basin Committee, 1953). The rate at Loess Hills, 12.8 m/1000 yr, is one of the highest recorded previously (Schumm, 1977). The maximum deflation in Bailey County also is 19 times the average maximum rate of denudation expected in large drainage basins (Schumm, 1977). Direct comparison of these figures is somewhat artificial, but it does illustrate the relative intensity of local deflation around structures in the Bailey County study area. Most of the structures are located south of Muleshoe along the edge of the Blackwater Draw sand dune belt, which



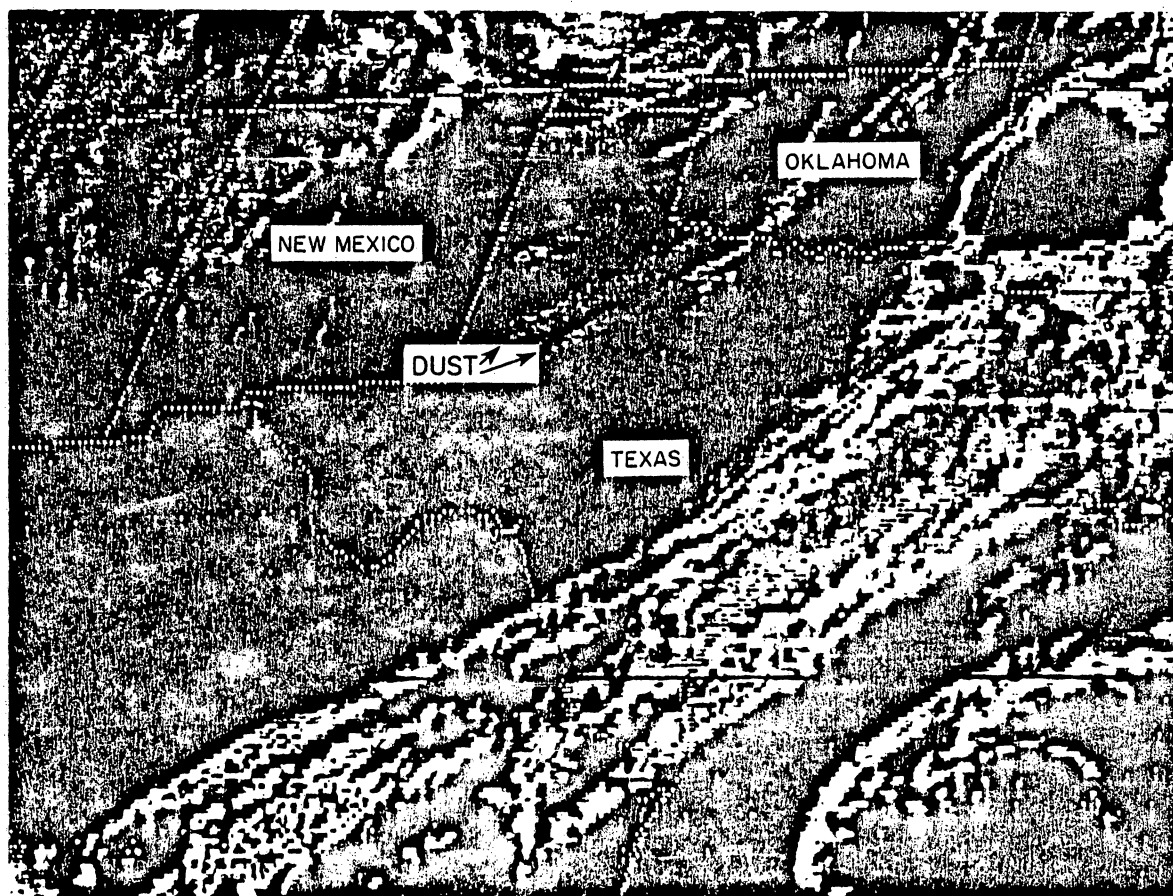
trends east-west (fig. 174). The soils are sandy loams subject to severe wind erosion (Girdner and others, 1963). Without irrigation these soils are poorly to only moderately well suited to cultivation, yet early settlers attempted dry-land farming. Abandonment of numerous homesteads during the "Dust Bowl" days in the mid-1930's and the extended drought of the mid-1950's attests to the severity of this problem.

The exceptional amount of deflation around these foundations must be considered a "worst-case" condition caused by the increased disturbance of soils associated with construction and habitation of the structures. Not surprisingly, most of the buildings exhibit maximum deflation on their north and northwest sides, the directions from which storm winds originate in the spring (Sidwell, 1938; Johnson, 1965). On those sections of land converted to range, cattle seeking shade further disturbed the vegetation and substrate, particularly on the north and west sides, thereby increasing the potential deflation of soils.

Rates of deflation shown in table 30 were calculated relative to the dates of construction of these buildings. At some sites most of the deflation may have resulted from individual severe wind storms such as those that affected the region on March 25-26, 1935, March 2-3, 1956, and February 23-24, 1977 (McCauley and others, 1981; Bomar, 1983). If this is true, the average annual rates as calculated are minimal. Yet even these rates are greater than would be expected under natural conditions and almost certainly are not representative of soil loss regionally. They are, however, indicative of conditions at severely disturbed sites from which all groundcover has been removed. Thus, the effects of eolian processes, enhanced by land use, should be considered if siting and designing a facility for isolating long-lived nuclear waste. Mounds of mined salt and large, heavily trafficked areas at the construction site would be particularly vulnerable to redistribution of sediment unless provisions were made to retard this effect.



Figure 171. Effects of deflation resulting from agricultural practices. The field shown on the right (east) is approximately 0.8 m lower than the vegetated rangeland on the left (west). The rangeland is in the southeastern corner of Caprock Canyons State Park immediately north of Farm-to-Market Road 1065, approximately 6.8 km north of Quitaque, Briscoe County, Texas.



QA/1734

Figure 172. Infrared satellite image at 1800 GMT (12:00 noon CST) of a dust storm over the Texas Panhandle, April 2, 1982. The source of dust is the region of dry, sandy soils along the Texas-New Mexico border. Image provided by G.W. Bomar, Texas Department of Water Resources, Austin, Texas.



*a*



*b*

Figure 173. (a) Abandoned homestead, located 5.2 km north of Needmore, in Bailey County, Texas, along State Highway 214. The house was constructed in 1928, abandoned in 1940, and exhibits a maximum of 1.02 m of deflation around its concrete foundation. (b) Detail of exposed foundation, the lower half of which retains impressions of trowel marks and root traces. The concrete forming this part of the foundation was poured against the wall of a shallow excavation. The original ground level is indicated by the rim of concrete at the top of the 1-m scale bar.

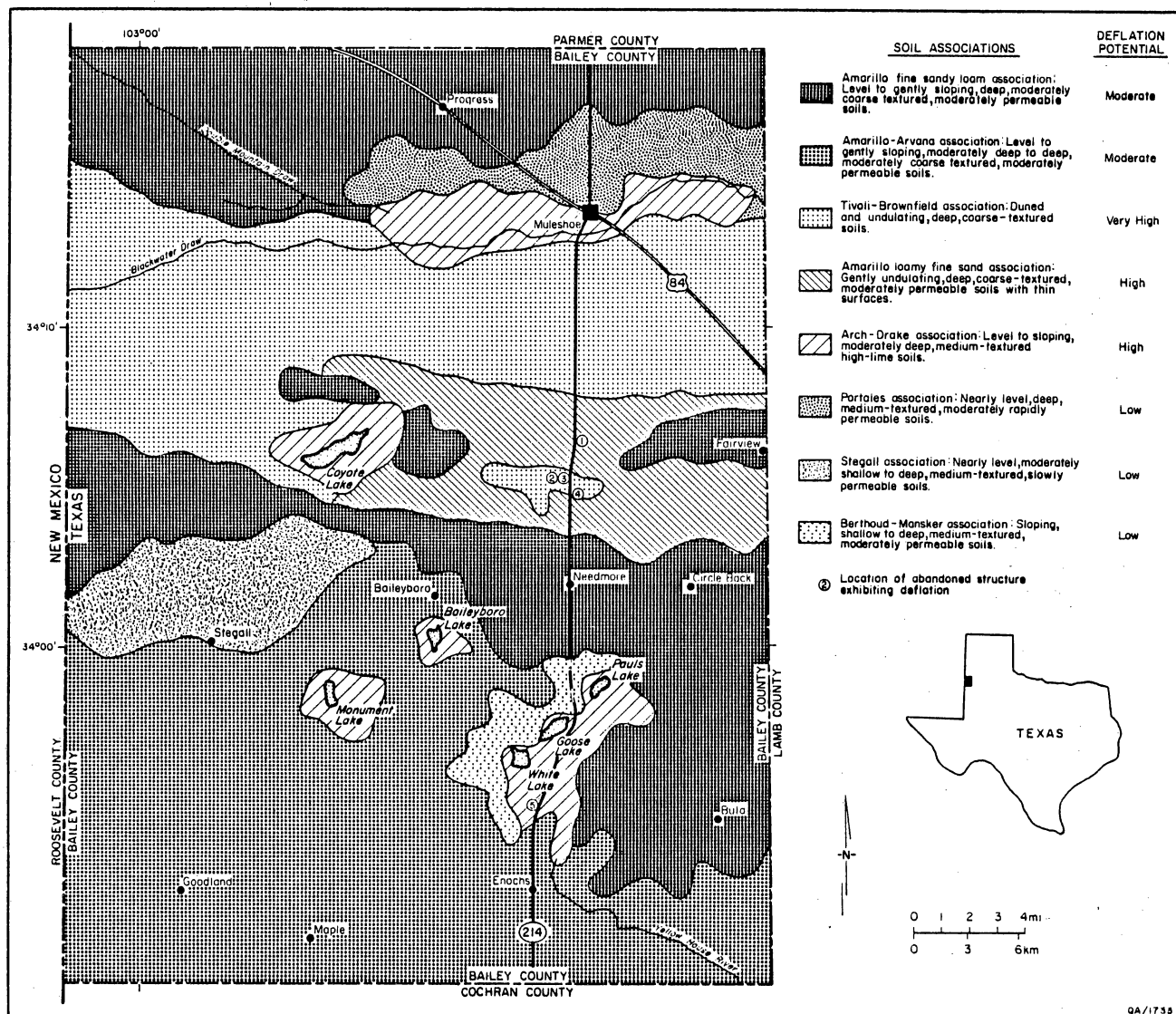


Figure 174. General soil map of Bailey County, Texas, showing deflation-prone soils and sand dunes south of Muleshoe (modified from Girdner and others, 1963). Numbers refer to the locations of abandoned structures at which deflation was measured (table 30). The building shown in figure 173 is number 4 in figure 174 and table 30. The Tivoli-Brownfield soil association corresponds to the sandhills along Blackwater Draw, a relict drainage feature.

Table 30. Mean annual rates of deflation from around the base of abandoned structures, Bailey County, Texas.

Building reference number	Construction date	Age (yr)	Maximum foundation exposure (mm)	Mean annual deflation (mm/yr)
1	1929	53	260	4.9
2	1930	52	390	7.5
3	1930	52	320	6.2
4	1928	54	1,020	18.9
5	1951	31	280	9.0

(For locations of numbered buildings see fig. 174.)

## ANALYSIS OF DUST-TRAP SAMPLES COLLECTED ON THE SOUTHERN HIGH PLAINS AND ADJACENT AREAS

Marcie D. Machenberg

*Preliminary data derived from six dust traps installed in the Southern High Plains and adjacent areas show that dust deposition varies locally and seasonally in response to natural and man-induced factors. Monthly rates of dustfall at individual stations ranged from 0.658 g/m<sup>2</sup> at Muleshoe National Wildlife Refuge to 13.441 g/m<sup>2</sup> at Palo Duro Canyon State Park. Dust deposition contributes significantly to aggradation of the High Plains surface.*

The Southern High Plains has been identified as the dustiest region in the contiguous U.S. (Orgill and Sehmel, 1976). Sources of dust are numerous and include desiccated playa bottoms, sand dunes, floodplains, plowed fields, overgrazed rangeland, and unpaved roads. Ambient dust deposition is a continuous process augmented by rapid influx of material during dust storms and precipitation events. This study focuses on the amount and characteristics of present-day ambient dustfall. This information is necessary to assess the influence of future eolian deposition and its effect on landscape evolution during the expected tenure of a high-level nuclear waste repository.

Six dust collectors, consisting of quart-sized glass canning jars with screened openings and glycerol as the trapping medium, were installed at previously established remote weather monitoring stations (fig. 175; two collectors are located at site number 4). The traps were designed to collect material deposited by gravitational settling and were mounted at heights of 135 to 147 cm above ground level. The collection sites were chosen to represent natural conditions as accurately as possible.

Dust collection was initiated in February 1983 and is expected to continue for 3 to 5 yr. Samples are collected monthly ( $29 \pm 3$  days) and analyzed for dust quantity, mineralogic composition, and grain-size distribution. Dustfall values are reported in g/m<sup>2</sup>/month (American Society for Testing and Materials, 1979).

Preliminary results show that the quantity of dust varies greatly among stations (fig. 176). As regional weather patterns are fairly homogeneous over this physiographic

province, local differences in soils, land-use practices, vegetation density, topography, and local wind flow account for the variations.

The Palo Duro site collects significantly greater amounts of dust owing to its geographic setting. The collector is situated 5 m below the top of the eastern Caprock Escarpment. Locally, the escarpment is a nearly vertical drop of 130 m. The "scarp effect" (Bowen and Findley, 1974) causes wind speeds to increase dramatically as currents are forced up the escarpment, thereby increasing the dust-entrainment capacity of winds. Wind velocity drops suddenly at the top of the escarpment, as flow spreads laterally across the High Plains surface. Much of the entrained material then falls from suspension and accumulates near the escarpment until remobilized by winds or runoff. The erosional competence of winds also increases with velocity. Not surprisingly, the Palo Duro station also collects a larger percentage of coarse eolian material than do the other stations (fig. 177).

The increase in collected dustfall between April and May relative to previous months (fig. 176) is a seasonal effect attributable to the passage of frontal systems from the west, combined with agricultural practices. Large tracts of bare, unconsolidated soil resulting from spring plowing are ready sources of fine silt and clay during the windy months. Dust storms in the South-Central U.S. occur with greatest frequency in February, March, and April (McCauley and others, 1981; Orgill and Sehmel, 1976) and transport vast quantities of dust far from the source areas (see fig. 172).

Rainfall can cause fine particulates to be washed out of suspension (Smith and others, 1970; Yaalon and Ganor, 1973). In general, there is a positive correlation between dust deposition and monthly rainfall (fig. 178). It appears, however, that for each station there exists a rainfall "threshold," above which the effects of increased vegetation growth or soil dampening inhibit dust entrainment. More data are needed to quantify this effect.

Dust deposition has been and continues to be an active process on a worldwide basis (Yaalon and Ganor, 1973; Péwé, 1981) and especially on the Southern High Plains, as shown



by the preliminary results of this study. The contribution of dust to the processes of caliche formation, soil renewal, and topographic modification should be investigated further to assess its impact.

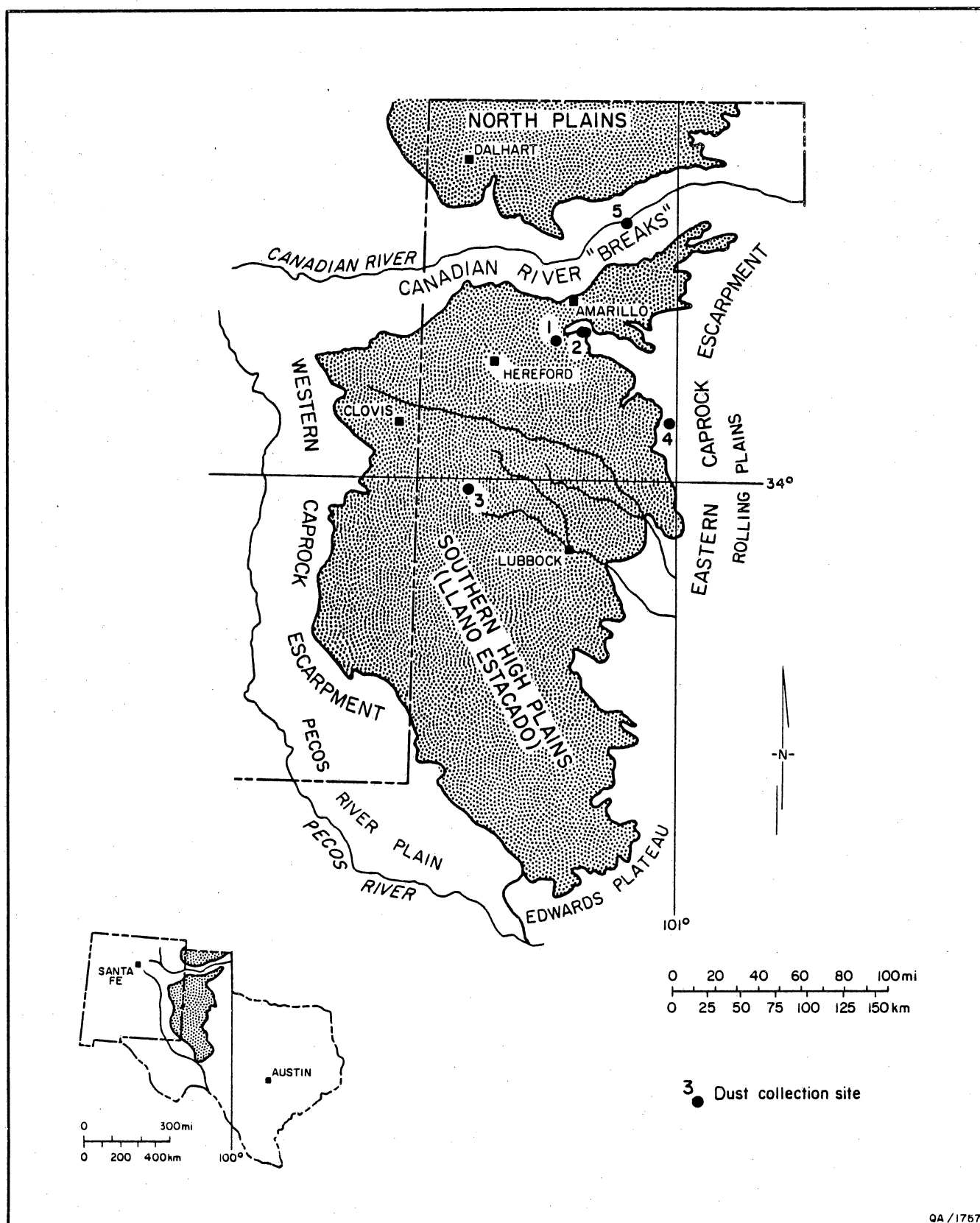


Figure 175. Physiography of the Texas Panhandle and location of dust collection sites: (1) Buffalo Lake National Wildlife Refuge; (2) Palo Duro Canyon State Park; (3) Muleshoe National Wildlife Refuge; (4) Caprock Canyons State Park (two traps); and (5) Lake Meredith National Recreation Area.

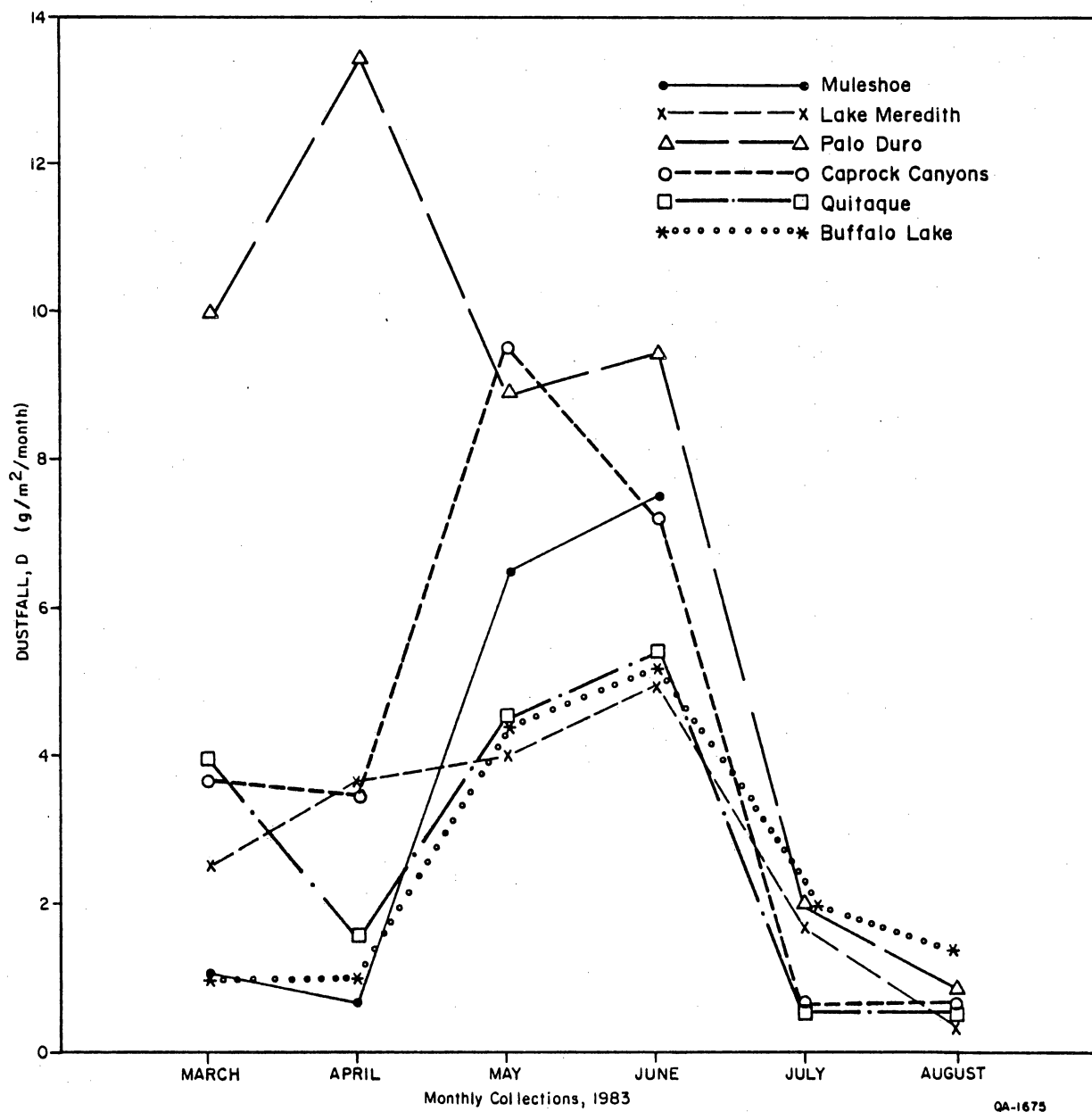
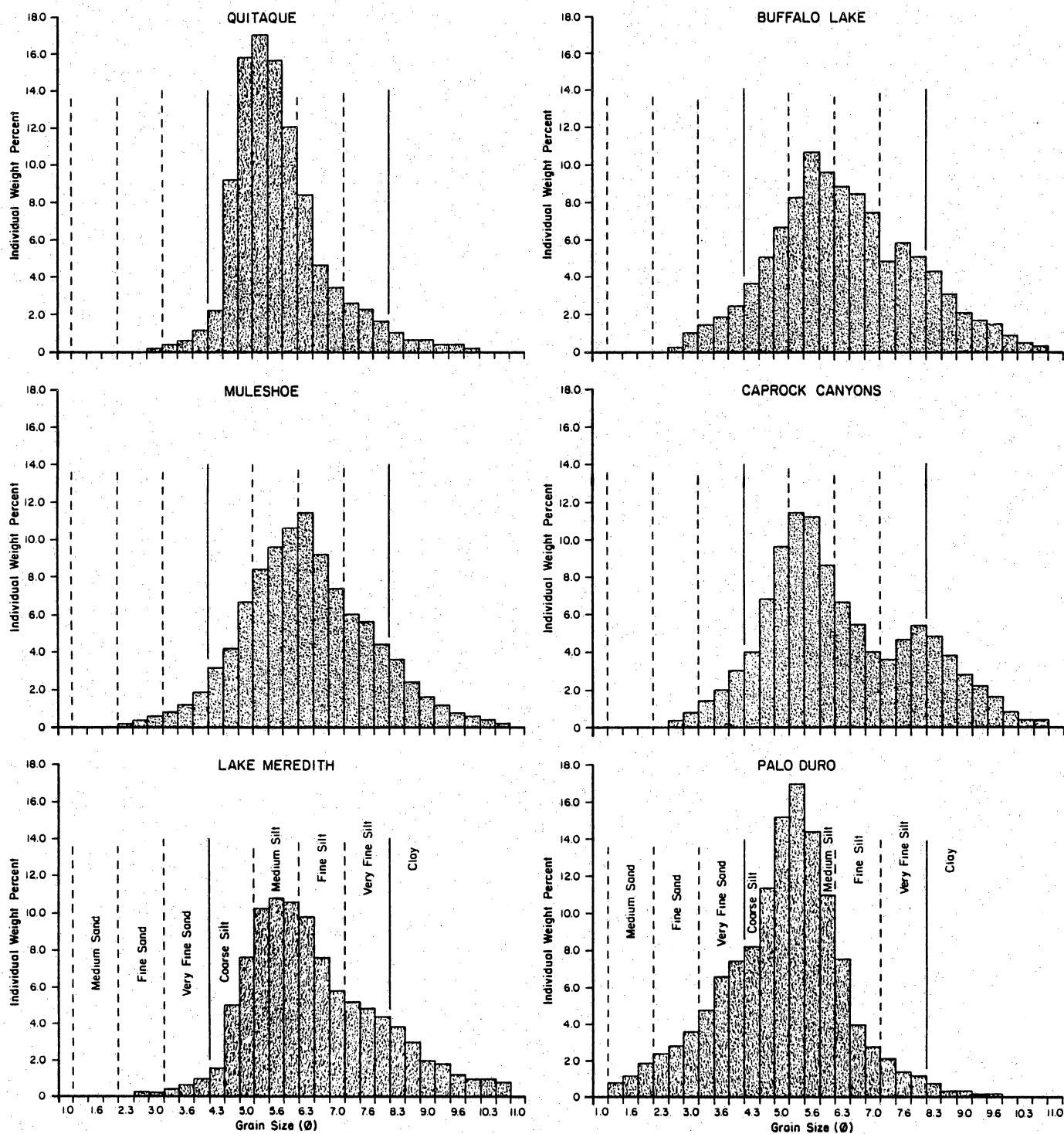


Figure 176. Monthly mean dustfall at six collection sites. Locations of collection sites are shown in figure 175. Horizontal scale is in phi ( $\phi$ ) units.  $\Phi = -\log_2 d$ , where  $d$  is the diameter of the sediment particle in millimeters.



QA / 1735

Figure 177. Grain-size distributions of dust samples collected in the Southern High Plains and adjacent areas. Location of collections sites are shown in figure 175.

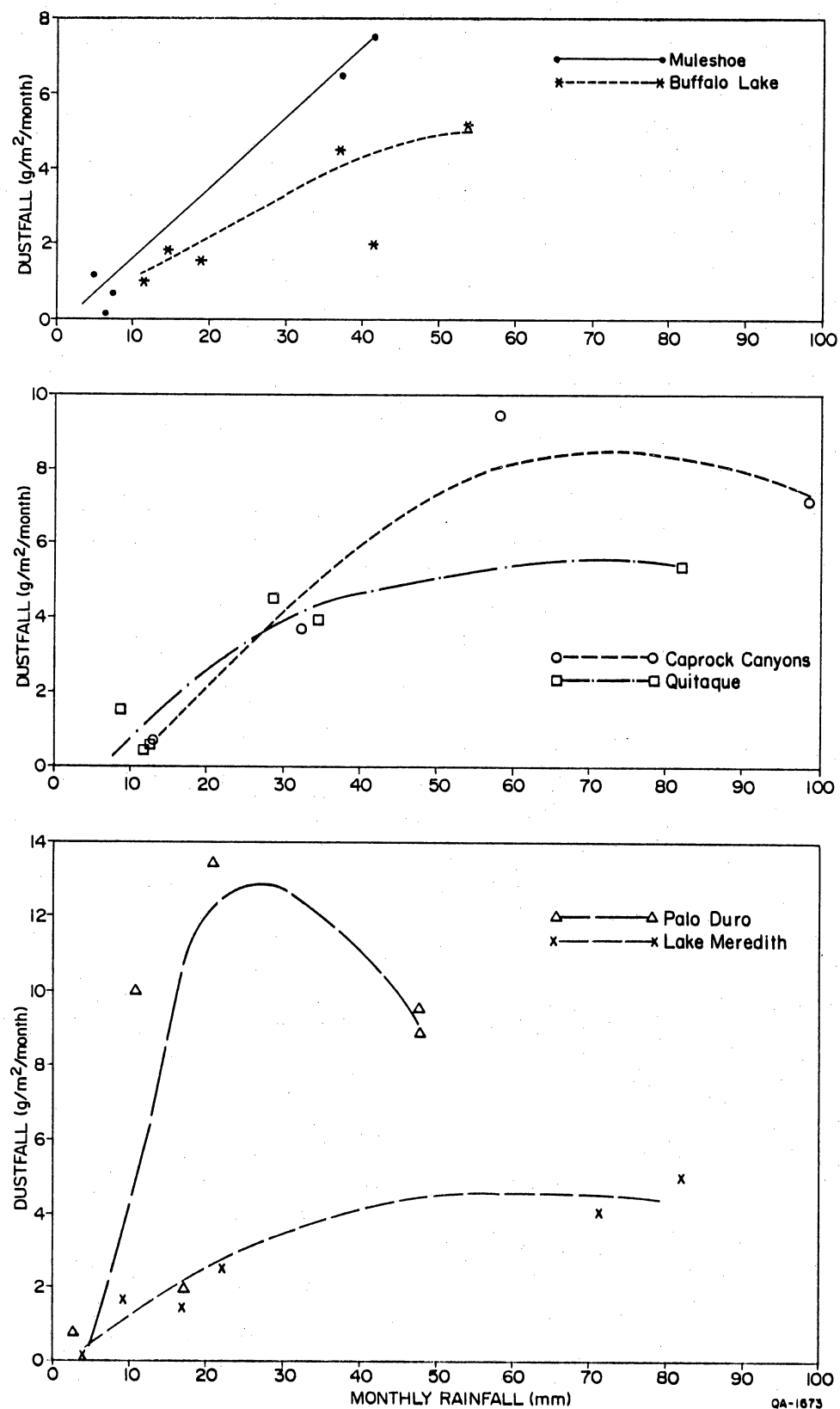


Figure 178. Relationship between monthly dustfall and rainfall. The variables are positively correlated up to a certain "threshold" rainfall value unique to each station.

## LATE QUATERNARY PALEOCLIMATOLOGY OF NORTHWESTERN TEXAS--IMPLICATIONS FOR DISPOSAL OF NUCLEAR WASTE

S. Christopher Caran and Raymond W. Neck

*During the past 15,000 yr the paleoclimate of the Southern High Plains has shifted from cool-wet to warm-wet to warm-dry. These changes are reflected in the sedimentology, pedology, and paleofauna of a laterally extensive, late Quaternary stratigraphic sequence in the contiguous Rolling Plains. Climatic variations on the scale of those disclosed by the geologic record could substantially alter regional patterns of erosion, deposition, and ground-water recharge.*

The paleoclimate of the Southern High Plains and adjacent areas (see fig. 158) has undergone marked changes since late Pleistocene time (Caran and McGookey, 1983). An extended period of relative climatic stability ("Woodfordian" climatic episode) was interrupted less than 15,000 yr ago by an interval of rapid, cyclical fluctuations of temperature and precipitation that increasingly diverged from preexisting conditions. This progression essentially culminated between 5,000 and 1,000 yr ago in a new interval of apparent stability corresponding to the modern climatic regime. The regional pattern of paleoclimatic change generally is consistent with trends recognized throughout the Southwest and worldwide, but circumstances in the present study area permit refinement of the record covering roughly the last 15,000 yr.

A thick wedge of fluvial, eolian, pedogenic, and lacustrine deposits covers a large area of the western Rolling Plains along the margin of the Southern High Plains (Caran and Baumgardner, this volume) (see fig. 158). This complex stratigraphic sequence is the product of nearly continuous deposition from late Pleistocene through Holocene time. The climatic history of this period is recorded in these strata as serial variations in faunas and environments of deposition. Such variations are well represented in deposits on the Rolling Plains and in comparable, apparently isochronous, deposits on the High Plains.

Figure 179 is a generalized measured section depicting the alluvial sequence at the Lake Theo archeological site (site number 41BI70) in southeastern Briscoe County, Texas (see fig. 178). This section is representative of the preliminary stratigraphic model of late

Quaternary deposition throughout the region proposed by Caran and Baumgardner (this volume). The Lake Theo site is located east of the Caprock Escarpment, which divides the High Plains (to the west) from the Rolling Plains. The pedology, paleofauna, and genetic stratigraphy of these deposits, as well as the archeology of cultural remains, have been studied by a number of investigators (Harrison and Killen, 1978; Johnson and others, 1982; Caran and McGookey, 1983). Strata at Lake Theo have been dated by radiocarbon analysis of organic humates (Johnson and others, 1982). These dates and others obtained during the present study are shown in figure 179.

The regional paleoclimate has been reconstructed using geologic evidence from many sites, including Lake Theo, where chronostratigraphic control is excellent. Cool, wet, equable conditions prevailed across the Southern High Plains and contiguous Rolling Plains during the late Pleistocene Epoch. Much of the western Rolling Plains was aggrading owing to rapid deposition of coarse sands and gravels with weakly developed soils (basal component of Caran and Baumgardner, this volume). Similar sediments with more strongly developed soils were accumulating along major drainages on the High Plains (Wendorf, 1961). Palynological analyses of some of these deposits show that mixed hardwood-conifer woodlands had undergone moderate expansion across the plains of North Texas (compare with Oldfield and Schoenwetter, 1964; 1970).

The expansion of woodlands influenced the composition of late Wisconsinan molluscan faunas studied by Pierce (1975), Neck (1978), and Johnson and others (1982). The faunas include many terrestrial gastropods now found far to the north, east, or at higher elevations to the west of the Southern High Plains, and most of these require a cool, moist climate and partial woodland cover. Relatively cool, moist conditions and accessible woodland habitats also were favored by Pleistocene mammals (Rancholabrean fauna) of the region, including a mixture of extinct grazers and large browsers (notably Equus cf. E. conversidens, Bison antiquus, Camelops sp., and at least one proboscidean), as well as a moderately diverse component of microvertebrates that today have divergent ranges

(Dalquest, 1964, 1965; Black, 1974; Harrison and Killen, 1978; Johnson and others, 1982). Artifacts of Paleoindians (Clovis culture) have been found at a few sites in association with the remains of extinct late Pleistocene mammals (Haynes, 1964; Black, 1974).

Beginning 11,000 to 13,000 yr ago, the regional paleoclimate began to change, becoming considerably warmer and slightly drier. By about 8,000 yr ago, the area may have been almost as warm as under modern climatic conditions. Evidence of this trend is seen in the rapid disappearance of most northern and western (montane) elements of the molluscan fauna and a corresponding increase in taxa with a more southerly range (Pierce, 1975; Johnson and others, 1982). Woodlands were reduced and the extinction or extirpation of much of the Rancholabrean fauna was complete by about 8,000 yr ago (Johnson and others, 1982). Beard (1973) independently defined essentially the same climatic chronology on the basis of replacement of cold-water planktonic foraminifera by a warm-water fauna throughout the Gulf of Mexico. On the Rolling Plains, the prevalence of lacustrine deposits dating from this period indicates the continuing availability of moisture. Beds of diatomite (deposited in perennial fresh-water lakes and marshes) at a number of localities on the High Plains (Sellards, 1952; Johnson, 1974) may be synchronous with strata of lacustrine origin in the Rolling Plains. Artifacts of Folsom and Plainview types have been found in these and correlative deposits. The climate of this interval essentially corresponds to the "Twocreekan" and "Greatlakean" climatic episodes (Evenson and others, 1976) and possibly to the San Jon Pluvial climate (Judson, 1953; Wendorf, 1961).

From 8,000 to at least 5,000 and probably 3,000 yr ago, the climate grew steadily warmer and much drier (Hypsithermal climatic episode), with perhaps one or more brief intervals of more moderate conditions (Holliday, 1982). The dry conditions eliminated those few lingering northern and eastern components of the early Holocene molluscan fauna, some of which might have tolerated the high temperatures if conditions had remained wet (Pierce, 1975; Neck, 1978). The vertebrates, too, were reduced essentially to the modern, indigenous fauna by 5,000 yr ago (Johnson and others, 1982). Deposition was

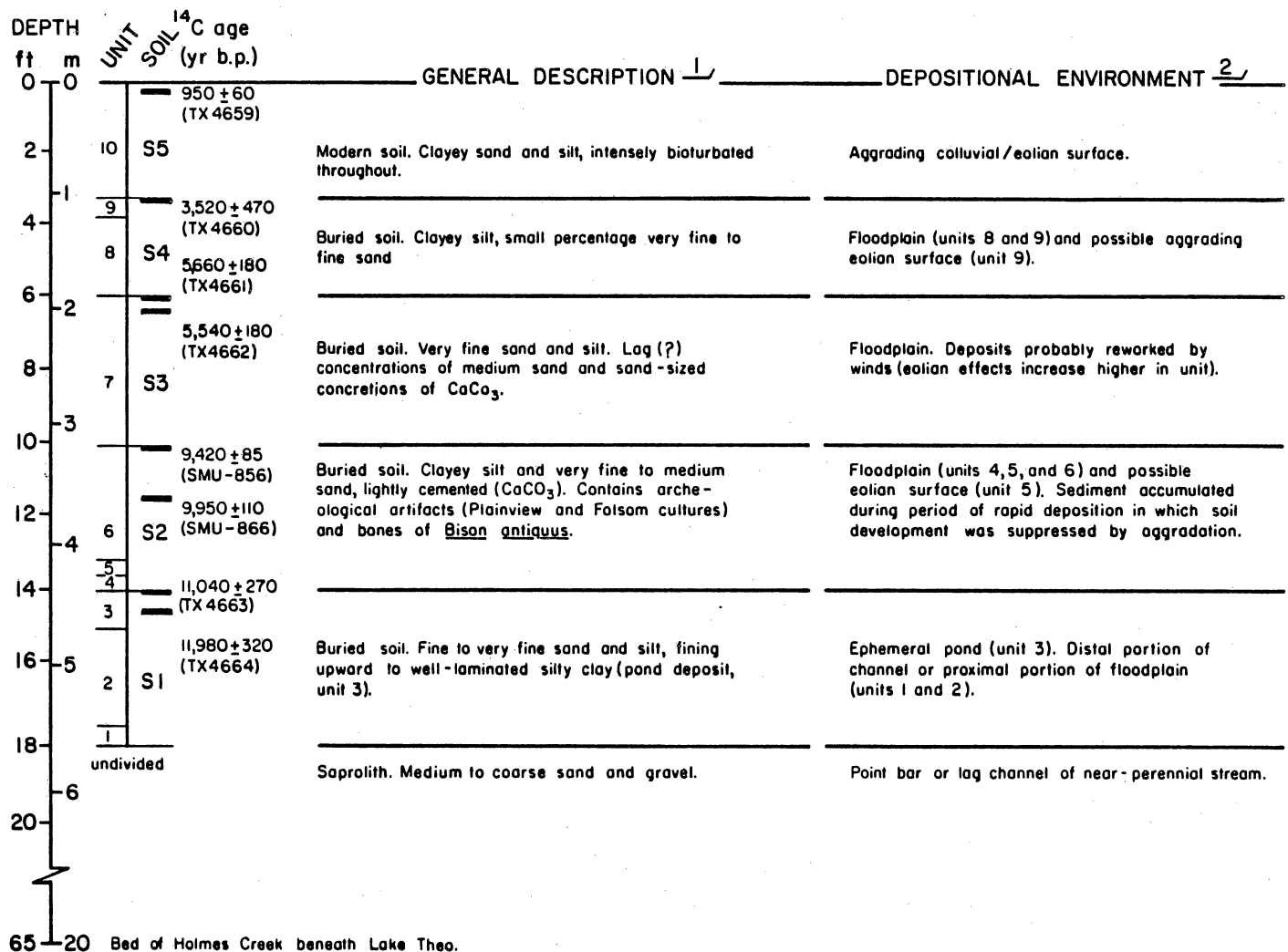


intermittent, as suggested by the stacking of moderately to strongly developed paleosols in many sections (Caran and Baumgardner, this volume). Waning fluvial activity (within confined channels probably corresponding very nearly to the modern drainage network), erosion, and eolian winnowing and deposition, as well as pedogenesis, clearly are in evidence in the upper part of the section at Lake Theo (fig. 179) and elsewhere throughout the Rolling Plains and High Plains (Holliday, 1983; Caran and McGookey, 1983).

During the period from 3,000 yr ago to the present, the prevailing climate (extended "Neoglacial" climatic episode and modern climate) has been very similar to that of today except for two intervals. These exceptions, discussed below, appear to have been temporary excursions from relatively stable conditions. Uplands throughout the region were dominated by eolian deposition, whereas denudation and incision may have increased within the valleys. Other than effects of human activity (extirpation and introduction of species), particularly since the middle 1800's, the fauna and flora of the region have undergone no major changes. Yet from about 2,600 to 1,000 yr ago, precipitation increased at least locally (Hall, 1982a and b; 1983). As a result, the range of some mesic hardwoods and relict colonies of small mammals (particularly Microtus ochrogaster) was maintained or even slightly extended. These colonies disappeared at the beginning of the present millenium. The range of drought-intolerant woody plants also was reduced such that today mesic flora are restricted to riparian corridors along major streams and to sheltered canyons with ample seepage. A second respite may have occurred during the "Little Ice Age" from about 650 to 150 yr ago, when temperatures were lower and effective moisture, if not precipitation, presumably increased. The temporarily colder temperatures may have eliminated one species from the molluscan fauna of the region, but this is uncertain (Neck, 1978).

The nature, distribution, and magnitude of climatic fluctuations during the last 15,000 yr have striking implications for the geologically foreseeable future. Global temperatures have varied cyclically at intervals of 10,000 to 30,000 yr since late

Sangamonian time (Kukla and others, 1981). This history is very similar to the preliminary reconstruction developed for the High Plains of Texas, as summarized by Caran and McGookey (1983). However, lesser changes have occurred much more frequently and erratically, and even these have had a significant effect on deposition, erosion, and the moisture available for infiltration and recharge. On this basis, significant deviation from the present climate could occur within 10,000 yr and probably should be expected within 20,000 yr. The magnitude of these changes would probably approximate that of fluctuations inferred from the late Quaternary record of northwestern Texas. But the rate and direction (warmer or cooler, drier or wetter) of climatic changes are difficult to predict, particularly when considering the possible effects of human enterprises over that period, such as deliberate or unintended manipulation of weather. A detailed reconstruction of the regional paleoclimate, emphasizing the record of late Pleistocene to Holocene events, would provide a reliable basis from which to develop alternate climatic scenarios for the future.



<sup>1</sup> For more detailed description see Johnson and others (1982).  
<sup>2</sup> From Caran and McGookey (1983)

QA-1700

Figure 179. Generalized measured section through late Quaternary deposits, Lake Theo archeological site (site number 41BI70), Caprock Canyons State Park, southeastern Briscoe County, Texas. Radiocarbon analyses performed at Southern Methodist University (SMU-856 and -866) were reported by Johnson and others (1982). All other analyses of radiocarbon were performed at The University of Texas Radiocarbon Laboratory (TX4659 to 4664) and have not been published previously.

## HISTORIC SEISMICITY IN AND AROUND THE TEXAS PANHANDLE

Wayne D. Pennington and Scott D. Davis

*At least 20 earthquakes have occurred in the Texas Panhandle north of 34°N since 1907. The largest earthquakes had magnitudes up to 4.8, and the maximum intensities throughout the Panhandle have ranged from IV to VI (Modified Mercalli), corresponding to accelerations from 6.8 cm/s<sup>2</sup> to more than 31.6 cm/s<sup>2</sup>.*

The record of seismicity in the Texas Panhandle dates from 1907, when the first reported event occurred near Amarillo. Since that time, numerous events have been reported or instrumentally recorded from the Panhandle. In the most complete survey of seismicity in the Panhandle (north of 34° latitude) to be undertaken, 20 earthquakes were identified from 1907 through April 1983. Slightly more than half of the events have locations determined from felt reports, and the others, from instrumental locations (fig. 180).

In the process of identifying earthquakes, reviewed contemporary newspaper accounts, weather bulletins, seismological reports, and other sources. Several reported events were found to be in error. Specifically, the published locations of some events are erroneous by tens or hundreds of kilometers; one event was in fact a sonic boom, and one "event" near the Panhandle resulted from spurious data reported from seismological observatories nearby.

The largest earthquakes in the Texas Panhandle had magnitudes of 4.7 to 4.8 (determined by maximum intensity and felt areas); there were five such events between 1917 and 1951. Since instrumental recording became widespread in about 1962, only two events of magnitude greater than 4.0 have occurred (table 31). Although some of the earthquakes reported have been assigned magnitudes of 3.0 or less, the detection threshold is probably considerably higher. As evidence, it is noted that a magnitude 3.4 event in 1983 would have been undetected by conventional procedures had there not been a specific interest in the modern seismicity. Because this interest did not exist until recently, it is

probable that many earthquakes of magnitudes up to 3.5 have gone unrecognized, and it is likely that some larger events have been missed as well.

All of the earthquakes in the Texas Panhandle appear at present to be natural and not induced. A high level of activity near Snyder, Texas (33°N, 101°W), south of the study area is clearly associated with injection of fluids for secondary recovery of hydrocarbons; at least 22 events with magnitude greater than 3.0 have occurred there since 1977. Although there are some injection fields in the Texas Panhandle, none of them appear to be associated with the seismicity. Current research suggests that under appropriate conditions extraction of gas can result in the same seismicity as that observed in the Gulf Coast region of Texas. The primary requirement of active growth faulting is absent in the Panhandle, and gas production will probably not influence seismicity there. Thus, most if not all of the seismicity in the Panhandle is apparently "natural."

The depths of earthquake hypocenters are unknown in all but one case. The 1974 Oklahoma-Texas border event probably lies at  $10 \pm 3$  km (Herrmann, 1979), placing it in the "basement" rock. Comparisons of felt areas of other events with the 1974 event, the 3-km-deep Snyder event of 1978, and other Central United States earthquakes for which depths are known, suggest that most Panhandle earthquakes are 3 to 15 km deep and may be either in the basement or in sedimentary structures above it. Several basement structural features are possible sources of Panhandle seismicity, particularly those associated with the Amarillo Uplift, but the specific features that may be responsible for the seismicity are unknown.

At least six earthquakes in neighboring regions with Modified Mercalli Intensities of up to V have been felt in the Texas Panhandle. Some Texas wells were damaged by the 1964 Alaskan earthquake (Miller and Redell, 1964). A final hazard assessment for any Panhandle waste repository site must include possible effects of regional earthquakes and of local seismic events.

A preliminary map has been prepared (fig. 181), showing the maximum intensities (Modified Mercalli) felt throughout the Texas Panhandle since 1907. In this map, isoseismal lines were drawn for all felt earthquakes in and near the Panhandle; we interpolated between points where necessary. In addition, some reports of anomalously high-intensity events were discarded when the reports appeared isolated within a region of consistently lower intensity reports for the same event.

A site-specific hazard assessment requires further work, but a simple evaluation of the maximum accelerations that occurred throughout the Panhandle during the last 76 years can be performed, utilizing a simple intensity-acceleration function (Richter, 1958; p. 140):

$$\log a = \frac{I}{3} - \frac{1}{2}$$

The accelerations corresponding to specific intensities observed in the Panhandle range from 6.8 cm/s<sup>2</sup> to more than 31.6 cm/s<sup>2</sup>. More detailed estimates of expected accelerations should be performed using specific attenuation laws appropriate for the High Plains and for specific active features when they can be identified.

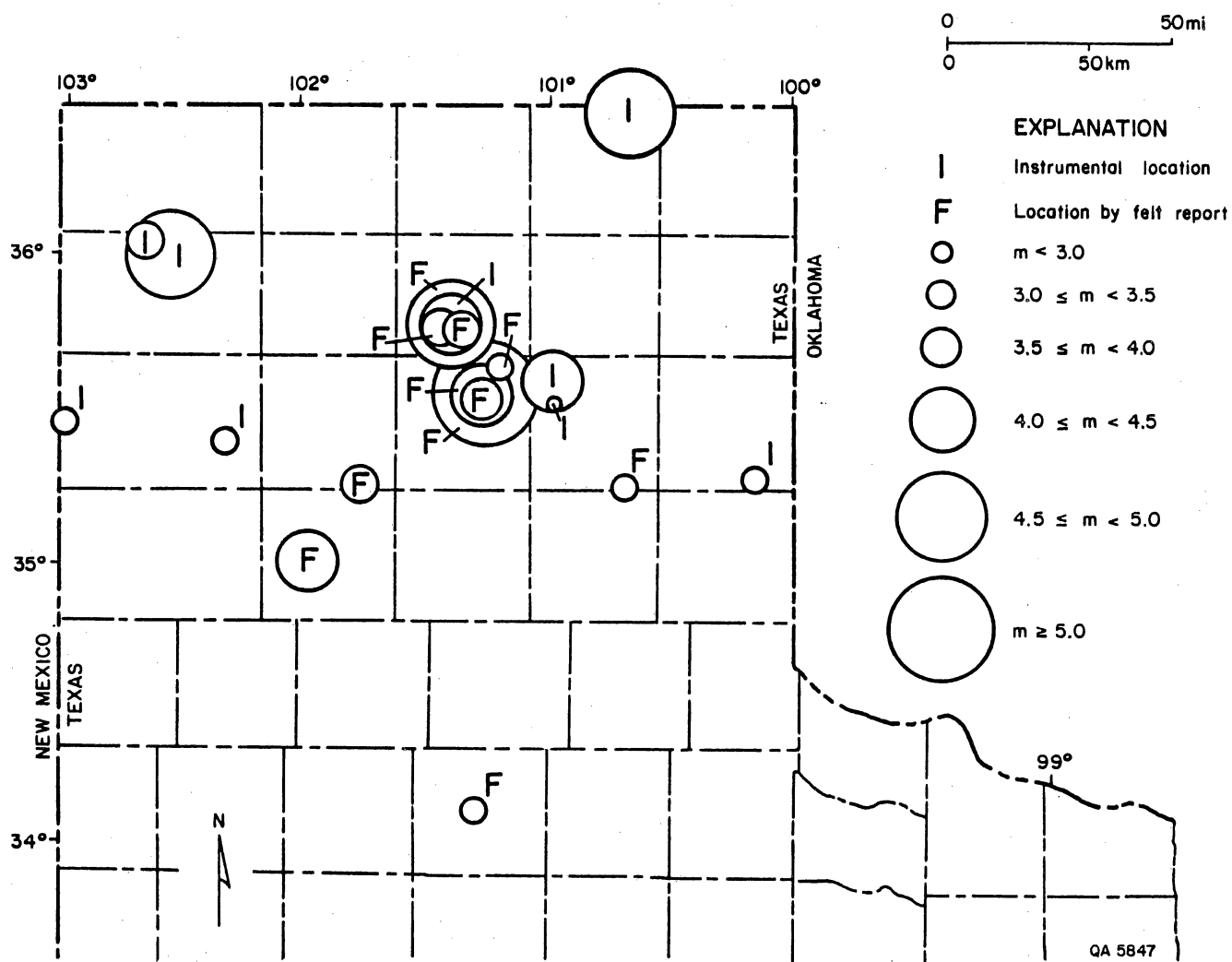


Figure 180. Epicentral locations, Texas Panhandle and vicinity.

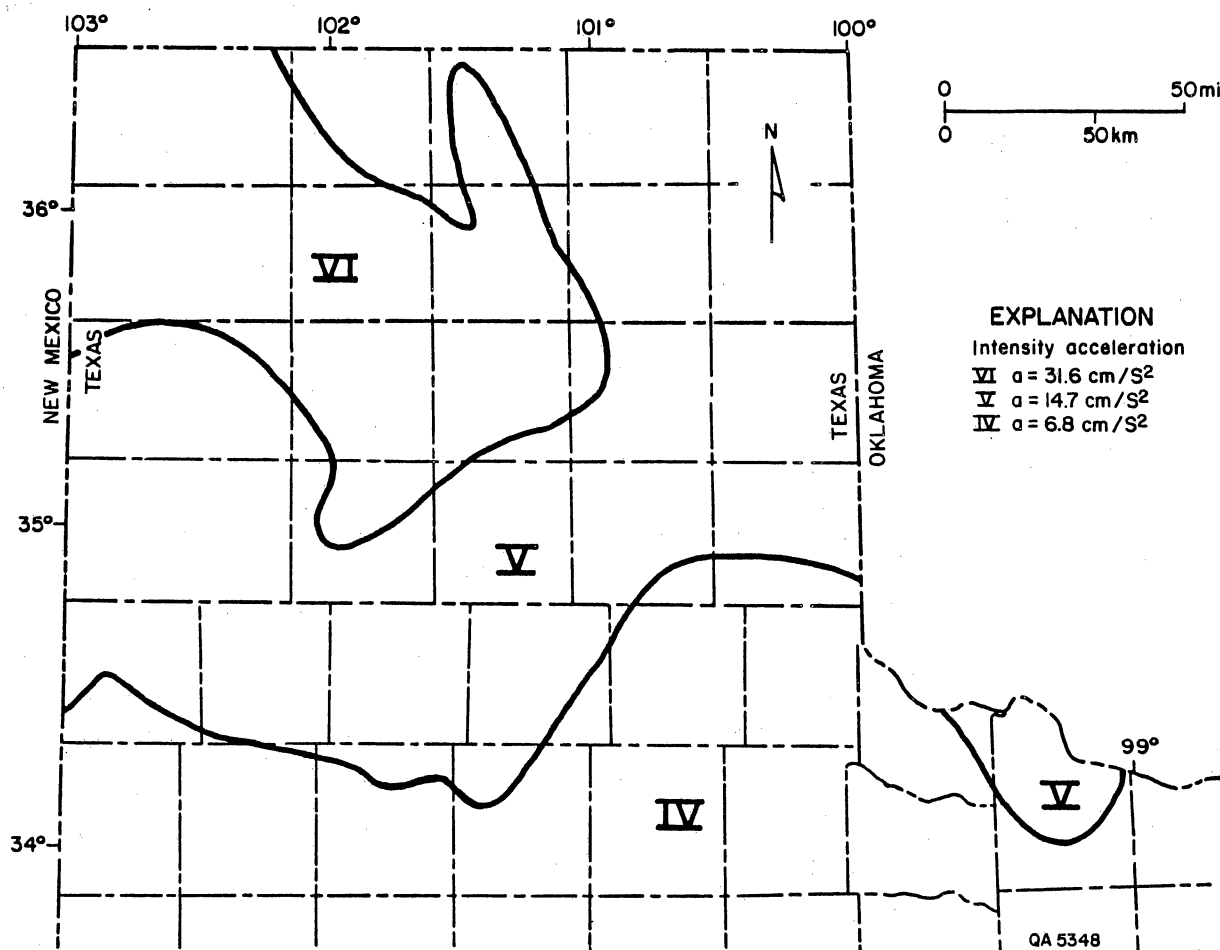


Figure 181. Maximum seismic intensities (modified Mercalli) in the Texas Panhandle from earthquakes in the Panhandle and nearby regions. Maximum accelerations are indicated, making use of the relationship

$$\log a = \frac{I}{3} - \frac{1}{2} \quad (\text{Richter, 1958; p. 140}).$$



Table 31. Historical seismicity of the Texas Panhandle in the area bounded by 100°W-103°W, 34°N-36.5°N; 1907 to April 1983.

Year	Month	Day	Origin time (UTC)	Latitude °N	Longitude °W	F/I	Magnitude	Felt area (km <sup>2</sup> )	MMI	General location
1907	04		00	35.2	101.8	F	3.6		V	Amarillo
1917	03	28	19:56	35.4	101.3	F	4.2	5,000	VI	Panhandle
1925	07	29	11:30	34.5	101.2	F	3.3		IV	Silverton
1925	07	30	08	35.4	101.3	F	3.5		III-IV	Panhandle
1925	07	30	12:17	35.4	101.3	F	5.1	700,000	VI	Panhandle
1925	07	31	18	35.5	101.1	F	3.0		III	White Deer
1936	06	19	21	35.2	100.7	F	3.0	>600	III	Clarendon
1936	06	20	03:13:37	35.7	101.4	F	3.92	23,000	III-IV	Borger
1936	06	20	03:18:27	35.7	101.4	F	3.9	23,000	III-IV	Borger
1936	06	20	03:24:06	35.7	101.4	F	4.8	110,000	VI	Borger
1948	03	12	04:29:00	36.0	102.5	I	4.9	300,000	VI	Dalhart
1951	06	20	18:37:10	35.0	102.0	F	4.4	65,000	V	Amarillo
1966	04	21	14:14:12	35.4	103.0	I	3.4			TX-NM border
1966	07	20	09:04:58.4	35.7	101.2	I	4.2	30,000	V	Borger
1974	02	15	13:33:49.2	36.5	100.7	I	4.5	120,000	V	OK-TX border
1980	02	21	20:42:02	35.3	101.1	I	2.9			Pampa
1980	06	09	22:37:10	35.5	101.1	I	4.3	44,000	V	Pampa
1982	10	14	12:52:46	36.1	102.6	I	3.9	8,200	III	Dalhart
1982	11	07	00:04:19	35.2	100.2	I	3.1			Wheeler County
1983	04	03	04:55:24	35.32	102.38	I	3.4			Oldham County

F = Location determined by felt reports

I = Location determined instrumentally

MMI = Maximum Modified Mercalli intensity

UTC = Coordinated Universal Time

## REFERENCES

- Ahlbrandt, T. S., 1979, Textural parameters of eolian deposits, in A study of global sand seas: U.S. Geological Survey Professional Paper 1052, p. 21-51.
- Ahlbrandt, T. S., and Fryberger, S. G., 1981, Sedimentary features and significance of interdune deposits, in Ethridge, F. G., and Flores, R. M., eds., Recent and ancient nonmarine depositional environments: models for exploration: Society of Economic Paleontologists and Mineralogists Special Publication 31, p. 293-314.
- American Society for Testing and Materials, 1979, Standard method for collection and analysis of dustfall (settleable particulates): ASTM D1739-70, Annual Book of ASTM Standards, Part 23, p. 536-539.
- Angino, E. E., and Hambleton, W. W., 1971, Final report: geology and hydrology of the proposed Lyons, Kansas, radioactive waste repository site: AEC/UC Subcontract 3484, March 1971.
- Aydin, A., and Nur, A., 1982, Evolution of pull-apart basins and their scale independence: Tectonics, v. 1, no. 1, p. 91-105.
- Baker, C. L., 1915, Geology and underground waters of the northern Llano Estacado: University of Texas, Austin, Bureau of Economic Geology, Bulletin 57, 225 p.
- Baldwin, B., and Muehlberger, W. R., 1959, Geologic studies of Union County, New Mexico: New Mexico Bureau of Mines and Mineral Resources Bulletin 63, 171 p.
- Barnes, V. E., and Eifler, G. K., 1968, Geologic atlas of Texas, Plainview sheet: The University of Texas at Austin, Bureau of Economic Geology, scale 1:250,000.
- Barrett, M. E., and Kirschner, C. E., 1979, Depositional systems in the Rinconada Formation (Precambrian), Taos County, New Mexico: New Mexico Geological Society Guidebook, 20th field conference, p. 121-126.
- Bassett, R. L., and Bentley, M. E., 1983, Deep brine aquifers in the Palo Duro Basin: regional flow and geochemical constraints: The University of Texas at Austin, Bureau of Economic Geology Report of Investigations No. 130, 59 p.

- Bassett, R. L., and Palmer, D. P., 1981, Clay mineralogy of Permian evaporites, Palo Duro Basin, Texas Panhandle, in Gustavson, T. C., and others, Geology and geohydrology of the Palo Duro Basin, Texas Panhandle, a report on the progress of nuclear waste isolation feasibility studies (1980): The University of Texas at Austin, Bureau of Economic Geology Geological Circular 81-3, p. 108-118.
- Bassett, R. L., and Roedder, E., 1981, Water content of Palo Duro salt, Randall and Swisher County cores, in Gustavson, T. C., and others, Geology and geohydrology of the Palo Duro Basin, Texas Panhandle, a report on the progress of nuclear waste isolation feasibility studies (1980): The University of Texas at Austin, Bureau of Economic Geology Geological Circular 81-3, p. 119-122.
- Bassett, W. A., 1959, The origin of the vermiculite deposit at Libby, Montana: American Mineralogist, v. 44, p. 282-299.
- Baumgardner, R. W., Jr., Hoadley, A. D., and Goldstein, A. G., 1982, Formation of the Wink Sink, a salt dissolution and collapse feature: The University of Texas at Austin, Bureau of Economic Geology Report of Investigations No. 114, 38 p.
- Beard, J. H., 1973, Pleistocene-Holocene boundary and Wisconsinan substages, Gulf of Mexico: Geological Society of America Memoir 136, p. 277-316.
- Bentley, M. E., 1981, Regional hydraulics of brine aquifers, Palo Duro and Dalhart Basins, Texas, in Gustavson, T. C., and others, Geology and geohydrology of the Palo Duro Basin, Texas Panhandle, a report on the progress of nuclear waste isolation feasibility studies (1980): The University of Texas at Austin, Bureau of Economic Geology Geological Circular 81-3, p. 93-101.
- Black, C. C., ed., 1974, History and prehistory of Lubbock Lake site: Lubbock, West Texas Museum Association, The Museum Journal, v. 15, p. 1-160.
- Blalock, H. M., Jr., 1972, Social statistics: New York, McGraw-Hill, 582 p.
- Bomar, G. W., 1983, Texas weather: Austin, University of Texas Press, 265 p.

- Bond, D. C., 1972, Hydrodynamics in deep aquifers of the Illinois basin: Illinois State Geological Survey Circular 470, 51 p.
- Boone, J. L., 1979, Lake margin depositional systems of the Dockum Group (Upper Triassic) in Tule Canyon, Texas Panhandle: The University of Texas at Austin, Master's thesis, 147 p.
- Borneman, E., and Doveton, J. H., 1983, Lithofacies mapping of Viola Limestone in south-central Kansas, based on wireline logs: American Association of Petroleum Geologists Bulletin, v. 67, no. 4, p. 609-623.
- Bowen, A. J., and Findley, D., 1974, Measurements of the mean wind flow over various escarpment shapes, in Proceedings, Fifth Australasian Conference on Hydraulics and Fluid Mechanics: New Zealand, University of Canterbury, p. 211-223.
- Bramlette, M. N., 1929, Natural etching of detrital garnet: American Mineralogist, v. 14, p. 336-337.
- Brune, G., 1981, Springs of Texas, vol. 1: Branch-Smith Inc., Fort Worth, Texas, 566 p.
- Bruning, J. L., and Kintz, B. L., 1977, Computational handbook of statistics: Glenview, Ill., Scott, Foresman, and Company, 308 p.
- Buck, A., Burkers, J. P., and Rhoderick, J. E., 1981, Examination of ERDA-10 grout specimens at different ages: ONWI-341 Technical Report, 25 p.
- Budnik, R. T., and Smith, Dale, 1982, Regional stratigraphic framework of the Texas Panhandle, in Gustavson, T. C., and others, Geology and geohydrology of the Palo Duro Basin, Texas Panhandle, a report on the progress of nuclear waste isolation feasibility studies (1981): The University of Texas at Austin, Bureau of Economic Geology Geological Circular 82-7, p. 38-86.
- Bureau of Economic Geology, 1982, Site characterization report, section 5.7.3 isotopic and regional hydrochemistry: Submitted to DOE 10-26-82 under contract number DE-AC97- 80ET46615, p. 33-42.

- \_\_\_\_\_ 1983a, Characterization status report, section 5.7.3 isotopic and regional hydro-chemistry: Submitted to DOE 2-28-83 under contract number DE-AC97-83WM46651, p. 10-11.
- \_\_\_\_\_ 1983b, Characterization status report, section 5.6.3 potentiometric levels: Submitted to DOE 2-28-83 under contract number DE-AC97-83WM46651, p. 9.
- Burke, J. A., Schmidt, A. W., and Campbell, R. L., Jr., 1969, The litho-porosity cross plot--a method of determining rock characteristics for computation of log data: *The Log Analyst*, v. 10, no. 6, p. 25-43.
- Campbell, I. A., and Honsaker, J. L., 1982, Variability in badlands erosion; problems of scale and threshold identification, in Thorn, C. E., ed., *Space and time in geomorphology*: Boston, Binghamton Symposia in Geomorphology, International Series No. 12, Allen and Unwin, 379 p.
- Caran, S. C., and Baumgardner, R. W., Jr., 1985, Radiocarbon age of Quaternary deposits, western Rolling Plains of Texas: The University of Texas at Austin, Bureau of Economic Geology Open-File Report WTWI-OF-1985-1, 6 p.
- Caran, S. C., and McGookey, D. A., 1983, Quaternary paleoclimatology of the Texas High Plains--preliminary summary, in Gustavson, T. C., and others, *Geology and geohydrology of the Palo Duro Basin, Texas Panhandle, a report on the progress of nuclear waste isolation feasibility studies (1982)*: The University of Texas at Austin, Bureau of Economic Geology Geological Circular 83-4, p. 142-146.
- Carroll, D., 1969, *Clay minerals: a guide to their X-ray identification*: Geological Society of America Special Paper 126, 80 p.
- Chapin, C. E., and Seager, W. R., 1975, Evolution of the Rio Grande Rift in the Socorro and Las Cruces areas, in Seager, W. R., Clemms, R. E., and Callender, J. F., eds., *Las Cruces Country: New Mexico Geological Society Guidebook, 26th field conference*, p. 237-321.

- Cheney, M. G., Dott, R. H., Hake, B. F., Moore, R. C., Newell, N. D., Thomas, H. D., and Tomlinson, C. W., 1945, Classification of Mississippian and Pennsylvanian rocks of North America: American Association of Petroleum Geologists Bulletin, v. 29, p. 125-169.
- Christensen, C. L., and Peterson, E. W., 1981, The Bell Canyon test summary report: Sandia National Laboratories Report SAND80-1375, 53 p.
- Collins, E. W., 1983a, Joints and joint densities at Caprock Canyons State Park, Briscoe County, Texas Panhandle (abs.): Geological Society of America, Abstracts with Programs, v. 15, no. 1, p. 3.
- \_\_\_\_\_, 1983b, Joint density of Permian strata at Caprock Canyons State Park, Briscoe County, Texas Panhandle, in Gustavson, T. C., and others, Geology and geohydrology of the Palo Duro Basin, Texas Panhandle, a report on the progress of nuclear waste isolation feasibility studies (1982): The University of Texas at Austin, Bureau of Economic Geology Geological Circular 83-4, p. 36-40.
- Collinson, C. W., Rexroad, C. B., and Thompson, T. L., 1971, Conodont zonation of the North American Mississippian: Geological Society of America Memoir 127, p. 353-394.
- Collinson, C. W., Scott, A. J., and Rexroad, C. B., 1962, Six charts showing biostratigraphic zones and correlations based on conodonts from the Devonian and Mississippian rocks of the upper Mississippi Valley: Illinois Geological Survey Circular 328, 32 p.
- Culler, F. L., 1971, Technical status of the radioactive waste repository--a demonstration project for solid radioactive waste disposal: ORNL Contract Report No. 4680, p. 34-36.
- Cunningham, B. J., 1969, Identification and division of the pre-Pennsylvanian sediments--western Anadarko Basin, in Pre-Pennsylvanian geology of the western Anadarko Basin: Panhandle Geological Society, p. 7-26.

- Dalquest, W. W., 1964, A new Pleistocene local fauna from Motley County, Texas: Kansas Academy of Science Transactions, v. 67, no. 3, p. 499-505.
- \_\_\_\_\_ 1965, New Pleistocene formation and local fauna from Hardeman County, Texas: Journal of Paleontology, v. 39, no. 1, p. 63-79.
- Dott, R. H., 1941, Regional stratigraphy of mid-continent: American Association of Petroleum Geologists Bulletin, v. 25, p. 1619-1705.
- Douglas, L. A., 1977, Vermiculites, in Dixon, J. B., and Weed, S. B., eds., Minerals in soil environments: Madison, Soil Science Society of America, p. 259-292.
- Dunbar, C. O., and others, 1960, Correlation of the Permian formations of North America: Geological Society of America Bulletin, v. 71, p. 1763-1806.
- Dutro, J. T., Jr., Gordon, M., Jr., and Huddle, J. W., 1979, Paleontological zonation of the Mississippian System, in Craig, L. C., and Connor, C. W., Paleotectonic investigations of the Mississippian system in the United States: U.S. Geological Survey Professional Paper 1010 S, p. 407-429.
- Dutton, A. R., 1983, Regional ground-water flow system of the San Andres Formation, West Texas and eastern New Mexico, in Gustavson, T. C., and others, Geology and geohydrology of the Palo Duro Basin, Texas Panhandle, a report on the progress of nuclear waste isolation feasibility studies (1982): The University of Texas at Austin, Bureau of Economic Geology Geological Circular 83-4, p. 97-101.
- Dutton, A. R., 1985, Hydrologic testing in the salt-dissolution zone of the Palo Duro Basin, Texas Panhandle: The University of Texas at Austin, Bureau of Economic Geology, Open-File Report OF-WTWI-1985-35 prepared for the U.S. Department of Energy under contract no. DE-AC97-83WM46651, 31 p.
- Dutton, A. R., and Orr, E. D., 1985, Hydrogeology and hydrochemical facies of the San Andres Formation in eastern New Mexico and the Texas Panhandle: The University of Texas at Austin, Bureau of Economic Geology Open-File Report OF-WTWI-1985-2.

- Dutton, S. P., 1980a, Depositional systems and hydrocarbon resource potential of the Pennsylvanian System, Palo Duro and Dalhart Basins, Texas Panhandle: The University of Texas at Austin, Bureau of Economic Geology Geological Circular 80-8, 49 p.
- \_\_\_\_\_ 1980b, Petroleum source rock potential and thermal maturity, Palo Duro Basin, Texas: The University of Texas at Austin, Bureau of Economic Geology Geological Circular 80-10, 48 p.
- Dutton, S. P., Goldstein, A. G., and Ruppel, S. C., 1982, Petroleum potential of the Palo Duro Basin, Texas Panhandle: The University of Texas at Austin, Bureau of Economic Geology Report of Investigations No. 123, 87 p.
- Eaton, G., 1980, Geophysical and geological characteristics of the crust of the Basin and Range province, in Burchfiel, B. C., Oliver, J. E., and Silver, L. T., panel chairmen, Continental tectonics: The National Research Council, p. 96-113.
- Emmett, W. W., 1965, The Vigil Network: methods of measurement and a sampling of data collected: IASH Publication 66, p. 89-106.
- Epstein, A. G., Epstein, J. B., and Harris, L. D., 1977, Conodont color alteration--an index to organic metamorphism: U. S. Geological Survey Professional Paper 995, 27 p.
- Evenson, E. B., Farrand, W. R., Eschman, D. F., Mickelson, D. M., and Maher, L. J., 1976, Greatlakean substage--a replacement for Valderan substage in the Lake Michigan Basin: Quaternary Research, v. 6, p. 411-424.
- Fader, S. W., 1975, Land subsidence caused by dissolution of salt near four oil and gas wells in central Kansas: U.S. Geological Survey, Water Research Investigations 27-75, 28 p.
- Federal Interagency River Basin Committee, 1953, Summary of reservoir sedimentation surveys for the United States through 1950: Washington, D.C., Subcommittee on Sedimentation, Sedimentation Bulletin 5, 31 p.



- Fertl, W. H., 1981, Openhole crossplot concepts--a powerful technique in well log analysis: *Journal of Petroleum Technology*, v. 33, no. 3, p. 535-549.
- Finley, R. J., and Baumgardner, R. W., Jr., 1981, Sedimentology and basin morphometry of the Little Red River Basin: insights into retreat of the Eastern Caprock Escarpment, Texas Panhandle, in Gustavson, T. C., and others, Geology and geohydrology of the Palo Duro Basin, Texas Panhandle, a report on the progress of nuclear waste isolation feasibility studies (1980): Bureau of Economic Geology Geological Circular 81-3, p. 148-151.
- Finley, R. J., and Gustavson, T. C., 1980, Climatic controls on erosion in the Rolling Plains and along the Caprock Escarpment of the Texas Panhandle: The University of Texas at Austin, Bureau of Economic Geology Geological Circular 80-11, 50 p.
- \_\_\_\_\_ 1981, Lineament analysis based on Landsat imagery, Texas Panhandle: The University of Texas at Austin, Bureau of Economic Geology Geological Circular 81-5, 37 p.
- \_\_\_\_\_ 1982, Geomorphic effects of a 10-year storm on a small drainage basin in the Texas Panhandle: *Earth Surface Processes and Landforms*, v. 8, p. 63-77.
- Finley, R. J., and Howard, R. C., 1981, Slope process monitoring and data analysis, Texas Panhandle, in Gustavson, T. C., and others, Geology and geohydrology of the Palo Duro Basin, Texas Panhandle, a report on the progress of nuclear waste isolation feasibility studies (1980): The University of Texas at Austin, Bureau of Economic Geology Geological Circular 81-3, p. 144-147.
- Fisher, R. S., and Kreidler, C. W., 1983, Bromide content of halite in core from Upper and Lower San Andres, Glorieta, and Upper and Lower Clear Fork Formations, DOE -Gruy Federal No. 1 Rex White Well, Randall County, Texas, in Gustavson, T. C., and others, Geology and geohydrology of the Palo Duro Basin, Texas Panhandle, a report on the progress of nuclear waste isolation feasibility studies (1982): The University of Texas at Austin, Bureau of Economic Geology Geological Circular 83-4.

- Flawn, P. T., 1956, Basement rocks of Texas and southeast New Mexico: University of Texas, Austin, Bureau of Economic Geology Publication 5605, 261 p.
- Flawn, P. T., Goldstein, August, Jr., King, P. B., and Weaver, C. E., 1961, The Ouachita System: University of Texas, Austin, Bureau of Economic Geology Publication 6120, 401 p.
- Fogg, G. E., and Senger, R. K., 1985, Automatic generation of ground-water flow nets using numerical models, *Ground Water*, v. 23, no. 3, p. 336-344.
- Folk, R. L., 1966, A review of grain-size parameters: *Sedimentology*, v. 6, p. 73-93.
- \_\_\_\_\_ 1971, Longitudinal dunes of the northwestern edge of the Simpson desert, Northern Territory, Australia, 1. Geomorphology and grain size relationships: *Sedimentology*, v. 16, p. 5-54.
- \_\_\_\_\_ 1974, Petrology of sedimentary rocks: Austin, Hemphill Publishing Company, 182 p.
- Freeze, R. A., and Cherry, J. A., 1979, Ground water: Englewood Cliffs, New Jersey, Prentice-Hall, 604 p.
- Friedman, G. M., 1979, Address of the retiring president of the International Association of Sedimentologists: differences in size distributions of populations of particles among sands of various origins: *Sedimentology*, v. 26, p. 3-32.
- Frye, J. C., and Leonard, A. B., 1963, Pleistocene geology of the Red River Basin in Texas: University of Texas, Austin, Bureau of Economic Geology Report of Investigations No. 49, 37 p.
- GeoChem Laboratories, Inc., 1980, Source rock evaluation reference manual: Houston, Texas, commercial brochure.
- Girdner, C. L., Richardson, W. E., Rivers, E. D., Reed, G. L., Green, J. W., Lowe, D. R., and Nix, S. B., 1963, Soil survey of Bailey County, Texas: U.S. Department of Agriculture, Soil Conservation Service, Series 1959, No. 21, 67 p.

- Goldstein, A. G., 1982, Brittle deformation associated with salt dissolution, Palo Duro Basin, in Gustavson, T. C., and others, Geology and geohydrology of the Palo Duro Basin, Texas Panhandle: a report on the progress of nuclear waste isolation feasibility studies (1981): The University of Texas at Austin, Bureau of Economic Geology Geological Circular 82-7, p. 18-27.
- Goldstein, A. G., and Collins, E. W., 1984, Deformation of Permian strata overlying a zone of salt dissolution and collapse in the Texas Panhandle: *Geology*, v. 12, no. 5, p. 314-317.
- Gonzalez, R. A., and Woodward, C. A., 1973, Petrology and structure of Precambrian rocks of the Pedernal Hills, New Mexico: New Mexico Geological Society Guidebook, 23rd field conference, p. 144-147.
- Grambling, J. A., 1979, Precambrian geology of the Truchas Peaks region, north-central New Mexico, and some regional implications: New Mexico Geological Society Guidebook, 30th field conference, p. 135-143.
- Granata, G. E., 1981, Regional sedimentation of the Late Triassic Dockum Group, west Texas and eastern New Mexico: The University of Texas at Austin, Master's thesis, 198 p.
- Gravenor, C. P., and Leavitt, R. K., 1981, Experimental formation and significance of etch patterns on detrital garnets: *Canadian Journal of Earth Sciences*, v. 18, p. 765-775.
- Gustavson, T. C., 1982, Structural control of major drainage elements surrounding the Southern High Plains, in Gustavson, T. C., and others, Geology and geohydrology of the Palo Duro Basin, Texas Panhandle, a report on the progress of nuclear waste isolation feasibility studies (1981): The University of Texas at Austin, Bureau of Economic Geology Geological Circular 82-7, p. 176-182.
- Gustavson, T. C., and Budnik, R. T., 1985, Structural influences on geomorphic processes, physiographic features, and lithofacies, Texas Panhandle, technical issues in the siting of a nuclear waste repository: *Geology*, v. 13, p. 173-176.

- Gustavson, T. C., and Finley, R. J., 1985, Late Cenozoic geomorphic evolution of the Texas Panhandle and northeastern New Mexico--case studies of structural controls on regional drainage development: The University of Texas at Austin, Bureau of Economic Geology Report of Investigations No. 148, 42 p.
- Gustavson, T. C., Finley, R. J., and Baumgardner, R. W., Jr., 1981a, Retreat of the Caprock Escarpment and denudation of the Rolling Plains in the Texas Panhandle: Association of Engineering Geologists Bulletin, v. 18, no. 4, p. 413-422.
- Gustavson, T. C., Finley, R. J., Goldstein, A. G., McGowen, J. H., Baumgardner, R. W., Jr., and Ramondetta, P. J., 1981b, Selected aspects of the geology of the Palo Duro Basin, Texas Panhandle: The University of Texas at Austin, Bureau of Economic Geology, unpublished Field Trip Guidebook, 31 p.
- Gustavson, T. C., Finley, R. J., and McGillis, K. A., 1980, Regional dissolution of Permian salt in the Anadarko, Dalhart, and Palo Duro Basins of the Texas Panhandle: The University of Texas at Austin, Bureau of Economic Geology Report of Investigations No. 106, 39 p.
- Gustavson, T. C., Hoadley, A. D., and Simpkins, W. W., 1981c, Salt dissolution and collapse along the margin of the Southern High Plains, in Gustavson, T. C., and others, Geology and geohydrology of the Palo Duro Basin, Texas Panhandle, a report on the progress of nuclear waste isolation feasibility studies (1980): The University of Texas at Austin, Bureau of Economic Geology Geological Circular No. 81-3, p. 131-137.
- Gustavson, T. C., Simpkins, W. W., Alhades, A., and Hoadley, A. D., 1982, Evaporite dissolution and development of karst features on the Rolling Plains of the Texas Panhandle: Earth Surface Processes and Landforms, v. 7, p. 545-563.
- Haan, C. T., and Johnson, H. P., 1966, Rapid determination of hypsometric curves: Geological Society of America Bulletin, v. 77, p. 123-126.
- Haigh, M. J., 1977, The use of erosion pins in the study of slope evolution: British Geomorphology Research Group Technical Bulletin, no. 18, p. 31-49.

- Hall, S. A., 1982a, Buried trees, water-table fluctuations, and past climates in western Oklahoma (abs.): Geological Society of America, Abstracts with Programs, v. 14, no. 3, p. 113.
- \_\_\_\_\_ 1982b, Late Holocene paleoecology of the Southern Plains: Quaternary Research, v. 17, p. 391-407.
- \_\_\_\_\_ 1983, Geology of the Holocene sediments and buried trees of Carnegie Canyon, in Lintz, Christopher, and Hall, S. A., The geomorphology and archeology of Carnegie Canyon.
- Hambleton, W. W., 1972, The unsolved problem of nuclear wastes: MIT Technology Review, March/April, p. 15-19.
- Handford, C. R., 1979, Lower Permian depositional systems, in Dutton, S. P., and others, Geology and geohydrology of the Palo Duro Basin, Texas Panhandle, a report on the progress of nuclear waste isolation feasibility studies (1978): The University of Texas at Austin, Bureau of Economic Geology Geological Circular 79-1, p. 26-38.
- \_\_\_\_\_ 1981, Bromide geochemistry of Permian halite in the Randall County core, in Gustavson, T. C., and others, Geology and geohydrology of the Palo Duro Basin, Texas Panhandle, a report on the progress of nuclear waste isolation feasibility studies (1980): The University of Texas at Austin, Bureau of Economic Geology Geological Circular 81-3, p. 75-81.
- Harrison, B. R., and Killen, K. L., 1978, Lake Theo--a stratified, early man bison butchering and camp site, Briscoe County, Texas (archeological investigations, phase 2): Canyon, Texas, Panhandle-Plains Historical Museum Special Archeological Report 1, 108 p.
- Haynes, C. V., 1964, Fluted projectile points--their age and dispersion: Science, v. 145, p. 1408-1413.
- Herrmann, R. B., 1979, Surface wave focal mechanisms for eastern North American earthquakes with tectonic implications: Journal of Geophysical Research 84, 3543-3552.

- Holliday, V. T., 1982, Mid-Holocene climate of the Southern High Plains--geologic evidence (abs.): American Quaternary Association, Seventh Biennial Conference, Program and Abstracts, p. 107.
- \_\_\_\_\_, 1983, Stratigraphy and soils of the Lubbock Lake landmark area, in Holliday, V. T., ed., Guidebook to the central Llano Estacado: Lubbock, Texas Tech University, International Center for Arid and Semi-Arid Land Studies and The Museum, p. 25-80.
- Holser, W. T., 1979, Trace elements and isotopes in evaporites, in Burns, R. G., ed., Marine minerals: Mineralogical Society of America Short Course Notes, v. 6, p. 295-346.
- Hovorka, S. D., 1983a, Carbonate-anhydrite-halite cycles, San Andres Formation (Permian), Palo Duro Basin, Texas, in Shaw, R. L., and Pollan, B. J., eds., Permian Basin cores-a workshop: Midland, Texas, PBS-SEPM Core Workshop No. 2, p. 197-224.
- \_\_\_\_\_, 1983b, Dissolution and recrystallization fabrics in halite and the timing of their development, in Gustavson, T. C., and others, Geology and geohydrology of the Palo Duro Basin, Texas Panhandle, a report on the progress of nuclear waste isolation feasibility studies (1982): The University of Texas at Austin, Bureau of Economic Geology Geological Circular 83-4, p. 58-65.
- Hoy, R. N., and Gross, G. W., 1982, A baseline study of oxygen 18 and deuterium in the Roswell, New Mexico groundwater basin: New Mexico Water Research Institute, Report 144.
- Hunt, J. M., 1979, Petroleum geochemistry and geology: San Francisco, W. H. Freeman, 617 p.
- Intera Environmental Consultants, 1981, Consequence assessment of hydrological communication through borehole plugs: Sandia Contractor Report, SAND81-7164, 25 p.
- Jachens, R. C., and Holzer, T. L., 1982, Differential compaction mechanism for earth fissures near Casa Grande, Arizona: Geological Society of America Bulletin, v. 93, no. 10, p. 998-1012.

- Johnson, C. S., 1974, Geologic investigations at the Lubbock Lake site, in Black, C. C., ed., History and prehistory of Lubbock Lake site: Lubbock, West Texas Museum Association, The Museum Journal, v. 15, p. 79-105.
- Johnson, Eileen, Holliday, V. T., and Neck, R. W., 1982, Lake Theo--late Quaternary environmental data and new Plainview (Paleoindian) date: North American Archeologist, v. 3, no. 2, p. 113-137.
- Johnson, K. S., 1979, Anomalous brines in Permian Flowerpot shale at Crowell Brine Dam, Red River Chloride Control Project area, North-Central Texas: submitted to U.S. Army Corps of Engineers, Tulsa District, Oklahoma.
- Johnson, W. C., 1965, Wind in the southwestern Great Plains: U.S. Department of Agriculture, Agricultural Research Service, Conservation Research Report No. 6, 65 p.
- Judson, H. E., 1953, Geology of the San Jon site, eastern New Mexico: Smithsonian Miscellaneous Collection, v. 121, no. 1, p. 1-70.
- Keith, M. L., and Anderson, G. M., 1963, Radiocarbon dating--fictitious results with mollusk shells: Science, v. 141, p. 634-637.
- Kelley, V. C., 1977, Geology of the Albuquerque basin, New Mexico: New Mexico Bureau of Mines and Mineral Resources, Memoir 33, 60 p.
- \_\_\_\_\_, 1979, Tectonics, middle Rio Grande Rift, New Mexico, in Riecker, R. E., ed., Rio Grande Rift: tectonics and magmatism: American Geophysical Union, p. 57-70.
- Kessler, E., Alexander, D. Y., and Rarick, J. F., 1978, Dust storms from the U.S. High Plains in late winter 1977--search for cause and implications: Proceedings of the Oklahoma Academy of Science, v. 58, p. 116-128.
- Kharaka, Y. K., and Barnes, I., 1973, SOLMNEQ: Solution-mineral equilibrium computations: NTIS Technical Report PB214-899, 82 p.
- King, P. B., 1942, Permian of West Texas and southeastern New Mexico: American Association of Petroleum Geologists Bulletin, v. 26, no. 4, p. 535-763.

- Kluth, P. B., and Coney, P. J., 1981, Plate tectonics of the Ancestral Rocky Mountains: *Geology*, v. 9, no. 1, p. 10-15.
- Knowles, T., Nordstrom, P., and Klemt, W. B., 1982, Evaluating the ground-water resources of the High Plains of Texas, final report: Texas Department of Water Resources, Publication LP-173, 4 v., 451 p.
- Kreitler, C. W., and Bassett, R. L., 1983, Chemical and isotopic composition of saline ground water and saline springs in the Rolling Plains east of the Ogallala Escarpment, in Gustavson, T. C., and others, *Geology and geohydrology of the Palo Duro Basin, Texas Panhandle, a report on the progress of nuclear waste isolation feasibility studies (1982)*: The University of Texas at Austin, Bureau of Economic Geology Geological Circular 83-4, p. 116-124.
- Kreitler, C. W., Fisher, R. S., Senger, R. K., Hovorka, S. D., and Dutton, A. R., 1985, Hydrology of an evaporite aquitard: Permian evaporite strata, Palo Duro Basin, Texas, in Simpson, E. S., Chairman, *Hydrogeology of rocks of low permeability: Proceedings, 17th International Congress, International Association of Hydrogeologists, January 7-12, 1985, Tucson, Arizona*, p. 150-168.
- Kukla, G., Berger, A., Lotti, R., and Brown, J., 1981, Orbital signature of interglacials: *Nature*, v. 290, p. 295-300.
- Lawrence, J. R., and Taylor, H. P., Jr., 1972, Hydrogen and oxygen systematics in weathering profiles: *Geochimica et Cosmochimica Acta*, v. 36, p. 1377-1393.
- MacCary, L. M., 1983, Geophysical logging in carbonate aquifers: *Ground Water*, v. 21, no. 3, p. 334-342.
- MacFadzean, T. B., 1973, Crossplotting--a neglected technique in log analysis: Society of Professional Well Log Analysts, 14th Annual Logging Symposium, Transactions, Section Y, p. 1-18.
- Mapel, W. J., Johnson, R. B., Bachman, G. O., and Varnes, K. L., 1979, Southern midcontinent and southern Rocky Mountains region, in *Paleotectonic investigations of*



- the Mississippian system in the United States: U.S. Geological Survey Professional Paper 1010 J, p. 161-187.
- McCauley, J. F., Breed, C. S., Grolier, M. J., and MacKinnon, D. J., 1981, The U.S. dust storm of February, 1977: Geological Society of America Special Paper 186, p. 123-147.
- McGillis, K. A., and Presley, M. W., 1981, Tansill, Salado, and Alibates Formations: Upper Permian evaporite/carbonate strata of the Texas Panhandle: The University of Texas at Austin, Bureau of Economic Geology Geological Circular 81-8, 31 p.
- McGookey, D. A., 1981, Application of Glorieta-Flowerpot facies analyses to map and distinguish between salt dissolution and facies transitions, western Amarillo Uplift and adjacent areas, in Gustavson, T. C., and others, Geology and geohydrology of the Palo Duro Basin, Texas Panhandle, a report on the progress of nuclear waste isolation feasibility studies (1980): The University of Texas at Austin, Bureau of Economic Geology Geological Circular 81-3, p. 156-165.
- McGookey, D. A., and Goldstein, A. G., 1982, Structural influence on deposition and deformation at the northwest margin of the Palo Duro Basin, in Gustavson, T. C., and others, Geology and geohydrology of the Palo Duro Basin, Texas Panhandle, a report on the progress of nuclear waste isolation feasibility studies (1981): The University of Texas at Austin, Bureau of Economic Geology Geological Circular 82-7, p. 28-37.
- McGookey, D. A., Gustavson, T. C., and Hoadley, A. D., 1985, Regional structural cross sections, Mid-Permian to Quaternary strata, Texas Panhandle and Eastern New Mexico: distribution of evaporites and areas of evaporite dissolution and collapse: The University of Texas at Austin, Bureau of Economic Geology Open-File Report OF-WTWI-1985-48, 20 p., 12 plates.
- McGowen, J. H., Granata, G. E., and Seni, S. J., 1979, Depositional framework of the lower Dockum Group (Triassic), Texas Panhandle: The University of Texas at Austin, Bureau of Economic Geology Report of Investigations No. 97, 60 p.

- McGowen, J. H., Seni, S. J., Andersen, R. L., and Thurwachter, J. E., 1980, Uranium resource evaluation, Lubbock Quadrangle, Texas: Prepared for the U.S. Department of Energy, Grand Junction, Colorado, Subcontract No. 78-133-E, 51 p.
- McKee, E. D., Crosby, E. J., Ferm, J. C., Keller, W. D., Schopf, J. M., Walker, T. R., Wanless, H. R., and Wright, C. R., 1975, Paleotectonic investigations of the Pennsylvanian System in the United States, part III, plates: U.S. Geological Survey Professional Paper 853.
- McLaren, Patrick, 1981, An interpretation of trends in grain size analysis: *Journal of Sedimentary Petrology*, v. 51, p. 611-624.
- McNeal, R. P., 1965, Hydrodynamics of the Permian Basin, in Young, A., and Galley, J. E., eds., *Fluids in subsurface environments*: American Association of Petroleum Geologists Memoir 4, p. 308-326.
- Miller, D. N., Jr., 1955, Hollow sanidine grains: stratigraphic marker for the Pierce Canyon Formation, West Texas and southeastern New Mexico: *Journal of Sedimentary Petrology*, v. 25, no. 3, p. 235-237.
- \_\_\_\_\_ 1966, Petrology of Pierce Canyon Redbeds, Delaware Basin, Texas and New Mexico: *American Association of Petroleum Geologists Bulletin*, v. 52, no. 2, p. 283-307.
- Miller, J. P., Montgomery, Arthur, and Sutherland, P. K., 1963, Geology of part of the southern Sangre de Cristo Mountains, New Mexico: New Mexico Bureau of Mines and Mineral Resources, Memoir 11, 106 p.
- Miller, W. D. and Redell, D. L., 1964, Alaskan earthquake damages Texas High Plains water wells: *American Geophysical Union Transactions*, v. 45, no. 4, p. 659-663.
- Mower, R. W., Hood, J. W., Cushman, R. L., Borton, R. L., and Galloway, S. E., 1964, An appraisal of potential ground-water salvage along the Pecos River between Acme and Artesia, New Mexico: U.S. Geological Survey Water-Supply Paper 1659, 98 p.

- Myers, B. N., 1969, Compilation of results of aquifer tests in Texas: Texas Water Development Board Report No. 98, 532 p.
- National Academy of Sciences, Committee on Radioactive Waste Management, 1970, Disposal of solid radioactive waste in bedded salt deposits: Washington, D.C., U.S. Government Printing Office, 28 p.
- Neck, R. W., 1978, Molluscan remains and environmental interpretations at the Lake Theo Folsom site (41BI70), Caprock Canyons State Park, Briscoe County, Texas, appendix in Harrison, B. R., and Killen, K. L., Lake Theo--a stratified, early man bison butchering and camp site, Briscoe County, Texas (archeological investigations, phase 2): Canyon, Texas, Panhandle-Plains Historical Museum Special Archeological Report 1, p. 92-98.
- Nelson, T. A., 1976, An automated rapid sediment analyser (ARSA): Sedimentology, v. 23, p. 867-872.
- Neuman, P. S., and Witherspoon, P. A., 1970, Finite element method of analyzing steady seepage with a free surface: Water Resources Research, v. 6, no. 3, p. 889-897.
- Nicholas, R. L., and Rosendal, R. A., 1975, Subsurface positive elements within the Ouachita foldbelt in Texas, and their relation to paleozoic cratonic margin: American Association of Petroleum Geologists Bulletin, v. 59, no. 2, p. 193-216.
- Nicholson, J. H., 1960, Geology of the Texas Panhandle, in Aspects of the geology of Texas, a symposium: University of Texas, Austin, Bureau of Economic Geology Publication No. 6017, p. 51-64.
- Nie, N. H., Hull, C.H., Jenkins, J. G., Steinbrenner, Karin, and But, D. H., 1975, Statistical package for the social sciences: New York, McGraw-Hill, 675 p.
- Nielsen, K. C., and Scott, T. E., Jr., 1979, Precambrian deformational history of the Picuris Mountains, New Mexico: New Mexico Geological Society Guidebook, 30th field conference, p. 113-120.

- Norton, P., 1954, A new Blaccan vertebrate locality: *Journal of Paleontology*, v. 28, p. 487.
- Office of Nuclear Waste Isolation (ONWI), 1979, The status of borehole plugging and shaft sealing for geologic isolation of radioactive waste: ONWI-15.
- Oldfield, F., and Schoenwetter, J., 1964, Late Quaternary environments and early man on the Southern High Plains: *Antiquity*, v. 38, p. 226-229.
- \_\_\_\_\_, 1970, Pollen analysis of late Pleistocene deposits in West Texas and eastern New Mexico: American Quaternary Association, Meeting Abstracts, p. 102.
- Orgill, M. M., and Sehmel, G. A., 1976, Frequency and diurnal variation of dust storms in the contiguous USA: *Atmospheric Environment*, v. 10, p. 813-825.
- Orr, E. D., and Dutton, A. R., 1983, An application of geostatistics to determine regional ground-water flow in the San Andres Formation, Texas and New Mexico: *Ground Water*, v. 21, no. 5, p. 619-624.
- Orr, E. D., and Kreidler, C. W., 1985, Interpretation of pressure-depth data from confined underpressured aquifers exemplified by the Deep-Basin Brine aquifer, Palo Duro Basin, Texas: *Water Resources Research*, v. 21, p. 533-544.
- Page, L. R., and Adams, J. E., 1940, Stratigraphy, eastern Midland Basin, Texas: *American Association of Petroleum Geologists Bulletin*, v. 24, p. 52-64.
- Palmer, D. P., 1981, Clay mineralogy of Permian sabkha sequences, Palo Duro Basin, Texas: The University of Texas at Austin, Master's thesis, 93 p.
- Patton, L. T., 1923, The geology of Potter County: University of Texas, Austin, Bureau of Economic Geology and Technology Bulletin 2330, 184 p.
- Péwé, T. L., 1981, Desert dust: an overview, in Péwé, T. L., ed., Desert dust: origin, characteristics, and effect on man: Geological Society of America Special Paper 186, p. 1-10.
- Pierce, H. G., 1975, Diversity of Late Cenozoic gastropods of the Southern High Plains: Texas Tech University, Ph.D dissertation, 267 p.

- Popkin, B. P., 1973, Ground-water resources of Hall and eastern Briscoe Counties, Texas: Texas Water Development Board Report 167, 84 p.
- Powell, B. N., and Fischer, J. F., 1976, Plutonic igneous geology of the Wichita magmatic province, Oklahoma: Oklahoma Geological Survey, Guidebook for field trip #2, south-central section, Geological Society of America.
- Powell, B. N., Gilbert, M. C., and Fischer, J. F., 1980, Lithostratigraphic classification of basement rocks of the Wichita province, Oklahoma: summary: Geological Society of America Bulletin, pt. 1, v. 91, p. 509-514.
- Presley, M. W., 1979a, Upper Permian evaporites and red beds, in Dutton, S. P., and others, Geology and geohydrology of the Palo Duro Basin, Texas Panhandle, a report on the progress of nuclear waste isolation feasibility studies (1978): The University of Texas at Austin, Bureau of Economic Geology Geological Circular 79-1, p. 39-49.
- \_\_\_\_\_ 1979b, Salt deposits, in Dutton, S. P., and others, Geology and geohydrology of the Palo Duro Basin, Texas Panhandle, a report on the progress of nuclear waste isolation feasibility studies (1978): The University of Texas at Austin, Bureau of Economic Geology Geological Circular 79-1, p. 50-56.
- \_\_\_\_\_ 1980, Upper Permian salt-bearing stratigraphic units, in Gustavson, T. C., and others, Geology and geohydrology of the Palo Duro Basin, Texas Panhandle, a report on the progress of nuclear waste isolation feasibility studies (1980): The University of Texas at Austin, Bureau of Economic Geology Geological Circular 80-7, p. 12-23.
- \_\_\_\_\_ 1981, San Andres salt stratigraphy and salt purity, in Gustavson, T. C., and others, Geology and geohydrology of the Palo Duro Basin, Texas Panhandle, a report on the progress of nuclear waste isolation feasibility studies (1981): The University of Texas at Austin, Bureau of Economic Geology Geological Circular 81-3, p. 33-40.
- Presley, M. W., and McGillis, K. A., 1982, Coastal evaporite and tidal-flat sediments of the Upper Clear Fork and Glorieta Formations, Texas Panhandle: The University of Texas at Austin, Bureau of Economic Geology Report of Investigations No. 115, 50 p.

- Rahmani, R. A., 1973, Grain surface etching features of some heavy minerals: *Journal of Sedimentary Petrology*, v. 43, p. 882-888.
- Railroad Commission of Texas, 1969, Docket No. 20-29, 540, application by Shell Oil Company for discovery allowable and new field designation of Manarte (Granite Wash, Upper) for Shell Alamosa 315 No. 2, Oldham County, Texas.
- \_\_\_\_\_ 1982, Docket no. 10-78, 609, application by Baker & Taylor Drilling Company for Discovery Allowable and New Field Designation of Hryhor (Granite Wash) for Baker & Taylor Aurora No. 1, Oldham County, Texas.
- Raymer, L. L., and Biggs, W. P., 1963, Matrix characteristics defined by porosity computations: *Society of Professional Well Log Analysts Symposium*, 21 p.
- Reagor, B. G., Stover, C. W., and Algermissen, S. T., 1982, Seismicity map of the State of Texas: U. S. Geological Survey Miscellaneous Field Studies Map MF-1388, scale 1:1,000,000.
- Richter, C. F., 1958, *Elementary seismology*: San Francisco, W. H. Freeman, 768 p.
- Robinson, P., 1972, Tertiary history, in Mallory, W. W., ed., *Geologic atlas of the Rocky Mountains*: Rocky Mountain Association of Geologists, p. 233-242.
- Rogatz, Henry, 1939, *Geology of the Texas Panhandle oil and gas field*: American Association of Petroleum Geologists Bulletin, v. 23, no. 7, p. 983-1053.
- Roth, R. I., Newell, N. D., and Burme, B. N., 1941, Permian pelecypods in the lower Quartermaster Formation, Texas: *Journal of Paleontology*, v. 15, no. 3, p. 312-317.
- Roy, D. M., and Grutzeck, M. W., 1982, DSU/WES interlaboratory study of experimental cementitious repository seal material: ONWI-324 Technical Report, 149 p.
- Roy, D. M., and Grutzeck, M. W., and Wakeley, L. D., 1982, Selection and durability of seal materials for a bedded salt repository: Topical report for ONWI, 157 p.
- Ruppel, S. C., and Hovorka, S. D., 1983a, Stratigraphic section along the northeastern margin of the Palo Duro Basin: core analysis of DOE - Stone and Webster No. 1 Sawyer test well, Donley County, Texas, in Gustavson, T. C., and others, *Geology and*

geohydrology of the Palo Duro Basin, Texas Panhandle, a report on the progress of nuclear waste isolation feasibility studies (1982): The University of Texas at Austin, Bureau of Economic Geology Geological Circular 83-4, p. 45-46.

\_\_\_\_\_ 1983b, Stratigraphic section along the northwestern margin of the Palo Duro Basin: core analysis of DOE - Stone and Webster No. 1 Mansfield test well, Oldham County, Texas, in Gustavson, T. C., and others, Geology and geohydrology of the Palo Duro Basin, Texas Panhandle, a report on the progress of nuclear waste isolation feasibility studies (1982): The University of Texas at Austin, Bureau of Economic Geology Geological Circular 83-4, p. 47-48.

Ruppel, S. C., and Ramondetta, P. J., 1982, Determination of salt purity using gamma-ray logs: San Andres Formation, Palo Duro Basin, in Gustavson, T. C., and others, Geology and geohydrology of the Palo Duro Basin, Texas Panhandle: a report on the progress of nuclear waste isolation feasibility studies (1982): The University of Texas at Austin, Bureau of Economic Geology Geological Circular 82-7, p. 183-199.

Sandburg, C. A., 1979, Devonian and Lower Mississippian conodont zonation of the Great Basin and Rocky Mountains: Brigham Young University Studies, v. 26, pt. 3.

Sarkar, A. K., Barnes, M. W., and Roy, D. M., 1982, Longevity of borehole and shaft sealing materials: thermodynamic properties of cements and related phases applied to depository sealing: ONWI-201 Technical Report, 48 p.

Schlumberger Limited, 1972, Log interpretation, volume I-principles: New York, Schlumberger Limited, 113 p.

\_\_\_\_\_ 1979, Log interpretation charts: New York, Schlumberger Limited, 97 p.

Schultz, G. F., ed., 1977, Field conference on Late Cenozoic biostratigraphy of the Texas Panhandle and adjacent Oklahoma: West Texas State University Killgore Research Center Special Publication no. 1, 165 p.

Schumm, S. A., 1963, Disparity between present rates of denudation and orogeny: U.S. Geological Survey Professional Paper 454, 13 p.

- \_\_\_\_\_ 1977, The fluvial system: New York, John Wiley, 338 p.
- Schwab, K. W., 1977, Source rock evaluation (visual kerogen): Houston, Geo-Strat, Inc., commercial brochure.
- Scott, G. R., 1975, Cenozoic surfaces and deposits in the southwestern Rocky Mountains, in Curtis, B. F., ed., Cenozoic history of the southern Rocky Mountains: Geological Society of America, Memoir 144, p. 277-248.
- Seager, W. R. and Morgan, P., 1979, Rio Grande rift in southern New Mexico, west Texas, and northern Chihuahua: in Reicker, R. E. (ed.) Rio Grande rift: Tectonics and Magnetism: Washington, D.C., American Geophysical Union, p. 87-106.
- Sellards, E. H., 1952, Early man in America--a study in prehistory: Austin, University of Texas Press, 211 p.
- Seni, S. J., 1978, Genetic stratigraphy of the Dockum Group (Triassic), Palo Duro Canyon, Panhandle, Texas: The University of Texas at Austin, Master's thesis, 157 p.
- \_\_\_\_\_ 1980, Sand-body geometry and depositional systems, Ogallala Formation, Texas: The University of Texas at Austin, Bureau of Economic Geology Report of Investigations No. 105, 36 p.
- Seni, S. J., McGowen, J. H., and Risner, R. S., 1980, Uranium resource evaluation, Amarillo quadrangle, Texas: U.S. Department of Energy, Grand Junction Office, Open-file Report GJQ-013 (81), 24 p.
- Shideler, G. L., 1976, A comparison of electronic particle counting and pipette techniques in routine mud analysis: Journal of Sedimentary Petrology, v. 46, no. 4, p. 1017-1025.
- Sidwell, R., 1938, Sand and dust storms in the vicinity of Lubbock, Texas: Economic Geography, v. 14, no. 1, p. 98-102.
- Simpkins, W. W., and Baumgardner, R. W., Jr., 1982, Stream incision and scarp retreat rates based on volcanic ash date from the Seymour Formation, in Gustavson, T. C., and others, Geology and geohydrology of the Palo Duro Basin, Texas Panhandle, a report on the progress of nuclear waste isolation feasibility studies (1981): The



University of Texas at Austin, Bureau of Economic Geology Geological Circular 82-7, p. 160-163.

Simpkins, W. W., and Gustavson, T. C., 1985, Erosion rates and processes in subhumid and semiarid climates, Texas Panhandle: statistical evaluation of field data: The University of Texas at Austin, Bureau of Economic Geology Open-File Report OF-WTWI-1985-13, 55 p.

Simpkins, W. W., Gustavson, T. C., Alhades, A. B., and Hoadley, A. D., 1981, Impact of evaporite dissolution and collapse on highways and other cultural features in the Texas Panhandle and eastern New Mexico: The University of Texas at Austin, Bureau of Economic Geology Geological Circular 81-4, 23 p.

Simpkins, W. W., Gustavson, T. C., and Finley, R. J., 1982, Erosion process studies in the Texas Panhandle--analysis of a two year data record, in Gustavson, T. C., and others, Geology and geohydrology of the Palo Duro Basin, Texas Panhandle, a report on the progress of nuclear waste isolation feasibility studies (1981): The University of Texas at Austin, Bureau of Economic Geology Geological Circular 82-7, p. 168-175.

Simpson, G. S., 1976, Evidence of overgrowths on, and solution of, detrital garnets: Journal of Sedimentary Petrology, v. 46, p. 689-693.

Smith, D. A., Bassett, R. L., and Roberts, M. P., 1983, Potentiometric surface of the Wolfcampian aquifer, Palo Duro Basin, in Gustavson, T. C., and others, Geology and hydrology of the Palo Duro Basin (1982): The University of Texas at Austin, Bureau of Economic Geology Geological Circular 83-4, p. 94-96.

Smith, R. M., Twiss, P. C., Krauss, R. K., and Brown, M. J., 1970, Dust deposition in relation to site, season, and climatic variables: Soil Science Society of America, Proceedings, v. 34, p. 112-117.

Soderstrom, G. S., 1968, Stratigraphic relationships in the Palo Duro-Hardeman Basin area, in Basins of the Southwest, v. 1: West Texas Geological Society, p. 41-49.

- Stevens, P. R., 1974, Geohydrology of the Upper Brazos River Basin between Lubbock and Possum Kingdom Reservoir, Texas, with special reference to discharge of brine from springs and seeps: on file at U.S. Geological Survey, Water Resources Division, Austin, Texas (unpublished manuscript).
- Stone and Webster Engineering Corporation, 1983, Well completion report: dissolution zone water wells, Palo Duro Basin: Boston, Stone and Webster Engineering Corporation, 15 p.
- Stormer, J. C., Jr., 1972, Ages and nature of volcanic activity on the Southern High Plains, New Mexico and Colorado: Geological Society of America Bulletin, v. 83, no. 8, p. 2443-2448.
- Strahler, A. N., 1952, Hypsometric (area-altitude) analysis of erosional topography: Geological Society of America Bulletin, v. 63, p. 1117-1142.
- Thompson, T. L., and Goebel, E. D., 1969, Conodonts and stratigraphy of the Meramecian stage (upper Mississippian) in Kansas: Kansas Geological Survey Bulletin, v. 192, 56 p.
- Till, Roger, 1974, Statistical methods for the earth scientist: New York, Halstead Press, 154 p.
- Tissot, B. P., and Welte, D. H., 1978, Petroleum formation and occurrence: New York, Springer-Verlag, 538 p.
- Tóth, J., 1978, Gravity induced cross-formational flow of formation fluids, Red Earth Region, Alberta, Canada: analysis, patterns, and evolution: Water Resources Research, v. 14, no. 5, p. 805-843.
- \_\_\_\_\_, 1979, Patterns of dynamic pressure increment of formation-fluid flow in large drainage basins, exemplified by the Red Earth Region, Alberta, Canada: Bulletin of Canadian Petroleum Geology, v. 27, no. 1, p. 63-86.
- Tweto, Ogden, 1979, The Rio Grande Rift System in Colorado, in Riecker, R. E., ed., Rio Grande Rift: tectonics and magmatism: American Geophysical Union, p. 33-56.

- \_\_\_\_\_ 1980, Precambrian geology of Colorado: Colorado Geology, Rocky Mountain Association of Geologists, 1980 Symposium, p. 37-46.
- Viessman, Warren, Jr., Knapp, J. W., Lewis, C. L., and Harbaugh, T. F., 1977, Introduction to hydrology: New York, Harper and Row, 704 p.
- Wakeley, L. D., Roy, D. M., and Grutzeck, M. W., 1981, Experimental studies of seal materials for potential use in Los Medanos-type bedded salt repository: ONWI-325 Technical Report, 115 p.
- Walters, R. F., 1975, Salt dissolution in oil and gas test holes in central Kansas: Oak Ridge National Laboratory Contract Report.
- \_\_\_\_\_ 1978, Land subsidence in central Kansas related to salt dissolution: Kansas Geological Survey Bulletin, v. 214, 82 p.
- Weaver, C. E., and Pollard, L. D., 1973, The chemistry of clay minerals: Amsterdam, Elsevier, 213 p.
- Webb, W. P., 1931, The Great Plains: Boston, Ginn and Company, 525 p.
- Weeks, J. B., and Gutentag, E. D., 1981, Bedrock geology, altitude of base, and 1980 saturated thickness of the High Plains aquifer in parts of Colorado, Kansas, Nebraska, New Mexico, Oklahoma, South Dakota, Texas, and Wyoming: U.S. Geological Survey, Hydrologic Investigations Atlas HA-648, scale 1:250,000.
- Wendorf, Fred, 1961, An interpretation of late Pleistocene environments of the Llano Estacado, in Wendorf, Fred, ed., Paleoecology of the Llano Estacado: Albuquerque, Museum of New Mexico Press, Fort Burgwin Research Center Publication No. 1, p. 115-133.
- Whittemore, D. O., Basel, C. L., Galle, O. K., and Waugh, T. C., 1981, Geochemical identification of saltwater sources in the Smoky Hill River valley, MacPherson, Saline, and Dickinson Counties, Kansas: Kansas Geological Survey final report to the U.S. Army Corps of Engineers, 78 p.



- Williams, H., Turner, F. J., and Gilbert, C. M., 1954, Petrography: an introduction to the study of rocks in thin sections: San Francisco, W. H. Freeman, 406 p.
- Wirojanagud, P., Kreitler, C. W., and Smith, D. A., 1986, Numerical modeling of regional ground-water flow in the Deep-Basin Brine aquifer of the Palo Duro Basin, Texas Panhandle: The University of Texas at Austin, Bureau of Economic Geology Report of Investigations No. 159, 68 p.
- Yaalon, D. H., and Ganor, E., 1973, The influence of dust on soils during the Quaternary: Soil Science, v. 116, no. 3, p. 146-155.